Response of Deep Foundations to Seismic Loads in Alabama

By

Kevin Marshall Kane

A thesis submitted to the Graduate Faculty of
Auburn University
in partial fulfillment of the
requirements for the Degree of
Master of Science

Auburn, Alabama
December 14, 2013

Keywords: pile, buckling, scour, soil-foundation-structure interaction

Approved by

J. Brian Anderson, Chair, Associate Professor of Civil Engineering
Justin Marshall, Assistant Professor of Civil Engineering
Robert Barnes, James J. Mallet Associate Professor of Civil Engineering

ABSTRACT

Deep foundations are commonly used as foundation elements for bridges in Alabama. Due to the implementation of the American Association of State Highway and Transportation Officials (AASHTO) Load and Resistance Factor Design (LRFD) Bridge Design Specifications, design of critical and essential bridges will be significantly impacted for the moderate seismic design category of Alabama.

Five bridge case studies were provided by the Alabama Department of Transportation (ALDOT) to evaluate the response of typical foundations used for critical and essential bridges. FB-MultiPier, a program that couples nonlinear structural finite element analysis with nonlinear static soil models, was used to model both the soil and structure (both foundation elements and substructure components) of each case history. These models were loaded with a suite of scaled time-history events to simulate an earthquake. Displacement at the top of the pier and ground surface was recorded, as well as maximum shear force, bending moment, and demand/capacity (D/C) ratio distribution along the length of the driven pile, drilled shaft, or column. The maximum shear force, bending moment, and D/C ratio distributions indicated where the plastic hinge zones could be expected to form in the structure. FB-MultiPier was also used to develop a family of foundation response curves that were used in SAP2000 to evaluate the performance of the case histories.

Pile performance under combined scour and earthquake was reviewed and two different scour depth models were developed for one case history. Buckling criteria for foundations in soft clay or liquefiable soil were also reviewed and compared to two case histories.

It was found that scour depth appears to affect the dynamic response of the bridge pier. The pier modeled with 25% scour depth performed worse (structurally) than the same pier modeled with 100% scour depth. This was due to large displacements at the ground surface and large bending moments developing below the ground surface. The pier founded in soft clay over rock performed poorly due to structural failure in the foundations. This was due to flexure failure of the piles. It was also found that drilled shafts embedded in shallow bedrock tend to perform well depending on the natural frequency and structural period of the pier. Recommendations for further research address soil susceptibility to scour and liquefaction, full-scale dynamic load testing, and correlations between the natural and structural period of a bridge pier and its performance during an earthquake event.

ACKNOWLEDGMENTS

First, I would like to thank God for the many blessings He has bestowed upon me throughout my life. It is through Him that all things are possible. I want to thank Dr. Brian Anderson for his guidance throughout this process and giving me the opportunity to further my education. He is not only a mentor but a friend in which I greatly appreciate. I also want to thank Dr. Justin Marshall and Dr. Robert Barnes for their guidance and contributions for this project.

Thank you to the Alabama Department of Transportation for funding this study. Thank you to Kaye Chancellor and Tim Colquett, representatives of ALDOT, for their help throughout this project. Thanks to Jordan Panzer and Jordan Law for their collaborative efforts during this project. I also would like to thank my fellow students and professors who have helped me throughout my career, here at Auburn.

I want to thank my wonderful girlfriend, Haley Grant. Her support, compassion, and patience throughout this process were unwavering. Finally, I want to thank my parents, Carl and Cathy Kane for their never-ending support, guidance, and love throughout my life. I am extremely blessed to have them as parents.

TABLE OF CONTENTS

LIST OF TABLES

LIST OF FIGURES

Chapter 1

INTRODUCTION

Due to the implementation of the AASHTO LRFD Bridge Design Specifications (LRFD Specification) (AASHTO 2013), design of bridges will be significantly impacted for the moderate seismic design category[1] (SDC) of Alabama. Since the AASHTO Standard Specification for Highway Bridges (Standard Specification) (AASHTO 2002) was last updated, there has been a significant amount of geotechnical and seismic hazard mapping research. Under the Standard Specification, Alabama was almost entirely classified as SDC A, which requires minimum detailing and no additional analysis for bridge design. The Standard Specification seismic hazard map showing peak ground acceleration (PGA) is shown in Figure 1.1.

[1] SDC, seismic hazard, and seismic zone all have the same meaning and are used frequently throughout literature. To be consistent, SDC will be used in accordance with the 2009 AASHTO Guide Specifications for LRFD Seismic Bridge Design (Guide Specification).

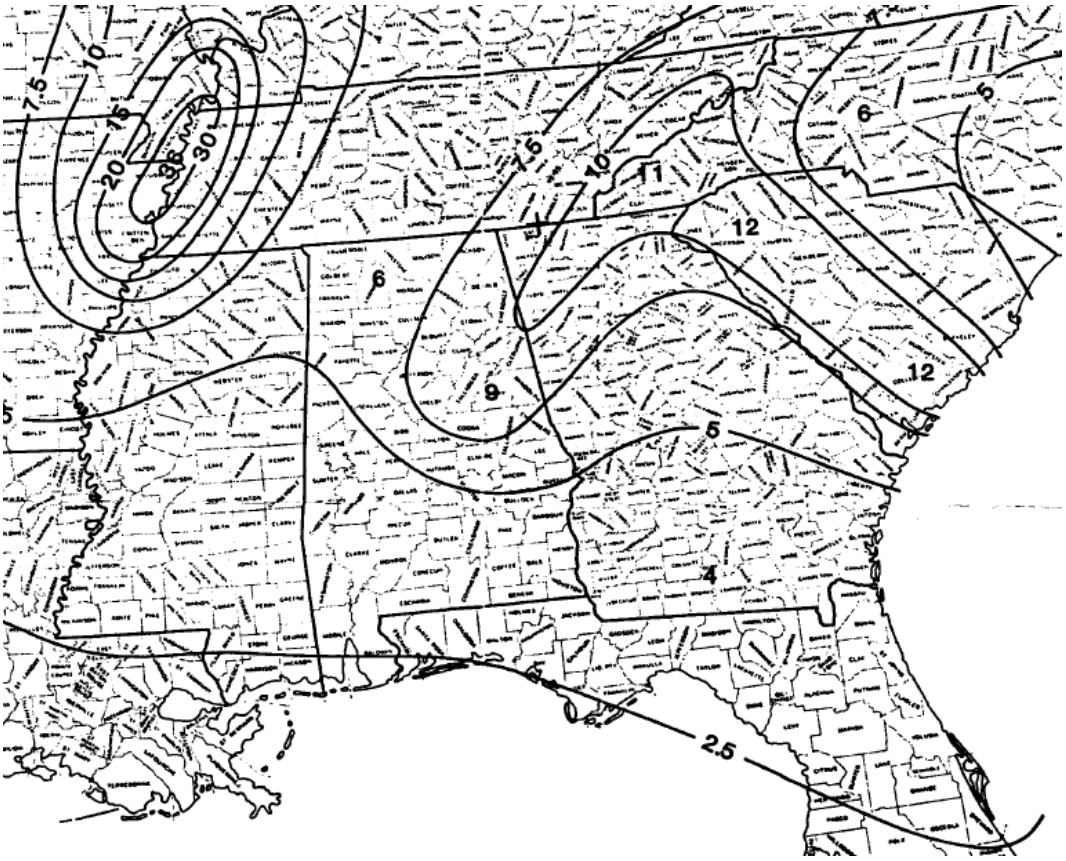

Figure 1.1. Standard Specification for PGA (%g) for a 500 year return period (AASHTO 2002)

The LRFD Specification seismic hazard maps have been significantly modified because of two primary changes: (1) the design level earthquake has increased from a 500-year return period to a 1000-year return period, and (2) the sources associated with Alabama seismicity, the New Madrid Seismic Zone and the East Tennessee Seismic Zone, have been further studied, which has consequently increased the PGA values for the state (Coulston, 2011). In addition, the methodology to determine the SDC now includes the geotechnical Site Class. Figure 1.2 shows the seismic hazard map for the LRFD Specification. In comparison to Figure 1.1, Figure 1.2 shows a greater level of

detail. Subsequently, the PGA has increased significantly in certain areas, especially in the northern half of the state.

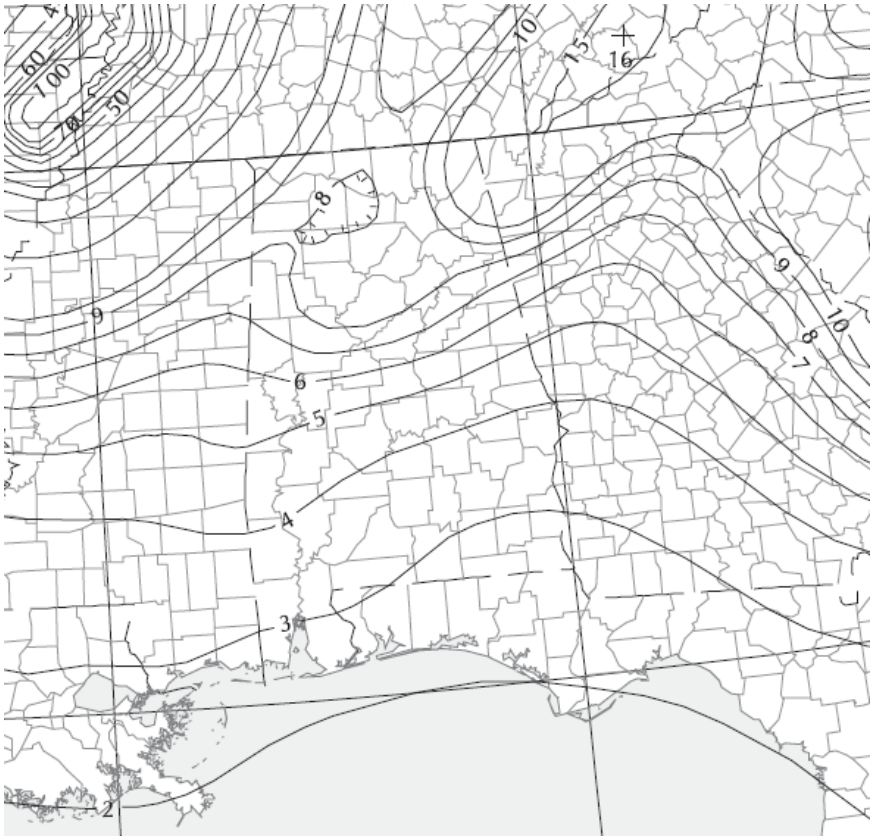

Figure 1.2. LRFD Specification for PGA for 1000-yr return period (AASHTO 2009)

1.1 Objectives

The primary objective of this research was to evaluate the response of deep foundations to seismic loads in Alabama. The specific objectives of the project included the following:

- Determine if ALDOTs current typical critical and essential bridge design, specifically regarding the foundation elements, are suitable for seismic design in Alabama.
- Determine the effects (if any) that scour and liquefaction have on driven piles and drilled shafts during an earthquake event.
- Review other state DOT's seismic design practices.

1.2 Scope of Work

A comprehensive review of deep foundation literature and design methods for seismic design was conducted along with a survey of other state DOTs to review their approach to seismic design of bridge foundations.

Substructure analysis was completed and static foundation response curves were developed. These curves were used in SAP2000 to represent the foundations for the bridges (Panzer 2013). A direct analysis was conducted in which a bridge bent was modeled for each case history and two scour cases for one of the case histories were modeled: 25% and 100% of scour depth. A suite of scaled time-history events developed by Panzer (2013) was used to load the bent dynamically. Displacements at the top of the bent and the ground surface were recorded, as well as maximum shear force, bending moment and demand/capacity (D/C) ratio distributions.

The results of the direct analyses were compared to the literature review findings and discussed. Recommendations for future research were also made.

Chapter 2

BACKGROUND

Chapter 2 provides background information on the relevant topics that this project encompassed. Previous research conducted by Auburn University and methods for determining liquefaction potential are presented and discussed. Soil-foundation-structure interaction is discussed in detail as well as different analysis methods for determining the foundation response. An overview of the computer software that was used to conduct the analysis methods is provided. This also includes methods for determining soil parameters needed and an overview of the dynamic analysis options available in the program. Finally, a brief overview of FHWA GEC-3 (Kavazanjian et al. 2011) is given, which summarizes several key points of emphasis for geotechnical considerations in seismic analysis and design.

2.1 Previous Research

A preliminary study (Coulston 2011) funded by the Auburn University Highway Research Center at Auburn University (HRC) was conducted to determine whether a set of economical bridge design standards, applicable to all hazards in the state, would be feasible. It was decided by ALDOT that its Bridge Bureau will use the Guide Specification for LRFD Seismic Bridge Design (Guide Specification), which is a displacement-based seismic design guideline, as an alternative to the LRFD Specification force-based seismic design provisions. The HRC study showed the Guide Specification to be simpler and more economical. However, the Guide Specification is only applicable

to Ordinary bridges, not Critical and Essential bridges. As part of the ongoing research by ALDOT, the design of Critical and Essential bridges are to be investigated and validated. Each class has a specific seismic design philosophy that was adopted by AASHTO:

A) Critical Bridge

A critical bridge is expected to remain open to all traffic, including emergency vehicles, and for defense and security purposes after the design earthquake (large rare earthquake with a 1000-year return period) (Kavazanjian et al. 2011).

B) Essential Bridge

An essential bridge is expected to be usable by emergency vehicles and for security and defense purposes after the design earthquake (Kavazanjian et al. 2011).

C) Ordinary Bridge

Bridges that don't fall under the critical or essential class are ordinary bridges. These bridges are designed to allow significant structural damage after the design earthquake (Kavazanjian et al. 2011).

The HRC study also found that a single design standard would not be feasible and further investigation was needed, including evaluating the response of deep foundations to seismic loads.

The primary concern for design of bridges to seismic events is the substructure elements, the superstructure-to-substructure connection (including the webwall or diaphragm braces), and the foundations (Coulston 2011). Damage is expected to occur at specific ductile elements without causing collapse for design level events (Coulston 2011). For the moderate hazard of Alabama, the substructure should be designed to be

the ductile link, whereas the other previously mentioned elements are to remain elastic (Coulston 2011). Figure 2.1 illustrates this behavior.

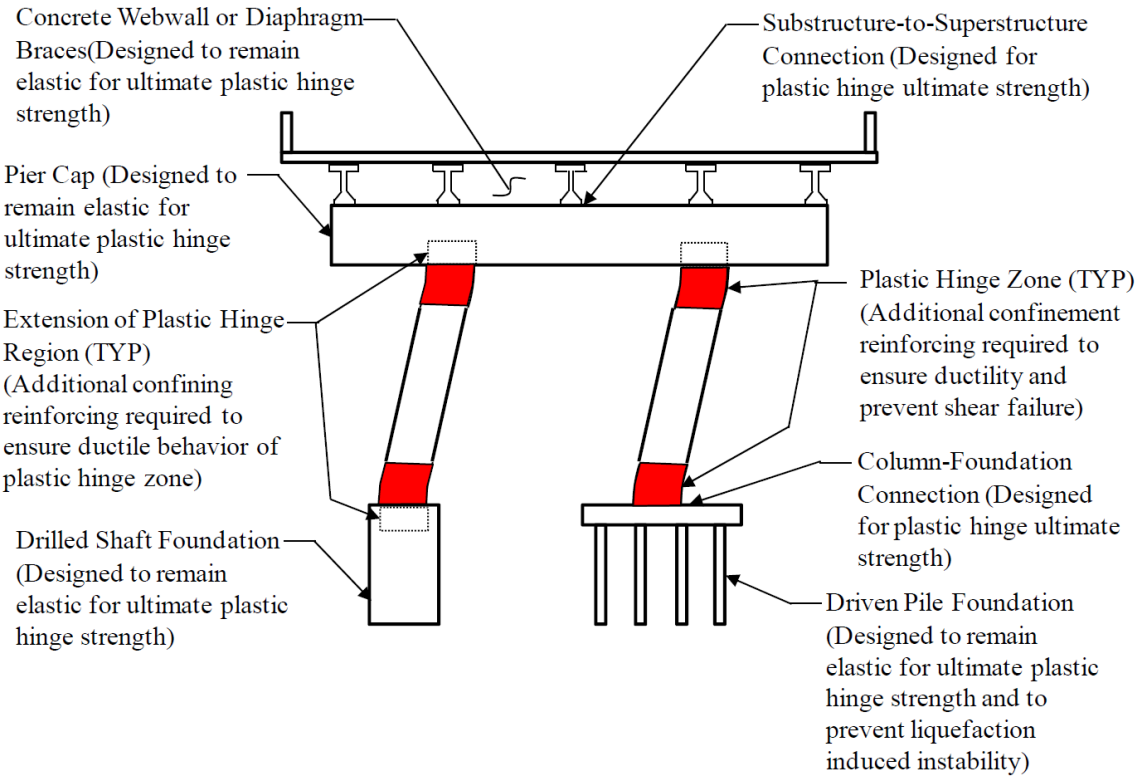

Figure 2.1. Inelastic behavior of bridge elements in design level seismic event (Coulston 2011)

As previously mentioned in Chapter 1, the method for determining the SDC has significantly changed since the Standard Specification was last updated. According to Coulston (2011), SDC B would likely be the highest design category to occur in Alabama. Figure 2.1 shows the design spectrum for several major cities in Alabama based on assuming Site Class D, which is the default soil condition for preliminary design. The different Site Class definitions are displayed in Table 2.1. Site class is determined by averaging the shear wave velocity, shear strength, or N-value throughout the top 100 feet of soil and/or rock. See AASHTO (2009) for further details. The

criterion for determining the SDC for a given site/area is shown in Table 2.2. Referring to Figure 2.2, the largest spectral acceleration at a period of one second (SA_1) is about 0.18, which is well below the threshold of SDC C, 0.30.

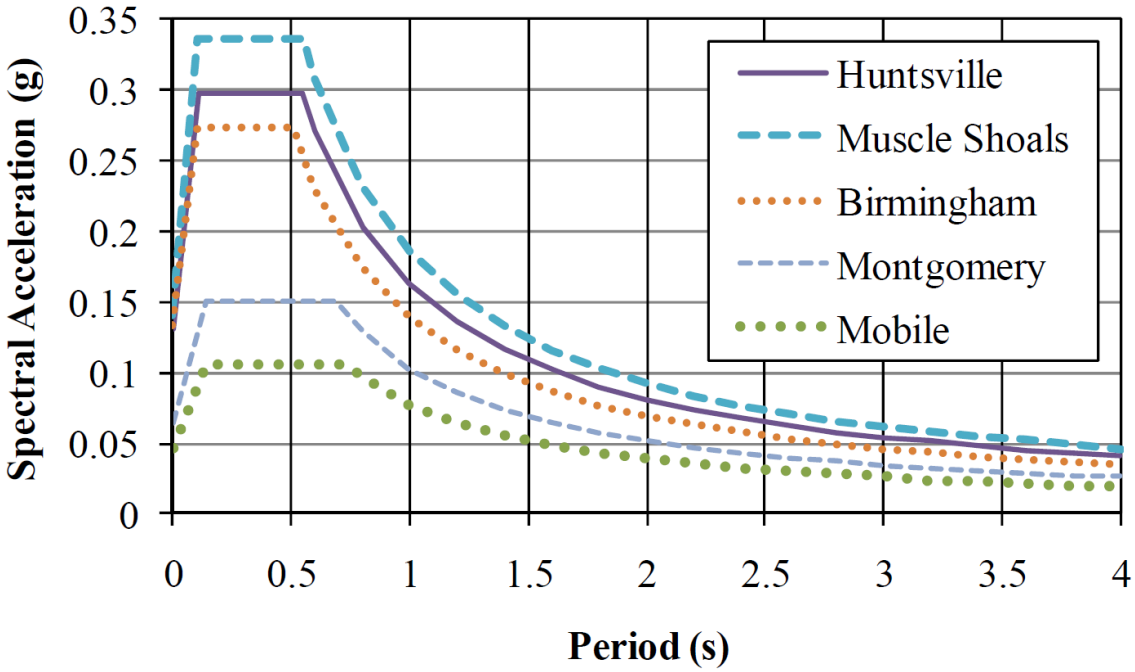

Figure 2.2. Design level seismic hazard curves for select Alabama cities (Coulston 2011)

Table 2.1 – Site class definitions (AASHTO 2009)

Site Class	Soil Type and Profile
A	Hard Rock with measured shear wave velocity, $\overline{v_s}$ > 5000 ft/sec
B	Rock with 2500 ft/sec < $\overline{v_s}$ < 5000 ft/sec
C	Very dense soil and soil rock with 1200 ft/sec < $\overline{v_s}$ < 2500 ft/sec, or with either $\overline{N}$ > 50 blows/ft or $\overline{s_u}$ > 2.0 ksf
D	Stiff soil with 600 ft/sec < $\overline{v_s}$ < 1200 ft/sec, or with either 15 blows/ft < $\overline{N}$ < 50 blows/ft or 1.0 < $\overline{s_u}$ < 2.0 ksf
E	Soil profile with $\overline{v_s}$ < 600 ft/sec, or with either $\overline{N}$ < 15 blows/ft or $\overline{s_u}$ < 1.0 ksf, or any profile with more than 10 ft of soft clay defined as soil with PI > 20, w > 40%, and $\overline{s_u}$ < 0.5 ksf
F	Soil requiring site-specific ground motion response evaluations, such as: Peats of highly organic clays (H > 10 ft of peat or highly organic clay, where H = thickness of soil) Very high plasticity clays (H > 25 ft with PI > 75 Very thick soft/medium stiff clays (H > 120 ft)

Exceptions:
Where the soil properties are not known in sufficient detail to determine the site class, a site investigation shall be undertaken sufficient to determine the site class. Site Class E and F could be present at the site or in the event that Site Class E or F is established by geotechnical data.

Where:
$\overline{v_s}$ = average shear wave velocity for the upper 100 ft of the soil profile as defined in Article 3.4.2.2
$\overline{N}$ = average standard penetration test (SPT) blow count (blows/ft) (ASTM D 1586) for the upper 100 ft of the soil profile as defined in Article 3.4.2.2
$\overline{s_u}$ = average undrained shear strength in ksf (ASTM D 2166 or D 2850) for the upper 100 ft of the soil profile as defined in Article 3.4.2.2
PI = plasticity index (ASTM D 4318)
w = moisture content (ASTM D 2216)

Table 2.2 – Partitions for seismic design categories A, B, C, and D (AASHTO 2009)

Value of SA_1	SDC
SA_1 < 0.15	A
0.15 < SA_1 < 0.30	B
0.30 < SA_1 < 0.50	C
0.50 < SA_1	D
Where: SA_1 = Spectral acceleration at a period of 1 second	

Currently, the Guide Specification (displacement-based procedure) does not allow for design of Critical and Essential bridges. There are three classes of bridges: (A) Critical, (B) Essential, and (C) Other (sometimes called Ordinary) Bridges (in descending order of importance) (Kavazanjian et al. 2011).

2.2 Evaluation of Liquefaction Potential

During an earthquake, insitu soils may be susceptible to liquefaction. Liquefaction typically occurs when saturated cohesionless soil undergoes undrained loading conditions which generate excess pore water pressures (Kramer, 1996). This increase in pore water pressure subsequently decreases soil shear strength and stability; the soil then mobilizes until it reaches a state of equilibrium. There are two general modes of liquefaction that can occur: (A) flow liquefaction and (B) cyclic mobility (lateral spreading) (Kramer, 1996).

A) Flow Liquefaction

Flow liquefaction produces the most dramatic effects of the two, flow failures (or landslides), which occur on sloping ground. Flow liquefaction occurs when the shear stress required for static equilibrium is greater than the shear strength of the soil (Kramer, 1996). The soil then "flows" under the influence of gravity until it reaches a stable condition. These can often be catastrophic, destroying structures and killing people in its path. Figure 2.3 shows an example of damage caused by flow liquefaction.

Figure 2.3. Flow liquefaction damage to a road in Japan during an offshore earthquake in 2007 (USGS, 2008)

B) Lateral Spreading

Lateral Spreading, on the other hand, occurs on gently sloping ground or flat ground near water when the static shear stress is less than the shear strength of the liquefied soil (Kramer 1996). These deformations can occur well after ground shaking has ceased, depending on the length of time required to reach static equilibrium (Kramer 1996). This mode can be destructive as well, causing bridges to collapse and excessive settlement of structures. Figure 2.4 shows a collapsed bridge due to lateral spreading.

Figure 2.4. Collapse of the showa bridge in the 1964 Niigata, Japan earthquake (NGDC as referenced in Kavazanjian et al. 2011)

Because both modes of liquefaction can cause significant structural damage to existing structures, an evaluation of liquefaction susceptibility is an important aspect of seismic design. Both modes of liquefaction can cause axial and lateral resistance of foundations to decrease significantly.

In a recent study (Ebersole and Perry 2008), liquefaction potential was mapped based on geologic age and origin using the Youd and Perkins (1978) method, which is shown in Table 2.3. This method is based on geologic conditions. Some geologic formations are inherently more susceptible to liquefaction than others. Figure 2.5 shows liquefaction susceptibility for Alabama. This map clearly indicates the relatively low potential for the northern part of the state. However, almost all of the areas that have a high potential for liquefaction are located near stream or river beds where alluvial

cohesionless deposits generally make up the soil stratigraphy and the soils have a high degree of saturation. This is important because many bridges are built to cross waterways.

Table 2.3 – Susceptibility of sedimentary deposits to liquefaction during strong shaking (Youd and Perkins 1978)

Type of deposit (1)	General distribution of cohesionless sediments in deposits (2)	Likelihood that Cohesionless Sediments, When Saturated, Would Be Susceptible to Liquefaction (by age of Deposit)			
		<500 yr (3)	Holocene (4)	Pleistocene (5)	Pre-Pleistocene (6)
(a) Continental Deposits					
River channel	Locally variable	Very high	High	Low	Very low
Flood plain	Locally variable	High	Moderate	Low	Very low
Alluvial fan and plain	Widespread	Moderate	Low	Low	Very low
Marine terraces and plains	Widespread	----	Low	Very low	Very low
Delta and fan-delta	Widespread	High	Moderate	Low	Very low
Lacustrine and playa	Variable High	Moderate	Low	Very low	
Colluvium	Variable High	Moderate	Low	Very low	
Talus	Widespread	Low	Low	Very low	Very low
Dunes	Widespread	High	Moderate	Low	Very low
Loess	Variable High	High	High	Unknown	
Glacial till	Variable Low	Low	Very low	Very low	
Tuff	Rare	Low	Low	Very low	Very low
Tephra	Widespread	High	High	?	?
Residual soils	Rare	Low	Low	Very low	Very low
Sebka	Locally variable	High	Moderate	Low	Very low
(b) Coastal Zone					
Delta	Widespread	Very high	High	Low	Very low
Esturine	Locally variable	High	Moderate	Low	Very low
Beach					
High wave energy	Widespread	Moderate	Low	Very low	Very low
Low wave energy	Widespread	High	Moderate	Low	Very low
Lagoonal	Locally variable	High	Moderate	Low	Very low
Fore shore	Locally variable	High	Moderate	Low	Very low
(c) Artificial					
Uncompacted fill	Variable	Very high	----	----	----
Compacted fill	Variable	Low	----	----	----

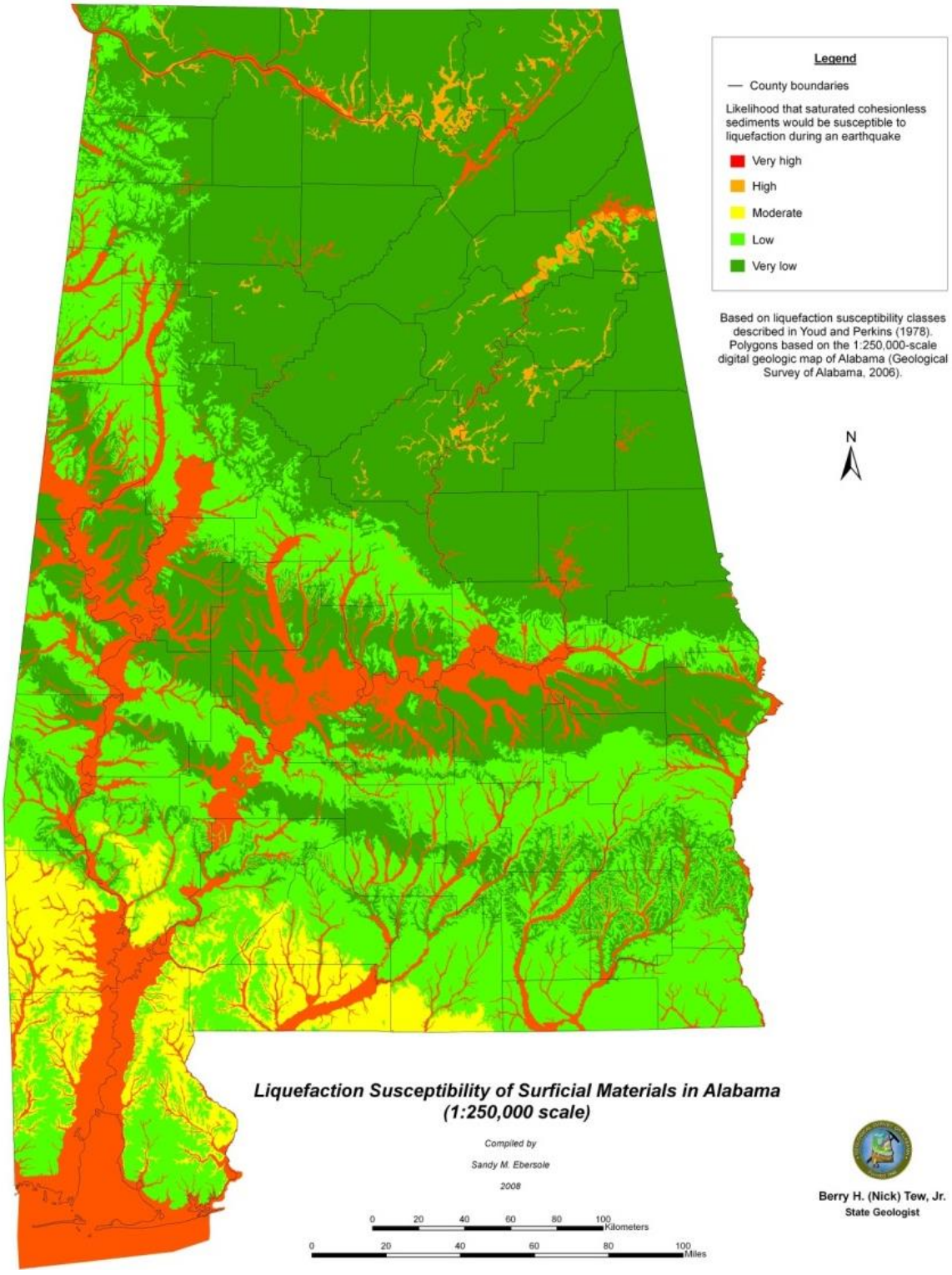

Figure 2.5. Liquefaction susceptibility of Alabama based on Youd and Perkins 1978 (Ebersole and Perry 2008).

Table 2.4 presents the Guide Specification requirements for liquefaction for each SDC. It should be noted that Kavazanjian et al. (2011) recommended that a liquefaction evaluation for SDC B was not necessary.

Table 2.4 – Liquefaction evaluation requirements for each SDC (AASHTO 2009)

Value of SA_1	**SDC**	**Liquefaction Evaluation Required?**
SA_1 < 0.15	A	No
0.15 < SA_1 < 0.30	B	Should be considered for certain conditions
0.30 < SA_1 < 0.50	C	Yes
0.50 < SA_1	D	Yes
Where: SA_1 = Spectral acceleration at a period of 1 second		

If the site is deemed to have a high potential for liquefaction, a formal liquefaction evaluation should be done in most cases. Referring to Figure 2.4, most of the areas that have a high potential for liquefaction are located in the southern part of the state, which has a low sesmic hazard (SDC A). However, the potential for liquefaction should always be considered in a SDC B, especially in regard to bridges near waterways in the northern part of the state. The Simplified Procedure, originally developed by Seed and Idris (1982) is one of the most common method used to evaluate liquefaction potential and is recommended to use should the engineer deem it necessary. It has been revised since its initial development and is presented in Kavazanjian et al. (2011). It should be noted that the Simplified Procedure should be primarily used for sites with moderate to strong ground motions (0.2 g < a_{max} < 0.5 g) (Kavazanjian et al. 2011).

2.3 Soil-Foundation-Structure Interaction

Understanding how the global system of any problem works is an important step in analysis and design of systems and structures. In this case, the global system is the bridge pier and surrounding elements, which can be broken into two main components:

the soil and structure. The presence of a constructed facility modifies the free-field ground motion at the base of the structure and typically reduces it (Kavazanjian et al. 2011). Free-field ground motion is the natural ground motion one would feel standing on undisturbed earth during an earthquake event. The interaction between the soil and the structure is commonly referred to as soil-structure interaction (SSI). The structure can be further broken down into two separate components: foundation and above-ground structure. The above-ground structure in the case of the type of bridge under consideration is the pier column(s) and cap, and the bridge deck. The interaction of the system is more properly described as soil-foundation-structure interaction (SFSI) which will be used throughout this document (Kavazanjian et al. 2011). There are two sources of SFSI: kinematic interaction and inertial interaction. Both interactions occur during an earthquake event and are complex. The foundation is loaded kinematically by the earthquake, and then the structure begins to move, causing inertial forces to be transferred from the structure to the foundation.

2.3.1 Kinematic Interaction

Kinematic interaction directly interplays both the soil and foundation system, making this interaction the more complex of the two (Bhattacharya 2003). Before the superstructure begins to oscillate, the piles may be forced, by the soil, to displace depending on the flexural stiffness (EI) of the pile (Bhattacharya 2003). The motion difference between the pile and the free-field motion can induce bending moments in the pile (Bhattacharya 2003). Kinematic interaction is often ignored in analysis because it is negligible for flexible piles in competent soils and tends to reduce the above-ground structural motion for stiff piles (Kavazanjian et al. 2011). In most applications, kinematic

interaction response analysis is not feasible because it leads to large numerical models (Kavazanjian et al. 2011). However, it can prove to limit conservatism, and could reduce costs associated with constructing the bridge.

2.3.2 Inertial Interaction

Inertial interaction takes place as the structure begins to move, and the magnitude of the inertial forces depends upon the fundamental period of the structure and the frequency content of the ground motions (Kavazanjian et al. 2011). These inertia forces of the structure are transferred to the foundation system as lateral forces, vertical forces and bending moments. To model inertial interaction for deep foundations, an equivalent cantilever or spring-dashpot model is used to represent the foundation (Kavazanjian et al. 2011). Figure 2.6 shows a generalized form of the inertial interaction model for deep foundations. This is a simple approach and is done often. However, it cannot account for the bending moment distribution in the pile, and, for each of the five relevant degrees of freedom (DOF) (2 translational and 3 rotational), the length of the equivalent cantilever (or point of fixity) may be different (Kavazanjian et al. 2011).

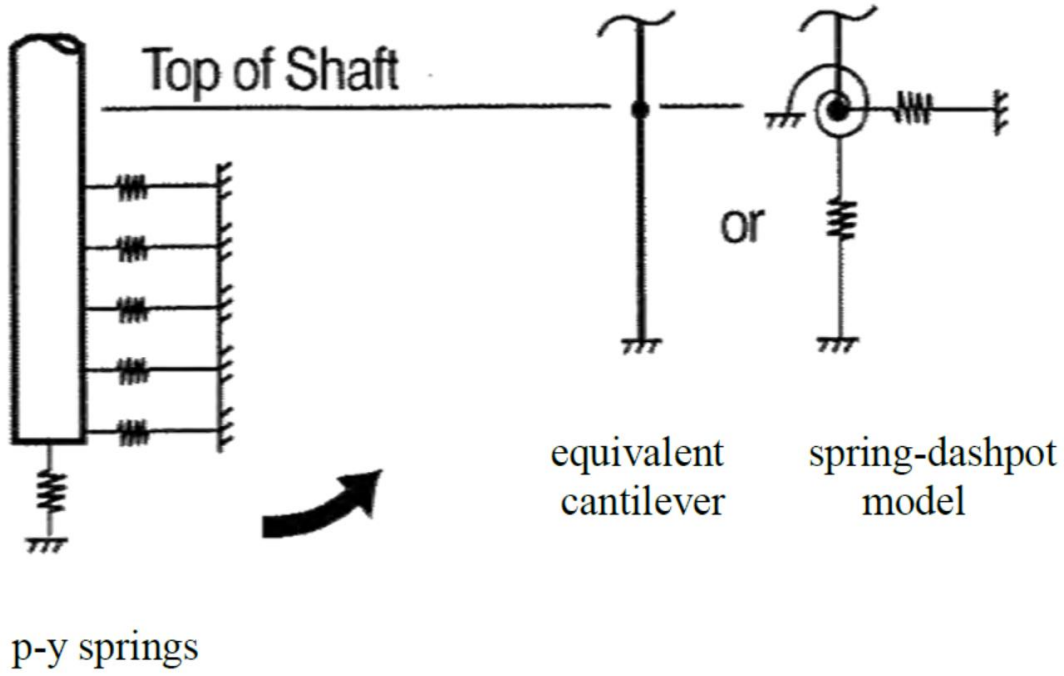

Figure 2.6. Inertial interaction model for deep foundations (Kavazanjian et al. 2011)

2.3.3 Seismic and Dynamic Response Analysis Methods

The two most common methods that are used to analyze the seismic response of bridge foundations are substructure analysis and direct analysis. For both methods, several factors must be considered: soil stratigraphy and strength parameters, water table elevation, foundation types and lengths, pile cap design (if applicable), and different geotechnical hazards such as scour and liquefaction. Each project is different and the analysis may or may not need to include consideration for other geotechnical hazards besides an earthquake. Thoughtful consideration must be given to all possibilities before implementing an analysis program.

Depending on what type of abutment is present, there are different resisting mechanisms, including mobilization of the abutment back-wall, that contribute to the resistance of a bridge to an earthquake event. For further detail, see Kavazanjian et al. (2011).

2.3.3.1 Substructure Analysis

Substructure modeling is the simpler and the more common method of the two. The most common way to determine the foundation stiffness is by using a computer program, such as LPILE or FB-MultiPier, that uses the p-y method to determine soil response, then extrapolate the stiffness so that it represents a group stiffness (if necessary). Since the extrapolation method was not used in this project, it is not covered. See Kavazanjian et al. (2011), for a more detailed discussion. While this is widely accepted, there is software capable of modeling pile groups more accurately such as GROUP and FB-MultiPier (which was used for this research project). Greater detail about FB-MultiPier and the p-y method is covered in section 2.4 of this chapter.

There are six DOF for a foundation system and the stiffness of the foundation for each degree must be known or estimated. The DOF are axial and bi-lateral translation (u, v, and w) and rotation (Θ_X, Θ_Y, and Θ_Z) about each of the three axes. Sometimes, it may be appropriate to assume some DOF are fixed, and therefore, they do not need to be evaluated, such as axial translation or torsional rotation. To determine the response of the foundation, a static response analysis is done at the pile head or pile cap head. See Figure 2.7 for a representation of substructure modeling. In this case, it was assumed the pile head was fixed within the cap, therefore they were modeled together. One question that is usually asked when determining the response is whether the axial dead load should be included in the lateral and rotational push-over analysis. Lam and Martin (1986) concluded the following:

> *For convenience in design or analysis, the axial soil support characteristics are assumed to be independent of the lateral soil support*

characteristics. This is justified because lateral soil reactions are usually concentrated along the top 5 or 10 pile diameters whereas almost all of the axial soil resistance is developed at greater depths. Therefore, the axial and lateral soil support behavior can be studied and analyzed separately.

The end result of a static foundation response analysis is a family of force/moment versus displacement/rotation response curves that represent the pile head or the top of a pile group in a structural model. These curves are almost always nonlinear. The structural and geotechnical engineer must communicate effectively as where to properly apply the springs and in what fashion. Figure 2.8 shows an example of a foundation stiffness curve.

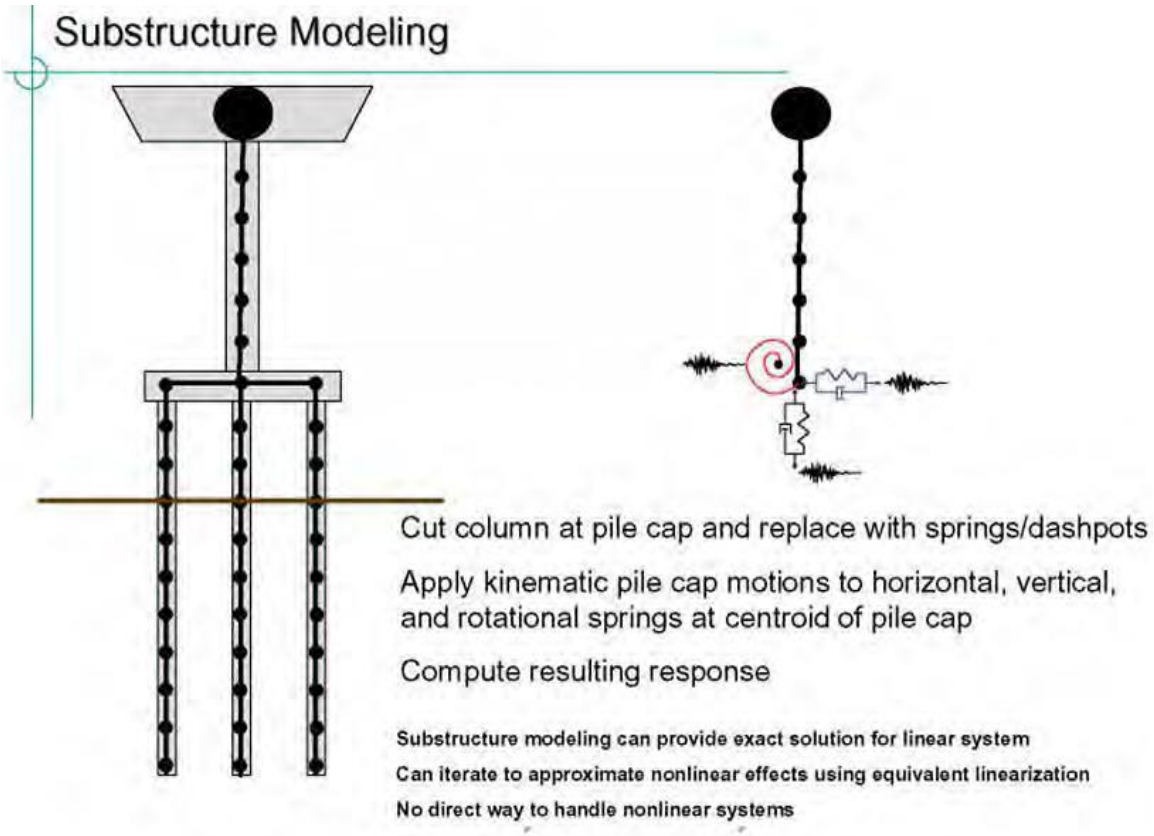

Figure 2.7. Foundation substructure model for kinematic analysis (Kavazanjian et al. 2011)

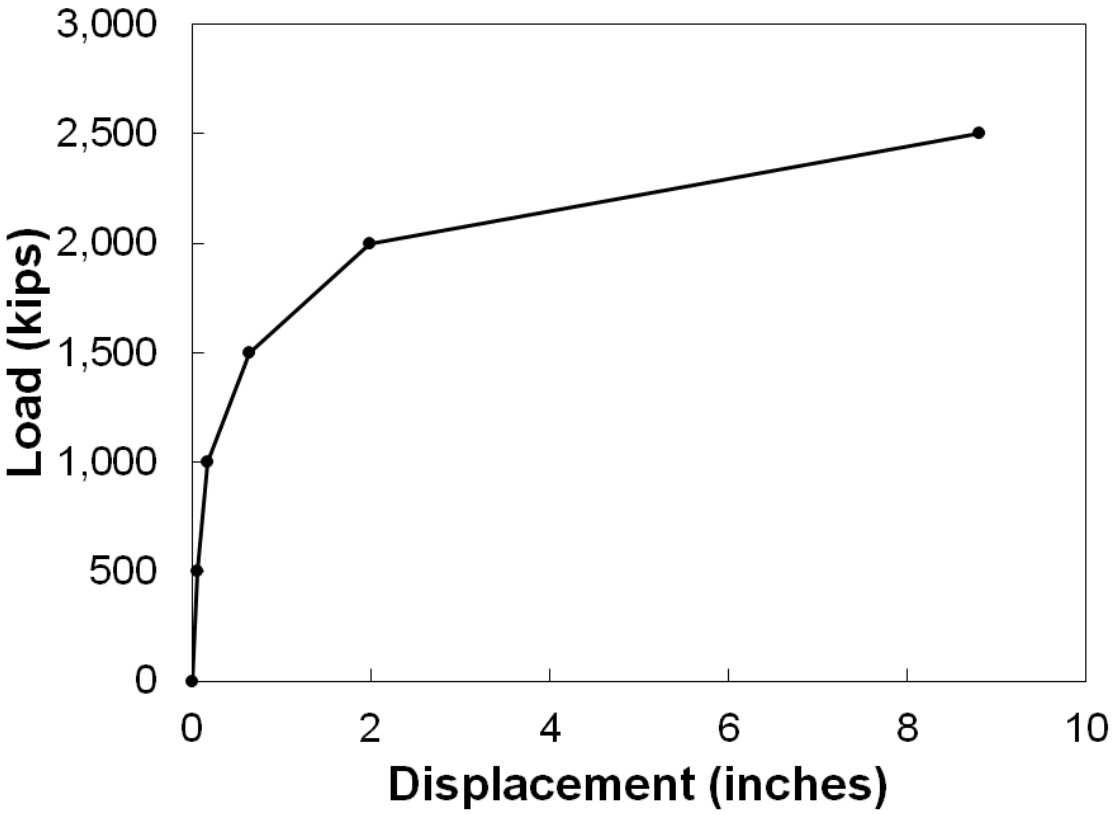

Figure 2.8. Example of a foundation stiffness curve

2.3.3.2 Direct Analysis

Direct analysis is not done in most applications. It is simply too time consuming and complicated to be used for every project, and most institutions or companies cannot afford the type of software that is best suited to run this method of analysis. Direct analysis builds on that of substructure modeling. However, time-history or response spectrum functions, structure configuration, and dead loads must also be input into the program. See section 2.4 for more detail on these topics. Figure 2.9 shows a detailed representation of direct analysis.

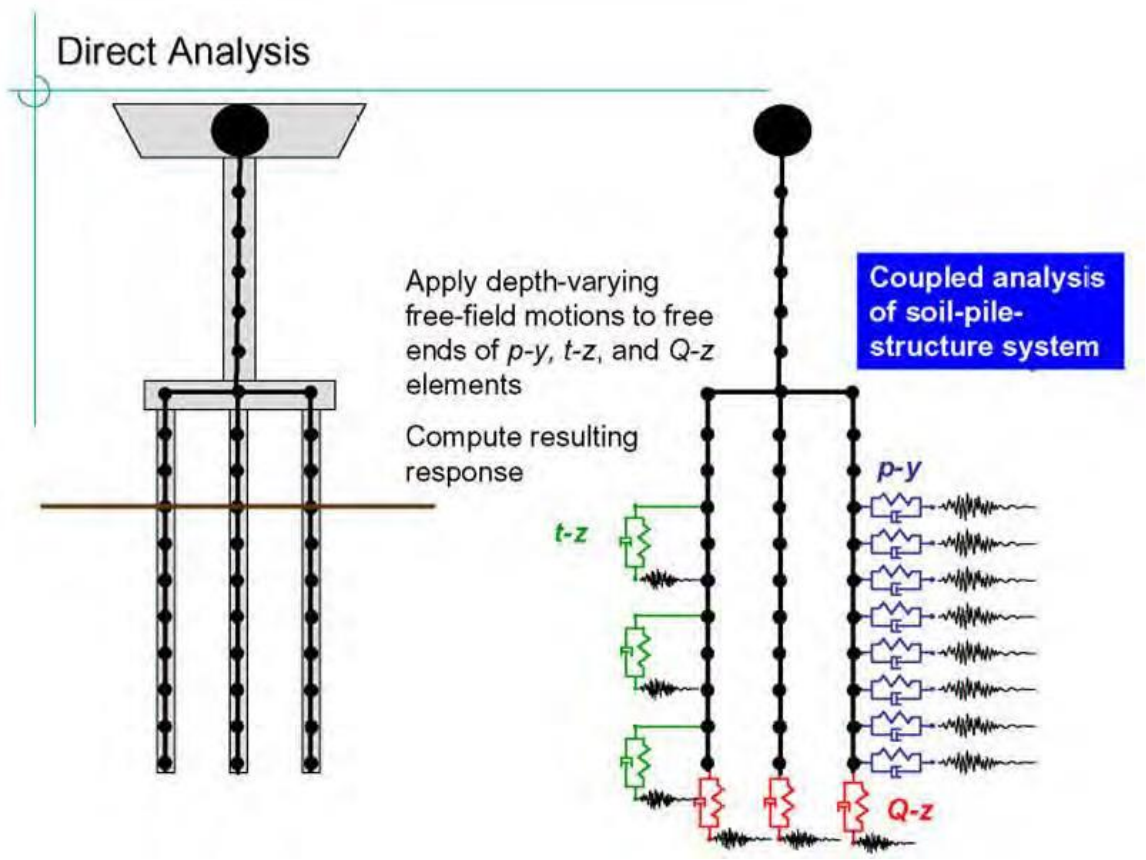

Figure 2.9. Direct (or Total) soil-foundation-structure kinematic interaction model (Kavazanjian et al. 2011)

2.4 Computer Programs

While there are several programs that can perform substructure analysis, such as LPile (Ensoft 2013(b)) and GROUP (Ensoft 2013(a)), FB-MultiPier (BSI 2013(b)) is capable of doing both substructure and direct analysis. This was an important factor in deciding which program to use.

2.4.1 Overview of FB-MultiPier

FB-MultiPier is a hybrid finite element analysis program developed by the Bridge Software Institute (BSI), which is headquartered at the University of Florida in Gainesville, FL. It is capable of modeling multiple bridge pier structures that are interconnected by single representative bridge spans. The full structure can be subjected

to a full array of AASHTO load types in a static analysis or time varying load functions in a dynamic analysis (BSI 2013(b)).

The structural elements that it is capable of simulating include foundation element(s) (piles and drilled shafts), pile cap(s), column, and pier cap. All of the structural elements can be uniquely modeled by the user. The program also provides standard sections for many common foundation elements (H-pile, drilled shaft, prestressed concrete pile, pipe pile, etc.). For the soil-foundation interaction, FB-MultiPier uses axial (t-z, Q-z), lateral (p-y), and torsional (T-θ) nonlinear spring functions (soil springs). It uses 2-node finite elements below the ground surface to model the pile, placing the corresponding axial, lateral, and torsional soil springs at each element. The number of 2-node finite elements can be varied from five to fifty below the ground and for the free length of the pile (if any). FB-MultiPier employs several soil spring functions to characterize the soil stiffness as well as the capability to enter a customized set of ten curve points if none of the default soil springs are suitable.

FB-MultiPier uses an iterative solution method to solve for the structural displacements. This method follows a secant approach where FB-MultiPier finds the stiffness of the soil and structure for a computed set of displacements, assembles a stiffness matrix, and then solves for a new set of displacements. Convergence is achieved when the system is in static equilibrium. This is determined by comparison of the magnitude of the highest out-of-balance nodal force and the tolerance defined by the user in the input file. If the highest out-of-balance force is lower than the tolerance, the system is in static equilibrium and the program terminates. If the program did not converge, it is likely due to one of three reasons: (1) structural failure, (2) soil failure, or

(3) numerical instability. Structural failure occurs when a plastic hinge develops within the model and the shaft/column/pile cannot distribute the load any longer and subsequently, does not converge to a solution. Soil failure occurs when the displacements of the soil springs are large enough that the soil cannot absorb any more load. This leads to large out-of-balance forces. Numerical instability can occur from a combination of things within the model such as secondary moment effects, time stepping issues, corrupt input data, etc. The output files are a good indication of what causes the model to fail (especially the last time-step) and should always be reviewed.

When first opening FB-MultiPier, the user must open an existing file or select a new problem type. If a new problem type is selected, a default file is automatically loaded and displayed (BSI 2013(b)). Figure 2.10 shows the home screen of FB-MultiPier. The top left window is the Model Data window where most of the information is entered (BSI 2013(b)). The top right window is the Pile Edit window and it shows the pile group in plan. The bottom left window is the Soil Edit window where the soil stratigraphy is shown. A 3-D view of the pier structure is shown in the bottom right pane. This graphical user interface allows the user to see the development of the model as it is being built, which can help find mistakes and accelerate the process (BSI 2013(b)).

The following sections provide a brief introduction to the system processes and various models employed by FB-MultiPier and are taken (in most part) from the FB-MultiPier User's Manual (user's manual) (BSI 2013(b)). Refer to the user's manual for further details and relevant information.

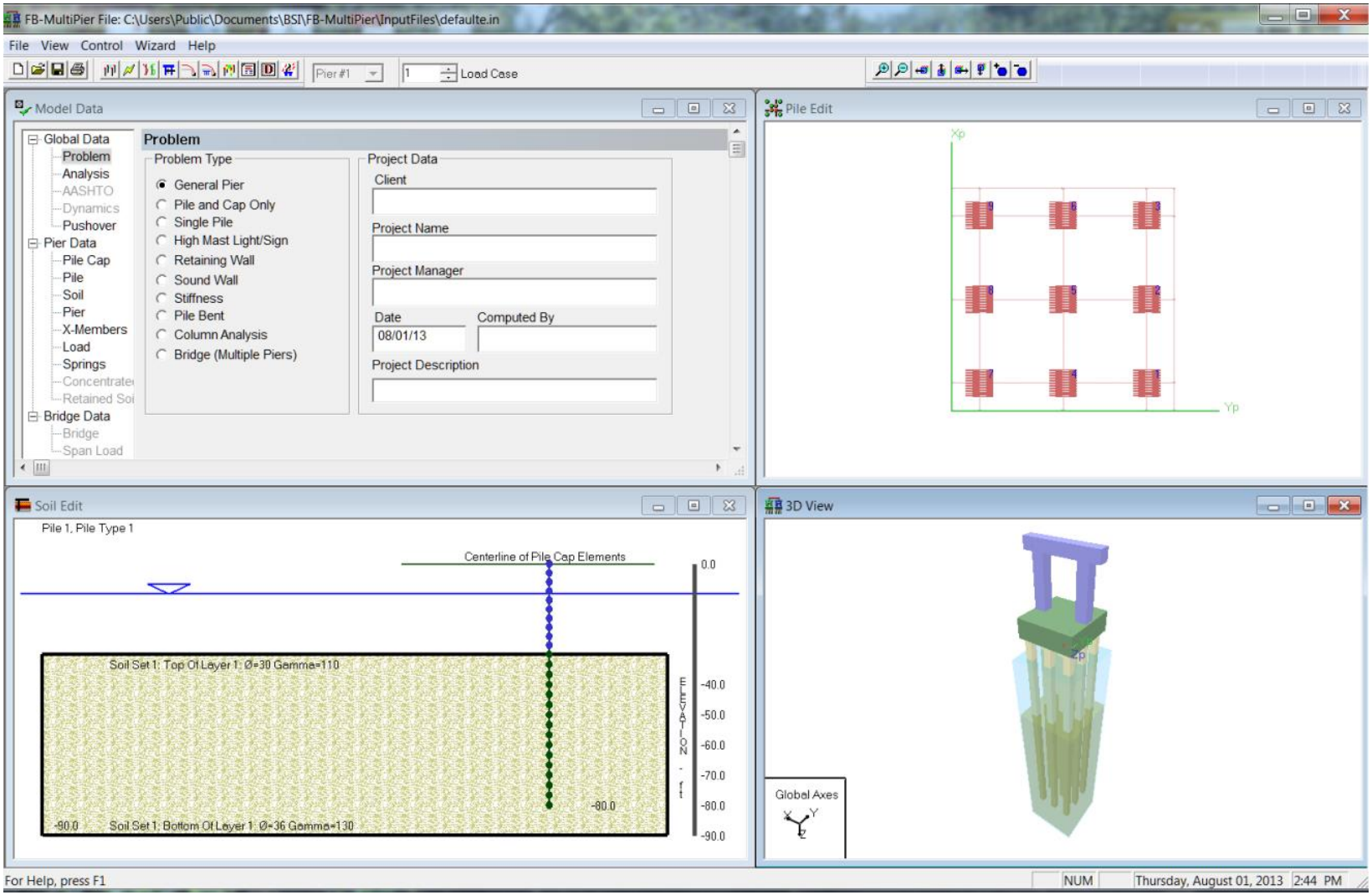

Figure 2.10. FB-MultiPier editor window

2.4.2 Soil Modeling

FB-MultiPier is capable of modeling multiple soil sets and layers within a model. This is important as site conditions can vary within a few feet. There are several important soil properties that are required as input parameters within the program such as: Young's modulus, Poisson's ratio, shear modulus, angle of internal friction, undrained strength, subgrade modulus, and the water table elevation (BSI 2013(b)). However, depending on what soil model is selected, other properties, such as shear strain, unit skin friction and ultimate tip resistance may be required. The user's manual provides various recommendations for estimating soil properties and for brevity, they are not presented in this document. A brief description of each soil model is given. More detailed information can be found in the user's manual (BSI 2013(b)).

It should be noted that for both lateral and axial (skin and base resistance) interaction, American Petroleum Institute's (API) clay and sand models are also available in FB-MultiPier. For further detail regarding these models, see API (1997).

2.4.2.1 Lateral

For the lateral soil-pile interaction, FB-MultiPier employs six different p-y models to choose from as well as a user defined option. This includes: (A) Matlock's Soft Clay Below Water Table, (B) Reese's Stiff clay Below Water Table, (C) Reese and Welch's Stiff Clay Above Water Table, (D) Sand of Reese, Cox, and Koop, (E) O'Neill's Sand, (F) O'Neill's Clay, and (G) Limestone (McVay).

A) Matlock's Soft Clay Below Water Table

Matlock (1970) developed curves for soft clay below the water table for both static and cyclic loading conditions. This representation requires the unit weight, γ;

undrained strength, s_u; and strain at 50% of the failure load of an unconfined compression test, ε_{50}, of the soil to be input for both programs. Figures 2.11 and 2.12 are representations of the curves.

B) Reese's Stiff Clay Below Water Table

Figures 2.13 and 2.14 are the p-y curves for stiff clay below the water table developed by Reese et al. (1975). The soil parameters necessary to develop this curve are subgrade modulus, k; unit weight, γ; undrained strength, s_u; and the strain at 50% of the failure stress in an unconfined compression test, ε_{50}. Figure 2.13 is the static case and Figure 2.14 is the cyclic case.

C) Reese and Welch's Stiff Clay Above Water Table

Reese and Welch's (1972) p-y curves are for stiff clay above the water table. This model requires the input of unit Weight, γ; undrained strength, s_u; and the strain at 50 % of the failure stress in an unconfined compression test, ε_{50}. Note that the cyclic curve is dependent upon the number of cycles. Figure 2.15 is the static model and Figure 2.16 is the cyclic model.

D) Sand of Reese, Cox, and Koop

Reese, Cox, and Koop (1974) developed a model for sands in general. This model requires subgrade modulus, k; effective unit Weight, γ'; and the angle of internal friction, φ, for the soil. Figure 2.17 is both the static and cyclic model for sand.

E) O'Neill's Sand

O'Neill and Murchison (1983) developed a model similar to Reese et al. (1974) for the lateral soil pile interaction for sand. Similarly, this model requires the input of

subgrade modulus, k; effective unit Weight, γ'; and angle of internal friction, φ, for the soil. Figure 2.18 shows O'Neill's p-y curve for sand.

F) O'Neill's Clay

O'Neill and Gazioglu (1984) developed a model for clay. This model requires the input of undrained strength, s_u; the strain at 50% of the failure stress in an unconfined compression test, ε_{50}; and the strain at failure in an unconfined compression test, ε_{100}. Figure 2.19 shows the static curve and Figure 2.20 shows the cyclic curve.

G) Limestone (McVay)

McVay and Niraula. (2004) developed a model for rock with characteristics of Florida limestone. The model requires the input of unconfined compressive strength, q_u. This model was based on twelve lateral load tests conducted in a centrifuge. It should be noted that the report (McVay and Niraula 2004) recommends that full scale field tests be conducted to validate the curves. Figure 2.21 shows the normalized curves from the tests conducted.

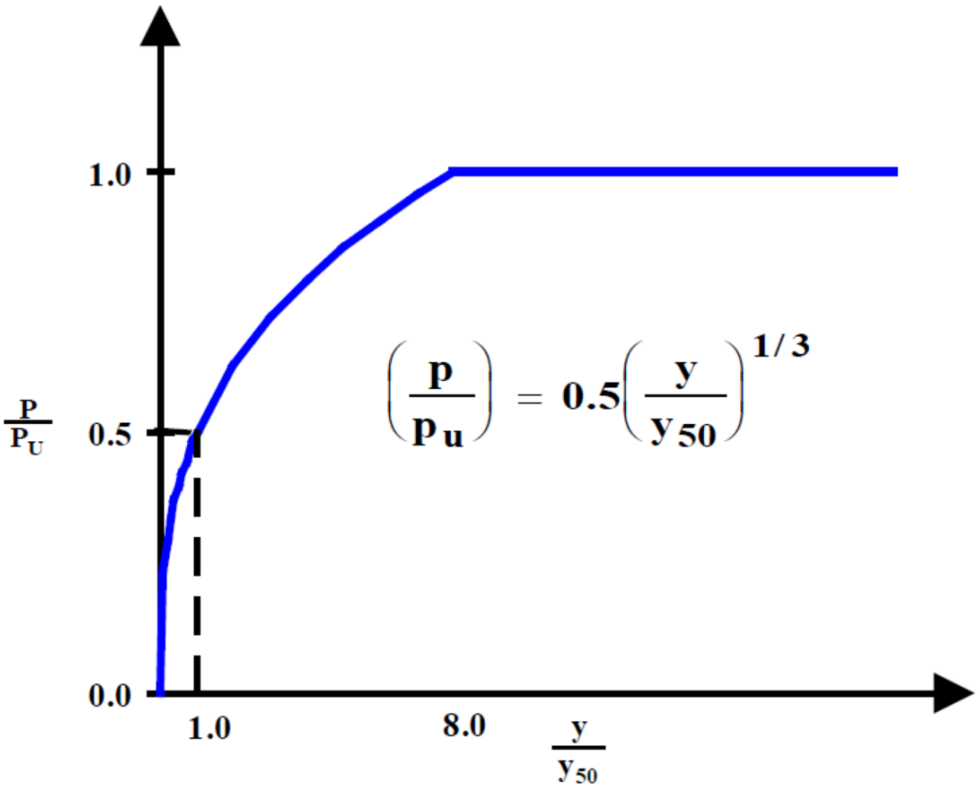

Figure 2.11. Matlock's static curve for soft clay (Matlock 1970)

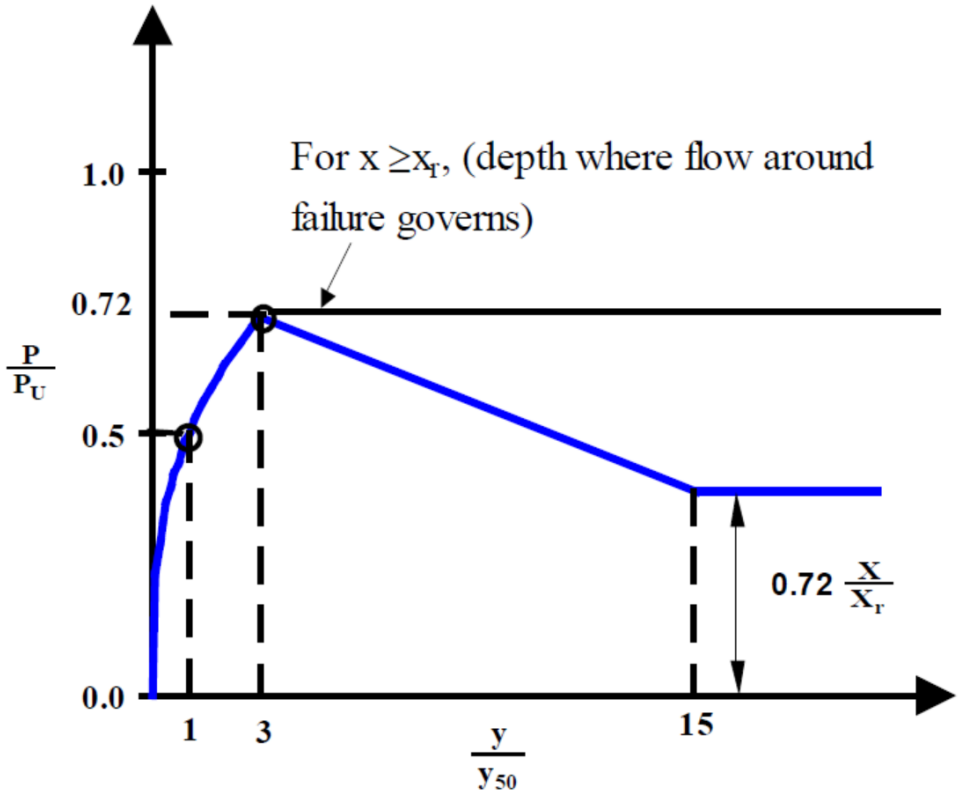

Figure 2.12. Matlock's cyclic curve for soft clay (Matlock 1970)

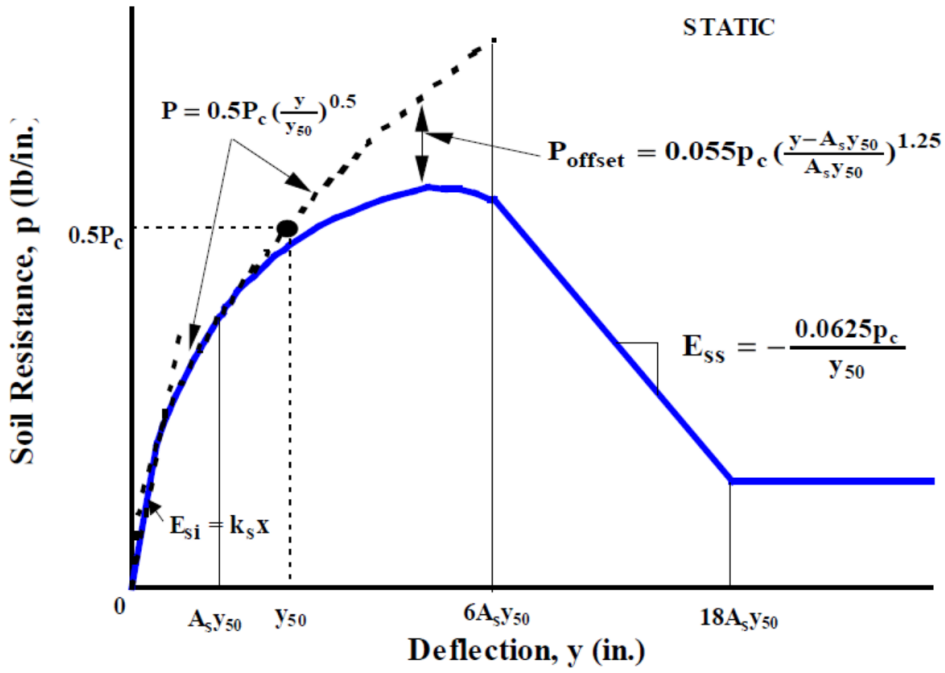

Figure 2.13. Reese's static curve for stiff clay below the water table (after Reese et al. 1975)

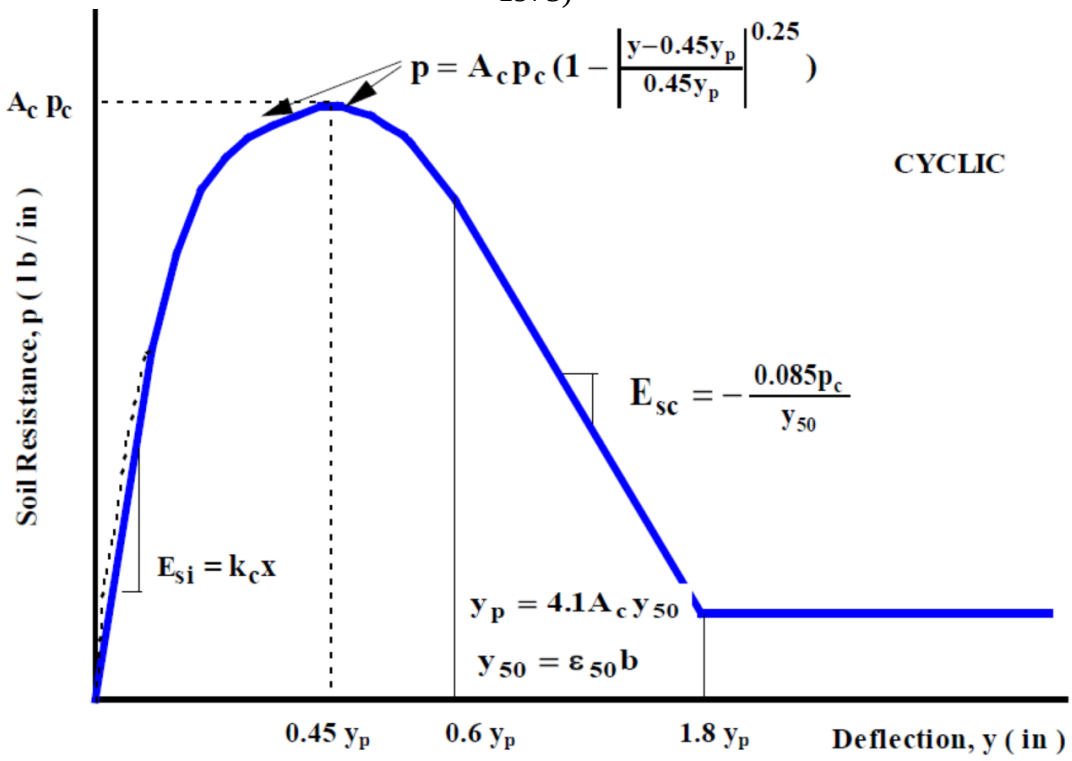

Figure 2.14. Reese's cyclic curve for stiff clay below the bater table (after Reese et al. 1975)

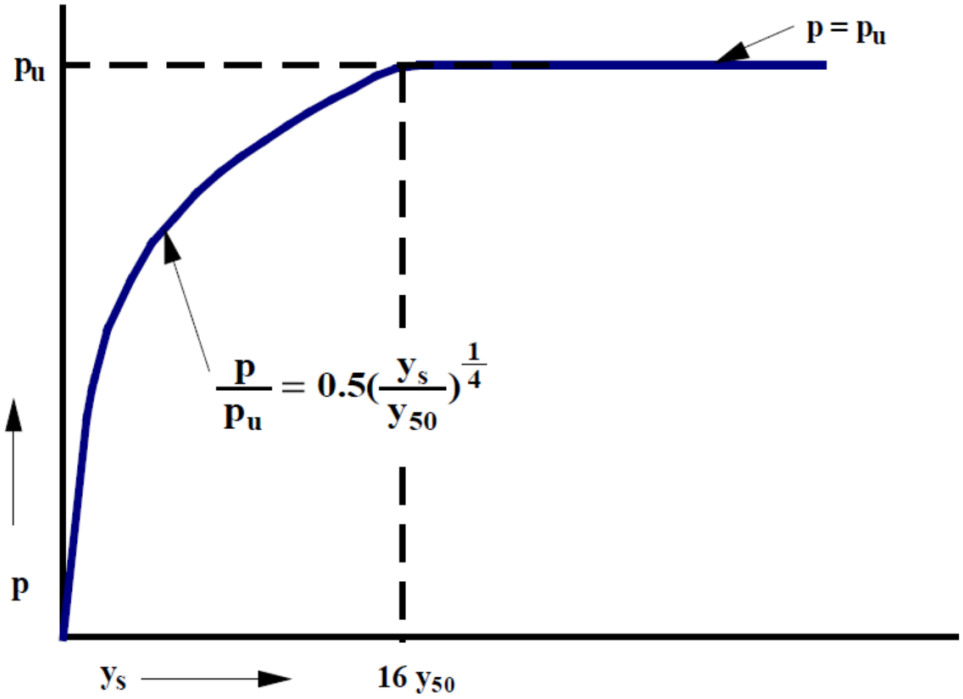

Figure 2.15. Reese and Welch's static curve for stiff clay above water table (Reese and Welch 1972)

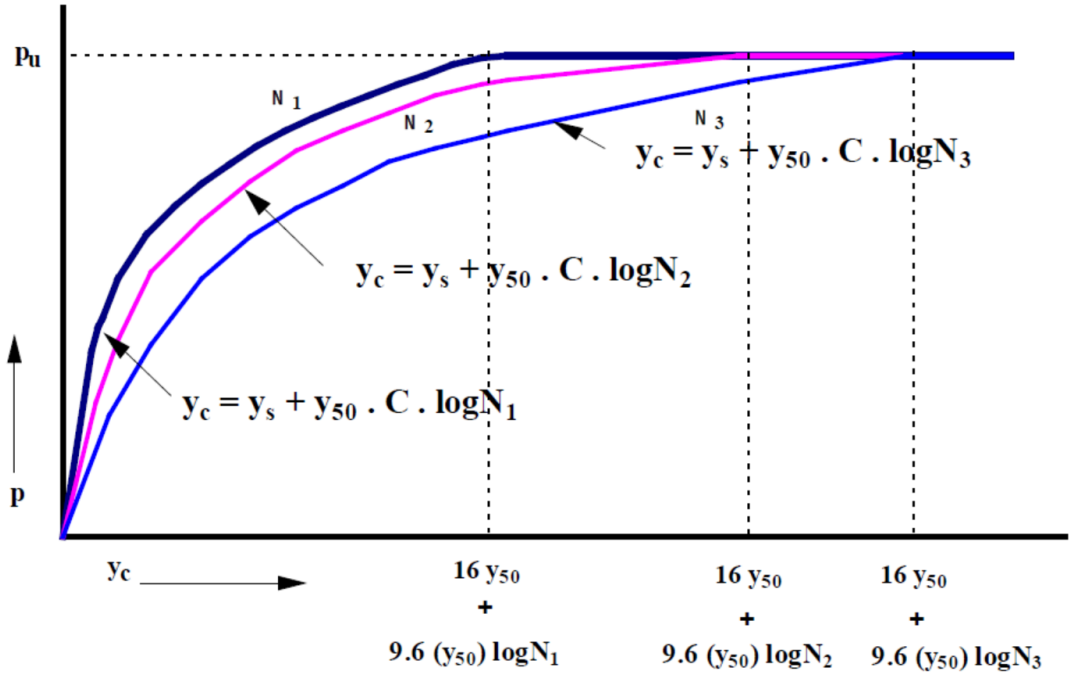

Figure 2.16. Reese and Welch's cyclic curve for stiff clay above water table (Reese and Welch 1972)

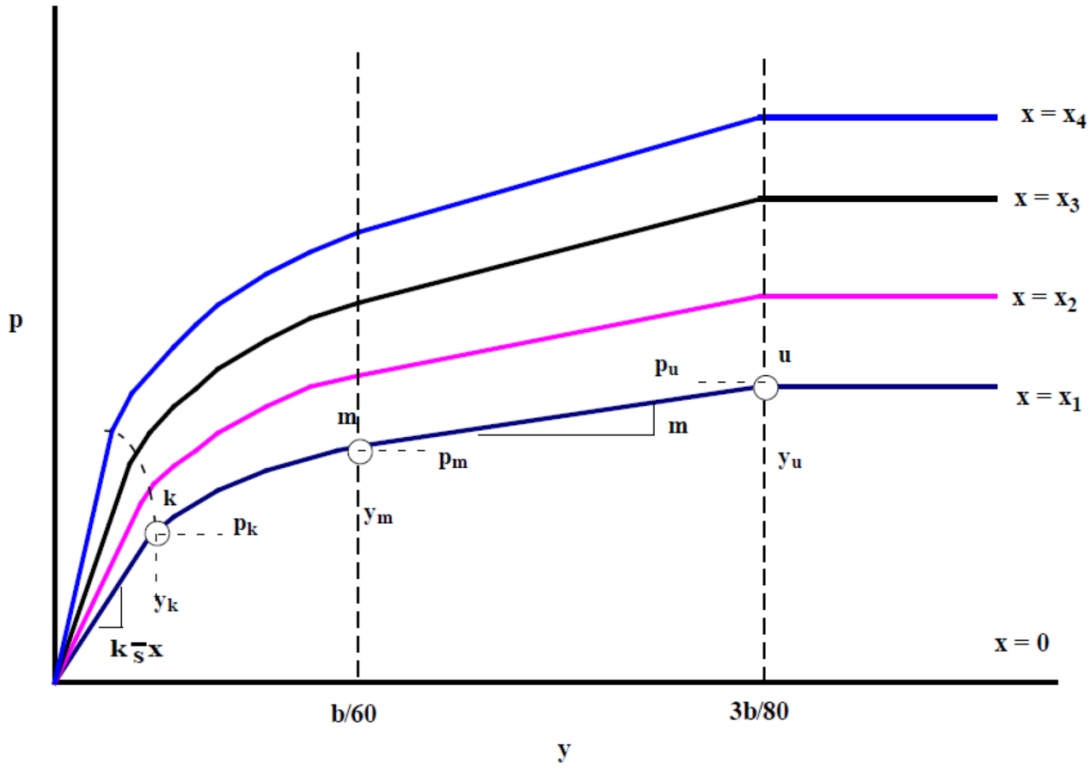

Figure 2.17. P-y curves for sand (Reese, Cox and Koop 1975)

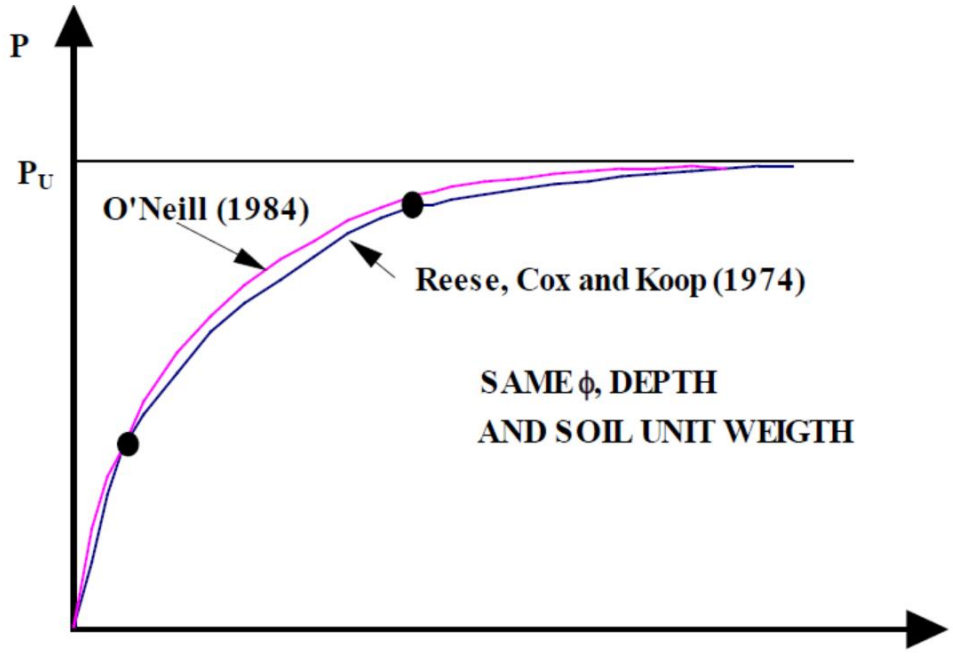

Figure 2.18. O'Neill's p-y curve for sand (O'Neil and Murchison 1983)

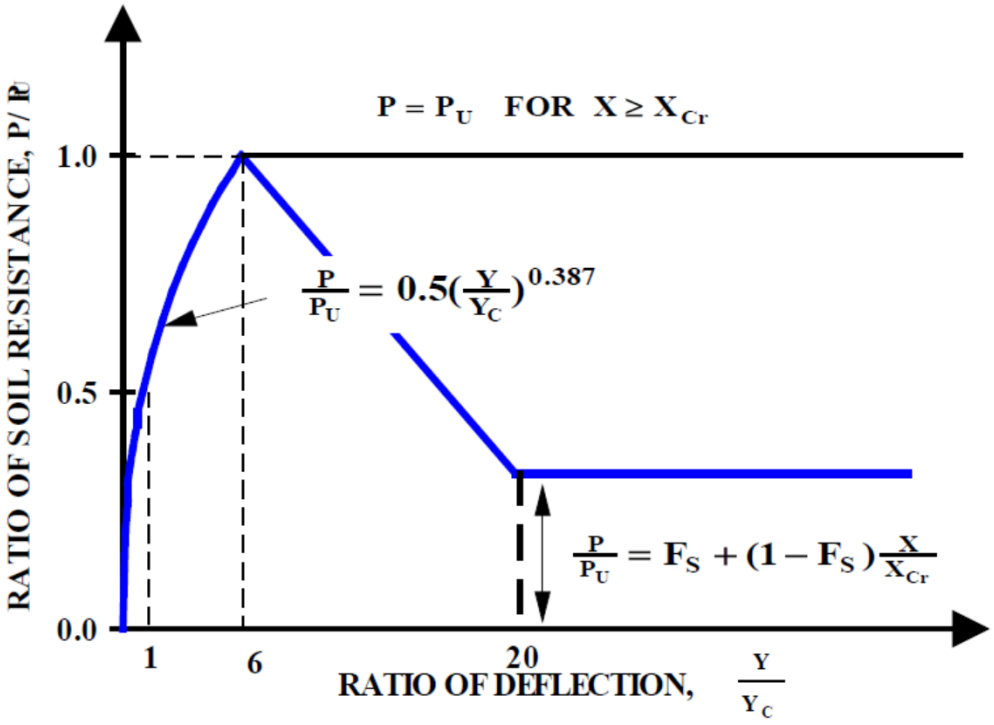

Figure 2.19. O'Neil's static p-y curve for clay (O'Neill and Gazioglu 1984)

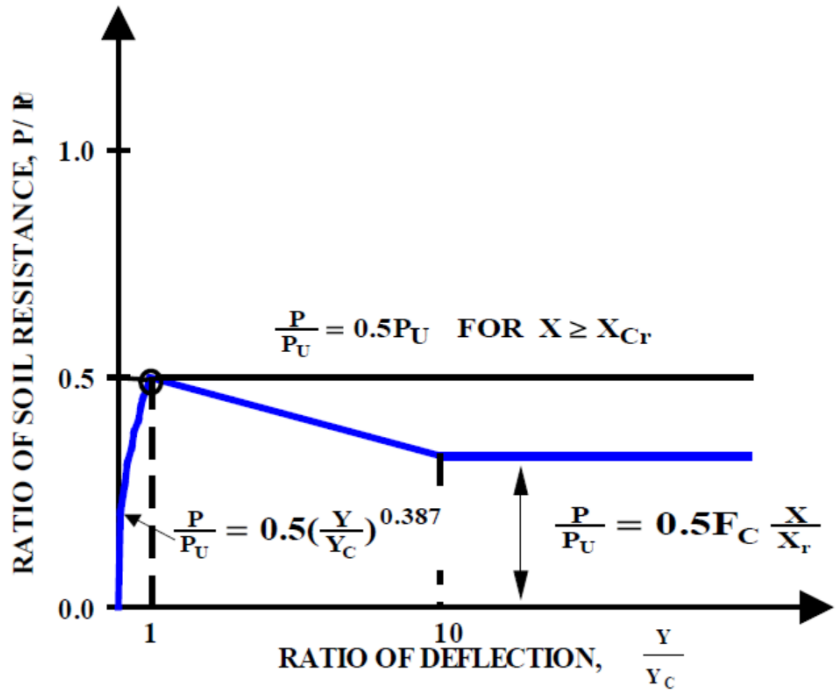

Figure 2.20. O'Neil's cyclic curve for clay (O'Neill and Gazioglu 1984)

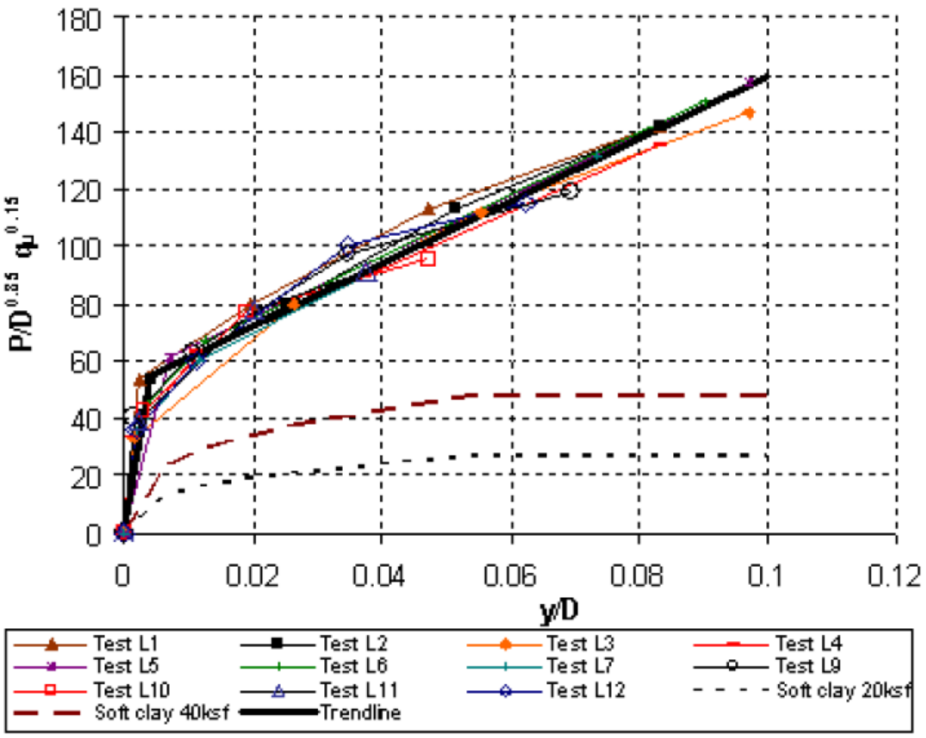

Figure 2.21. McVay's normalized p-y curves corrected for side shear for limestone (McVay and Niraula 2004)

2.4.2.2 Axial

For the axial soil-pile interaction (this section excludes tip resistance), FB-MultiPier employs three models as well as the user defined option. These include: (A) driven piles, (B) drilled and cast insitu piles/shafts, and (C) axial skin resistance for limestone (McVay).

A) Driven Piles

This model is for both cohesive and cohesionless soil. The user must supply the initial shear modulus, G_i; Poisson's ratio, ν; and the maximum shear stress between the pile and soil at the depth in question, τ_f. Figure 2.22 shows the axial T-z curve for a pile.

B) Drilled and Cast Insitu Piles/Shafts

The T-z curves used are based on the recommendations found in Wang and Reese (1993). They are based on trend lines and computed for each node. There are three models provided for the following soil types: sand, clay and intermediate geomaterials (IGM). For both the sand and clay models, no additional soil properties are needed. Figures 2.23 and 2.24 present the sand and clay trend lines. The IGM model is taken directly from FHWA's Load Transfer for Drilled Shafts in Intermediate Geomaterials (O'Neill 1996). The user must supply the mass modulus, E_m; modulus ratio, E_m/E_i; surface condition; split tensile strength of the pile concrete; unit Weight of the pile concrete γ_{con}; and the slump of the pile concrete. Refer to the FB-MultiPier user manual for more details.

C) Axial Skin Resistance for Limestone (McVay)

This model is taken from McVay and Niraula (2004) as previously mentioned. The user must supply the ultimate unit skin friction, f_{max}. The curves are based on tests performed on 6 feet diameter drilled shaft embedded 18 feet into rock. Figure 2.25 shows the comparison of the normalized T-z curves.

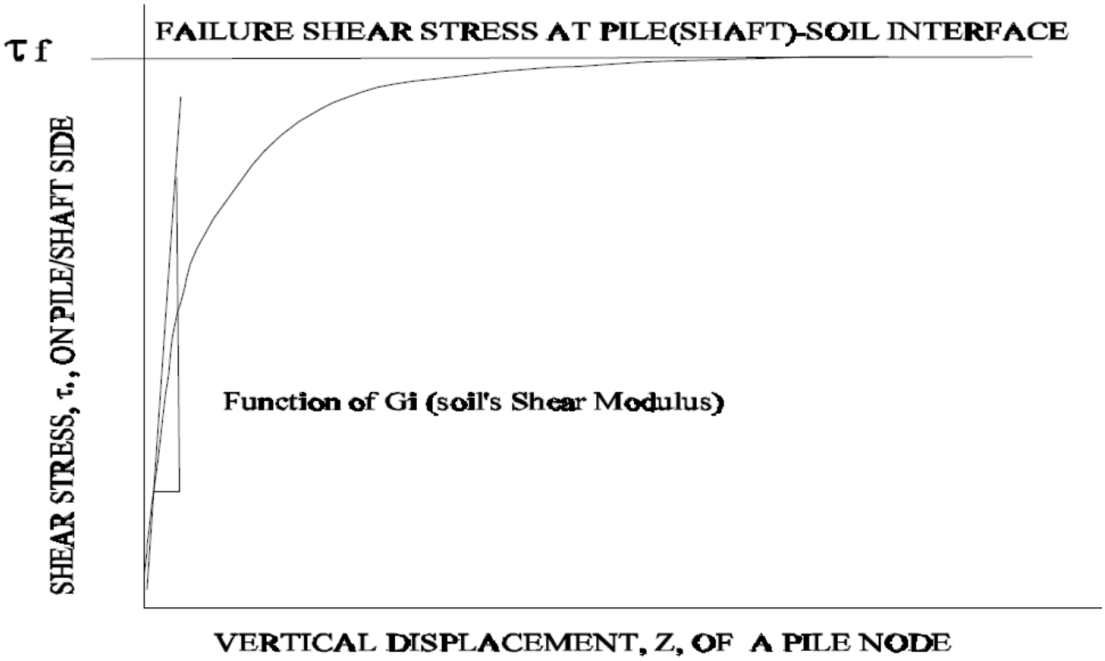

Figure 2.22. Axial T-z curve for pile/shaft (McVay et al. 1989)

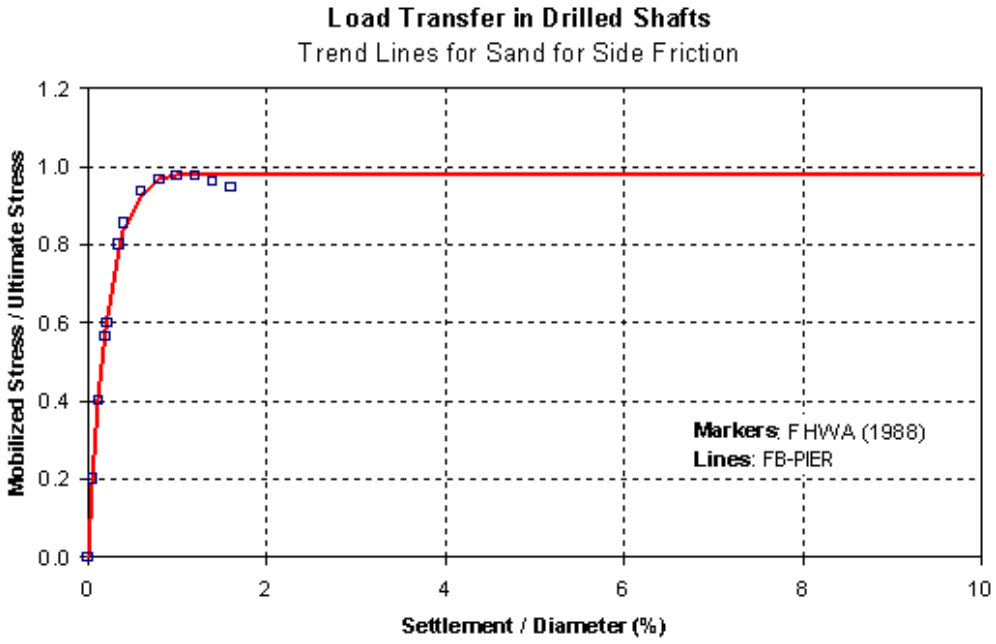

Figure 2.23. Trend lines for drilled shaft side resistance in sand (BSI 2013(b), and Reese and O'Neill 1988)

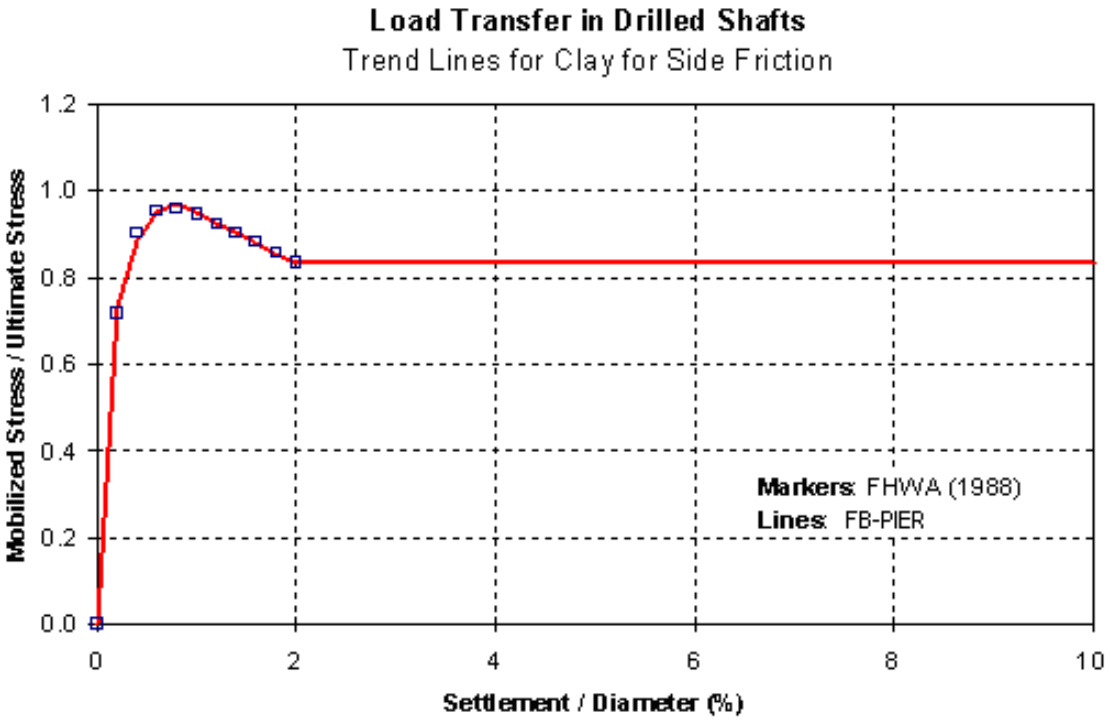

Figure 2.24. Trend lines for drilled shaft aide resistance in clay (BSI 2013(b), and Reese and O'Neill 1988)

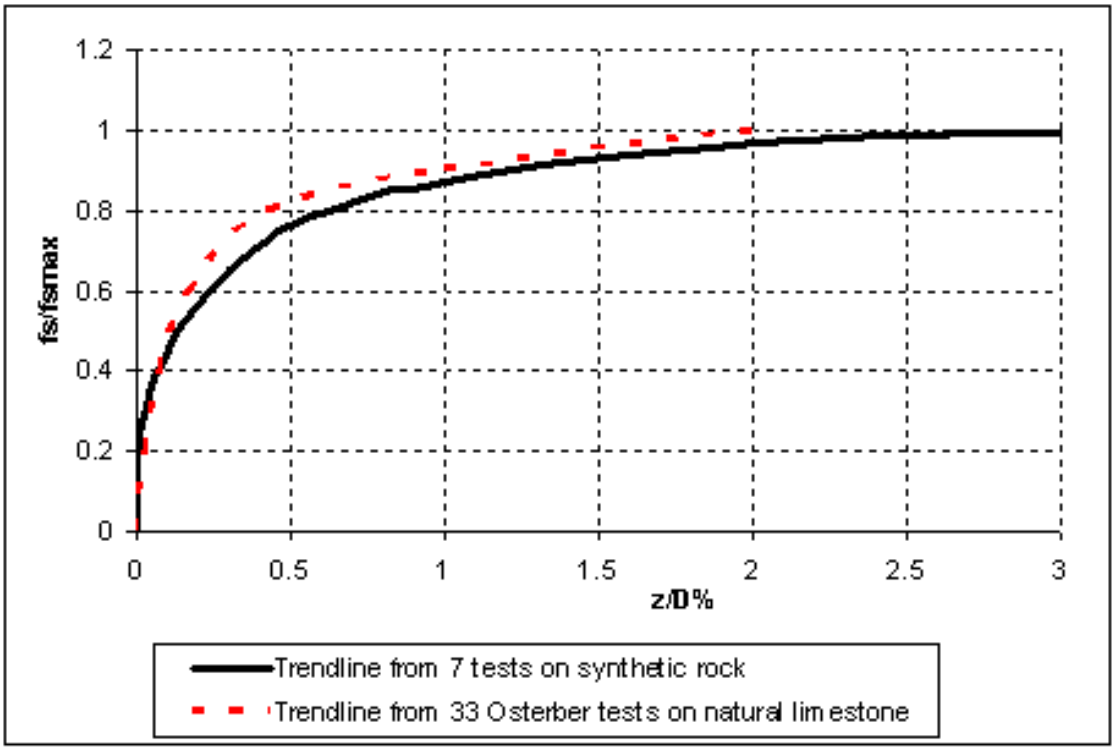

Figure 2.25. Comparison of normalized T-z curves for limestone (BSI 2013(b), Kim 2001, and McVay and Niraula 2004)

2.4.2.3 Torsional

FB-MultiPier uses two models to account for the non-linear torsional (T-θ) behavior of the soil: a hyperbolic curve and a user defined curve. The initial slope of the hyperbolic curve is a function of the shear modulus, G; and the ultimate value is based upon the ultimate shear stress at the soil-pile interface. Figure 2.26 shows a hyperbolic representation of the T-θ curve.

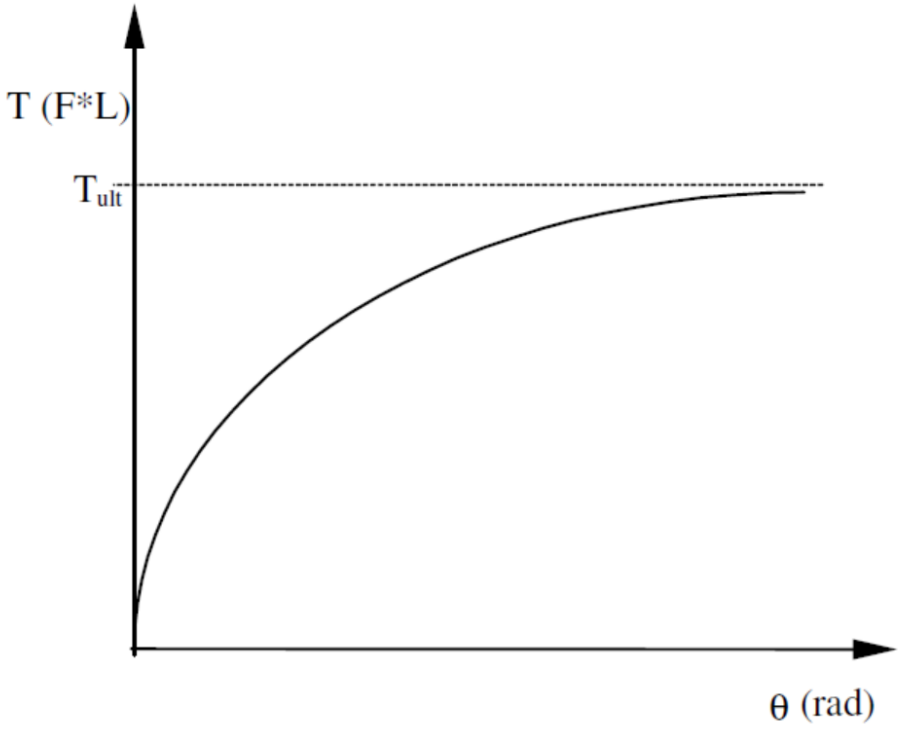

Figure 2.26. Hyperbolic representation of T-Θ curve (BSI 2013(b))

2.4.2.4 Tip

FB-MultiPier uses two axial base resistance (or Tip) Q-z models as well as a user defined curve. These models include: (A) driven pile, and (B) drilled and cast insitu

piles/shafts. For every model in FB-MultiPier, the pile must be embedded in a soil element. The amount of embedment does not matter for axial analysis. That is not to say it does not matter for lateral analysis, however.

A) Driven Pile

The nonlinear Q-z model used in FB-MultiPier is a function of the ultimate tip resistance, Q_f; initial shear modulus, G_i; and Poisson's ratio, ν. Figure 2.27 shows the Q-z curve for driven pile. The model used is from McVay (1989).

B) Drilled and Cast Insitu piles/shafts

The drilled and cast insitu pile/shafts Q-z curves are based on the recommendation given by Reese and Wang, 1993. They are based on trend lines and computed for each node. Trend lines are provided for sand, clay, and IGM. For sand and clay, the uncorrected SPT blow count and the undrained shear strength, s_u, is required respectively. For IGM, the mass modulus, E_m , is required. See the user's manual for more information regarding IGM modeling. Figures 2.28 and 2.29 show the trend lines for sand and clay respectively.

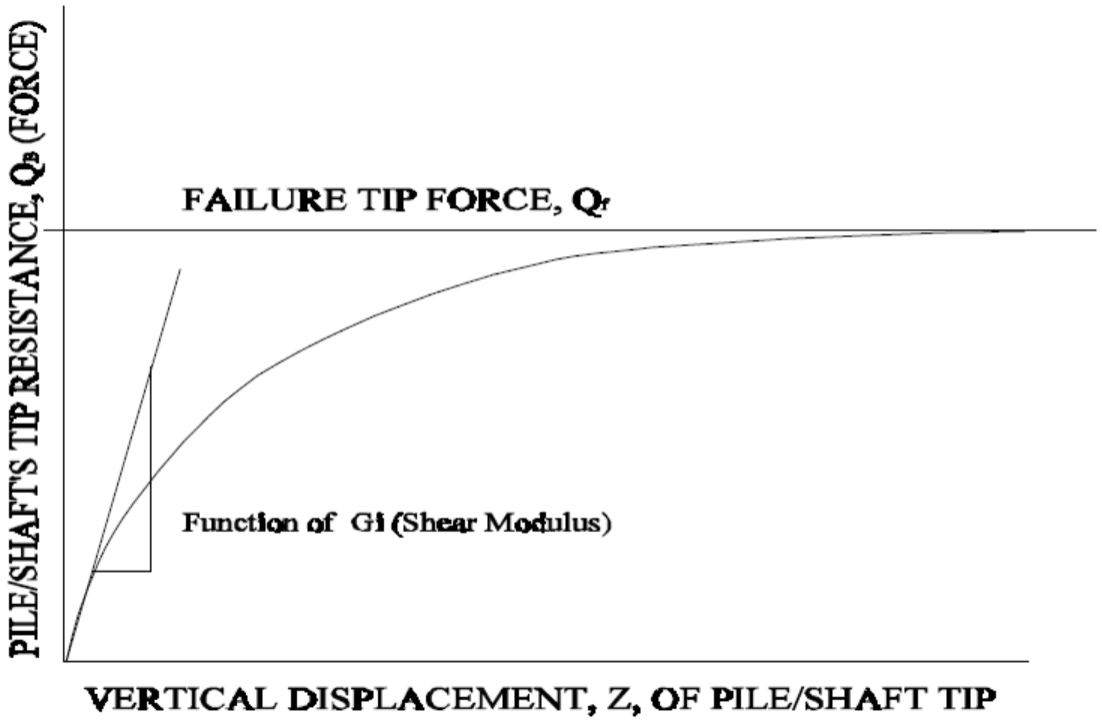

Figure 2.27. Axial Q-z curve for driven pile (BSI 2013(b))

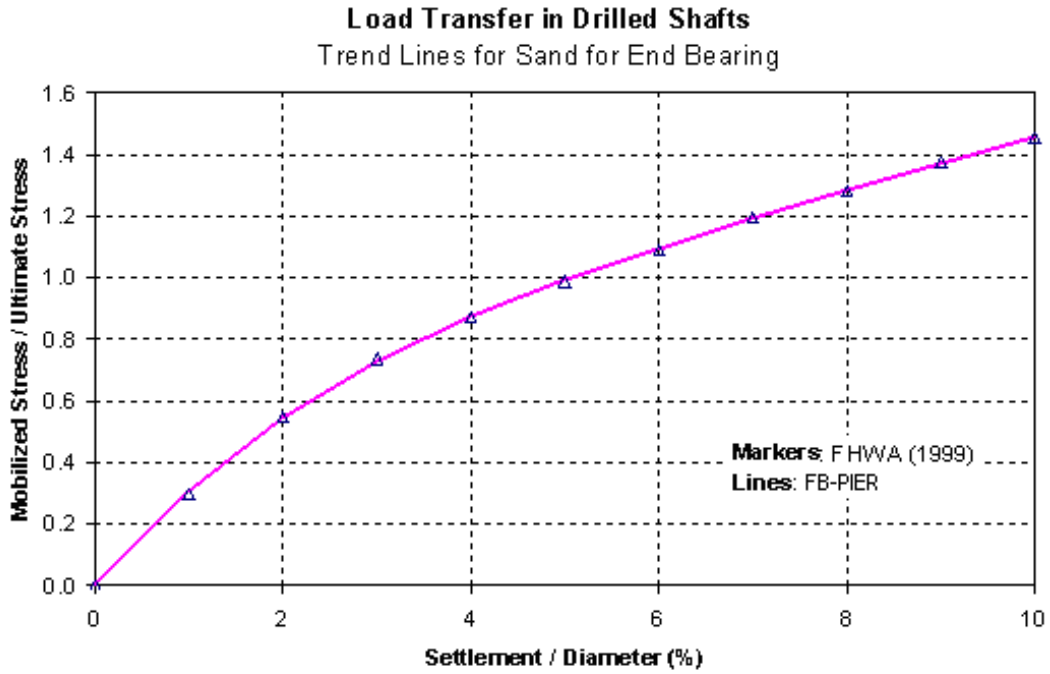

Figure 2.28. Trend Lines for drilled shaft end bearings in sand (BSI 2013(b), and O'Neill and Reese 1999)

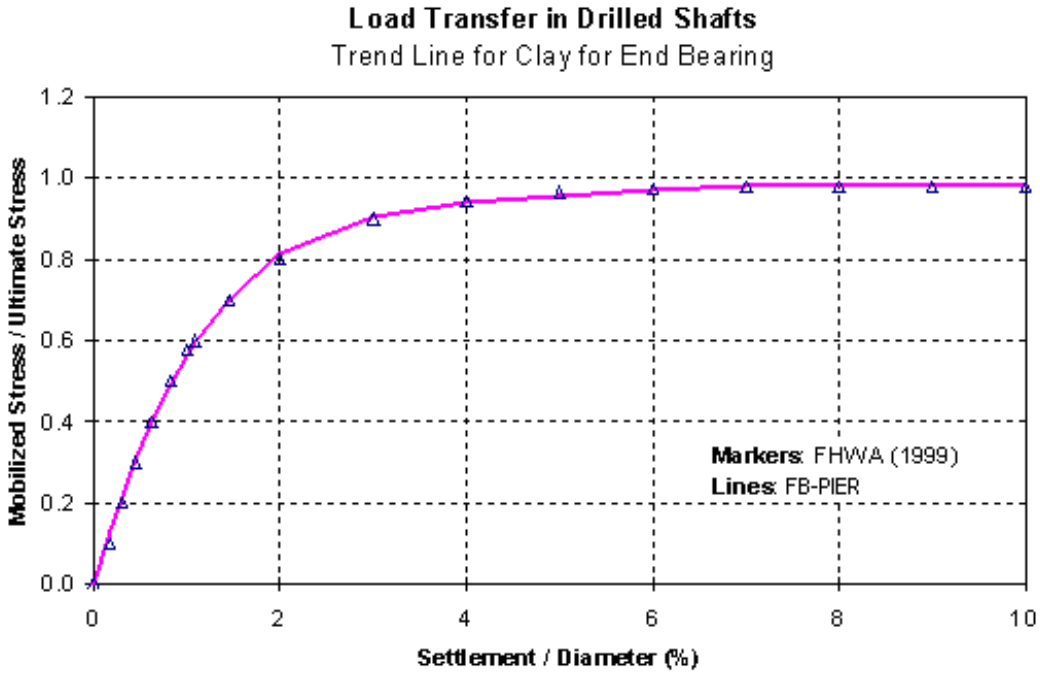

Figure 2.29. Trend lines for drilled shaft end bearings in clay (BSI 2013(b), and O'Neill and Reese 1999)

2.4.2.5 Input Parameters

One of the most important aspects of any computer program analysis is the input parameters used. There are many correlations, charts, tables, etc., to determine the soil parameters necessary for FB-MultiPier. The input parameters needed to be determined for this project, and sources used to determine parameters are shown in Table 2.5. The shear strength correlations referenced are primarily based on the SPT N-value, which is commonly used to determine soil strength and consistency.

Table 2.5 – Input parameters needed for FB-MultiPier

γ	unit Weight (Terzaghi and Peck 1968)
ϕ	angle of internal friction (Peck et al., 1974); (Barton 1973, and Hoek & Bray 1977, as referenced in Mayne et al. 2001)
S_u and q_u	undrained shear strength and unconfined compressive strength (Kulhawy and Mayne 1990)
ε_{50}	strain at 50% of the failure stress in an unconfined compression test (Reese and Wang 1993)
ε_{100}	strain at 100% of the failure stress in an unconfined compression test (In the absence of testing, experience shows that ε_{100} is somewhere between 7 and 15 % or roughly twice that of ε_{50})
k	subgrade modulus (Reese and Wang 1993)
G	initial shear modulus (PL_AID,1989)
τ_f	unit skin friction (BSI 2013(a))
Q_{tip}	axial bearing failure (BSI 2013(a) after Schmertmann (1967))
ν	Poisson's ratio (BSI 2013(b))
N	SPT N-value (Value determined based on Standard Penetration Test)

2.4.3 Structural Modeling

FB-MultiPier is capable of modeling complex structural components. The structural components are modeled by inputting the pier geometry (pier height, pier cap cantilever length, column spacing and offset, number of piers, and pier cap slope), cross-section parameters, and taper data (if applicable). Figure 2.30 shows the pier data edit window. The program has default cross sections or the user can model a custom one. The cross section can be modeled as one of two types: gross properties and full cross section. The gross properties option requires the specification of the resulting sectional

properties. This can be cumbersome when modeling complex reinforced concrete cross sections. The full cross section option requires reinforcement details and material properties. The sectional properties are calculated internally. Figure 2.31 and 2.32 show the gross properties and full cross section windows within the program. Figure 2.33 shows the reinforcement specification window. The user has the option of specifying reinforcement by custom designation or by percentage of gross area.

The program can conduct linear or non-linear analysis for both the pile and pier (column and cap). If linear behavior is selected, it is assumed the behavior is purely linear elastic and deflections do not cause secondary moments (BSI 2013(b)). If non-linear analysis is selected, the program accounts for second order effects (p-delta) as well as stiffness changes within the structure, such as cracking of concrete, and it uses either user defined or default stress-strain curves (BSI 2013(b)). P-delta effects occur when the axial force becomes eccentric within the element due to displacements of one end of the element relative to the other, causing an out-of-balance moment within the member (BSI 2013(b)). The default non-linear stress strain curve of concrete is a function of compressive strength and the Young's modulus of elasticity of the concrete. The default stress-strain curve for mild steel, such as an H-pile, is elastic-perfectly plastic and a function of Young's modulus of elasticity and the yield strength. These default stress-strain curves are shown in Figures 2.34 and 2.35. Concrete modulus is also needed for developing the concrete models in FB-MultiPier. Equation 2.1 presents the concrete modulus equation given by ACI (2011) for normal weight concrete:

$$E_c = 57{,}000\sqrt{f_c'} \tag{2.1}$$

where:

E_c = modulus of elasticity of concrete (lb/in^2)
f_c' = specified 28-day compressive strength of concrete (lb/in^2)

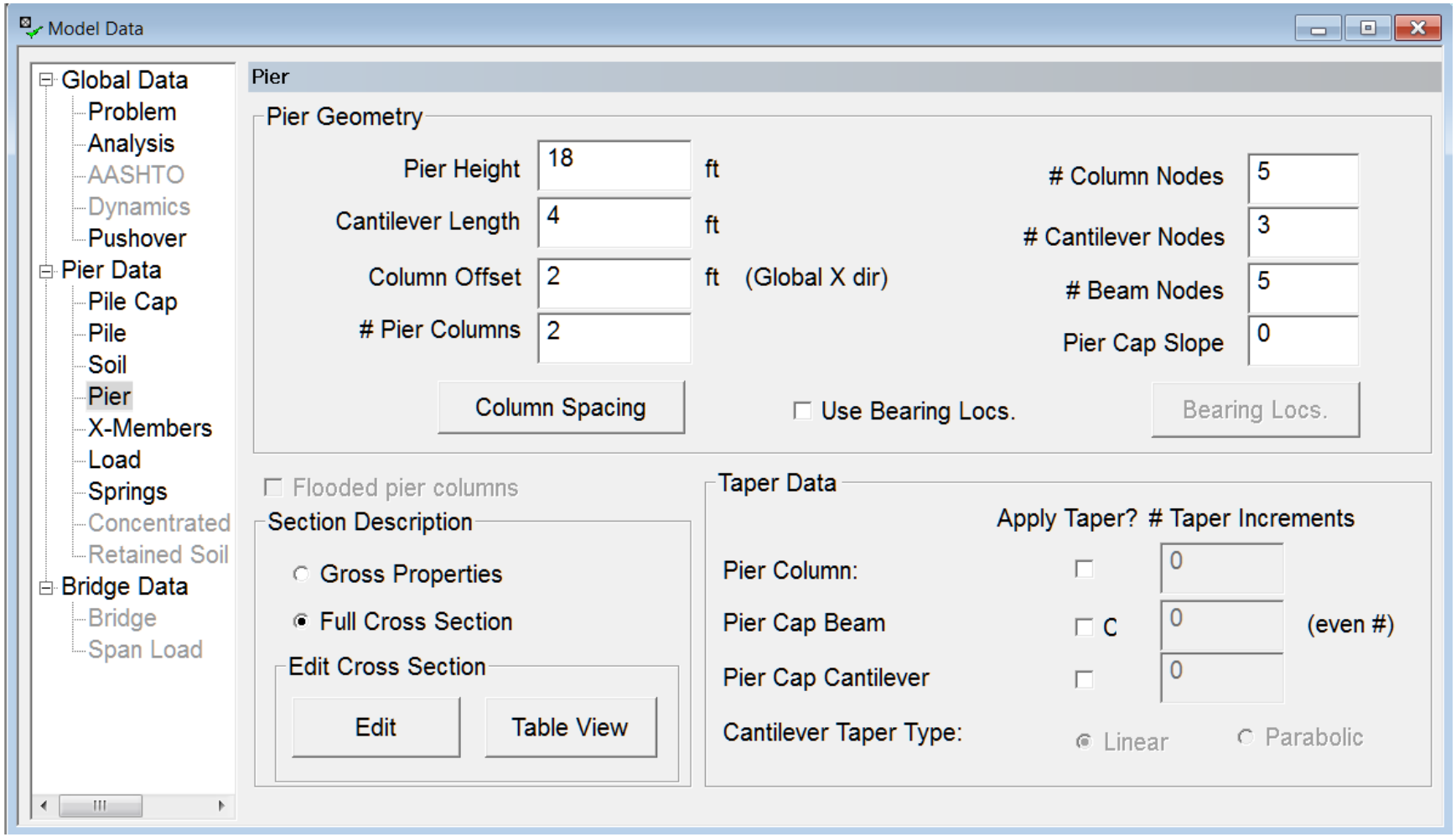

Figure 2.30. Pier data edit window

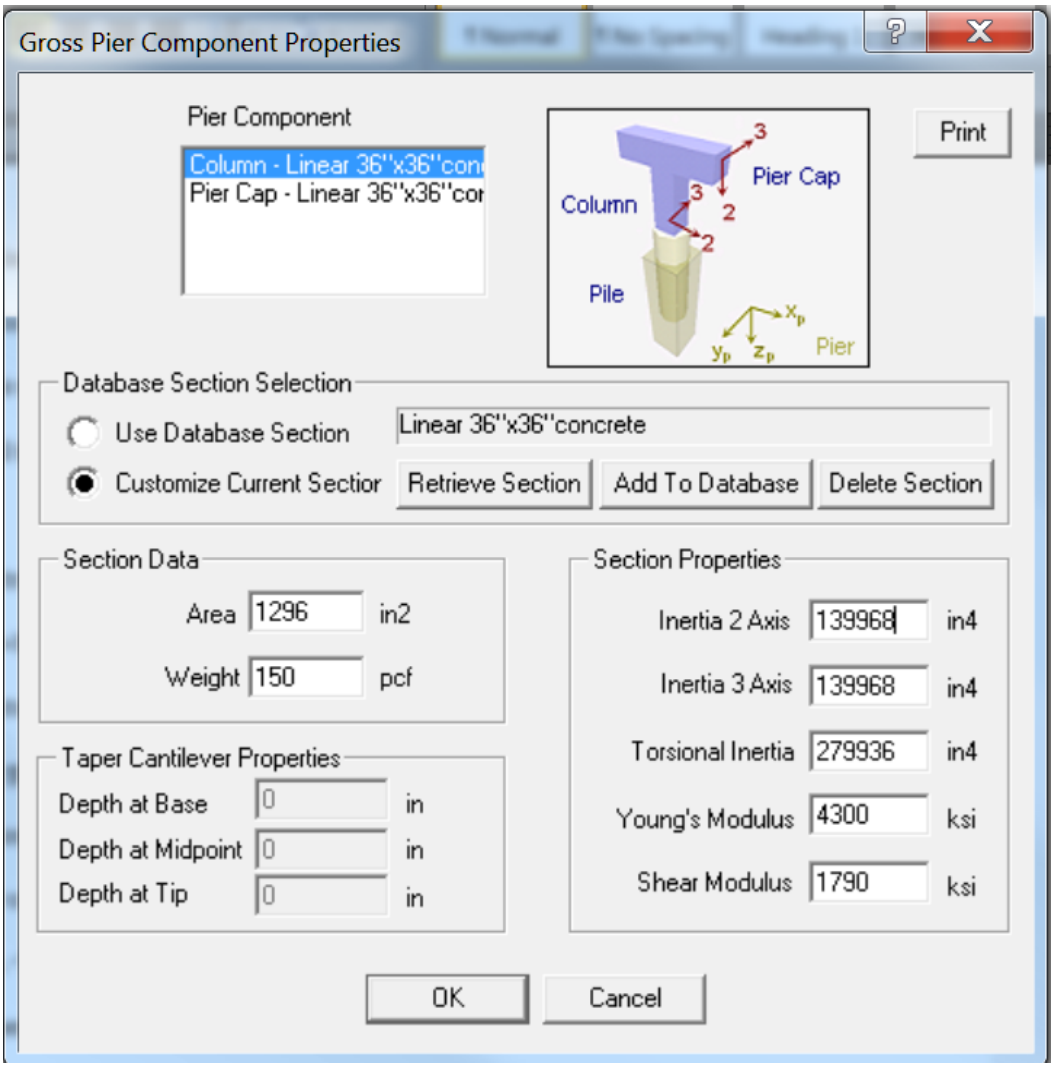

Figure 2.31. Gross properties window

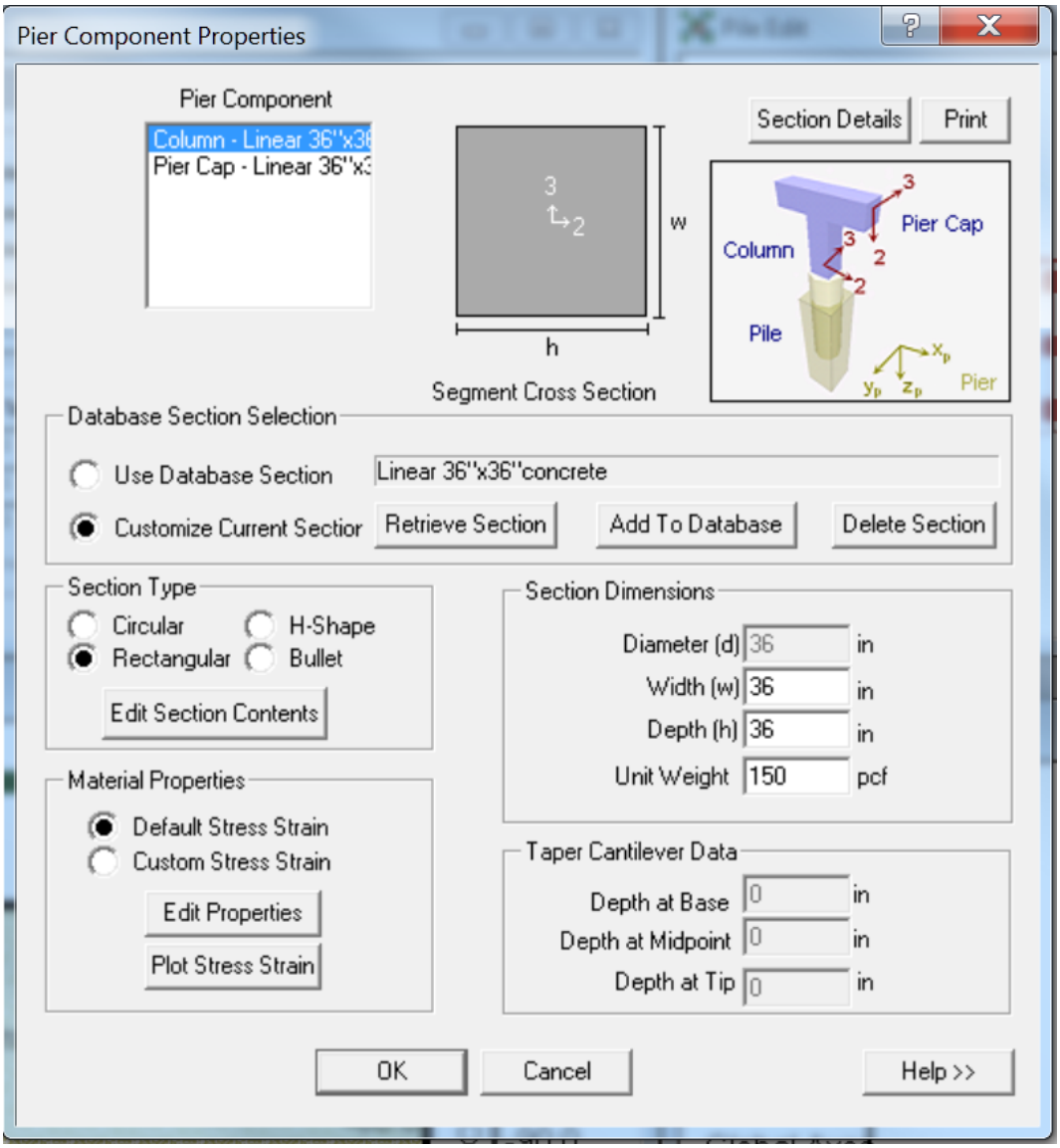

Figure 2.32. Full cross section properties window

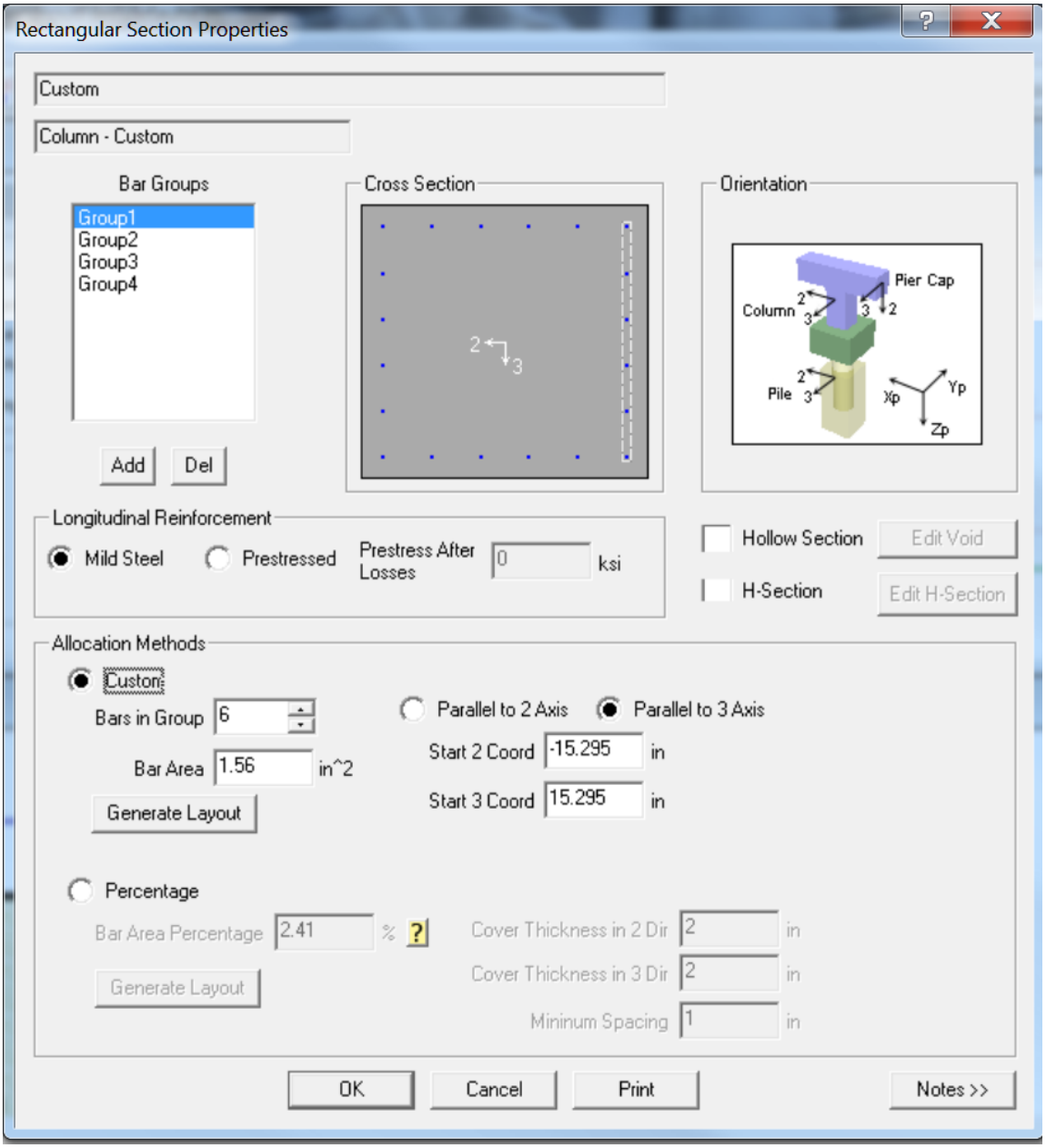

Figure 2.33. Reinforcement specification window

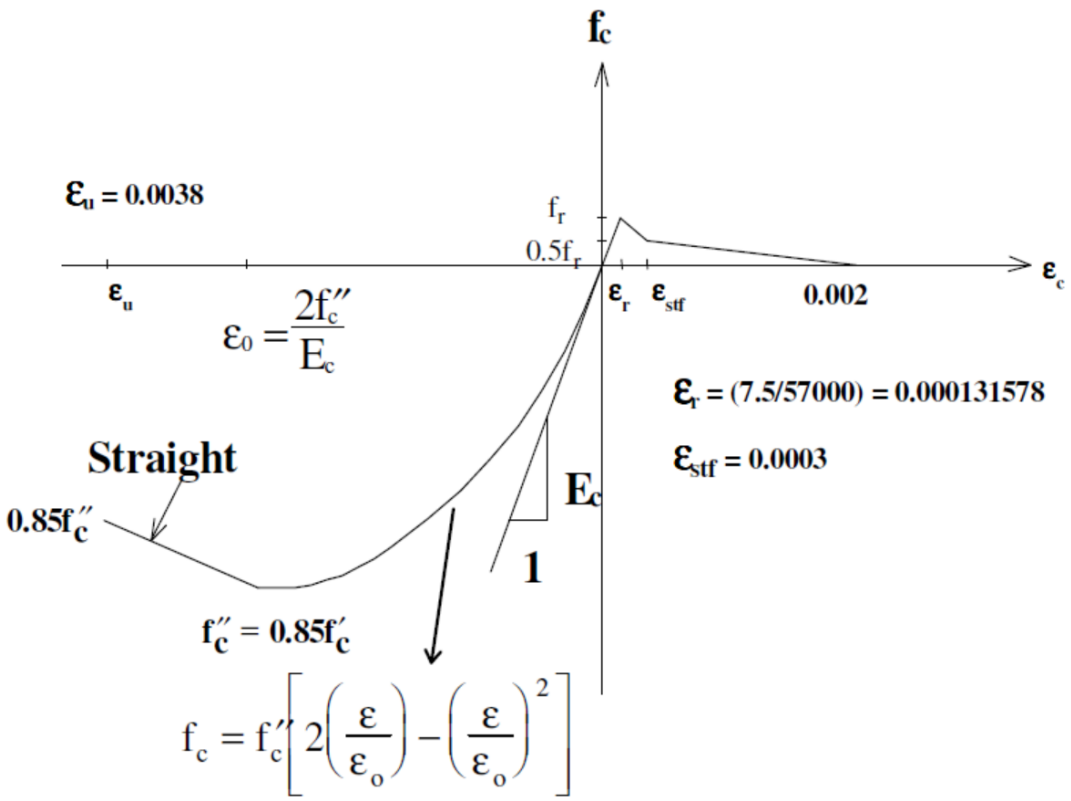

Figure 2.34. Hognestad model for concrete (Hognestad et al. 1955)

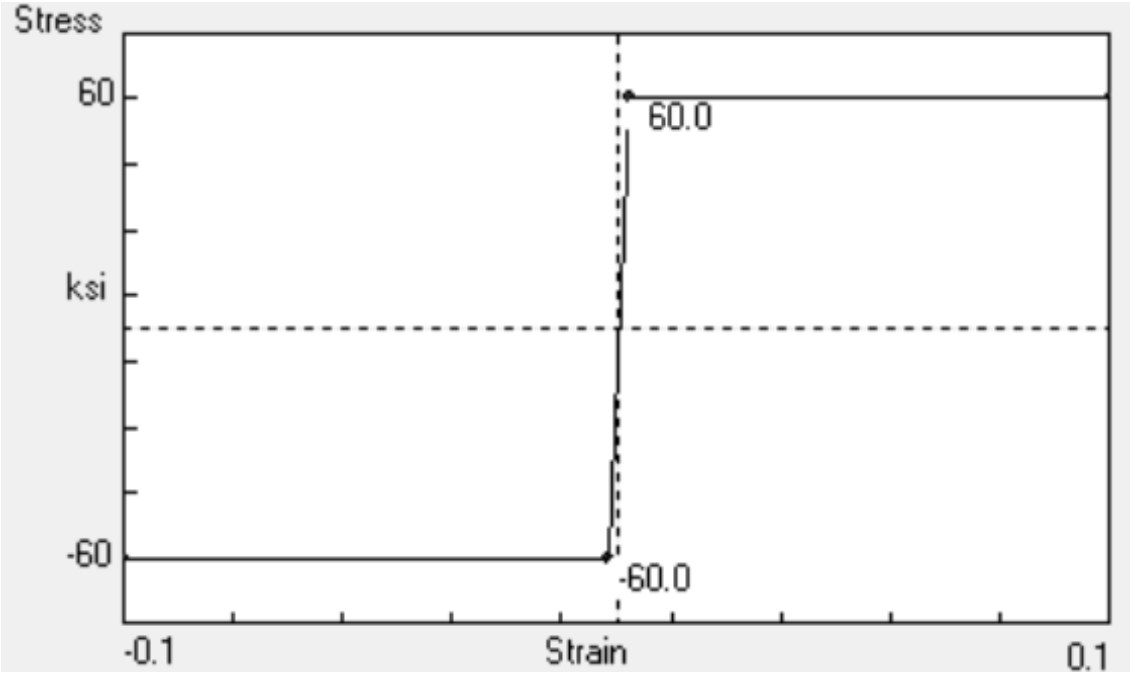

Figure 2.35. Default stress-strain curve for 60 ksi steel (BSI 2013(b))

2.4.4 Foundation Modeling

The foundation elements are modeled like that of the structure elements as previously mentioned. There are default options as well as a user defined option available. The option to model multiple pile sets is also available. For example, if the design calls for one drilled shaft tip elevation at 250 feet and the other at 265 feet, FB-MultiPier can specify 2 (or more) pile sets. This is an important option, as tip elevations or pile types can be different for a large pier structure.

2.4.5 Pile Cap Modeling

The pile cap is modeled based on the concrete's Young's modulus of elasticity, Poisson's ratio, thickness, and unit weight of the pile cap material (usually concrete). To avoid stress concentrations at the base column node where it connects to the pile, FB-MultiPier spreads the load to the four adjacent nodes on the pile cap using rigid connectors built in to the program (BSI 2013(b)). The user has the option to choose whether to treat the pile-to-cap connection as pinned or rigid (referred within the program as fixed).

The pile cap can also be a factor in lateral and axial capacity within the program. A simple parametric study was done to compare a pile cap just above the ground surface and a fully embedded pile cap. It was found that the lateral deflections decreased significantly when the pile cap was embedded. Though this is generally correct, the soil resistance around the pile cap may change during construction depending on the techniques used and depth of embedment. Therefore, it is up to the engineer to determine the "as built" strength of the soil surrounding the pile cap. In the analysis edit window, the option to include axial bearing effects of the pile cap is available. It is to the

discretion of the engineer whether to use it or not. Typically, pile foundations are designed with the assumption that the axial forces would be resisted by the piles alone.

2.4.6 Pile Group Effects

Lateral and axial resistance of soil for a group of piles is typically not equal to the sum of the individual resistances relative to each pile (BSI 2013(b)). Generally, the soil resistance to a pile within a group is less than the same individual pile (not in a group). This difference in resistance of soil to a pile within a group is a function of the pile center-to-center (c-c) spacing and location within the group (Brown et al. 1988). Lateral group effects are typically handled by use of p-y multipliers. P-y multipliers are used to degrade the p-y curve to account for the "shadowing" effect (i.e., loss of soil resistance of piles in the trailing rows) (Brown et al. 1988). When a pile group is loaded, the front row (or lead row) carries a larger proportion of the load, whereas the trailing rows carry less of a proportion. Figure 2.36 shows an illustration of a generalized pile group interaction when laterally loaded.

FB-MultiPier provides the user with three options: (1) use default p-y multipliers, (2) user defined p-y multipliers, or (3) do not use p-y multipliers. The default p-y multipliers are based on the recommendation by Brown et al. (1988). The default multipliers used in FB-MultiPier for lateral loading are: 0.8, 0.4, 0.3, 0.2, 0.2, ….0.3, where 0.8 is the lead row and 0.3 is the trail row value (BSI 2013(b)). These values are recommended by Brown et al. (1988) to be used for 3D spacing. Note that if there are four rows, the trail multiplier would be 0.2, whereas if there were ten rows, the trail multiplier would be 0.3. For 5D spacing, Brown et al. (1988) recommends using the following p-y multipliers: 1.0, 0.85, 0.7, 0.7, …, 0.7, where 1.0 is the lead row and 0.7 is

the trail row value. BSI (2013(b)) also recommended using the same p-y multipliers for battered piles. It is also important to note that FB-MultiPier will apply the p-y multipliers to the correct pile rows (lead to trail) based on which direction the piles move (not based on which direction the initial load is applied) (BSI 2013(b)). For dynamic analysis, this means that as a pile is moving back and forth, the p-y multipliers will be updated each time the piles change the direction of displacement.

FB-MultiPier also considers group efficiency for axial loads. Group efficiency for axial loads is the ratio of the amount of axial load the group can resist relative to the sum of the single pile resistances that make up the group. Typically, driven pile group efficiencies are greater than one because the soil consolidates during driving, which increases the soil axial resistance. The user has the option to input an efficiency factor other than one. Otherwise the default factor is one. See Hannigan et al. (2006) for recommendations for axial group efficiency factors.

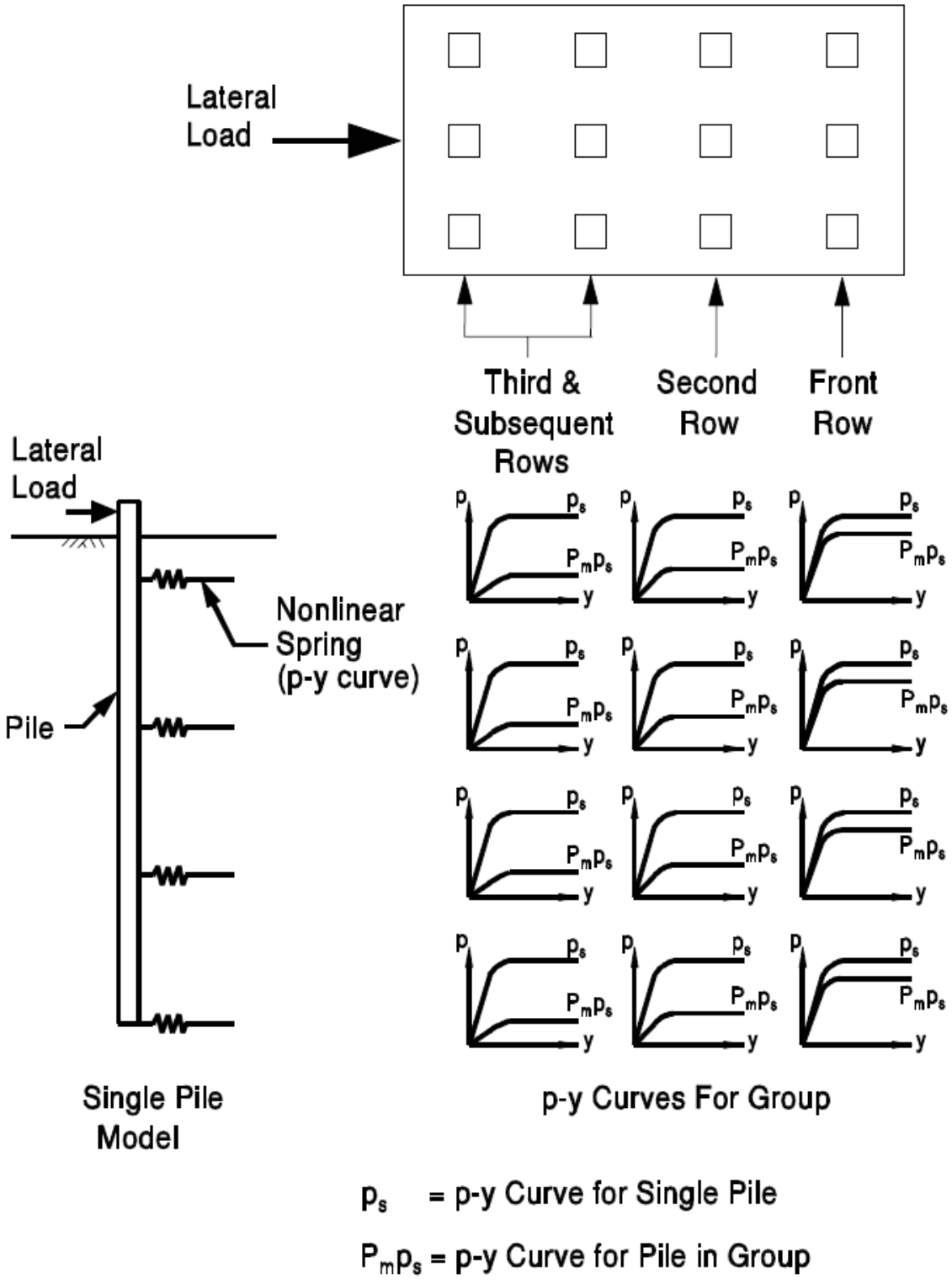

Figure 2.36. Illustration of p-y multiplier concept for lateral group analysis (Hannigan et al. 2006)

2.4.7 Dynamic Analysis Methods

There are two methods that FB-MultiPier employs to predict the dynamic response of a system: transient dynamic (time-history) analysis and modal response analysis. Both dynamic analysis options are briefly discussed herein. For more detail on either analysis type, see Fernandes (1999).

2.4.7.1 Time-History Analysis

FB-MultiPier uses time-history analysis to simulate the structural response under an earthquake event. This is done by loading an earthquake record into the program. FB-MultiPier has built in functions and also allows the user to upload their own. The functions can be either applied as load versus time or acceleration versus time. The "load versus time" functions are generally for impact analysis such as a barge impact.

Time-history analysis allows significant inertial and damping effects to be considered when determining the structural response. This done by using implicit time integration algorithms to obtain a numerical solution to the equation of motion:

$$[M]\{\ddot{x}\} + [C]\{\dot{x}\} + [K]\{x\} = \{F(t)\} \tag{2.2}$$

where:

$[M]$ = mass matrix
$\{\ddot{x}\}$ = nodal acceleration vector
$[C]$ = damping matrix
$\{\dot{x}\}$ = nodal velocity vector
$[K]$ = stiffness matrix
$\{x\}$ = nodal displacement vector
$\{F(t)\}$ = external force vector

FB-MultiPier has the option of using either the Newmark or Wilson-Θ method to determine the numerical solution of Equation 2.2 by using discrete time increments

specified by the user. Typically, the same time step is used in that of the time function. It is possible, however, to use a larger time step to reduce analysis time if the time-history event is long. This skips over some time steps and may miss a few peaks, but generally it is not significant in the overall response of the structure. For more detail regarding time-history analysis, see Fernandes (1999).

2.4.7.2 Modal Response Analysis

Modal response analysis performs a response spectrum analysis of the structure in its equilibrium position (BSI 2013(b)). The equilibrium position being the response of the system after it was statically loaded. Figure 2.37 shows the cycle for how modal analysis is conducted within FB-MultiPier. To perform modal analysis, FB-MultiPier requires the number of modes in which to run and a spectral acceleration function (acceleration versus frequency). Global damping factors can be applied if applicable. Fernandes (1999) describes the modal analysis process within FB-MultiPier:

> *In the first cycle the earthquake is applied to the structure and the initial forces at the base of the piers are computed. Initially the springs that represent the foundation are considered very stiff, to simulate fixed supports. Then for each column a vector of six forces is generated, the three forces F_x, F_y, and F_z in the x, y and z directions, and the three respective moments. Then each of these forces is applied to the foundation, one at a time, like in a regular static analysis. This will produce three displacements, d_X, d_Y, and d_Z, in the x, y, and z directions, and three respective rotations, θ_X, θ_Y, and θ_Z, at the base of each column.... After all six forces are applied we have the six by six flexibility*

matrix for the foundation, one (flexibility matrix) for each column. Inverting this matrix we obtain the new stiffness for the foundation, which becomes the foundation springs for the base of each pier for the next cycle.

Note that the force vectors generated represent the foundation response. Once two consecutive forces are within the user defined tolerance, the program terminates. Note that in this analysis, the structure is considered linear, but the springs generated for each cycle will have characteristics of nonlinear behavior (Fernandes 1999).

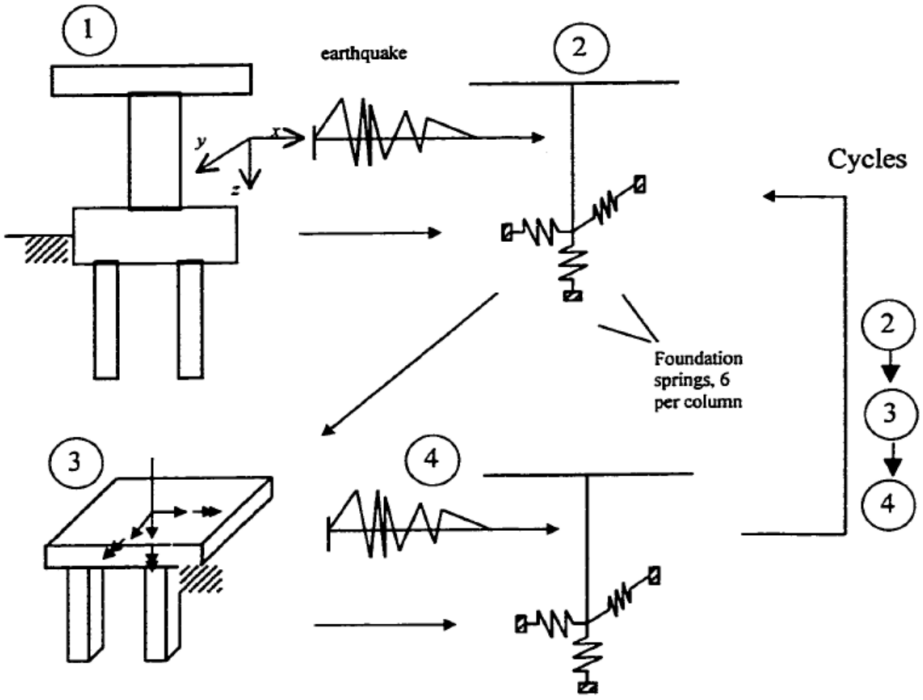

Figure 2.37. Modal analysis process for a bridge pier within FB-MultiPier (Fernandes 1999)

2.4.7.3 Damping

Damping is a complex and important part of structural response during dynamic loading. It reduces the free motion vibrations in an oscillatory system. Damping effects in a real system, such as a bridge, are due to friction, air resistance, or other external or internal (within the damped system) physical mechanisms. FB-MultiPier employs Rayleigh mass and stiffness damping factors in time-history analysis. In the initial development of the dynamic analysis option in FB-MultiPier (Brown et al. 2001), Rayleigh mass and stiffness damping factors for the pier, piles, and soil were determined based on field tests correlated to the program results. The Rayleigh damping factors used in Brown et al. (2001) are presented in Table 2.6. From Equation 2.3, we can expand the damping matrix, [C], as:

$$[C] = \alpha[K] + \beta[M] \tag{2.3}$$

where:

α = stiffness proportional damping constant
$[K]$ = stiffness matrix
β = mass proportional damping constant
$[M]$ = mass matrix

Table 2.6 – Rayleigh damping factors used in Brown et al. (2001)

	Mass (α)	Stiffness (β)
Pier	0.04	0.01
Piles	0.001 (steel)	0.001 (steel)
Soil	0.015	0.015

2.4.7.4 Dynamic Relaxation

Dynamic relaxation within FB-MultiPier accounts for a static dead load before the transient dynamic load is applied. Static analysis of the structure is conducted before the dynamic load is applied and a new stiffness matrix and nodal displacement vector are obtained through the static analysis once the system is in equilibrium (BSI 2013(b)). This new initial stiffness and nodal displacement vector is then used in the dynamic time-history analysis. If this option is not used, it will apply the dead load as an impact load simultaneously with the dynamic load (BSI 2013(b)). This can exaggerate the dynamic structural response, and therefore, any assessment made based on that response is unreliable (BSI 2013(b)).

2.4.8 FB-MultiPier Limitations

While FB-MultiPier is a very powerful program, there are several limitations that the user should be aware of. These limitations can affect the quality of the output. Therefore, it is important to understand them to properly interpret the output generated. Most of these limitations directly affect the dynamic analysis.

- FB-MultiPier can only apply 100 percent of the ground motion in the X, Y or Z direction (or a combination of the three). It cannot apply, for example, 30 percent in the X direction and 70 percent in the Y direction.
- There is an apparent limitation in the number of decimal places the time and acceleration values can be in the ".acc" input files. If the time step was originally 0.005 seconds, duplicating numbers would be read by the

program due to rounding by the program. Also, if the time step was 0.01 seconds and the time history function is over 100 seconds long, the program would only recognize numbers to the accuracy of 0.1. For example, the program would read 100 until 100.05, and then read 100.05 as 100.1 and so forth until it reached 101.05. This can cause numerical error within the program.

- FB-MultiPier has a memory restriction of 4GB. This is too low for a dynamic model with many piles and structural members, and causes the program to crash due to insufficient memory capacity. Increasing the time step was an option to lower the amount of memory needed for analysis. BSI is currently in the process of correcting this memory restriction.
- Batch mode cannot be used when using the dynamic relaxation option. The program will not start the dynamic analysis after the static analysis is completed to use the new stiffness matrix and displacements. BSI is currently in the process of correcting this issue.

2.5 FHWA LRFD Seismic Analysis and Design of Bridge Foundations

Recently, the FHWA sponsored the revision of GEC-3 (Kavazanjian et al. 2011), to include the LRFD guidelines developed by AASHTO. Along with Kavazanjian et al. (2011), a course was developed (Kavazanjian et al. 2012) that aims to illustrate the principles and methodologies for LRFD seismic analysis and design of geotechnical features and structural foundations for bridges (Kavazanjian et al. 2012). Three design examples were presented to show the procedures that need to be addressed in the seismic design process in accordance

with AASHTO specifications for LRFD seismic design (Kavazanjian et al. 2012). There are several points of emphasis pertaining to geotechnical considerations that were addressed in Kavazanjian et al. (2012) document:

1. Development of the acceleration response spectrum for use in structural design, including adjustment for local site conditions.
2. Deaggregation of the seismic hazard to get the earthquake magnitude for seismic stability analysis.
3. Evaluation of lateral pile stiffness (p-y behavior) for the piles for both the abutments and the central piers (substructure analysis)
4. Evaluation of vertical pile capacity (including uplift) and spring stiffness for both abutment and central pier piles (substructure analysis).
5. Evaluation of the seismic stability of the abutment slope.
6. Evaluate the seismic passive resistance and spring stiffness of the abutment wall.
7. Evaluate liquefaction and lateral spreading potential of slopes at the abutments.
8. Evaluation of the bearing capacity, sliding resistance and spring stiffness of the pier and abutment footings (if applicable).

All of these points of emphasis are discussed in detail in Kavazanjian et al. (2011).

Chapter 3

LITERATURE REVIEW

Chapter 3 is a summary of literature to explain deep foundation (referred to as pile in this chapter) behavior during an earthquake event. Pile failure modes that are possible during an earthquake event are presented and discussed, as well as case histories of past pile performance during earthquake events. Finally, pile performance and recommendations are reviewed and discussed for the combined effect of earthquake and scour.

3.1 Pile Failure Modes

During an earthquake, deep foundations have the capacity to perform well and maintain overall stability. However, it is important to understand the different failure modes a pile can undergo during an earthquake. This allows the engineer to design the proper foundation while accounting for the different failure modes that could occur. Pile failure can occur in several different ways. The mechanisms of pile failure are shear force and flexure failure, and excessive settlement, all of which can be induced by several different modes. There are two primary categories of pile failure during an earthquake: (a) pile failure without liquefaction-induced phenomena and (b) pile failure with liquefaction-induced phenomena (Wei et al. 2008). A brief description of each category is presented:

A) Pile failure with no liquefaction-induced phenomena

1) Failure due to the inertial force of the superstructure

Ishihara (1997) described this as the 'top down effect' because the inertial force exerted by the superstructure is transferred down to the upper portion of the pile, inducing large bending moments at the pile cap and pile head(s). Therefore, most of the damage and pile failure is located at joints between the pile cap and pile head or at the top of the pile (Wei et al. 2008).

2) Failure at the interface of soft and hard soil layers (Wei et al. 2008)

Excessive bending moment and shear force can also develop at the interface of two distinct soil layers of differing strength (i.e. a large deposit of soft clay over very dense sand). Wei et al. (2008) also states that the p-y curve method, which is commonly used to determine the response of deep foundations, cannot reflect the actual situation that occurs between the two soil layers; therefore, careful consideration and proper engineering judgment should be used to determine the most representative response of a deep foundation system in this situation.

3) Pile settlement due to thixotropy

Thixotropy is a unique phenomenon that generally occurs in flocculated clayey soil. Thixotropy is a time-dependent process that occurs when the soil is softened due to remolding of the soil skeleton that is induced by a dynamic loading; it then returns to its original, harder state after the loading is over and the particles realign (McCarthy 2007). Thixotropy of soft soil can occur during an earthquake, therefore, the axial resistance of the soil can be greatly reduced which could cause excessive settlement.

4) Retaining wall or embankment near pile foundations (Wei et al. 2008)

Earthquakes can cause retaining wall or embankment failures without the soil liquefying (i.e. tension cracks, etc.) during and after the event. The soil could induce large passive pressures on the pile foundation should the soil mobilize, which could lead to excessive bending moment and ultimately structural failure of the pile.

B) Pile failure with liquefaction-induced phenomena (Wei et al. 2008)

1) Failure without lateral spreading

If the soil liquefies, but does not undergo lateral spreading, it can create non-uniform distributions in liquefied strength and thickness of the soil (Wei et al. 2008). The load distribution of the structure can become eccentric which could lead to differential settlement. However, if the distribution of soil strength and thickness are uniform, the pile could still fail at the liquefied and non-liquefied soil interface due to the inertial loading of the structure (Wei et al. 2008).

2) Failure with lateral spreading

Bridges often span rivers. The soil profile of these areas often includes liquefiable sand and silt layers sloping towards the river (Wei et al. 2008). If the liquefied soil is present below the ground surface, the non-liquefiable soil (crust) above the liquefied layer can place a significant amount of passive pressure on the pile foundations as the liquefied soil displaces the top layer during liquefaction (Berrill et al. 2001). This results in increased shear and bending at the pile head and cap. The lateral and axial resistance of the soil also drastically decreases, and the pile can become unstable. The main cause for pile failure during an

earthquake is thought to be due to lateral spreading around the pile according to a report published by National Research Council (NRC) Committee on Earthquake Engineering (1985). They go on to claim that lateral spreading is responsible for more damage during an earthquake than any other mode of ground failure due to liquefaction. This failure mechanism is widely accepted and has been used as the explanation for pile failure in many earthquakes (Bhattacharya 2003).

Another failure mechanism that can develop during an earthquake that does not necessarily lie within the two categories previously described is pile buckling. Typically, buckling is accounted for in design by considering: (a) piles in very soft clay, (b) during installation by driving, and (c) partially exposed piles such as offshore platforms or jetties (Fleming et al., 1992) Recently there has been research (Bhattacharya et al. (2004), Knappett and Madabhushi (2005), Kimura and Tokimatsu (2005), and Shanker et al. (2007)) suggesting that this is an important aspect of pile foundation design for earthquake loading and should be accounted for (Bhattacharya et al. 2008). Buckling is only a problem if there is not sufficient lateral restraint to keep the pile from displacing laterally. This can happen when soil liquefies and the effective stress is zero. The easiest concept to describe buckling is that the axial design load P_{des} must be less than the critical buckling load P_{cr}. Euler's formula for calculating P_{cr} is shown as equation 3.1:

$$P_{cr} = \frac{\pi^2}{L_{eff}^2} EI \tag{3.1}$$

where:

P_{cr}	=	critical buckling load (kips)
L_{eff}	=	effective length of the pile in the liquefiable or soft clay region. See Figure 3.1 for an explanation of the different boundary conditions. Some designers may prefer to increase the effective length by a few diameters to account for imperfect fixity in the non-liquefying layer (Bhattacharya 2003) (in)
E	=	modulus of elasticity (ksi)
I	=	cross-sectional area moment of inertia (in^4)

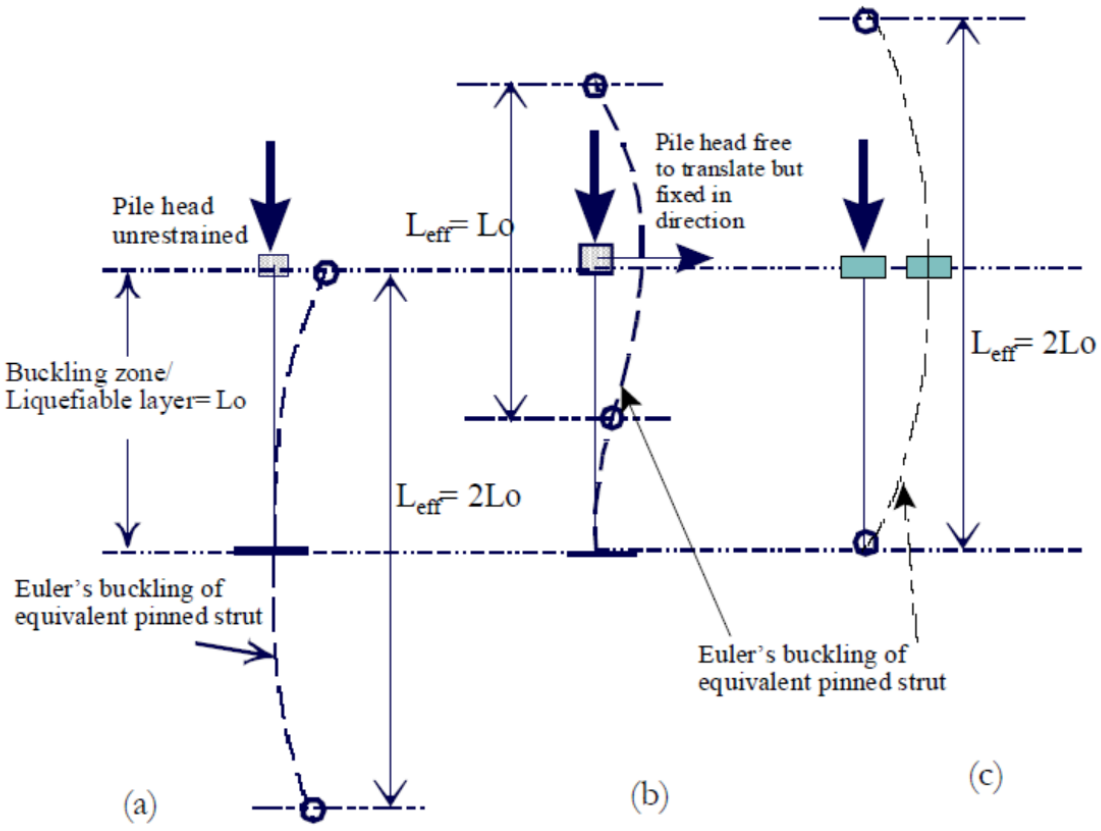

Figure 3.1. Concept of effective length of pile for different boundary conditions (Bhattacharya 2003).

The engineer must estimate the height of the liquefiable layer (or resulting free length of the pile) and the pile head and tip condition. L_{eff} is also different for each direction of buckling (longitudinal and transverse). Typically, a drilled shaft embedded into rock will have an estimated L_{eff} of 2 times the free length (Figure 3.1(a)) (length

from rock line to pile cap) in the longitudinal direction; whereas, in the transverse direction, L_{eff} is most likely the same as the free length (assumed that the pier cap and column connection is rigid [fixed]). For driven piles, a pinned connection is typically assumed for piles driven to bedrock (small embedment) and a fixed connection at the pile head embedded into the footing (Figure 3.1(c)). Therefore, L_{eff} is 2 times the length of the pile. However, if stiff soil is in the upper or lower portion of the soil profile, partial fixity should be considered which would change L_{eff}.

3.2 Pile Performance in Liquefied Soil and Soft Clay

The Bhattacharya (2003) document was a primary source for pile buckling (see previous section), past pile performance (case histories) during an earthquake, and centrifuge testing and should be referred to for further detail.

3.2.1 Case Histories

Pile foundations have been known to have both good and bad performance during an earthquake event. Bhattacharya (2003) presents a summary of fourteen case histories of pile performance. The pile types included in the case studies are reinforced concrete (drilled shafts), prestressed concrete piles, and steel pipe piles. It was not conclusive that one pile type out-performed another. They are presented in Table 3.1. There are two important ratios that Bhattacharya discusses that are helpful in the design and selection of pile types and sizes: P_{des}/P_{cr} (P_{des} is the design axial load for the pile) and L_{eff}/r_{min} (also known as effective slenderness ratio). Equation 3.2 shows how to calculate r_{min}:

$$r_{min} = \sqrt{\frac{I}{A}} \tag{3.2}$$

where:

r_{min} = minimum radius of gyration of the pile section about any axis of bending (in)
I = minimum cross-sectional area moment of inertia (in^4)
A = area of the pile section (in^2)

Bhattacharya (2003) noted that the piles that failed had a P_{des}/P_{cr} ratio between 0.5 and 1.0; he then hypothesized that a pile having a P_{des}/P_{cr} ratio of 0.5 or less would most likely perform well during an earthquake event. Bhattacharya also hypothesized that if the effective slenderness ratio is 50 or less, the pile is likely to perform well. These hypotheses were based on fourteen case studies presented in Table 3.1. Figure 3.2 shows the slenderness ratio threshold of 50 and the case history values are shown for comparison. Figure 3.3 shows the P_{des}/P_{cr} thresholds of 0.5 and 1.0 with the case histories plotted for comparison. It should also be noted that the piles that performed well in the case histories reviewed had a P_{des}/P_{cr} ratio less than 0.1.

Table 3.1 – Summary of pile performances (after Bhattacharya 2003)

Case History and Reference	**L* (m)**	**L_0** (m)**	**Pile Section/Type**	**Framing Action/β*** Value**	**L_{eff} (m)**	**r_{min} (m)**	**L_{eff}/r_{min}**	**P_{des} (MN)**	**P_{cr} (MN)**	**P_{des}/P_{cr}**	**Lateral Spreading Observed?**	**Performance**
10 storey-Hokuriku building, 1964 Niigata earthquake, Hamada (1992)	12	5	0.4m dia reinforced concrete (RCC)	Large piled raft with basement, 1	5	0.1	50	0.77	12.4	0.062	Yes	Good
Landing bridge, 1987 Edgecumbe earthquake, Berrill et al (2001)	9	4	0.4m square prestressed concrete (PSC)	Raked piles, no sway frame, 0.5	2	0.12	17	0.62	139	0.004	Yes	Good
14 storey building in American park, 1995 Kobe earthquake, Tokimatsu et al (1996)	33	11	2.5m dia RCC	Large pile group and large pile dia, 1.0	11	0.63	19	18	3915	0.005	Yes	Good
Kobe Shimim hospital, 1995 Kobe earthquake, Soga (1997)	30	6.2	0.66m dia Steel tube	Large piled raft with basement, 1.0	6.2	0.23	27	3	91	0.033	No	Good
Hanshin expressway pier, 1995 Kobe earthquake, Ishihara (1997)	41	15.9	1.5m dia RCC	Small group (22 piles), 1.0	15.9	0.38	42	14	305	0.046	Yes	Good
LPG tank 101, Kobe earthquake, Ishihara (1997)	27	15	1.1m dia RCC	Large piled raft, 1.0	15	0.28	53	4.1	79	0.052	Yes	Good
N.H.K building, 1964 Niigata earthquake, Hamada (1992)	12	9.3	0.35m dia RCC	Groups tied by flexible beam, Less embedment at pile tip, 2.0	18.6	0.09	207	0.43	0.52	0.827	Yes	Poor

Table 3.1 – Summary of pile performances (continued) (after Bhattacharya 2003)

Case History and Reference	**L* (m)**	**L_0** (m)**	**Pile Section/Type**	**Framing Action/β*** Value**	**L_{eff} (m)**	**r_{min} (m)**	**L_{eff}/r_{min}**	**P_{des} (MN)**	**P_{cr} (MN)**	**P_{des}/P_{cr}**	**Lateral Spreading Observed?**	**Performance**
NFCH building, 1964 Niigata earthquake, Hamada (1992)	9	7	0.35m dia RCC hollow	Groups tied by flexible beam, Less embedment at pile tip, 2.0	14	0.10	140	0.29	0.82	0.354	Yes	Poor
Showa bridge, 1964 Niigata earthquake, Hamada (1992)	25	19	0.6m dia Steel tube	A single row of piles, 2.0	38	0.21	181	0.96	1.1	0.873	Yes	Poor
Yachiyo Bridge, 1964 Niigata earthquake, Hamada (1992)	11	8	0.3m dia RCC	Isolated footing, 2.0	16	0.08	200	0.34	0.39	0.872	Yes	Poor
Gaiko Ware House, 1983 Chubu earthquake, Hamada (1992)	18	14	0.6m dia PSC hollow	Isolated footing, 2.0	28	0.16	175	1.47	1.61	0.913	Yes	Poor
4 storey fire house, 1995 Kobe earthquake, Tokimatsu et al (1996)	30	16.4	0.4m dia PSC	Groups tied by beam, 1.0	16.4	0.10	161	0.89	1.15	0.774	Yes	Poor
3 storied building at Fukae, 1995 Kobe earthquake, Tokimatsu et al (1998)	20	16	0.4m dia PSC hollow	Groups tied by beam, 1.0	16	0.12	133	0.72	1.02	0.706	Yes	Poor
LPG tank 106,107 – 1995 Kobe earthquake, Ishihara (1997)	20	15	0.3m dia RCC hollow	Groups tied by beam, 1.0	15	0.08	187	0.46	0.38	1.211	No	Poor

*L = Length of the pile; **L_0 = Length of pile in liquefiable region/bucking zone; ***β = Factor for estimating L_{eff}, where $L_{eff} = \beta L_0$

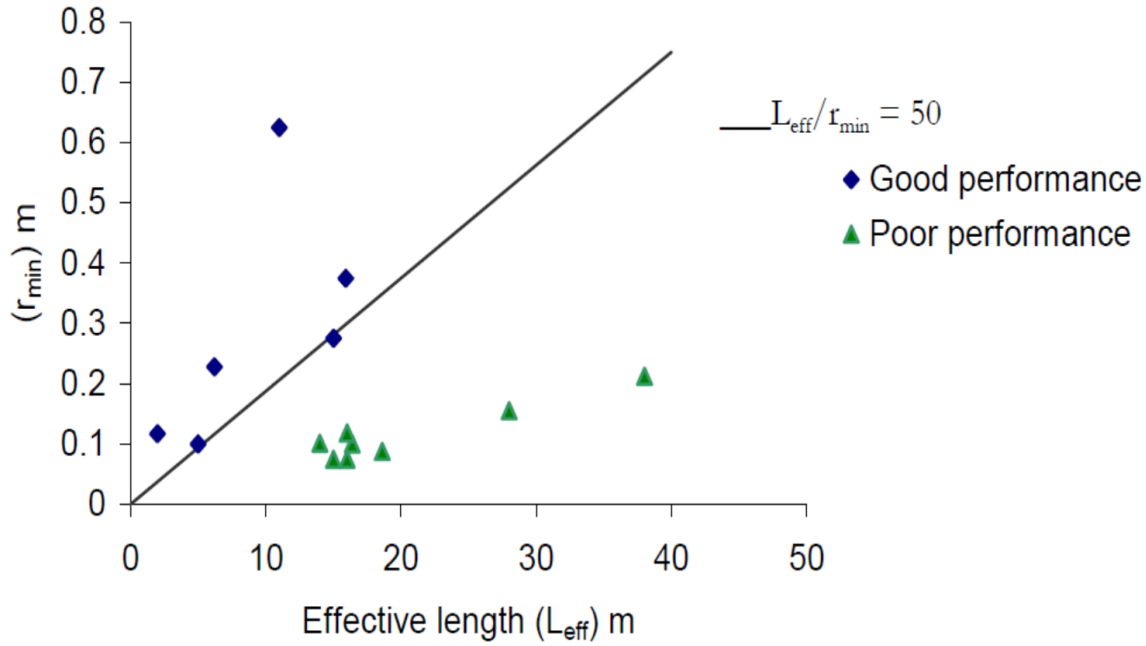

Figure 3.2. r_{min} versus L_{eff} for piles studied (Bhattacharya 2003)

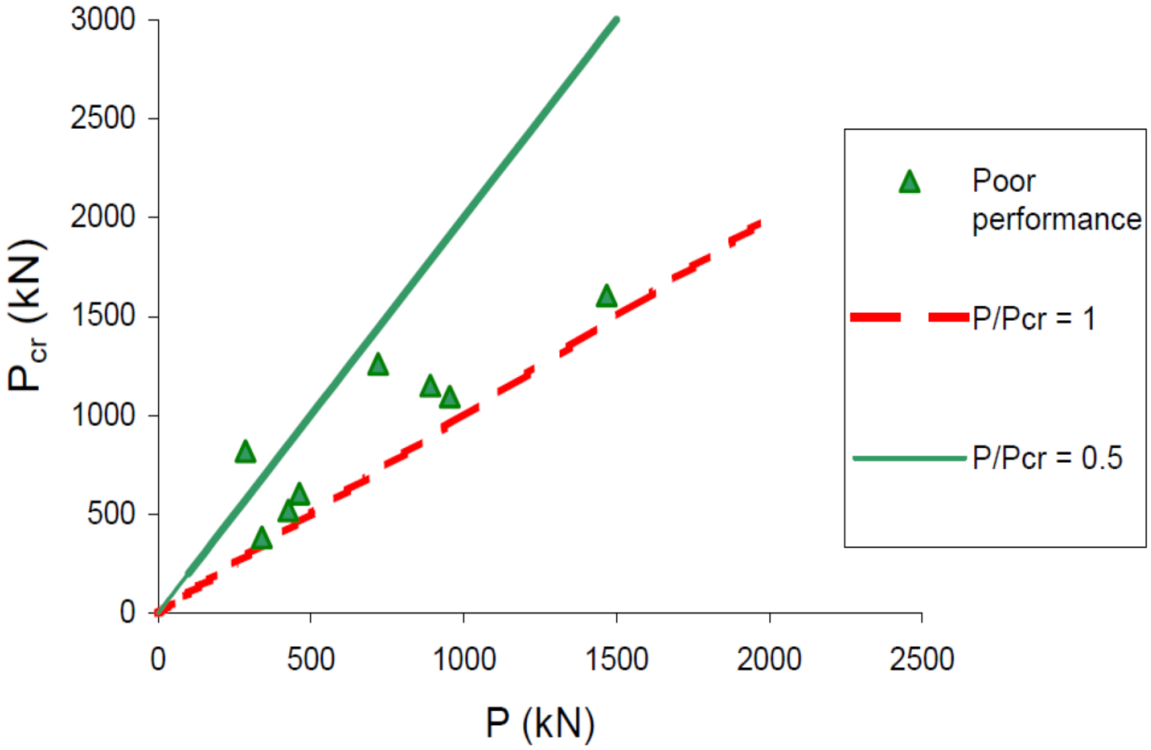

Figure 3.3. Plot of the pile foundations that performed poorly as a function of P_{cr} versus P_{des} (Bhattacharya 2003)

3.2.2 Centrifuge Testing

To verify that a P_{des}/P_{cr} ratio of 0.5 or less and a slenderness ratio of 50 or less would indicate good pile performance during an earthquake, Bhattacharya (2003) conducted a series of centrifuge tests with different control parameters and soil conditions. Figure 3.4 shows the set-up for the centrifuge test. Table 3.2 shows the properties of the model (one used in the centrifuge tests) and prototype piles. The model pile was 7 times stronger than an equivalent concrete pile and 1.5 times stronger than an equivalent steel pile in terms of plastic moment (M_p)

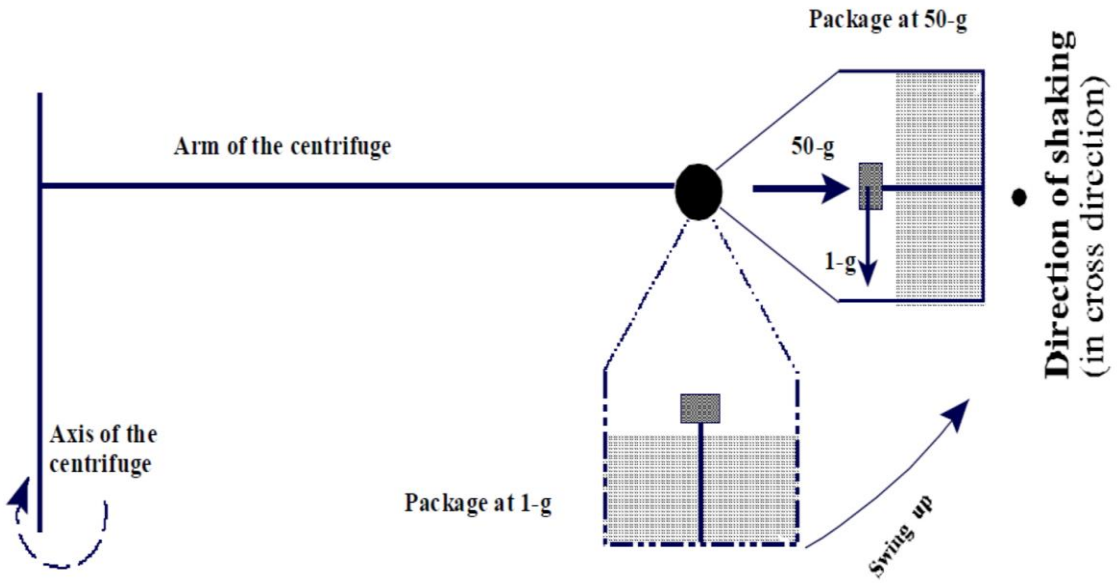

Figure 3.4. Schematic of forces acting on the model pile (Bhattacharya 2003)

Table 3.2 – Properties of the model and prototype pile (Bhattacharya 2003)

Properties	**Model**	**Prototype Section (50-g)**
Material	Aluminium Alloy (Dural)	Aluminium Alloy (Dural)
E (Young's Modulus)	70 GPa	70 GPa
Outside Diameter	9.3 mm	465 mm
Inside Diameter	8.5 mm	425 mm
r_{min} of the section	3.1 mm	155 mm
Yield Stress	250 MPa	250 MPa
Plastic Moment Capacity (M_p)	8175 Nmm	$8175 \times 50^3 = 1021.8$kNm
EI of the Section	7.77×10^6 Nmm^2	$7.77 \times 10^6 \times 50^4 = 48.6 \times 10^3$ kNm^2

The centrifuge test results verified the hypothesis Bhattacharya (2003) proposed for pile performance criteria based on the P_{des}/P_{cr} ratio, which was based on the case histories presented in section 3.2.1. Figure 3.5 presents the results of the centrifuge testing. Table 3.3 also shows the results of each pile performance during the tests. Test SB-05 was not included because the results were identical to test SB-04. It was not conclusive that the slenderness ratio has a direct effect on the pile performance. This is clear when comparing Pile 3 to Piles 4, 5, and 6, as the slenderness ratio of Pile 3 is less than that of Piles 4, 5, and 6, but still failed during the centrifuge test. However, Pile 9 had a slenderness ratio less than 50 (29) and did not fail. Note that P_{cr} also takes into account the axial load applied to the column and L_{eff}, whereas the slenderness ratio is based solely on geometry of the column. However, the slenderness ratio could still be used as a guide to determine shaft, column, or pile section.

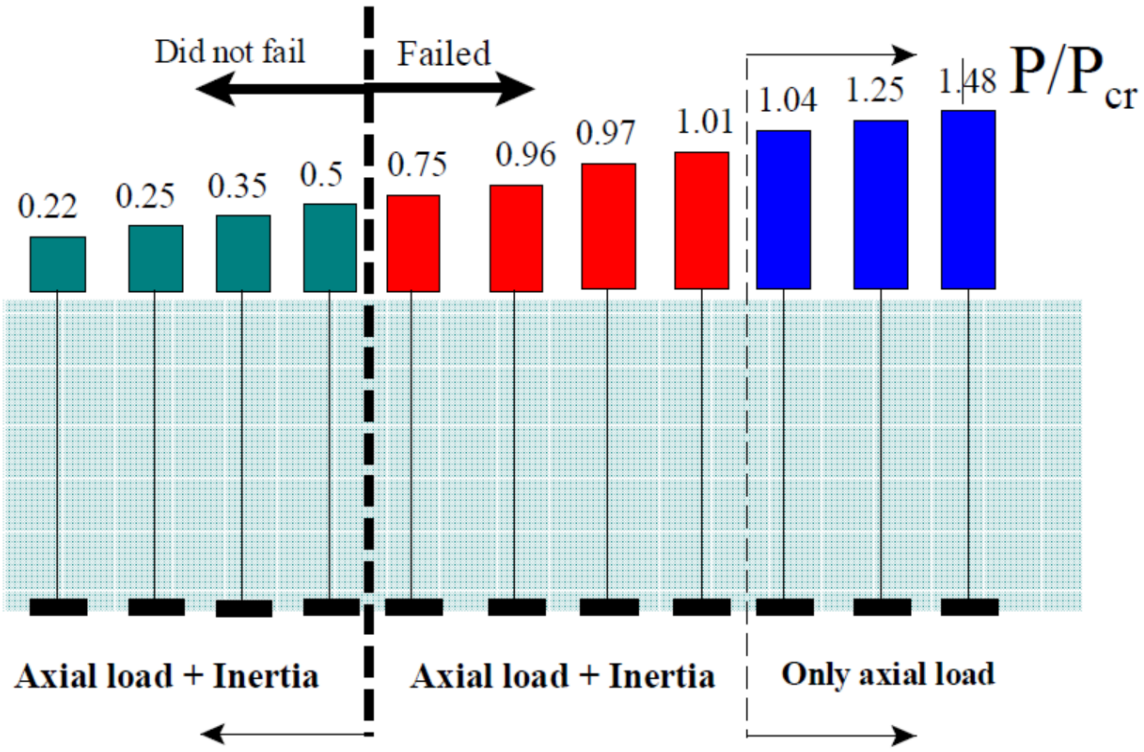

Figure 3.5. Schematic representation of the centrifuge test results (Bhattacharya 2003)

Table 3.3 – Performance of the piles during the centrifuge tests (Bhattacharya 2003)

Test ID	Pile ID	Head Mass (kg)	Max Load P (N)	P/A (MPa)	Leff (Leff/rmin)	P/Pcr	Remarks
SB-02 Pile length = 160mm r_{min} =3.1mm A=9.7 mm^2	1	1.96	768	79	L_{eff} = 355mm (114)	0.97	Failed at 40-g during swing up
	2	1.56	642	65	L_{eff} = 350mm (113)	1.01	Failed at 42-g during swing up
	3	1.26	617	63	L_{eff} = 345mm (111)	0.97	Failed during earthquake
SB-03 Pile length = 180mm r_{min} =3.1mm A = 11.2 mm^2	4	0.60	294	26.3	L_{eff} = 372mm (120)	0.50	Did not collapse
	5	0.45	220	19.7	L_{eff} = 370mm (119)	0.35	Did not collapse
	6	0.23	113	10.1	L_{eff} = 370mm (119)	0.22	Did not collapse
SB-04 Pile length = 180mm r_{min} = 3.1mm A = 11.2 mm^2	7	1.25	610	54.5	L_{eff} = 420mm (135)	1.04	Failed during earthquake
	8	1.78	872	78	L_{eff} = 445mm (144)	1.48	Failed during earthquake
	9	4.68	2249	201	L_{eff} = 90mm (29)	0.25	Did not collapse
SB-06 Pile length = 180mm r_{min} = 3.1mm A = 11.2 mm_2	10	1.50	735	65.6	L_{eff} = 445mm (144)	1.25	Failed during earthquake
	11	0.55	269	24	L_{eff} = 370mm (119)	0.46	Did not collapse
	12	0.90	441	39.4	L_{eff} = 378mm (122)	0.75	Failed during earthquake

3.3 Pile Performance under the combined Effect of Earthquake and Scour

The combined effect of flood-induced scour and earthquake hazards is a complex problem. There are three components of scour that should be considered: (a) long-term aggradation and degradation, (b) contraction scour, and (c) local scour (Ghosn et al. 2003). Aggradation and degradation is long-term elevation change due to deposition or erosion of the streambed of the waterway. Contraction scour is often due to the bridge embankments constricting the main channel (causes water to accelerate). Local scour occurs when the water around the bridge piers accelerates in concurrence with rising water levels (Ghosn et al. 2003).

Because of the uncertainty of when an earthquake will occur, it is possible that the soil could scour around a bridge before or even during an earthquake. One of the major questions is how much scour to account for during the design process. If the insitu soil is susceptible to scour, the lateral stiffness of the foundation can be significantly reduced by the lack of soil resistance. However, scour can possibly reduce the applied inertial forces, which could also reduce the demand for lateral capacity (Ghosn et al. 2003). This means that scour has the potential to be both harmful and beneficial to bridge response during an earthquake; therefore, it is important to check different scenarios.

In Ghosn et al. (2003), the authors suggest using a scour factor of 0.25 (25% of the maximum anticipated scour depth be used in design) when combining scour and earthquake events. This was based on the fact that the inertial forces are partially offset by the reduction in soil resistance capacity due to scour. They presented the following load combination:

$$\text{Extreme Event VI:} \quad 1.25\,DC + 1.00\,EQ; \\ 0.25\,SC$$

where:

DC = Dead Load
EQ = Earthquake Load
SC = Design Scour Depth

The second recommendation they provide is to design the foundations so that they are twice the length of the scour depth. This recommendation attempts to ensure that the resistance capacity needed to resist an earthquake event will not be reduced below the demand. However, some instances may necessitate longer foundation lengths, and this recommendation should be a minimum controlling factor when considering scour in design. It should be noted that the design scour depth used in the Ghosn et al. (2003) is based on Richardson and Davis (1995).

Chapter 4

MODEL GENERATION

Five bridge piers[2] were modeled in FB-MultiPier to evaluate the response to seismic loading. Each pier was modeled using a bridge design provided by ALDOT. All of these bridges have been built and are in use in the state of Alabama. Each bridge is located in a different county; therefore, each bridge will be referred to by the county name. Figure 4.1 shows the locations of the bridges throughout the state. For each bridge, the middle bridge pier was used for the response analysis. A representative soil profile was developed using the lower bound of the boring log data (SPT N-values). In some instances, multiple boring logs were taken at the same bent location, but to the right and left of the centerline of the bridge. In this case, both boring logs were used to develop the profile by taking the lower bound of each layer (if layer matching between boring logs was relatively good). Before the bridge piers were modeled in FB-MultiPier, the soil profiles were developed. Soil layer type and elevation, water table elevation, and soil properties were all recorded in a spreadsheet, along with the type of lateral, axial, torsional, and tip models used in FB-MultiPier.

It was determined that the abutments cannot be used to resist longitudinal displacements because the gap between the girders and the abutment walls are 4 inches or greater for each bridge. This gap prevents the use of the passive earth pressure behind the abutment wall from mobilizing in a seismic event, which would provide longitudinal

[2] Pier and bent have the same meaning in this document and are used interchangeably throughout.

resistance. If integral abutments are used, the passive pressure could be relied on to resist longitudinal displacements.

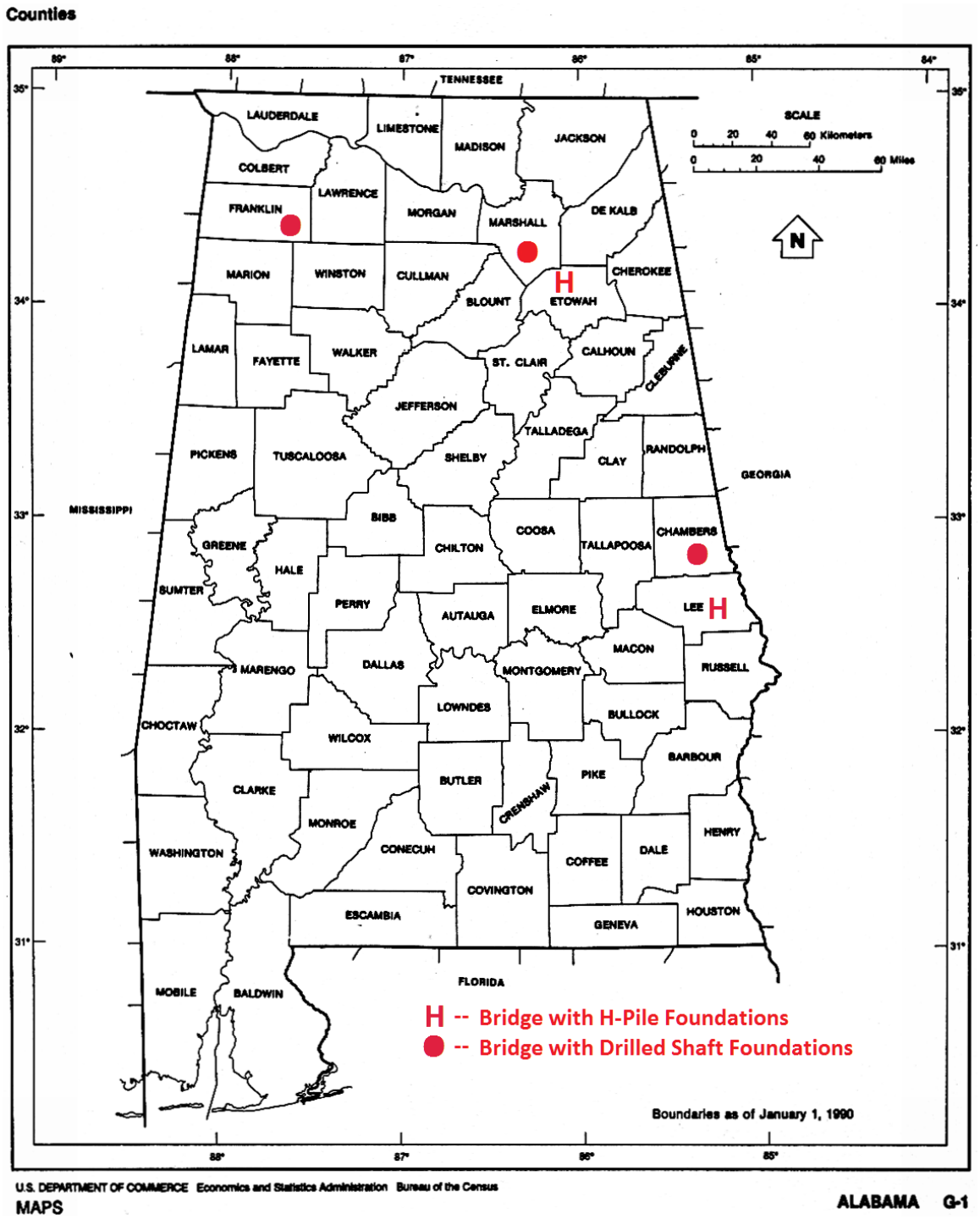

Figure 4.1. Map of Alabama Counties with bridge locations (modified after Yellow Maps 2010)

4.1 Time-History Events

Ten time-history events were used in the analysis and can be found in Appendix A. These original time-history events are records of free-field ground acceleration versus time of an actual earthquake event. The original time-history events were modified using scale factors to represent an earthquake that would be typical in Alabama. There were two different scale factors used for each time-history, North and North Maximum Considered Earthquake (NMCE). For further detail regarding the modification factors and development of the time history events used, see Panzer (2013). Each one was applied longitudinally and transversely separately for each bridge case. Figure 4.2 shows the scaled Coalinga North time-history event used in dynamic analysis. See Appendix A for all of the scaled time-history events. All time-history events included 20-30 seconds of time when acceleration is equal to zero after the strong shaking. This is to show the bridge response after the event. Table 4.1 shows the time steps used for every time-history for each model. The Lee County time step had to be increased due to the file size limitations for the output files.

Table 4.1 – Time steps used for each time-history for each model

	Time Step used (sec)				
	Chambers	**Etowah**	**Franklin**	**Lee**	**Marshall**
Coalinga North	0.01	0.01	0.01	0.03	0.01
Imperial Valley NMCE and North	0.01	0.01	0.01	0.03	0.01
Kobe NMCE and North	0.01	0.01	0.01	0.03	0.01
Kocaeli NMCE and North	0.01	0.01	0.01	0.04	0.01
Kocaeli2 NMCE and North	0.01	0.01	0.01	0.02	0.01
Landers NMCE and North	0.02	0.02	0.02	0.04	0.02
LSM North	0.01	0.01	0.01	0.04	0.01
NPS North	0.01	0.01	0.01	0.02	0.01
SanFernando NMCE and North	0.01	0.01	0.01	0.03	0.01
SanFernando2 NMCE and North	0.01	0.01	0.01	0.03	0.01

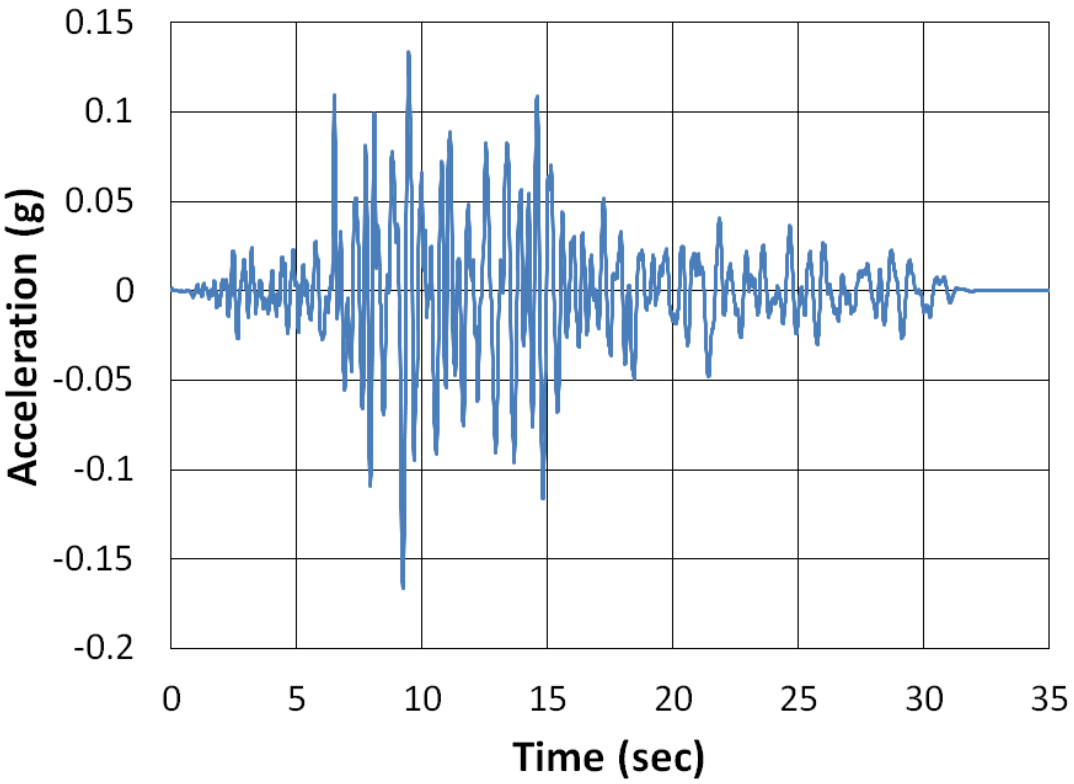

Figure 4.2. Scaled Coalinga North earthquake time-history event

4.2 Dynamic Analysis Options Used within FB-MultiPier

4.2.1 Dynamic Analysis Method Used

Time-history analysis was used to evaluate the dynamic structural response of the bridge piers modeled. There are three time stepping options available: average acceleration (Newmark), linear acceleration (Newmark), and Wilson-θ. The average acceleration option was used because it is typically more stable from a computational standpoint, and is one of the most effective and popular implicit techniques used for structural dynamic problems (Hughes and Belytschko 1983).

4.2.2 Damping Analysis

For each model, Eigenvector analysis was conducted using FB-MultiPier's modal analysis option to determine the natural period and the circular frequency of the pier.

Then, a classic sine wave time-history curve was developed for each model and run using the Rayleigh damping factor values for the pier previously shown in Table 2.17. Mass and stiffness damping factors for the piles and soil were ignored in this analysis for simplicity (and consistency) and due to lack of information regarding cyclic response of the soil for each case history. This approach was accepted as reasonable because it is conservative to ignore the damping effects of the soil and piles. However, it was noticed that if zero is entered into any one of the six input boxes of the mass and stiffness damping factors, Rayleigh damping would not be considered at all within the program analysis. Therefore, a low mass and stiffness factor of 0.000001 was applied to both the piles and soil.

The displacement at the top of the pier versus time was plotted and the damping was calculated using the peak displacements that occurred once the amplitude of the sine wave time-history curve was zero. The sine wave curves were plotted so that the bridge would go through three cycles (time [in seconds] of three times the structural period) of the sine wave, then a circular frequency of zero was introduced for roughly 10 seconds. The equations used to develop the sine wave time-history curve and damping factors are shown as equations 4.1 and 4.2.

$$a_{sin} = \sin \omega t \tag{4.1}$$

$$\zeta = \frac{1}{2\pi j} \ln \frac{u_i}{u_{i+j}} \tag{4.2}$$

where:

a_{sin}	=	calculated acceleration used in the time-history function
ω	=	circular frequency
t	=	time in seconds
ζ	=	calculated damping ratio
j	=	number of peak after the first initial peak when acceleration is equal to zero
u_i	=	displacement recorded at the first initial peak when acceleration is equal to zero
u_{i+j}	=	displacement recorded at the j^{th} peak when acceleration is equal to zero

The calculated damping ratios for four of the six bridge piers were all within 1-4%; therefore, for simplicity, the initial damping factors were used for the dynamic analysis. The Marshall county bridge was not included because the damping ratios were extremely high. This is believed to be because of the large strut that is used to connect the columns of the bent. Figure 4.3 and 4.4 show Chambers County 100% scour sine wave and displacement versus time at the top of the pier respectively in the longitudinal direction. Figure 4.5 and 4.6 show the Marshall County sine wave and displacement versus time at the top of the pier respectively in the longitudinal direction to show contrast between the two. Refer to Appendix B for the results of each bridge for damping analysis. Table 4.2 shows the average calculated damping factors for both the longitudinal and transverse directions respectively for each bridge.

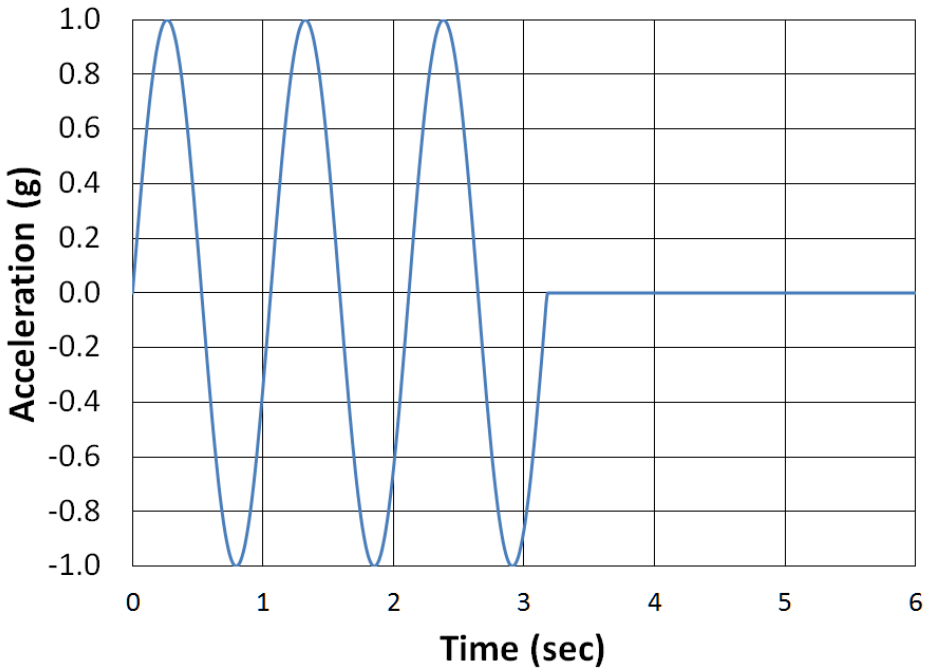

Figure 4.3. Chambers County 100% scour longitudinal sine wave time-history

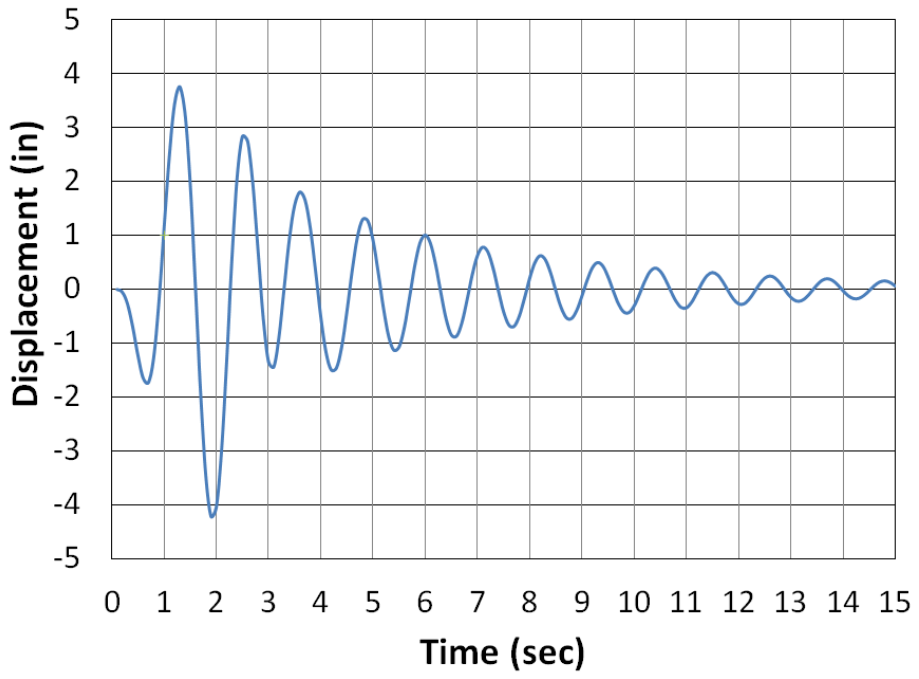

Figure 4.4. Chambers County 100% scour longitudinal displacement versus time at the top of the pier

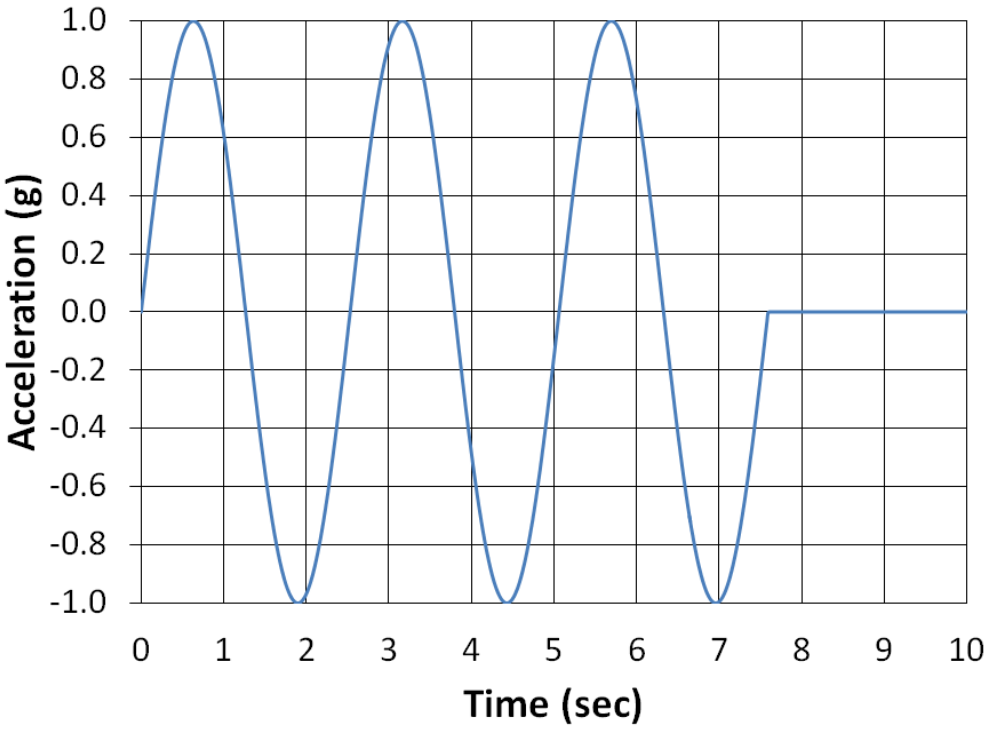

Figure 4.5. Marshall County longitudinal sine wave time-history

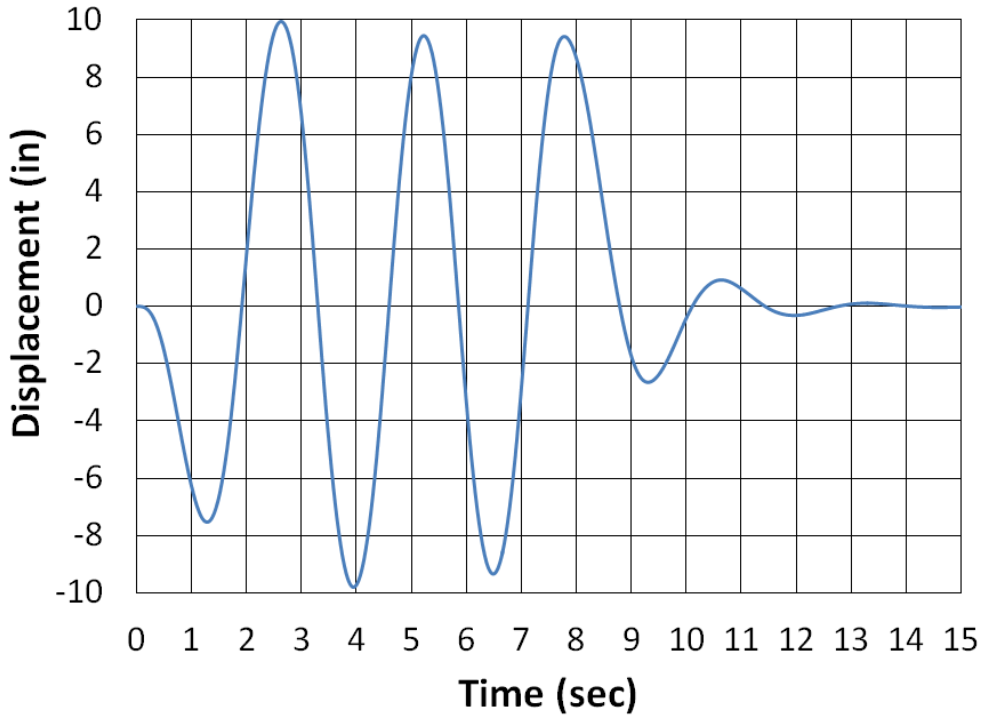

Figure 4.6. Marshall County longitudinal displacement versus time at the top of the pier

Table 4.2 – Frequency, structural period, and calculated average damping ratios for each bridge

	Longitudinal			Transverse		
Bridge	**Frequency (rad/sec)**	**Period (sec)**	**Percent Damping**	**Frequency (rad/sec)**	**Period (sec)**	**Percent Damping**
Chambers 25%	6.454	0.974	0.25%	11.455	0.549	0.2%
Chambers 100%	5.935	1.059	3.96%	10.724	0.586	3.18%
Etowah	4.307	1.459	2.14%	7.551	0.832	1.70%
Franklin	7.566	0.83	2.1%	12.725	0.494	1.2%
Lee	5.492	1.144	1.92%	8.958	0.701	2.82%
Marshall	2.483	2.531	N/A	0.707	0.889	N/A

4.3 Dead Load and Discrete Mass

Dead loads and discrete masses were applied to each direct analysis model. This was done to account for the weight of the bridge deck and girders. Factored live load was not taken into account for this analysis. Dead loads were calculated based on typical cross sections given and the standard unit weight of normalweight, reinforced concrete (150 pcf). The discrete masses were calculated using the dead weight divided by the acceleration of gravity (386.2 in/sec^2). The dead load was applied in the z (vertical) direction and the discrete masses were applied in the x and y (horizontal) direction because vertical acceleration was not used for the case studies. The dead weight was applied to each bearing pad location, whereas the discrete masses were applied in between the bearing pad locations. The bearing pad locations were taken from the center line of each girder in the typical cross section provided in the subsequent sections for each case study. Therefore, the dead load used to calculate each discrete mass was the combination of the loads on each bearing pad. The reason for applying dead loads at each bearing pad is because in some cases, the spans supported by the bent were different

lengths and therefore the dead load applied to the pads would be different on each side of the bent. Table 4.3 presents the dead loads and discrete masses used for each case study.

Table 4.3 – Dead loads and discrete masses used for each case study

Bearing Pad Location	Left Bearing Pad (kips)	Discrete Mass (kip-sec^2/in)	Right Bearing Pad (kips)
Chambers County			
Exterior	65	0.34	65
Interior (for all)	60	0.31	60
Exterior	65	0.34	65
Etowah County			
Exterior	130	0.67	116
Interior (for all)	105	0.54	82
Exterior	130	0.67	116
Franklin County			
Exterior	125	0.65	125
Interior (for all)	100	0.52	100
Exterior	125	0.65	125
Lee County			
Exterior	120	0.62	120
Interior (for all)	100	0.52	100
Exterior	120	0.62	120
Marshall County			
Exterior	120	0.62	120
Interior (for all)	110	0.57	110
Exterior	120	0.62	120

4.4 Chambers County

4.4.1 Background Information

The Chambers County Bridge is a bridge replacement project over Oseligee Creek. The total bridge span is 240 ft and rests on two abutments and two central piers. It is not skewed and has a total roadway width of 32 ft and 9 in. See Figure 4.7 and 4.8 for the plan and elevation views and the bridge deck cross section. The foundations used for both the abutments and piers are drilled shafts. Because the abutments were not modeled, they are not discussed. Bent 3 was modeled in FB-MultiPier. Bent 2 and 3 are built the same but with slightly different tip elevations. Both have similar soil conditions.

Bent 3 consists of a pier cap and two shafts. The shafts are 3.5 ft in diameter with twelve No. 11 longitudinal reinforcing bars. Figure 4.9, 4.10, and 4.11 show Bent 3 elevation view, the shaft cross-section, and the pier cap cross section respectively.

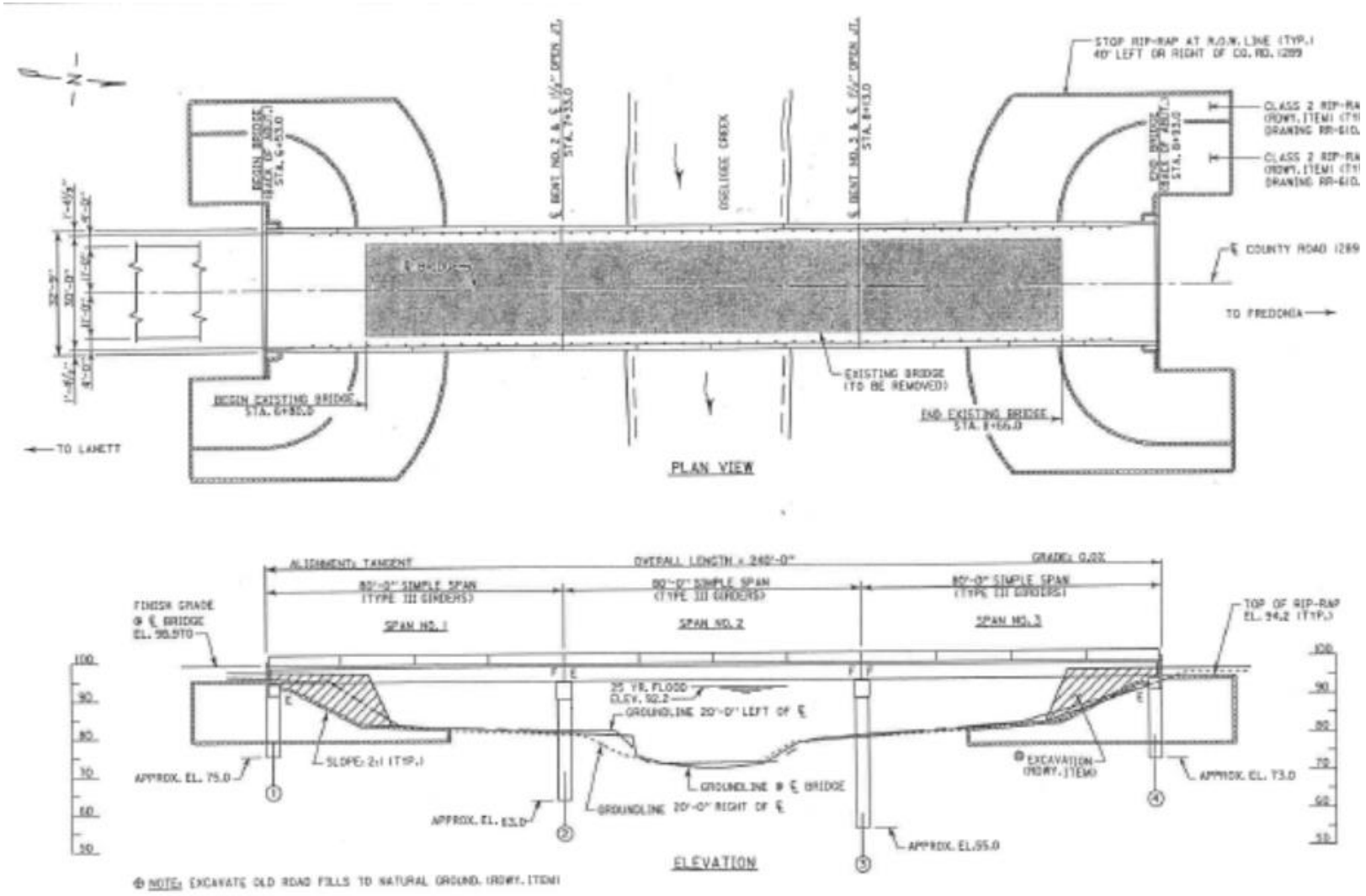

Figure 4.7. Chambers County bridge plan and elevation view (ALDOT 2008)

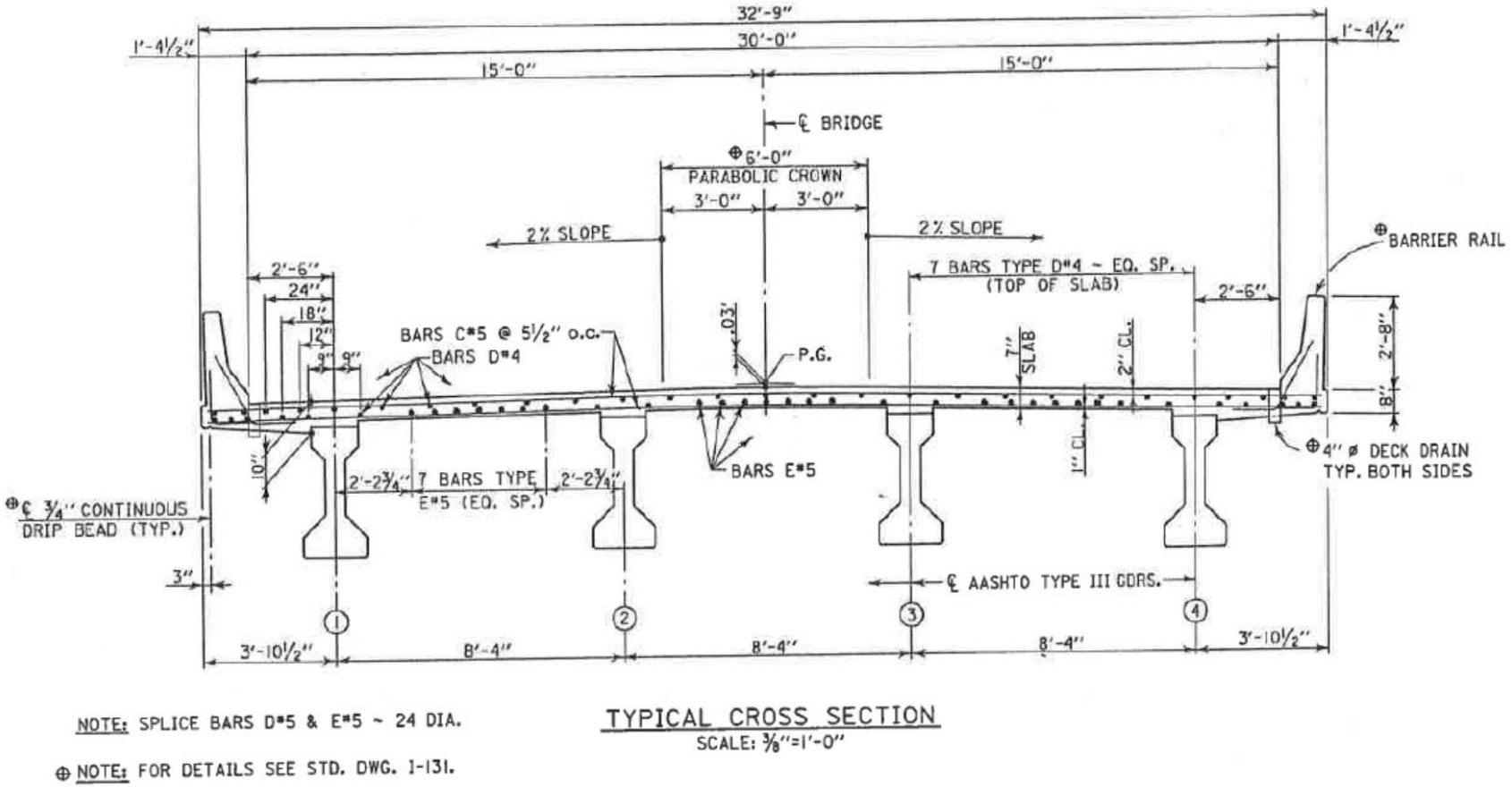

NOTE: SPLICE BARS D*5 & E*5 ~ 24 DIA.

⊕ NOTE: FOR DETAILS SEE STD. DWG. 1-131.

TYPICAL CROSS SECTION

SCALE: ⅜"=1'-0"

Figure 4.8. Chambers County typical bridge deck cross section (ALDOT 2008)

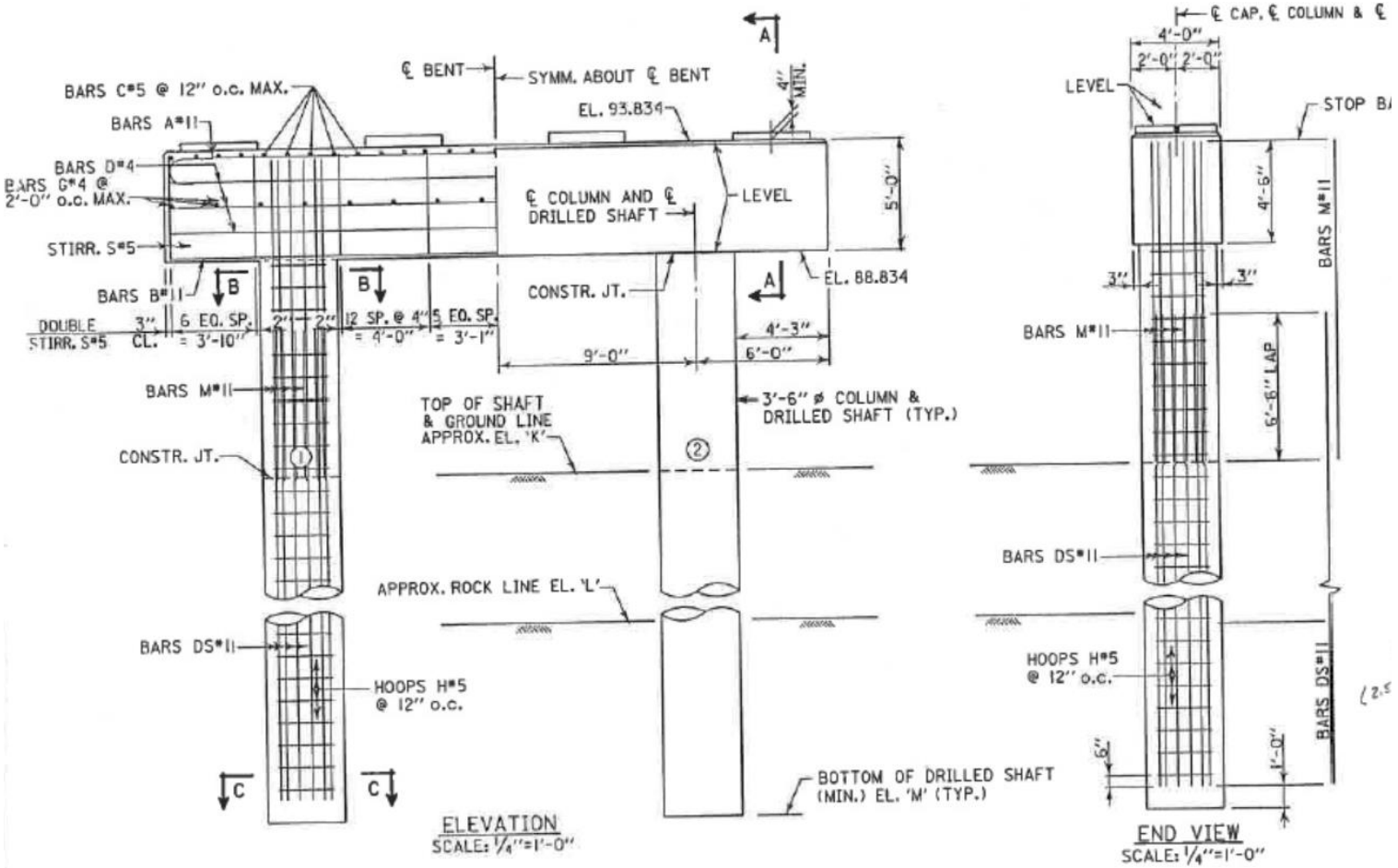

ELEVATION TABLE			
LOCATION	'K'	'L'	'M'
BENT#2	81.2	70.9	63.0
BENT#3	79.2	63.0	55.0

Figure 4.9. Chambers County Bent 3 elevation and end view (ALDOT 2008)

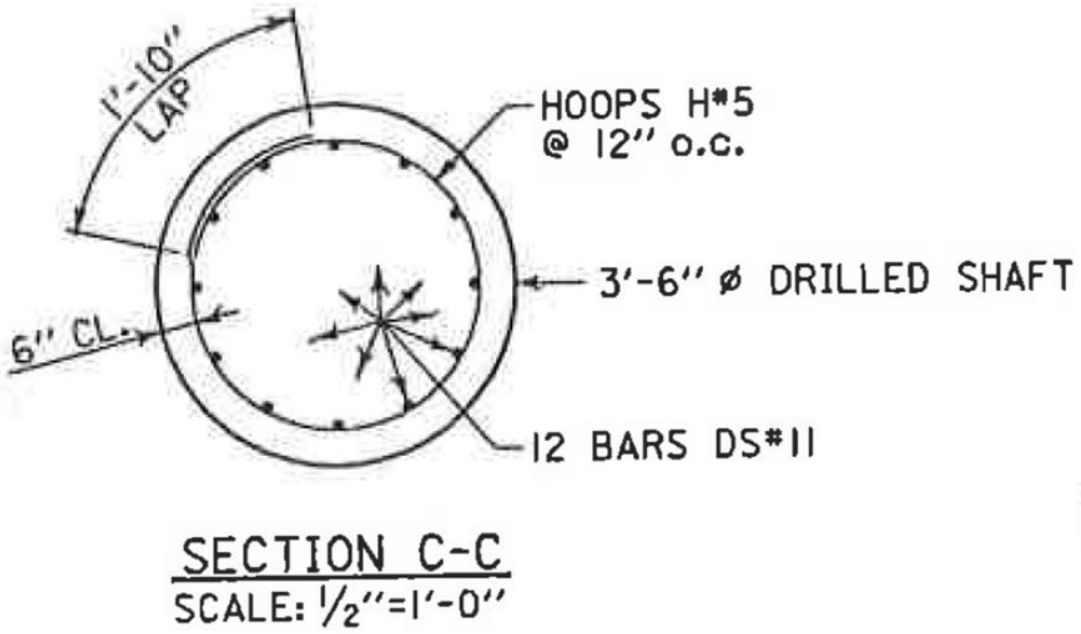

Figure 4.10. Chambers County cross section of drilled shaft (ALDOT 2008)

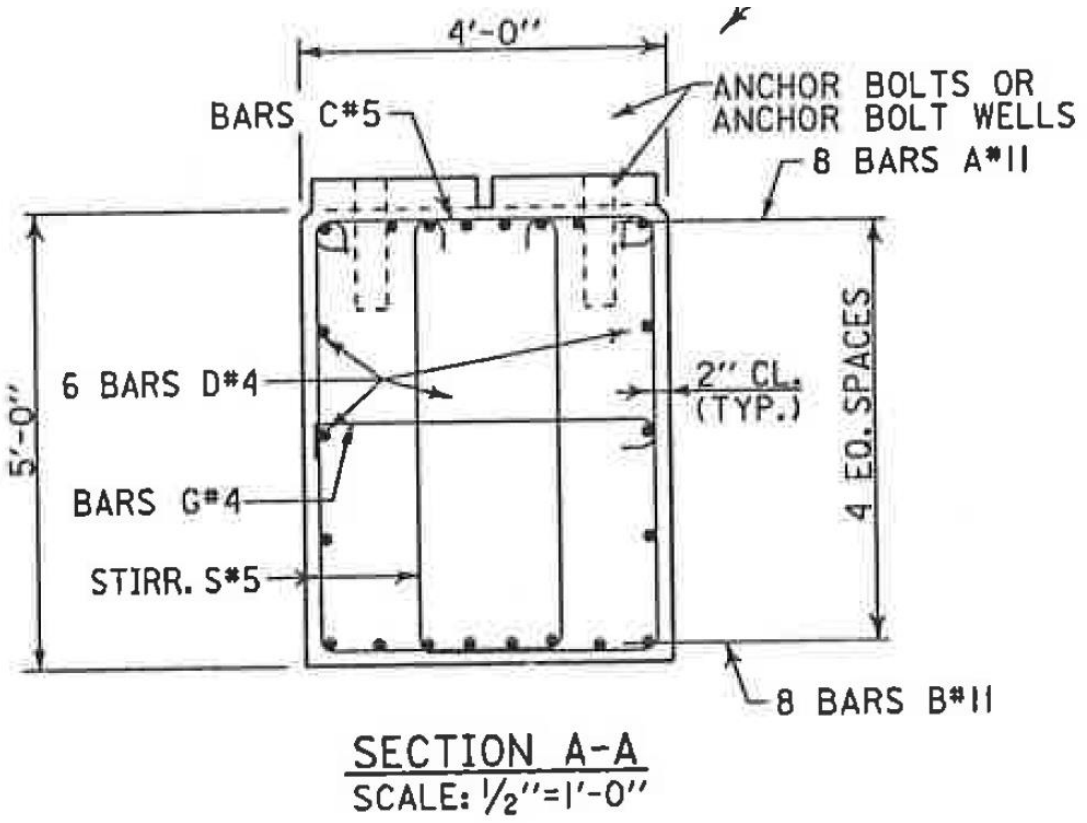

Figure 4.11. Chambers County Bent 3 pier cap cross section (ALDOT 2008)

4.4.2 Soil Modeling

A formal site investigation, using the standard penetration test (SPT) and rock coring, was conducted by the Bureau of Materials and Tests within ALDOT. According to the geotechnical report, the site is located in the Southern Piedmont Upland district and underlain by Ropes Creek Amphibolite and the Agricola Schist of Precambrian to Paleozoic age (ALDOT 2008). The ground water table (GWT) elevation at Bent 3 was found to be that of the water elevation of Osiligee Creek at 72 ft (ALDOT 2008). There is roughly 16 feet of top soil that was assumed to scour to bedrock at an elevation of 63 ft. Static analysis of the lateral capacity of the drilled shafts was done using LPile and the input parameters were included in the geotechnical report. The same input parameters were used in FB-MultiPier. However, some parameters that were needed for FB-MultiPier were not provided and had to be determined based on the boring logs. Figure 4.12 shows the idealized soil profile that was developed and used in FB-MultiPier. For the 25% scour case, the top 25% of the soil (above the bedrock) was simply removed from the existing conditions. The insitu soils were determined to be a site class E. However, if 100% scour is assumed, the site class would be C. Refer to Appendix C for the original boring logs and other relative information.

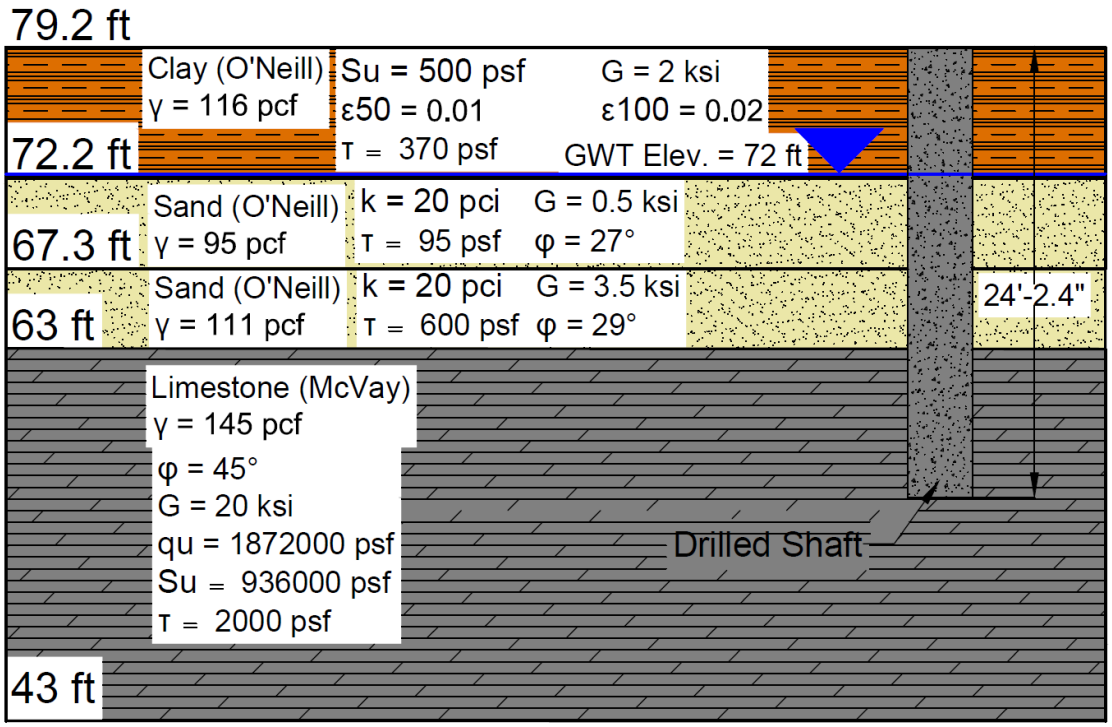

Figure 4.12. Chambers County idealized soil profile for Bent 3

4.5 Etowah County

4.5.1 Background Information

The Etowah County Bridge is a bridge replacement on I-59 south bound lanes over US-11 and Norfolk Southern Railroad. The total bridge span is 265 feet and rests on two abutments and one central pier (bent 2). It is skewed approximately 30° and has a total roadway width of 46 feet and 9 in. See Figure 4.13 and 4.14 for the plan and elevation views and the bridge deck cross section. The foundations used for both the abutments and piers are 12x53 H-piles. Because the abutments were not modeled, they are not discussed. Bent 2 was modeled in FB-MultiPier and consists of a pier cap and three columns that are each supported by pile footings. Figures 4.15, 4.16, and 4.17 show the Bent 2 elevation view, end view, and pier cap cross section. Figure 4.18 and 4.19 show the column cross section and pile footing layout respectively.

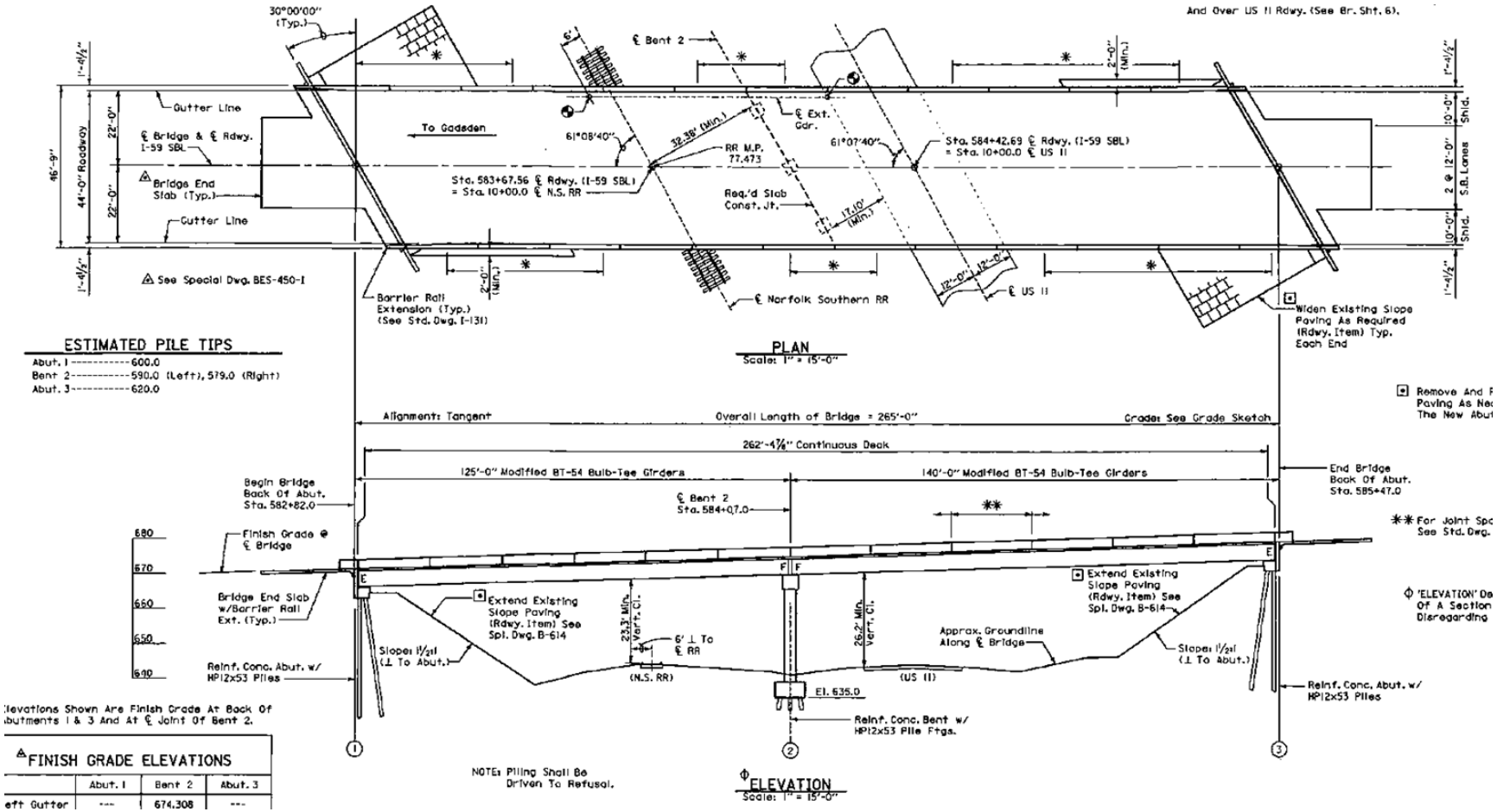

Figure 4.13. Etowah County bridge plan and elevation view (ALDOT 2011)

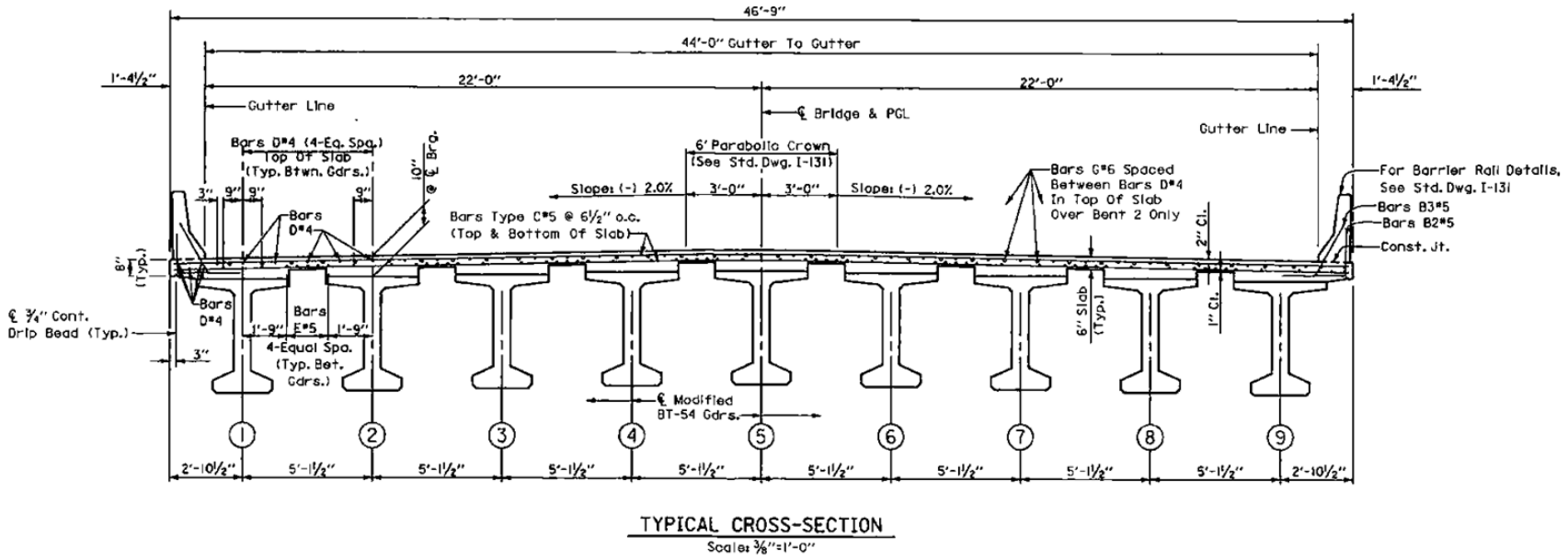

TYPICAL CROSS-SECTION
Scale: ⅜"=1'-0"

Figure 4.14. Etowah County typical bridge deck cross section (ALDOT 2011)

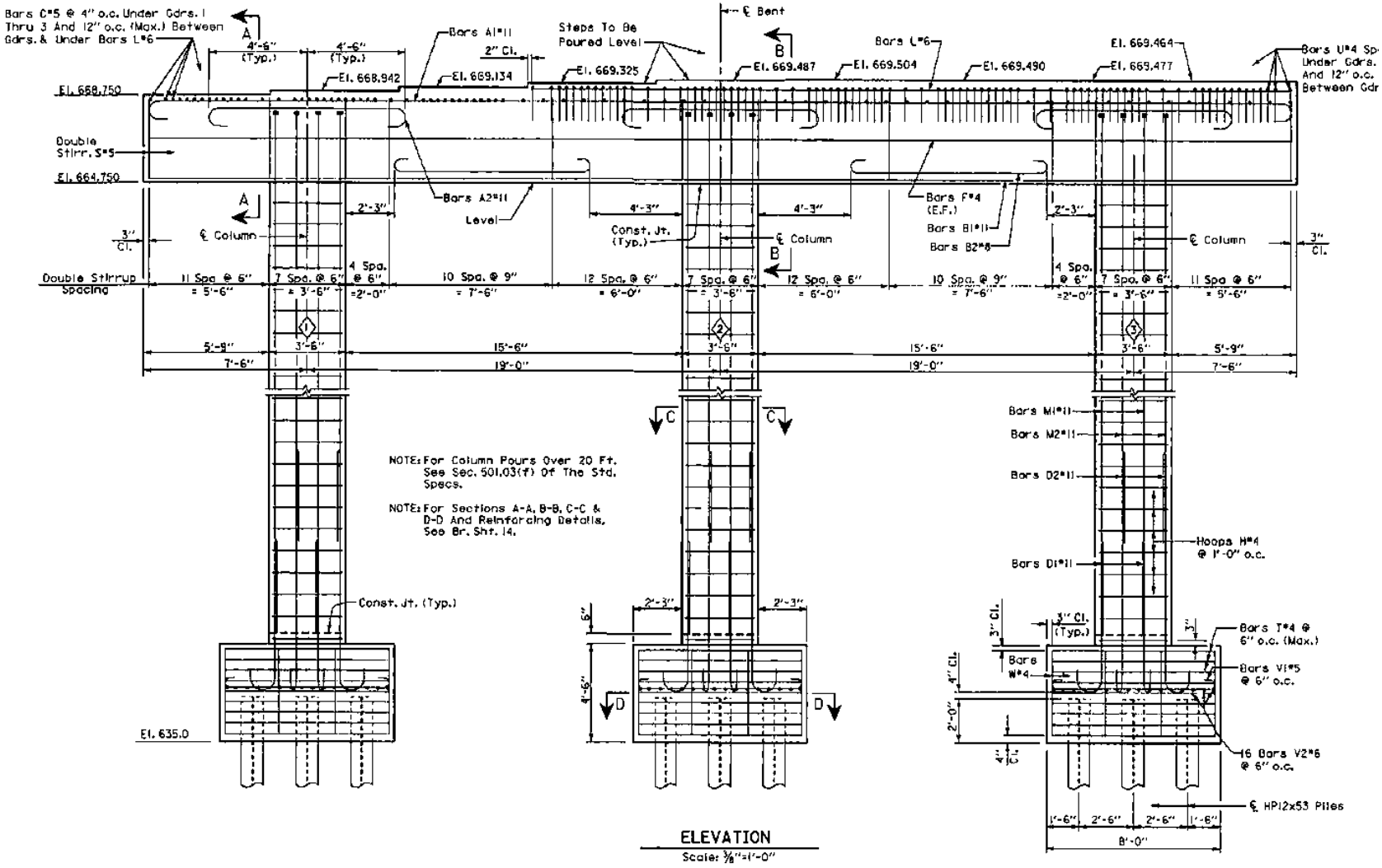

Figure 4.15. Etowah County Bent 2 elevation view (ALDOT 2011)

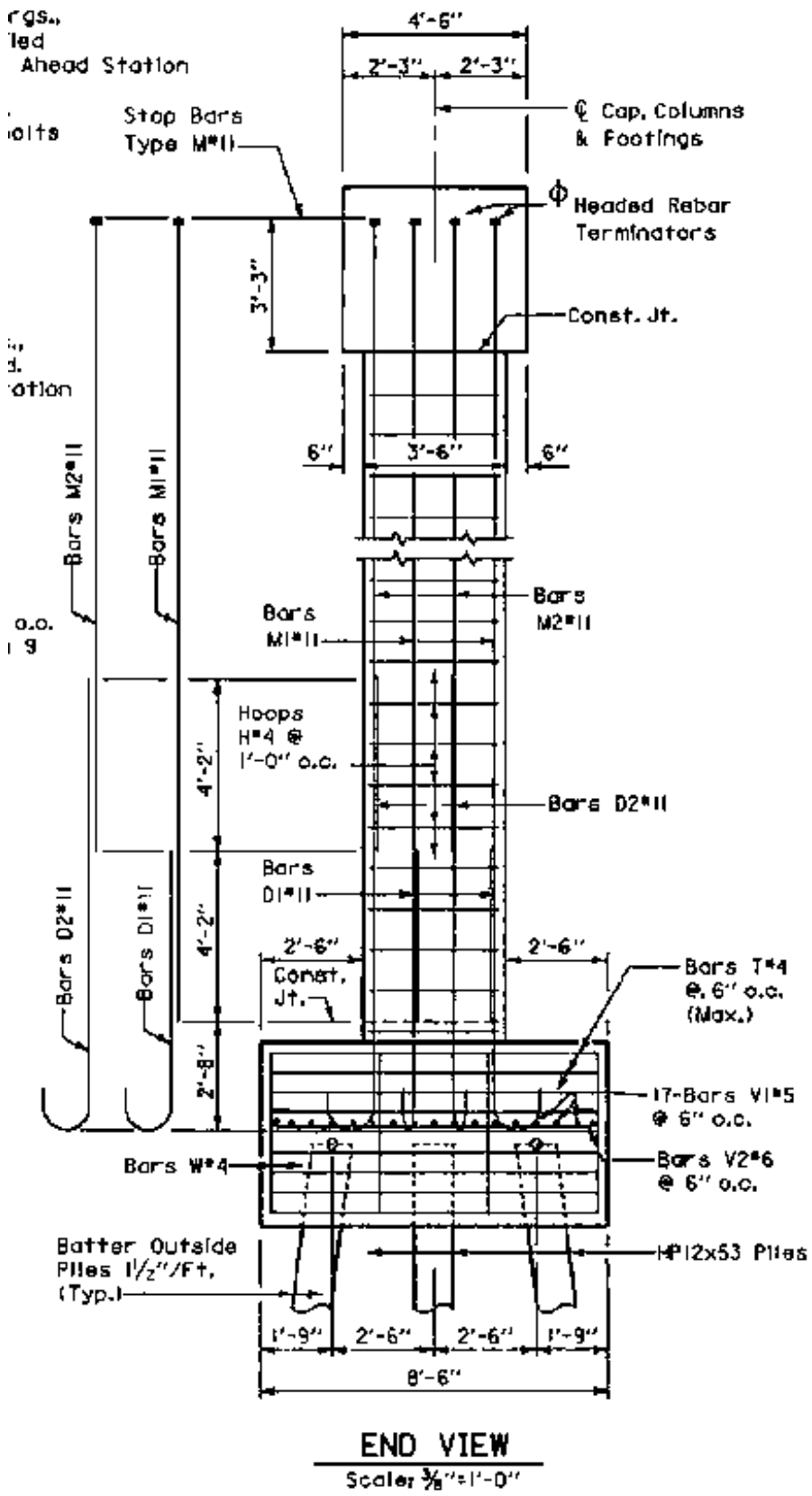

END VIEW

Scale: ⅜"=1'-0"

Figure 4.16. Etowah County Bent 2 end view (ALDOT 2011)

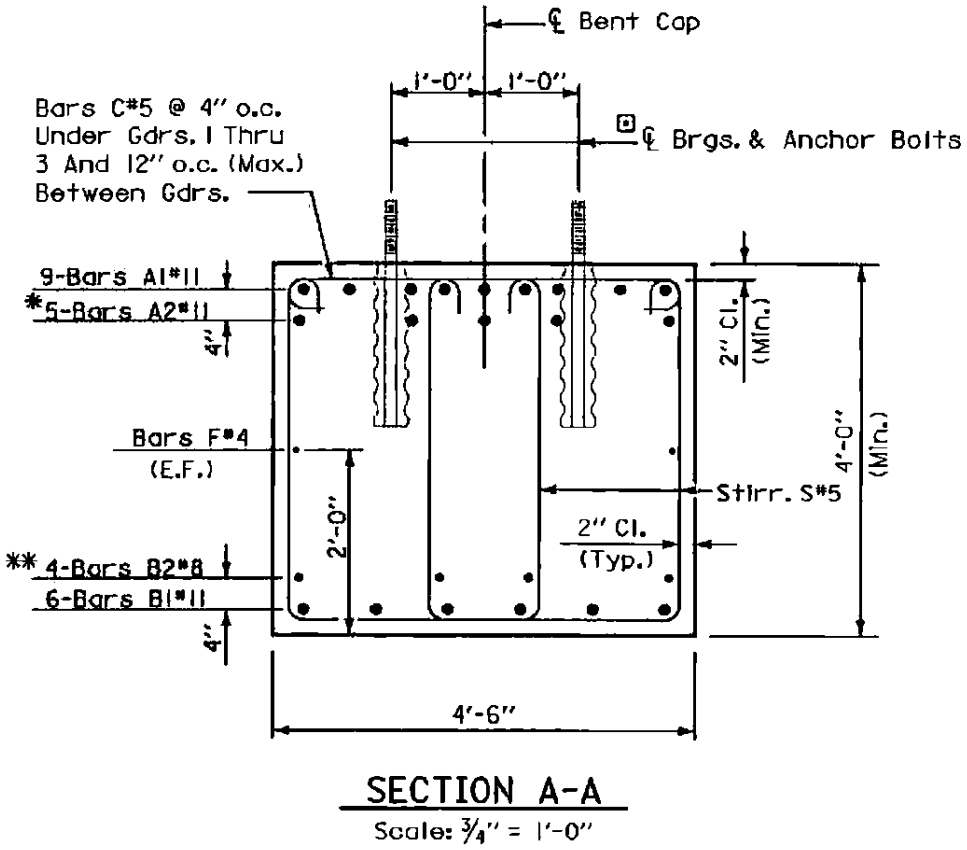

Figure 4.17. Etowah County Bent 2 pier cap cross section (ALDOT 2011)

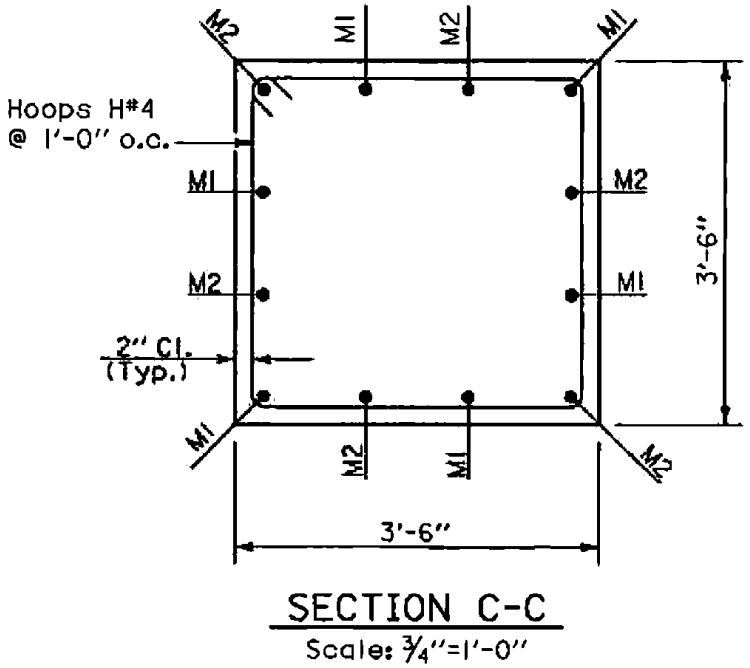

Figure 4.18. Etowah County Bent 2 column cross section (ALDOT 2011)

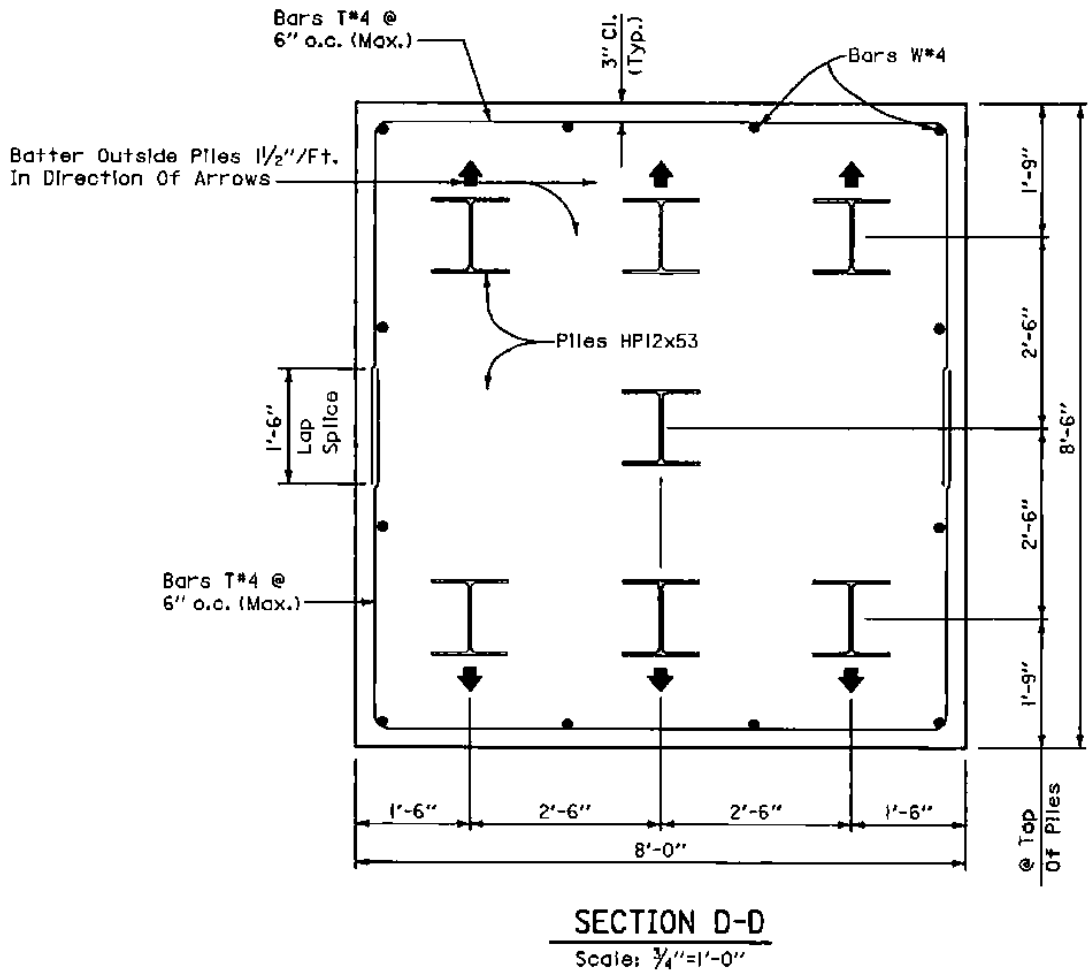

Figure 4.19. Etowah County Bent 2 typical pile footing layout (ALDOT 2011)

4.5.2 Soil Modeling

A formal site investigation, using the SPT and rock coring, was conducted by Terracon (formerly Gallet and Associates). According to the geotechnical report, the site is at or very near the contact between Bangor Limestone and Monteagle Limestone deposits. Bangor Limestone consists of medium-gray bioclastic and oolitic limestone containing interbeds of dusky red and olive green mudstone (Gallet 2008). The Monteagle Limestone deposit consists of light-gray oolitic limestone containing

interbedded argillaceous, bioclastic, or dolomitic limestone, dolomite, and medium gray shale (Gallet 2008).

The GWT elevation at Bent 2 was recorded as 620 feet during the initial site investigation (Gallet 2008). The boring logs taken near bent 2 indicated that insitu soils consist of approximately 50 feet of soft clay from the ground surface. A void was then encountered for roughly 15 feet until limestone bedrock was reached at an approximate depth of 65 feet (578.5 feet elevation). All input parameters needed for FB-MultiPier were determined based on the boring logs and rock core testing. The mobilized end bearing resistance (referred to as axial bearing failure in FB-MultiPier) was determined using FB-Deep. All relative information regarding input parameters for Etowah County used in FB-Deep are in Appendix C. Figure 4.20 shows the idealized soil profile that was developed and used in FB-MultiPier. The insitu soils were determined to be a site class E. Refer to Appendix D for the original boring logs as well.

Default p-y multipliers were used for lateral analysis in Etowah models. A pile group efficiency of 1.0 was used for the axial analysis based on recommendations made by Hannigan et al. (2006). The pile cap, in this case, was buried several feet below the ground surface.

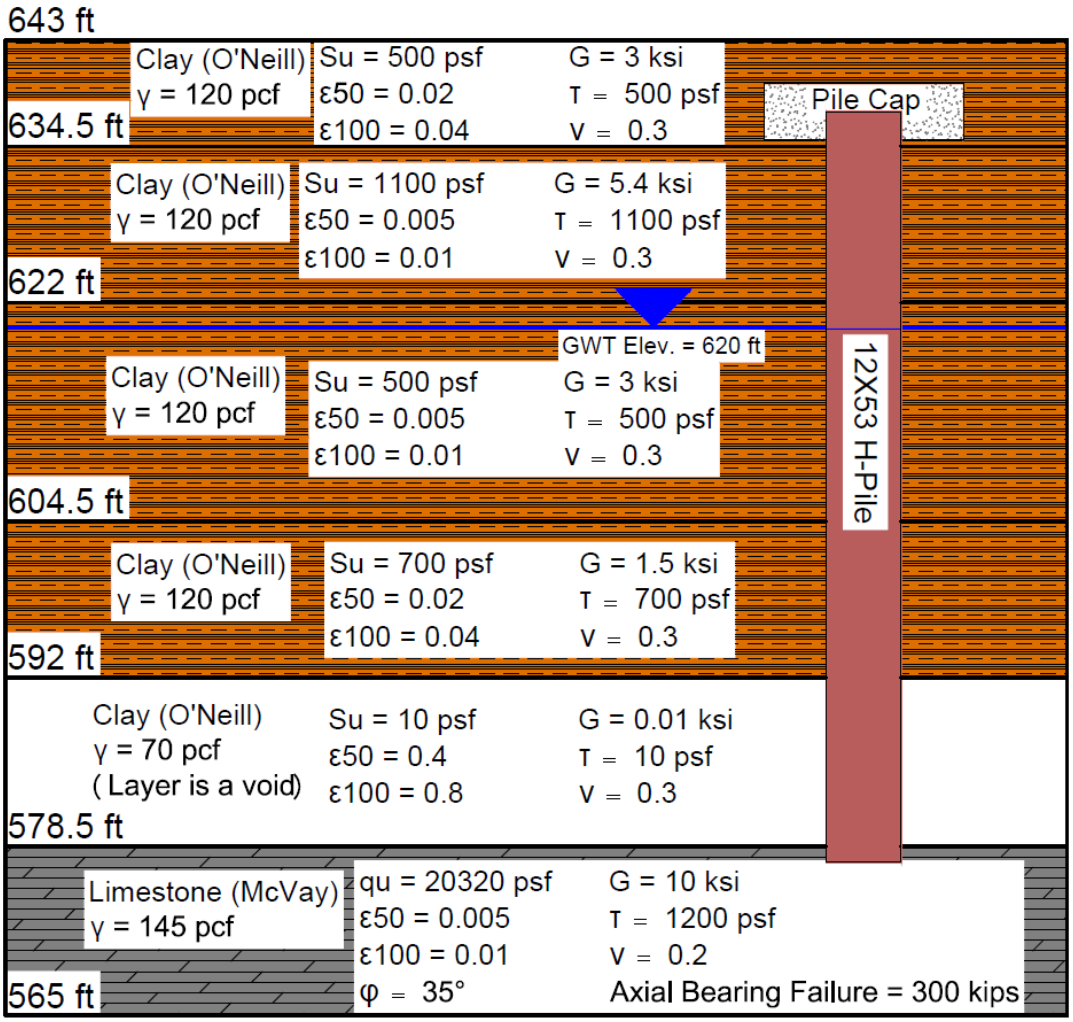

Figure 4.20. Etowah County idealized soil profile

4.6 Franklin County

4.6.1 Background Information

The Franklin County Bridge is a bridge over Little Bear Creek on the east bound lane of S.R 24 (Corridor V). The total bridge span is 300 ft and rests on two abutments and two central piers. It is not skewed and has a total roadway width of 42 ft and 9 in. See Figure 4.21 and 4.22 for the plan and elevation views and the bridge deck cross section. The foundations used for both the abutments and piers are drilled shafts. Because the abutments were not modeled, they are not discussed. Bent 3 was modeled in FB-MultiPier. Bent 2 and 3 are built the same but with slightly different tip elevations

and soil conditions. Bent 3 consists of a pier cap and two shafts. The shafts are 4.5 ft in diameter with twelve No. 11 longitudinal reinforcing bars above the ground surface, and 5 ft in diameter with the same reinforcement alignment below the ground surface. Figure 4.23 and 4.24 shows the Bent 3 elevation view and pier cap cross section. The pier cap was modeled as flat on top due to program capabilities. Figure 4.25 and 4.26 show the shaft cross section.

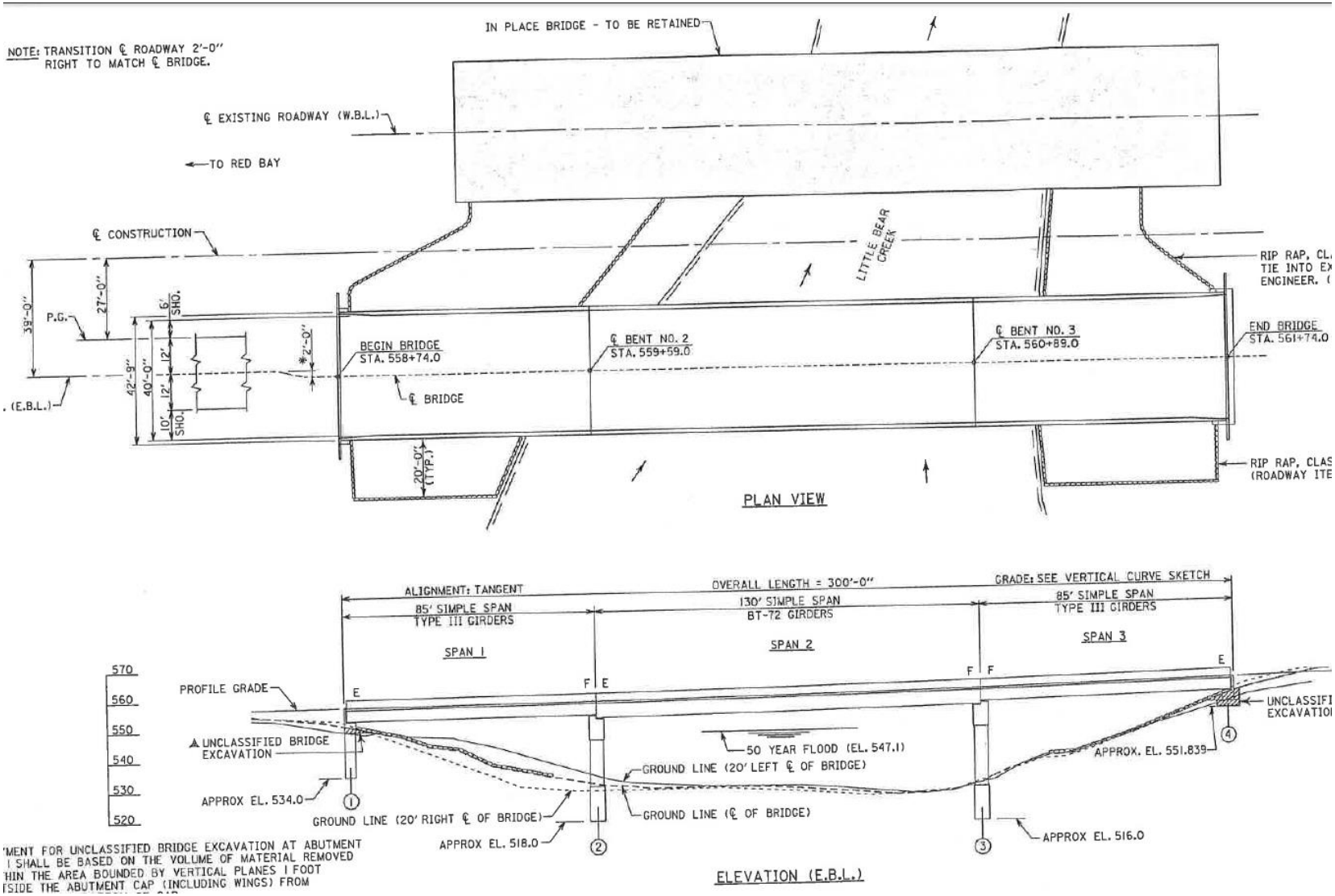

Figure 4.21. Franklin County bridge plan and elevation views (ALDOT 2005)

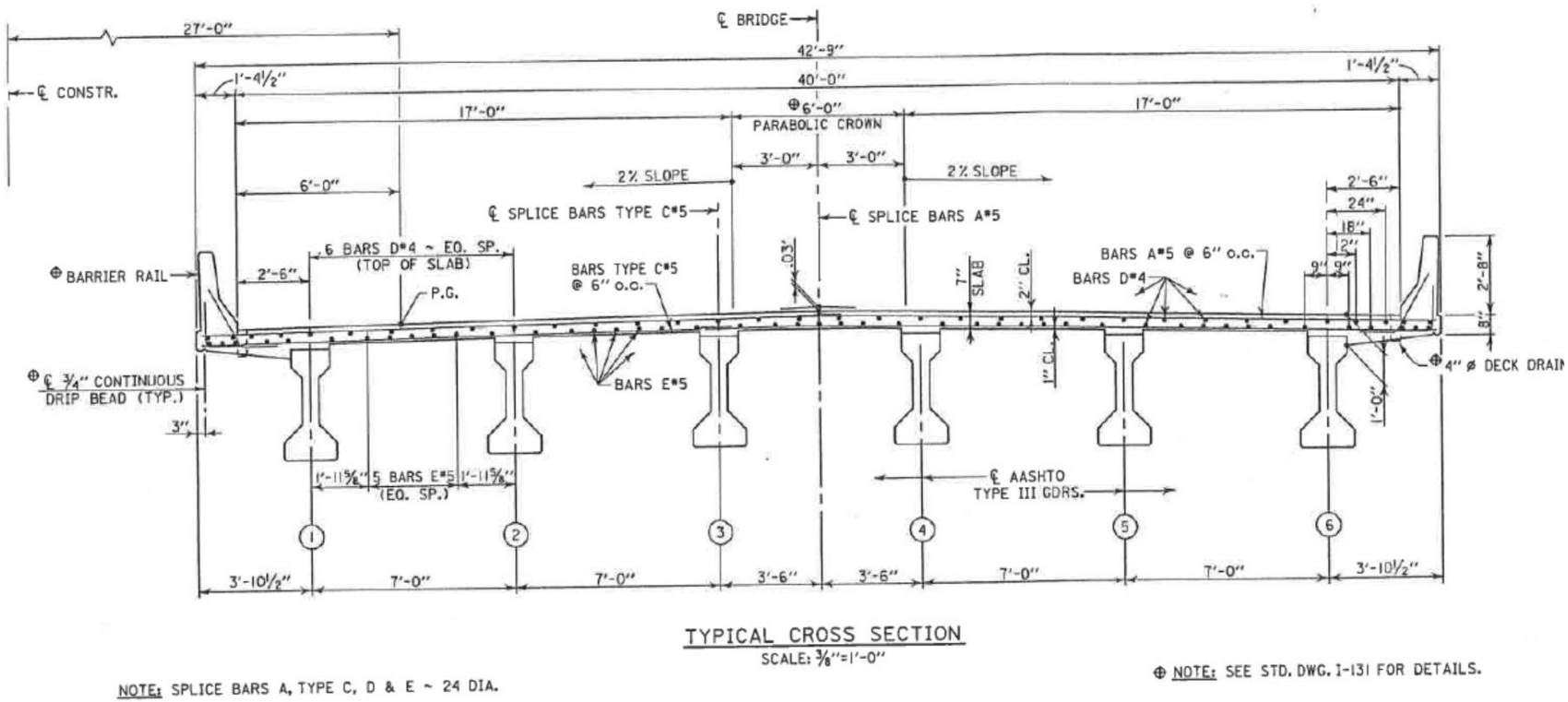

TYPICAL CROSS SECTION

SCALE: ⅜"=1'-0"

NOTE: SPLICE BARS A, TYPE C, D & E ~ 24 DIA.

⊕ NOTE: SEE STD. DWG. I-131 FOR DETAILS.

Figure 4.22. Franklin County typical bridge deck cross section (ALDOT 2005)

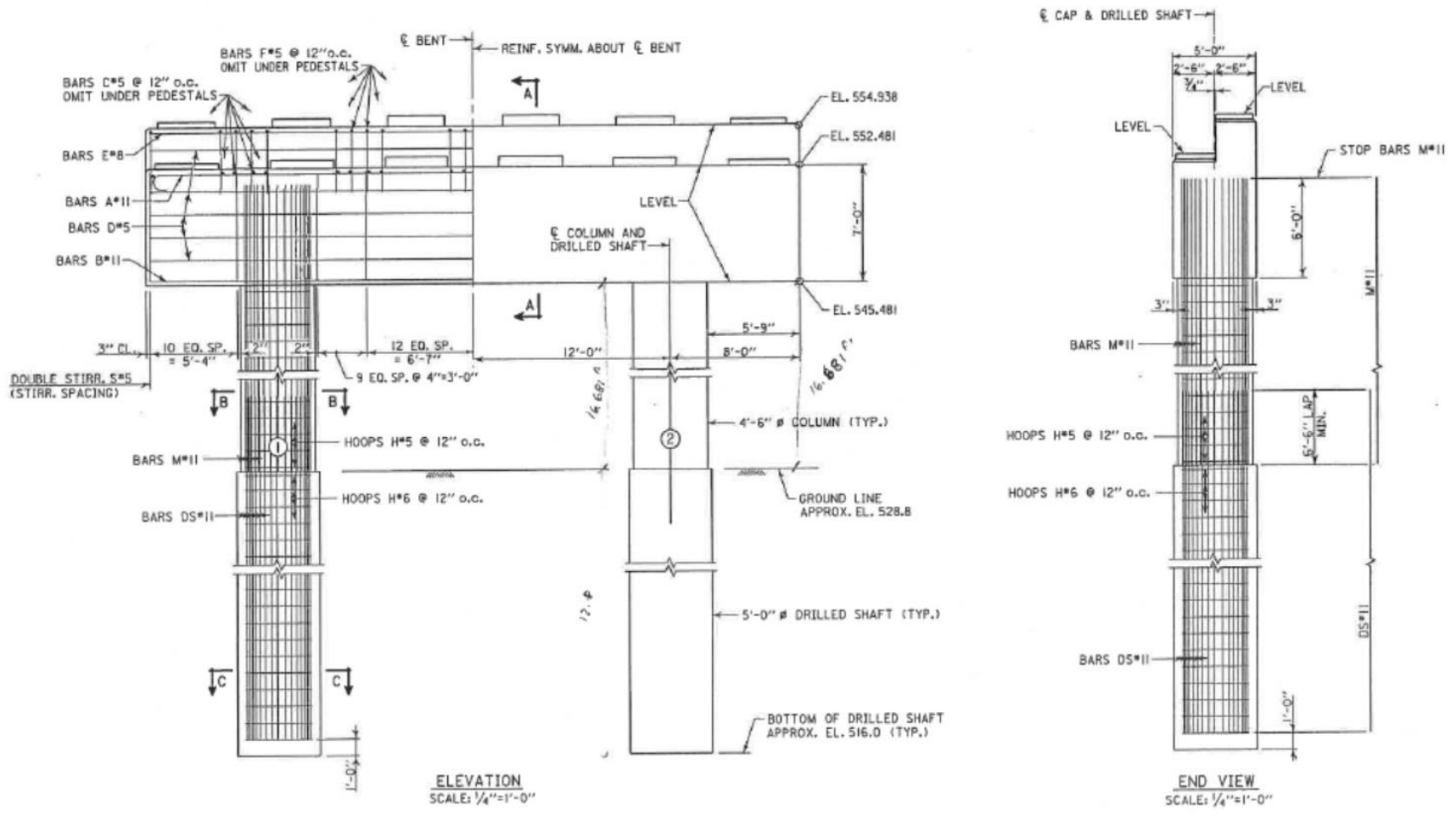

Figure 4.23. Franklin County Bent 3 elevation and end view (ALDOT 2005)

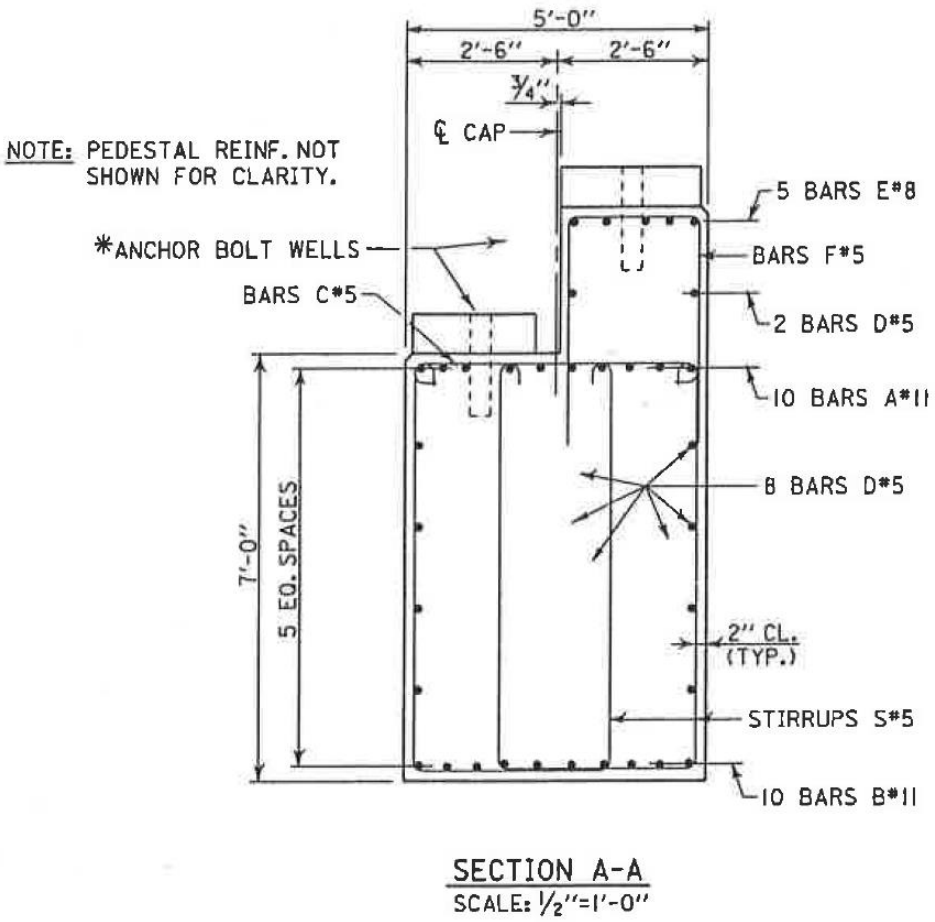

Figure 4.24. Franklin County pier cap cross section (ALDOT 2005)

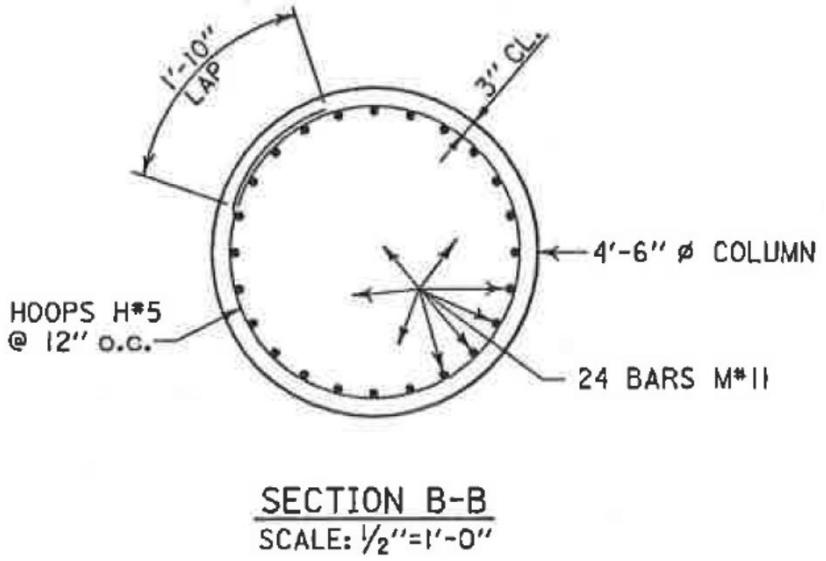

Figure 4.25. Franklin County above ground column cross section (ALDOT 2005)

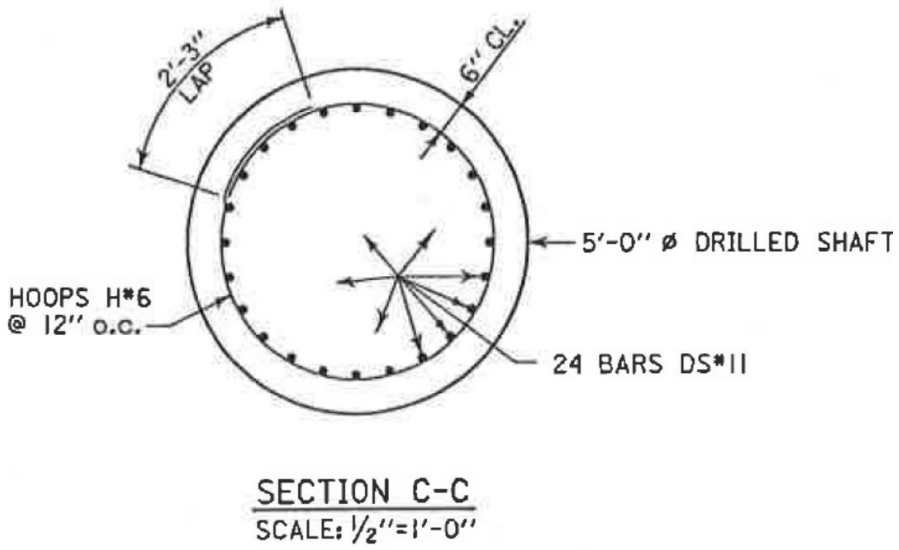

Figure 4.26. Franklin County below ground drilled shaft cross section (ALDOT 2005)

4.6.2 Soil Modeling

A formal site investigation, using the SPT and rock coring, was conducted by the Bureau of Materials and Tests within ALDOT. According to the geotechnical report, the site is located in the Moulton Valley district of the Highland Rim physiographic section and underlain by Bangor Limestone of Mississippian age (ALDOT 2005). The GWT elevation at Bent 3 was recorded as 528 ft at a 24 hour reading after the initial site investigation (ALDOT 2005). There is roughly 3 ft of top soil that was assumed to scour to bedrock at an elevation of 525.6 ft. Static analysis of the lateral capacity of the drilled shafts was done using LPile and the input parameters were included in the geotechnical report. The same input parameters were used in FB-MultiPier. However, some parameters that were needed for FB-MultiPier were not provided and had to be determined based on the boring logs. Figure 4.27 shows the idealized soil profile that was developed and used in FB-MultiPier. The soft clay layer was not included in the analysis, but shown here for reference. Due to the bedrock being very close to the

surface, the soil is a site class C. Refer to Appendix E for the original boring logs and input parameters.

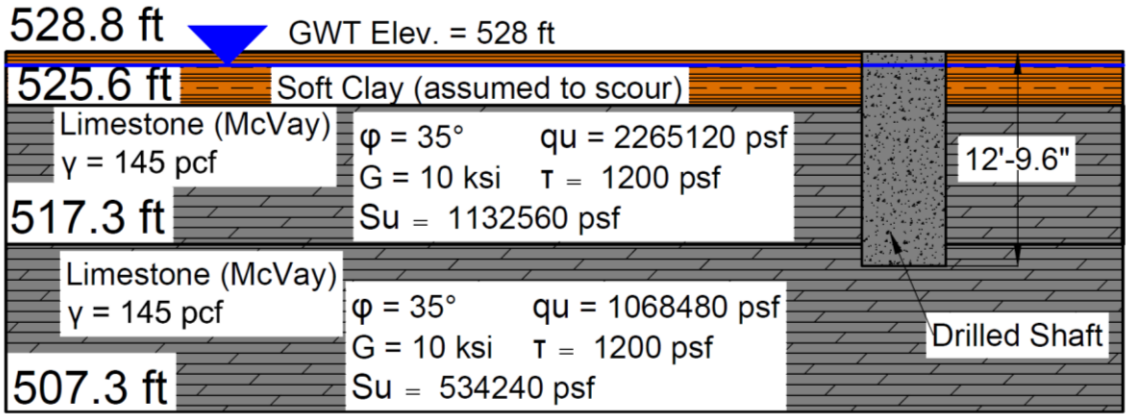

Figure 4.27. Franklin County idealized soil profile

4.7 Lee County

4.7.1 Background Information

The Lee County Bridge is a bridge replacement for Bent Creek Road over I-85. The total bridge span is 270 feet and rests on two abutments and one central pier (bent 2). It is not skewed and has a total roadway width of 80 feet and 9 in. See Figure 4.28 and 4.29 for the plan and elevation views and Figure 4.30 for the bridge deck cross section. The foundations used for both the abutments and piers are 12x53 H-piles. Because the abutments were not modeled, they are not discussed. Bent 2 was modeled in FB-MultiPier and consists of a pier cap and three columns that are each supported by pile footings. The bridge was built in two stages to avoid closing the existing road. The bridge was modeled in FB-MultiPier as one bent, however, due to program limitations. Figure 4.30 and 4.31 show the Bent 2 stage one and two elevation view. Figure 4.32 shows the bent 2 stage one and two end view, and Figure 4.33 and 4.34 show the column and pier cap cross sections and the pile footing layout respectively.

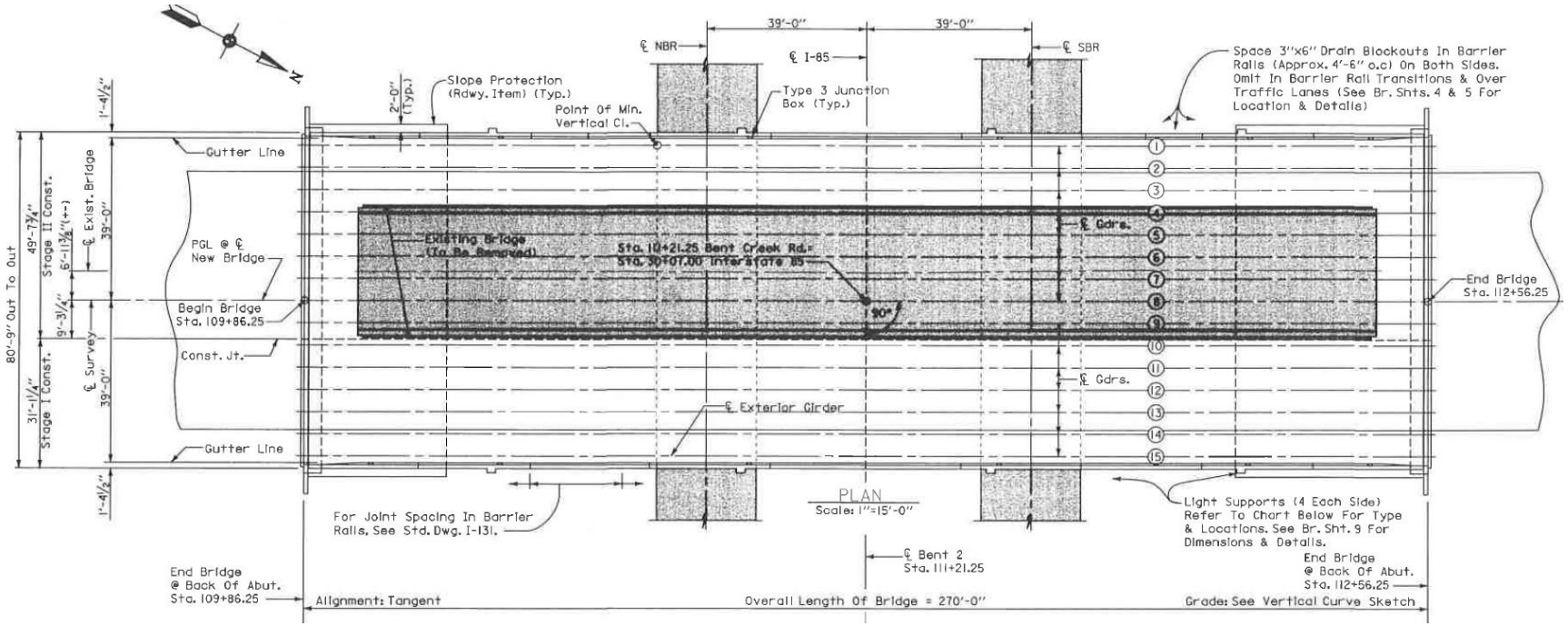

Figure 4.28. Lee County bridge plan view (ALDOT 2006)

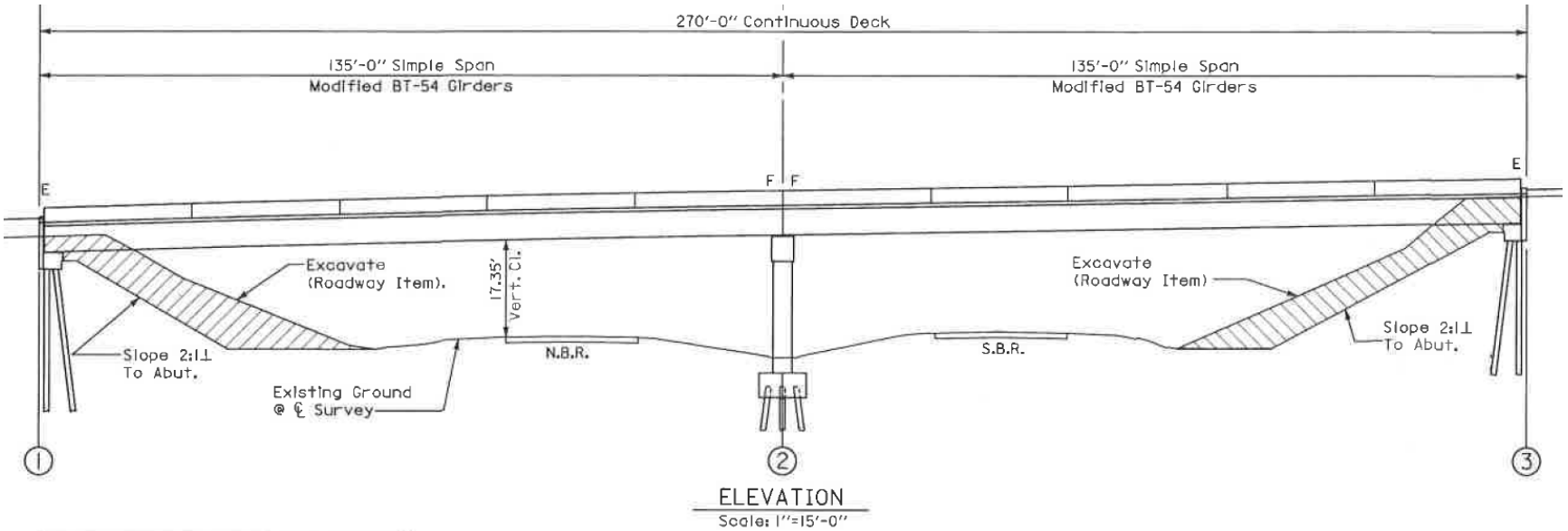

Figure 4.29. Lee County bridge elevation view (ALDOT 2006)

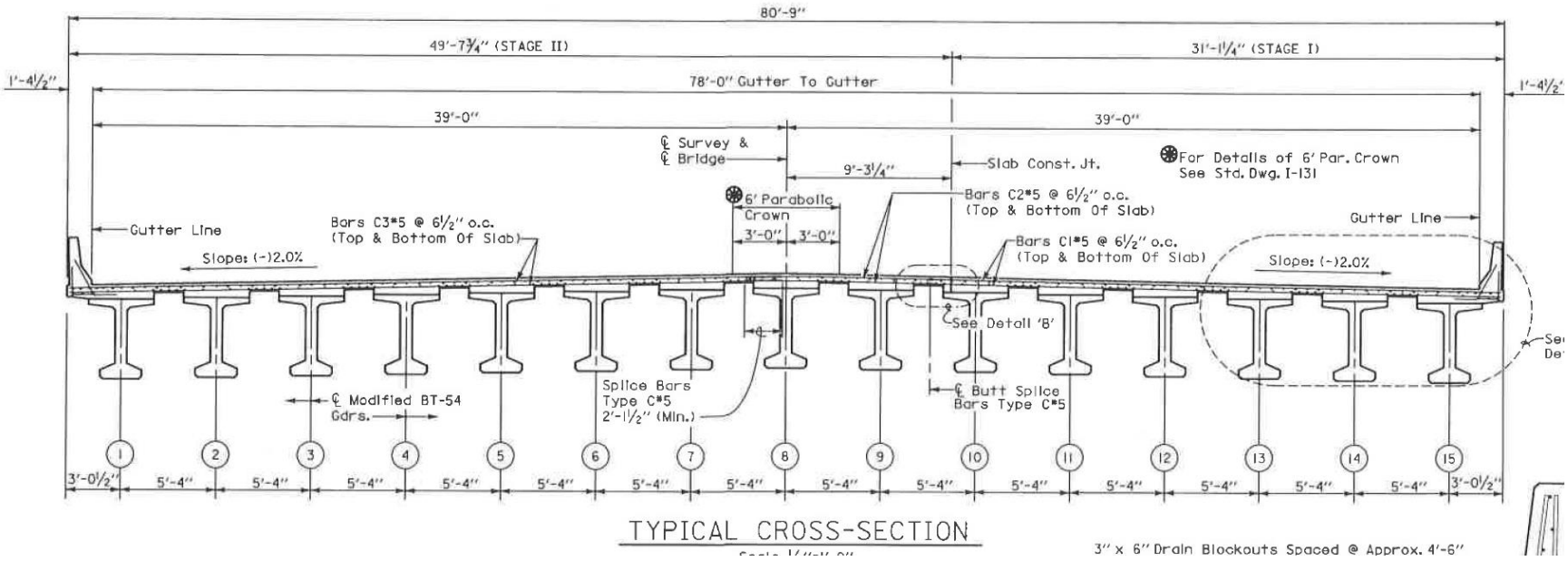

Figure 4.30. Lee County typical bridge deck cross section (ALDOT 2006)

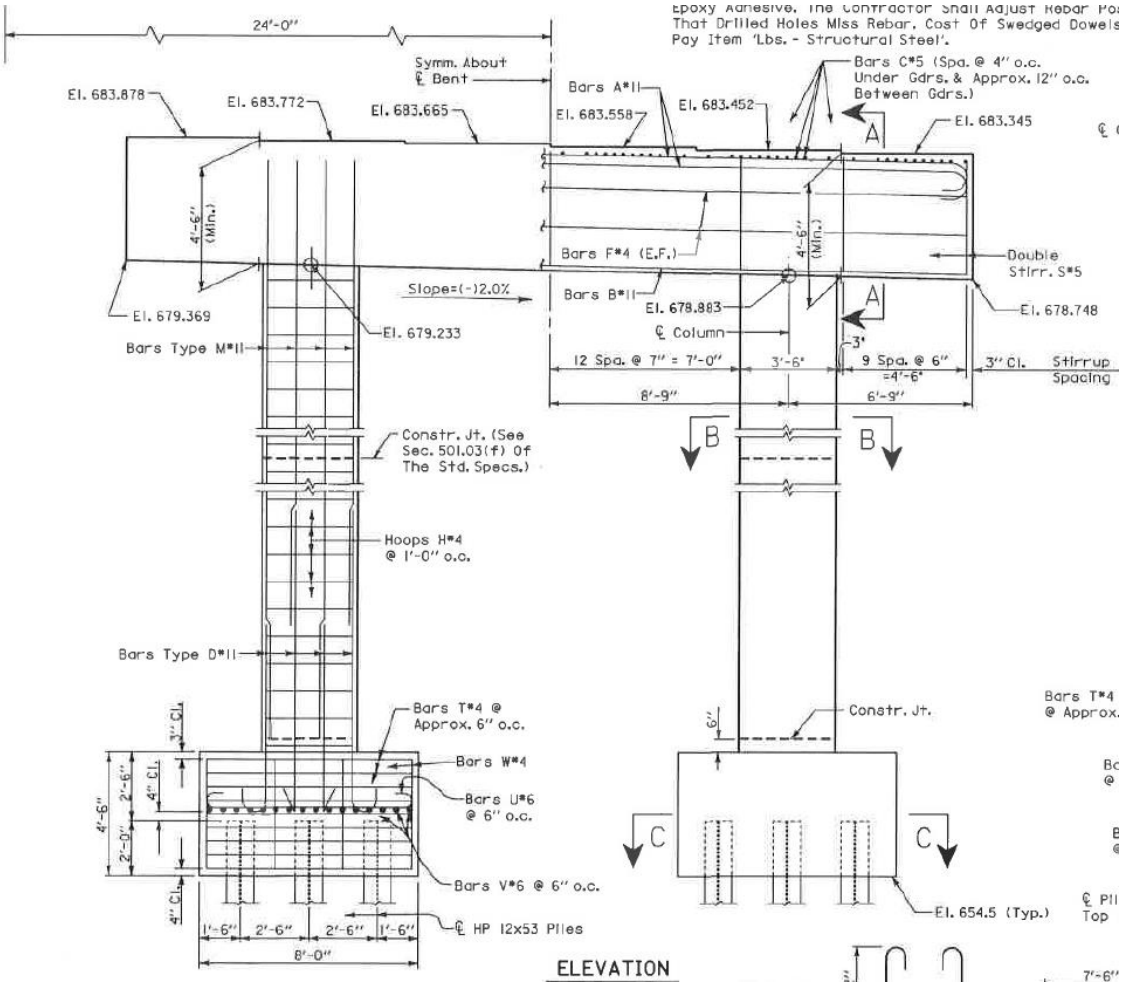

Figure 4.31. Lee County Bent 2 stage one elevation view (ALDOT 2006)

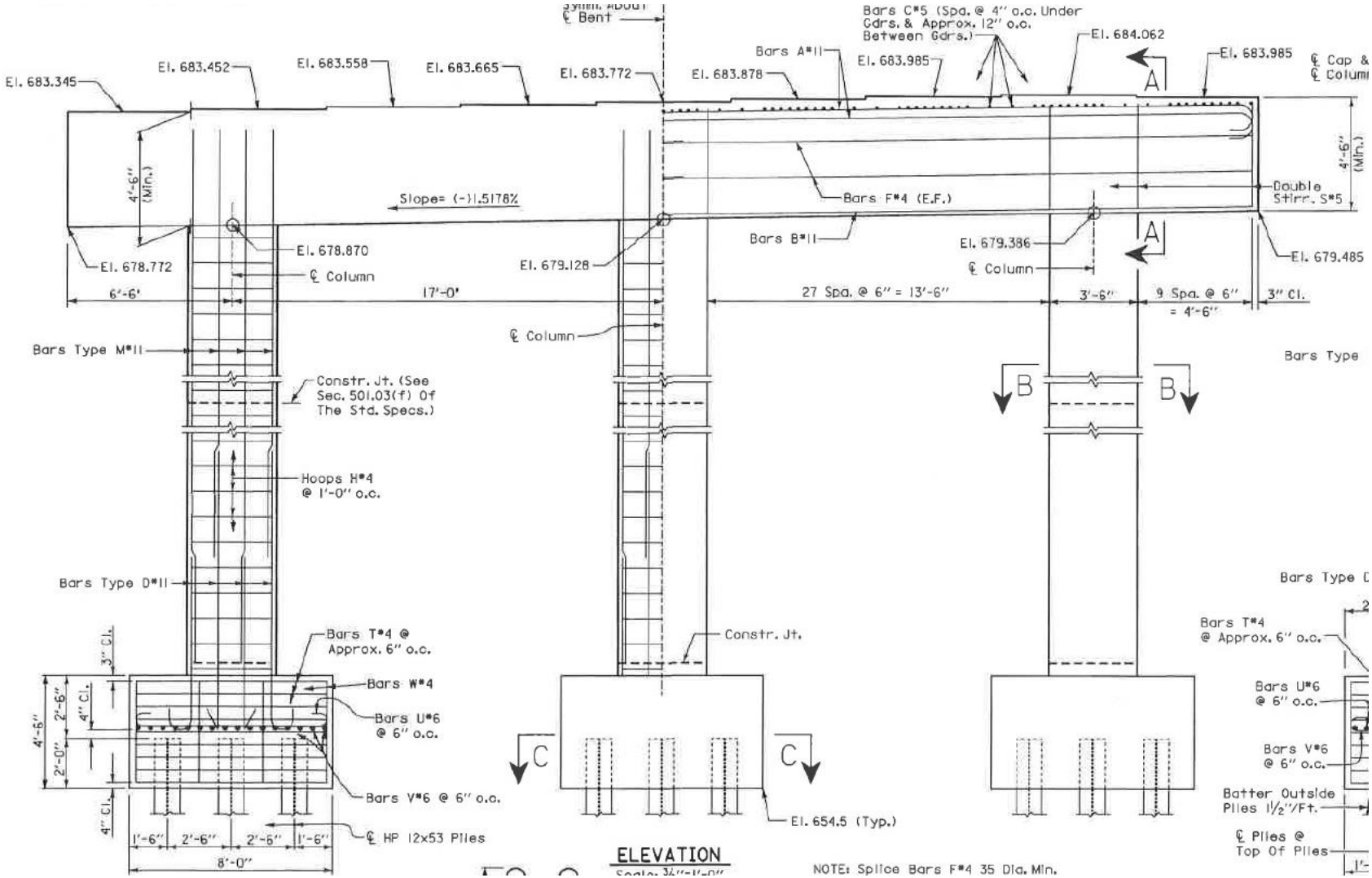

Figure 4.32. Lee County Bent 2 stage two elevation view (ALDOT 2006)

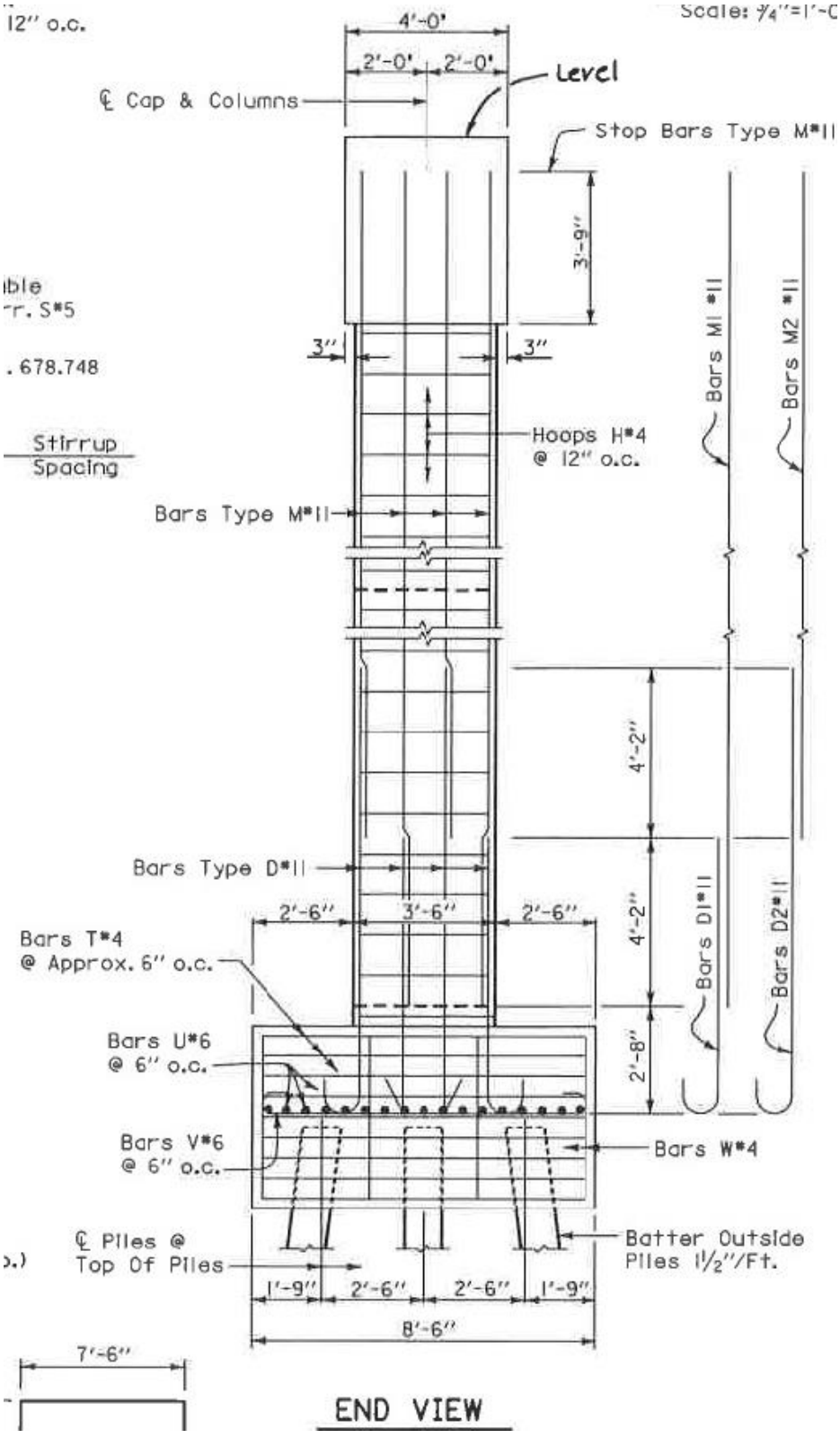

Figure 4.33. Lee County Bent 2 stage one and two end view (ALDOT 2006)

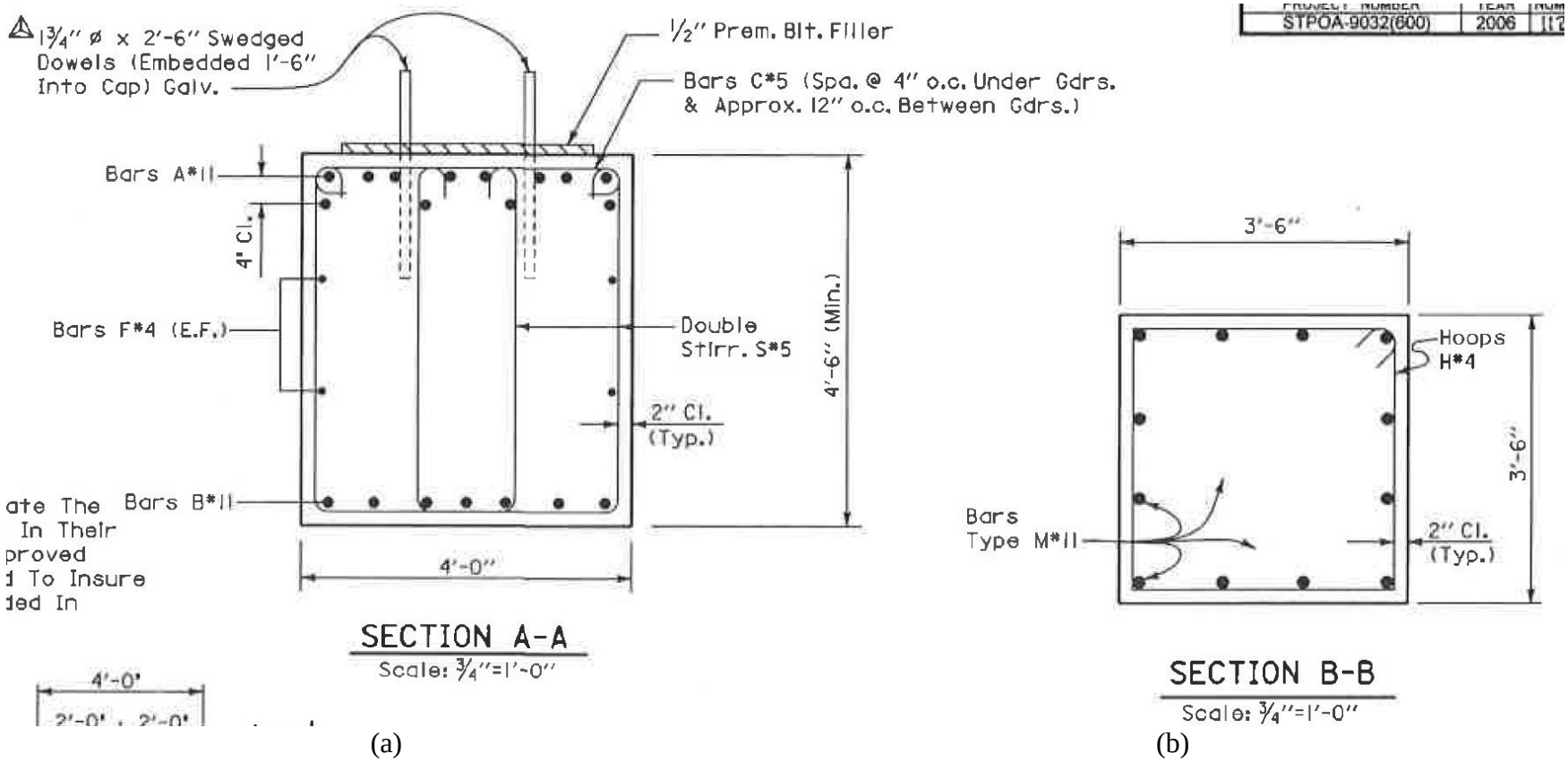

Figure 4.34. Lee County Bent 2 (a) pier cap and (b) column cross section (ALDOT 2006)

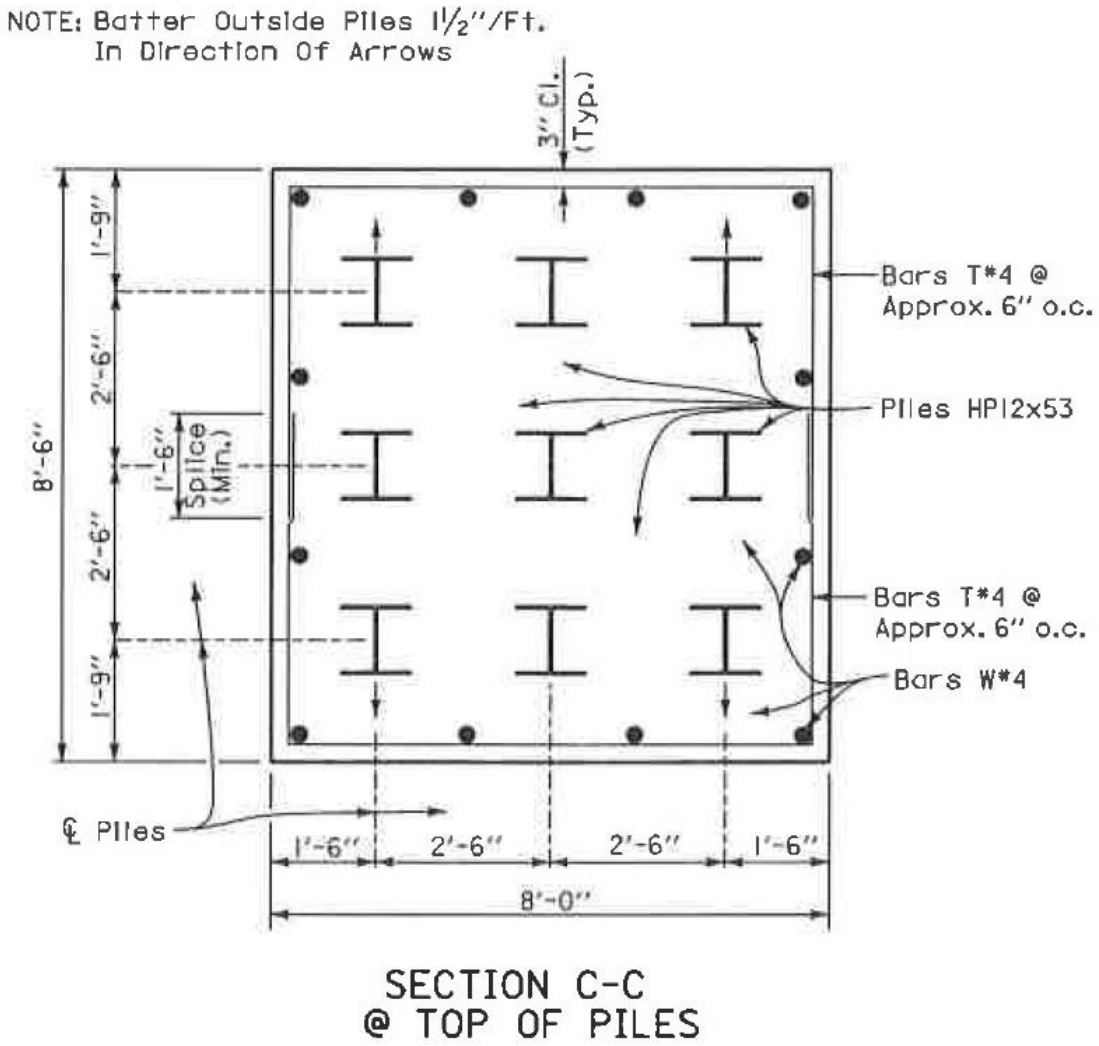

Figure 4.35. Lee County Bent 2 pile footing layout (ALDOT 2006)

4.7.2 Soil Modeling

A formal site investigation, using the SPT and rock coring, was conducted by the Bureau of Materials and Tests within ALDOT. According to the geotechnical report, the site is in the Southern Piedmont Upland district of the Piedmont Upland physigraphic section. The project is located in the Towaliga fault zone and is underlain by blastomylonite which is schist and gneiss that has been pulverized by the lateral movement of the fault (ALDOT 2006).

The GWT elevation at Bent 2 at 24 hours after drilling was estimated to be 655 feet elevation during the initial site investigation (ALDOT 2006). The boring logs taken near bent 2 indicated that insitu soils consist of approximately 30 feet of stiff sandy silt from the ground surface underlain by hard weathered gneiss. All input parameters needed for FB-MultiPier were determined based on the boring logs and rock core testing. The axial bearing failure (or mobilized end bearing) was determined using FB-Deep. All relative information regarding input parameters for Lee County used in FB-Deep are in Appendix F. Figure 4.36 shows the idealized soil profile that was developed and used in FB-MultiPier. The insitu soils were determined to be a site class D. Refer to Appendix F for the original boring logs.

Default p-y multipliers were used for lateral analysis in the Lee County models. It was determined that these were adequate for use. A pile group efficiency of 1 was used for the axial analysis. For driven piles, axial group efficiency can be greater than 1 in some cases, due to densification of the surrounding soil during pile driving.

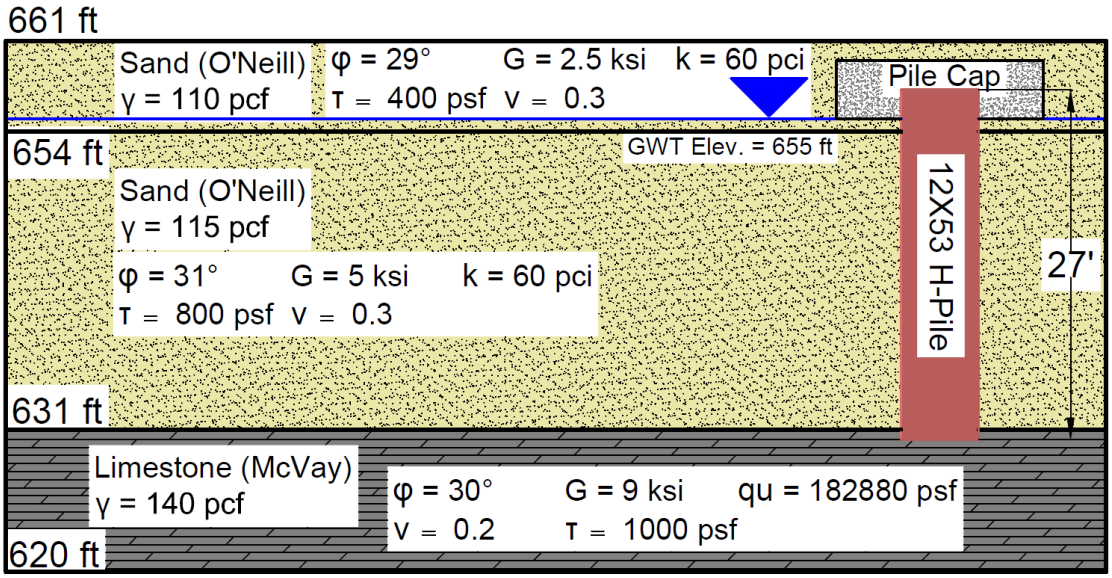

Figure 4.36. Lee County idealized soil profile

4.8 Marshall County

4.8.1 Background Information

The Marshall County Bridge provided by ALDOT is a bridge over Scarham Creek on State Route 75 (south bound lane). The total bridge span is 520 ft and rests on two abutments and three central piers. It is not skewed and has a total roadway width of 40 ft. See Figure 4.37 and 4.38 for the plan and elevation views and the bridge deck cross section. The foundations used for both the abutments and piers are drilled shafts. Because the abutments were not modeled, they are not discussed. The foundations for Bents 2, 3, and 4 were modeled in FB-MultiPier to develop static stiffness response curves for the SAP model. All of the bents were modeled using the same soil profile, which was the lower bound. Bent 2 and 4 have the same section properties; therefore, one model was developed to represent both bents. Bent 3 has a larger shaft diameter than that of Bents 2 and 3 was the bent modeled for direct analysis.

The shafts for Bent 2 and 4 are 5 ft in diameter with 24 No. 11 longitudinal reinforcing bars above the ground surface, and 5.5 ft in diameter with the same reinforcement alignment below the ground surface. Figure 4.39 shows the Bent 2 shaft elevations only and Figure 4.40 shows the shaft cross sections. The shafts for Bent 3 are 6 ft in diameter with 32 No. 11 longitudinal reinforcing bars above the ground surface, and 6.5 ft in diameter with the same reinforcement alignment below the ground surface. Figures 4.41, 4.42, and 4.43 show the Bent 3 elevation view, pier cap cross section, and strut cross section. Figure 4.44 shows the shaft cross sections.

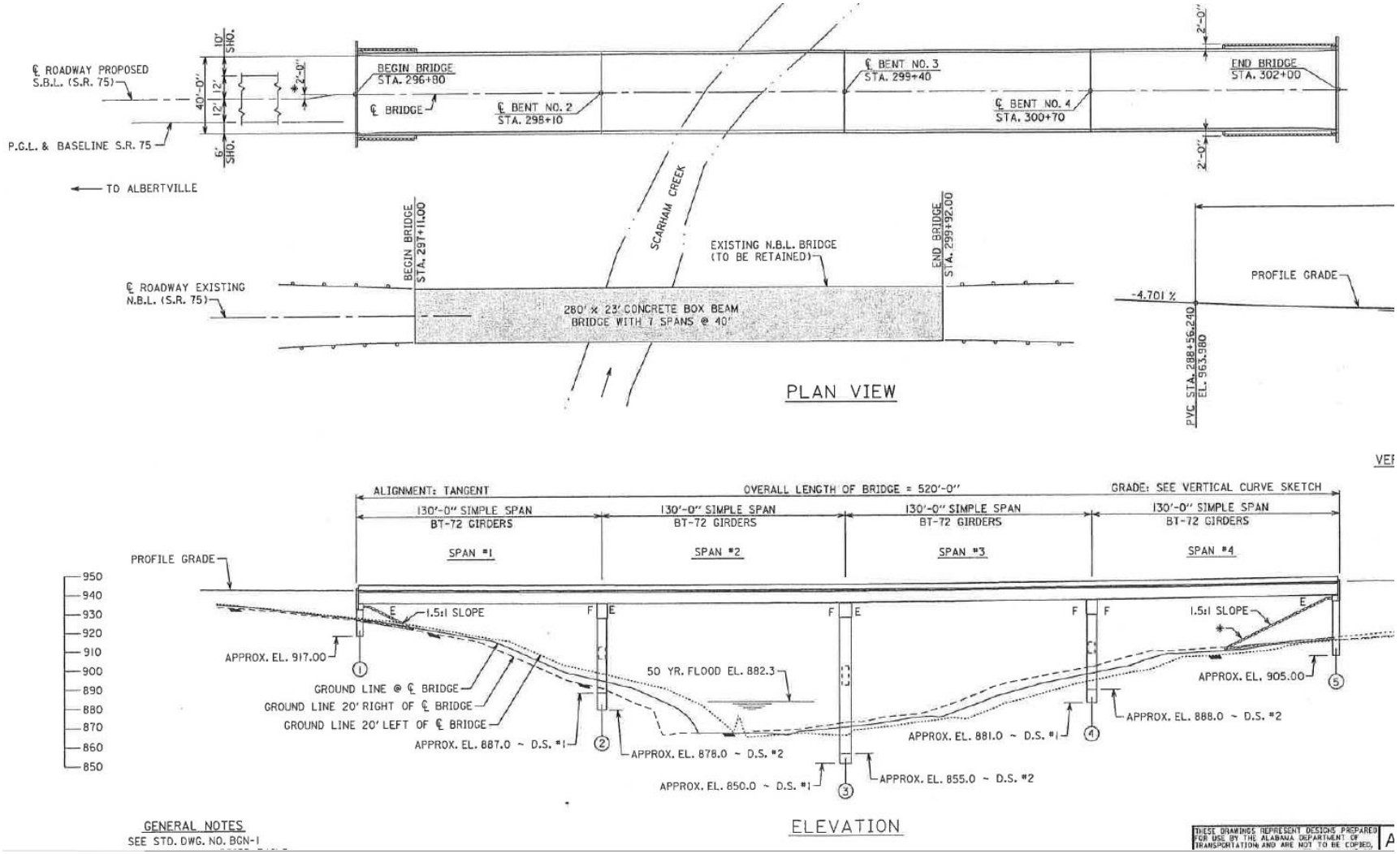

Figure 4.37. Marshall County bridge plan and elevation view (ALDOT 2003)

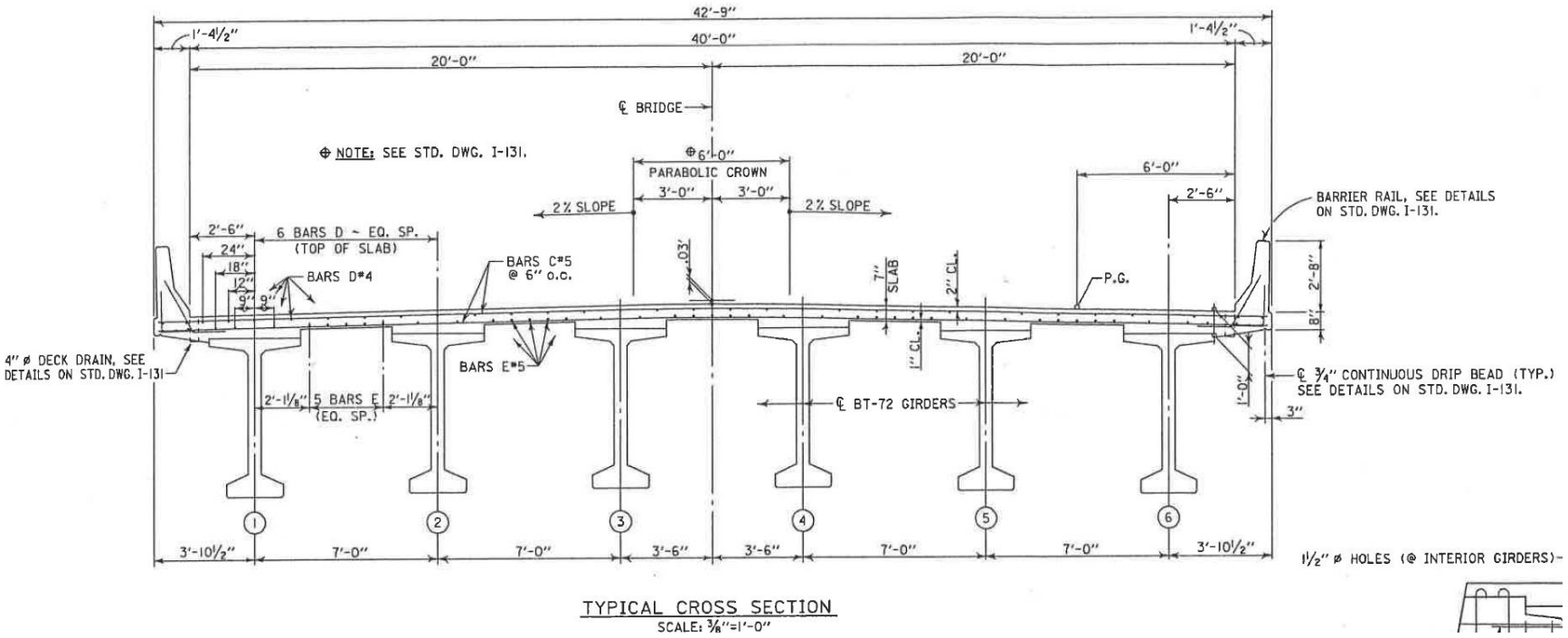

TYPICAL CROSS SECTION
SCALE: ⅜"=1'-0"

Figure 4.38. Marshall County typical bridge deck cross section (ALDOT 2003)

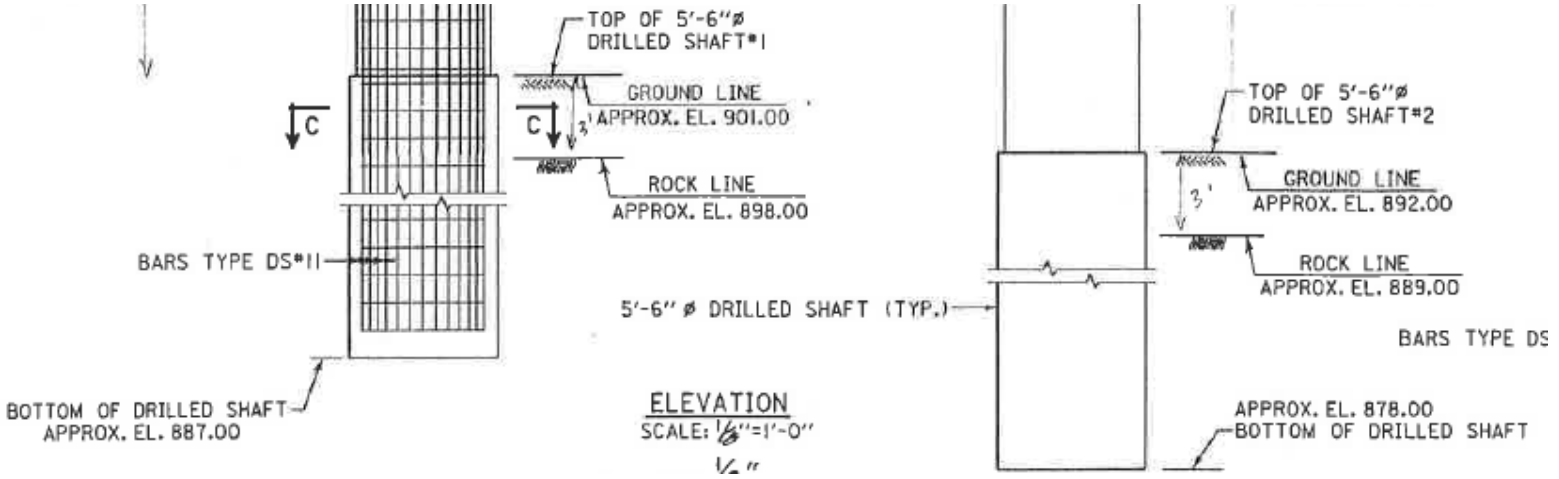

Figure 4.39. Marshall County Bent 2 shaft elevations (ALDOT 2003)

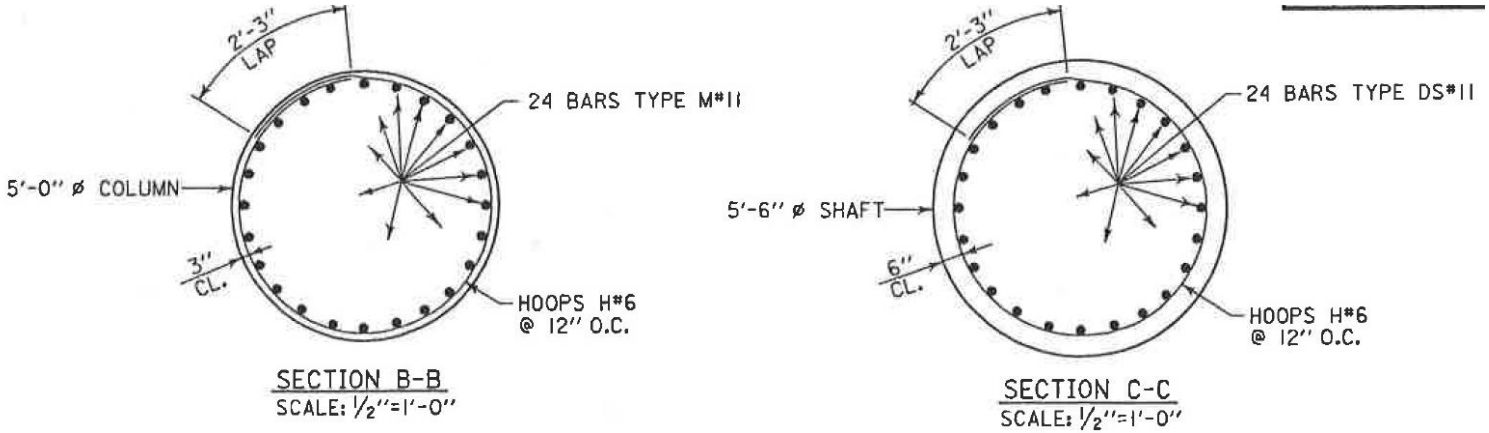

Figure 4.40. Marshall County Bent 2 (a) above ground and (b) below ground column and shaft cross section (ALDOT 2003)

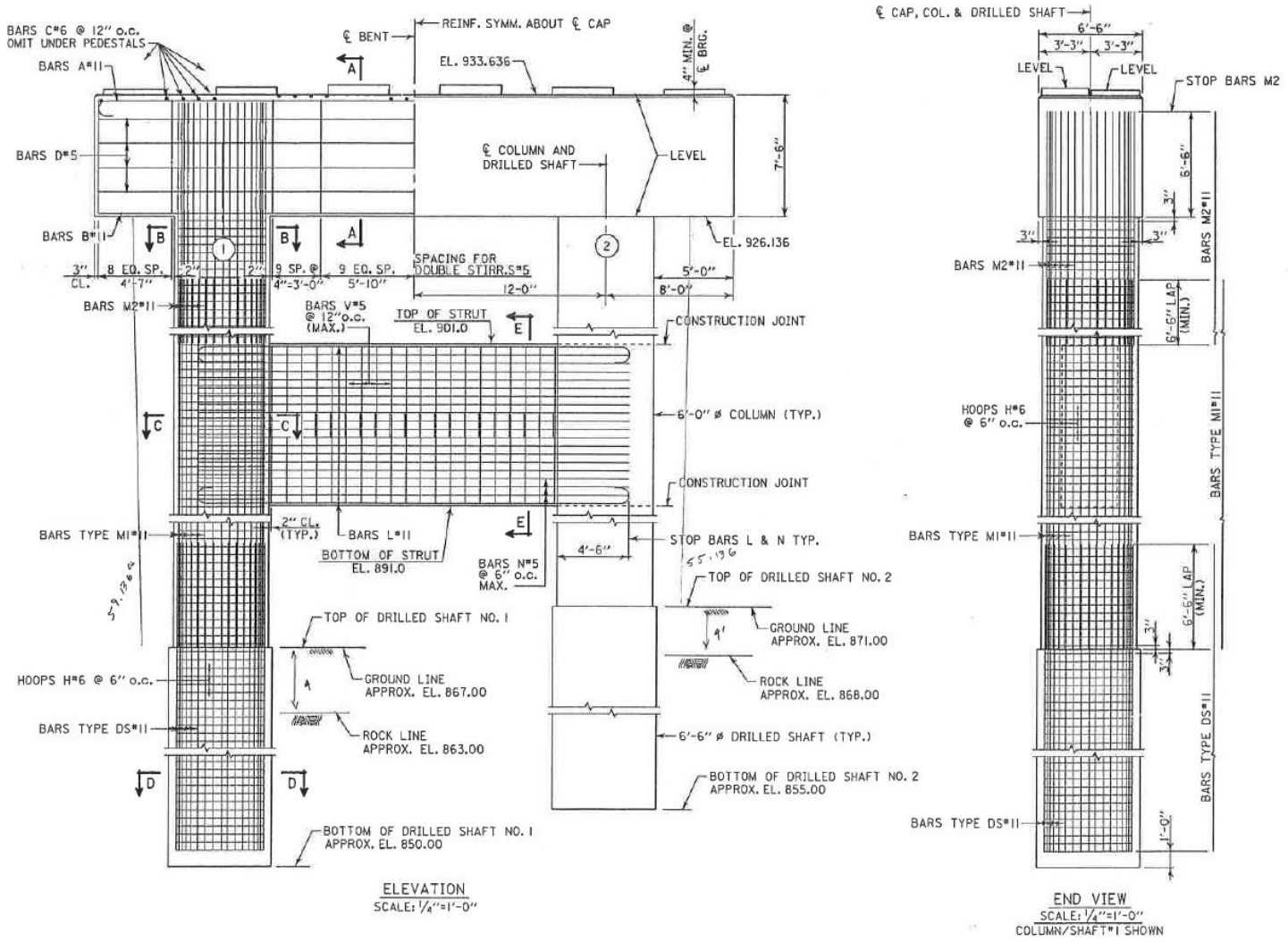

Figure 4.41. Marshall County Bent 3 elevation and end view (ALDOT 2003)

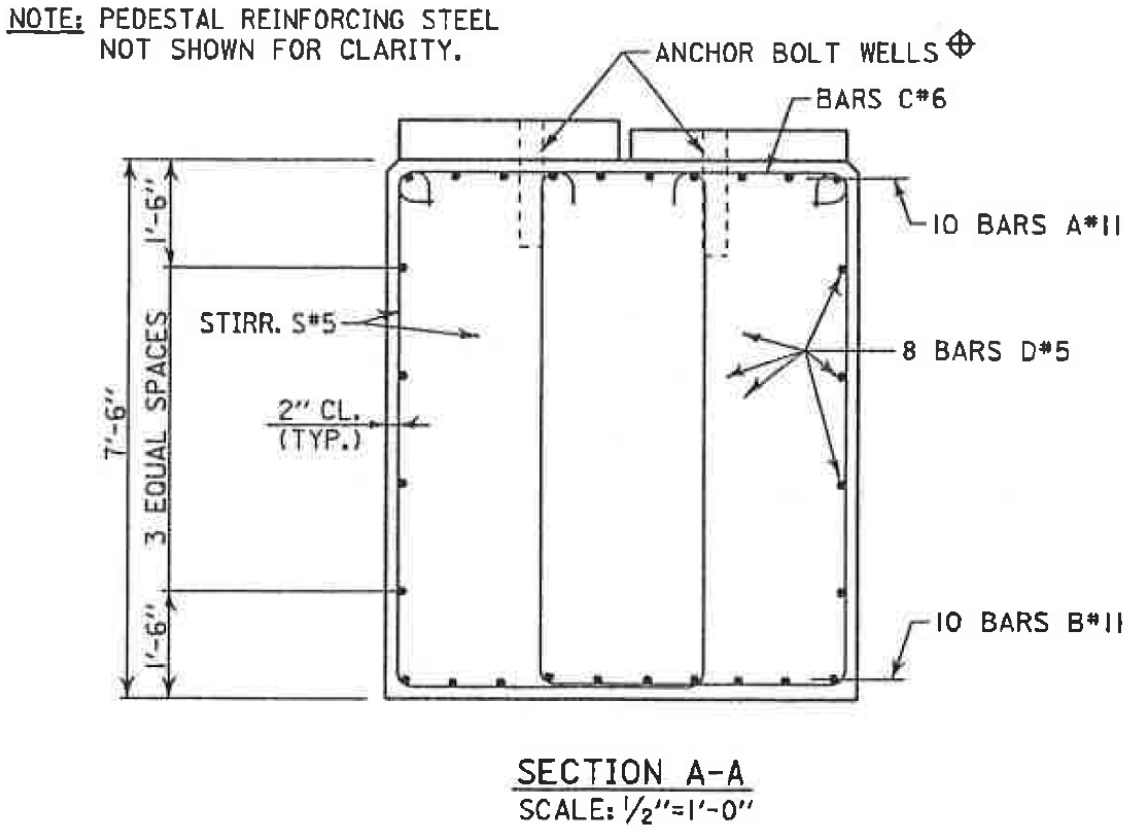

Figure 4.42. Marshall County Bent 3 pier cap cross section (ALDOT 2003)

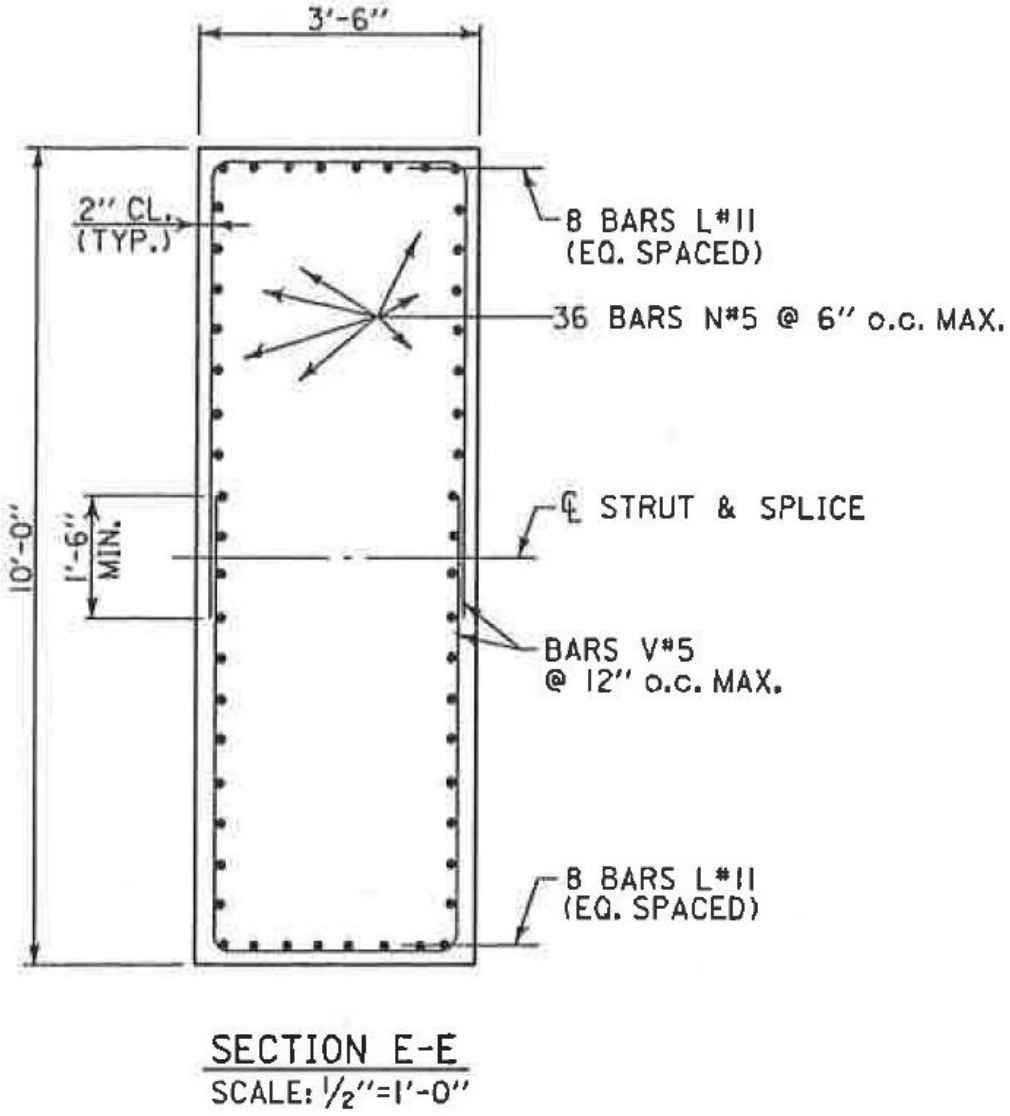

Figure 4.43. Marshall County Bent 3 strut cross section (ALDOT 2003)

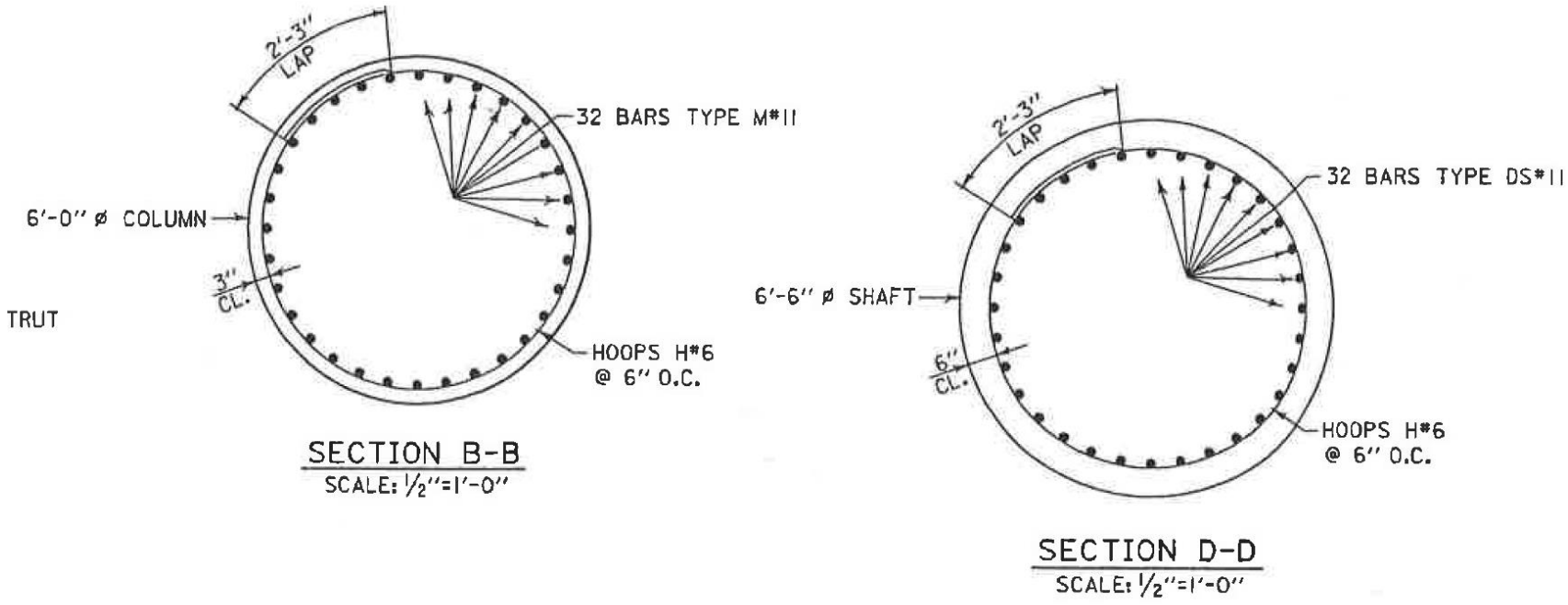

(a) (b)

Figure 4.44. Marshall County Bent 3 (a) above ground and (b) below ground column and shaft cross section (ALDOT 2003)

4.8.2 Soil Modeling

A formal site investigation, using the SPT and rock coring, was conducted by the Bureau of Materials and Tests within ALDOT. According to the geotechnical report, the site is located in the Sand Mountain district of the Cumberland Plateau physiographic section and underlain by Pottsville Formation of Pennsylvanian age (ALDOT 2003). The Pottsville Formation consists of over 400 feet of brown gray thin- to thick-bedded sandstone, gray shale, siltstone, conglomerate, and coal beds (ALDOT 2003). The GWT elevation at Bent 3 was recorded as 860 feet at a 24 hour reading after the initial site investigation (ALDOT 2003). There was not a GWT elevation recorded for Bents 2 and 4. There is roughly 3-4 ft of top soil that was assumed to scour to bedrock at all of the bents. The elevations for Bent 2 and 4 can be seen on Figure 4.38. However, it should be noted that only the shaft length and free length is critical for Bents 2 and 4. Uniaxial compression testing was done at different stations and depths. The lowest value was used as a representative unconfined compressive strength. All other input parameters needed for FB-MultiPier were determined based on the boring logs. Figure 4.45 shows the idealized soil profile that was developed and used in FB-MultiPier (elevations shown are for Bent 3). The same soil parameters were used for all the bents. The soft clay layer was not included in the analysis, but shown here for reference. Due to the bedrock being very close to the surface, the soil is a site class C. Refer to Appendix G for the original boring logs and input parameters. Note that the multiple elevations in Figure 4.45 refer to the elevations of the soil profile at each drilled shaft for Bent 3. Refer to Figure 4.41 for elevation difference at each shaft.

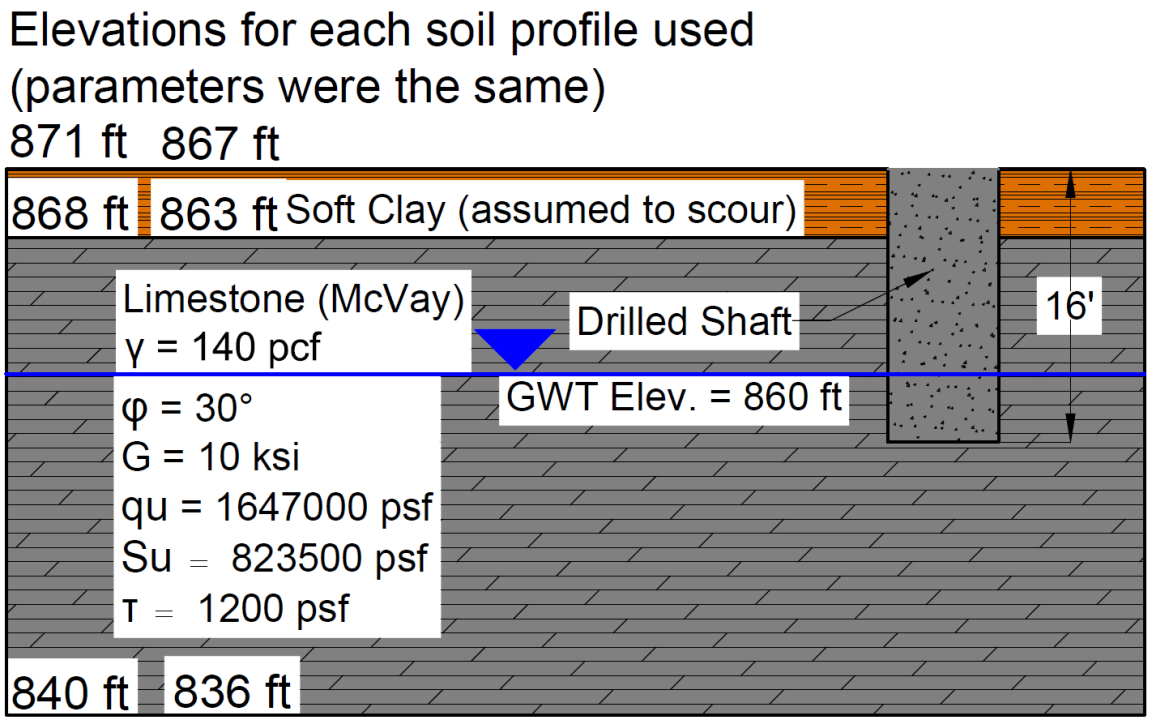

Figure 4.45. Marshall County idealized soil profile

Chapter 5

SUBSTRUCTURE ANALYSIS RESULTS AND DISCUSSION

Static foundation response curves for each bridge were developed to represent the foundations for the SAP2000 models (Panzer 2013). Each foundation was represented with a family of six non-linear curves. The curves were developed using FB-MultiPier. The six curves include the response curves for the forces in the F_X, F_Y, and F_Z directions, as well as the moments in the M_X, M_Y, and M_Z directions (see Figure 5.1). Referring to Chapter 2, section 2.5, the points of emphasis covered in substructure analysis are 3 and 4 which include evaluating the lateral and vertical stiffness of the shafts or pile groups, excluding uplift and abutment response.

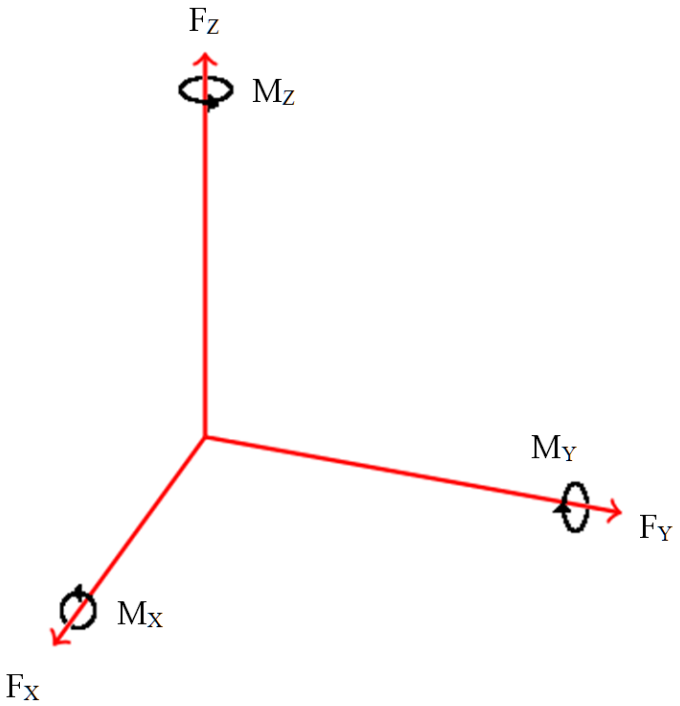

Figure 5.1. Force and moment directions

One representative set of curves was developed for each bridge case except for the Marshall County Bridge. Bents 2 and 4 of this bridge had smaller drilled shaft sizes; therefore, a separate response curve family for both bents was developed to adequately represent the foundations. The abutments were modeled as fixed in the F_Z direction for the SAP2000 models. Refer to Panzer (2013) for further detail regarding abutment foundation modeling.

The loading of each foundation was applied at the center-most point. For the Lee and Etowah County Bridges (H-Pile foundations), the center of the pile cap was the point of loading. The point of loading for the drilled shaft bridge foundations was always in the center of the shaft, but the elevation differed. The Chambers County Bridge bent does not change in diameter; therefore, the loads were applied to the shaft at the rock line. The 100% scour case was the only model used for SAP2000 analysis, and is the only one presented here. The Franklin and Marshall County Bridges had an increased diameter of 6 inches at the elevation of the soil. The point of loading was applied at the elevation where the increase in shaft size occurs. The case with dead load applied was also evaluated for comparison to the recommendation given by Lam and Martin (1986). Dead load was not included to develop the response curve, F_Z, however. Figures 5.2, 5.3, 5.5, 5.6, and 5.8 present the static foundation response curves developed for each case history. Also, pile group layouts are shown for the Etowah and Lee County models (see figure 5.4 and 5.7).

5.1 Chambers County 100% Scour

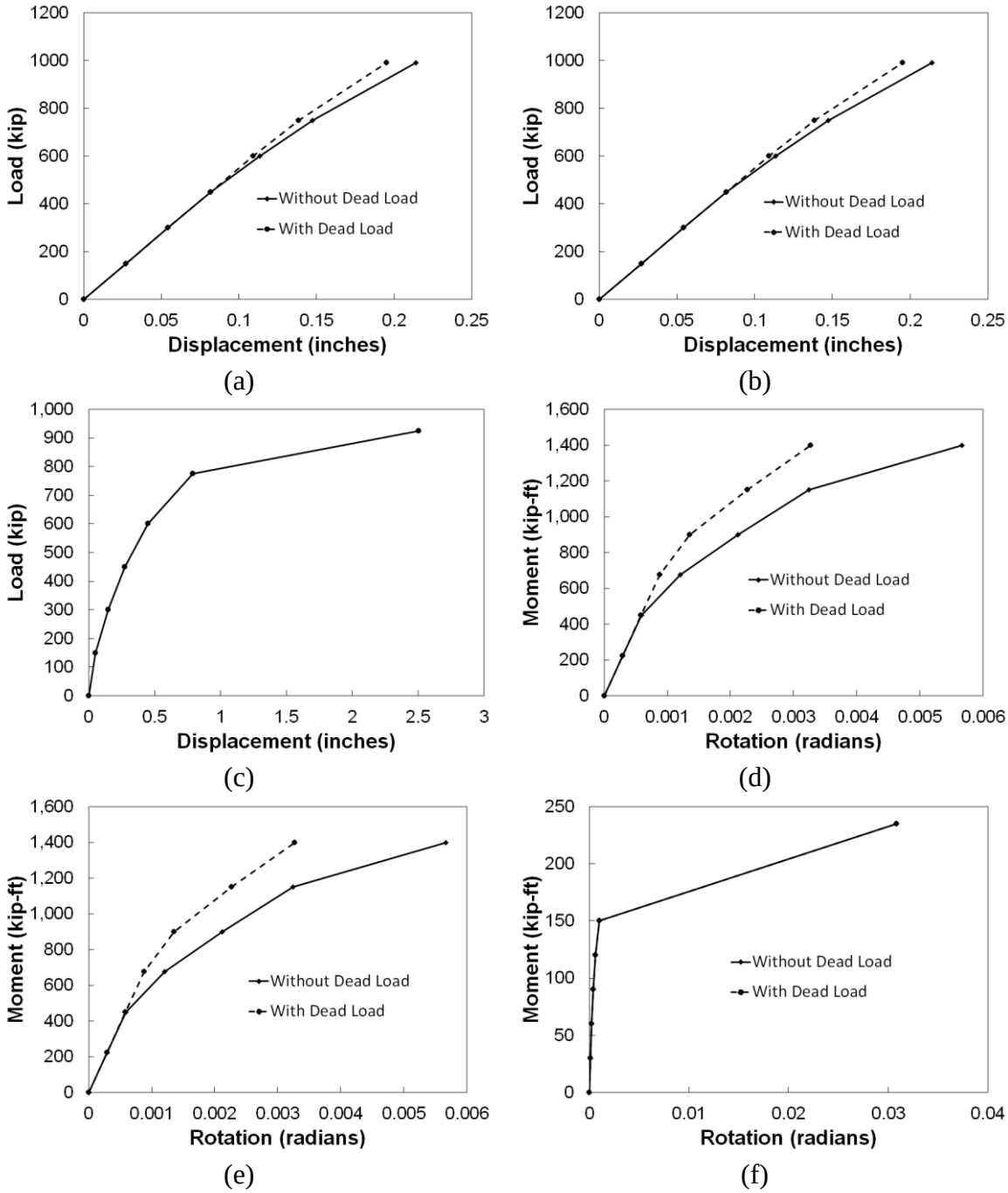

Figure 5.2. Chambers County foundation response curves for (a) F_X, (b) F_Y, (c) F_Z, (d) M_X, (e) M_Y, and (f) M_Z

5.2 Etowah County

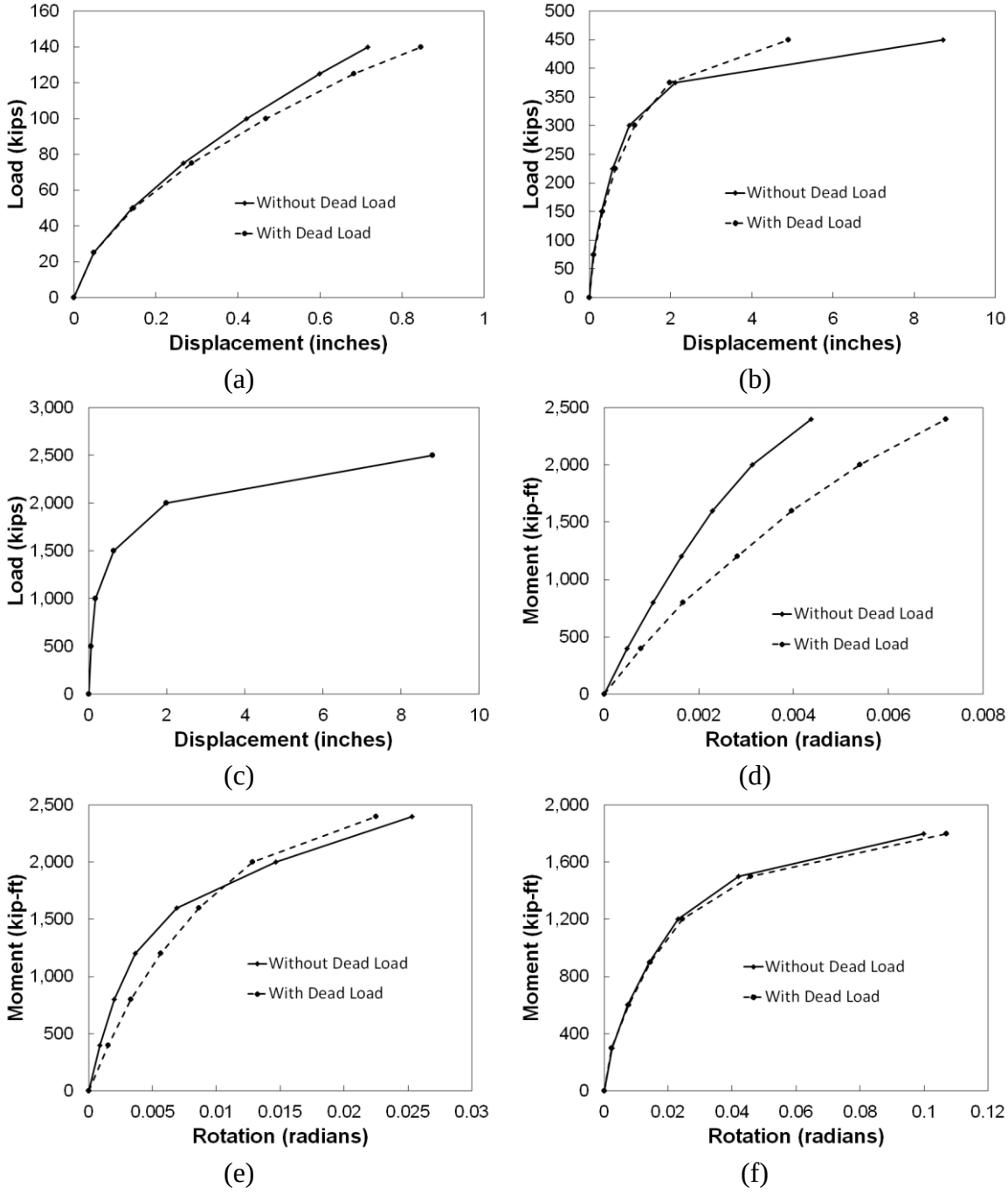

Figure 5.3. Etowah County foundation response curves for (a) F_X, (b) F_Y, (c) F_Z, (d) M_X, (e) M_Y, and (f) M_Z

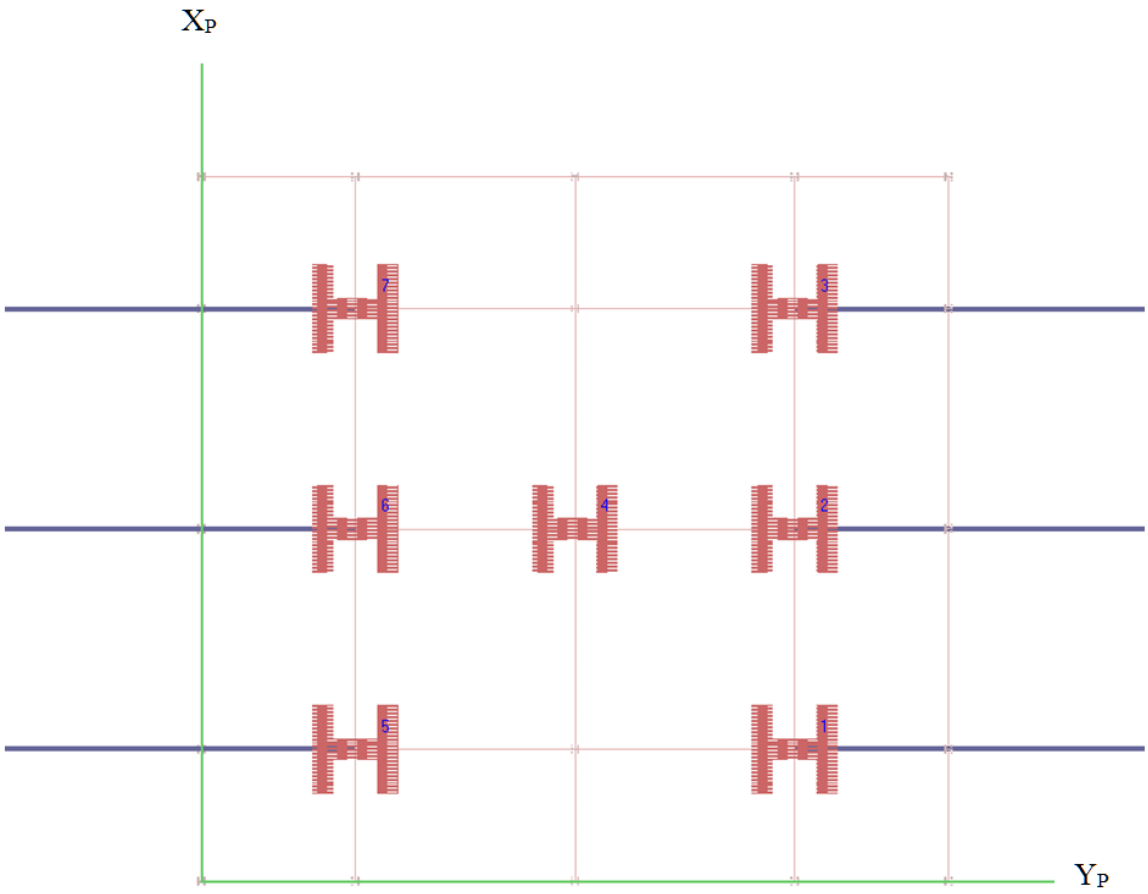

Figure 5.4. Etowah County pile group layout and direction

5.3 Franklin County

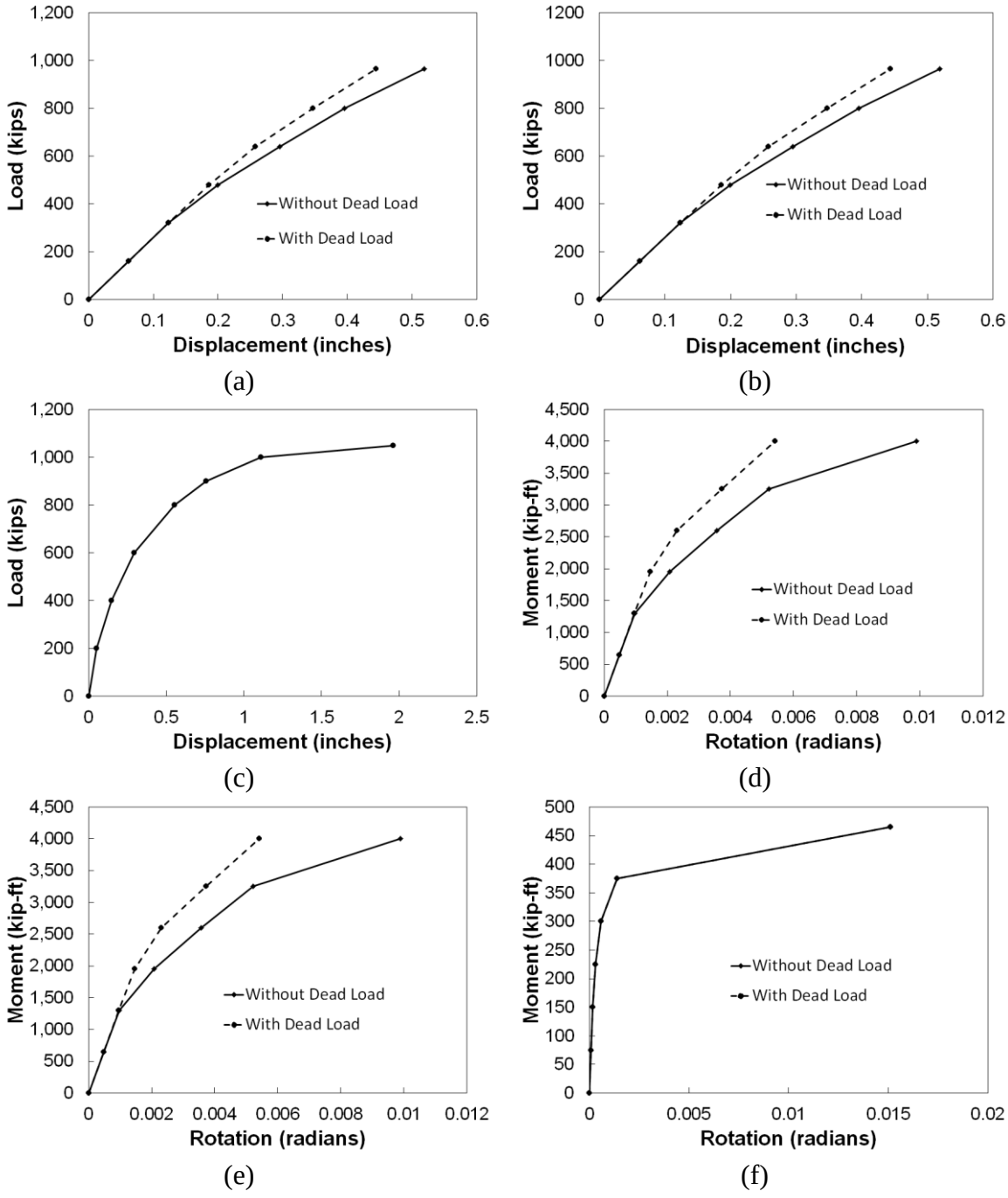

Figure 5.5. Franklin County foundation response curves for (a) F_X, (b) F_Y, (c) F_Z, (d) M_X, (e) M_Y, and (f) M_Z

5.4 Lee County

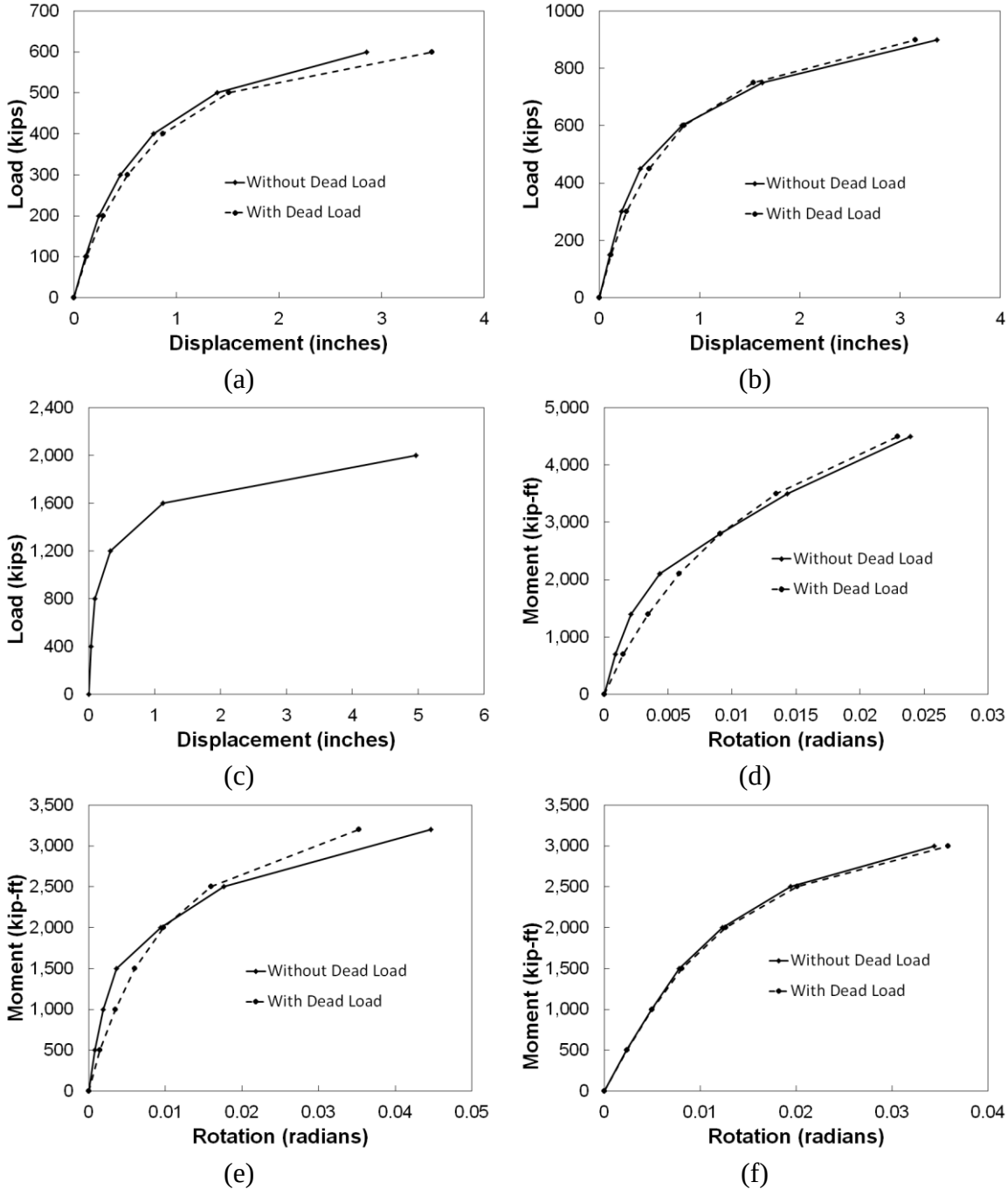

Figure 5.6. Lee County foundation response curves for (a) F_X, (b) F_Y, (c) F_Z, (d) M_X, (e) M_Y, and (f) M_Z

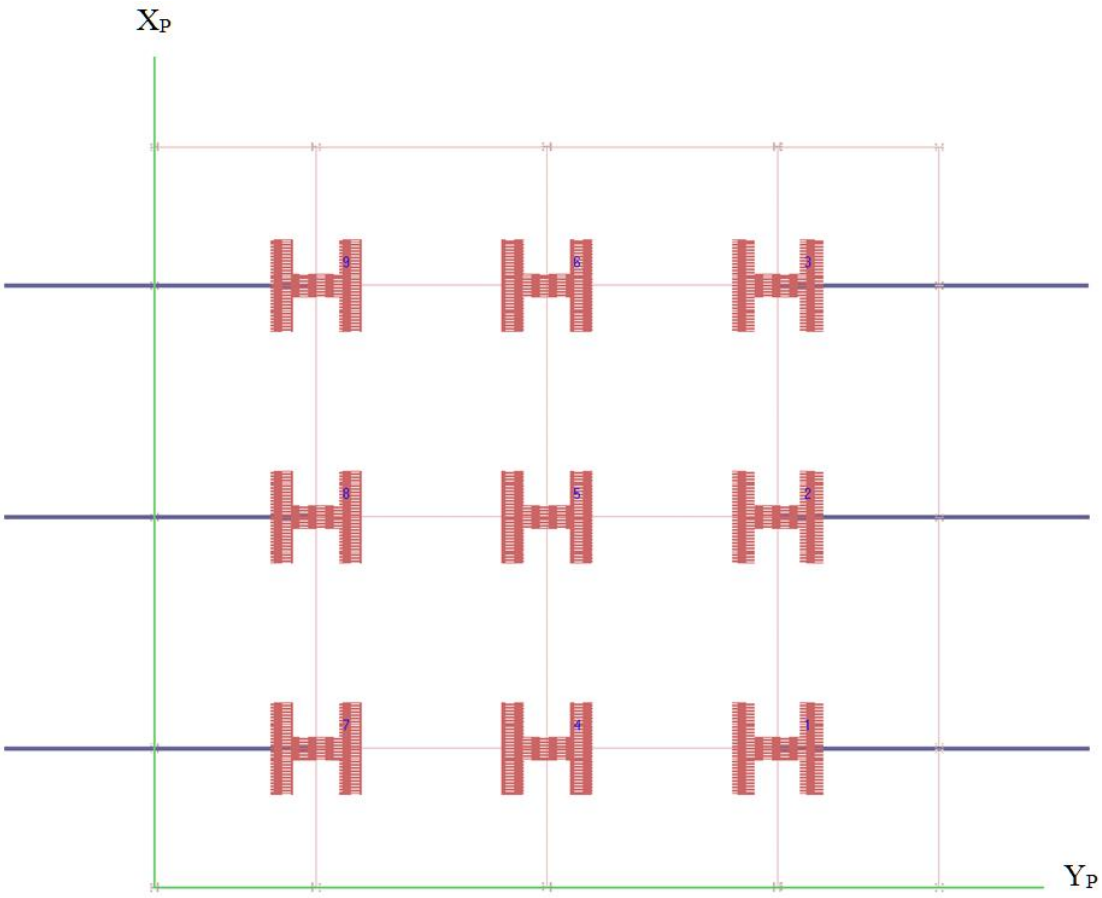

Figure 5.7. Lee County pile group layout and direction

5.5 Marshall County

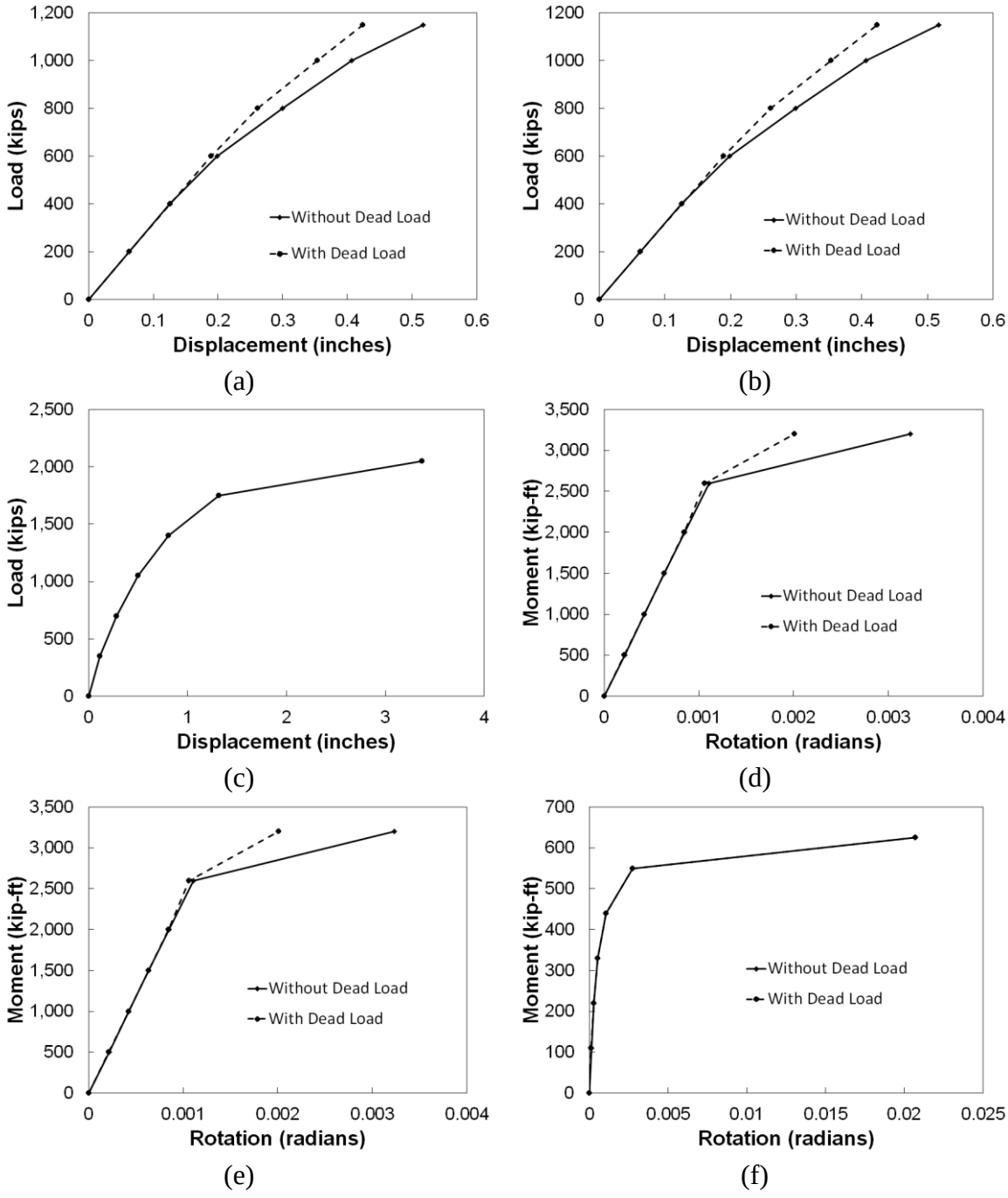

Figure 5.8. Marshall County Bents 2 and 4 foundation response curves for (a) F_X, (b) F_Y, (c) F_Z, (d) M_X, (e) M_Y, and (f) M_Z

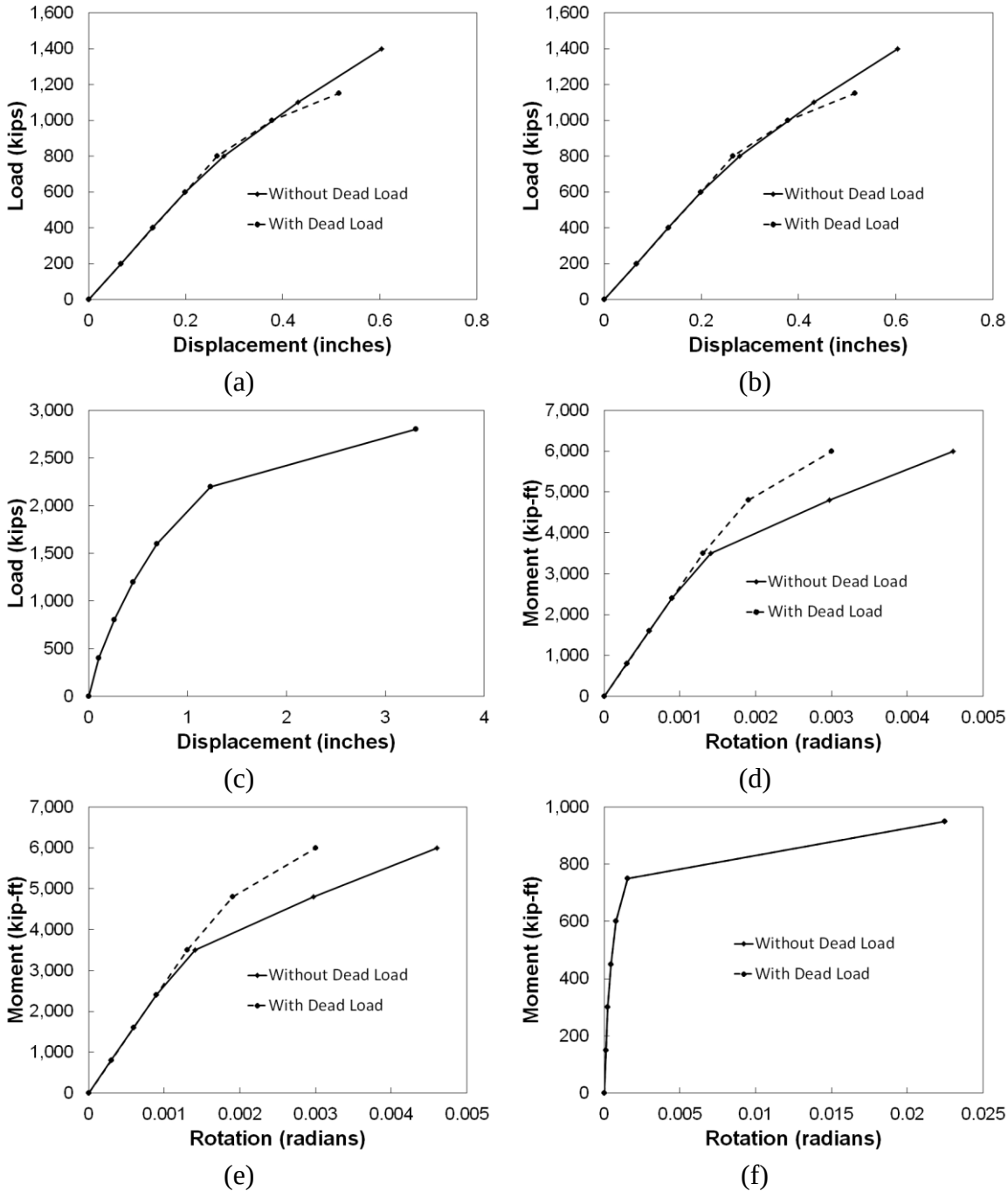

Figure 5.9. Marshall County Bent 3 foundation response curves for (a) F_X, (b) F_Y, (c) F_Z, (d) M_X, (e) M_Y, and (f) M_Z

5.6 Discussion

As mentioned in chapter 2, the most common way to develop the spring stiffness is without taking into account the dead load. Generally, the dead load increased the stiffness or made no difference at all, making the recommendation by Lam and Martin (1986) conservative. However, the rotational stiffness about the X-axis decreased in the Etowah County model when the dead load was applied. It is difficult to discern exactly why this occurred. However, one possibility is that the added weight caused the battered piles to be more susceptible to bending. This is because the axial load distributed to the piles increased. For this research, the response curves with dead load applied were applied to the SAP2000 models (Panzer 2013) to more accurately represent foundation behavior.

Chapter 6

DIRECT ANALYSIS RESULTS AND DISCUSSION

The results from the direct analysis of the five bridge case studies are presented. For each bridge, the earthquake time-history used and the displacement at the top of the pier and the head of the shaft or pile footing was recorded. The largest shear force, bending moment, and D/C ratio distribution for a shaft or pile is also presented for one time step. This time step is indicated by a black vertical line on the time-history plots. Note that the D/C ratio is based on the axial-force D/C (which is a function of bending moment). For the failed models, the time step in which these distributions are taken at are not necessarily the last time step before the program terminated. Typically, the last time step before failure is numerically flawed and inconclusive; therefore, the time-step with the next largest shear force and bending moment are shown. This is to give an indication of where the shear forces and bending moments are developing relative to the ground surface or rock line.

There were 17 scaled time-history events used for each bridge case in each direction (longitudinal and transverse): Coalinga North, Imperial Valley NMCE and North, Kobe NMCE and North, Kocaeli NMCE and North, Kocaeli2 NMCE and North, Landers NMCE and North, LSM North, NPS North, San Fernando NMCE and North, and San Fernando2 NMCE and North. All results are presented in Appendix H. The following presents a discussion of each case history and its overall performance, as well as a selection of detailed results and tabular summary for each case history. The case

histories provided did not have liquefaction potential; therefore, a liquefaction case was not explicitly done. However, parallels from the Etowah County case history can be drawn due to the weak insitu soil that the foundations are embedded.

The results overview table indicates how the structure performed based on whether the program converged or not. If the model did not converge, the performance was described as "failed," and a probable cause of failure (structural, soil, or numerical instability) was provided (refer back to section 2.4.1). The time of occurrence that the maximum forces were generated is provided for each model, as well as the location of the maximum values along the shaft, pile, or column to compare to the elevation of the ground surface or pier cap.

6.1 Chambers County 25% Scour Discussion

The Chambers County 25% scour Bridge performed poorly, overall. Most of the failed models were suspected to have failed because of either structural failure or soil failure. Soil failure is likely due to large displacements that the soil spring undergoes. These displacements can become so large that the soil can no longer resist the lateral forces and the out-of-balance forces become extremely large. Referring back to the soil profile for Chambers County (Figure 4.12), the soil layers over rock are relatively weak, which suggests that large displacements at the ground surface are not unlikely to occur. Also, there is an interface of soft and hard soils (as discussed in section 3.1). The maximum bending moments appeared to develop above the rock line, but below the ground surface line. This is important because typically, bridges are detailed to develop a plastic hinge at the ground surface and at the pier cap/column connection because that is inherently the most likely place it will occur. This is to allow enough ductility so the

structure does not collapse (see section 2.1). If damage occurs at those hinge zones, it also allows the damage to be identified and repaired without excavating to the damaged areas. The models that were loaded in the transverse direction generally showed that the largest moment and D/C ratio were at the top of the bent where the column connects to the pier cap. This is a desired plastic hinge zone location. However, large moments and D/C ratios were still developing well below the ground surface, which could possibly develop into plastic hinge zones as well.

It is difficult to discern whether scour, the soft/hard soil interface, or a combination of the two had the most impact of the bridge bent performance. Liquefaction was not taken into account for this model. However, there are two cohesionless layers that could have the potential to liquefy; however, the scouring effect is a similar loss in soil resitance and is compared for the Chambers County 100% scour case, which is in section 6.2. Tables 6.1 and 6.2 show an overview of the results; this includes the location of the maximum shear force, bending moment and D/C ratio along the drilled shaft. The highlighted rows correspond to the selected results shown in Figures 6.1 – 6.4. The ground surface indicates the ground surface after 25% scour. Note that the rock line is approximately at an elevation of 63 feet. The kink that typically occurs around elevation 63 seen in the shear force, bending moment, and D/C distributions indicates this drastic change in soil resistance.

6.1.1 Longitudinal Results

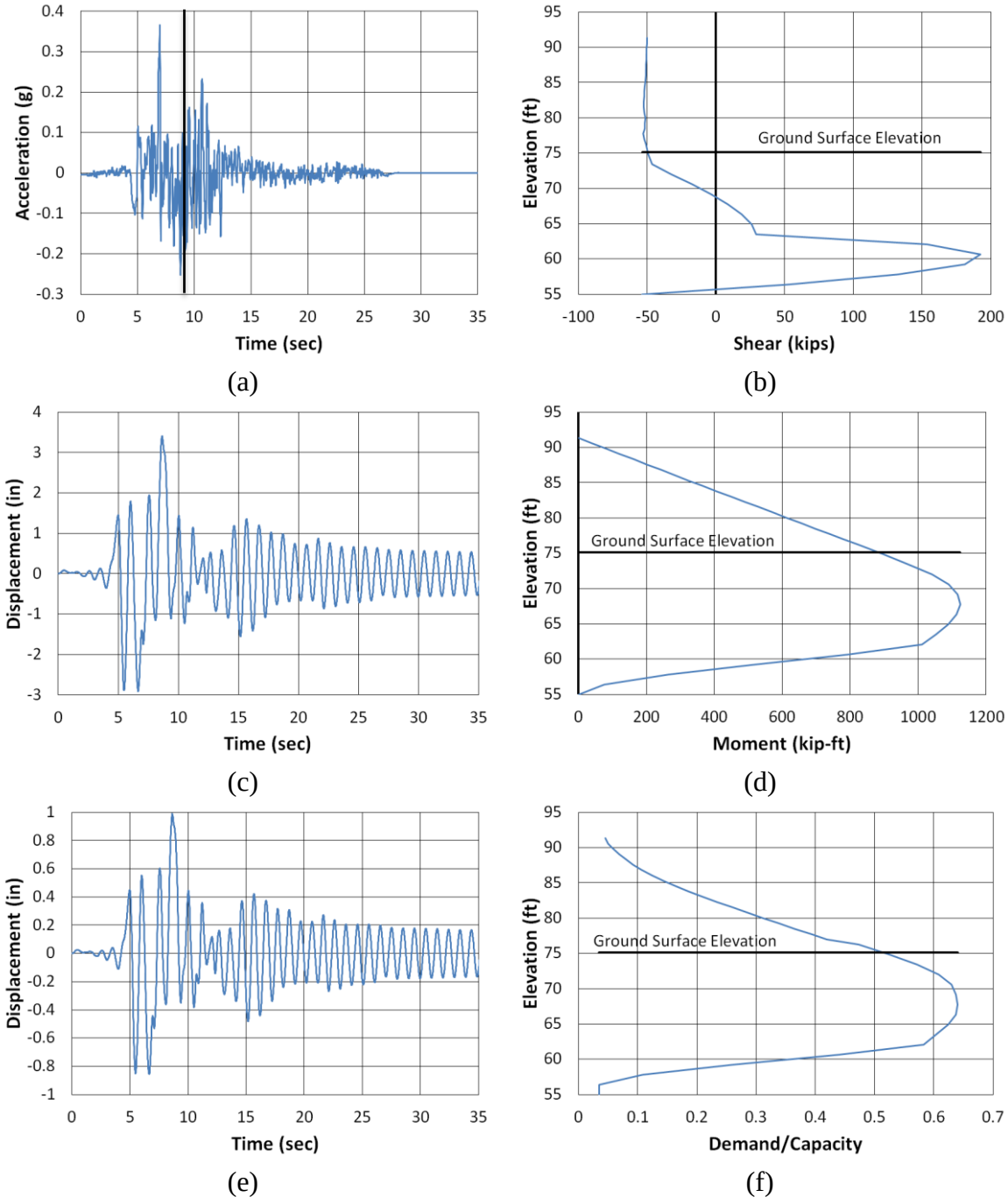

Figure 6.1. Chambers County 25% scour longitudinal Kocaeli2 NMCE (a) time-history event, (b) shear distribution, (c) top of pier displacement, (d) moment distribution, (e) ground surface displacement, and (f) demand capacity ratio

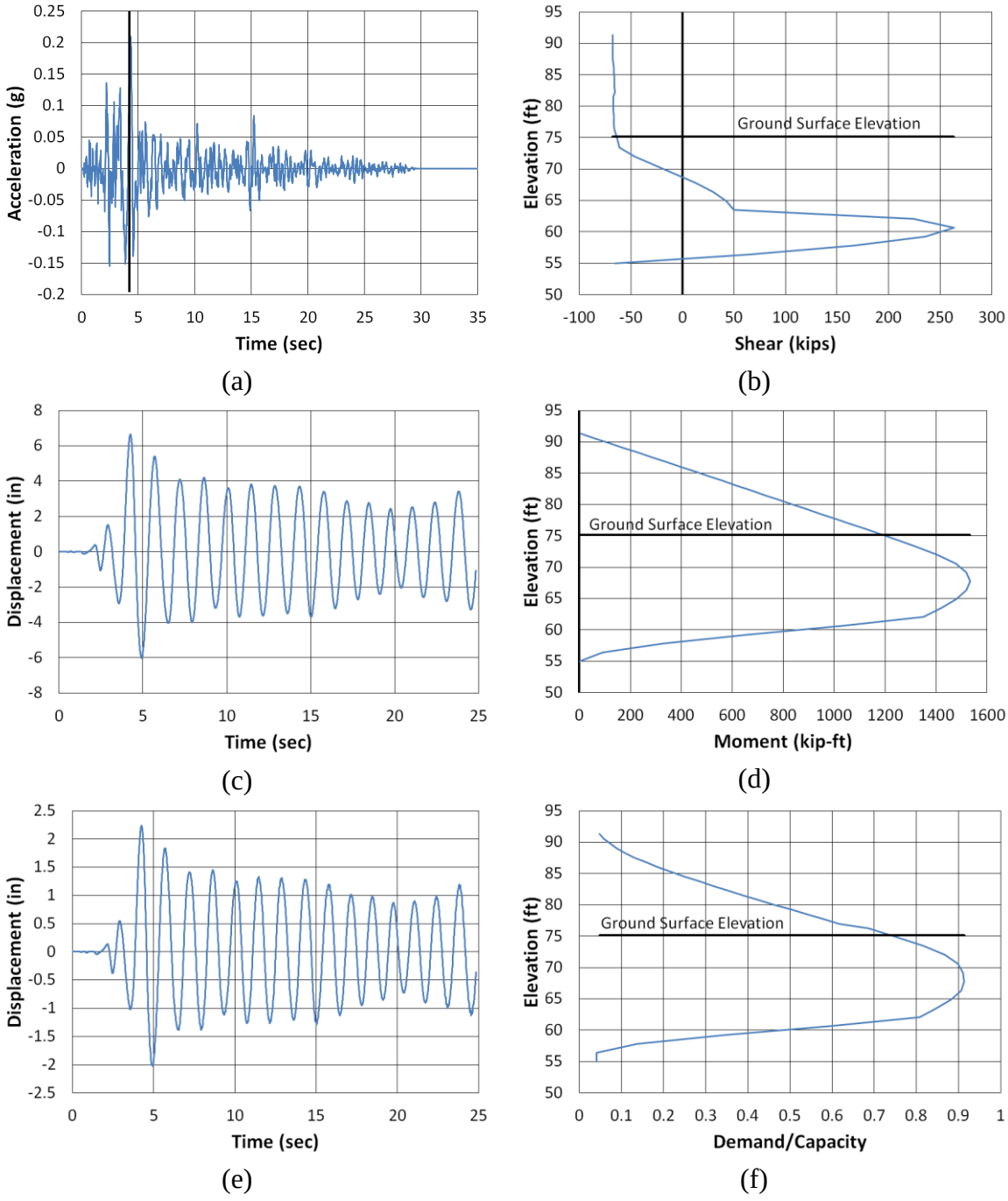

Figure 6.2. Chambers County 25% scour longitudinal San Fernando2 NMCE (a) time-history event, (b) shear distribution, (c) top of pier displacement, (d) moment distribution, (e) ground surface displacement, and (f) demand capacity ratio

Table 6.1 – Results overview for Chambers 25% scour longitudinal models (highlighted ones are shown in Figures 6.1 and 6.2)

Chambers 25% Scour Longitudinal Earthquake Event	Performance	Plastic Hinge Developed	Location of Plastic Hinge (ft)	Probable Cause of Failure	Time of Occurrence (sec)	Maximum Shear (kip)	Elevation of Shear Occurrence (ft)	Maximum Moment (kip-ft)	Elevation of Moment Occurrence (ft)	Maximum D/C Ratio	Elevation of D/C Occurrence (ft)
Coalinga North	Failed	Yes*	77	Structural	24.03	233	61	1409	68	0.83**	68
Imperial Valley NMCE	Failed	Yes	75	Structural	28.85	1344	76	956	77	1.20	73
Imperial Valley North	Failed	Yes*	77	Structural	16.79	241	61	1416	68	0.83**	68
Kobe NMCE	Failed	No	--	Soil	21.05	270	61	1563	68	0.93	68
Kobe North	Failed	No	--	Numerical Instability	10.57	57	77	1213	68	0.70	68
Kocaeli NMCE	Failed	No	--	Soil	26.33	282	61	1635	68	0.97	68
Kocaeli North	Survived	No	--	--	24.4	172	61	991	68	0.56	68
Kocaeli2 NMCE	Survived	No	--	--	8.64	193	61	1123	68	0.64	68
Kocaeli2 North	Survived	No	--	--	6.5	156	61	873	68	0.47	66
Landers NMCE	Failed	No	--	Soil	25.52	280	61	1630	68	0.98	69
Landers North	Failed	No	--	Soil	38.24	234	65	1651	66	0.90	69
LSM North	Failed	Yes*	65	Structural	10.34	141	61	779	66	0.41**	65
NPS North	Survived	No	--	--	7.95	135	61	737	66	0.39	65
SanFernando NMCE	Survived	No	--	--	5.57	282	61	1601	68	0.94	68
SanFernando North	Failed	No	--	Structural	5.43	276	61	1594	68	0.93	68
SanFernando2 NMCE	Failed	Yes*	66	Structural	4.27	263	61	1533	68	0.91**	68
SanFernando2 North	Failed	Yes	73	Structural	4.2	221	61	1284	68	0.75**	68
Percent Survived	29%										

* Plastic Hinge developed at last time step

** D/C ratio not at last time step

6.1.2 Transverse Results

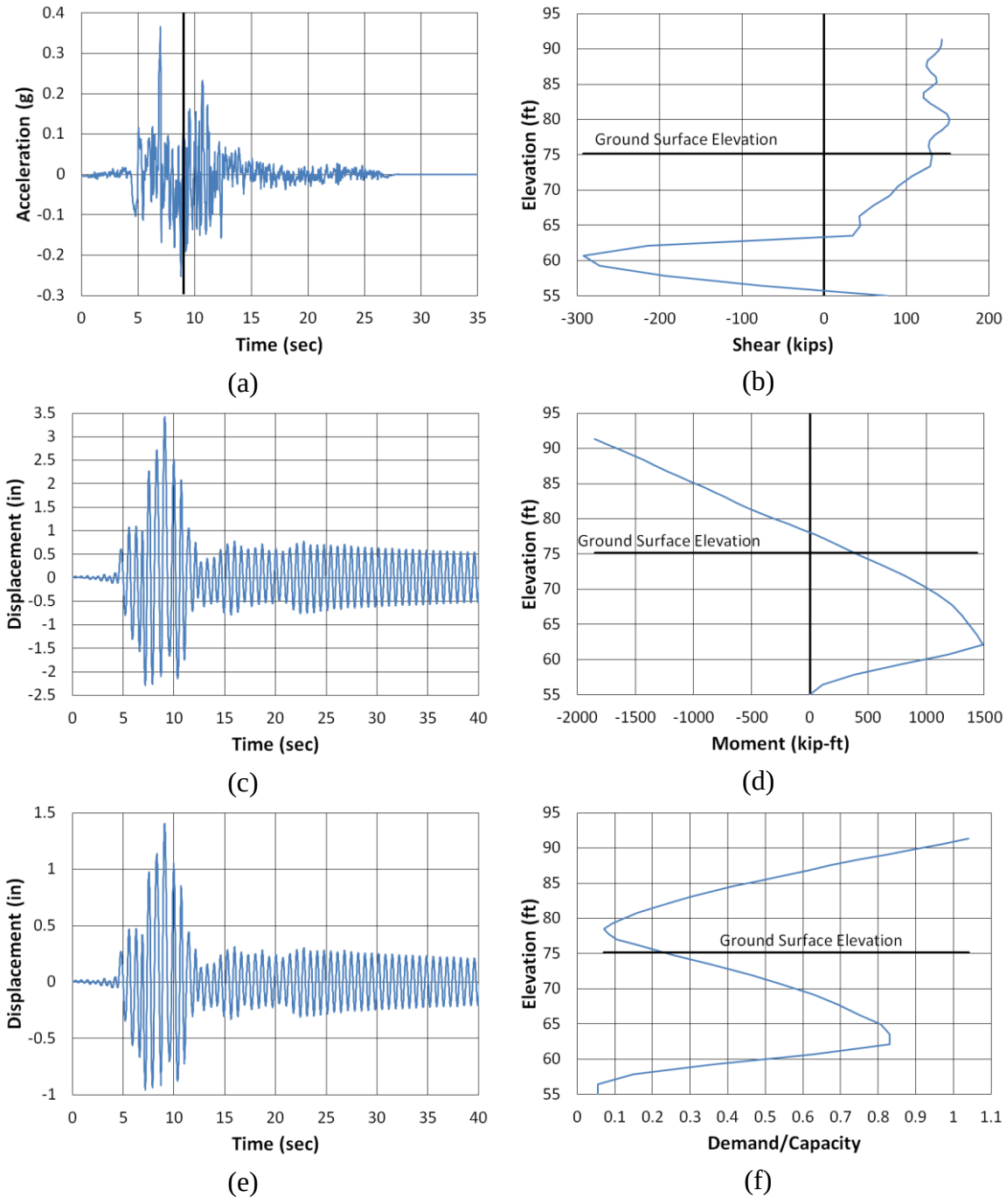

Figure 6.3. Chambers County 25% scour transverse Kocaeli2 NMCE (a) time-history event, (b) shear distribution, (c) top of pier displacement, (d) moment distribution, (e) ground surface displacement, and (f) demand capacity ratio

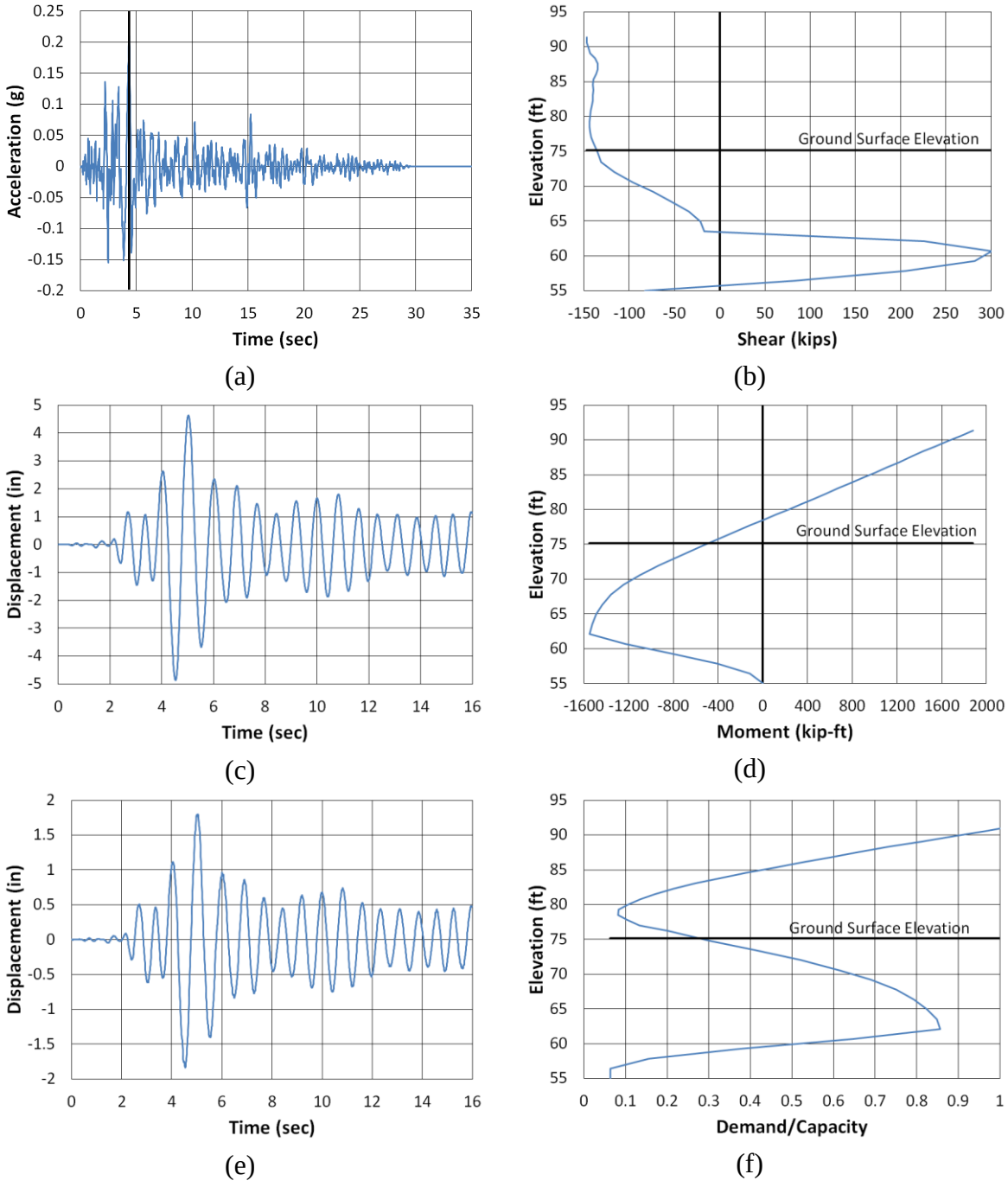

Figure 6.4. Chambers County 25% scour transverse San Fernando2 NMCE (a) time-history event, (b) shear distribution, (c) top of pier displacement, (d) moment distribution, (e) ground surface displacement, and (f) demand capacity ratio

Table 6.2 – Results overview for Chambers 25% scour transverse models (highlighted ones are shown in Figures 6.3 and 6.4)

Chambers 25% Scour Transverse Earthquake Event	Performance	Plastic Hinge Developed	Location of Plastic Hinge (ft)	Probable Cause of Failure	Time of Occurrence (sec)	Maximum Shear (kip)	Elevation of Shear Occurrence (ft)	Maximum Moment (kip-ft)	Elevation of Moment Occurrence (ft)	Maximum D/C Ratio	Elevation of D/C Occurrence (ft)
Coalinga North	Failed	No	--	Structural	10.8	254	61	1757	91	0.98	91
Imperial Valley NMCE	Failed	No	--	Structural	13.97	232	61	1639	91	0.97	91
Imperial Valley North	Failed	No	--	Structural	15.37	197	59	1380	91	0.71	91
Kobe NMCE	Failed	Yes	90*	Structural	8.46	240	61	1747	91	0.95**	91
Kobe North	Survived	No	--	--	6.19	176	59	1195	91	0.61	91
Kocaeli NMCE	Failed	No	--	Structural	29.08	290	61	1811	91	1.03	91
Kocaeli North	Failed	No	--	Structural	29.02	274	61	1826	91	1.04	91
Kocaeli2 NMCE	Survived	No	--	--	9.09	293	61	1851	91	1.04	91
Kocaeli2 North	Failed	No	--	Structural	8.95	261	61	1831	91	1.00	91
Landers N-MCE	Failed	Yes	91	Structural	18.64	265	59	1892	91	1.00	91
Landers North	Failed	No	--	Structural	24.38	222	59	1879	91	0.99	91
LSM North	Survived	No	--	--	15.65	52	59	359	91	0.15	91
NPS North	Failed	No	--	Structural	8.89	242	61	1755	91	0.97	91
SanFernando NMCE	Survived	No	--	--	5	241	61	1674	91	0.92	91
SanFernando North	Failed	No	--	Structural	5.06	250	61	1739	91	0.95	91
SanFernando2 NMCE	Failed	No	--	Structural	4.42	301	61	1878	91	1.04	91
SanFernando2 North	Survived	No	--	--	4.88	286	61	1888	91	1.04	91
Percent Survived	29%										

* Plastic hinge developed at last time step

** D/C ratio not at last time step

6.2 Chambers County 100% Scour Discussion

The Chambers 100% scour model performed well, overall. The three models that failed all used NMCE scaled time-history events, which are of larger magnitude and, typically, more harmful than the North scaled time-histories. The North scaled events are more representative of what the state of Alabama would generally experience.

The 100% scour model performed much better than the 25% scour model (based on structural performance of the bent). This shows the importance of checking both scenarios because it is difficult to determine which case could be worse. Figures 6.5 and 6.6 show the longitudinal Kocaeli2 results for the Chambers 25% and 100% scour cases, respectively. These figures compare the location of the maximum shear forces and bending moments that are developing within the model. It is clear that there is a possibility of plastic hinges developing beneath the ground surface in the 25% scour case; whereas, the plastic hinges would most likely develop at the rock line or slightly above for the 100% scour case.

Table 6.3 presents the results overview of all the longitudinal models, and figures 6.7 and 6.8 show a selection of longitudinal detailed results. The transverse models showed that the hinge zones would most likely develop at the column/pier cap interface or at the rock line. This is important because it shows that the plastic hinge zones are developing at the desired locations. See Table 6.4 for the results overview and figures 6.9 and 6.10 for a selection of transverse detailed results.

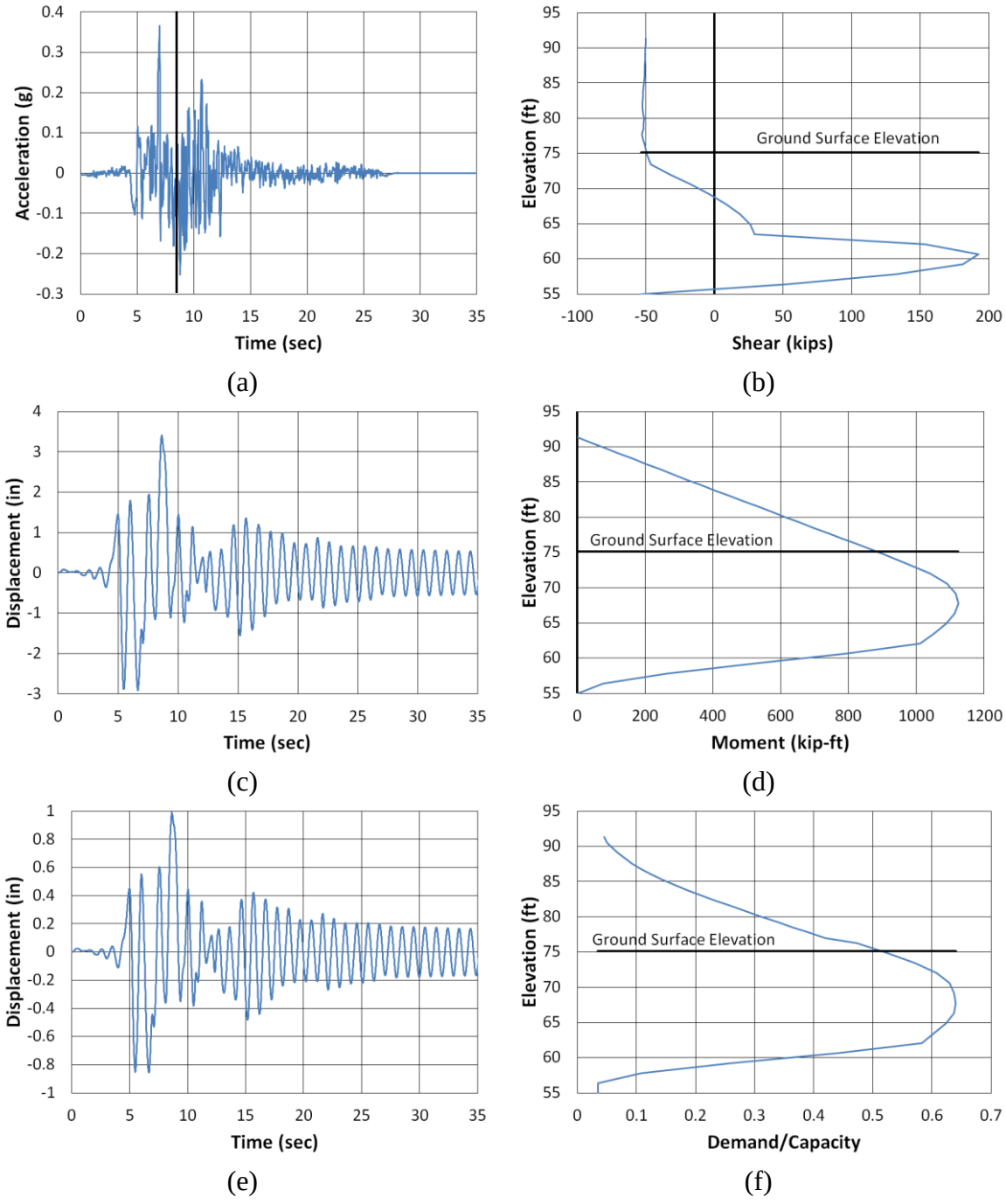

Figure 6.5. Chambers County 25% scour longitudinal Kocaeli2 NMCE (a) time-history event, (b) shear distribution, (c) top of pier displacement, (d) moment distribution, (e) ground surface displacement, and (f) demand capacity ratio

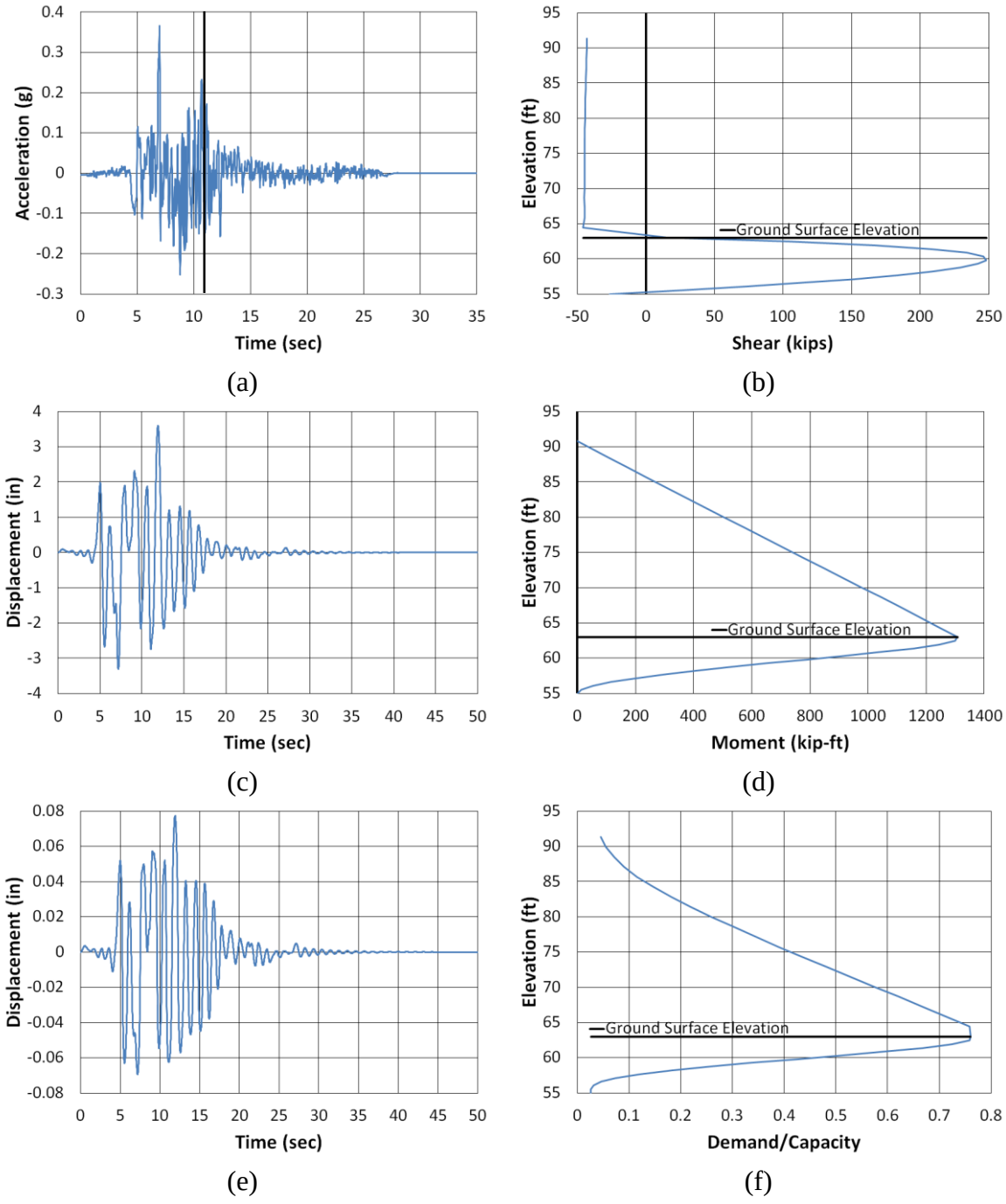

Figure 6.6. Chambers County 100% Scour Longitudinal Kocaeli2 NMCE (a) time-history event, (b) shear distribution, (c) top of pier displacement, (d) moment distribution, (e) ground surface displacement, and (f) demand capacity ratio

6.2.1 Longitudinal Results

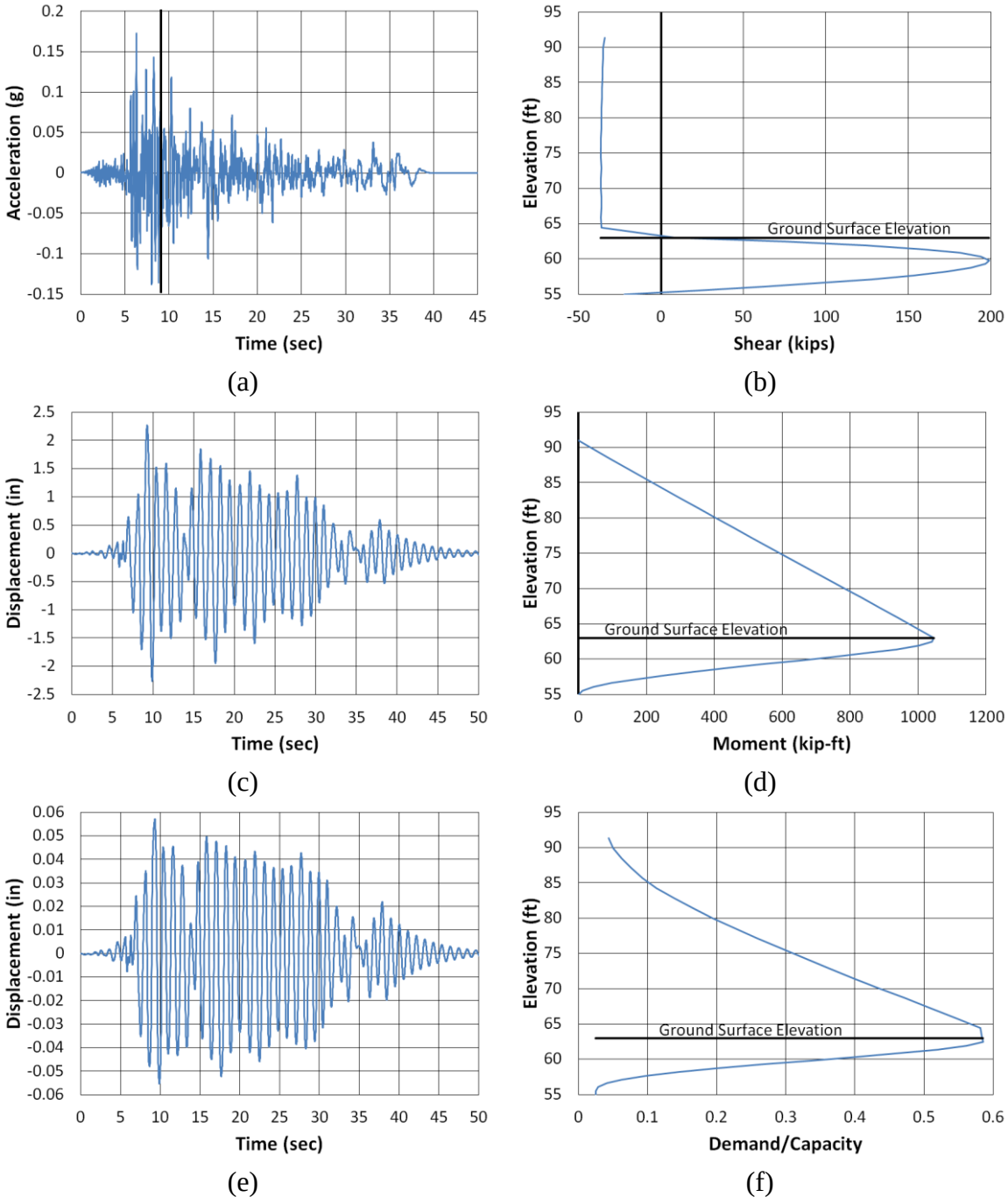

Figure 6.7. Chambers County 100% scour longitudinal Imperial Valley North (a) time-history event, (b) shear distribution, (c) top of pier displacement, (d) moment distribution, (e) ground surface displacement, and (f) demand capacity ratio

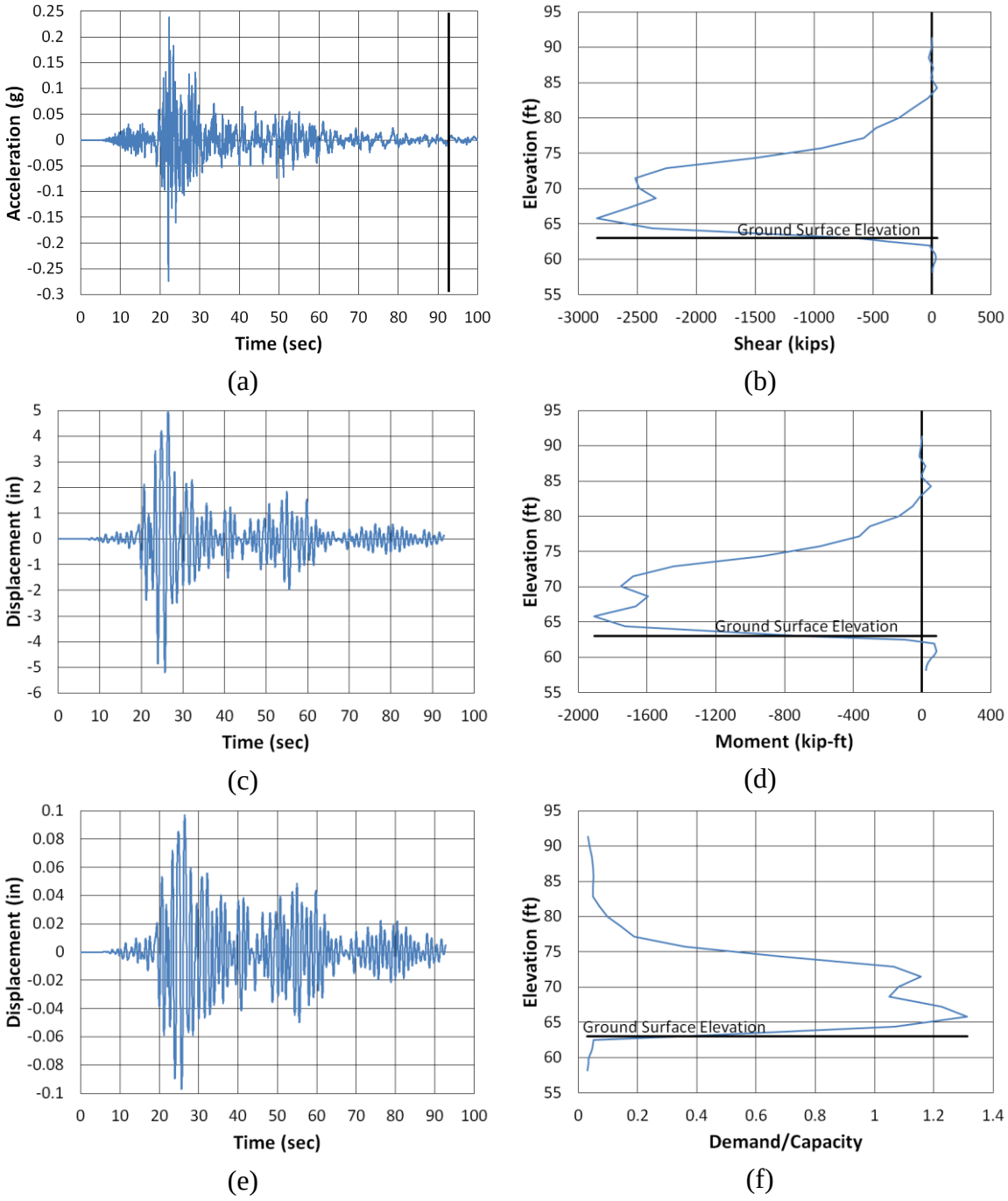

Figure 6.8. Chambers County 100% scour longitudinal Kocaeli NMCE (a) time-history event, (b) shear distribution, (c) top of pier displacement, (d) moment distribution, (e) ground surface displacement, and (f) demand capacity ratio

Table 6.3 – Results overview for Chambers 100% scour longitudinal models (highlighted ones are shown in Figures 6.5 and 6.6)

Chambers 100% Scour Longitudinal Earthquake Event	Performance	Plastic Hinge Developed	Location of Plastic Hinge (ft)	Probable Cause of Failure	Time of Occurrence (sec)	Maximum Shear (kip)	Elevation of Shear Occurrence (ft)	Maximum Moment (kip-ft)	Elevation of Moment Occurrence (ft)	Maximum D/C Ratio	Elevation of D/C Occurrence (ft)
Coalinga North	Survived	No	--	--	12.87	222	60	1165	63	0.67	62
Imperial Valley NMCE	Survived	No	--	--	9.36	226	60	1190	63	0.67	62
Imperial Valley North	Survived	No	--	--	9.29	199	70	1045	63	0.59	62
Kobe NMCE	Survived	No	--	--	10.59	241	60	1265	63	0.74	63
Kobe North	Survived	No	--	--	7.22	185	60	971	63	0.52	62
Kocaeli NMCE	Failed	Yes	65.83	Structural	92.82	2848	66	1908	66	1.31	66
Kocaeli North	Survived	No	--	--	24.44	211	60	1111	63	0.62	62
Kocaeli2 NMCE	Survived	No	--	--	11.91	248	60	1308	63	0.76	63
Kocaeli2 North	Survived	No	--	--	5.47	179	60	941	63	0.51	62
Landers NMCE	Survived	No	--	--	25.38	292	60	1534	63	0.91	63
Landers North	Survived	No	--	--	24.42	259	60	1364	63	0.80	63
LSM North	Survived	No	--	--	10.9	81	59	419	63	0.17	62
NPS North	Survived	No	--	--	7.96	145	60	755	63	0.40	62
SanFernando NMCE	Survived	No	--	--	7.68	293	60	1555	63	0.92	63
SanFernando North	Survived	No	--	--	7.66	286	60	1500	63	0.91	63
SanFernando2 NMCE	Survived	No	--	--	4.26	296	60	1556	63	0.93	63
SanFernando2 North	Survived	No	--	--	4.23	261	60	1376	63	0.80	63
Percent Survived	94.12%										

6.2.2 Transverse Results

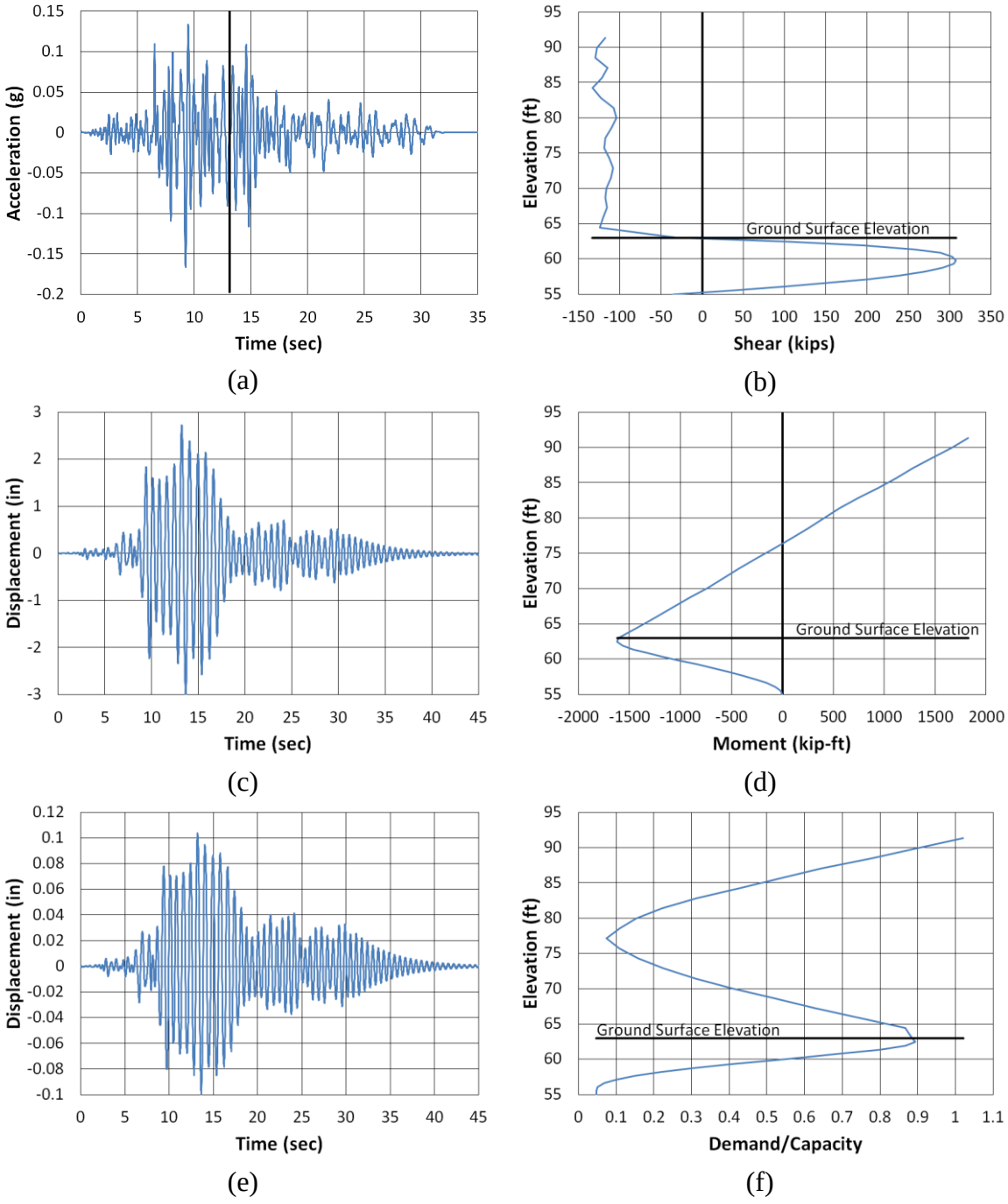

Figure 6.9. Chambers County 100% scour transverse Coalinga North (a) time-history event, (b) shear distribution, (c) top of pier displacement, (d) moment distribution, (e) ground surface displacement, and (f) demand capacity ratio

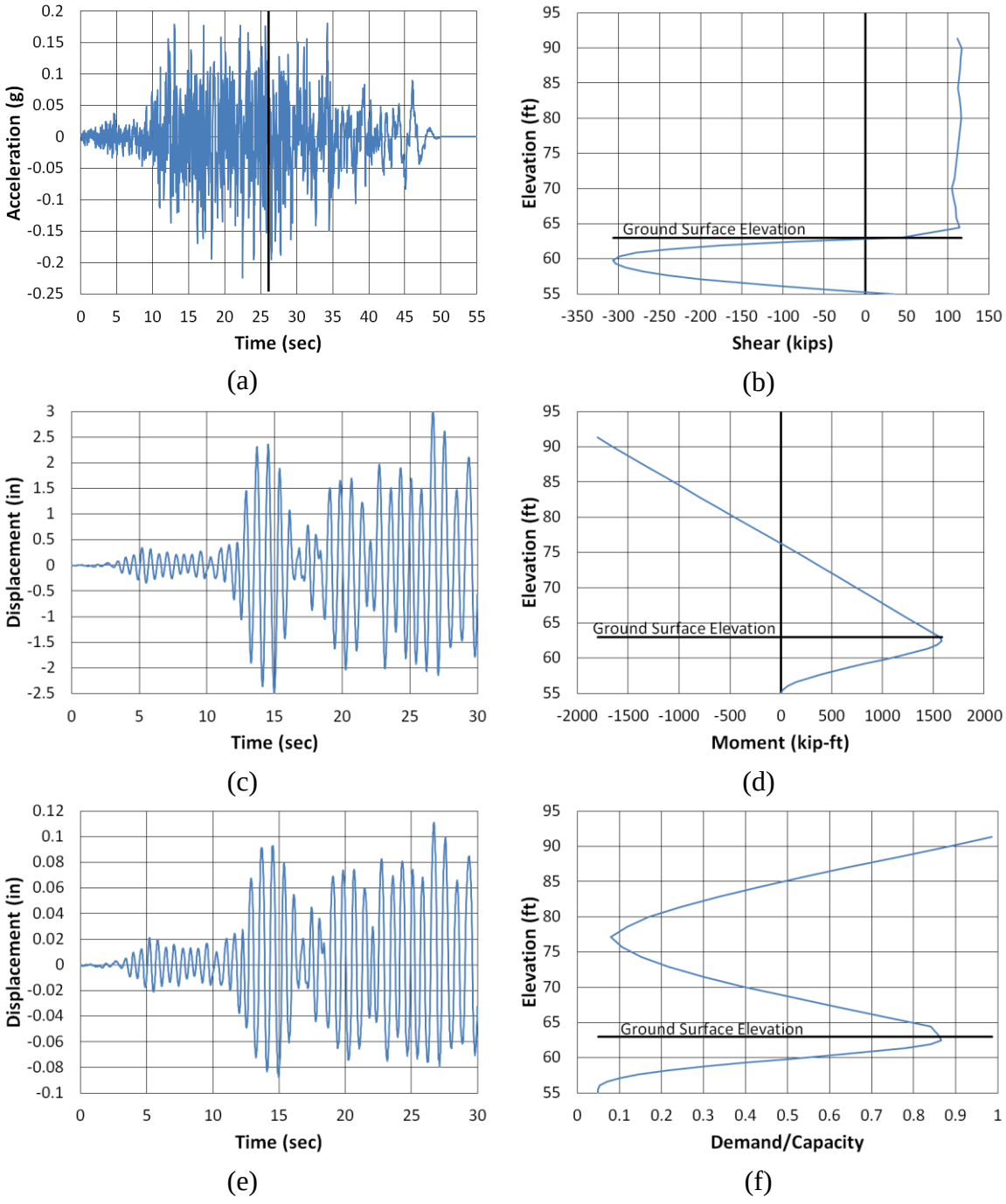

Figure 6.10. Chambers County 100% scour transverse Landers NMCE (a) time-history event, (b) shear distribution, (c) top of pier displacement, (d) moment distribution, (e) ground surface displacement, and (f) demand capacity ratio

Table 6.4 – Results overview for Chambers 100% Scour transverse models (highlighted ones are shown in Figures 6.7 and 6.8)

Chambers 100% Scour Transverse Earthquake Event	Performance	Plastic Hinge Developed	Location of Plastic Hinge (ft)	Probable Cause of Failure	Time of Occurrence (sec)	Maximum Shear (kip)	Elevation of Shear Occurrence (ft)	Maximum Moment (kip-ft)	Elevation of Moment Occurrence (ft)	Maximum D/C Ratio	Elevation of D/C Occurrence (ft)
Coalinga North	Survived	No	--	--	13.64	308	60	1824	91	1.02	91
Imperial Valley NMCE	Survived	No	--	--	10.52	272	60	1618	91	0.89	91
Imperial Valley North	Survived	No	--	--	10.42	229	59	1295	91	0.67	91
Kobe NMCE	Survived	No	--	--	11.04	238	60	1381	91	0.75	91
Kobe North	Survived	No	--	--	6.26	192	59	1076	91	0.57	91
Kocaeli NMCE	Failed	No	--	Structural	22.65	329	60	1822	91	1.06	91
Kocaeli North	Survived	No	--	--	29.87	263	60	1565	91	0.87	91
Kocaeli2 NMCE	Survived	No	--	--	8.99	287	60	1642	91	0.91	91
Kocaeli2 North	Survived	No	--	--	8.99	249	60	1422	91	0.76	91
Landers NMCE	Failed	No	--	Structural	26.66	307	60	1802	91	0.99	91
Landers North	Survived	No	--	--	20.32	248	59	1419	91	0.77	91
LSM North	Survived	No	--	--	5.05	51	59	292	91	0.11	91
NPS North	Survived	No	--	--	8.54	239	60	1418	91	0.78	91
SanFernando NMCE	Survived	No	--	--	2.81	209	59	1203	91	0.61	91
SanFernando North	Survived	No	--	--	4.98	214	59	1221	91	0.65	91
SanFernando2 NMCE	Survived	No	--	--	4.51	346	60	1899	91	1.05	91
SanFernando2 North	Survived	No	--	--	4.89	319	60	1816	91	1.01	91
Percent Survived	88%										

6.3 Etowah County Discussion

The Etowah County bridge models performed poorly. Moreover, the piles were the main cause of failure. See Table 6.7 and 6.8 for an overview of the longitudinal and transverse results, respectively. The models suggested that the piles were failing in bending. This is thought to be a buckling problem due to several factors. The length of the piles was approximately 60 feet (including embedment into the pile cap) and the width of the pile is only 12.045 inches. Referring back to Figure 4.20 in Chapter 4, the soil profile of Etowah County, it is apparent that the insitu soils are relatively weak (shear strength is 700 psf or less in lower layers). There is also a void layer that is almost 15 feet in depth, which does not provide any lateral resistance.

To determine if the problem is, in fact, most likely buckling, equation 3.1, presented in Chapter 3, was used to check Bhattacharya's (2003) recommendation that a P_{des}/P_{cr} ratio of greater than 0.5 indicated that buckling may be an issue. Table 6.5 shows the assumptions made to calculate the ratios.

Table 6.5 – Assumptions used in buckling analysis for Etowah County

L_{eff}	100	ft
E	29000	ksi
I	393	in^4
Section Area of H-pile	15.5	in^2
P_{cr}	78	kips
r_{min}	5.04	in
P_{column}	680	kips/column
No. of piles/column	7	
$FS_{(assumed)}$	2	
P_{des}/pile	194	kips

L_{eff} was determined based on the assumption that the pile is pinned at the rock line and fixed at the pile cap. Therefore, the depth of the soft soil region, which was

estimated as roughly 50 feet, was multiplied by a factor of 2 to estimate the effective length. The largest moment of inertia was used because the bending was about the axis it was calculated. This also was a conservative assumption. The load per column was based on the dead loads from the bridge deck. The load of the pier cap, column, and pile cap were not included as it only increased the P_{des}/P_{cr} ratio. A pile efficiency of one was assumed for each pile. Table 6.6 summarizes the calculations made.

Table 6.6 – Etowah County P_{des}/P_{cr} and L_{eff}/r_{min} results

P_{des}/P_{cr}	2.49
L_{eff}/r_{min}	238

Based from these calculations, buckling is most likely the main cause for pile failure for the Etowah County bridge models. It is also important to note that the transverse models were failing about the same axis as the longitudinal models. This suggests that it was failing regardless of which direction the load function was applied. Figure 6.11 shows the pile number layout for the model. Figures 6.12 – 6.14 show the displacements at the top of the pier and pile cap, along with the shear force, bending moment and D/C ratio distributions for the length of the pile. Note that these distributions are all below the ground surface. Figure 6.15 shows the displacement at the top of the pier and pile cap, as well as the shear force, bending moment, and D/C ratio distribution along the length of the column.

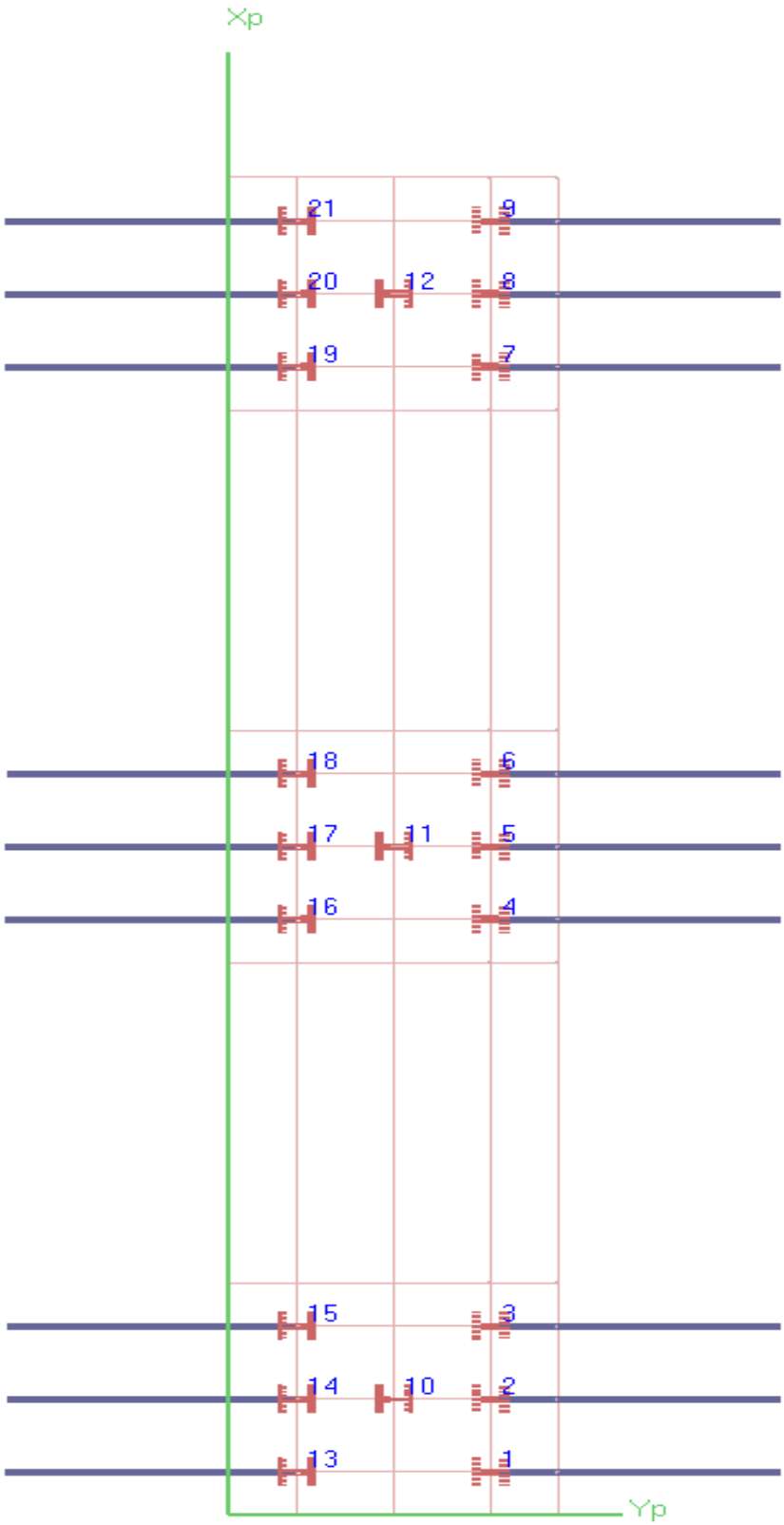

Figure 6.11. Etowah County FB-MultiPier pile number layout

6.3.1 Longitudinal Results

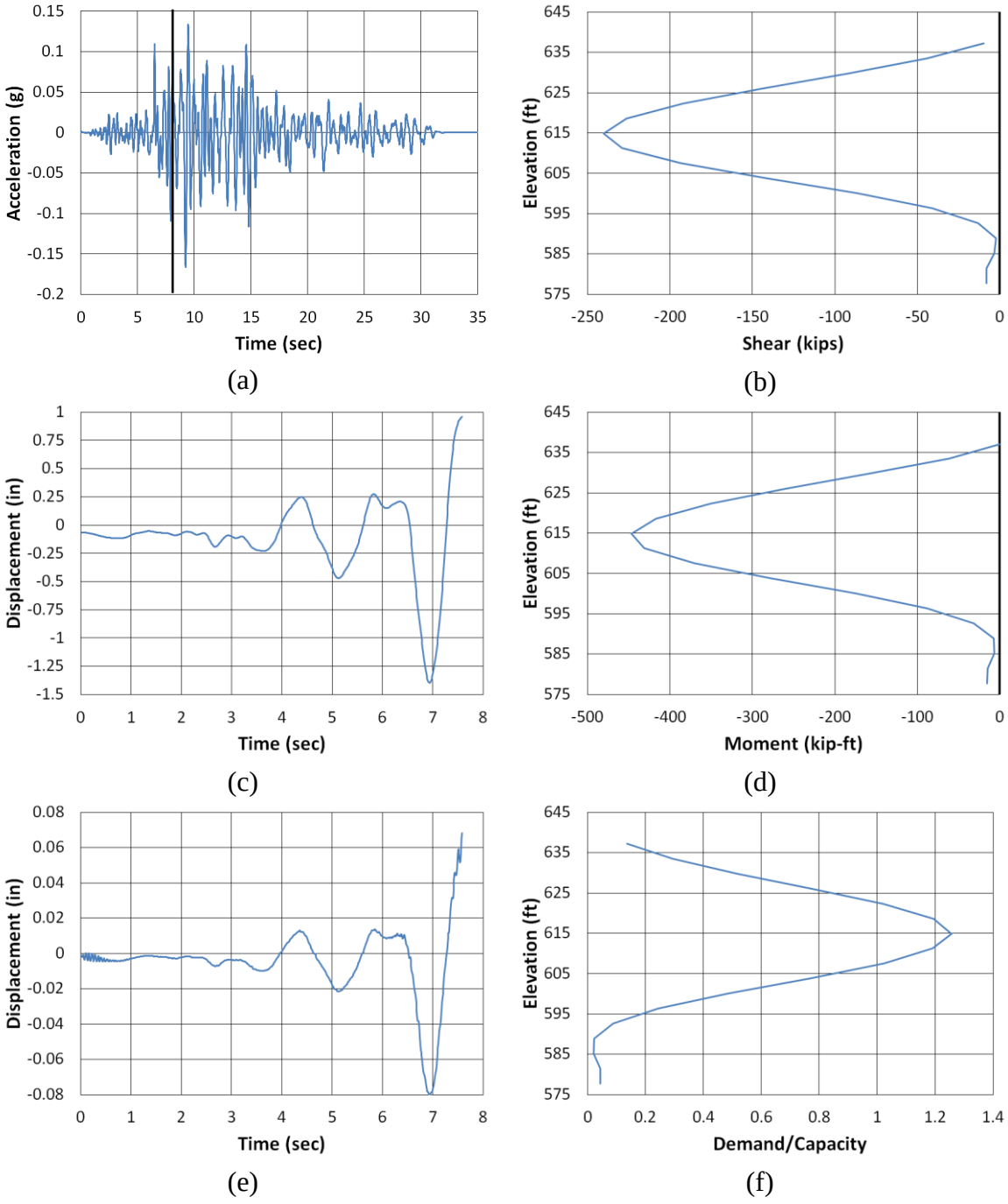

Figure 6.12. Etowah County longitudinal Coalinga North (a) time-history event, (b) shear distribution, (c) top of pier displacement, (d) moment distribution, (e) ground surface displacement, and (f) demand capacity ratio

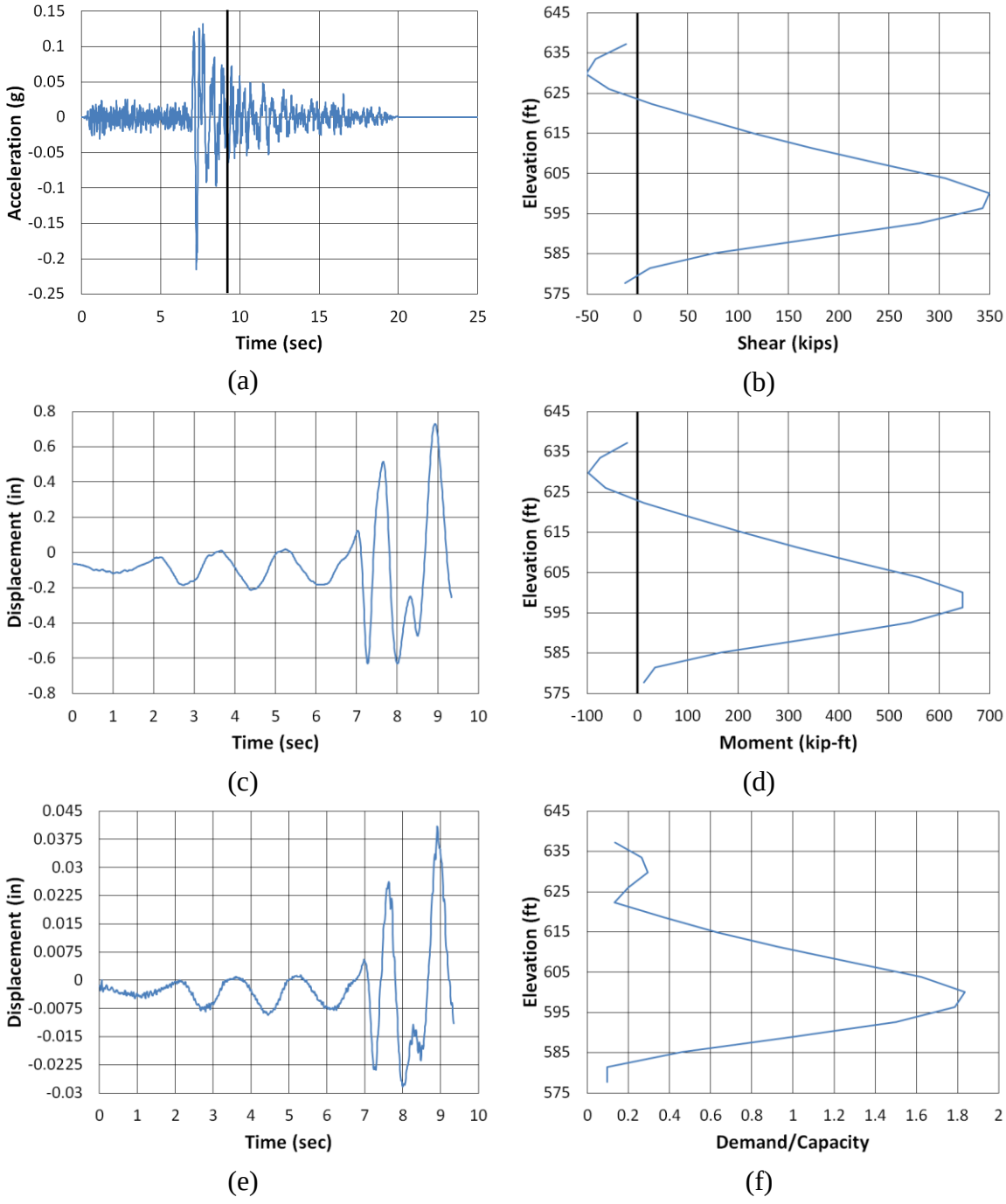

Figure 6.13. Etowah County longitudinal NPS North (a) time-history event, (b) shear distribution, (c) top of pier displacement, (d) moment distribution, (e) ground surface displacement, and (f) demand capacity ratio

Table 6.7 – Results overview for Etowah County longitudinal models (highlighted ones are shown in Figures 6.9 and 6.10)

Etowah Longitudinal Earthquake Event	Performance	Plastic Hinge Developed	Location of Plastic Hinge (ft)	Pile No.	Probable Cause of Failure	Time of Occurrence (sec)	Maximum Shear (kip)	Elevation of Shear Occurrence (ft)	Maximum Moment (kip-ft)	Elevation of Moment Occurrence (ft)	Maximum D/C Ratio	Elevation of D/C Occurrence (ft)
Coalinga North	Failed	Yes	615	14	Structural	7.58	240	615	447	615	1.26	615
Imperial Valley NMCE	Failed	Yes	600	9	Structural	9.17	329	600	608	596	1.74	600
Imperial Valley North	Failed	Yes	596	6	Structural	9.26	339	596	649	596	1.80	596
Kobe N-MCE	Failed	Yes	615	14	Structural	7.69	347	615	650	615	1.80	615
Kobe North	Failed	No	--	--	Structural	6.51	54	581	361	585	1.00	585
Kocaeli NMCE	Failed	Yes	600	7	Structural	9.45	353	600	658	600	1.85	600
Kocaeli North	Failed	Yes	615	1	Structural	9.34	328	615	619	615	1.72	615
Kocaeli2 N-MCE	Failed	Yes	615	14	Structural	7.86	-359	615	-672	615	1.86	615
Kocaeli2 North	Failed	Yes	615	18	Structural	7.74	323	615	602	615	1.70	615
Landers N-MCE	Failed	No	--	--	Structural	28.26	30	581	346	589	0.97	589
Landers North	Failed	No	--	--	Structural	22.8	36	581	332	589	0.93	589
LSM North	Failed	Yes	615	14	Structural	7.77	330	615	622	615	1.72	615
NPS North	Failed	Yes	600	7	Structural	9.34	350	600	647	600	1.84	600
SanFernando NMCE	Failed	Yes	596	9	Structural	9.1	352	596	663	596	1.84	596
SanFernando North	Failed	Yes	611	14	Structural	7.61	308	611	596	611	1.66	611
SanFernando2 N-MCE	Failed	Yes	615	14	Structural	7.84	359	615	676	615	1.87	615
SanFernando2 North	Failed	Yes	615	14	Structural	7.89	360	615	673	615	1.87	615
Percent Survived	0%											

6.3.2 Transverse Results

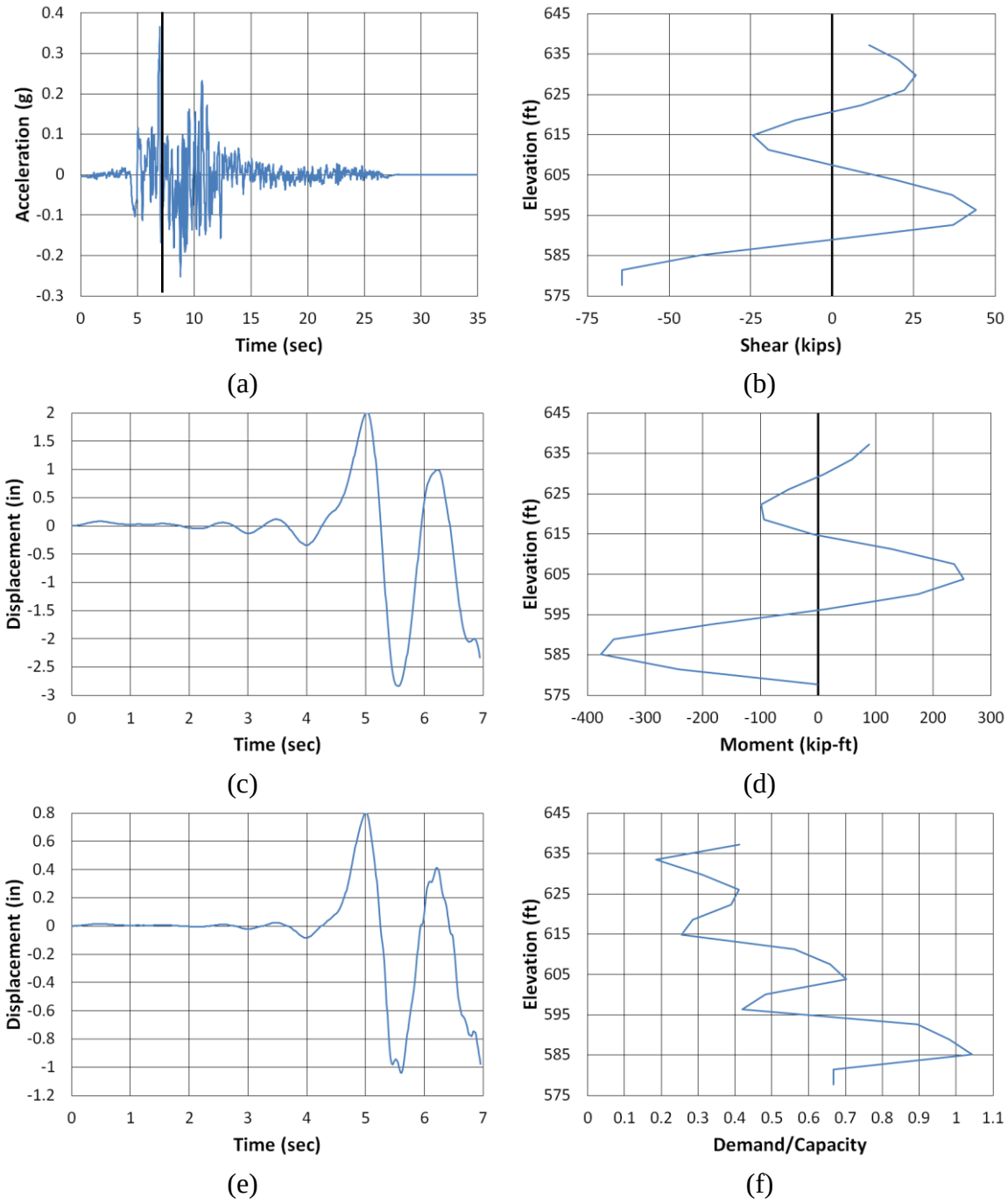

Figure 6.14. Etowah County transverse Kocaeli2 NMCE (a) time-history event, (b) shear distribution, (c) top of pier displacement, (d) moment distribution, (e) ground surface displacement, and (f) demand capacity ratio

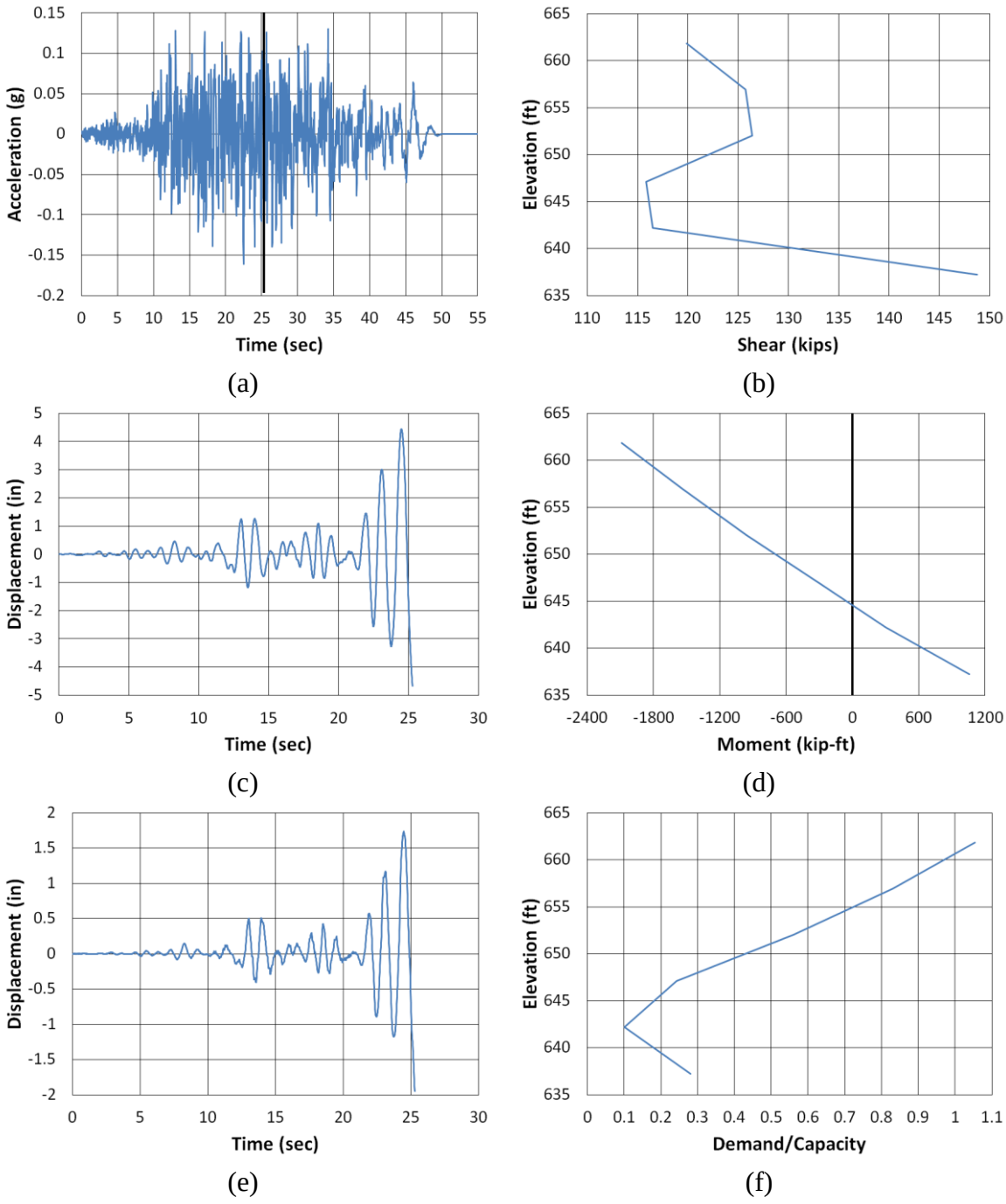

Figure 6.15. Etowah County transverse Landers North (column) (a) time-history event, (b) shear distribution, (c) top of pier displacement, (d) moment distribution, (e) ground surface displacement, and (f) demand capacity ratio

Table 6.8 – Results overview for Etowah County transverse models (highlighted ones are shown in Figures 6.12 and 6.13)

Etowah Transverse Earthquake Event	Performance	Plastic Hinge Developed	Location of Plastic Hinge (ft)	Pile/Column No.	Probable Cause of Failure	Time of Occurrence (sec)	Maximum Shear (kip)	Elevation of Shear Occurrence (ft)	Maximum Moment (kip-ft)	Elevation of Moment Occurrence (ft)	Maximum Demand Capacity Ratio	Elevation of D/C Occurrence (ft)
Coalinga North	Failed	Yes	615	16	Structural	7.8	331	615	607	615	1.76	615
Imperial Valley NMCE	Failed	Yes	600	7	Structural	9.24	333	596	622	596	1.75	600
Imperial Valley North	Failed	Yes	600	6	Structural	9.24	335	600	618	600	1.77	600
Kobe NMCE	Failed	Yes	585	4	Structural	6.54	62	581	366	585	1.01	585
Kobe North	Failed	No	--	--	Structural	6.7	39	581	357	589	0.99	589
Kocaeli NMCE	Failed	Yes	596	7	Structural	9.4	348	596	656	596	1.82	596
Kocaeli North	Failed	Yes	615	1	Structural	9.38	349	615	656	615	1.82	614
Kocaeli2 NMCE	Failed	Yes	585	3	Structural	6.95	64	681	377	585	1.04	585
Kocaeli2 North	Failed	Yes	615	17	Structural	7.76	311	615	573	615	1.64	615
Landers NMCE	Failed	No	--	--	Structural	25.8	43	581	343	589	0.96	589
Landers North	Column Failed	Yes	667	3	Structural (column)	25.28	149	637	2088	662	1.05	662
LSM North	Failed	Yes	615	14	Structural	7.68	325	615	607	615	1.70	615
NPS North	Failed	Yes	600	7	Structural	9.35	345	600	646	600	1.79	600
SanFernando NMCE	Failed	Yes	596	1	Structural	9.16	331	596	631	596	1.75	596
SanFernando North	Failed	Yes	615	17	Structural	7.63	335	615	627	615	1.75	615
SanFernando2 NMCE	Failed	Yes	615	18	Structural	7.69	292	615	540	619	1.66	615
SanFernando2 North	Failed	Yes	615	21	Structural	7.55	219	615	336	622	1.50	615
Percent Survived	0%											

6.4 Franklin County Discussion

The Franklin county bridge models performed fair, overall. Most of the models that failed were NMCE earthquake events, which are the higher magnitude events. See Table 6.9 and 6.10 for the longitudinal and transverse results, repsectively. Figures 6.16 – 6.19 present a selection of detailed results. Only one model (San Fernando2 NMCE Longitudinal) showed a plastic hinge developing due to structural failure (see Figure 6.17). Note that the change in D/C ratio distribution at elevation 530 feet is due to the change in shaft size, which is consistent with what is to be expected (lower capacity for a smaller shaft size). When the model does not show a plastic hinge zone developing in the last time step before it fails, it is difficult to discern whether the failure was structural, or numerical. Soil failure is unlikely because the drilled shafts are embedded into bedrock. If the last time step shows large bending moments and shear forces, and D/C ratios are approaching one, then structural failure may be a likely cause that the model failed. Otherwise, it could be due to numerical instability within the model. However, the bending moment and D/C ratio distributions for Franklin County show that if the structure does fail, it is likely the failure will occur in the desired plastic hinge zones and not in the foundations. Liquefaction was not taken into account for this model because of the thin layer of soil over bedrock.

6.4.1 Longitudinal Results

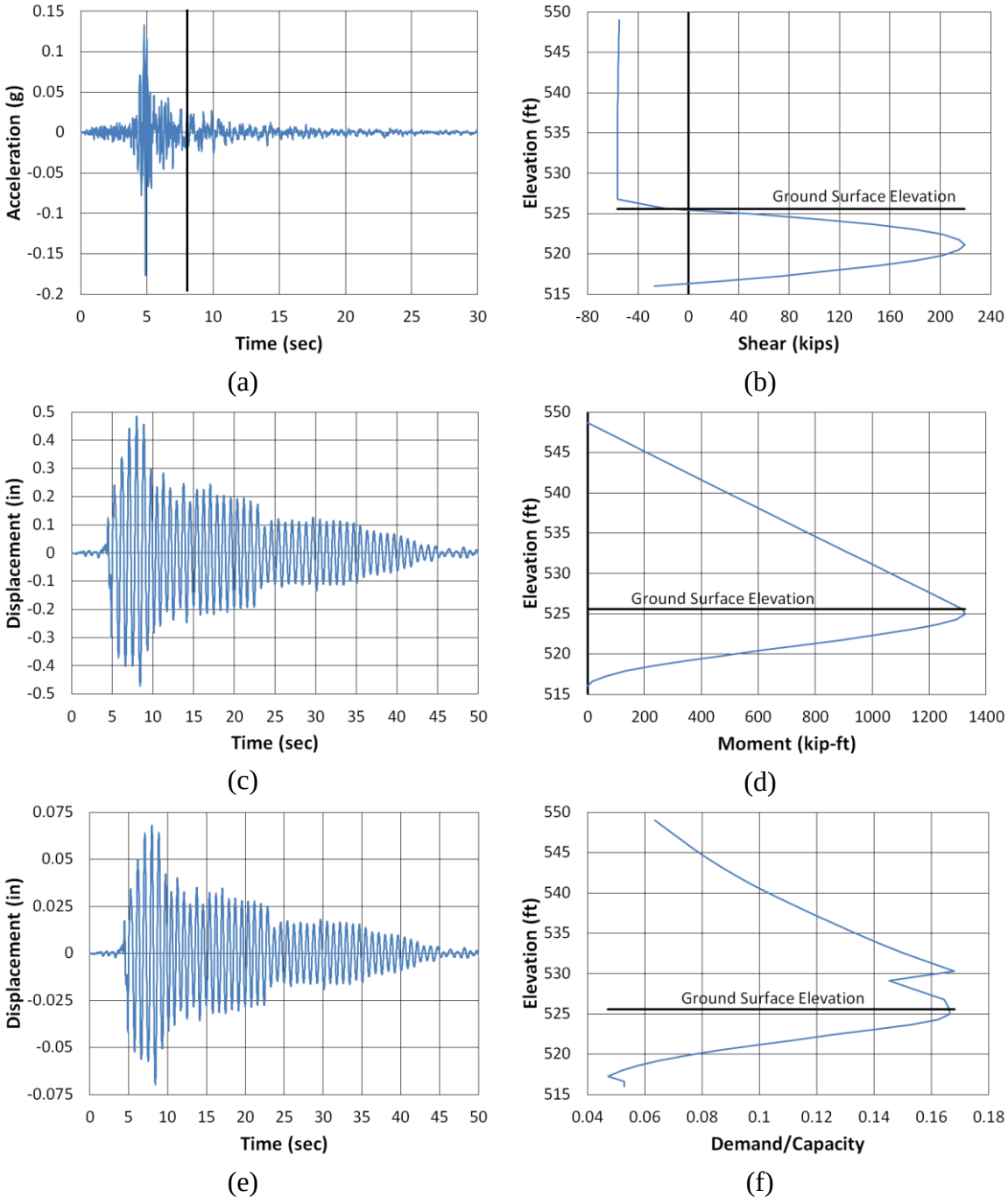

Figure 6.16. Franklin County longitudinal LSM North (a) time-history event, (b) shear distribution, (c) top of pier displacement, (d) moment distribution, (e) ground surface displacement, and (f) demand capacity ratio

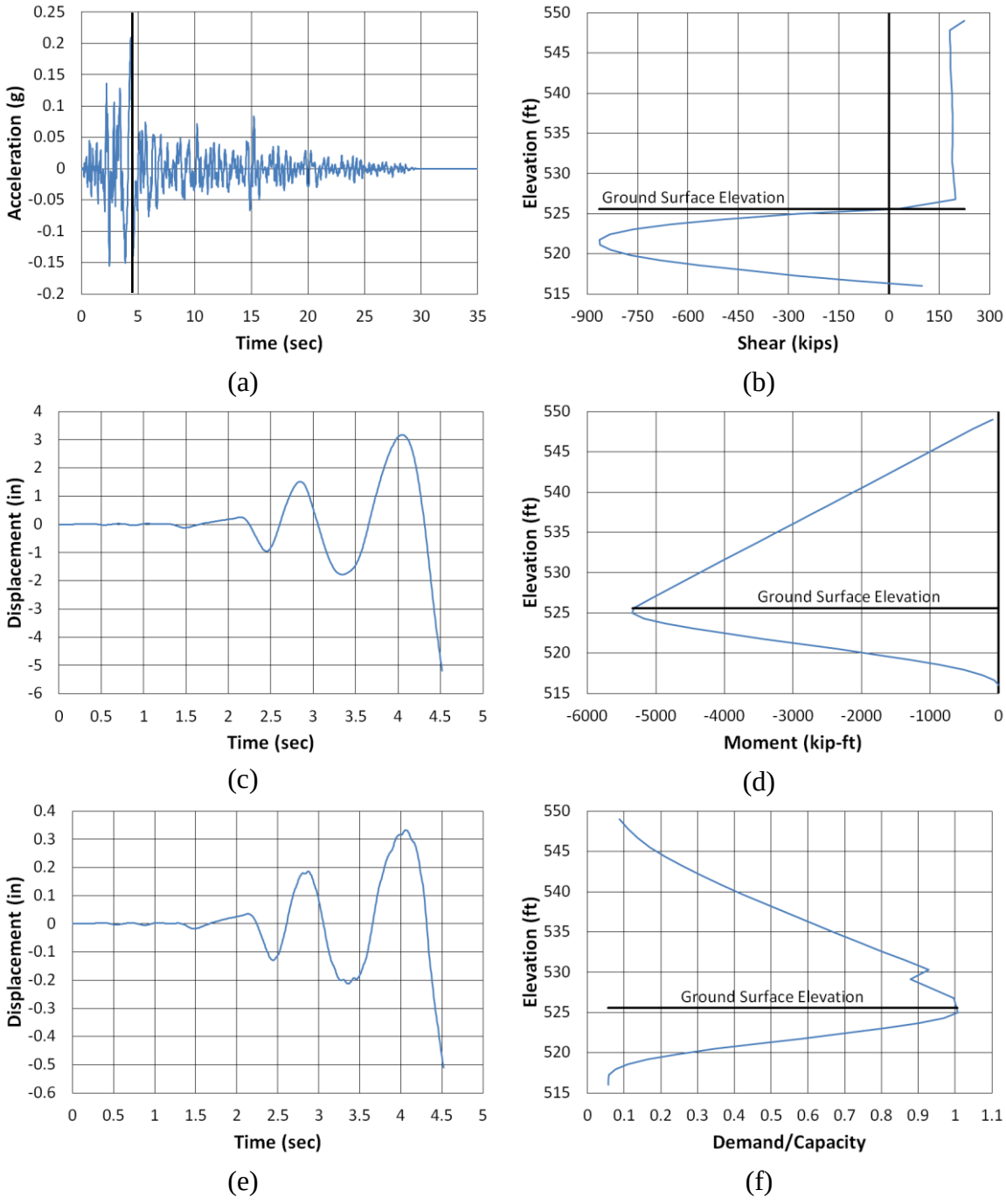

Figure 6.17. Franklin County longitudinal San Fernando2 NMCE (a) time-history event, (b) shear distribution, (c) top of pier displacement, (d) moment distribution, (e) ground surface displacement, and (f) demand capacity ratio

Table 6.9 – Results overview for Franklin County longitudinal models (highlighted ones are shown in Figures 6.14 and 6.15)

Franklin Longitudinal Earthquake Event	Performance	Plastic Hinge Developed	Location of Plastic Hinge (ft)	Probable Cause of Failure	Time of Occurrence (sec)	Maximum Shear (kip)	Elevation of Shear Occurrence (ft)	Maximum Moment (kip-ft)	Elevation of Moment Occurrence (ft)	Maximum D/C Ratio	Elevation of D/C Occurrence (ft)
Coalinga North	Survived	No	--	--	24.79	518	522	3138	525	0.54	526
Imperial Valley NMCE	Failed	No	--	Structural	15.77	865	522	5300	525	1.00	525
Imperial Valley North	Survived	No	--	--	21.14	423	521	2563	525	0.41	525
Kobe NMCE	Failed	No	--	Structural	13.08	823	522	5069	525	0.92	525
Kobe North	Survived	No	--	--	11.76	565	521	3450	525	0.58	525
Kocaeli NMCE	Failed	No	--	Structural	23.89	845	522	5238	525	0.99	525
Kocaeli North	Failed	No	--	Structural	23.88	826	522	5107	525	0.96	525
Kocaeli2 NMCE	Survived	No	--	--	7.28	729	522	4505	525	0.91	525
Kocaeli2 North	Survived	No	--	--	7.24	767	521	4729	525	0.90	525
Landers NMCE	Failed	No	--	Structural	22.98	868	521	5394	525	0.99	525
Landers North	Failed	No	--	Structural	23.44	845	522	5142	525	0.94	525
LSM North	Survived	No	--	--	7.99	219	521	1326	525	0.17	530
NPS North	Survived	No	--	--	8.34	486	521	2960	525	0.50	525
SanFernando NMCE	Survived	No	--	--	9.19	845	521	5215	525	0.99	525
SanFernando North	Survived	No	--	--	9.04	724	521	4473	525	0.90	525
SanFernando2 NMCE	Failed	Yes	525	Structural	4.52	864	521	5341	525	1.01	525
SanFernando2 North	Survived	No	--	--	6.25	756	522	4692	525	0.97	525
Percent Survived	59%										

6.4.2 Transverse Results

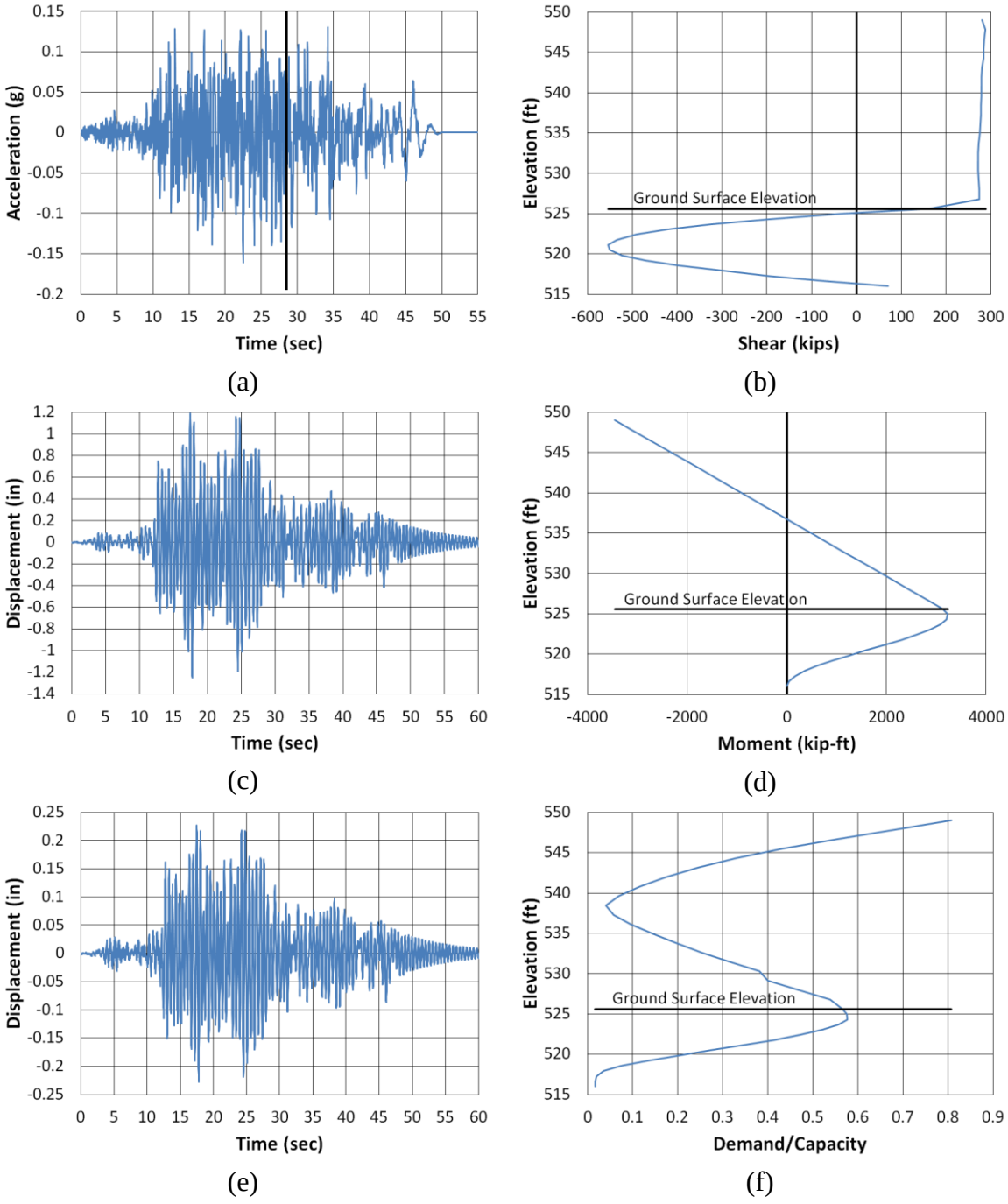

Figure 6.18. Franklin County transverse Landers North (a) time-history event, (b) shear distribution, (c) top of pier displacement, (d) moment distribution, (e) ground surface displacement, and (f) demand capacity ratio

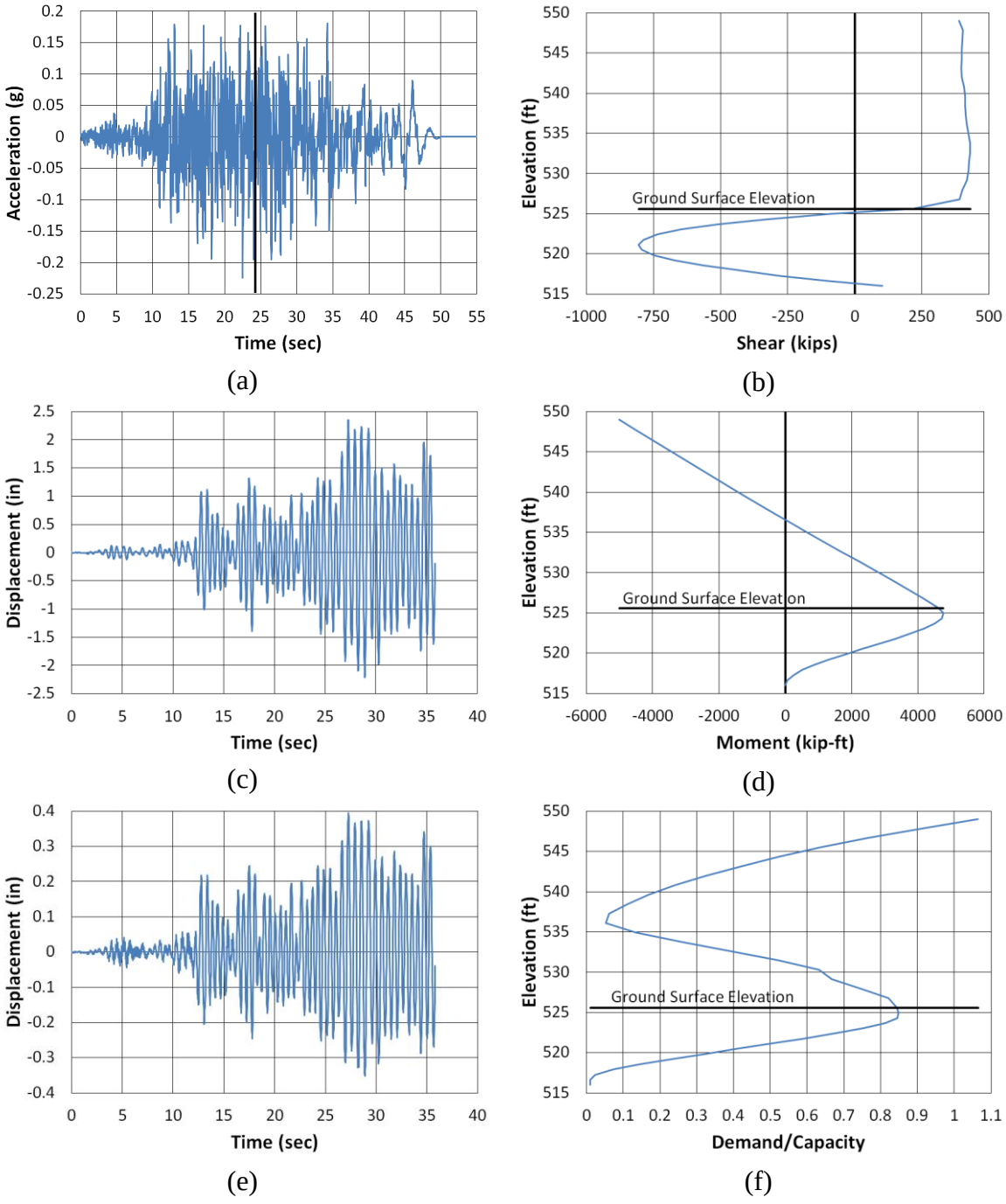

Figure 6.19. Franklin County transverse Landers NMCE (a) time-history event, (b) shear distribution, (c) top of pier displacement, (d) moment distribution, (e) ground surface displacement, and (f) demand capacity ratio

Table 6.10 – Results overview for Franklin County transverse models (highlighted ones are shown in Figures 6.16 and 6.17)

Franklin Transverse Earthquake Event	Performance	Plastic Hinge Developed	Location of Plastic Hinge (ft)	Probable Cause of Failure	Time of Occurrence (sec)	Maximum Shear (kip)	Elevation of Shear Occurrence (ft)	Maximum Moment (kip-ft)	Elevation of Moment Occurrence (ft)	Maximum Demand Capacity Ratio	Elevation of D/C Occurrence (ft)
Coalinga North	Failed	No	--	Structural	13.03	818	521	5279	549	1.04	549
Imperial Valley NMCE	Failed	No	--	Numerical Instability	20.09	609	521	3804	549	0.69	549
Imperial Valley North	Survived	No	--	--	8.73	433	521	2793	549	0.50	549
Kobe N-MCE	Survived	No	--	--	9.69	917	521	5350	549	1.06	549
Kobe North	Survived	No	--	--	12.8	593	521	3906	549	0.77	549
Kocaeli NMCE	Failed	No	--	Structural	22.61	855	521	5490	549	1.07	549
Kocaeli North	Survived	No	--	--	22.89	705	521	4634	549	0.90	549
Kocaeli2 NMCE	Failed	No	--	Structural	8.03	894	521	5402	549	1.07	549
Kocaeli2 North	Survived	No	--	--	11.69	671	521	4536	549	0.91	549
Landers NMCE	Failed	No	--	Structural	28.58	806	521	5011	549	1.07	549
Landers North	Survived	No	--	--	24.24	554	521	3454	549	0.81	549
LSM North	Survived	No	--	--	5.99	153	520	1467	549	0.25	549
NPS North	Failed	No	--	Structural	11.68	787	521	5183	549	1.02	549
SanFernando NMCE	Failed	No	--	Structural	7.3	807	521	5184	549	1.03	549
SanFernando North	Survived	No	--	--	3.41	629	521	4382	549	0.89	549
SanFernando2 NMCE	Survived	No	--	--	3.85	742	521	4612	549	0.89	549
SanFernando2 North	Survived	No	--	--	4.83	588	521	3945	549	0.75	549
Percent Survived	59%										

6.5 Lee County Discussion

The Lee county bridge models performed well. None of the models failed in the longitudinal or transverse direction. See Table 6.13 and 6.14 for an overview of the longitudinal and transverse results, respectively. Like the Etowah County bridge, the Lee County bridge foundations are H-piles. Referring to Figure 4.36 in chapter 4, the soil profile for Lee County was saturated cohesionless soil over bedrock. Based on Figure 2.5, the potential for liquefaction is low in this part of the state, and therefore, was not considered for this analysis. The depth to rock was about half of that of Etowah County, and the soil had moderate strength. For comparison, buckling analysis was done for the Lee County model as well. Table 6.11 shows the assumptions made.

Table 6.11 – Assumptions used in buckling analysis for Lee County

L_{eff}	50	ft
E	29000	ksi
I	393	in^4
Section Area of H-pile	15.5	in^2
P_{cr}	312	kips
r_{min}	5.04	in
P_{column}	725	kips/pile footing
No. of piles/column	9	
$FS_{(assumed)}$	2	
P_{des}/pile	161	kips

The free length of the pile was estimated as 25 feet. L_{eff} was determined by multiplying the free length by 2. This is because the pile is assumed to be pinned at the rock layer and fixed at the pile cap. Instead of using just the bridge deck dead load, the column and pile footing load was also taken into account. The section properties remained the same as Etowah. Pile efficiency of 1 was assumed and the number of piles for each footing is nine. Table 6.12 summarizes the calculations made.

Table 6.12 – Lee County P_{des}/P_{cr} and L_{eff}/r_{min} results

P_{des}/P_{cr}	0.52
L_{eff}/r_{min}	119

Based from these calculations, buckling could be an issue for the Lee County model. It is important to note that when evaluating the buckling stability of a pile embedded in cohesionless soils, it is assumed that the soil liquefied and lateral resistance is basically zero. However, it should be noted that even in a liquefied state, soil still possesses residual strength (which is typically low) that can be relied on. However, it is more conservative to assume the lateral resistance is zero. It should also be noted that for the Lee County models, the time steps were larger than the other models. This was due to FB-MultiPier's restriction of memory that could be used for analysis at the time these models were run. The file sizes were simply too big for the program to access during analysis and the program would crash. Therefore, the time steps were increased to decrease the size of the output files being created. The increase in time steps is not thought to have a significant impact on the analysis, as the time steps were still relatively small (greatest one being 0.05 seconds). Figures 6.20 – 6.23 show the displacements at the top of the pier and pile cap, along with the shear force, bending moment and D/C ratio distributions for the length of the pile. Note that these distributions are all below the ground surface. See Table 6.15 and 6.16 for an overview of the longitudinal and transverse results, respectively.

6.5.1 Longitudinal Results

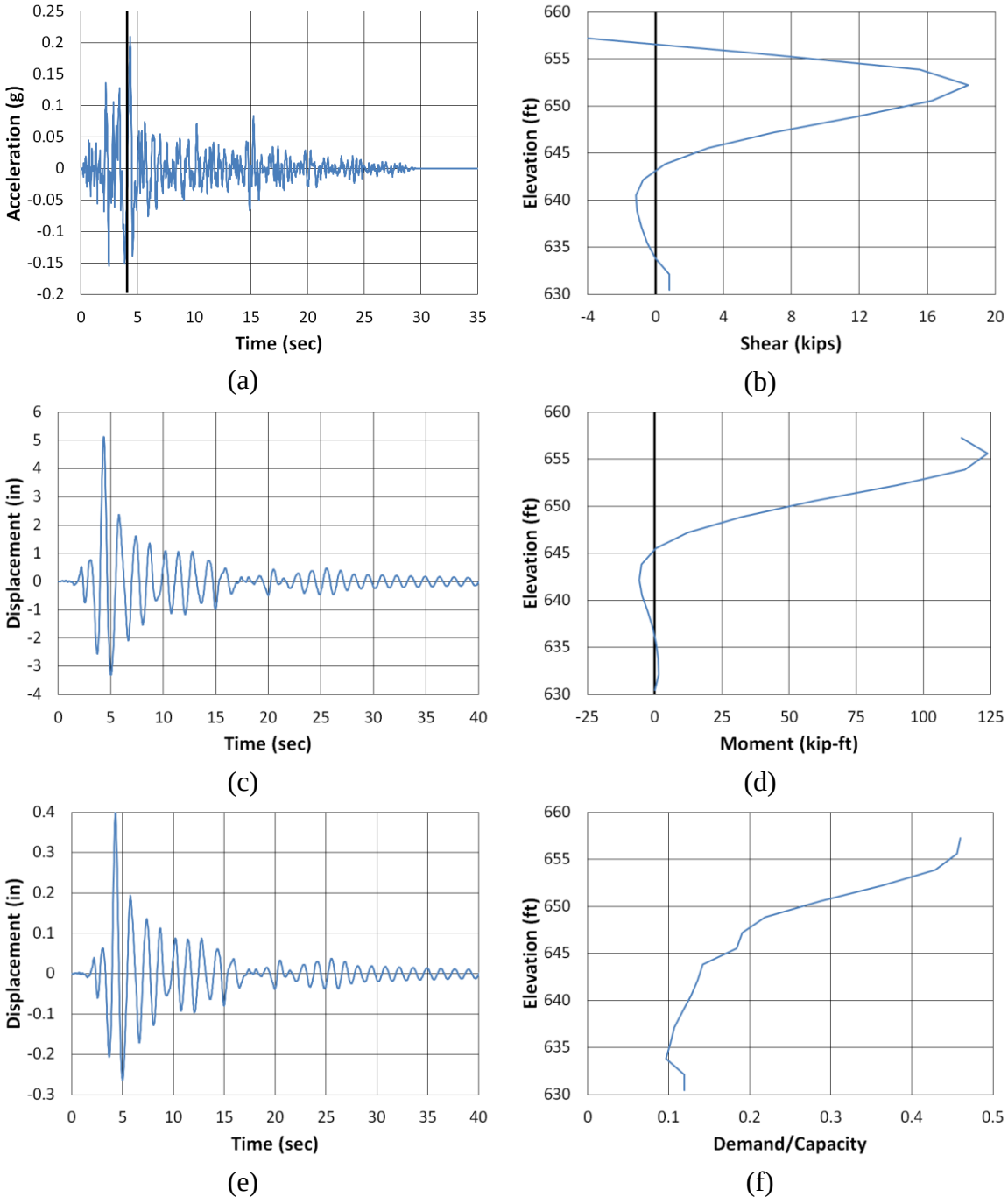

Figure 6.20. Lee County longitudinal San Fernando2 NMCE (a) time-history event, (b) shear distribution, (c) top of pier displacement, (d) moment distribution, (e) ground surface displacement, and (f) demand capacity ratio

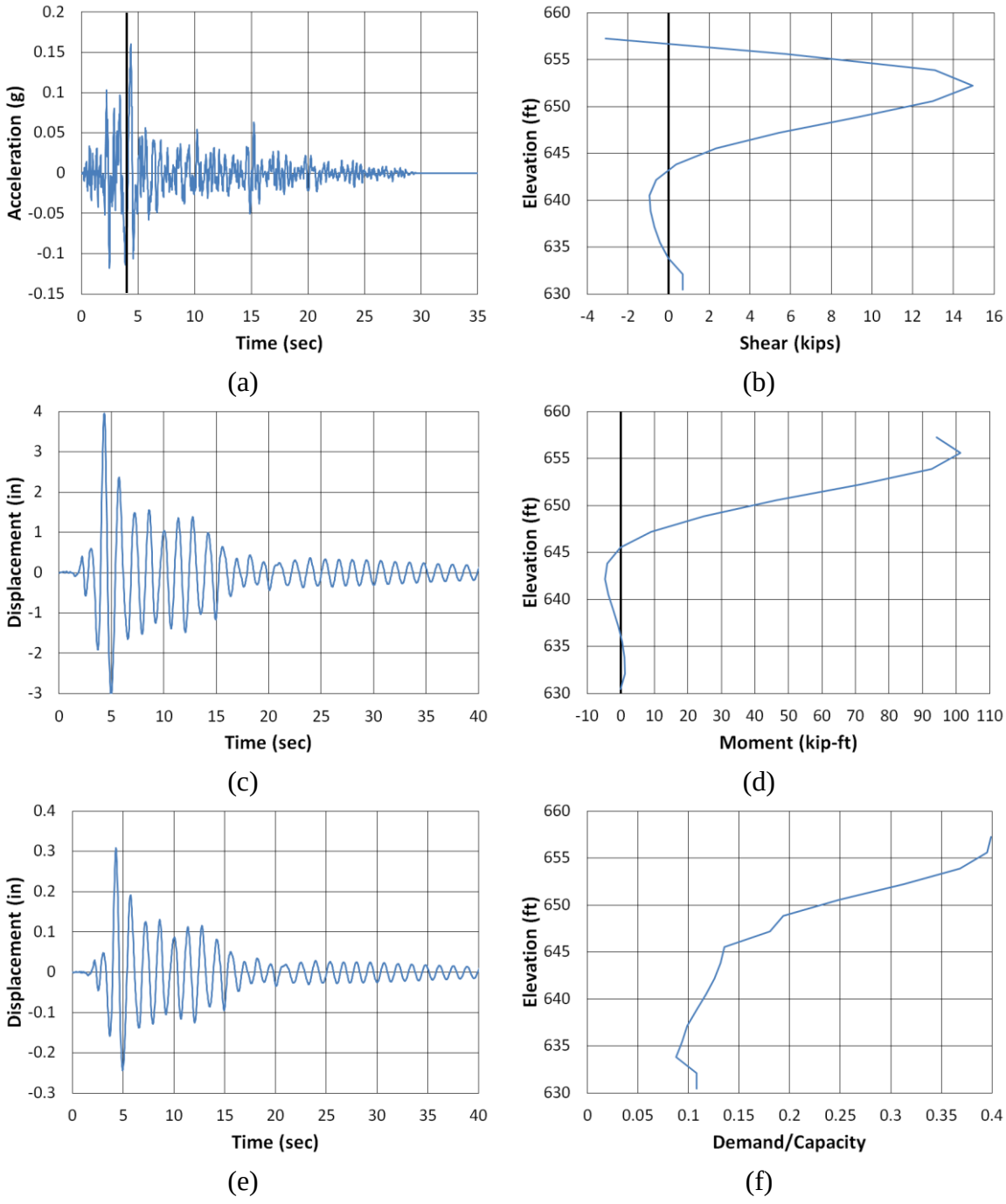

Figure 6.21. Lee County longitudinal San Fernando2 North (a) time-history event, (b) shear distribution, (c) top of pier displacement, (d) moment distribution, (e) ground surface displacement, and (f) demand capacity ratio

Table 6.13 – Results overview for Lee County longitudinal models (highlighted ones are shown in Figures 6.18 and 6.19)

Lee Longitudinal Earthquake Event	Performance	Plastic Hinge Developed	Time of Occurrence (sec)	Maximum Shear (kip)	Elevation of Shear Occurrence (ft)	Maximum Moment (kip-ft)	Elevation of Moment Occurrence (ft)	Maximum D/C Ratio	Elevation of D/C Occurrence (ft)
Coalinga North	Survived	No	13.98	21	657	124	657	0.43	657
Imperial Valley NMCE	Survived	No	34.68	17	652	117	656	0.44	657
Imperial Valley North	Survived	No	16.77	8	654	73	657	0.31	657
Kobe NMCE	Survived	No	8.76	27	652	176	656	0.60	657
Kobe North	Survived	No	9.42	14	652	125	657	0.46	657
Kocaeli NMCE	Survived	No	33.72	15	652	130	657	0.48	657
Kocaeli North	Survived	No	41.2	12	652	105	657	0.41	657
Kocaeli2 NMCE	Survived	No	8.5	26	652	174	656	0.59	657
Kocaeli2 North	Survived	No	7.24	12	652	105	657	0.41	657
Landers NMCE	Survived	No	30.72	19	652	173	657	0.58	657
Landers North	Survived	No	47.56	22	652	148	656	0.52	657
LSM North	Survived	No	8.96	3	656	22	657	0.15	657
NPS North	Survived	No	16.3	5	654	43	657	0.22	657
SanFernando NMCE	Survived	No	4.86	13	652	117	657	0.44	657
SanFernando North	Survived	No	4.86	12	652	111	657	0.42	657
SanFernando2 NMCE	Survived	No	4.32	18	652	124	656	0.46	657
SanFernando2 North	Survived	No	4.29	15	652	101	656	0.40	657
Percent Survived	100%								

6.5.2 Transverse Results

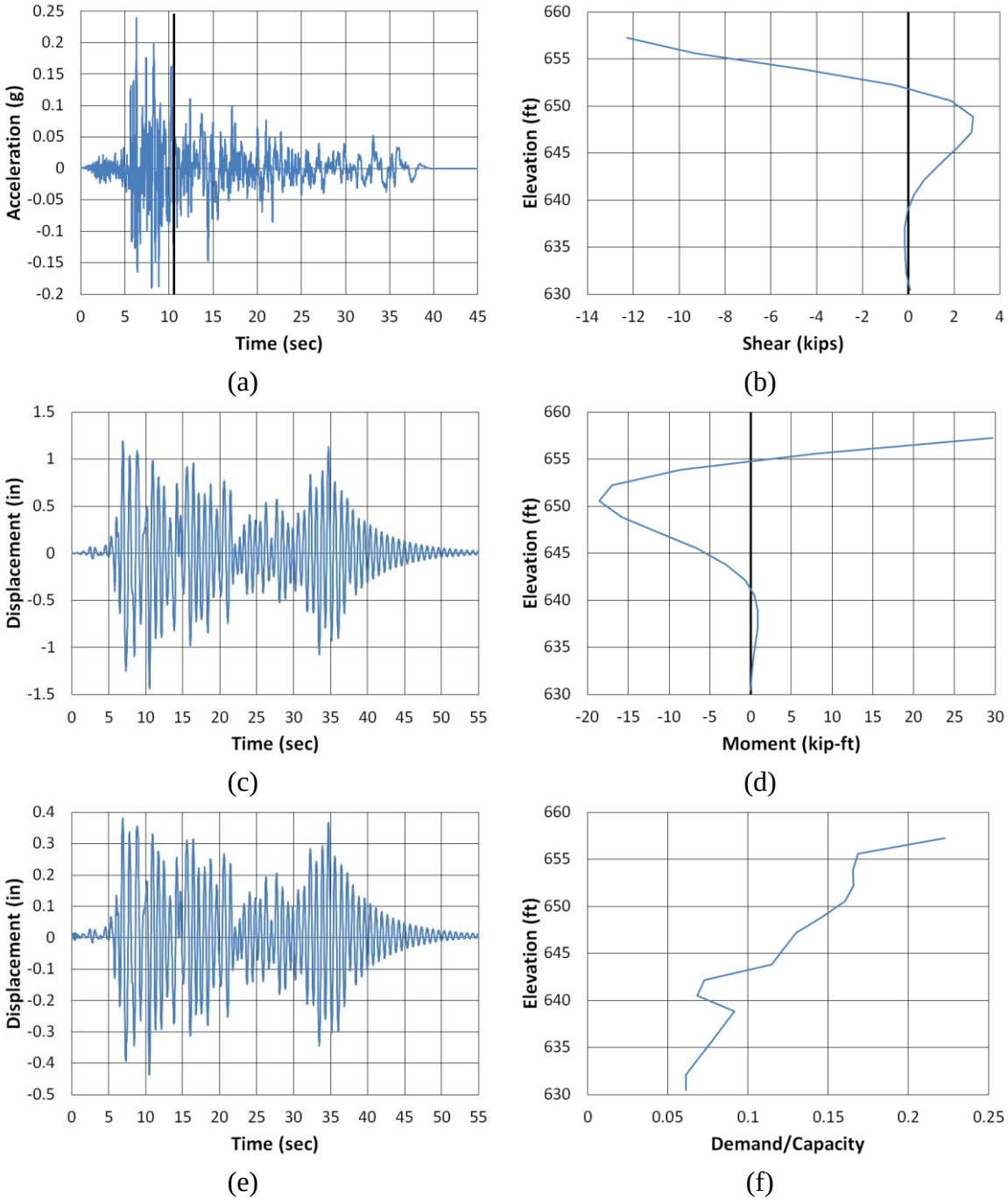

Figure 6.22. Lee County transverse Imperial Valley NMCE (a) time-history event, (b) shear distribution, (c) top of pier displacement, (d) moment distribution, (e) ground surface displacement, and (f) demand capacity ratio

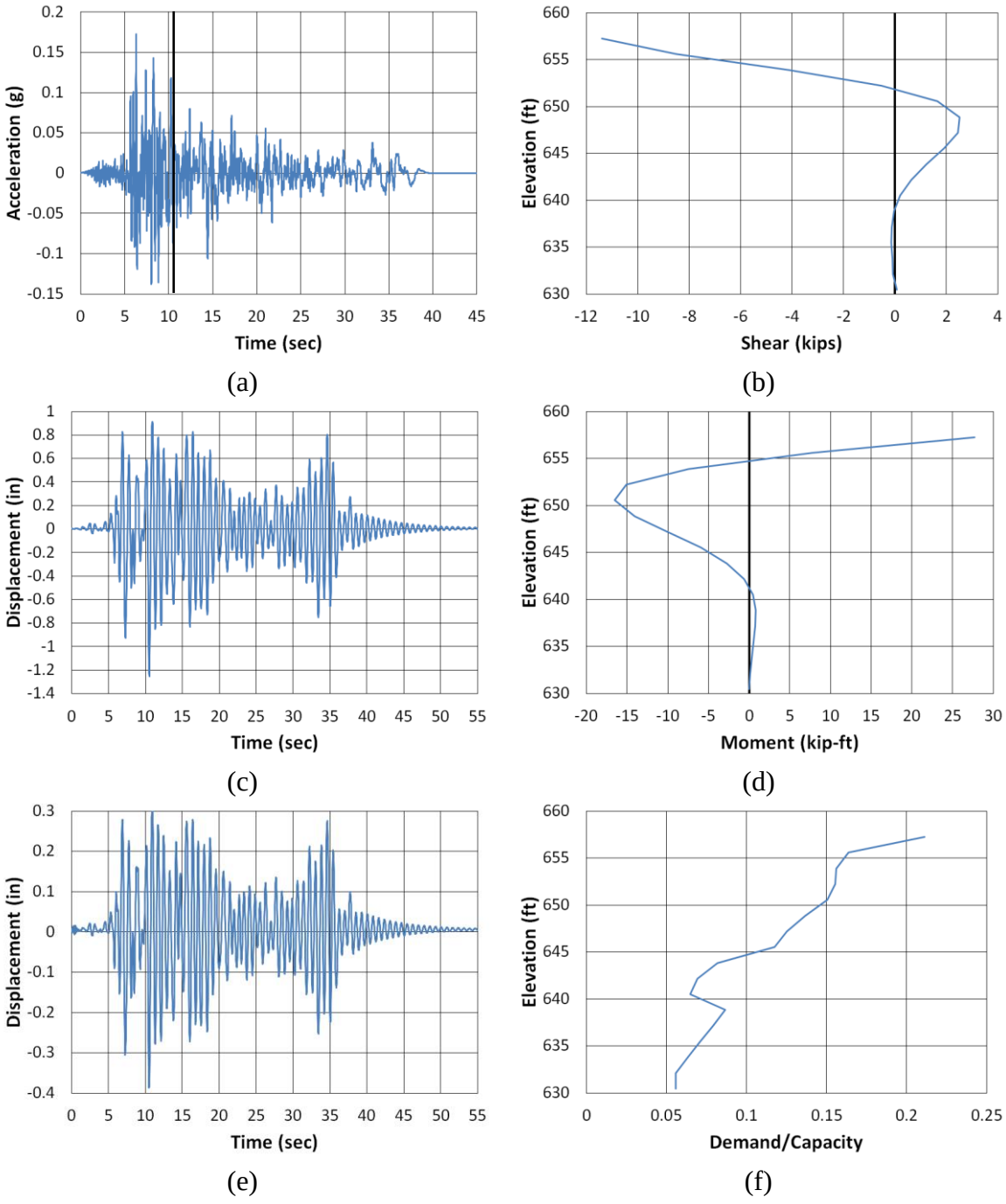

Figure 6.23. Lee County transverse Imperial Valley North (a) time-history event, (b) shear distribution, (c) top of pier displacement, (d) moment distribution, (e) ground surface displacement, and (f) demand capacity ratio

Table 6.14 – Results overview for Lee County transverse models (highlighted ones are shown in Figures 6.20 and 6.21)

Lee Transverse Earthquake Event	Performance	Plastic Hinge Developed	Time of Occurrence (sec)	Maximum Shear (kip)	Elevation of Shear Occurrence (ft)	Maximum Moment (kip-ft)	Elevation of Moment Occurrence (ft)	Maximum D/C Ratio	Elevation of D/C Occurrence (ft)
Coalinga North	Survived	No	7.32	29	657	65	657	0.41	657
Imperial Valley NMCE	Survived	No	10.47	12	657	30	657	0.22	657
Imperial Valley North	Survived	No	10.47	11	657	28	657	0.21	657
Kobe NMCE	Survived	No	6.06	34	657	74	657	0.46	657
Kobe North	Survived	No	8.25	32	657	71	657	0.45	657
Kocaeli NMCE	Survived	No	23.92	32	657	65	654	0.41	657
Kocaeli North	Survived	No	24.36	27	657	54	654	0.37	657
Kocaeli2 NMCE	Survived	No	7.24	31	657	61	654	0.38	656
Kocaeli2 North	Survived	No	7.06	18	657	47	657	0.32	657
Landers NMCE	Survived	No	22.92	30	657	62	654	0.41	656
Landers North	Survived	No	22.88	24	657	46	654	0.32	656
LSM North	Survived	No	5.76	3	657	7	657	0.11	657
NPS North	Survived	No	8.3	16	657	33	657	0.21	657
SanFernando NMCE	Survived	No	8.97	22	657	44	657	0.28	657
SanFernando North	Survived	No	9	17	657	42	657	0.30	657
SanFernando2 NMCE	Survived	No	5.13	26	657	62	654	0.40	656
SanFernando2 North	Survived	No	4.29	18	657	46	657	0.31	657
Percent Survived	100%								

6.6 Marshall County Discussion

The Marshall County bridge model performed well, overall. The longitudinal model seemed to have instability problems for some time-history events. This is most likely due to the large displacements that were generated. These displacements can cause secondary moments which can cause large out-of-balance forces to occur. See Table 6.15 and 6.16 for an overview of the longitudinal and transverse results, respectively. Figures 6.24 – 6.28 show the displacements at the top of the pier and ground surface, along with the shear force, bending moment and D/C ratio distributions for the length of the shaft.

Referring to Figure 6.25, the displacement when the acceleration is zero is nearly zero as well. However, the failed models showed that the bending moment and shear force were very high at the last time step, which then caused the model to fail. The Kobe NMCE and the Kocaeli2 NMCE models are thought to have failed due to numerical instability because the displacements were nearly zero for the last 35 seconds. The transverse models performed well. The strut provided extra stiffness in the transverse direction. For the longitudinal models, there is an indication that the strut's mass created some inertial effects within the model. The bending moment and D/C distributions show slight changes at the strut elevation, which indicates that the strut affected the response of the pier slightly in the longitudinal direction. This can be seen on the shear force distribution figures (more drastically in the transverse direction). The models also showed that the largest moment was developing at the rock line, which is a desired plastic hinge zone location. It should also be noted that the bent is very tall. The free length of the columns is approximately 60 feet, which can lead to large displacements at the top of

the pier, especially in the longitudinal direction. Liquefaction was not considered because the rock layer is very shallow on site and the thin soil layer is assumed to scour. Buckling was not checked for this model even though the pier was very tall (approximately 60 feet from the ground surface). This is because of the extra transverse resistance the strut provided and its overall performance when seismically loaded.

6.6.1 Longitudinal Results

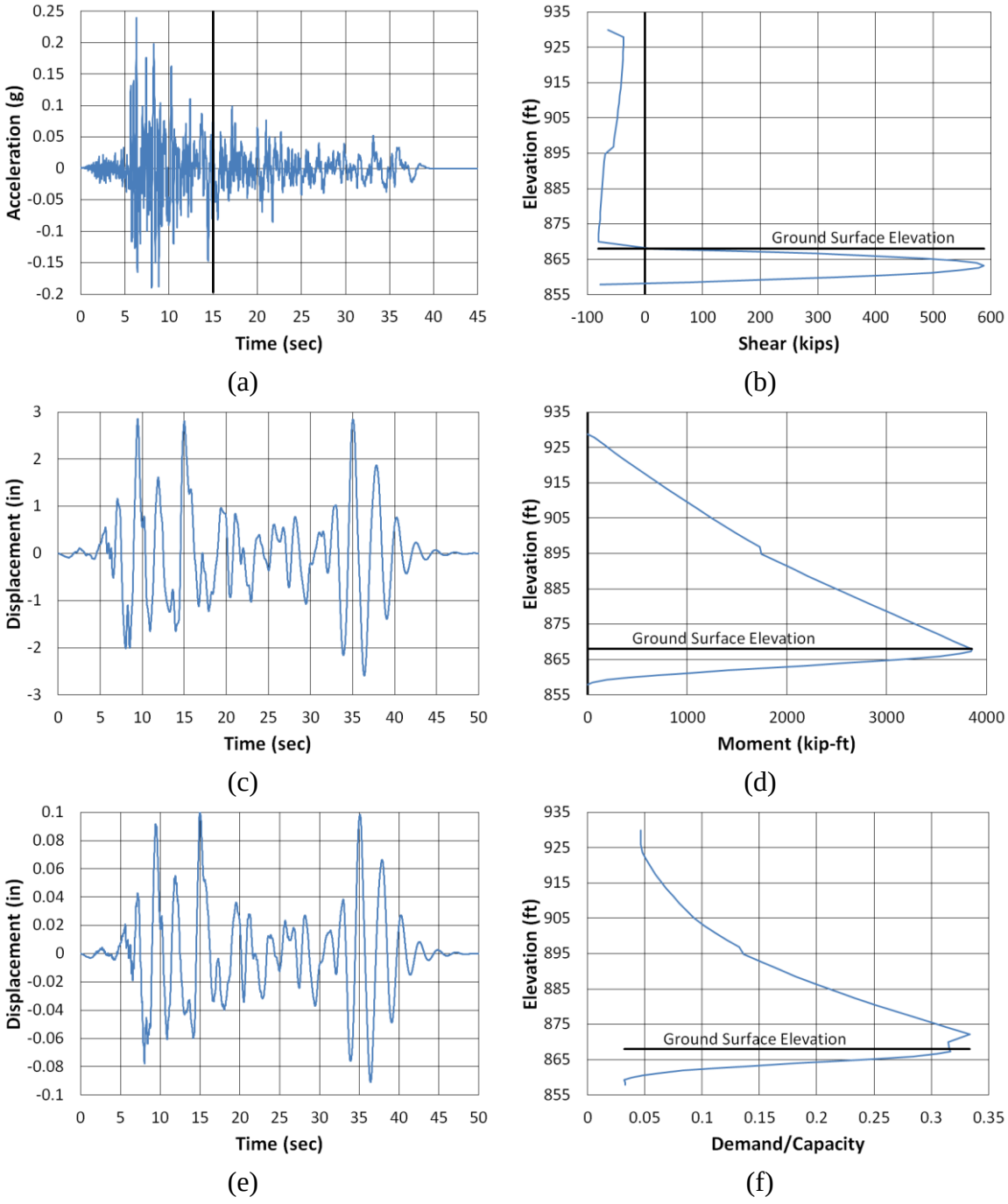

Figure 6.24. Marshall County longitudinal Imperial Valley NMCE (a) time-history event, (b) shear distribution, (c) top of pier displacement, (d) moment distribution, (e) ground surface displacement, and (f) demand capacity ratio

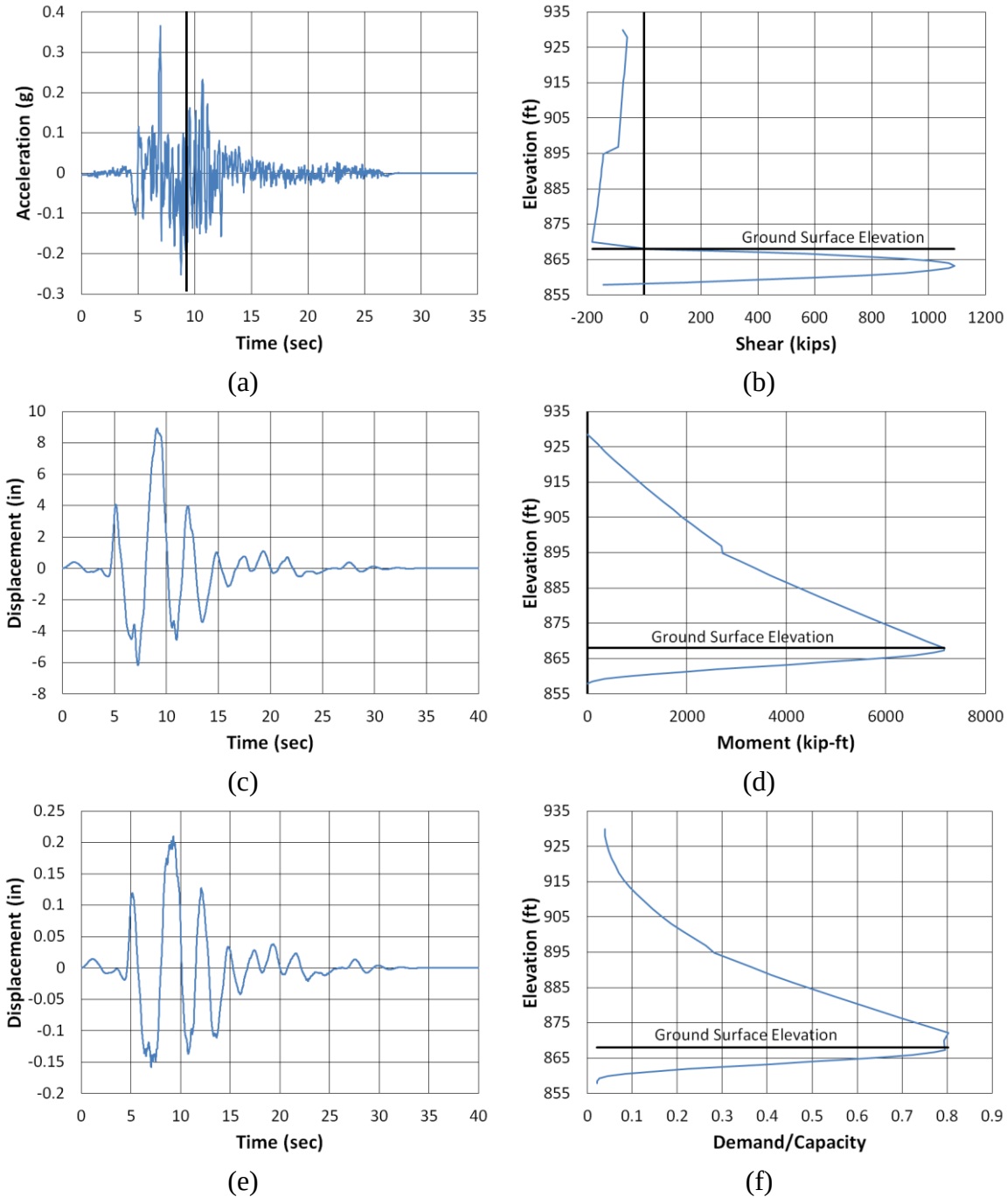

Figure 6.25. Marshall County longitudinal Kocaeli2 NMCE (As if Survived) (a) time-history event, (b) shear distribution, (c) top of pier displacement, (d) moment distribution, (e) ground surface displacement, and (f) demand capacity ratio

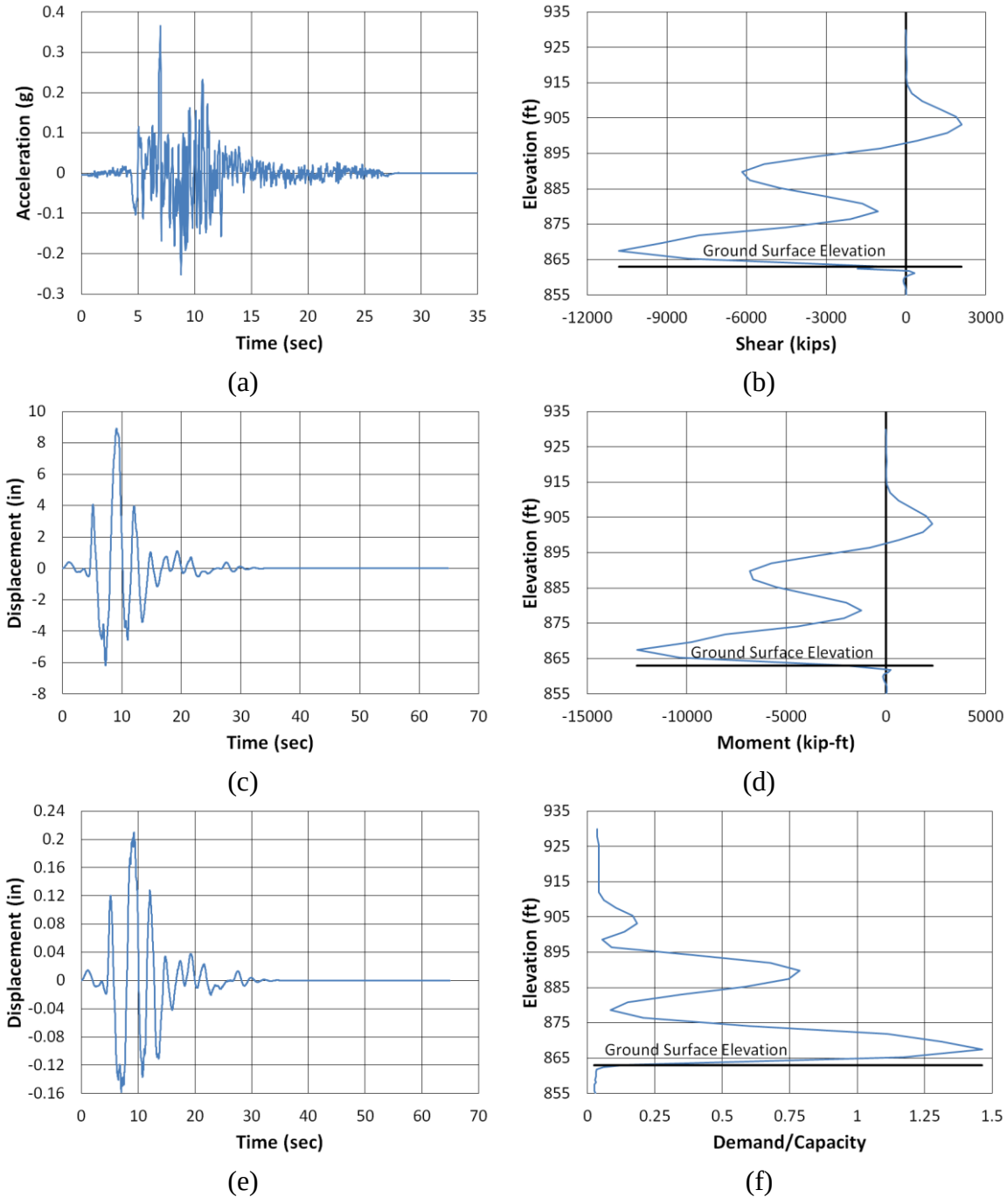

Figure 6.26. Marshall County longitudinal Kocaeli2 NMCE (failed at time 64.9 sec) (a) time-history event, (b) shear distribution, (c) top of pier displacement, (d) moment distribution, (e) ground surface displacement, and (f) demand capacity ratio

Table 6.15 – Results overview for Marshall County longitudinal models (highlighted ones are shown in Figures 6.22, 6.23 and 6.24)

Marshall Longitudinal Earthquake Event	Performance	Plastic Hinge Developed	Location of Plastic Hinge (ft)	Probable Cause of Failure	Time of Occurrence (sec)	Maximum Shear (kip)	Elevation of Shear Occurrence (ft)	Maximum Moment (kip-ft)	Elevation of Moment Occurrence (ft)	Maximum D/C Ratio	Elevation of D/C Occurrence (ft)
Coalinga North	Survived	No	--	--	19.99	248	863	1631	868	0.11	872
Imperial Valley NMCE	Survived	No	--	--	14.99	588	863	3855	868	0.33	872
Imperial Valley North	Survived	No	--	--	15	435	863	2858	868	0.22	872
Kobe NMCE	As if Survived	--	--	--	7.06	568	863	3782	868	0.38	872
Kobe NMCE	Failed	Yes	876	Numerical Instability	75.31	11240	876	13141	874	1.69	876
Kobe North	Survived	No	--	--	6.13	473	863	3103	868	0.29	872
Kocaeli NMCE	Failed	Yes	876	Structural	90.09	11637	876	12638	876	1.68	876
Kocaeli North	Survived	No	--	--	25.18	490	863	3227	868	0.26	872
Kocaeli2 NMCE	As if Survived	--	--	--	9.29	1091	863	7176	868	0.80	872
Kocaeli2 NMCE	Failed	Yes	867	Numerical Instability	64.9	10806	867	12507	867	1.46	867
Kocaeli2 North	Failed	Yes	876	Structural	69.7	12538	880	13868	880	1.79	880
Landers NMCE	Survived	No	--	--	46.8	953	863	6269	868	0.66	872
Landers North	Survived	No	--	--	46.74	791	863	5195	868	0.51	872
LSM North	Failed	Yes	881	Structural	92.94	12946	914	12997	879	1.88	814
NPS North	Survived	No	--	--	7.61	136	859	798	863	0.62	870
SanFernando NMCE	Survived	No	--	--	9.52	678	863	4444	868	0.41	872
SanFernando North	Survived	No	--	--	7.69	628	863	4111	868	0.41	872
SanFernando2 NMCE	Survived	No	--	--	4.27	537	863	3524	868	0.34	872
SanFernando2 North	Survived	No	--	--	4.27	420	863	2752	868	0.24	872
Percent Survived	71%										

6.6.2 Transverse Results

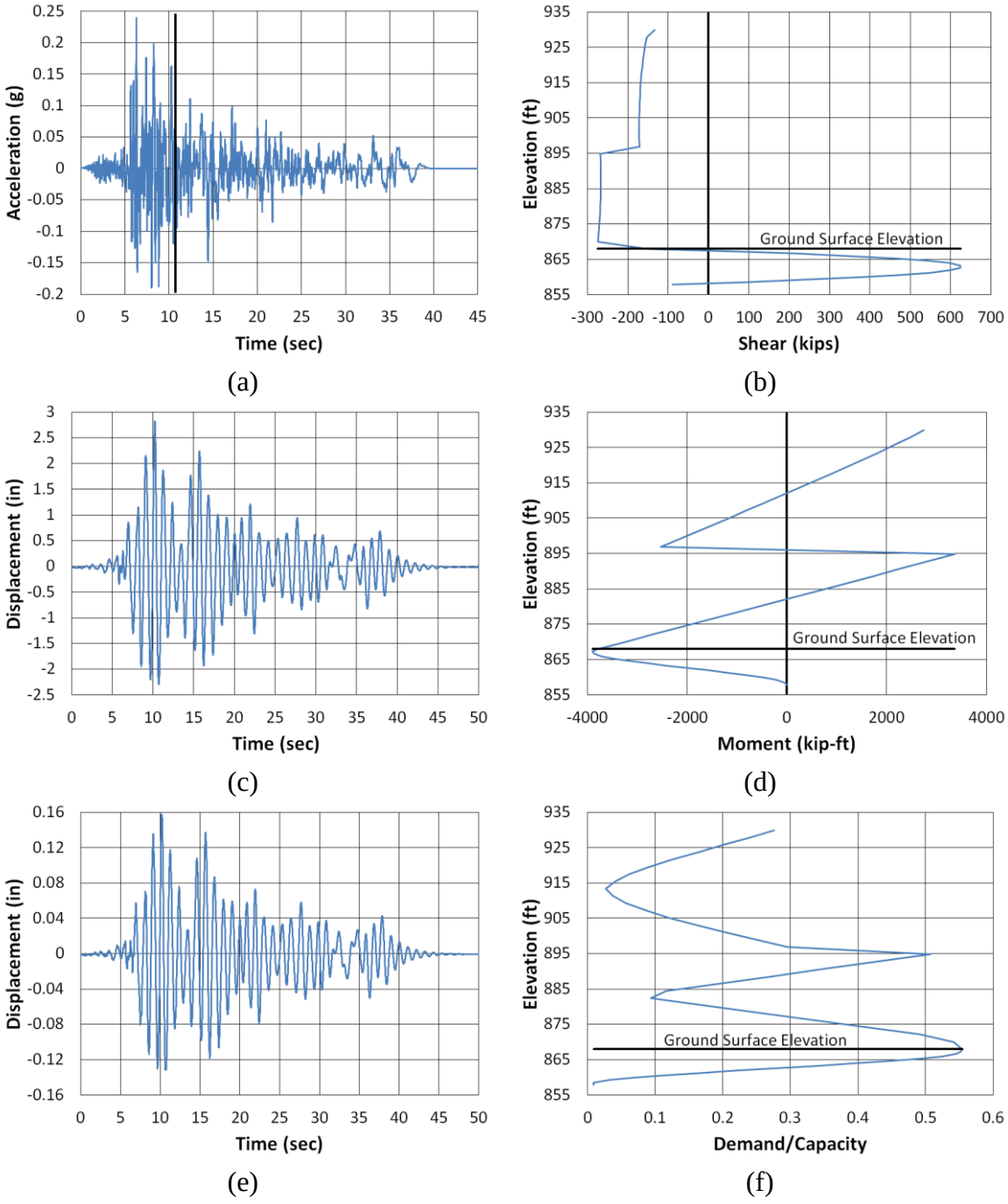

Figure 6.27. Marshall County transverse Imperial Valley NMCE (a) time-history event, (b) shear distribution, (c) top of pier displacement, (d) moment distribution, (e) ground surface displacement, and (f) demand capacity ratio

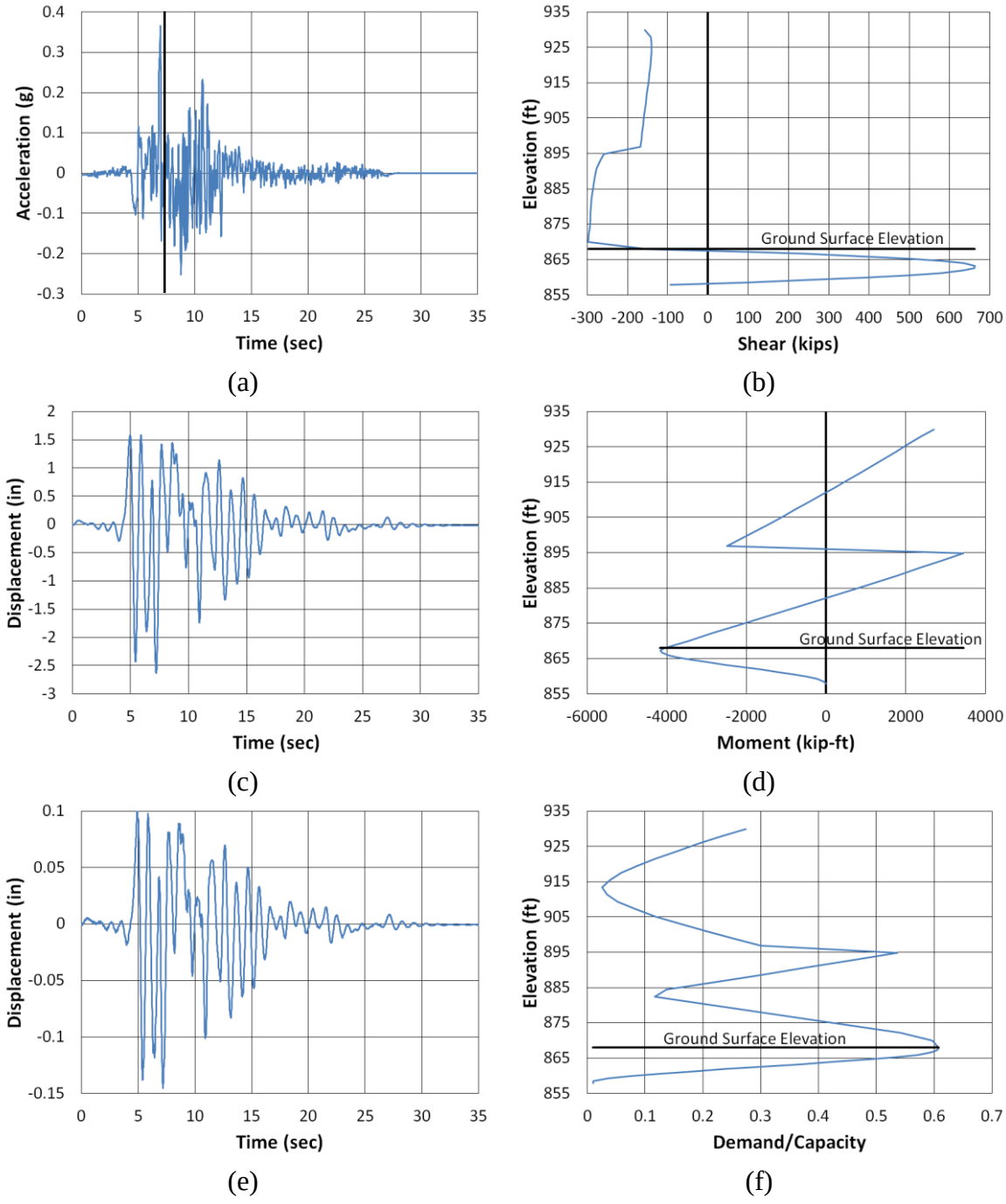

Figure 6.28. Franklin County longitudinal Kocaeli2 NMCE (failed) (a) time-history event, (b) shear distribution, (c) top of pier displacement, (d) moment distribution, (e) ground surface displacement, and (f) demand capacity ratio

Table 6.16 – Results overview for Marshall County transverse models (highlighted ones are shown in Figures 6.25 and 6.26)

Marshall Transverse Earthquake Event	Performance	Plastic Hinge Developed	Time of Occurrence (sec)	Maximum Shear (kip)	Elevation of Shear Occurrence (ft)	Maximum Moment (kip-ft)	Elevation of Moment Occurrence (ft)	Maximum D/C Ratio	Elevation of D/C Occurrence (ft)
Coalinga North	Survived	No	11.28	426	863	2656	867	0.31	867
Imperial Valley NMCE	Survived	No	10.73	625	863	3899	867	0.55	868
Imperial Valley North	Survived	No	10.68	513	863	3206	867	0.39	867
Kobe NMCE	Survived	No	10.35	589	863	3673	867	0.51	868
Kobe North	Survived	No	10.35	406	863	2525	867	0.28	867
Kocaeli NMCE	Survived	No	23.81	774	863	4861	867	0.71	868
Kocaeli North	Survived	No	23.8	574	863	3582	867	0.46	867
Kocaeli2 NMCE	Survived	No	7.22	663	863	4163	867	0.61	867
Kocaeli2 North	Survived	No	7.22	517	863	3220	867	0.43	867
Landers NMCE	Survived	No	23.48	770	863	4830	867	0.71	868
Landers North	Survived	No	23.4	638	862	3997	867	0.56	868
LSM North	Survived	No	10.83	131	863	811	867	0.05	895
NPS North	Survived	No	7.96	308	863	1921	867	0.19	867
SanFernando NMCE	Survived	No	3.23	641	863	4000	867	0.51	867
SanFernando North	Survived	No	3.23	612	863	3836	867	0.45	867
SanFernando2 NMCE	Survived	No	4.58	877	863	5562	867	0.82	868
SanFernando2 North	Survived	No	4.6	791	863	4991	867	0.74	868
Percent Survived	100%								

6.7 Direct Analysis Results Summary

Five bridge pier case histories were modeled in FB-MultiPier: Chambers County 25% and 100% scour, Etowah County, Franklin County, Lee County, and Marshall County. Dynamic analysis was run for each model using a suite of scaled earthquake time-history events.

The Chambers County case history was modeled for two cases: 25% scour and 100% scour. The Chambers County bridge bent for the 25% scour case performed poorly, overall. Most of the failed models were suspected to have failed because of either structural failure or soil failure. Soil failure is likely due to large displacements that the soil spring undergoes. The insitu soil above the rock line for the Chambers County case history was very weak and provided little lateral resistance. Bending moment and D/C ratio was typically largest below the ground surface and above the rock line in the longitudinal direction. In the transverse direction, it was largest at the column/pier cap connection. However, large bending moments were still developing below the ground surface. This suggests that plastic hinges may develop in these locations. If a plastic hinge developed under the ground surface, it would be difficult to identify and repair.

In comparison, the Chambers County bridge bent for the 100% scour case performed well, overall. The three models that failed all used NMCE scaled earthquake time-history events, which are of larger magnitude and, typically, more harmful than the North scaled time-histories. The North scale factor events are more representative of what the state of Alabama would generally experience. Bending moment and D/C ratio was typically largest at the rock line and column/pier cap connection when seismically

loaded in the longitudinal and transverse directions, respectively. This suggests that plastic hinges may develop in these locations, which would be ideal.

The Etowah County bridge pier models performed poorly due to pile failure. Every model failed due to structural failure within the H-pile foundations (specifically the battered piles). It appeared that the soft clay provided very little lateral resistance, causing the piles to buckle.

The Franklin County bridge bent models performed fair, overall. Most of the models that failed were subjected NMCE earthquake events, which are the higher magnitude events. Bending moment and D/C ratio was typically largest at the rock line and column/pier cap connection when seismically loaded in the longitudinal and transverse directions, respectively. This suggests that plastic hinges may develop in these locations, which would be ideal.

The Lee County bridge pier models performed well, overall. All of the models survived the earthquake event they were subjected to. The moderate strength cohesionless soil seemed to provide adequate lateral resistance. The highest D/C ratio for any pile was 0.6. The bending moment and D/C ratio in the columns were largest at the column base and the column/pier cap connection in the longitudinal and transverse directions, respectively. This suggests that plastic hinges are most likely to form at these locations.

The Marshall County bridge bent models performed well, overall. Bending moment and D/C ratio was typically largest at the rock line and column/pier cap connection when seismically loaded in the longitudinal and transverse directions, respectively. This suggests that plastic hinges may develop in these locations, which

would be ideal. Some displacements at the top of the pier were very large. This is expected because of the free length of the bent. Typically, structures with longer period tend to displace more that structures with shorter periods.

The major limitation to these models is that only one bridge pier was modeled. In the complete system for a bridge, interaction between the bridge deck, abutments, and other bridge piers (if applicable) is very important. The interaction between these components can possibly provide additional stiffness, which could reduce the inertial forces generated within the bridge piers. Without the interaction of the bridge deck, the displacements at the top of the pier are not completely accurate. However, these models provided an indication of where maximum shear forces and bending moments would develop within the bridge pier, specifically in the foundations. This subsequently suggests probable locations of plastic hinge zones that would develop, which is a key component of seismic design of bridges.

Chapter 7

STATE DOT SURVEY

As part of the research scope, several southeastern state DOTs were surveyed to compare their seismic design process, specifically to deep foundations, to ALDOT's current practice. The survey was sent to eleven states: Arkansas, Florida, Georgia, Kentucky, Louisiana, Mississippi, North Carolina (NC), South Carolina (SC), Tennessee, Virginia, and West Virginia. At the time of writing this document, three had replied: Arkansas, Kentucky, and South Carolina. Below is the survey submitted to the state DOTs:

1. Do you use/prefer driven piles, drilled shafts, spread footings, or a combination of the three for foundation design in a seismic area?
2. If driven piles are used for foundation design in a seismic area, what type(s) and configuration(s) is/are most often used? If it is a group configuration, please provide typical spacing, batter (if applicable), and driving criteria.
3. Is there a specific standard you use to determine if insitu soils on site are potentially susceptible to liquefaction (i.e. geologic age and origin, water table levels, fines content, etc.)?
4. Have you ever taken remedial measures to meet seismic standards (current foundations not adequate or weak soil layer is a concern), specifically in regards to the foundations? If so, what was done and why?

5. Have your foundation designs been validated through computer program modeling or some other method? If so, what program(s) did you use and how (combination of programs, run dynamic analysis or push-over analysis, etc.)?

7.1 Arkansas Survey Response

1. Since our bridge foundations in seismic zones are predominantly in soils with very deep overburden, we typically use driven trestle pile bents or pile footings. Drilled shafts may also be used, however, we have experienced difficulties in the past with construction procedures used in the placement of slurry-displaced drilled shafts; so. the majority of our seismic bridges are designed using piling.
2. Pile Types: Steel H-piles where significant depth of sand or clay exists over rock, Concrete piles in Seismic Zone 2 (assumed to also mean SDC B) or less, and Concrete-filled steel shell piles in all seismic zones.

   Pile Spacing: As required by design, but not less than LRFD Specification minimum requirements.

   Pile Batter: Typically use vertical piles unless other present or more frequently occurring design concerns such as earth pressure (end bents), bridge curvature, water velocity, etc. out weigh concerns from the extreme seismic event. When battered piling is used in seismic zones, the batter is minimized from our standard 4H:12V to 1.5H:12V.

   Driving Criteria: Ultimate bearing capacity is typically determined using a Wave Equation Analysis (WEAP) where hammer approval and bearing graph relationships are determined and provided for the Contractor's use.

3. Liquefaction susceptibility is determined by using the water table, soil type, and SPT blow counts from field sampling to calculate a factor of safety using a procedure developed by Youd and Idriss (2001).
4. No remedial measures have been taken on in-situ soil to date. Geosynthetic internal reinforcement is used in bridge embankments when required by design and minimum pile tip elevations may be specified to ensure pile tips are not established in a liquefiable layer. Pile buckling due to a longer unsupported length in liquefiable layers is not typically considered. Our liquefactions calculations often result in a combination of liquefiable and non-liquefiable layers. Some soil resistance is considered to be available during liquefaction and steel shell piles are concrete-filled to help resist buckling.
5. We model our bridges using the SEISAB program in conjunction with a response spectrum analysis and this provides us with the seismic forces to use in our foundation design for the extreme event case.

7.2 Kentucky Survey Response

1. We typically use driven piles in areas where seismic design is a consideration. However, the selection of foundation type is typically not governed by seismic design considerations. Due to considerations other than seismic design driven piles are typically the appropriate foundation type in the New Madrid Seismic Zone (NMSZ) where there are significant seismic design considerations. However, we would potentially use another foundation type such as drilled shafts or spread footings on bedrock if warranted by the site conditions.

2. We typically use steel piles (H or pipe) with a group configuration when we use driven piles. The spacings are typically 3 ft to 10 ft depending on loads, and whether pile is point bearing or friction. We typically avoid battered piles in seismic zones. Driving criteria would typically be determined using dynamic testing and in some cases only dynamic formulas. We are currently working on a bridge over Kentucky Lake (in the NMSZ) where we will be performing static and pseudo-static (i.e. Statnamic) testing in conjunction with dynamic testing to determine pile driving criteria.
3. Preliminary liquefaction assessments may be based on SPT blow counts, CPT testing, water table, and fines content. On our Lake Bridges Project (the previously-mentioned bridge over Kentucky Lake and a nearby bridge over Lake Barkley) rigorous liquefaction analyses were performed using site-specific ground motions, equivalent linear site response analyses using shear modulus values determined from in-situ and laboratory resonant column testing, and both CPT and SPT data. These analyses are generally based on the NCEER workshop recommendations as published in the American Society of Civil Engineers (ASCE) Journal (2001) (Youd and Idriss 2001).
4. On our Lake Bridges project we specified deep soil mixing (DSM) to mitigate against liquefaction due to the liquefaction predicted for a 2500 year seismic event. We had a single bidder that was significantly higher than the Engineer's estimate and the bid was rejected. Subsequently, the seismic design criteria were changed to design for the 1000 year event and DSM was no longer required. We re-let the project and construction is currently ongoing.

5. Foundations are sometimes modeled with GT STRUDL to estimate seismic response. On our Lake Bridge Projects, dynamic modeling using time histories are being performed using SAP and MIDAS. Push over analyses was also performed.

7.3 South Carolina Survey Response

1. South Carolina Department of Transportation (SCDOT) exclusively uses either driven piles or drilled shafts to support our bridges. Spread footings are not allowed at any location that will undergo soil Shear Strength Loss (SSL) (i.e. liquefaction). Deep foundations are designed to incorporate downdrag should settlement caused by SSL be present at the location.
2. SCDOT uses precast, prestressed concrete piles, H-piles and combination piles to support our bridges depending on the load (axial and lateral) and the soil that the foundations will be driven into. Our typical pile sizes are indicated in Table 7.1.

Table 7.1 – South Carolina's Typical Pile Types and Sizes

Pile Type	Size
Steel H-piles	HP 12x53 HP 14x73 HP 14x89 HP 14x117[1]
Steel Pipe Piles	16-inch[2] 18-inch[2] 20-inch[2] 24-inch[2]
Prestressed Concrete Piles[3]	18-inch 20-inch 24-inch 30-inch[4] 36-inch[4]
Combination Piles	18-inch[3] with W 8x58 stinger 20-inch[3] with HP 10x57 stinger 24-inch[3] with HP 12x53 stinger
[1]used where penetration is minimal and nominal capacity is large [2]wall thickness is ½ inch for all pipe pile sizes [3]prestressed concrete piles are square in section [4]these sizes are only allowed with the written approval of SCDOT	

Please note that the pipe piles are typically filled with concrete to improve seismic performance. Typically SCDOT uses pile bents for driven piles, with pile footings being used on a relatively limited basis. The piles are installed typically no closer than 3 diameters apart in the transverse direction. Driving criteria is based either on reaching a specified tip elevation or is based on achieving a specified nominal capacity. SCDOT also tries to indicate which loading condition controlled the design i.e. axial or lateral and static (strength) or seismic (extreme event). For drilled shafts, SCDOT typically uses a single drilled shaft supporting a single column with multiple columns supporting the bent (typically 3 to 5 columns) depending on the width of the bridge. We also have used hammer-head

type foundations before as well as drilled shaft footings [e.g. The Cooper River Bridge (Arthur Ravenel, Jr. Bridge) in Charleston, SC].

3. SCDOT has adopted the use of the Idriss and Boulanger (2008) procedure. We both screen the site for potential SSL as well as conduct a full SSL analysis. These procedures are contained in Chapter 13 of the SCDOT Geotechnical Design Manual (GDM) v. 1.1 (SCDOT 2010). A copy of this Chapter, as well as the entire GDM, is available at the SCDOT website. Please note that we are in the process of revising our GDM and would be willing to provide ALDOT a draft copy of our GDM for reference.
4. First, SCDOT does not retrofit bridges to meet seismic performance. Second, if SCDOT reviews the project, we do not allow deep foundations to be founded in liquefiable or soft clays that may undergo SSL during seismic shaking. Finally, we account for the movement of the end slope into the bridge either through acceptable movements and the necessary loads being applied to the bridge or through ground improvement. If slope stability is not an issue we would typically design the bridge to accommodate the downdrag on the piles by checking the pile capacity. If slope instability is an issue, we start using the cheapest and easiest ground improvement method we can (i.e. geogrid) and then proceed toward the most expensive ground improvement method e.g. DSM or some other in-situ modification. Our number one rule is no collapse of the bridge.
5. The designers use L-pile, CSiBridge (CSI 2013), Leap Bridge (RC-Pier).

   Dynamic analysis is run using CSiBridge; this program allows performing the response spectral analysis and the push-over analysis. The designer shall meet the

requirements of the Seismic Design Specifications. (Please note that this last answer was prepared by our Seismic Design Support Section).

7.4 State DOT Survey Summary

1. All states use driven piles for seismic design, but seismic hazard may not necessarily be the controlling factor in foundation selection and design. Arkansas primarily uses driven piles for seismic bridges. Kentucky generally uses driven piles as well; however, it is usually due to other considerations other than seismic hazard, and considers other foundation types is the it is warranted by the site conditions. SC exclusively uses driven piles and/or drilled shafts to support bridges in seismic hazard.
2. Each state uses a variety of driven piles. Most of the time, the selection of foundation type is dependent upon site conditions. Arkansas uses steel H-piles when significant depth of sand or clay to bedrock is present; concrete piles are used for seismic zone 2 (SDC B) or less, and steel pipe piles filled with concrete can be used for all seismic zones. Kentucky typically uses steel (H or pipe) piles when using driven piles. SC uses steel, concrete, or combination piles depending on local site conditions and are typically pile bents (not pile footings). Group spacing is typically what is recommended by design standards for all DOTs. SC did state that in the transverse direction, pile spacing is no less than three diameters. Arkansas decreased their typical batter slope (1.5H:12V) when in a seismic zone and Kentucky usually avoids battered piles all together in seismic areas. SC did not comment. Driving criteria is determined by WEAP analysis for Arkansas; Kentucky uses statnamic or dynamic (most likely Pile Driving

Analyzer [PDA]); and SC uses a specified tip elevation that must be reached or achieving a specified nominal capacity.

3. Liquefaction assessments are handled differently by all three states. Arkansas uses the Youd and Idriss (2001) procedure; whereas Kentucky generally conducts a preliminary assessment based on SPT and CPT testing, water table elevation and fines content. If further evaluation is needed, they perform analysis based on the NCEER workshop published in the ASCE Journal (2001) (Youd and Idriss 2001). SC adopted the Idriss and Boulanger (2008) procedure. They have also documented in the SCDOT GDM, a standardized procedure for the department to use (SCDOT 2010).
4. Remedial measures are generally not taken by any of the DOTs. Kentucky did order DSM to be done based on a 2500 year seismic event, but was eventually not economically feasible because the seismic event was lowered to 1000 year. SC makes an interesting point in that it does not allow deep foundations to be founded in soft clay or liquefiable sands if it was reviewed by the SCDOT. They did not expound on how they determine a suitable foundation selection and design for a site given those characteristics.
5. All three DOTs use computer programs to determine seismic response. SC's approach is very similar to part of this research project's scope. It uses LPILE to determine the foundation response, and then inputs the foundation springs into CSiBridge to perform a response spectral analysis as well as a static pushover analysis

.

Chapter 8

CONCLUSIONS AND RECOMMENDATIONS

The research is summarized including the literature review, substructure and direct analysis done in FB-MultiPier, and the state DOT survey. Conclusions were made based on those results and recommendations are provided to improve future research of deep foundation response to seismic and dynamic loads.

8.1 Summary of Work

ALDOT provided five case histories of bridges to determine the response of the foundations to seismic loads relative to Alabama. Substructure analysis was done and the response curves developed were used in SAP2000 to represent the foundations for the bridges. A bridge bent was then modeled for each case history and direct analysis was conducted. The Chambers County case history was modeled for two scour cases: 25% and 100% scour. A suite of scaled earthquake time-history events developed by Panzer (2013) was used to load the bent dynamically. Displacements at the top of the bent and the ground surface were recorded, as well as maximum shear force, bending moment and D/C ratio distributions. The results of the direct analysis were compared to the literature review and discussed. Finally, a survey was sent out to multiple state DOTs to review their approach to seismic design of bridge foundations.

8.2 Conclusions

Based on the research, the following conclusions were made on the response of deep foundations to seismic and dynamic loads.

- The drilled shaft case histories with drilled shafts embedded in shallow bedrock performed well, overall. If structural failure occurred (plastic hinge zones developed), they typically developed at the rock line (longitudinal direction) or column/pier cap connection (transverse).
- It appeared, based on the Chambers County case histories, that the 25% scour case was more detrimental to the performance of the drilled shaft foundations than the 100% scour case. Plastic hinge zones seemed to be developing below the ground surface in the 25% scour case due to the low lateral resistance provided by the soil layers above the bedrock.
- The driven pile case histories performed well when founded in competent soil (Lee County case history). However, the Etowah case history suggested that pile performance is poor when thick layers of soft clay are present, even in a moderate seismic hazard. Buckling, due to the lack of lateral resistance by the soil is most likely the cause of failure.
- Plastic hinge zones typically formed at the rock line in the longitudinal direction and at the pier cap in the transverse direction when the bed rock was shallow.
- If soft soils are present over rock, plastic hinges may form below the ground surface, but above the rock line.
- If driven piles are founded through soil that provides adequate lateral resistance, plastic hinges would most likely form at the base of the column or at the top of the pier cap for longitudinal and transverse directions, respectively.
- Deep foundations should be evaluated for buckling using the recommendation ($P_{des}/P_{cr} < 50$) made by Bhattacharya (2003).

- An alternative (or adaptive) foundation design should be considered for sites that have liquefiable or soft clay soils present.
- If seismic design is required, a detailed site investigation as well as laboratory tests should be conducted to more accurately estimate the soil parameters. This could potentially lead to a more efficient foundation design and reduce construction costs.
- In high seismic areas (relative to Alabama), shear wave velocity testing should be done. This could possibly lead to higher site classifications (A being the highest) which could lessen the seismic design requirements for critical and essential bridges in Alabama.
- Remedial measures are typically not taken by any of the states that responded to the survey.
- Though the likelihood of liquefaction occurring in Alabama is very low for most parts of the state, the potential for liquefaction should always be considered especially in regard to bridges near waterways in the northern part of the state.
- Soil data compiling of recent, past sites and future sites or bridge projects should be done to map site class and the SDC throughout the state. This can possibly expedite the design phase of future projects.
- It appeared that the models with a lower frequency and higher structural period performed better than those with a higher frequency and lower period.

8.3 Recommendations

There are several recommendations for foundation design considerations and future research on the response of deep foundations to seismic loading.

1. If scour is a possibility, deep foundations should be designed so that they are (at minimum) twice the length than the design scour depth (Ghosn et al. 2003).
2. Increase the drilled shaft diameter at the ground surface. If plastic hinges develop due to insufficient capacity, this will increase the likelihood of them developing at the ground surface.
3. Further scour analysis should be done for both drilled shaft and driven pile foundations. Multiple scour depths and soil types should be considered.
4. Soil susceptibility to scour within the state of Alabama should be further researched in order to better predict scour depths and behavior.
5. Further research regarding the structural period and frequency of a structure should be done to determine if there is a correlation to dynamic performance; and to determine if certain thresholds should be met for design standards.
6. Foundation response, using computer modeling, should be evaluated for liquefaction using residual soil strength to define the soil.
7. A full scale dynamic testing program coupled with direct analysis using a computer program (such as FB-MultiPier) should be conducted to better understand foundation response and to compare with FB-MultiPier's output results.

REFERENCES

American Concrete Institute (ACI) (2011) *Building Code Requirements for Structural Concrete (ACI 318-11) and Commentary*. American Concrete Institute, Farmington Hills, MI.

Alabama Department of Transportation (ALDOT) (2011). "Bridge Replacement on I-59 SBL over Norfolk Southern Railroad and US 11, Etowah County – Project No. STMAAF-I059 (342)," Bridge Drawings, Alabama Department of Transportation, Montgomery, AL.

ALDOT (2008). "Bridge Replacement Over Oseligee Creek on C.R. 1289, Chambers County – Project No. BR-IV20 (515)," Foundation Report and Bridge Drawings, Alabama Department of Transportation, Montgomery, AL.

ALDOT (2006). "Bridge Replacement on Bent Creek Road over I-85, Lee County – Project No. STPOA-9032 (600)," Foundation Report and Bridge Drawings, Alabama Department of Transportation, Montgomery, AL.

ALDOT (2005). "Bridge Over Little Bear Creek on E.B.L. of S.R. (Corridor V), Franklin County – Project No. APD-355 (501)," Foundation Report and Bridge Drawings, Alabama Department of Transportation, Montgomery, AL.

ALDOT (2003). "Bridge Replacement on SR 75 over Scarham Creek (S.B.L.), Marshall County – Project No. STPAA-0075 (502)," Foundation Report and Bridge Drawings, Alabama Department of Transportation, Montgomery, AL.

American Petroleum Institute (API) (1997). *Recommended Practice for Planning, Designing and Constructing Fixed Offshore Platforms – Load and Resistance Factor Design*, Washington D.C.

American Association of State Highway and Transportation Officials (AASHTO) (2013) *AASHTO LRFD Bridge Design Specifications,* Washington D.C.

AASHTO (2009) *AASHTO Guide Specification for LRFD Seismic Bridge Design,* Washington D.C.

AASHTO (2002) *AASHTO Standard Specification for Highway Bridges*, Washington D.C.

Bhattacharya, S., Madabhushi, S. P. G. and Bolton, M. D., (2004). "An Alternative Mechanism of Pile Failure in Liquefiable Deposits During Earthquakes." *Geotechnique,* 54(3), 203 – 213.

Bhattacharya, S. (2003). "Pile Instability During Earthquake Liquefaction," Ph.D. Dissertation, University of Cambridge, Cambridge, UK.

Berril, J.B., Christensen, S. A., Keenan, R. P., Okada, W. and Pettinga, J.R. (2001). "Case Studies of Lateral Spreading Forces on a Piled Foundation." *Geotechnique*, 51(6), 501-517.

Brown, D. A., O'Neill, M. W., Hoit, M., McVay, M., Naggar, M. H. El, Chakraborty, S., (2001). *Static and Dynamic Lateral Loading of Pile Groups.* Report 461, National Cooperative Highway Research Program, Washington D.C.

Brown, D. A., Morrison, C., and Reese, L. C. (1988). "Lateral Load Behavior of Pile Group in Sand." *Journal of Geotechnical Engineering*, 114(11), 1261 - 1276.

Bridge Software Institute (BSI) (2013)a. *FB-Deep v2.04*, Gainesville, Florida.

BSI (2013)b. *FB-MultiPier v4.18*, Gainesville, Florida

Coulston, P. (2011). "Influence of the LRFD Bridge Design Specifications on Seismic Design in Alabama." Master's Thesis, Auburn University, Auburn, Alabama.

CSI (Computers and Structures, Inc.) (2013). *CSiBridge*, Walnut Creek, CA.

Ebersole, Sandy M. and Perry, Shinisha L. (2008). "Seismic Amplification and Liquefaction Susceptibility Mapping in Alabama." Geological Survey of Alabama Open-File Report 0807, pp 21, 4 plates.

Ensoft, Inc. (2013)a. *GROUP v8.0 for windows*, Austin, Texas

Ensoft, Inc. (2013)b. *LPILE v6.0 for windows*, Austin, Texas

Fernandes, C. (1999). "Nonlinear Dynamic Analysis of Bridge Piers," Ph.D Dissertation, University of Florida, Gainesville, Florida.

Gallet & Associates (2008). "Bridge Replacement on I-59 SBL over Norfolk Southern Railroad and US 11, Etowah County – Project No. STMAAF-I059 (342)," Foundation Report, Terracon (formerly Gallet & Associates), Huntsville, AL.

Ghosn, M., Moses, F., and Wang, J. (2003). *Design of Highway Bridges of Extreme Events*. Report No. 489, National Cooperative Highway Research Program, Washington D.C.

Hannigan, P. J., Goble, G.G., Likins, G.E., and Rausche, F. (2006). *Design and Construction of Driven Pile Foundations, Reference Manual – Volume 1.* Report No. FHWA-NHI-05-042, Federal Highway Administration, Washington D.C.

Hognestad, E., Hanson, N. W. and McHenry, D. (1955) "Concrete stress distribution in ultimate strength design.". *Journal of the American Concrete Institute.* Part 1. 27(4), 455-479.

Hughes, T. J. R. and Belytschko, T. (1983). "A Precis of Developments in Computational Methods for Transient Analysis." *Journal of Applied Mechanics,* 50(12), 1033-1041.

Idriss, I. M. and Boulanger, R. W. (2008) *Soil Liquefaction During Earthquake.* Earthquake Engineering Research Institute, Oakland, California.

Ishihara, K. (1997). Terzaghi oration: "Geotechnical Aspects of the 1995 Kobe Earthquake." *Proceedings of ICSMFE,* Hamburg, 2047-2073.

Kavazanjian, E. Jr., Marsh, M. L., and Banks, G. (2012). *LRFD Seismic Analysis and Design of Transportation Geotechnical Features and Structural Foundations, Comprehensive Design Examples.* Report No. FHWA-NHI-11-075, NHI Course No. 132094, Federal highway Administration Washington D.C.

Kavazanjian, E. Jr., Wang, J. J., Martin, G. R., Shamsabadi, Anoosh, Lam, Ignatius, Dickenson, Stephen E., and Hung, Jeremy C. (2011). *Geotechnical Engineering Circular No. 3 – LRFD Seismic Analysis and Design of Transportation Geotechnical Features and Structural Foundations – Reference Manual.* Report No. FHWA-NHI-11-032, Federal Highway Administration, Washington D.C.

Kim, M. (2001). "Analysis of Osterberg and Statnamic Axial Load Testing and Conventional Lateral Load Testing." Master's Thesis, University of Florida, Gainesville, Florida.

Kimura, Y. and Tokimatsu, K. (2005). "Buckling Stress of Steel Pile with Vertical Load in Liquefied Soil." *Journal of Structural and Construction Engineering*, (595) 73-78.

Knappett, J. and Madabhushi, S. (2005) Modeling of Liquefaction-Induced Instability in Pile Groups. *Seismic Performance and Simulation of Pile Foundations in Liquefied and Laterally Spreading Ground*, 255-267.

Kramer, S. L. (1996). *Geotechnical Earthquake Engineering*. Prentice Hall, Inc., Upper Saddle River, NJ.

Kulhawy, F.H. and Mayne, P.W. (1990) *Manual on Estimating Soil Properties for Foundation Design*. Report No. EPRI EL-6800, Electric Power Research Institute, Palo Alto, California.

Lam, I., and Martin, G. (1986), *Seismic Design of Highway Bridge Foundations Vol. II – Design Procedures and Guidelines*. Report No. FHWA/RD-86/102, Federal Highway Administration, Washington D.C.

Matlock, H. (1970). "Correlations for Design of Laterally Loaded Piles in Soft Clay." Paper No. OTC 1204, *Proceedings, Second Annual Offshore Technology Conference,* Houston, Texas, Vol. 1. 577 - 594.

Mayne, P. W., Christopher, B. R., and DeJong, Jason (2001). *Subsurface Investigations – Geotechnical Site Investigations, Reference Manual.* Report No. FHWA-NHI-01-031, Federal Highway Administration, Washington D.C.

McCarthy, D. F. (2007). *Essentials of Soil Mechanics and Foundations: Basic Geotechnics*. Prentice Hall, Upper Saddle River, New Jersey.

McVay, M.C. and Niraula, L. (2004). *Development of P-y Curves for Large Diameter Piles/Drilled Shafts in Limestone for FBPIER.* University of Florida, Gainesville, FL.

McVay, M. C., O'Brien, M., Townsend, F. C., Bloomquist, D. G., and Caliendo, J. A. (1989) "Numerical Analysis of Vertically Loaded Pile Groups." *ASCE Foundation Engineering Congress*, Northwestern University, Illinois, 675-690.

National Research Council (NRC) (1985). *Liquefaction of Soils During Earthquakes*. Committee on Earthquake Engineering, Report No. CETS-EE-001, National Research Council, Washington D.C.

O'Neill, M. W. (1996). *Load Transfer for Drilled Shafts in Intermediate Geomaterials*. Report No. RD-95-172, Federal Highway Administration, Washington, D.C.

O'Neill, M.W. and Reese, L.C., (1999). *Drilled Shafts: Construction Procedures and Design Methods*. Report No. IF-99-025, Federal Highway Administration, Washington, D.C.

O'Neill, M. W. and Gazioglu, S. M. (1984). "Evaluation of P-y Relationships in Cohesive Soils." *Proceedings, Analysis and Design of Pile Foundations, ASCE Technical Council on Codes and Standards*, ASCE National Convention, San Francisco, California, 192-213.

O'Neil, M. W. and Murchison, J. M. (May, 1983) *An Evaluation of P-y Relationships in Sands.* Research Report No. GT-DF02-83, Department of Civil Engineering, University of Houston, Houston, Texas.

Panzer, J. (2013). "Evaluation of Critical and Essential Concrete Highway Bridges in a Moderate Seismic Hazard." Master's Thesis, Auburn University, Auburn, Alabama.

Peck, R. B., Hanson, W. E., and Thornburn, T. H. (1974). *Foundation Engineering.* John Wiley and Sons, New York.

Reese, L. C., and O'Neill, M. W. (1988). *Drilled Shafts: Construction Practices and Design Methods.* Report No, FHWA-HI-042, Federal Highway Administration, Washington, D. C.

Reese, L. C., Cox, W. R., and Koop, F. D. (1975). "Field Testing and Analysis of Laterally Loaded Piles in Stiff Clay," Paper No. OTC 2312, *Proceedings, Seventh Offshore Technology Conference*, Houston, Texas, 106 - 125.

Reese, L. C., and Wang, S. (1993) *Com624P- Laterally Loaded Pile Analysis Program for the Microcomputer Version 2.0*. Report No. FHWA-SA-91-048, Federal Highway Administration, Washington D.C.

Reese, L. C. and Welch, R. C. (1972). *Lateral Load Behavior of Drilled Shafts*, Research Report No. 3-5-65-99, conducted for Texas Highway Department and U.S. Department of Transportation, Federal Highway Administration, Bureau of Public Roads by Center for Highway Research, The University of Texas at Austin, Austin, Texas.

Reese, L. C., Cox, W. R., and Koop, F. D. (1975). "Field Testing and Analysis of Laterally Loaded Piles in Stiff Clay," Paper No. OTC 2312, *Proceedings, Seventh Offshore Technology Conference*, Houston, Texas.

Richardson, E.V., and Davis, S.R., (1995). *Evaluating Scour at Bridges,* Report No. FHWA-IP-90-017, Federal Highway Administration, Washington D.C.

SCDOT (2010). *Geotechnical Design Manual Version 1.1*, <http://www.scdot.org/doing/structural_Geotechnical.aspx>, July 18, 2013.

Schmertmann, J. H. (1975). "Measurement of Insitu Strength," *Proceedings, First Conference on Insitu Measurements of Soil Properties*, Vol. 2, Raleigh, NC, 57-138.

Schmertmann, J. H. (1967). *Guidelines For Use In The Soils Investigation and Design of Foundations For Bridge Structures In The State Of Florida.* Research Bulletin 121, Florida Department of Transportation, Tallahassee, Florida.

Seed, H.B. and Idriss, I.M. (1982). *Ground Motions and Soil Liquefaction During Earthquakes*. Earthquake Engineering Research Institute, Berkeley, California, 134.

Shanker, K., Basudhar, P., and Patra, N. (2007). "Buckling of Piles under Liquefied Soil Conditions," *Geotechnical and Geological Engineering*, 25(3), 303-313.

Terzaghi, K. and Peck, R. B. (1968). *Soil Mechanics in Engineering Practice*, 2nd Ed., Wiley, New York.

USGS (2008). "USGS Researchers Lead International Team Investigating Damage Caused by Offshore Earthquake Near World's Largest Nuclear Power Plant in Japan," <http://soundwaves.usgs.gov/2008/01/> (April 5, 2013).

Wei, X., Wang, Q., and Wang, J. (2008). "Damage Patterns and Failure Mechanisms of Bridge Pile Foundation Under Earthquake," *The 14th World Conference on Earthquake Engineering*, Beijing China,

Yellow Maps (2010). "Alabama Counties," <http://www.yellowmaps.com/maps/img/US/outline/alabama.gif> (December 12, 2012).

Youd, T. L., and Idriss, I. M.,(2001). "Liquefaction Resistance of Soils: Summary Report from the 1996 NCEER and 1998 NCEER/NSF Workshops on Evaluation of Liquefaction Resistance of Soils." *Journal of Geotechnical and Geoenvironmental Engineering*, American Society of Civil Engineers, 297-313

Youd, T.L. and Perkins, I.M. (1997). "Mapping of Liquefaction-Induced Ground Failure Potential." *Journal of the Geotechnical Engineering Division*, American Society of Civil Engineers, 104(4), 433-446.

Appendix A

TIME-HISTORY EVENTS

The time-history events used for direct analysis are presented. For graphical purposes, the 30-40 seconds when the acceleration is zero is not shown on the plots.

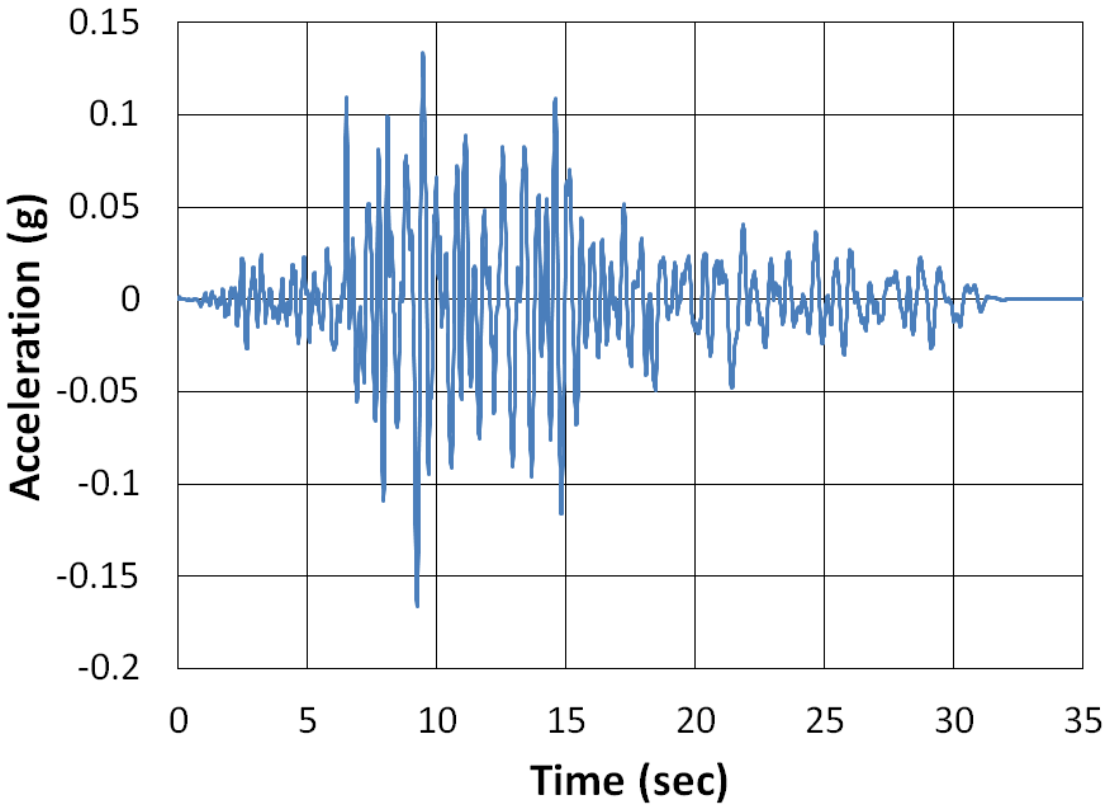

Figure A.1. Coalinga North time-history event

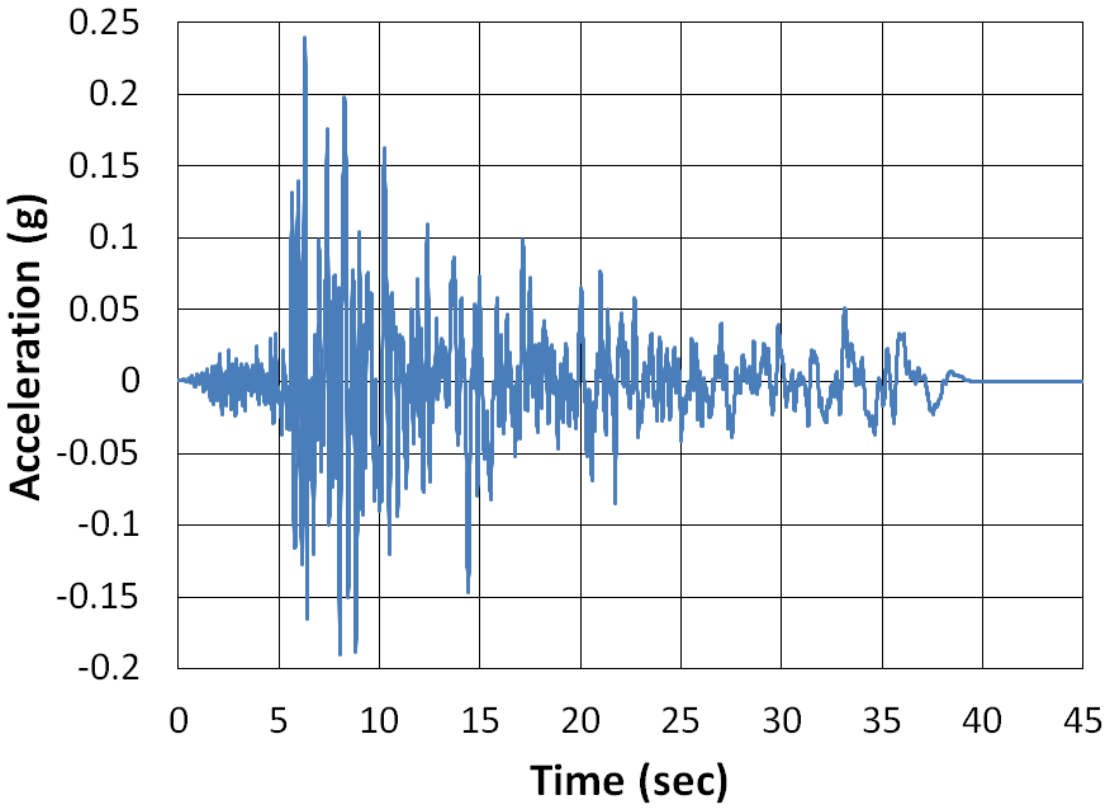

Figure A.2. Imperial Valley NMCE time-history event

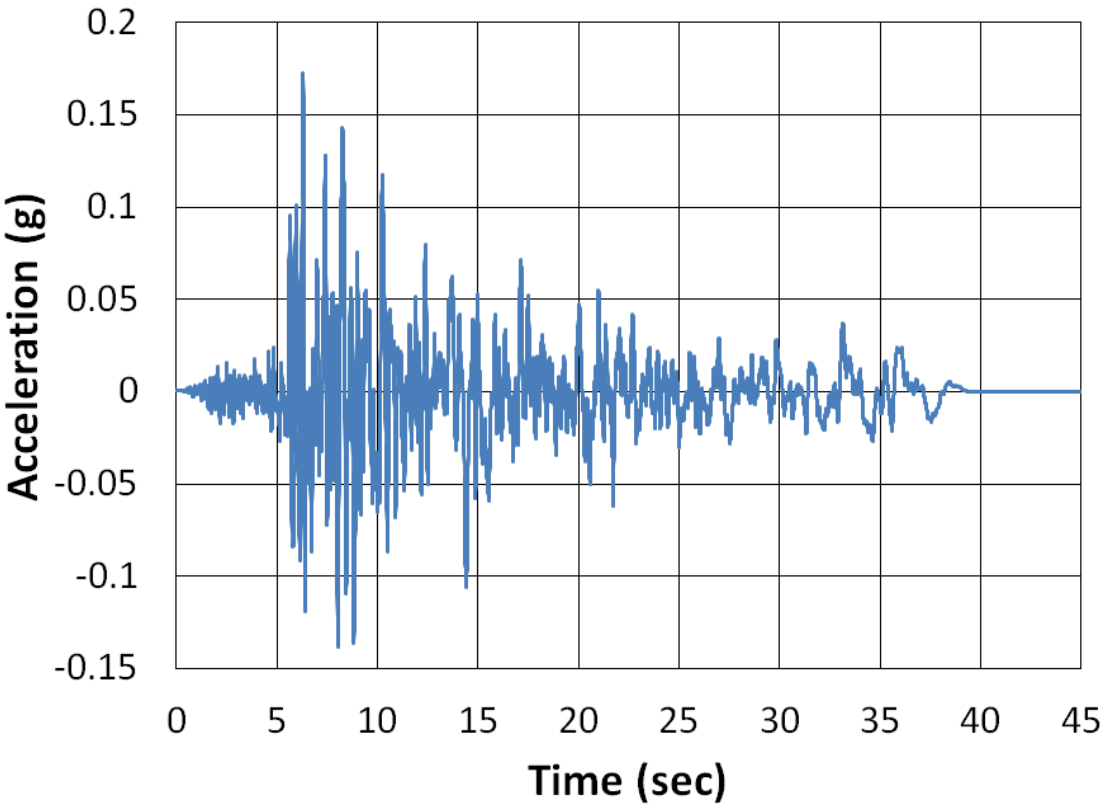

Figure A.3. Imperial Valley North time-history event

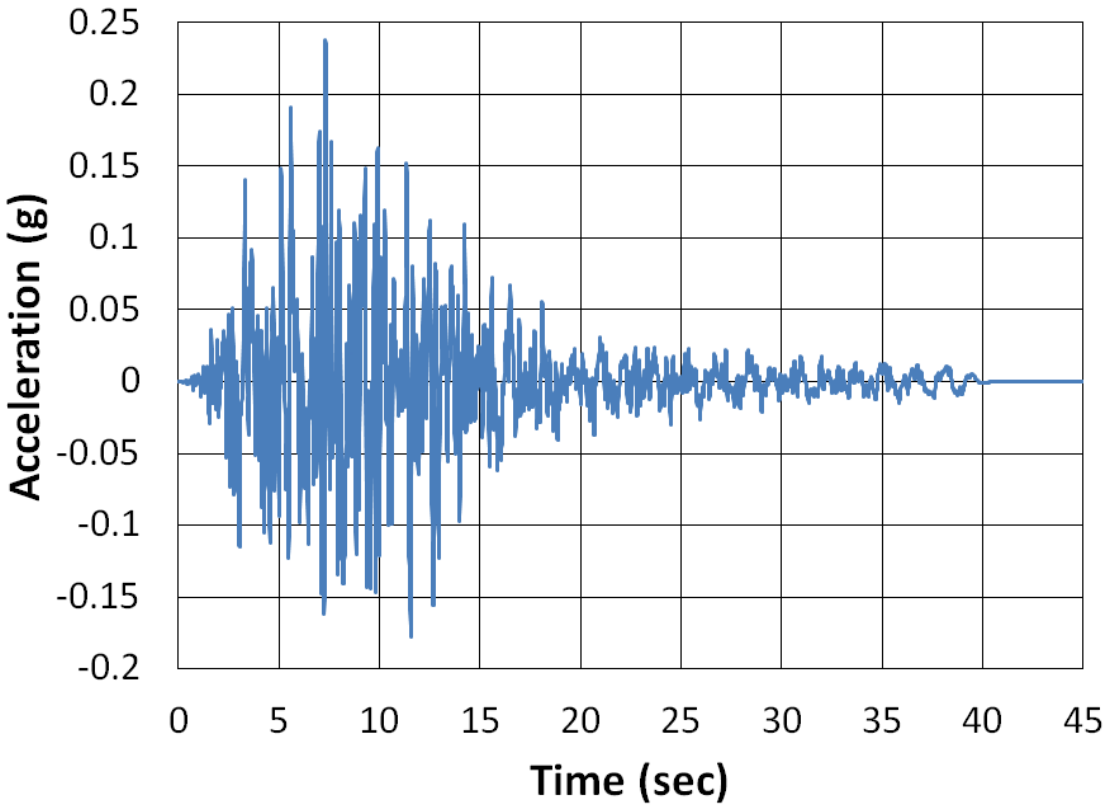

Figure A.4. Kobe NMCE time-history event

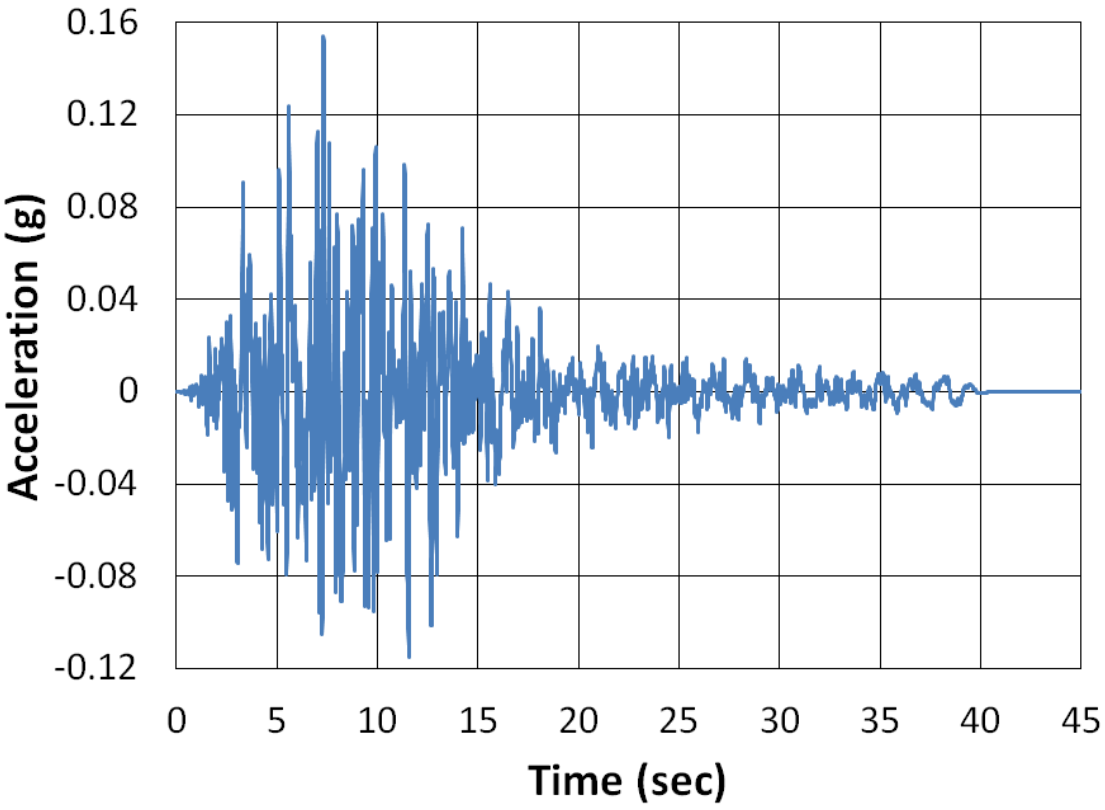

Figure A.5. Kobe North time-history event

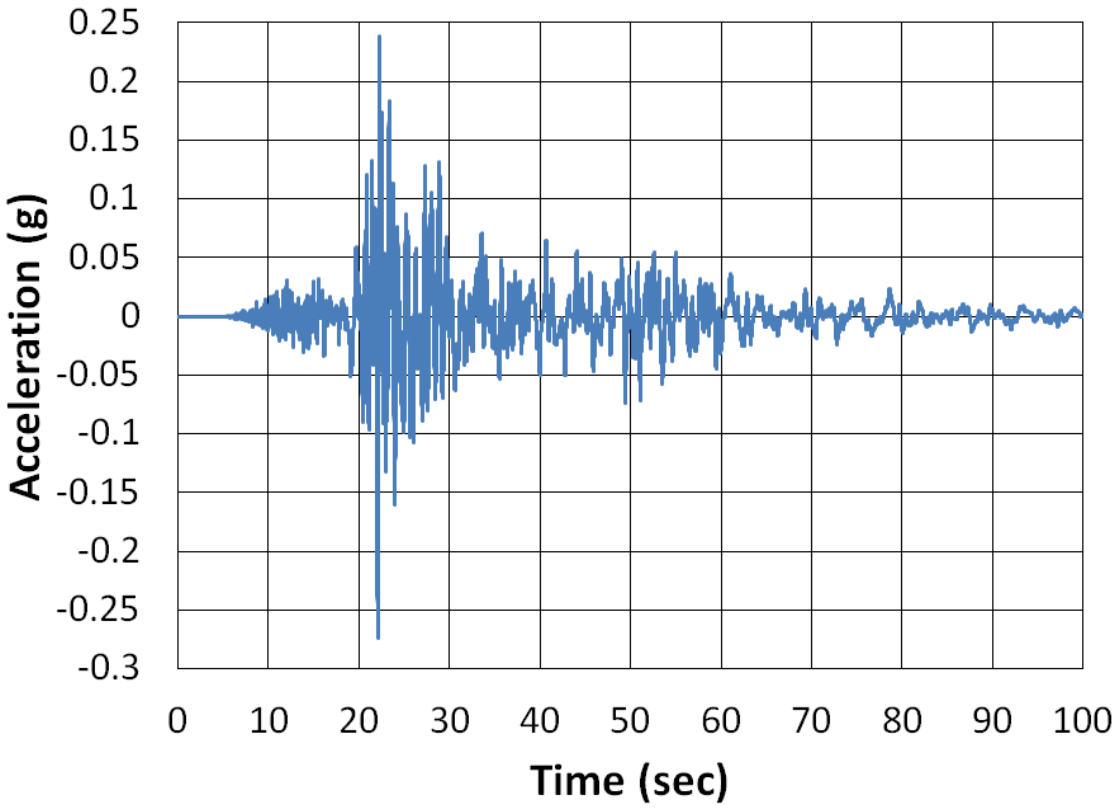

Figure A.6. Kocaeli NMCE time-history event

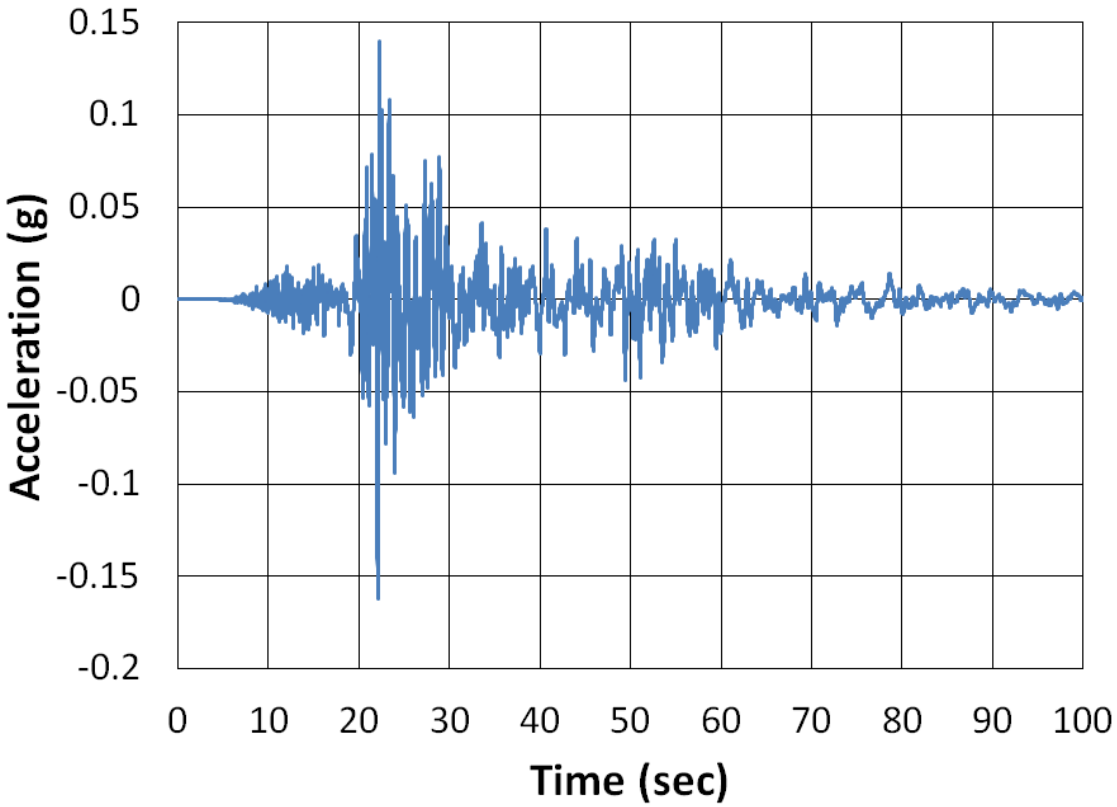

Figure A.7. Kocaeli North time-history event

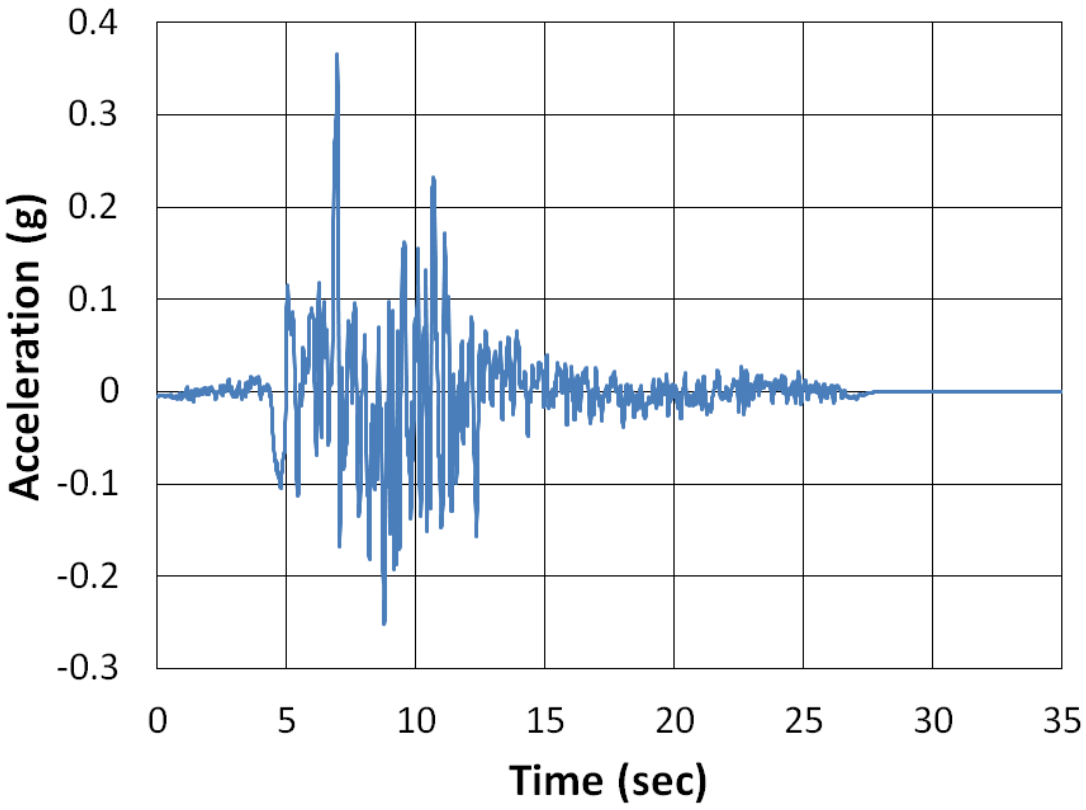

Figure A.8. Kocaeli2 NMCE time-history event

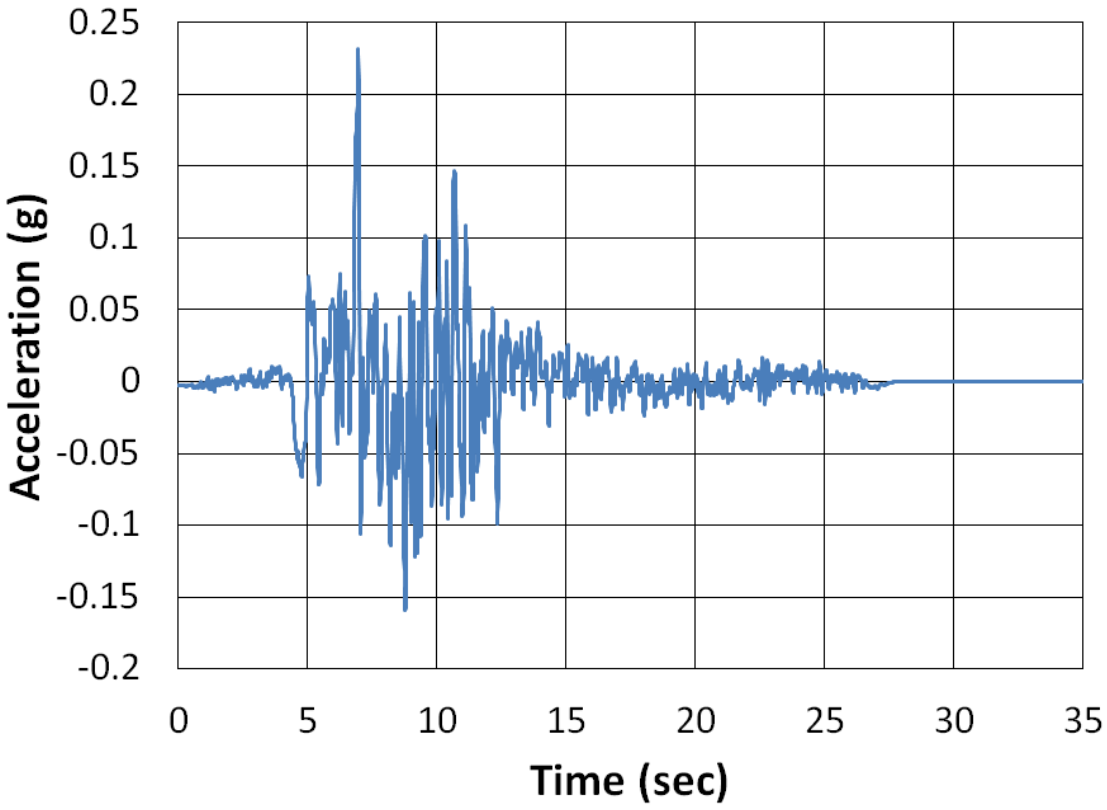

Figure A.9. Kocaeli2 North time-history event

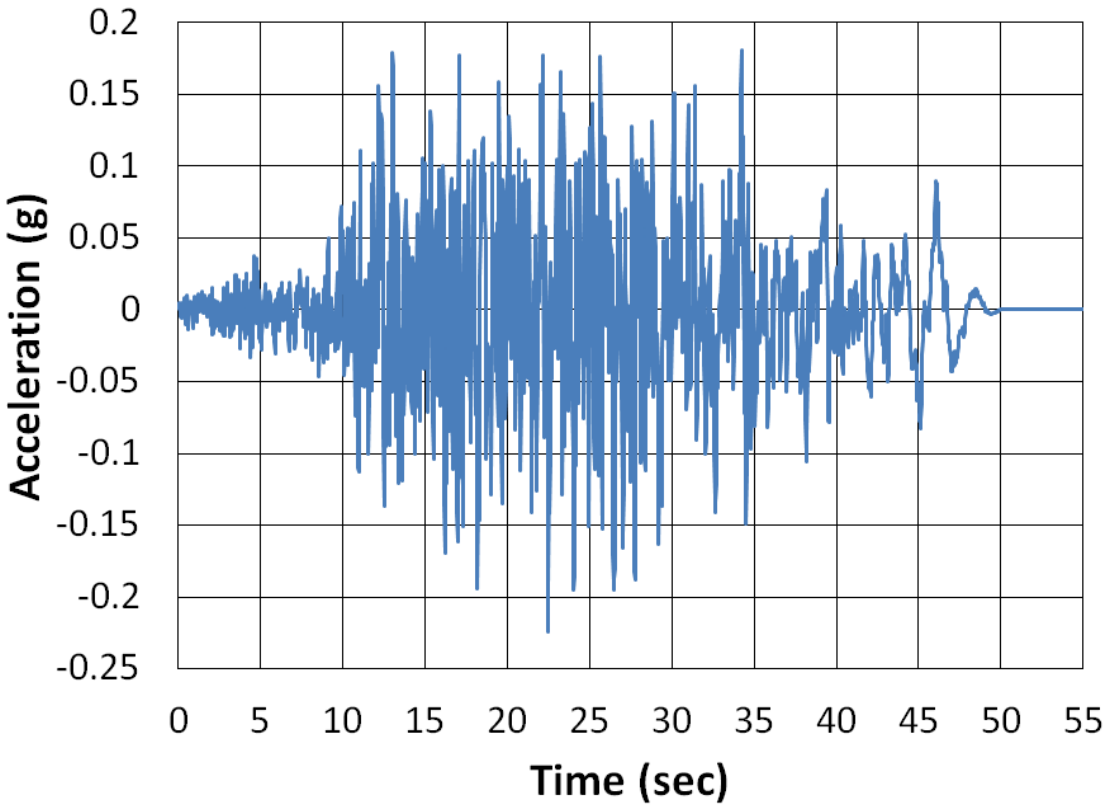

Figure A.10. Landers NMCE time-history event

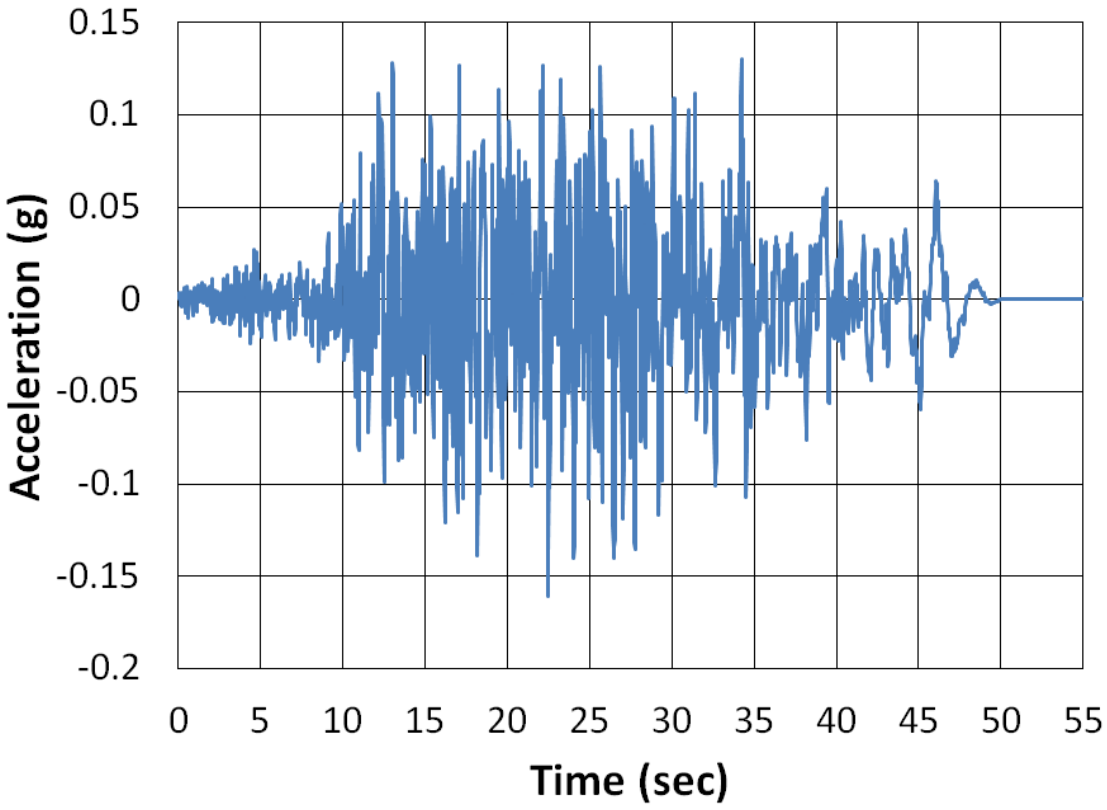

Figure A.11. Landers North time-history event

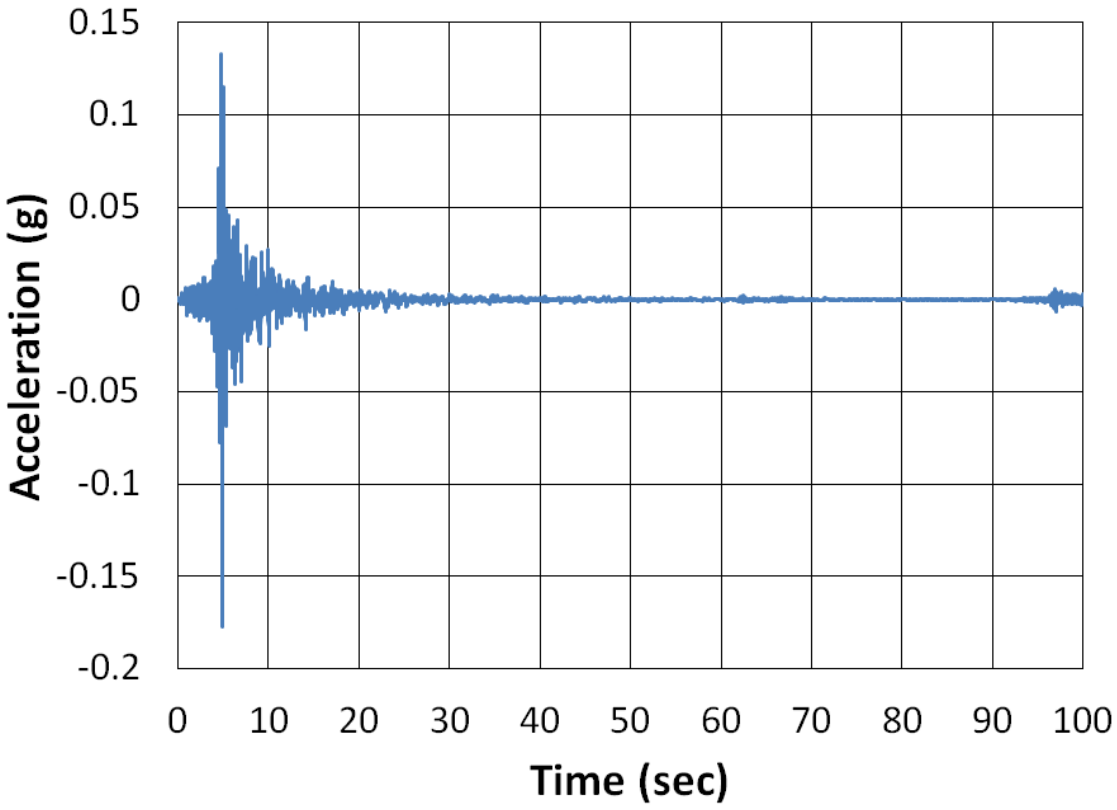

Figure A.12. LSM North time-history event

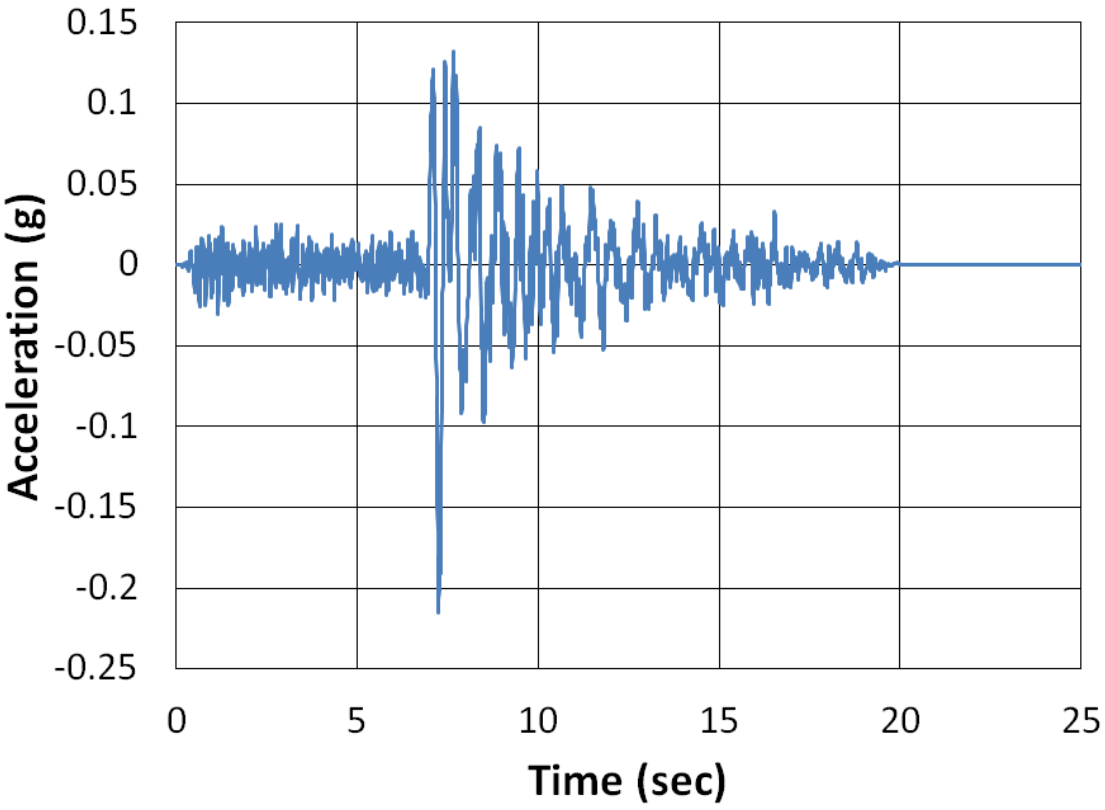

Figure A.13. NPS North time-history event

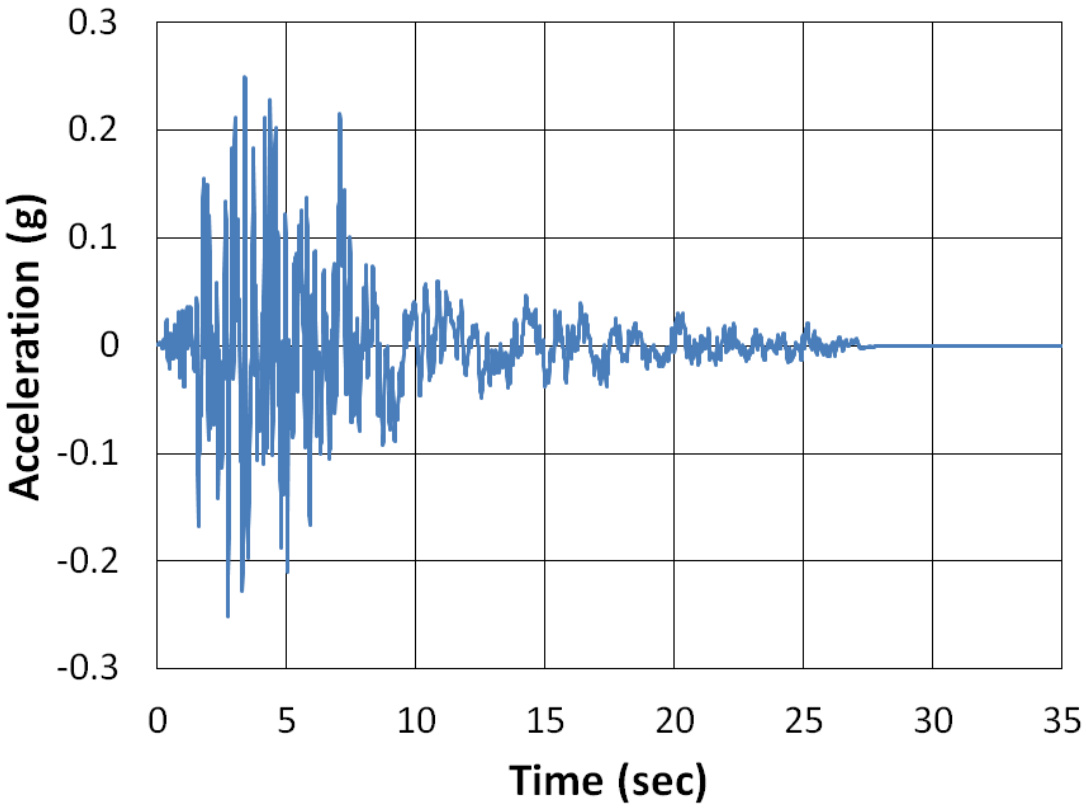

Figure A.14. San Fernando NMCE time-history event

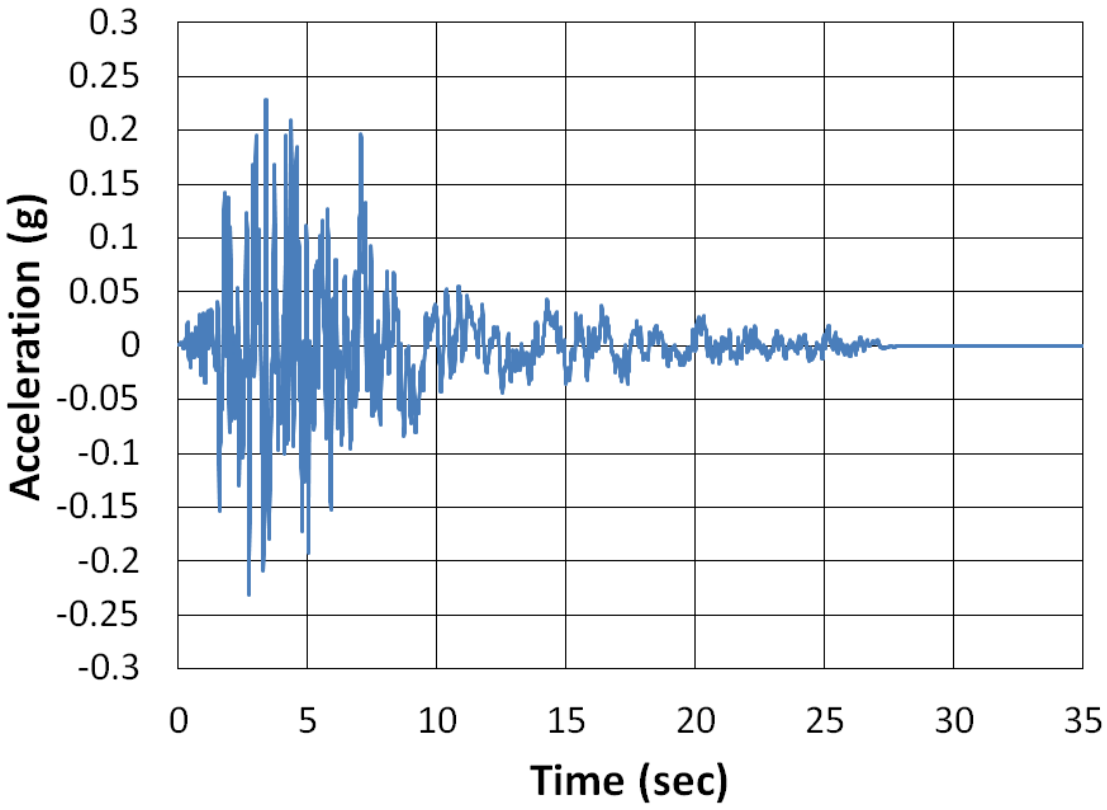

Figure A.15. San Fernando North time-history event

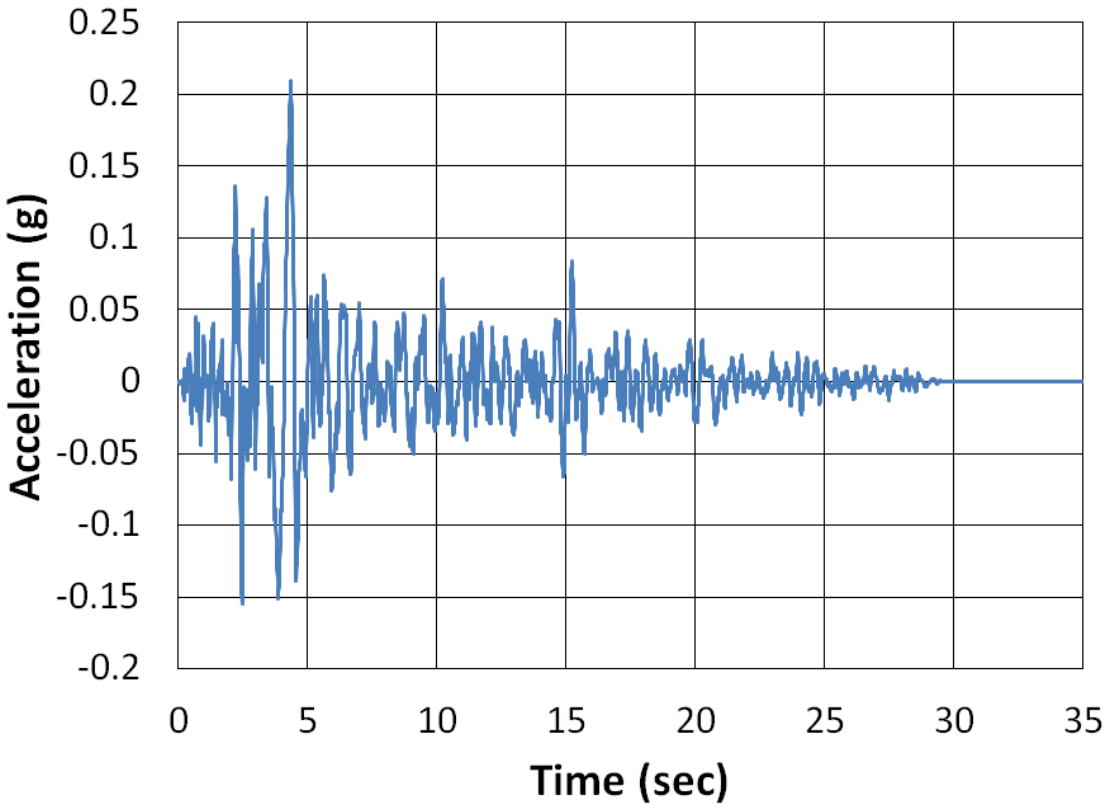

Figure A.16. San Fernando2 NMCE time-history event

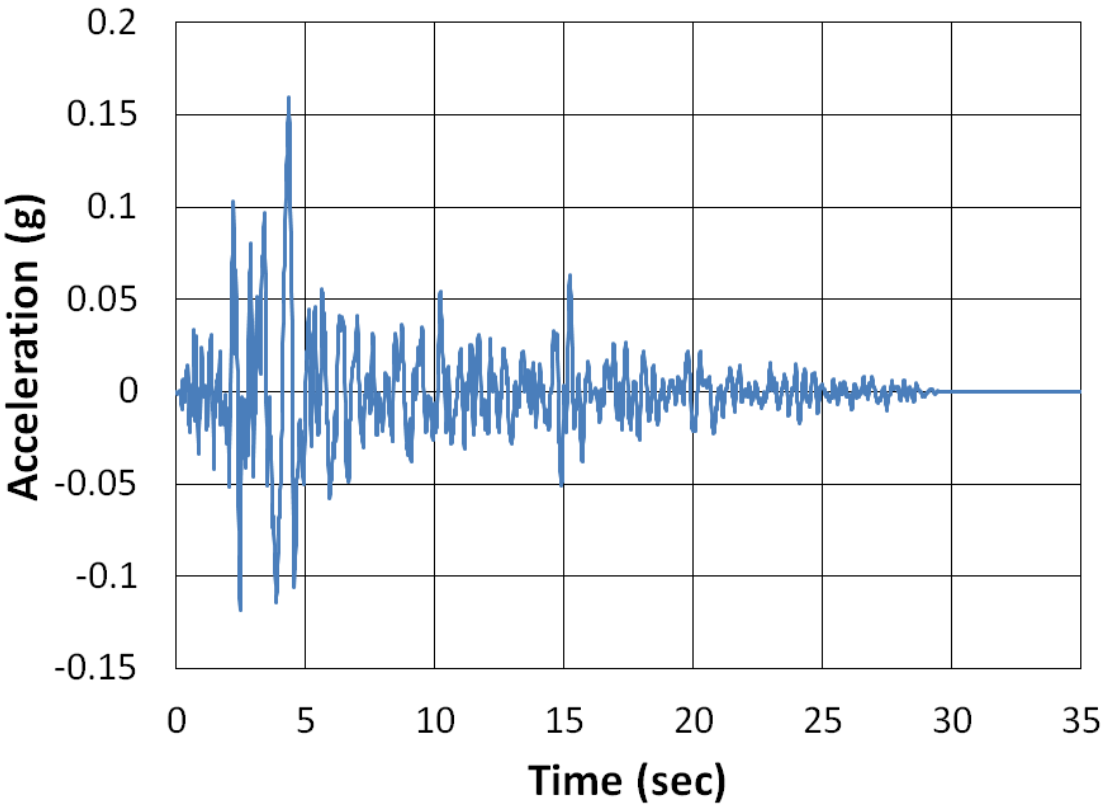

Figure A.17. San Fernando2 North time-history event

Appendix B

DAMPING ANALYSIS RESULTS

The damping analysis results are presented. The sine wave was used in FB-MultiPier to determine the response of the structure. Displacement versus time was then used to determine the percent damping of the system.

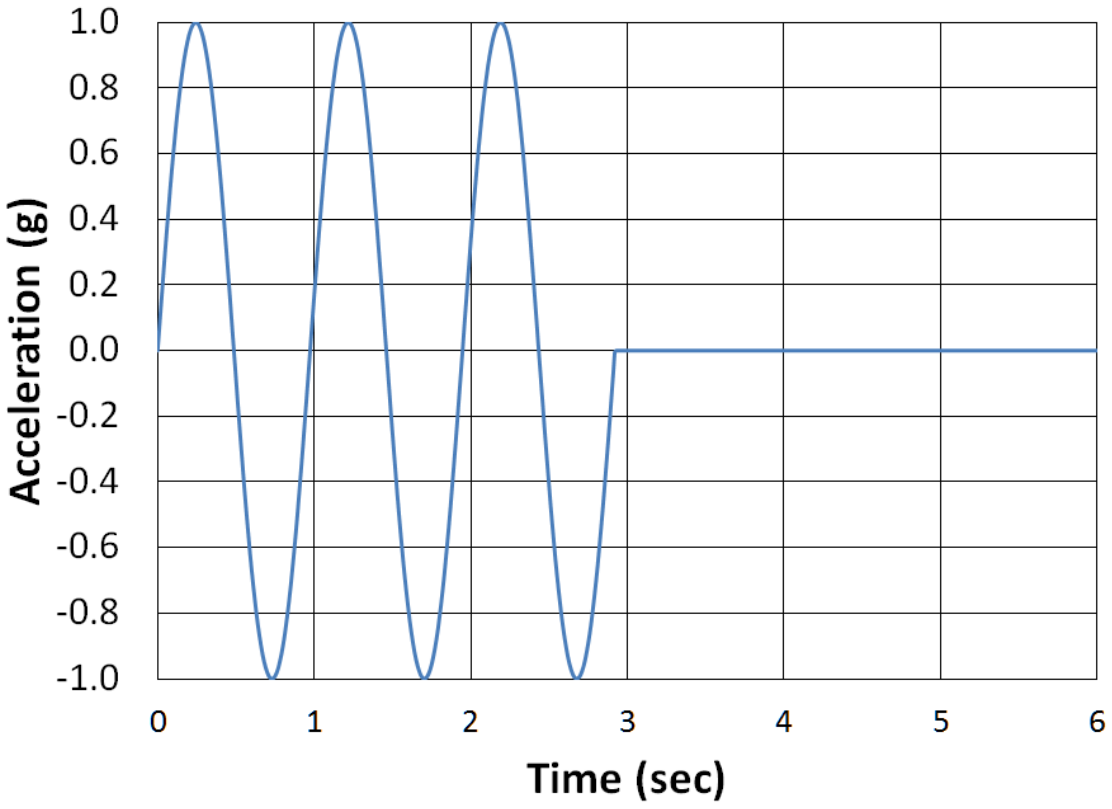

Figure B.1. Chambers County 25% Scour longitudinal sine wave time-history

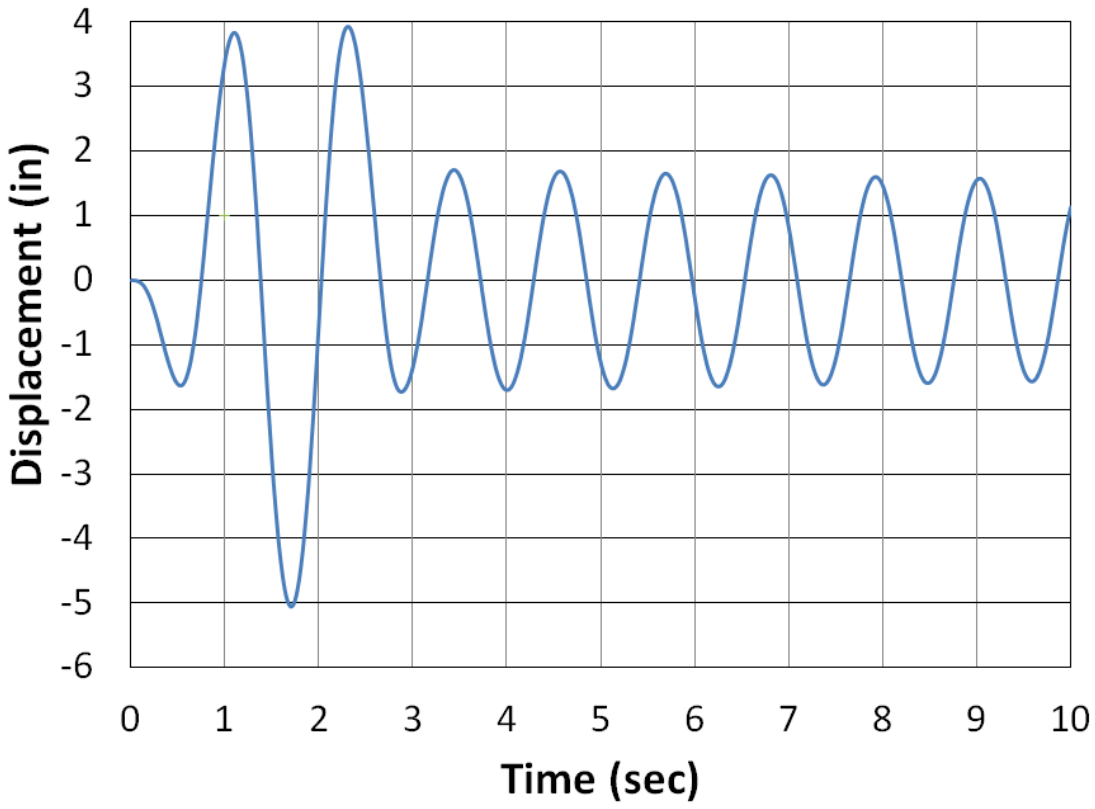

Figure B.2. Chambers County 25% scour longitudinal displacement versus time at the top of the pier

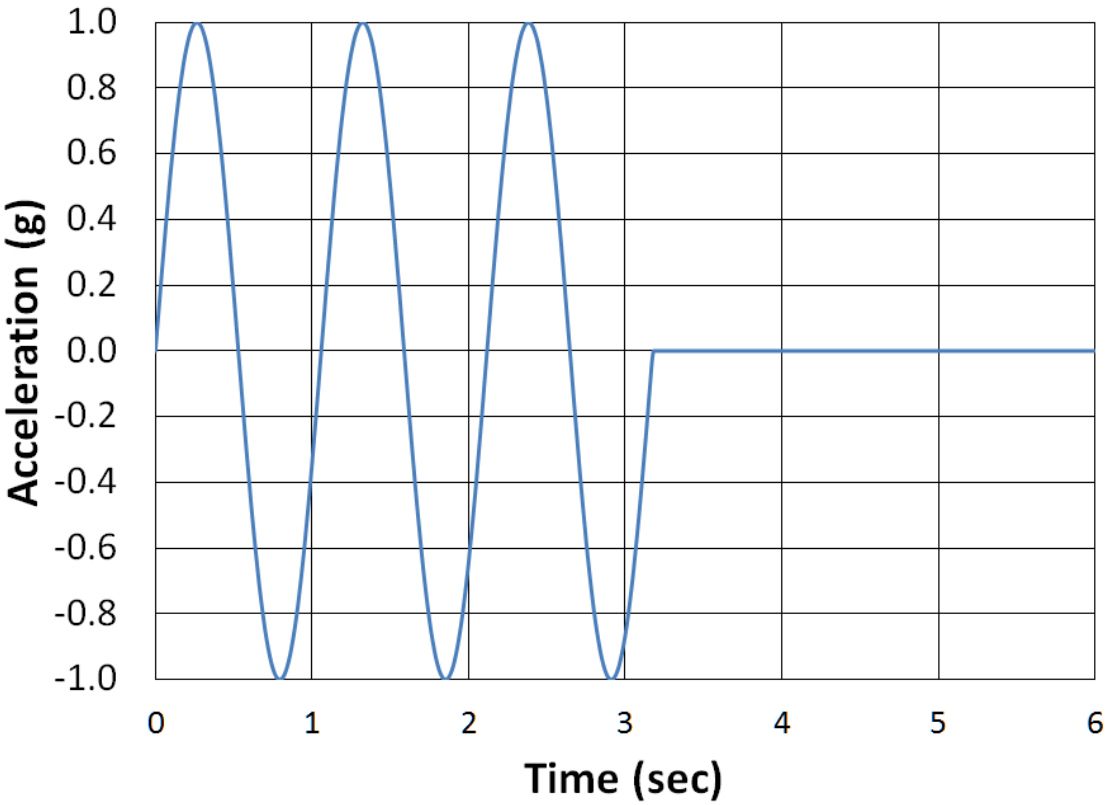

Figure B.3. Chambers County 100% Scour longitudinal sine wave time-history

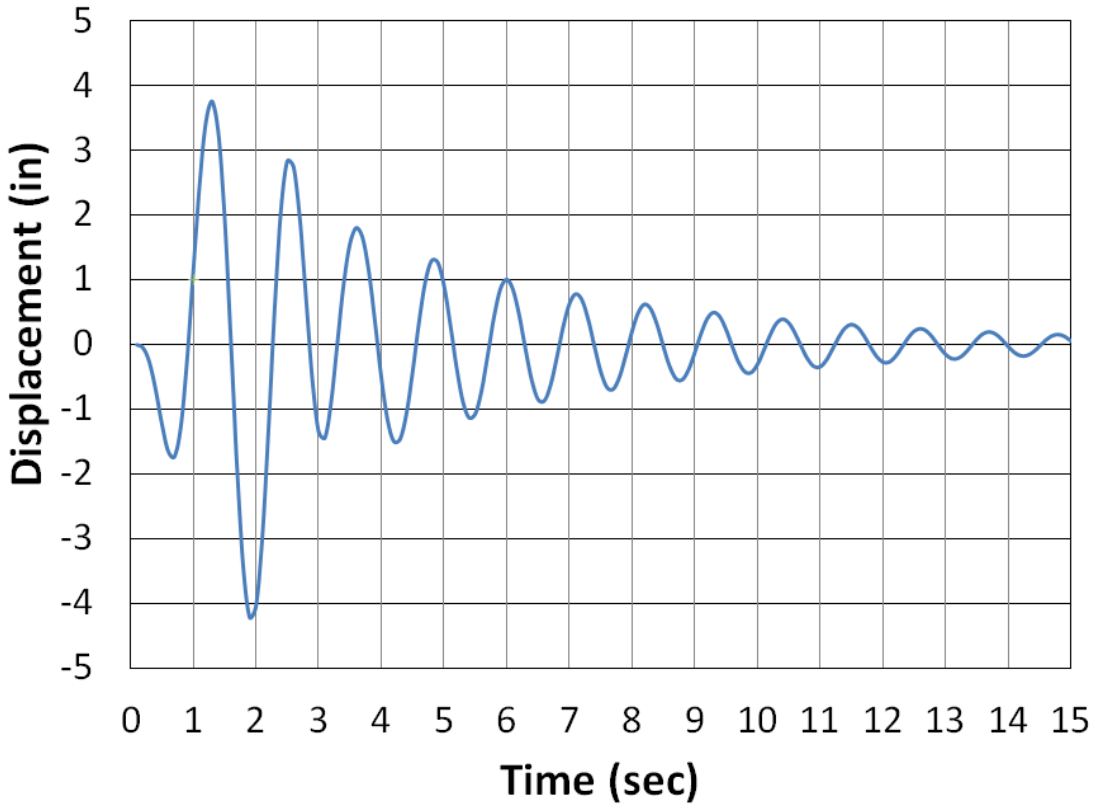

Figure B.4. Chambers County 100% scour longitudinal displacement versus time at the top of the pier

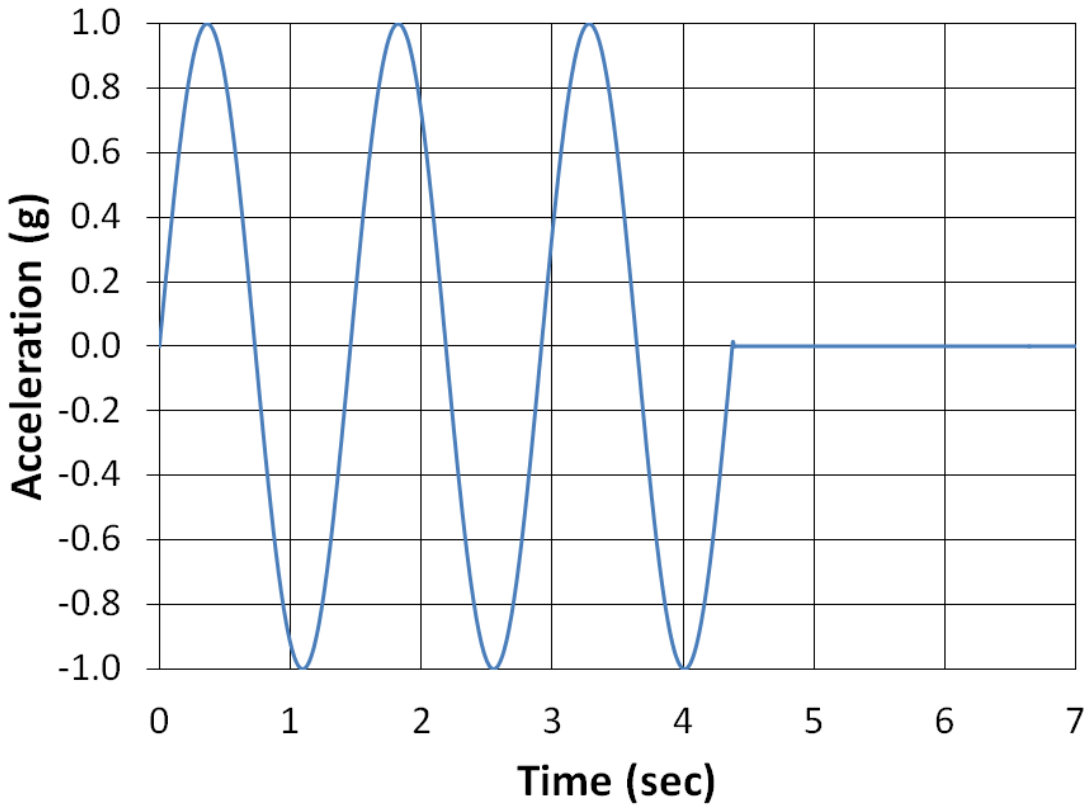

Figure B.5. Etowah County longitudinal sine wave time-history

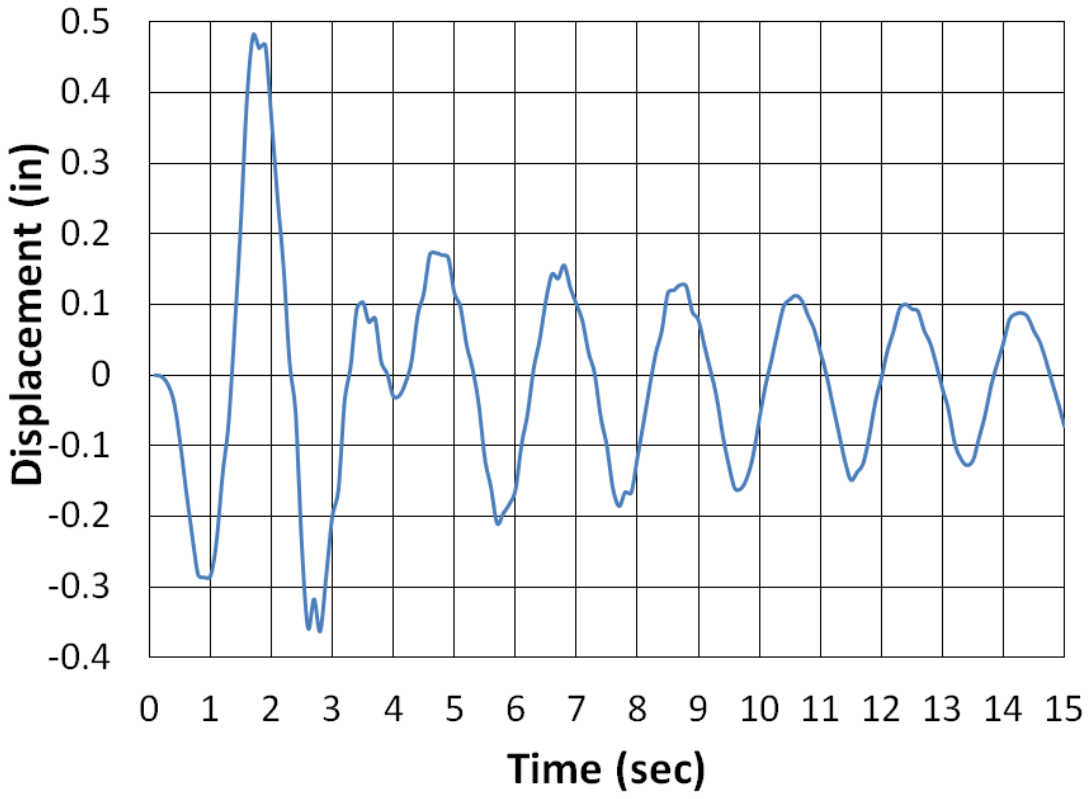

Figure B.6. Etowah County longitudinal displacement versus time at the top of the pier

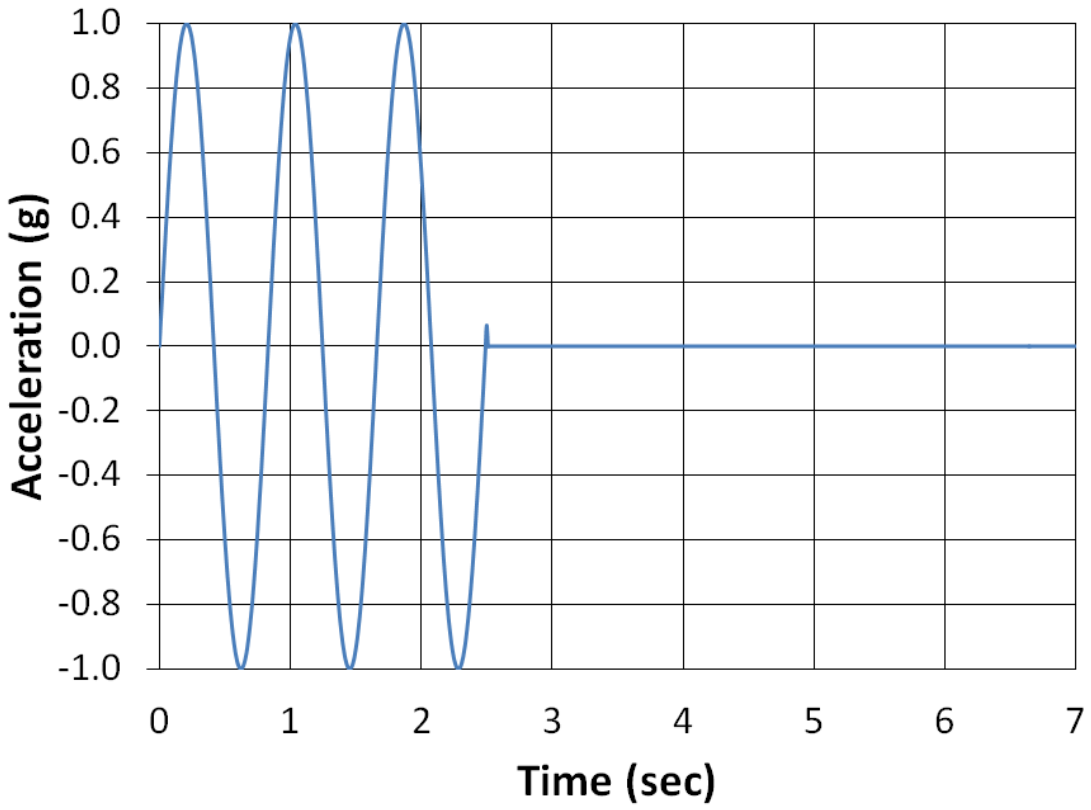

Figure B.7. Franklin County longitudinal sine wave time-history

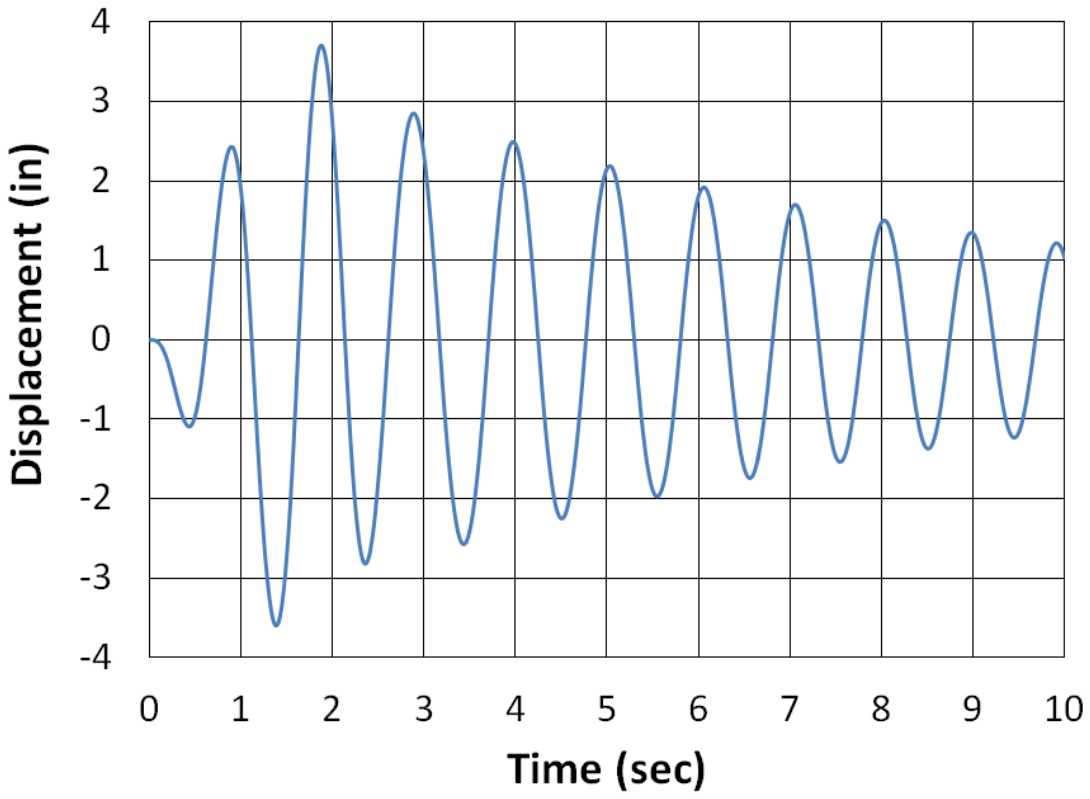

Figure B.8. Franklin County longitudinal displacement versus time at the top of the pier

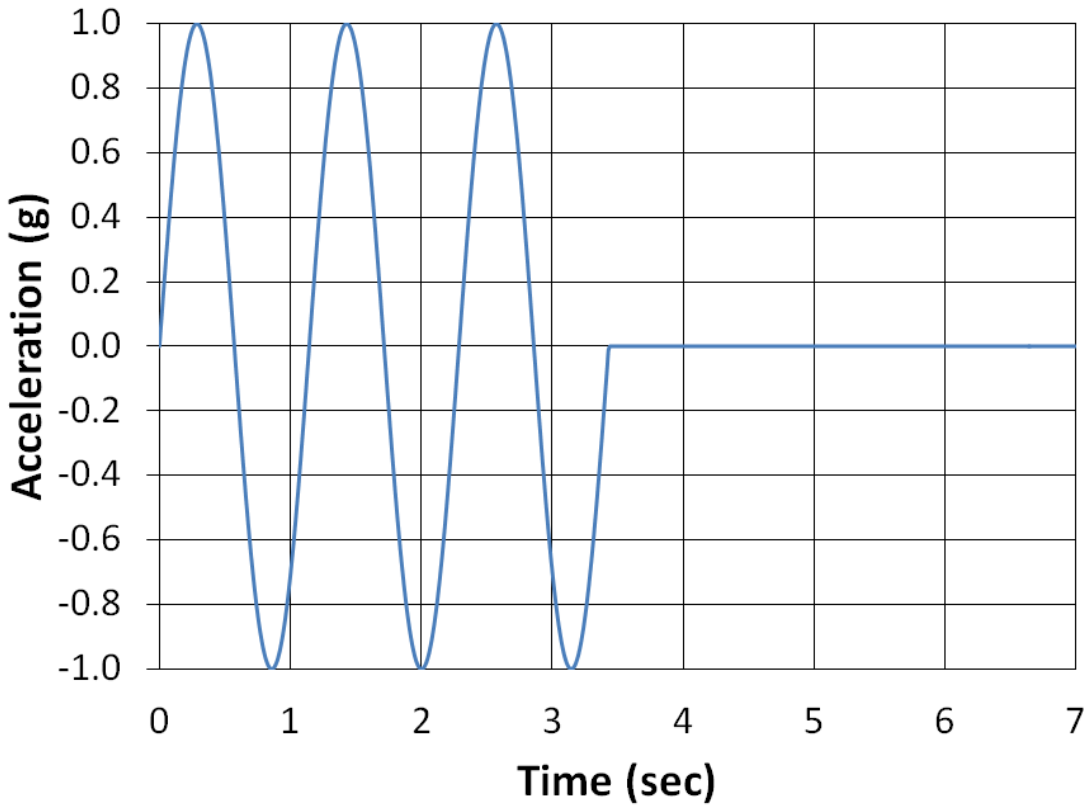

Figure B.9. Lee County longitudinal sine wave time-history

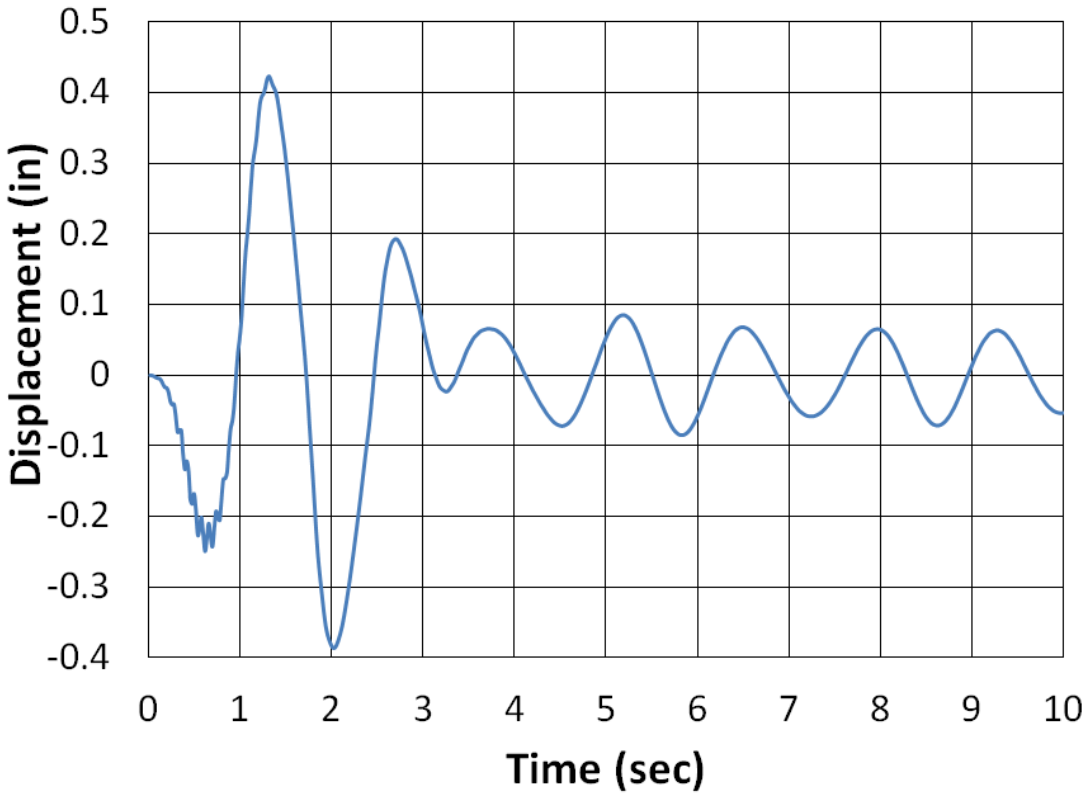

Figure B.10. Lee County longitudinal displacement versus time at the top of the pier

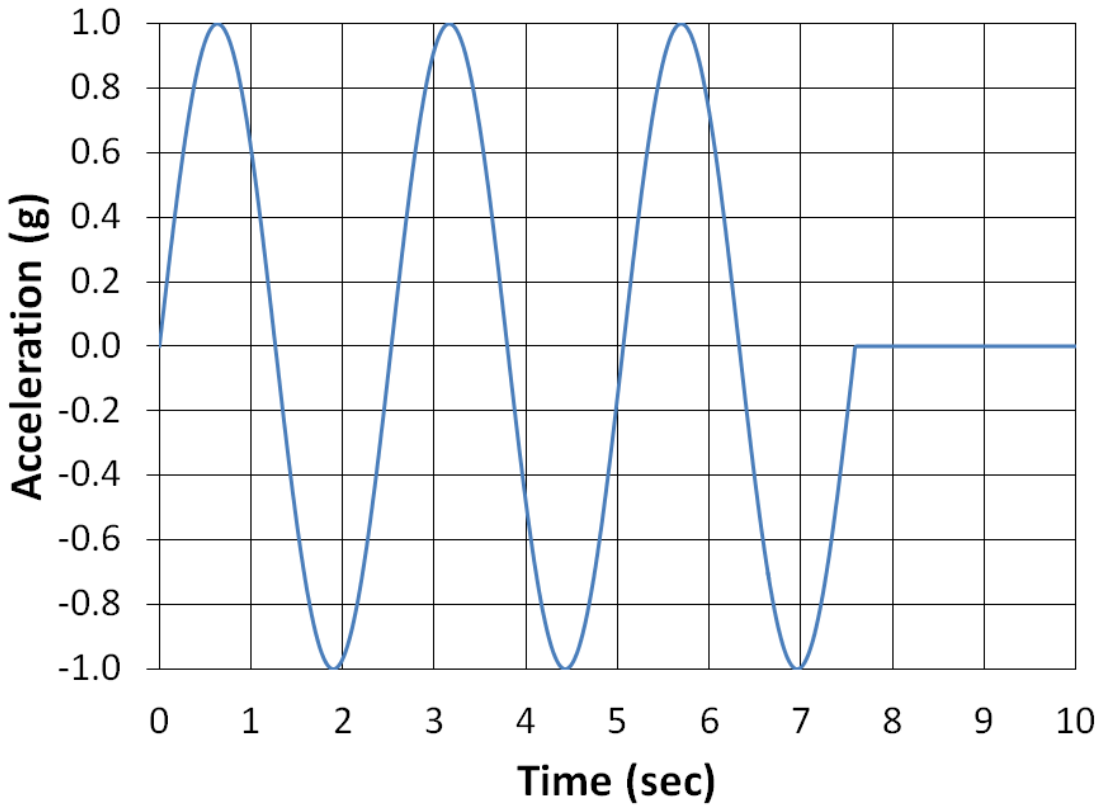

Figure B.11. Marshall County longitudinal sine wave time-history

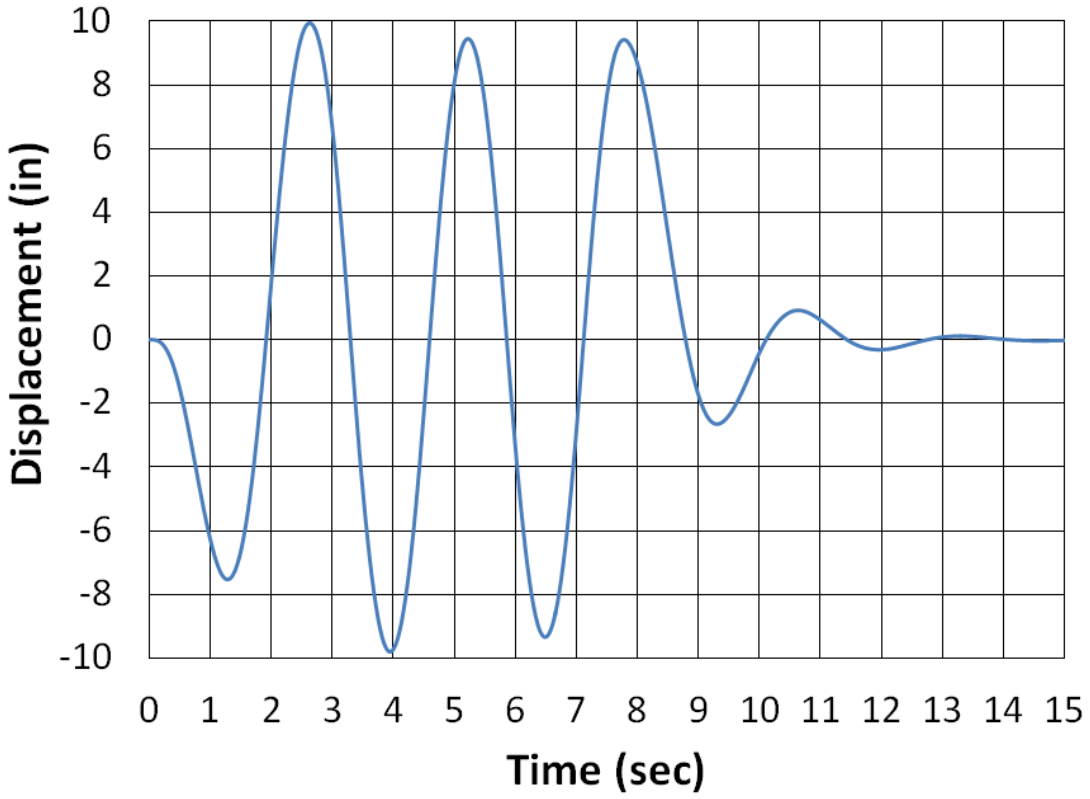

Figure B.12. Marshall County longitudinal displacement versus time at the top of the pier

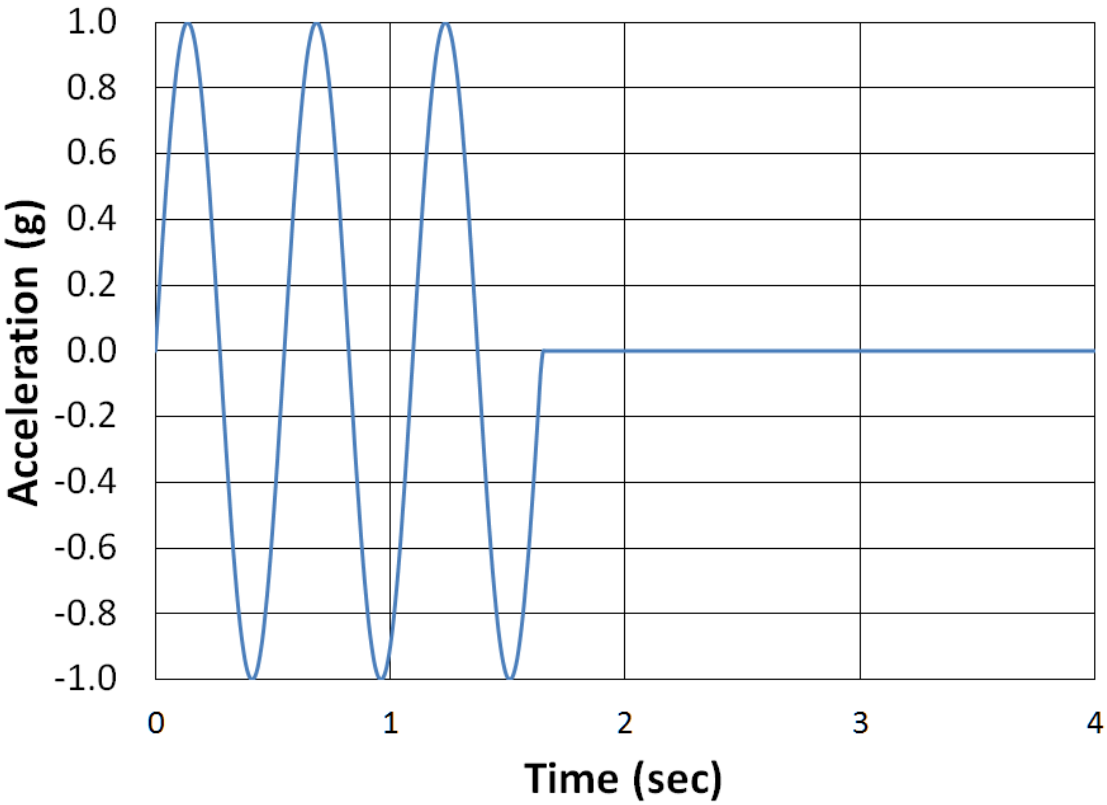

Figure B.13. Chambers County 25% scour transverse sine wave time-history

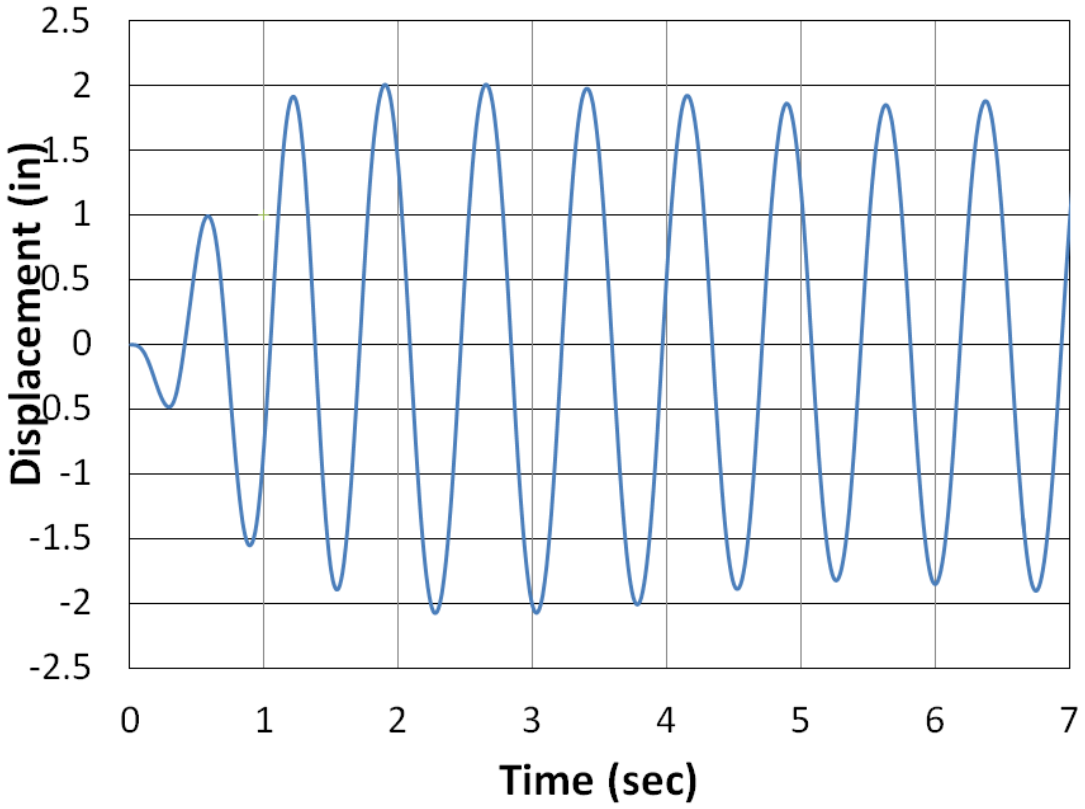

Figure B.14. Chambers County 25% scour transverse displacement versus time at the top of the pier

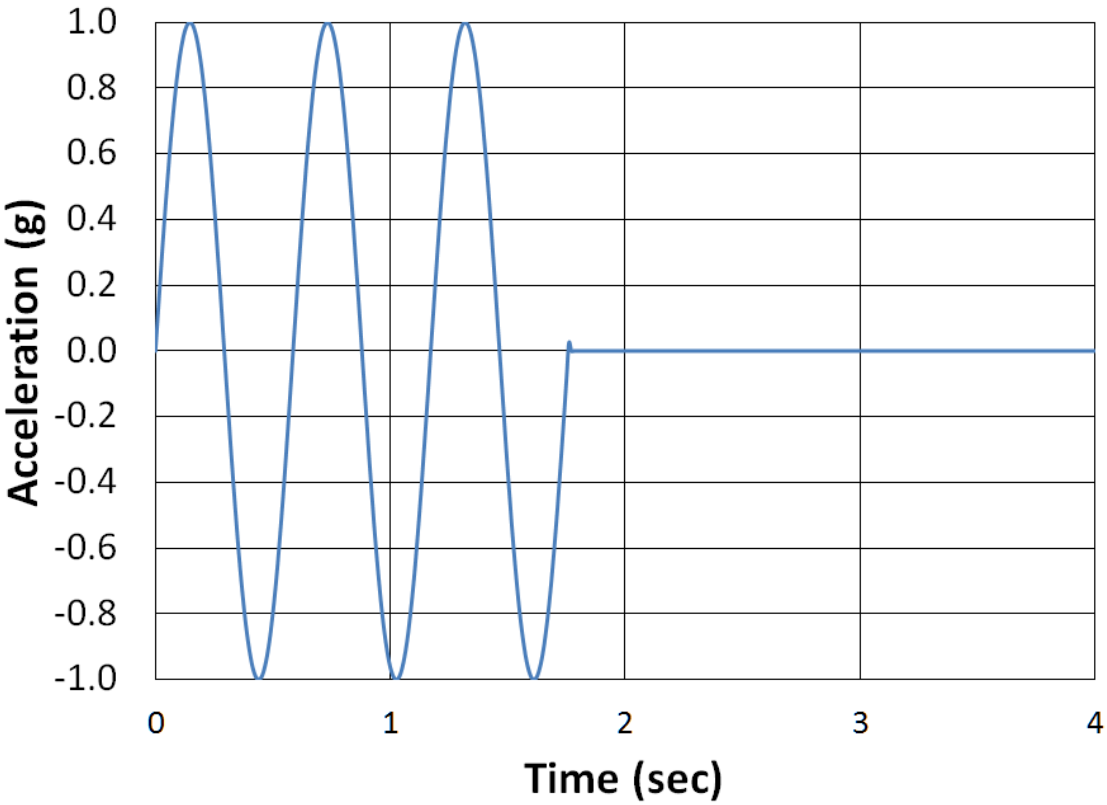

Figure B.15. Chambers County 100% scour transverse sine wave time-history

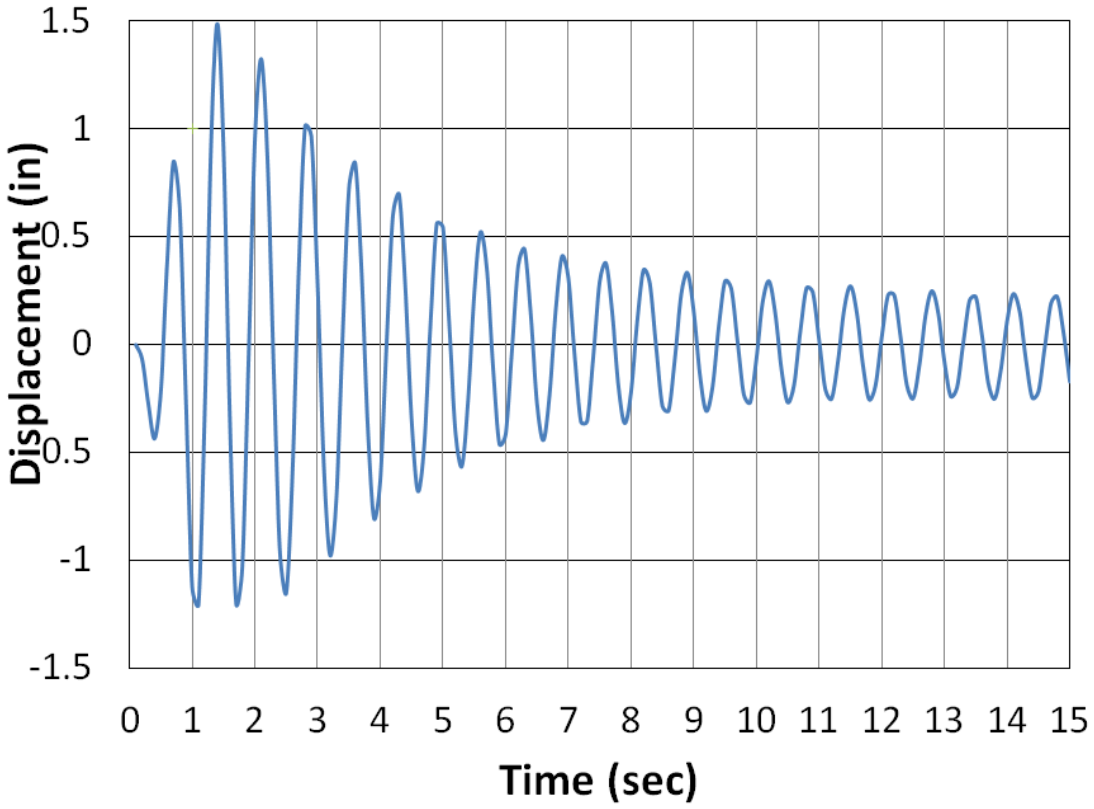

Figure B.16. Chambers County 100% scour transverse displacement versus time at the top of the pier

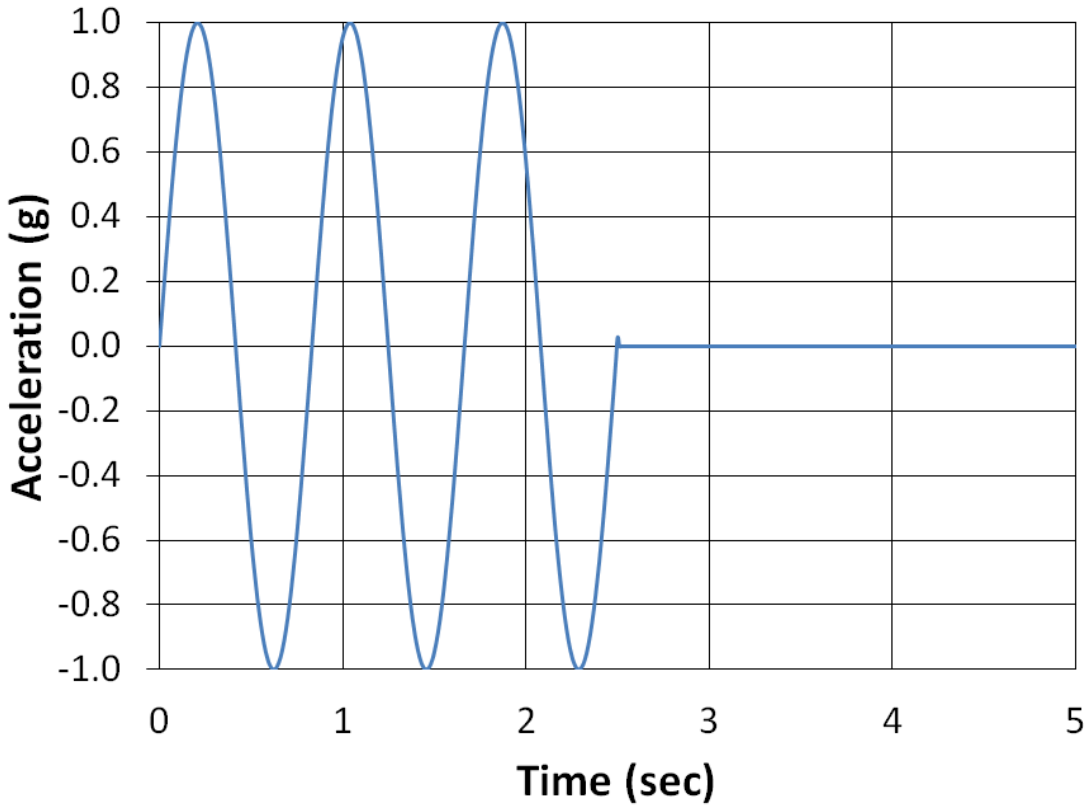

Figure B.17. Etowah County transverse sine wave time-history

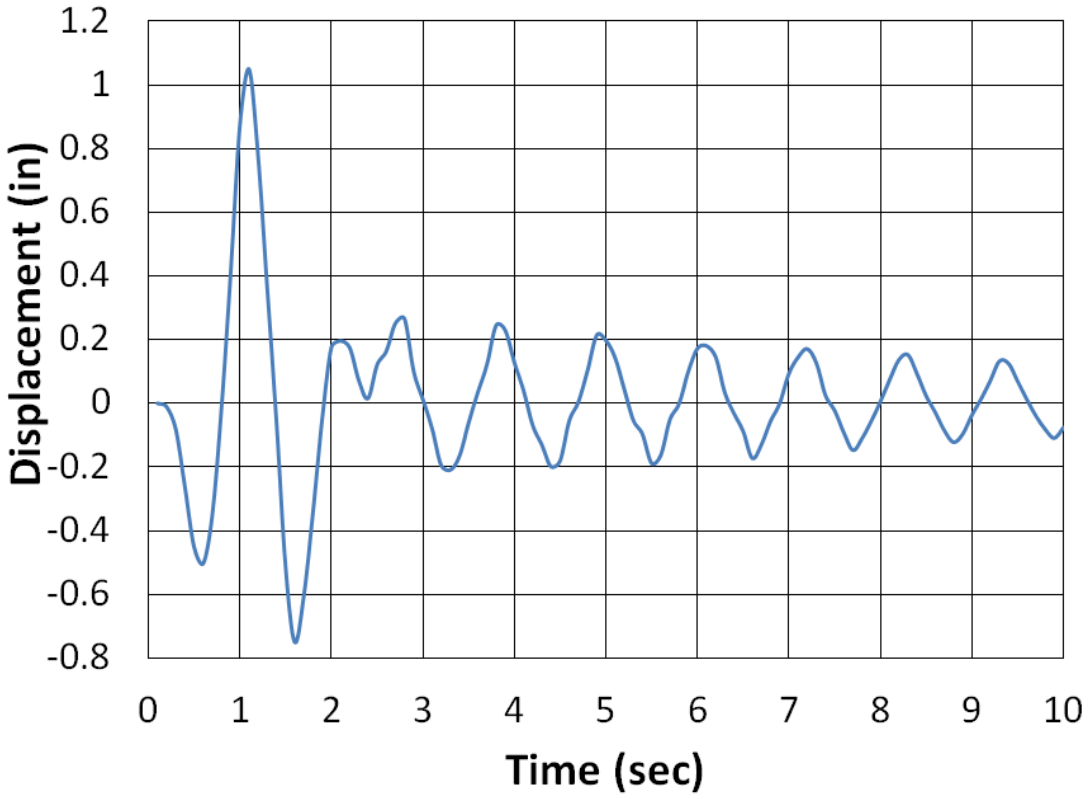

Figure B.18. Etowah County transverse displacement versus time at the top of the pier

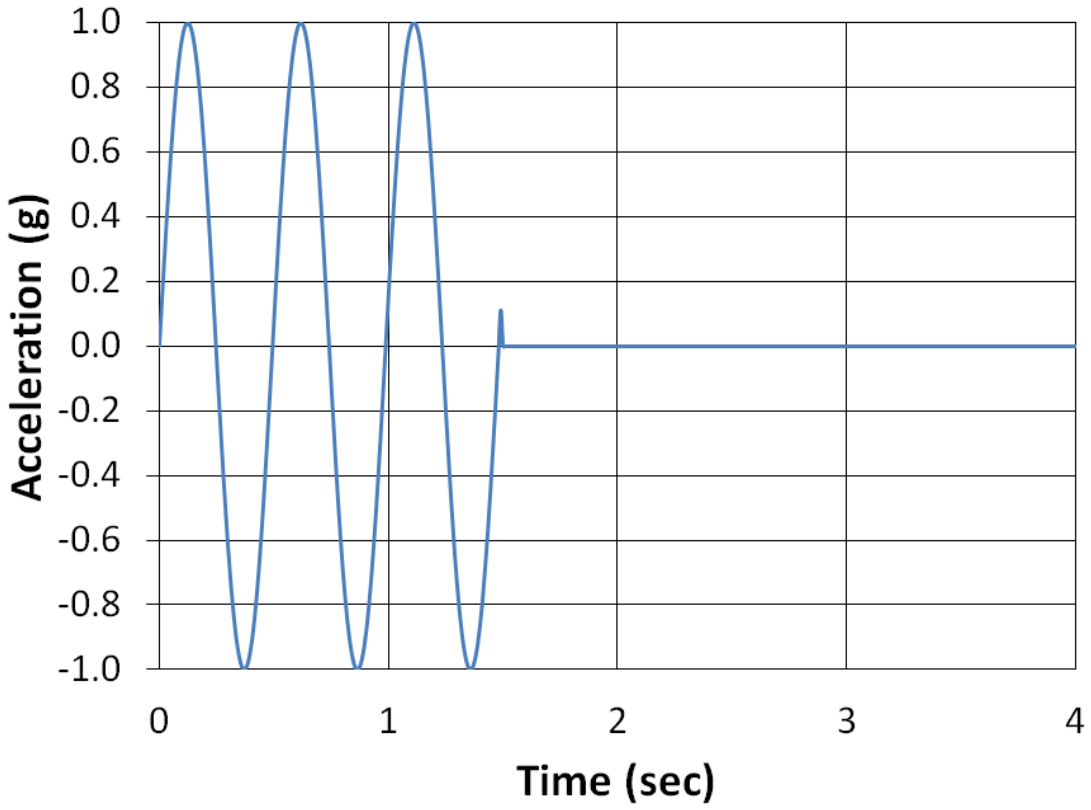

Figure B.19. Franklin County transverse sine wave time-history

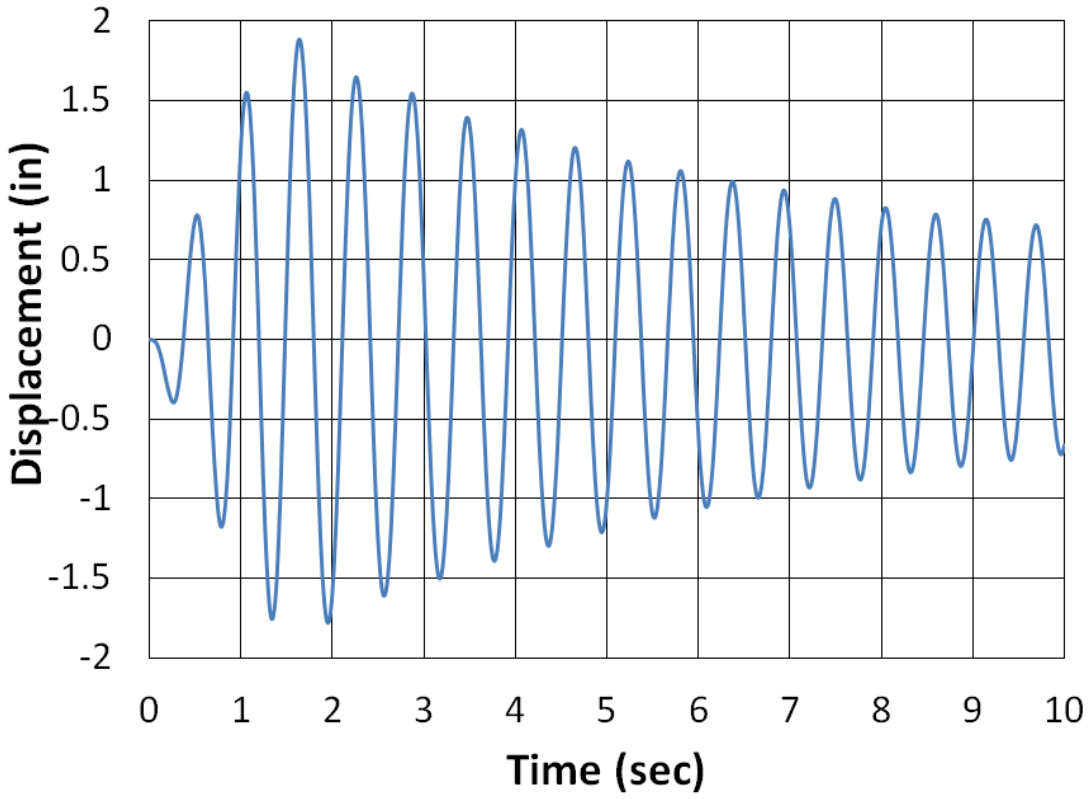

Figure B.20. Franklin County transverse displacement versus time at the top of the pier

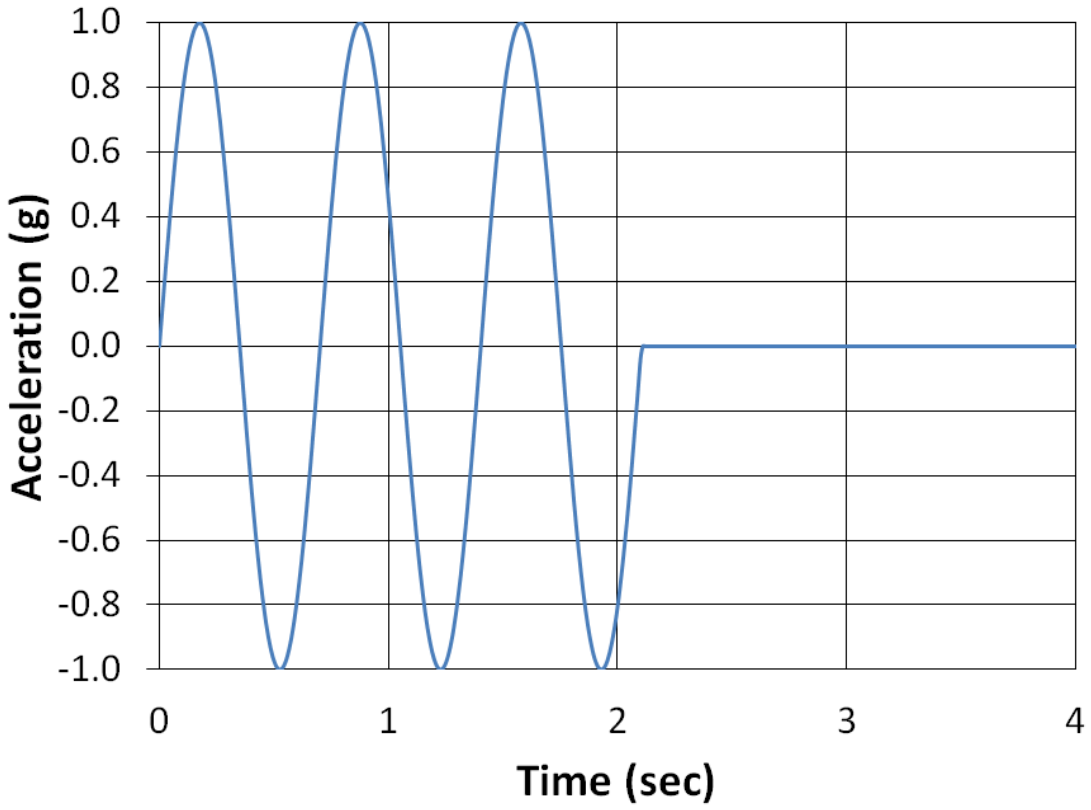

Figure B.21. Lee County transverse sine wave time-history

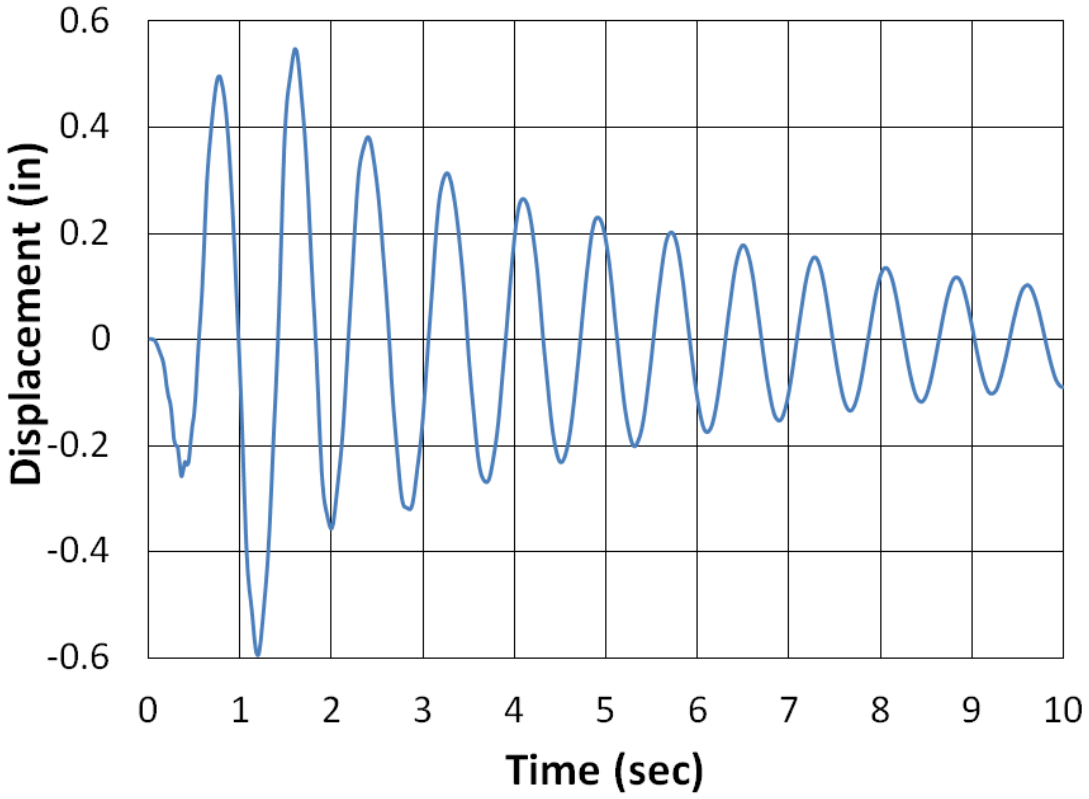

Figure B.22. Lee County transverse displacement versus time at the top of the pier

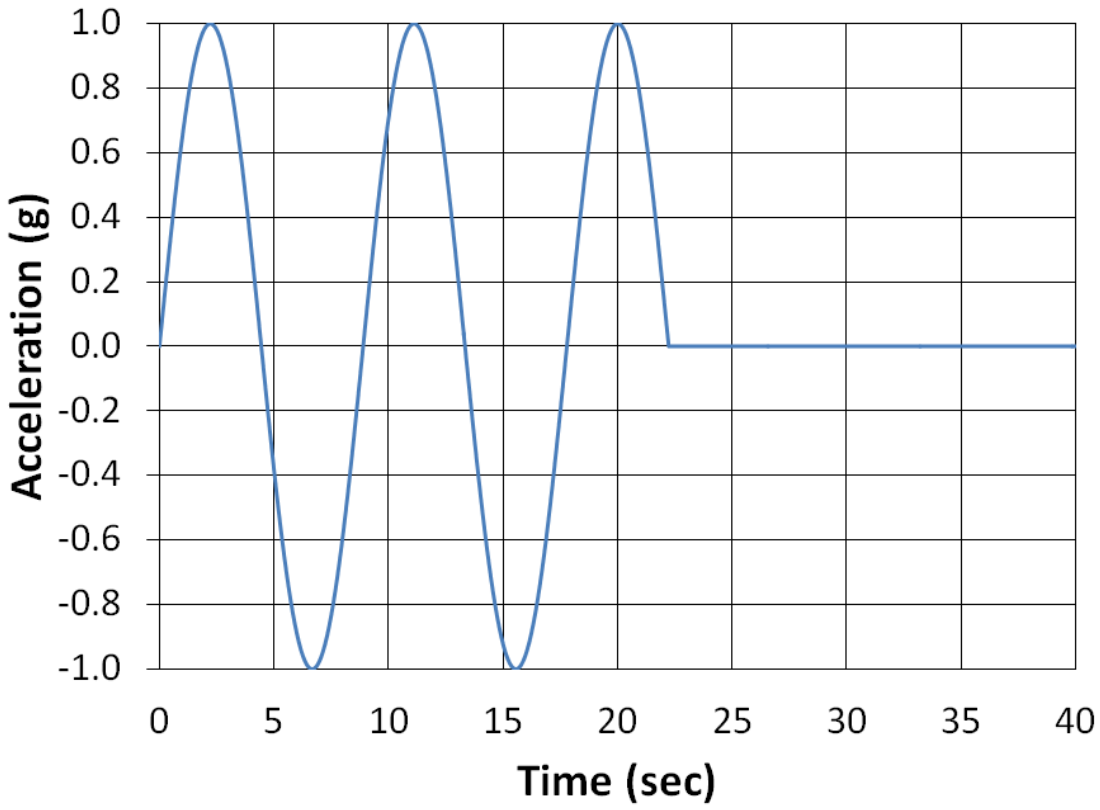

Figure B.23. Marshall County transverse sine wave time-history

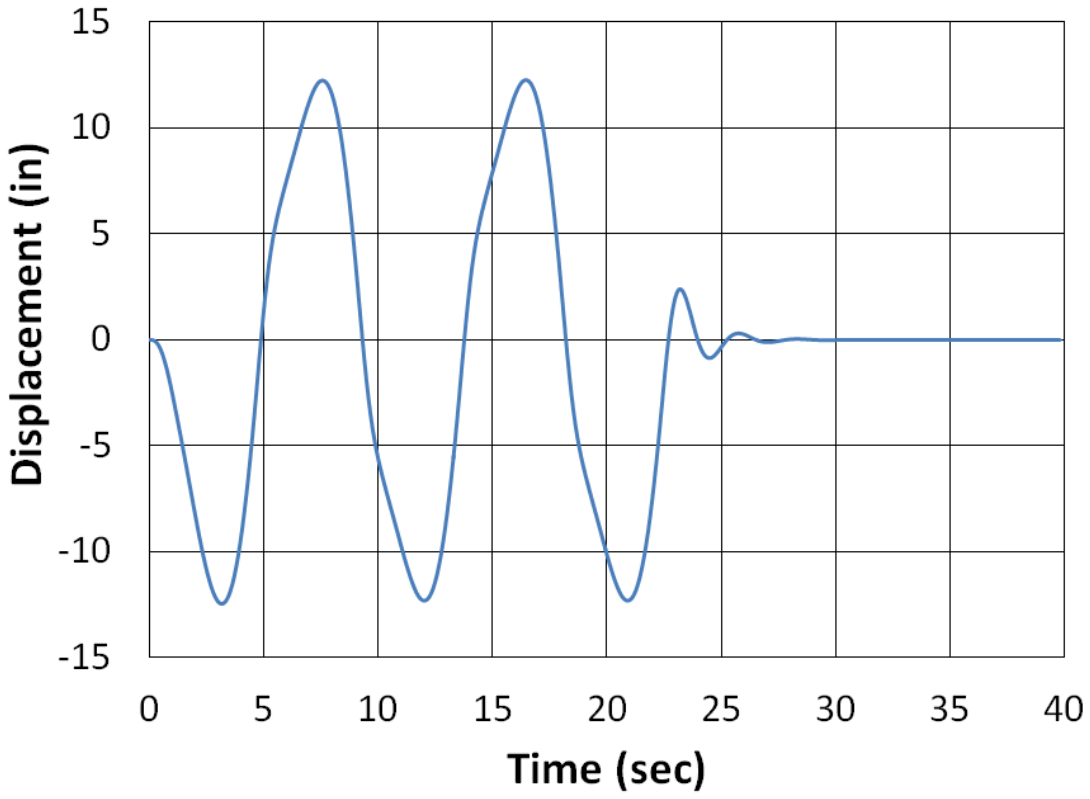

Figure B.24. Marshall County transverse displacement versus time at the top of the pier

Appendix C

CHAMBERS COUNTY BORING LOGS

Appendix C contains all relevant soil information regarding Chambers County that was used in developing the soil profile for FB-MultiPier.

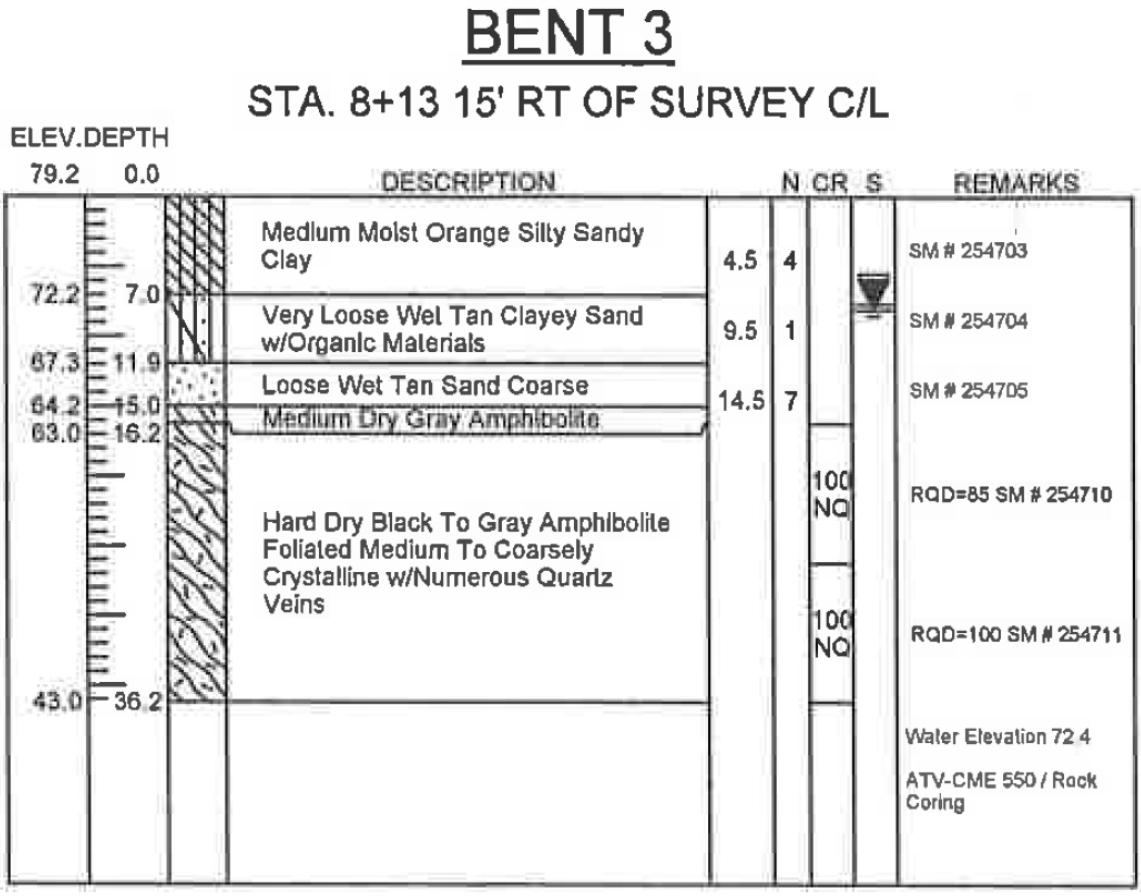

Figure C.1. Chambers County Bent 3 boring log (ALDOT 2008)

Table C.1 – Chambers County L-Pile Soils Input Data for the bents

Soil Criteria	Layer Thickness (in.)	Soil Modulus ($x10^3$ lb/in^3) k_s	k_c	Effective Unit Weight (lb/in^3)	Cohesion (lb/in^2)	Friction Angle ϕ (°)	Strain .5qu (E_{50})
Medium Moist Clay **Assumed to Scour**	84.0	100	-	0.067	3.47	-	0.01
Very Loose Wet Clay **Assumed to Scour**	58.8	20	20	0.019	-	27°	-
Loose Wet Clay **Assumed to Scour**	51.6	20	20	0.028	-	29°	-
Hard Dry Amphibolite	240.0	Em = 3.0E6 psi		0.084	6500	45°	0.001

Appendix D

ETOWAH COUNTY BORING LOGS

Appendix D contains all relevant soil information regarding Etowah County that was used in developing the soil profile for FB-MultiPier.

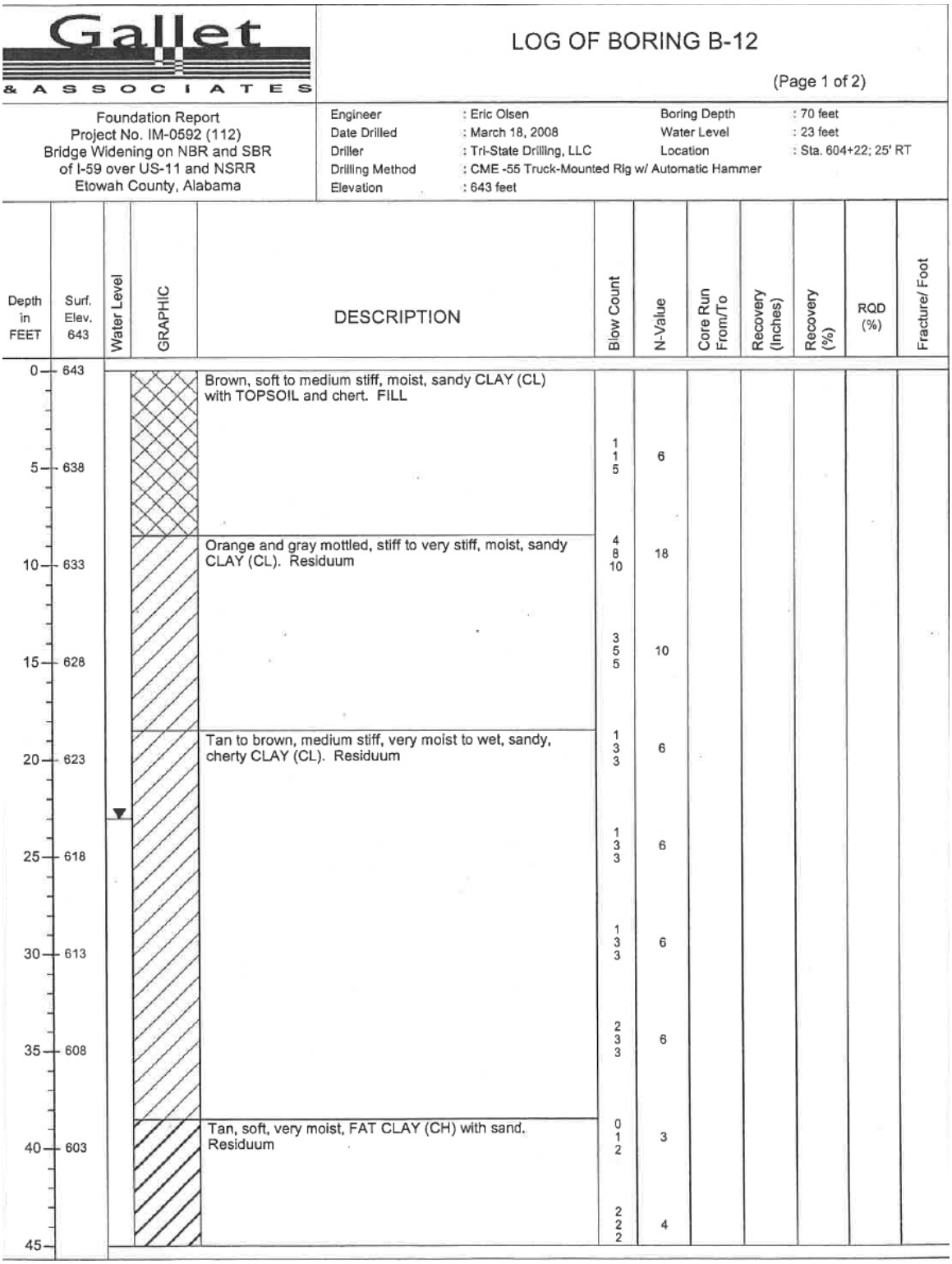

Figure D.1. Etowah County Bent 2 boring log (Gallet 2008)

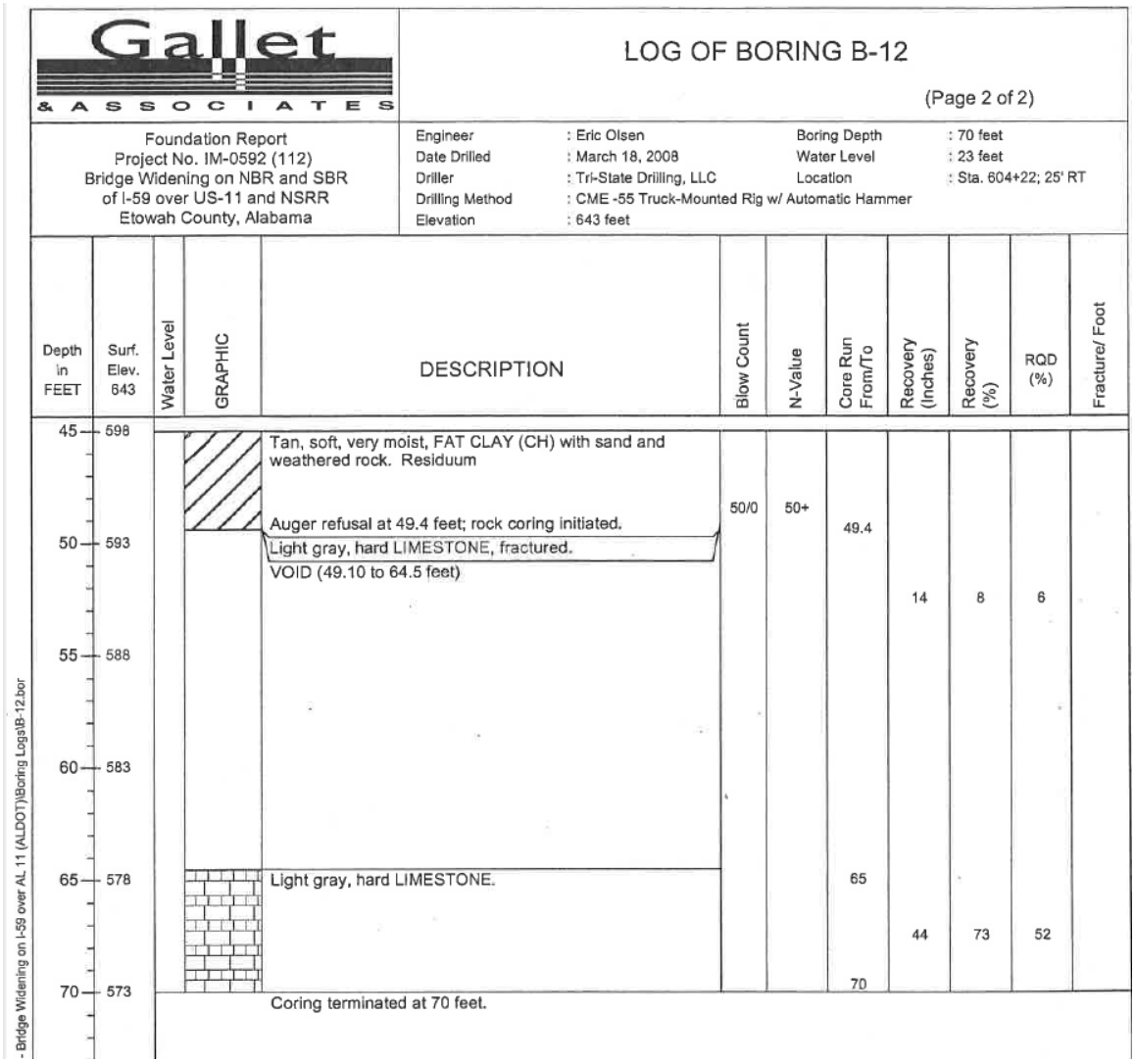

Figure D.2. Etowah County Bent 2 boring log (cont'd) (Gallet 2008)

Gallet & ASSOCIATES

LOG OF BORING B-13

(Page 1 of 2)

Foundation Report
Project No. IM-0592 (112)
Bridge Widening on NBR and SBR
of I-59 over US-11 and NSRR
Etowah County, Alabama

Engineer	: Eric Olsen	Boring Depth	: 52.4 feet
Date Drilled	: March 13, 2008	Water Level	: 23 feet
Driller	: Tri-State Drilling, LLC	Location	: Sta. 604+25; 28' LT
Drilling Method	: CME -55 Truck-Mounted Rig w/ Automatic Hammer		
Elevation	: 643 feet		

Depth in FEET	Surf. Elev. 643	Water Level	GRAPHIC	DESCRIPTION	Blow Count	N-Value	Core Run From/To	Recovery (Inches)	Recovery (%)	RQD (%)	Fracture/ Foot
0	643			Brown, soft to medium stiff, moist, sandy CLAY (CL) with TOPSOIL and chert. FILL	1 2 4	6					
5	638										
10	633			Orange and gray mottled, stiff to very stiff, moist, sandy CLAY (CL). Residuum	6 10 12	22					
15	628				5 10 15	25					
20	623	▼			5 11 15	26					
25	618			Tan to brown, stiff to medium stiff, wet, sandy, cherty CLAY (CL). Residuum	5 5 6	11					
30	613				3 2 3	5					
35	608				3 4 6	10					
40	603			Tan, soft, wet, FAT CLAY (CH) with sand. Residuum	1 1 1	2					
45					1 1 0	1					

Figure D.3. Etowah County Bent 2 boring log (Gallet 2008)

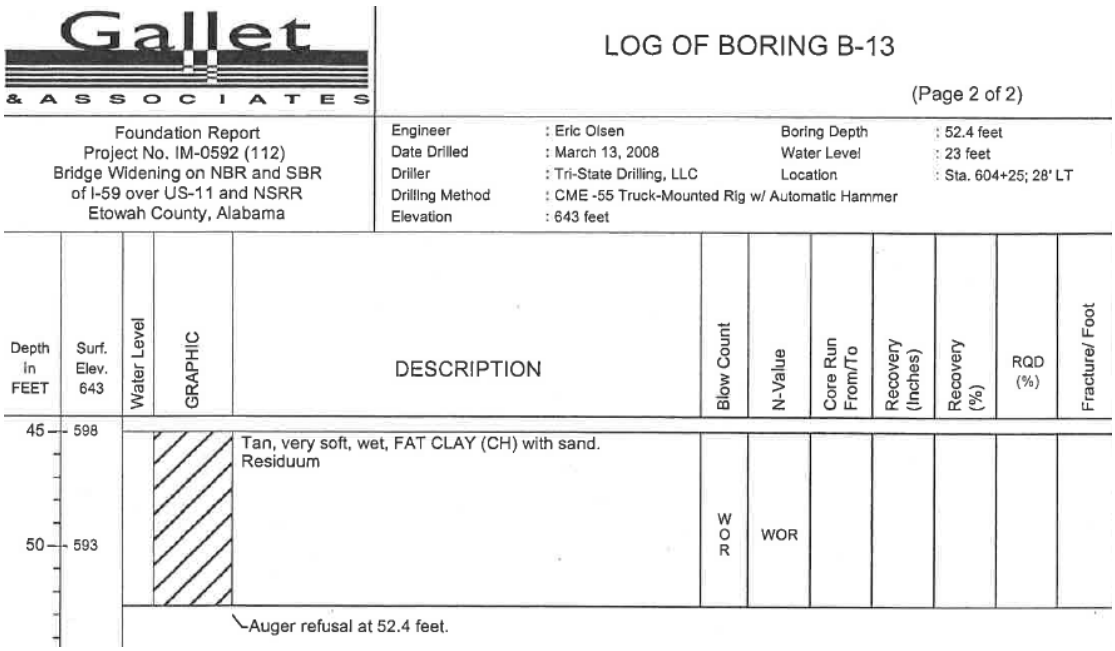

Figure D.4. Etowah County Bent 2 boring log (cont'd) (Gallet 2008)

Table D.1 – Etowah County soil input parameters for FB-Deep

No.	Depth (ft)	Soil Type	Soil Description	N. Blows (blow/ft)
1	0.000	1	Plastic Clay	6.000
2	2.750	1	Plastic Clay	14.000
3	15.520	1	Plastic Clay	6.000
4	33.750	1	Plastic Clay	3.000
5	45.250	1	Plastic Clay	0.000
6	58.750	4	Limestone, very shelly sand	50.000
7	67.250	4	Limestone, very shelly sand	50.000

FB-Deep Output:

PILE INFORMATION (Pile Length = 60.00 (ft))

Section Type: H-Section, Flange width = 12.05(in)
Section Depth = 12.05(in), True cross-sectional area = 15.50(in^2)
Length = 60.00(ft), Tip Elevation = 577.50(ft)
Unit Weight of Pile = 290.00(pcf), Weight of pile = 0.94(tons)

Skin friction capacity

Soil Layer Num.	Bottom Elev. (ft)	Average SPT Blows (Blows/ft)	Ult. Skin Friction (Tons)	Thick. (ft)	Soil Type
1	578.75	10.08	41.38	58.75	1- Plastic Clay
2	570.25	50.00	0.00	8.50	4- Lime Stone/Very shelly sand

(* IN LAYERS ABOVE BEARING LAYER)

Ultimate skin friction in layers above bearing layer = 41.38(tons)
Average SPT in Bearing layer above tip = 50.00(blow/ft)
Ultimate skin friction in bearing layer = 1.89(tons)
Corrected Ultimate skin friction in bearing layer = 1.81(tons)
Total Skin Friction = 43.19(tons)

End bearing capacity

ELEVATION (ft)	SPT Blows (Blows/ft)	UNIT E. B. (tsf)	
585.53	24.89	29.87	<-- 8B above pile tip
578.75	50.00	60.00	
577.50	50.00	60.00	<-- Pile tip elevation
573.99	50.00	60.00	<-- 3.5B below pile tip

Average unit end bearing above pile tip = 47.28(tsf)
Average unit end bearing below pile tip = 60.00(tsf)
Average unit end bearing in vicinity of pile tip = 53.64(tsf)

Critical depth of embedment in bearing layer = 6.02(ft)
Actual depth of embedment = 1.25(ft)

Maximum mobilized end bearing capacity = 52.85(tons)
Corrected mobilized end bearing capacity = 50.85(tons)

Pile Capacity

Estimated Davisson capacity	=	94.04(tons)
Allowable pile capacity	=	47.02(tons)
Ultimate pile capacity	=	144.89(tons)

Appendix E

FRANKLIN COUNTY BORING LOGS

Appendix E contains all relevant soil information regarding Franklin County that was used in developing the soil profile for FB-MultiPier.

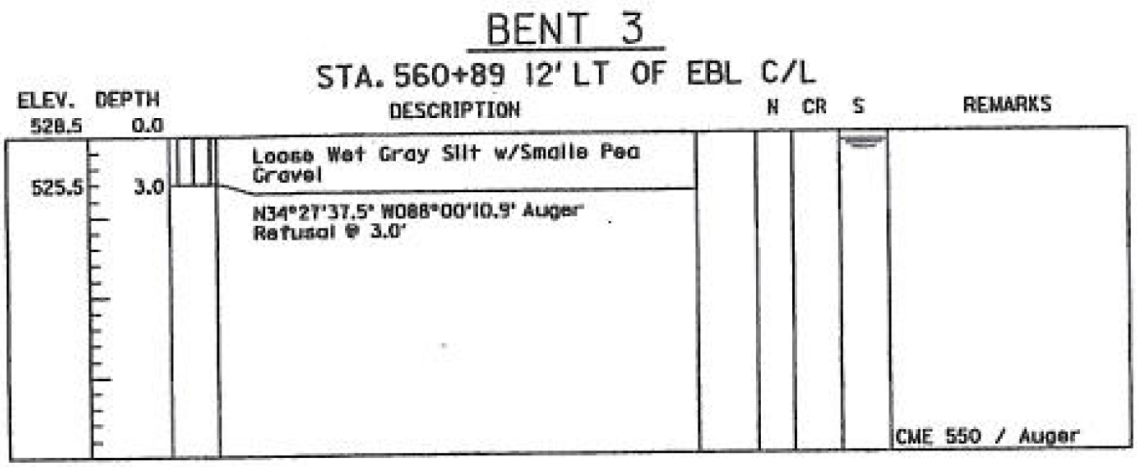

Figure E.1. Franklin County Bent 3 boring log (ALDOT 2005)

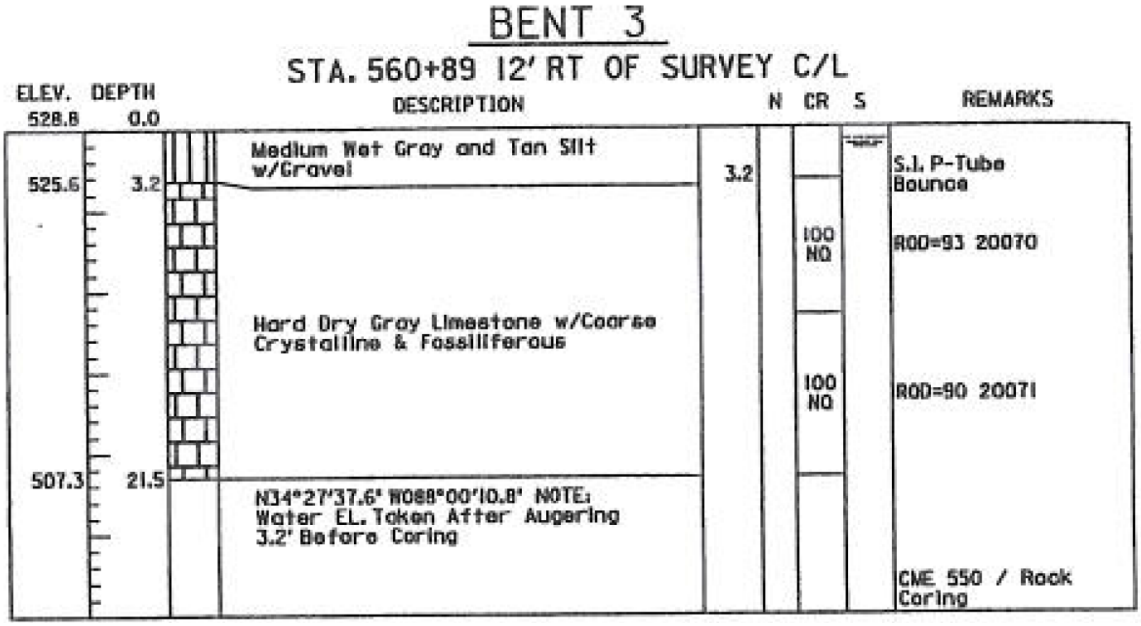

Figure E.2. Franklin County Bent 3 boring log (ALDOT 2005)

Table E.1—Franklin County L-Pile soil input data for Bent 3

Table 4C : L-Pile Soils Input Data for Bent 3							
Soil Criteria	Layer Thickness (in.)	Soil Modulus (pci) ks	kc	Effective Unit Weight (pci)	Cohesion (psi)	Friction Angle Φ (°)	Strain .5qu (E50)
Loose Silt w/Gravel	38.4	30	-	6.65x10^-2	1.74	-	0.02
Hard Limestone	99.6	Em=3x10^6		8.4x10^-2	7865	-	0.001
Hard Limestone	120	Em=1.6x10^6		8.4x10^-2	3710	-	0.001

Appendix F

LEE COUNTY BORING LOGS

Appendix F contains all relevant soil information regarding Lee County that was used in developing the soil profile for FB-MultiPier.

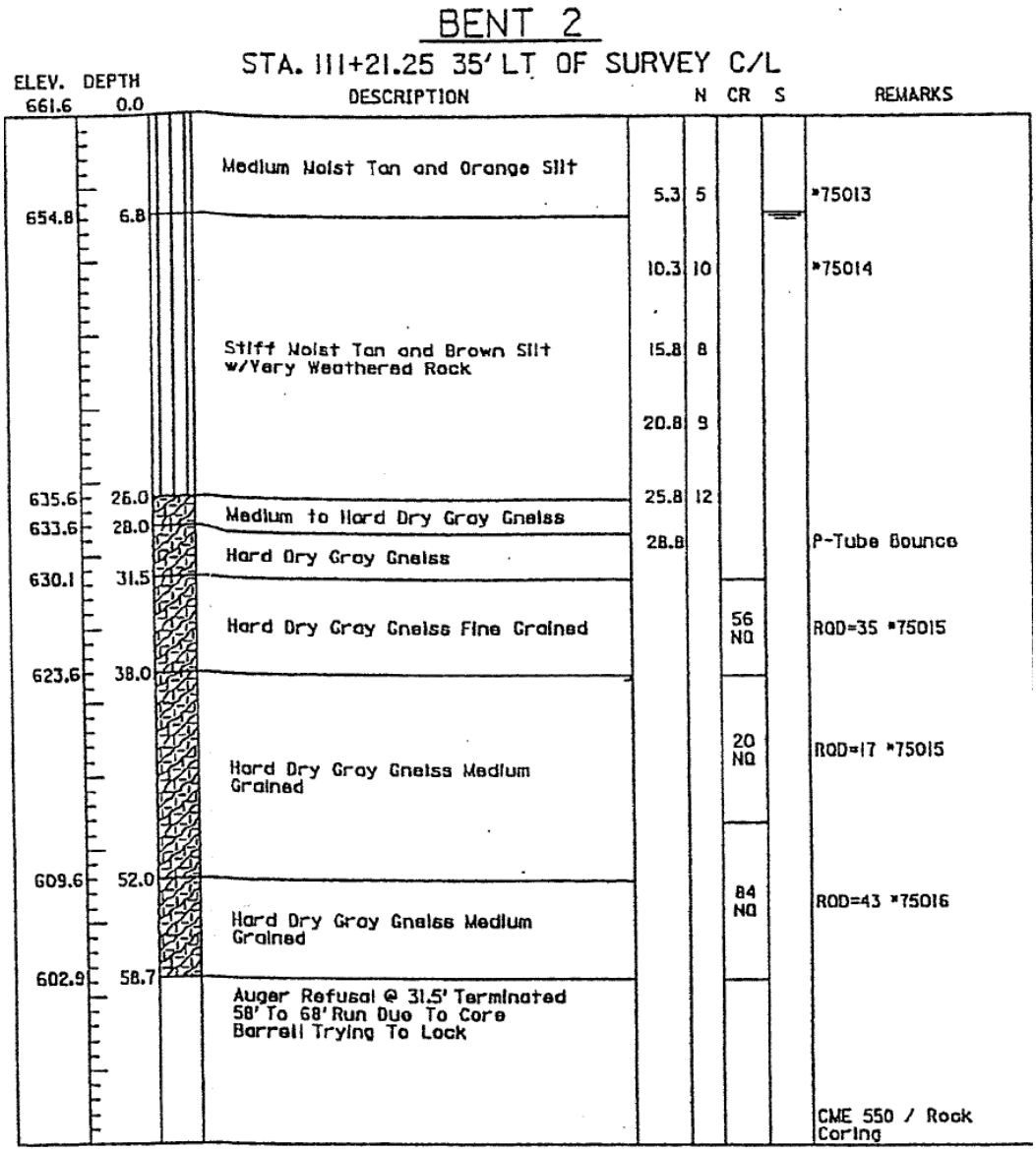

Figure F.1. Lee County Bent 2 boring log (ALDOT 2006)

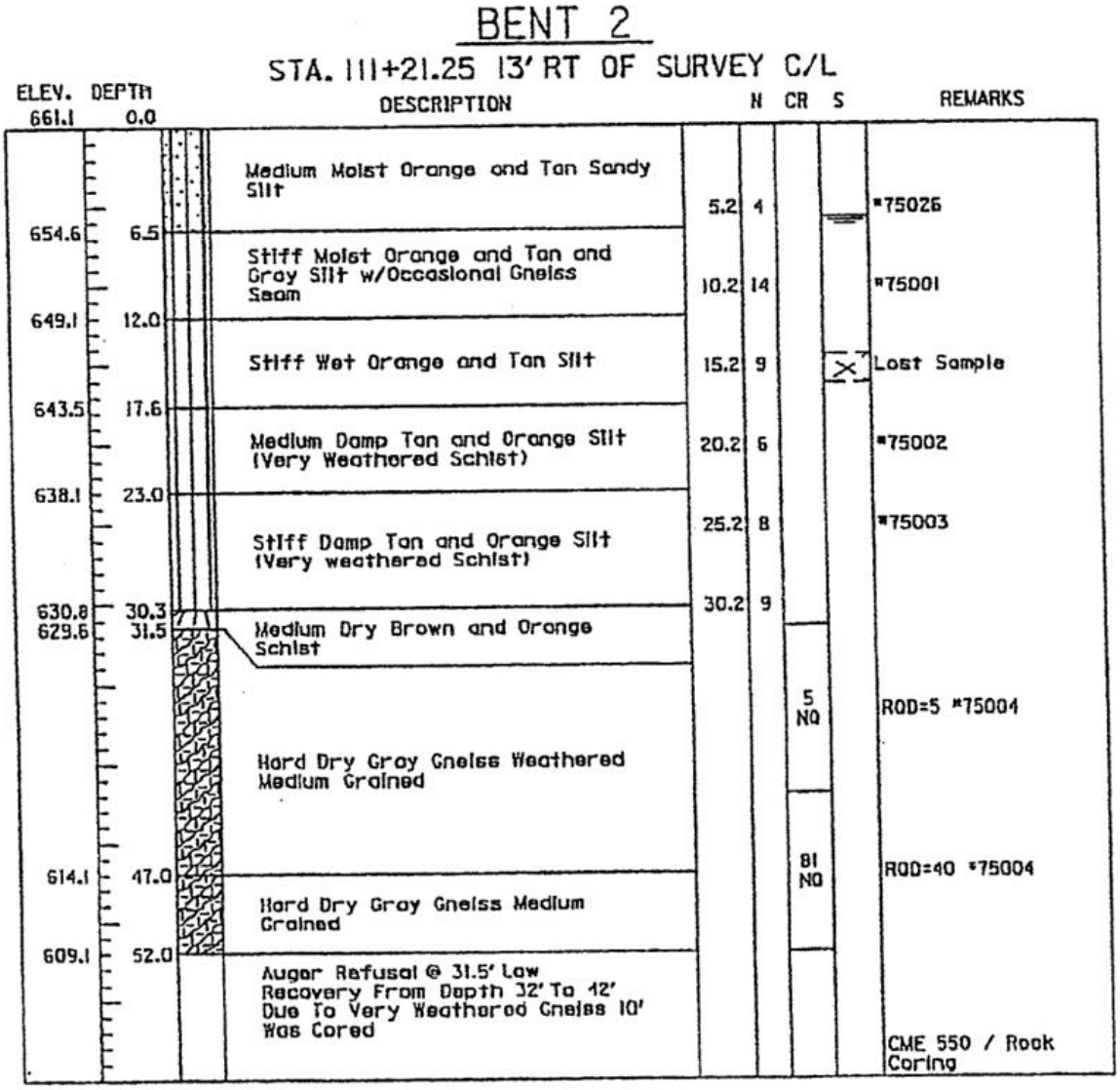

Figure F.1. Lee County Bent 2 boring log (ALDOT 2006)

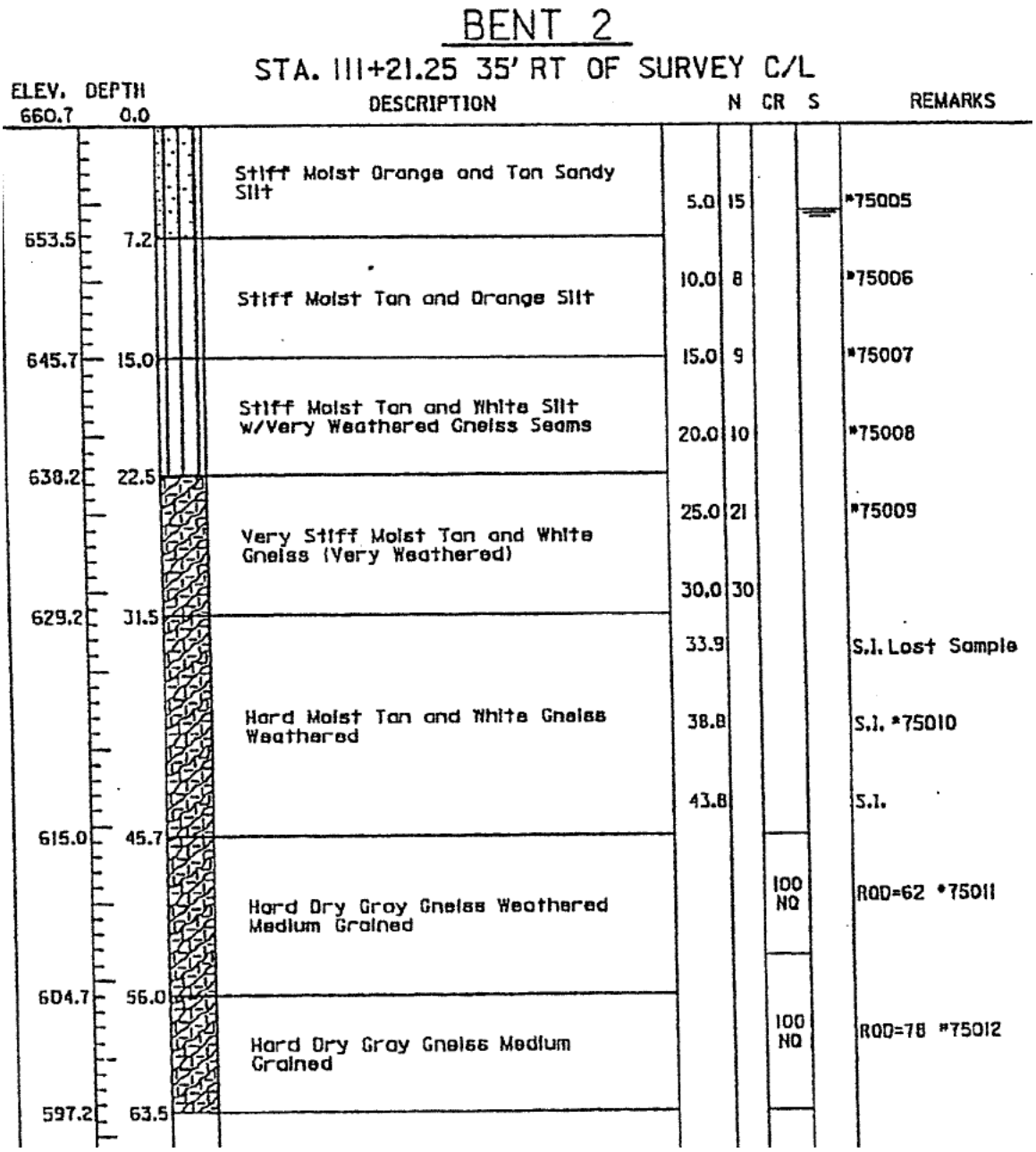

Figure F.3. Lee County Bent 2 boring log (ALDOT 2006)

Table F.1 – Lee County uniaxial compression testing results (boxed value is one used for FB-MultiPier) (ALDOT 2006)

SAMPLE	*STATION*	*DEPTH*	*LOAD (LBS)*	*PSI*
B2-35RT1	111+21.25, 35' RT	51.0'	34200	11000
B2-35RT2	111+21.25, 35' RT	63.0'	27800	8940
B2-35LT1	111+21.25, 35' LT	32.5'	34500	11090
B2-35LT2	111+21.25, 35' LT	38.3"	6560	2140
B2-13RT1	111+21.25, 13' RT	48.0'	3930	1270
A1-95RT1	109+86.25, 95' RT	45.7'	3250	1055

Table F.2. Lee County FB-Deep soil input parameters

No.	Depth (ft)	Soil Type	Soil Description	N. Blows (blow/ft)
1	0.000	2	Clay and silty Sand	5.000
2	7.000	2	Clay and silty Sand	10.000
3	29.500	4	Limestone, very shelly sand	30.000
4	41.000	4	Limestone, very shelly sand	30.000

FB-Deep Output:

PILE INFORMATION (Pile Length = 30.00 (ft))

Section Type: H-Section, Flange width = 12.05(in)
Section Depth = 12.05(in), True cross-sectional area = 15.50(in^2)
Length = 30.00(ft), Tip Elevation = 627.25(ft)
Unit Weight of Pile = 200.00(pcf), Weight of pile = 0.32(tons)

Skin friction capacity

Soil Layer Num.	Bottom Elev. (ft)	Average SPT Blows (Blows/ft)	Ult. Skin Friction (Tons)	Thick. (ft)	Soil Type
1	627.75	17.03	27.47	29.50	2- Clay and silty sand
2	616.25	30.00	0.00	11.50	4- Lime Stone/Very shelly sand

(* IN LAYERS ABOVE BEARING LAYER)

Ultimate skin friction in layers above bearing layer = 27.47(tons)
Average SPT in Bearing layer above tip = 30.00(blow/ft)
Ultimate skin friction in bearing layer = 0.45(tons)
Corrected Ultimate skin friction in bearing layer = 0.45(tons)
Total Skin Friction = 27.92(tons)

End bearing capacity

ELEVATION (ft)	SPT Blows (Blows/ft)	UNIT E. B. (tsf)	
635.28	23.31	25.74	<-- 8B above pile tip
627.75	30.00	36.00	
627.25	30.00	36.00	<-- Pile tip elevation
623.74	30.00	36.00	<-- 3.5B below pile tip

Average unit end bearing above pile tip	=	31.19(tsf)
Average unit end bearing below pile tip	=	36.00(tsf)
Average unit end bearing in vicinity of pile tip	=	33.59(tsf)
Critical depth of embedment in bearing layer	=	6.02(ft)
Actual depth of embedment	=	0.50(ft)
Maximum mobilized end bearing capacity	=	33.10(tons)
Corrected mobilized end bearing capacity	=	32.80(tons)

Pile Capacity

Estimated Davisson capacity	=	60.72(tons)
Allowable pile capacity	=	30.36(tons)
Ultimate pile capacity	=	93.53(tons)

Appendix G

MARSHALL COUNTY BORING LOGS

Appendix G contains all relevant soil information regarding Marshall County that was used in developing the soil profile for FB-MultiPier.

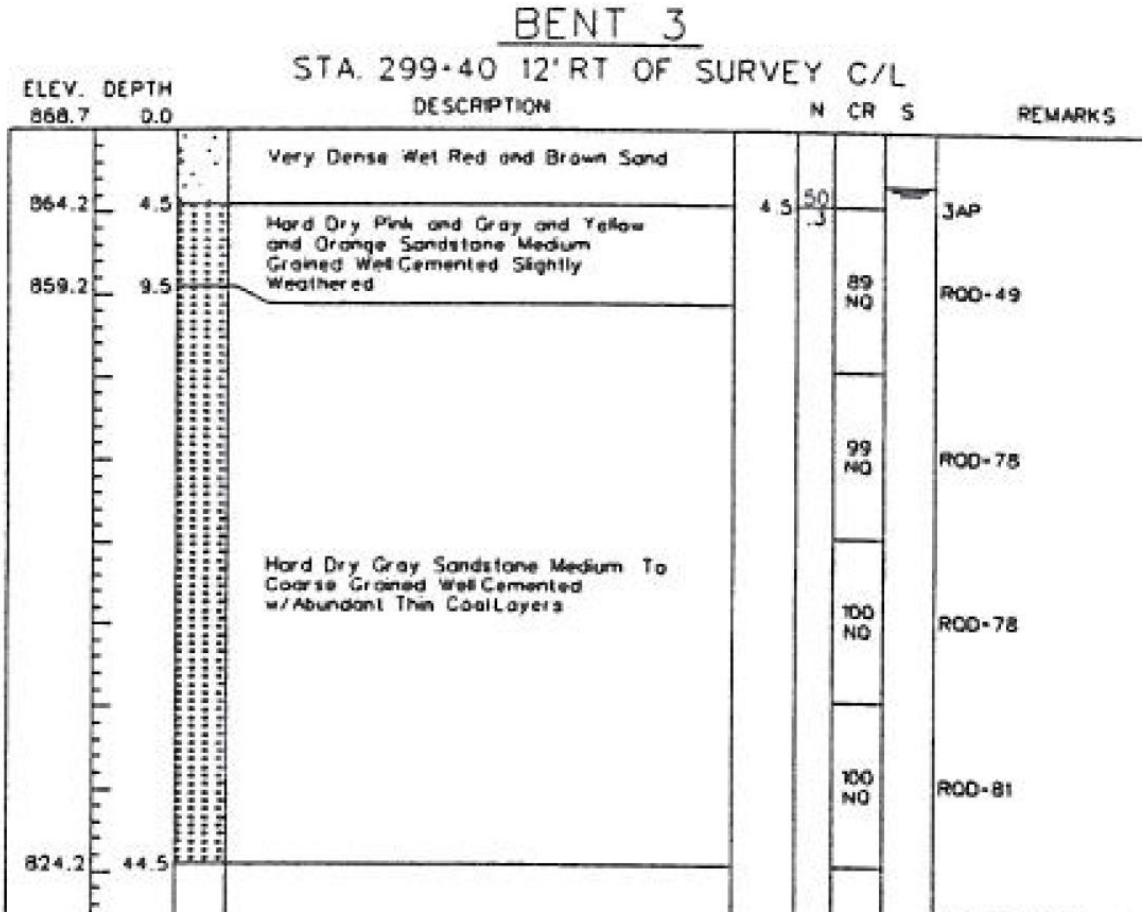

Figure G.1. Marshall County Bent 3 boring log (ALDOT 2003)

Table G.1 – Marshall County uniaxial compression test results (boxed value was used for FB-MultiPier) (ALDOT 2003)

SAMPLE	*STATION*	*DEPTH*	*HEIGHT (IN.)*	*DIAMETER (IN.)*	*CORR. FAC. (H/D RATIO)*	*AREA (IN.^{2})*	*LOAD (LBS)*	*PSI*
A1-1	296+80 CL	7.0'	3.774	1.987	(1.90)	3.101	69000	22200
A1-2	296+80 CL	37.0'	3.981	1.988	(2.00)	3.981	42200	13580
B2-1	298+10 24' LT	22.0'	4.015	1.986	(2.02)	3.098	35400	11440
B3-1	299+40 CL	43.0'	4.281	1.989	(2.15)	3.107	76500	24600
A5-1	302+00 24' LT	3.7'	4.008	1.989	(2.02)	3.107	60600	19510
A5-2	302+00 24' LT	31.5'	4.195	1.985	(2.11)	3.095	74900	24200

Appendix H

DIRECT ANALYSIS RESULTS

The results from the direct analysis are presented. This includes the time-history, top-of-pier and ground surface displacement, and shear, moment, and demand/capacity ratio distribution for the length of the pile, shaft, or column.

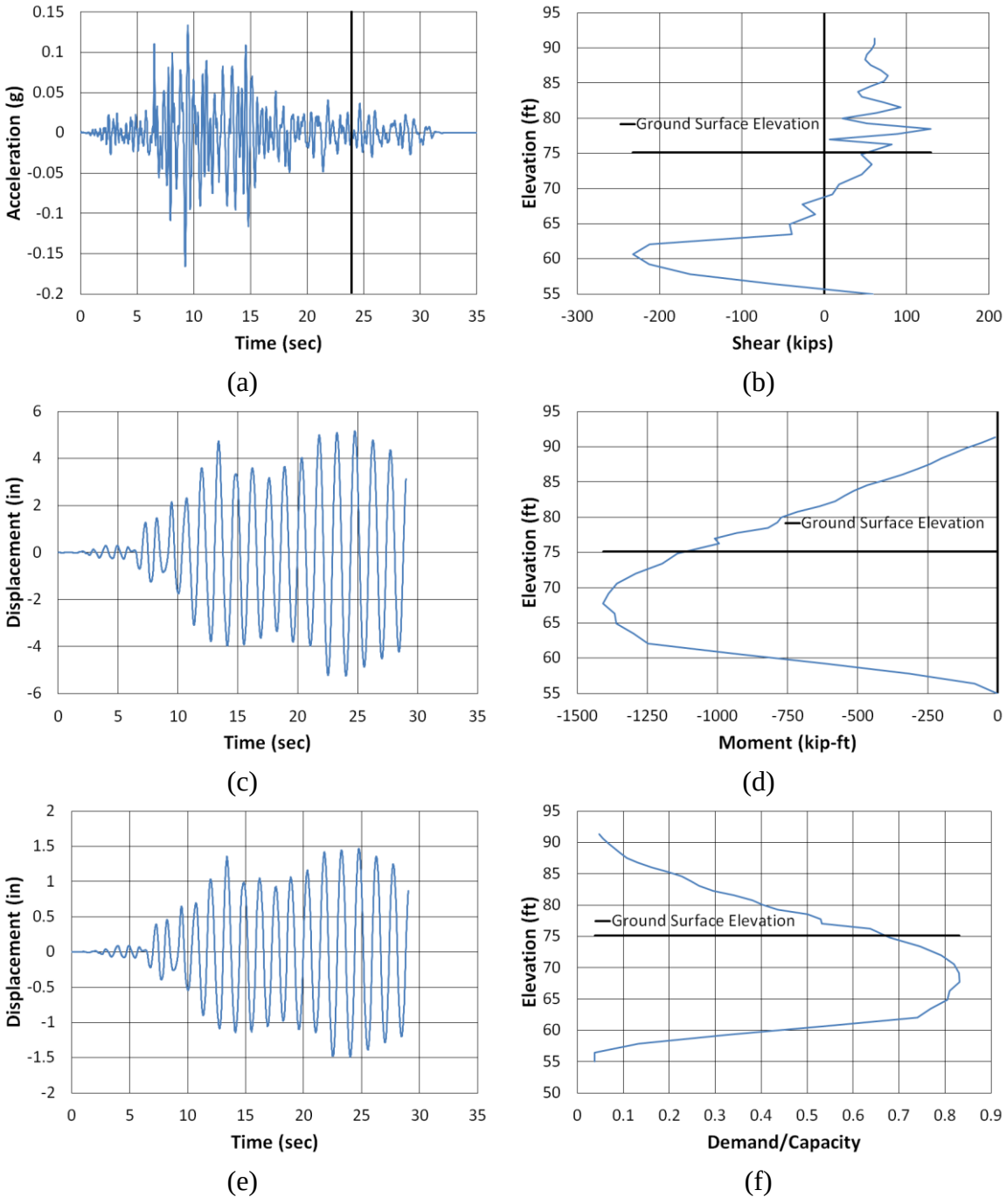

Figure B.1. Chambers County 25% Scour Longitudinal Coalinga North (a) time-history event, (b) shear distribution, (c) top of pier displacement, (d) moment distribution, (e) ground surface displacement, and (f) demand capacity ratio

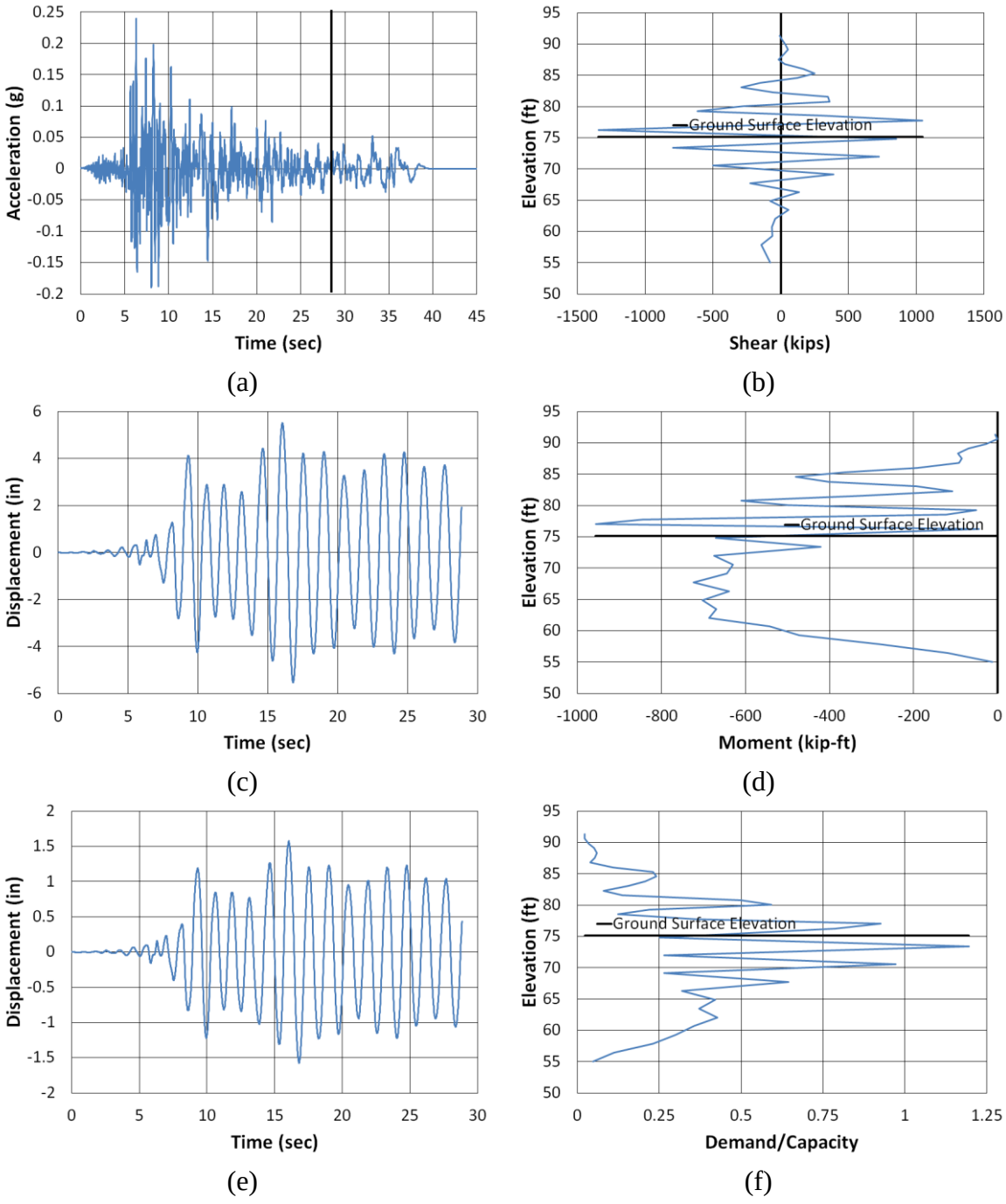

Figure B.2. Chambers County 25% Scour Longitudinal Imperial Valley NMCE (a) time-history event, (b) shear distribution, (c) top of pier displacement, (d) moment distribution, (e) ground surface displacement, and (f) demand capacity ratio

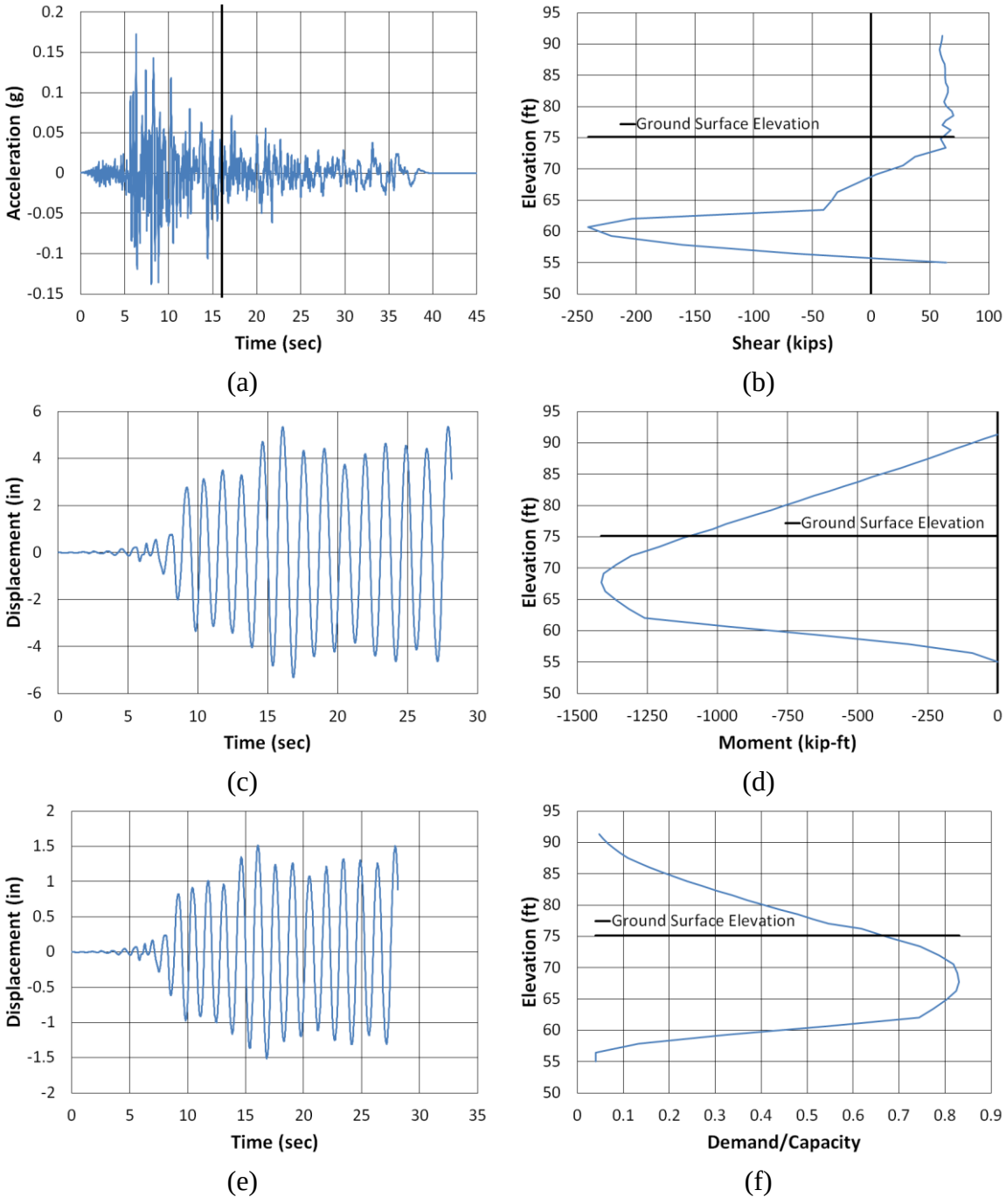

Figure B.3. Chambers County 25% Scour Longitudinal Imperial Valley North (a) time-history event, (b) shear distribution, (c) top of pier displacement, (d) moment distribution, (e) ground surface displacement, and (f) demand capacity ratio

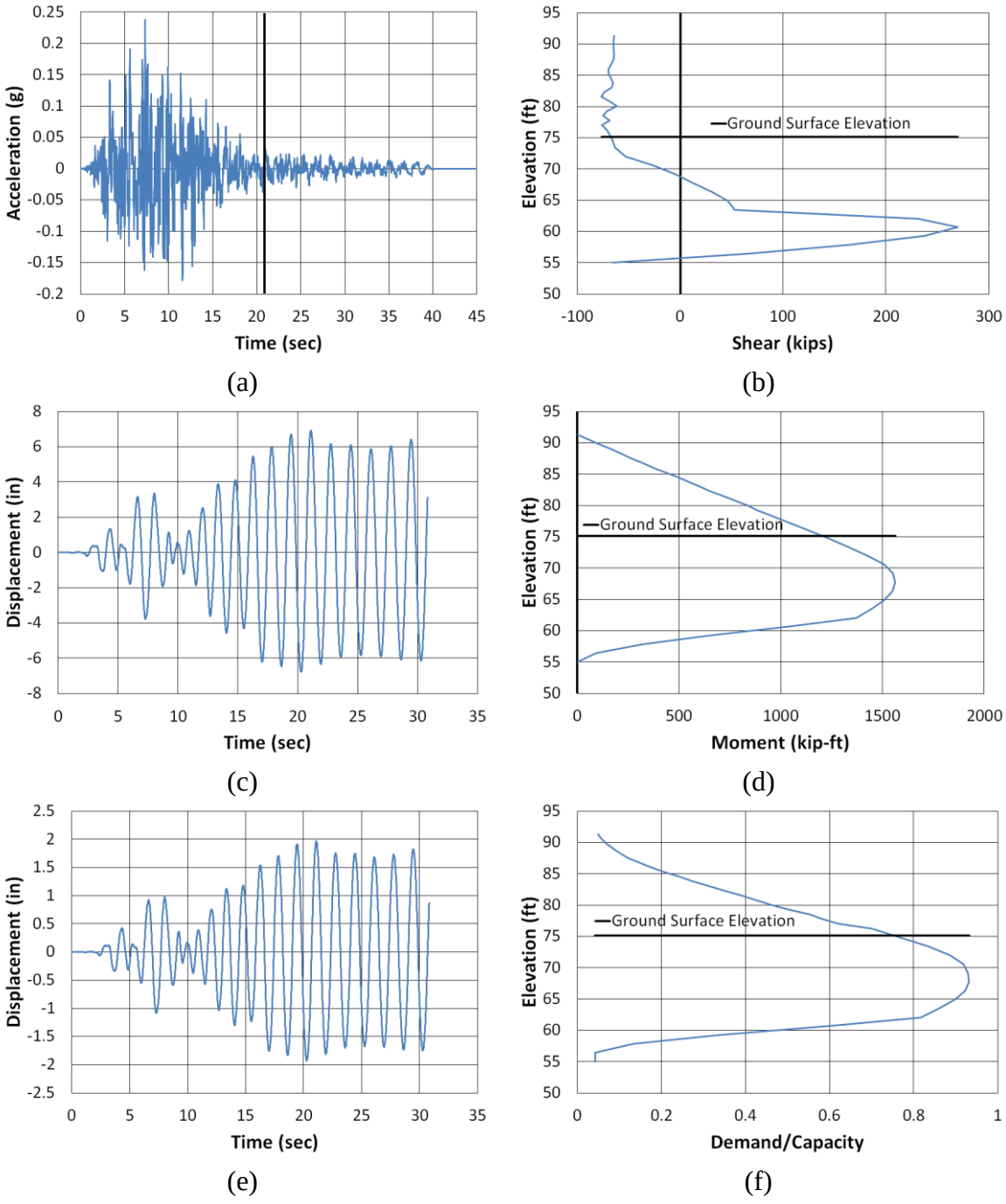

Figure B.4. Chambers County 25% Scour Longitudinal Kobe NMCE (a) time-history event, (b) shear distribution, (c) top of pier displacement, (d) moment distribution, (e) ground surface displacement, and (f) demand capacity ratio

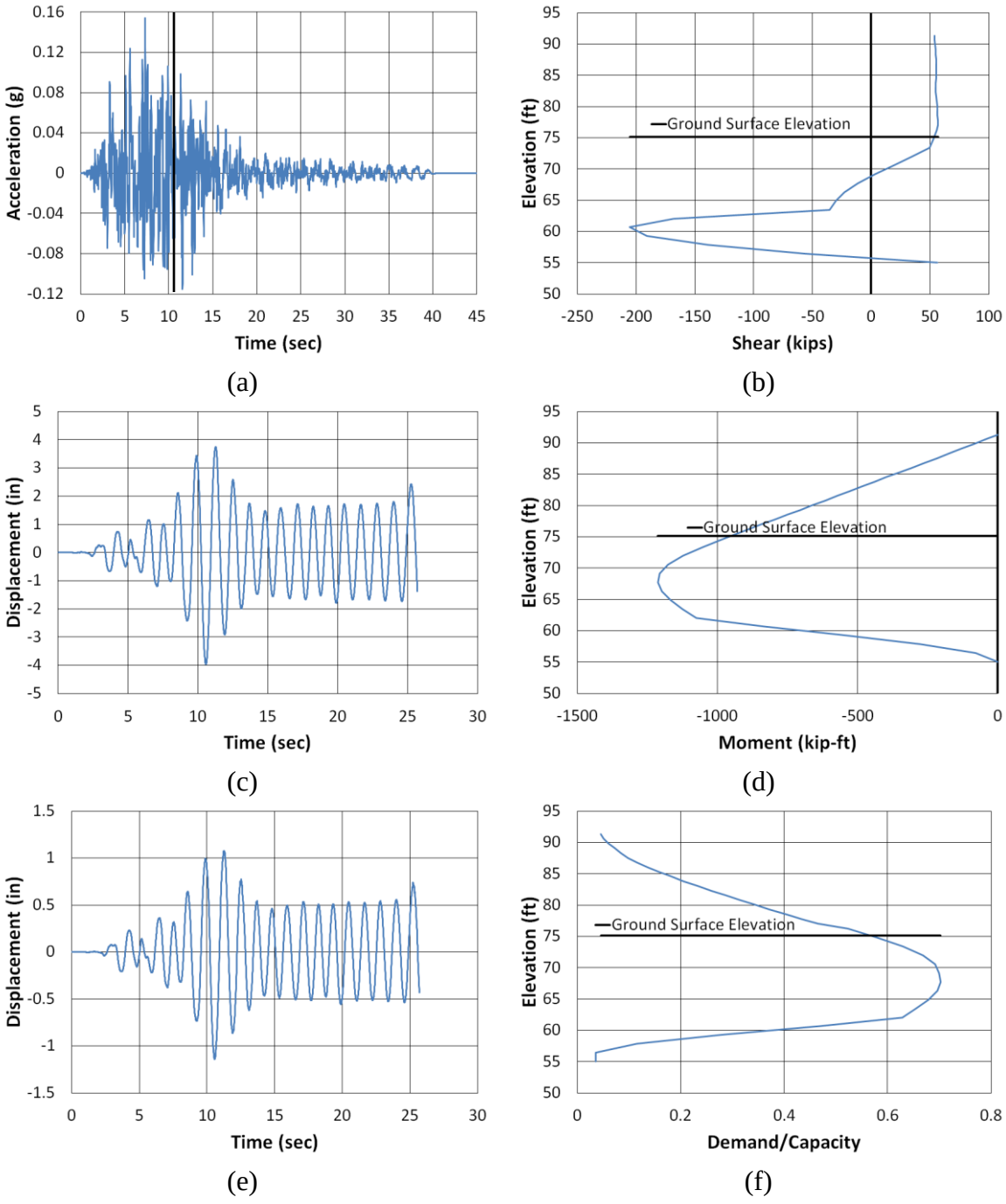

Figure B.5. Chambers County 25% Scour Longitudinal Kobe North (a) time-history event, (b) shear distribution, (c) top of pier displacement, (d) moment distribution, (e) ground surface displacement, and (f) demand capacity ratio

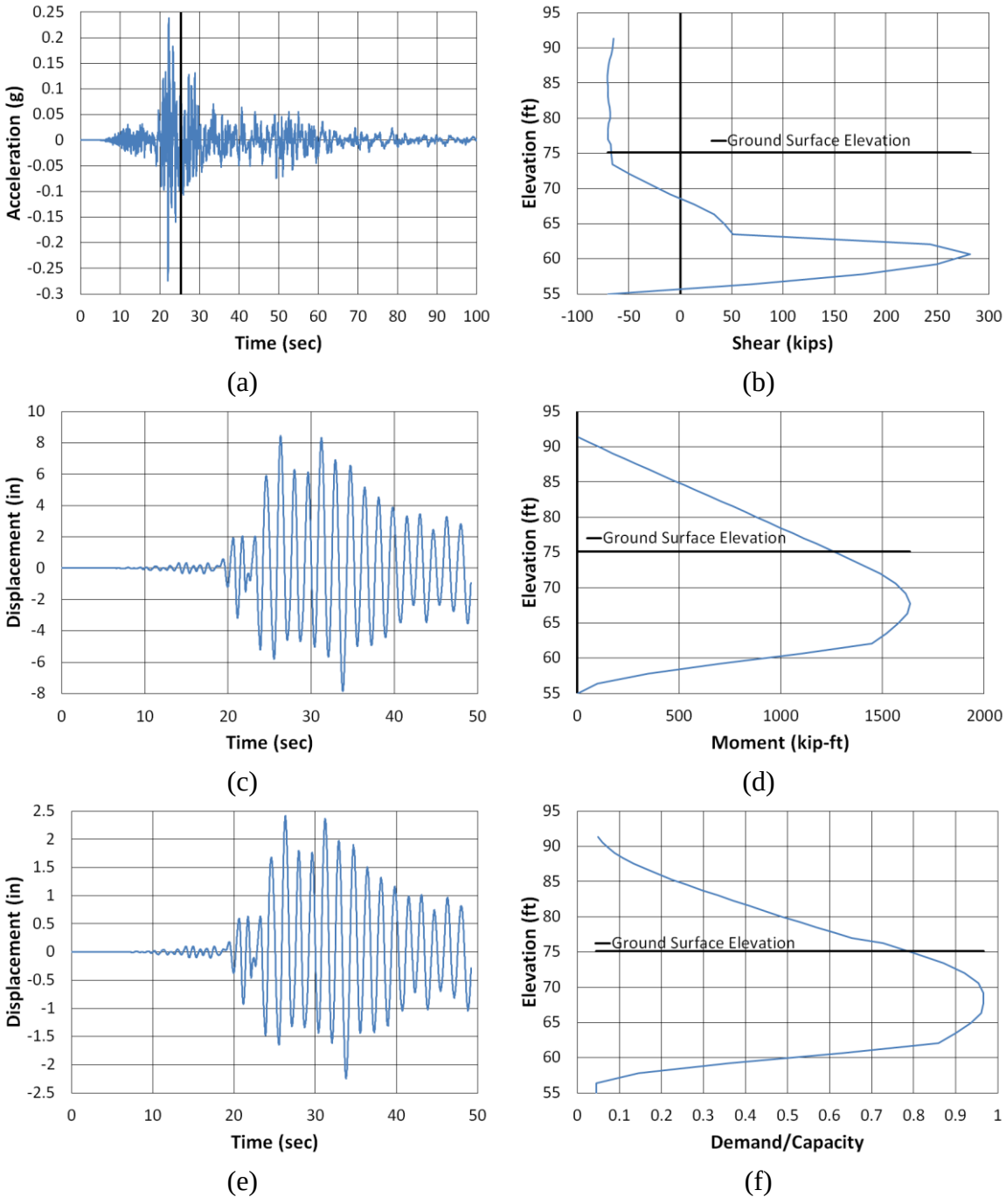

Figure B.6. Chambers County 25% Scour Longitudinal Kocaeli NMCE (a) time-history event, (b) shear distribution, (c) top of pier displacement, (d) moment distribution, (e) ground surface displacement, and (f) demand capacity ratio

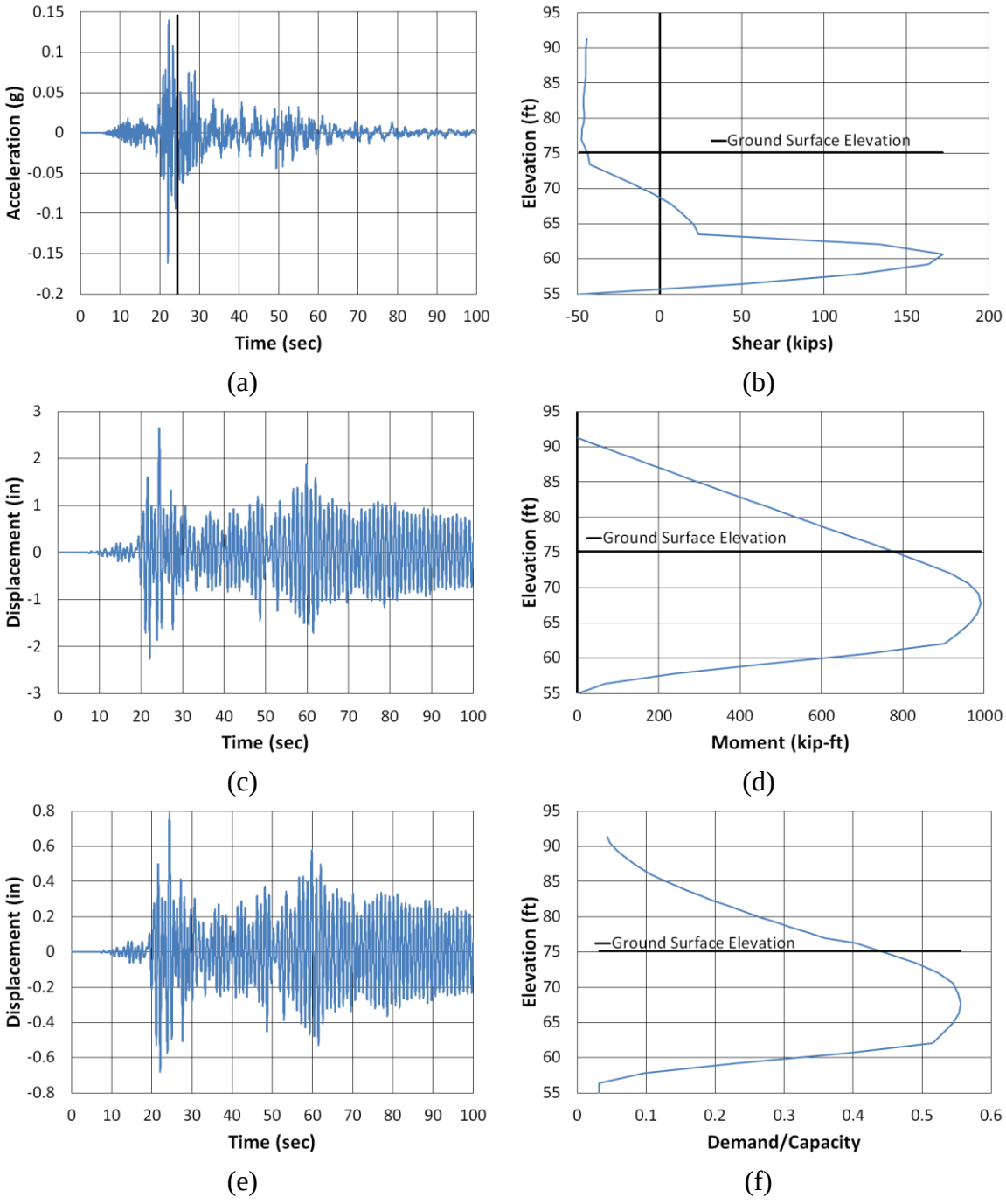

Figure B.7. Chambers County 25% Scour Longitudinal Kocaeli North (a) time-history event, (b) shear distribution, (c) top of pier displacement, (d) moment distribution, (e) ground surface displacement, and (f) demand capacity ratio

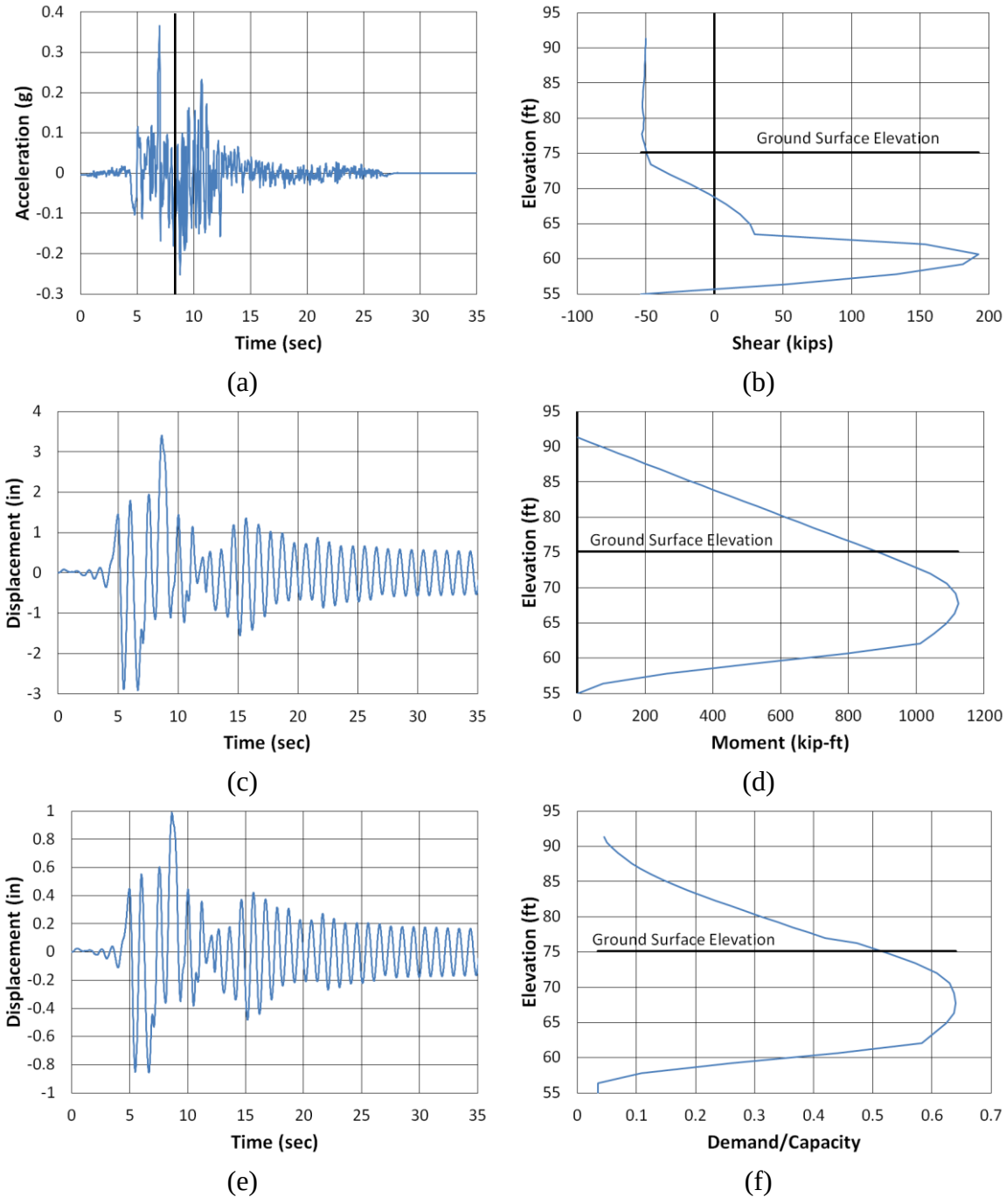

Figure B.8. Chambers County 25% Scour Longitudinal Kocaeli2 NMCE (a) time-history event, (b) shear distribution, (c) top of pier displacement, (d) moment distribution, (e) ground surface displacement, and (f) demand capacity ratio

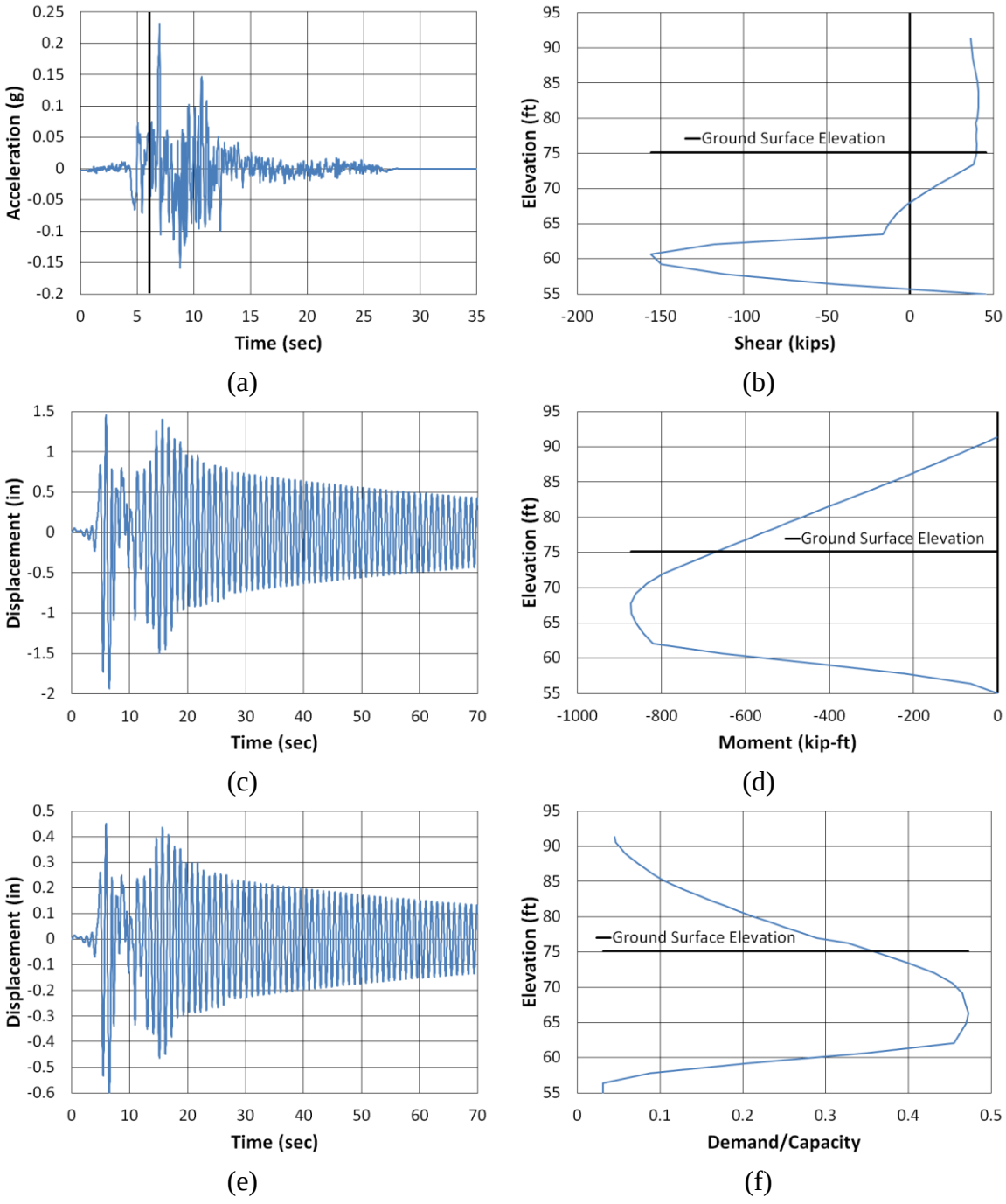

Figure B.9. Chambers County 25% Scour Longitudinal Kocaeli2 North (a) time-history event, (b) shear distribution, (c) top of pier displacement, (d) moment distribution, (e) ground surface displacement, and (f) demand capacity ratio

.

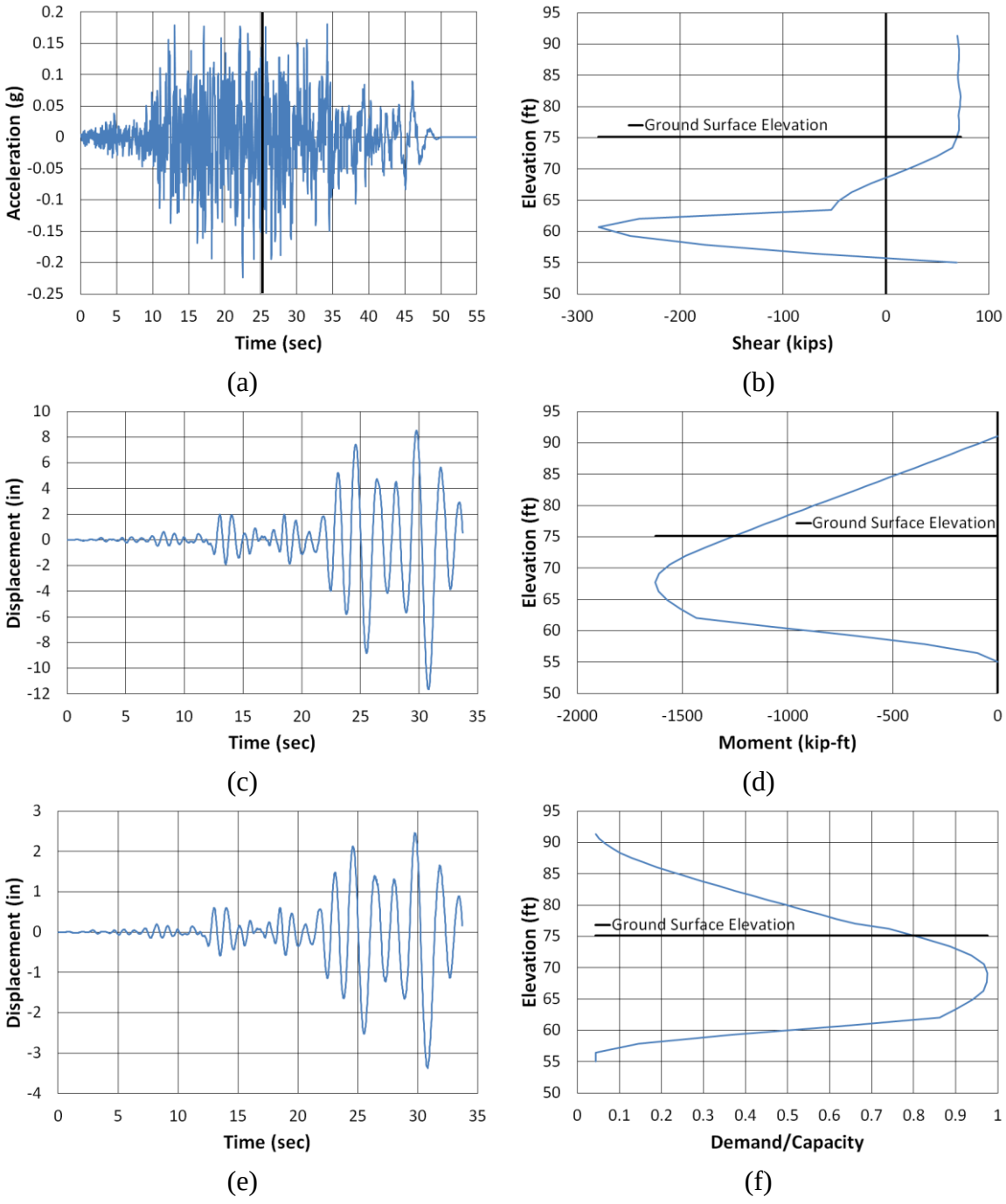

Figure B.10. Chambers County 25% Scour Longitudinal Landers NMCE (a) time-history event, (b) shear distribution, (c) top of pier displacement, (d) moment distribution, (e) ground surface displacement, and (f) demand capacity ratio

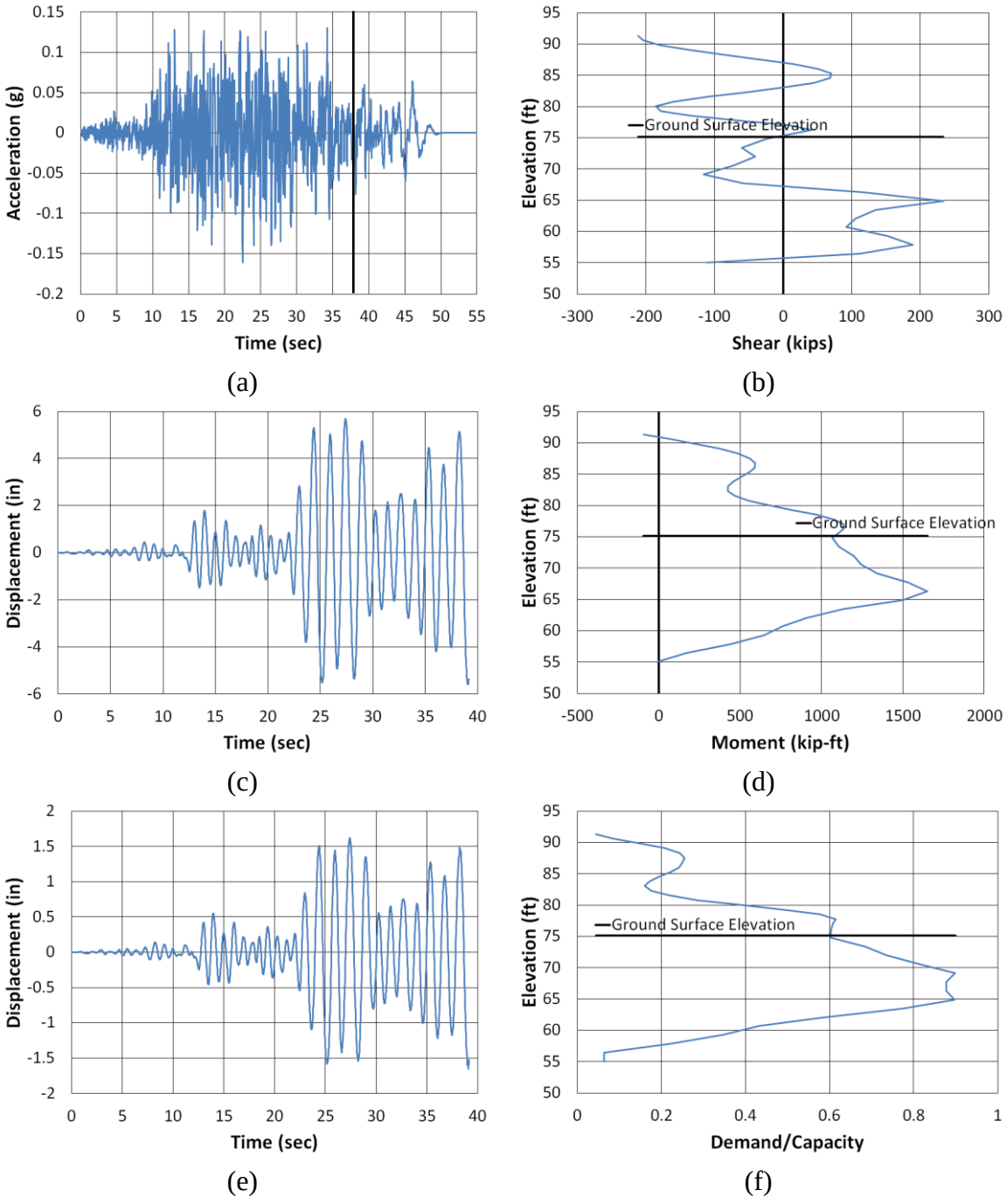

Figure B.11. Chambers County 25% Scour Longitudinal Landers North (a) time-history event, (b) shear distribution, (c) top of pier displacement, (d) moment distribution, (e) ground surface displacement, and (f) demand capacity ratio

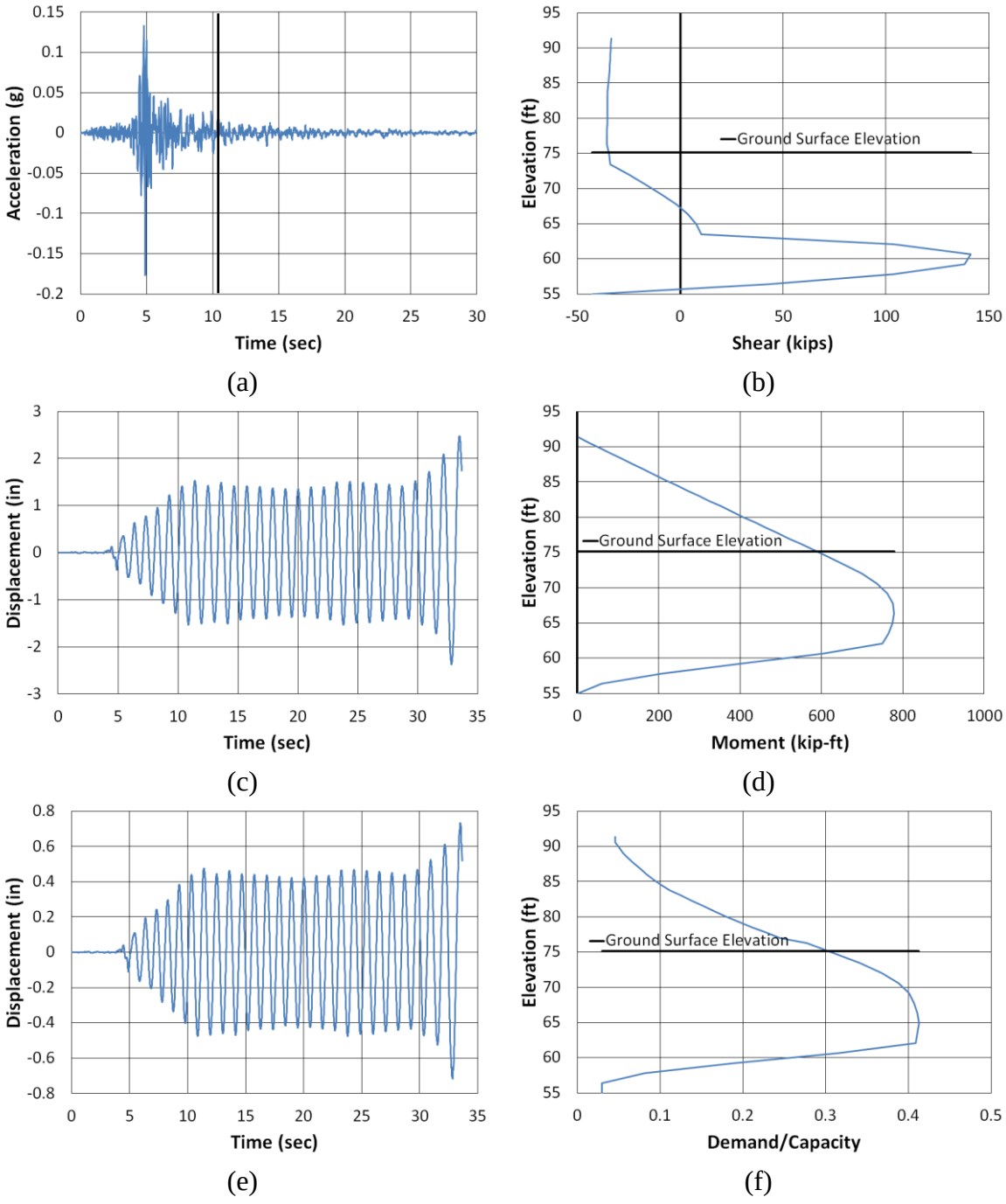

Figure B.12. Chambers County 25% Scour Longitudinal LSM North (a) time-history event, (b) shear distribution, (c) top of pier displacement, (d) moment distribution, (e) ground surface displacement, and (f) demand capacity ratio

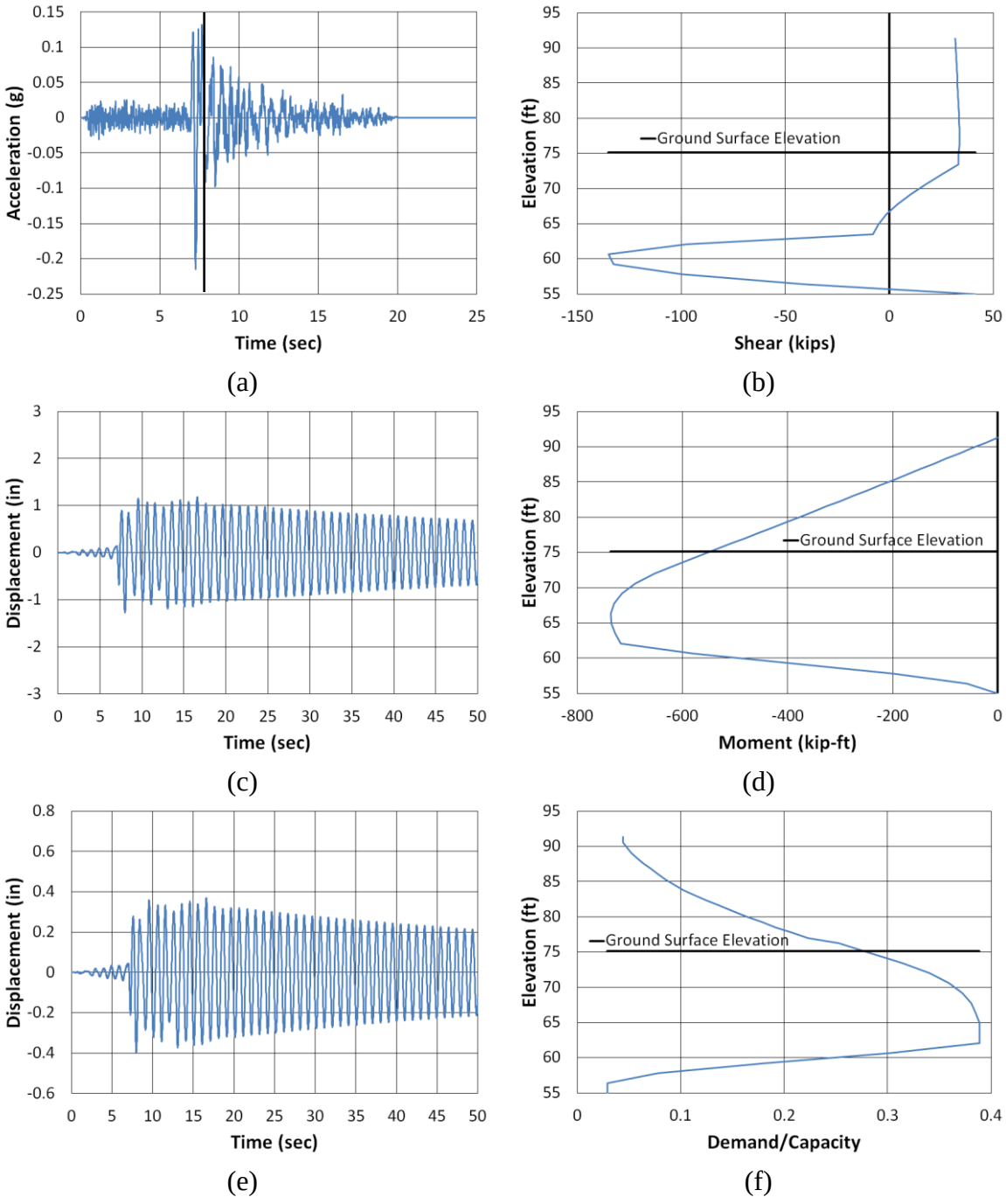

Figure B.13. Chambers County 25% Scour Longitudinal NPS North (a) time-history event, (b) shear distribution, (c) top of pier displacement, (d) moment distribution, (e) ground surface displacement, and (f) demand capacity ratio

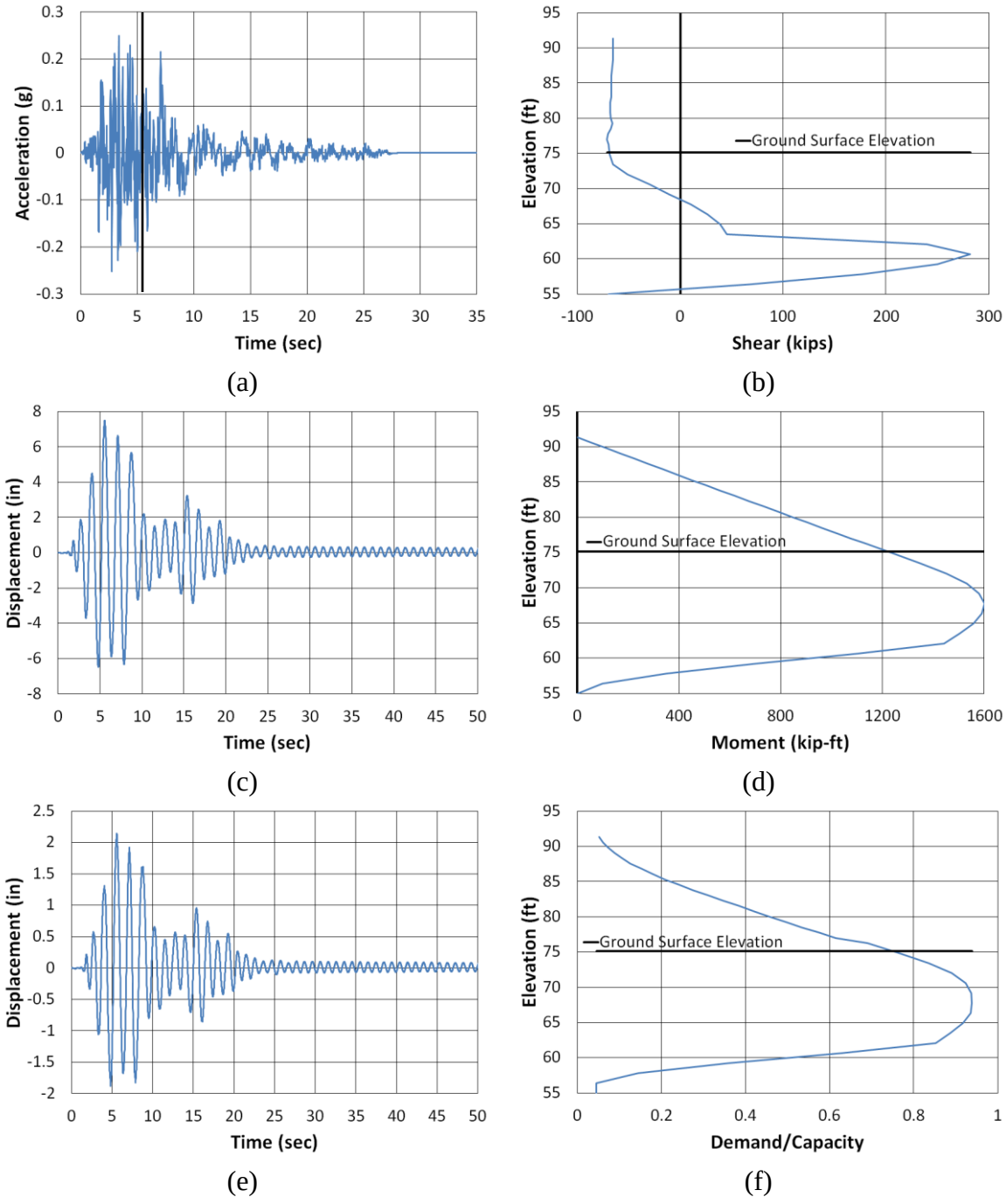

Figure B.14. Chambers County 25% Scour Longitudinal San Fernando NMCE (a) time-history event, (b) shear distribution, (c) top of pier displacement, (d) moment distribution, (e) ground surface displacement, and (f) demand capacity ratio

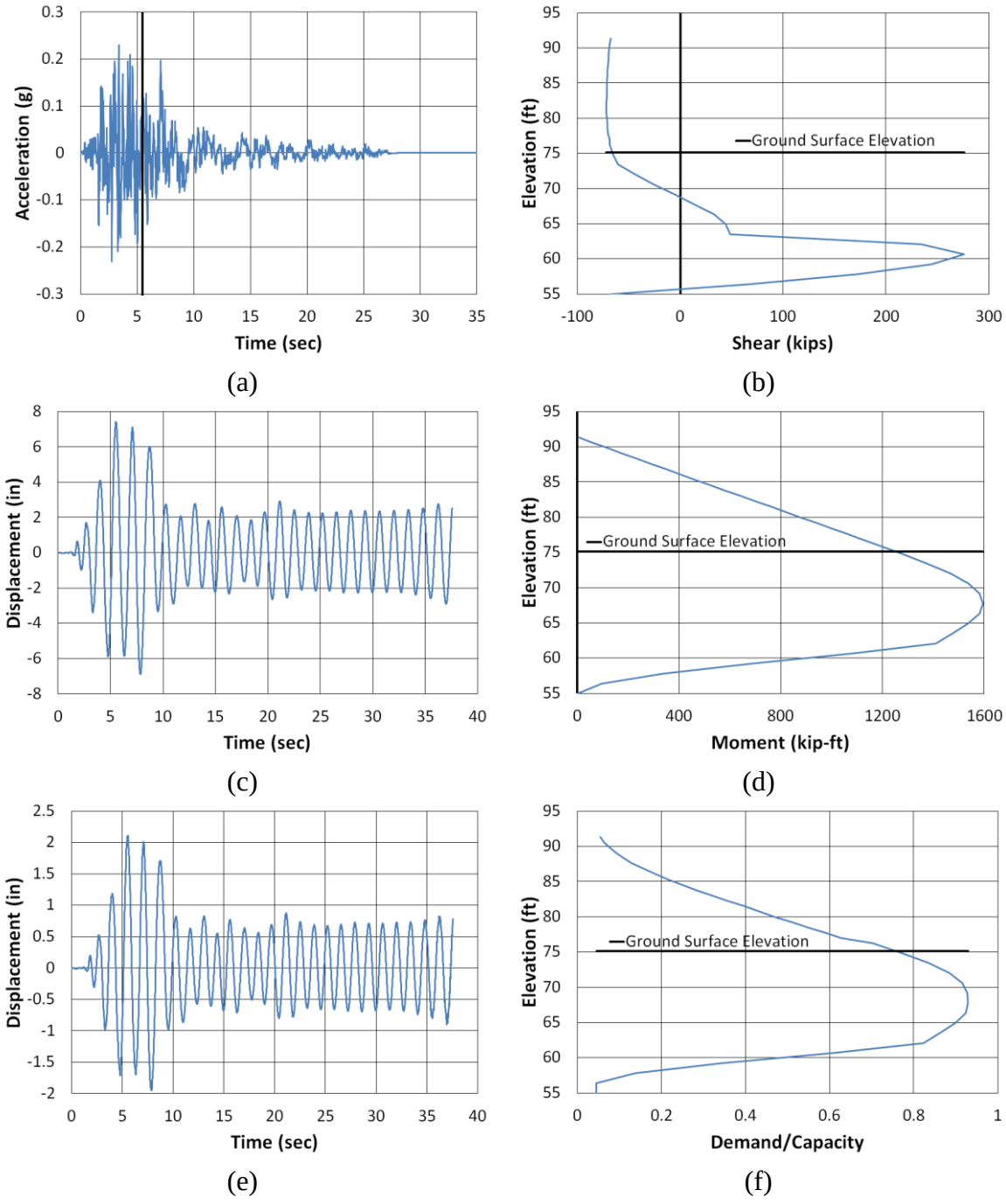

Figure B.15. Chambers County 25% Scour Longitudinal San Fernando North (a) time-history event, (b) shear distribution, (c) top of pier displacement, (d) moment distribution, (e) ground surface displacement, and (f) demand capacity ratio

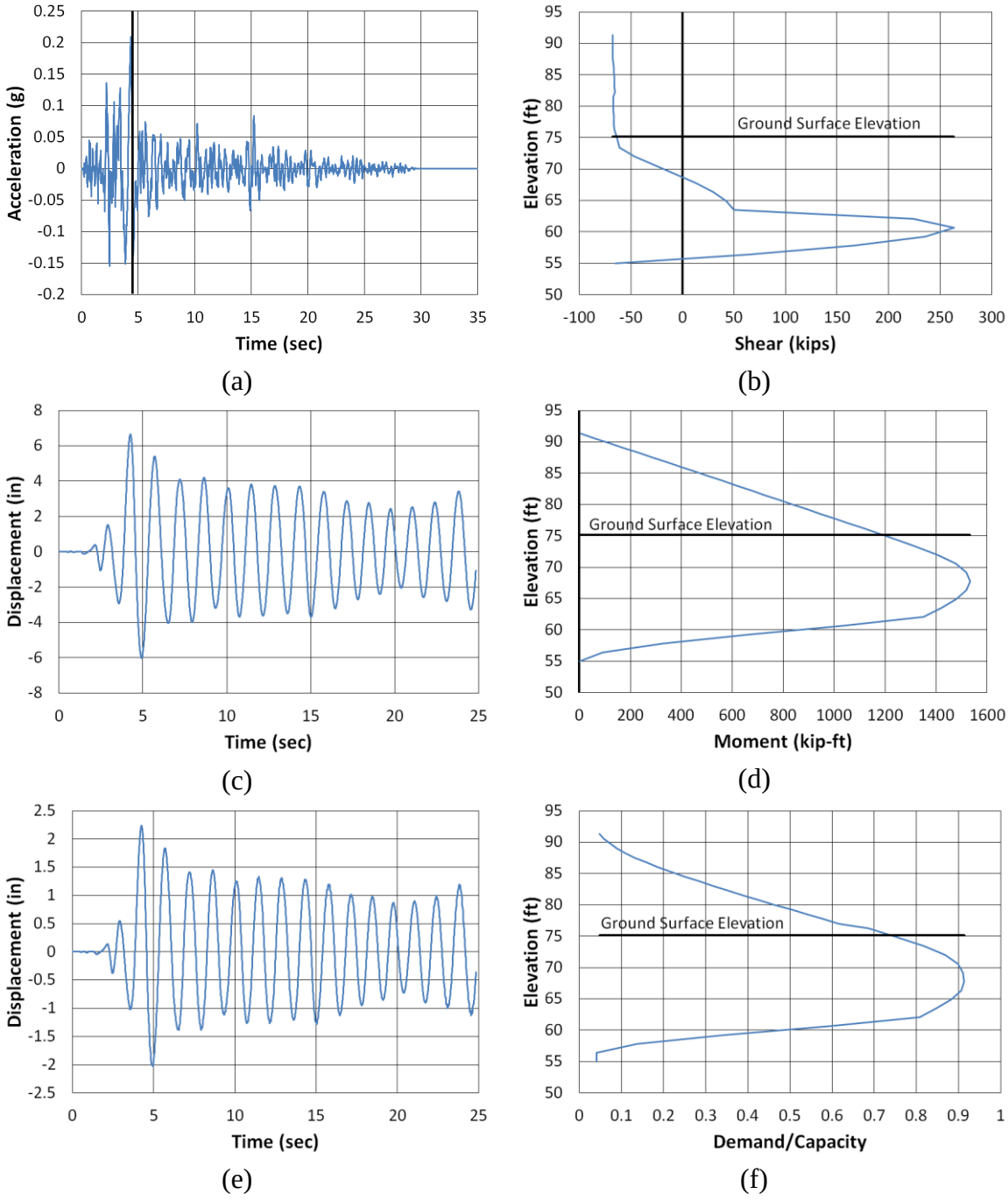

Figure B.16. Chambers County 25% Scour Longitudinal San Fernando2 NMCE (a) time-history event, (b) shear distribution, (c) top of pier displacement, (d) moment distribution, (e) ground surface displacement, and (f) demand capacity ratio

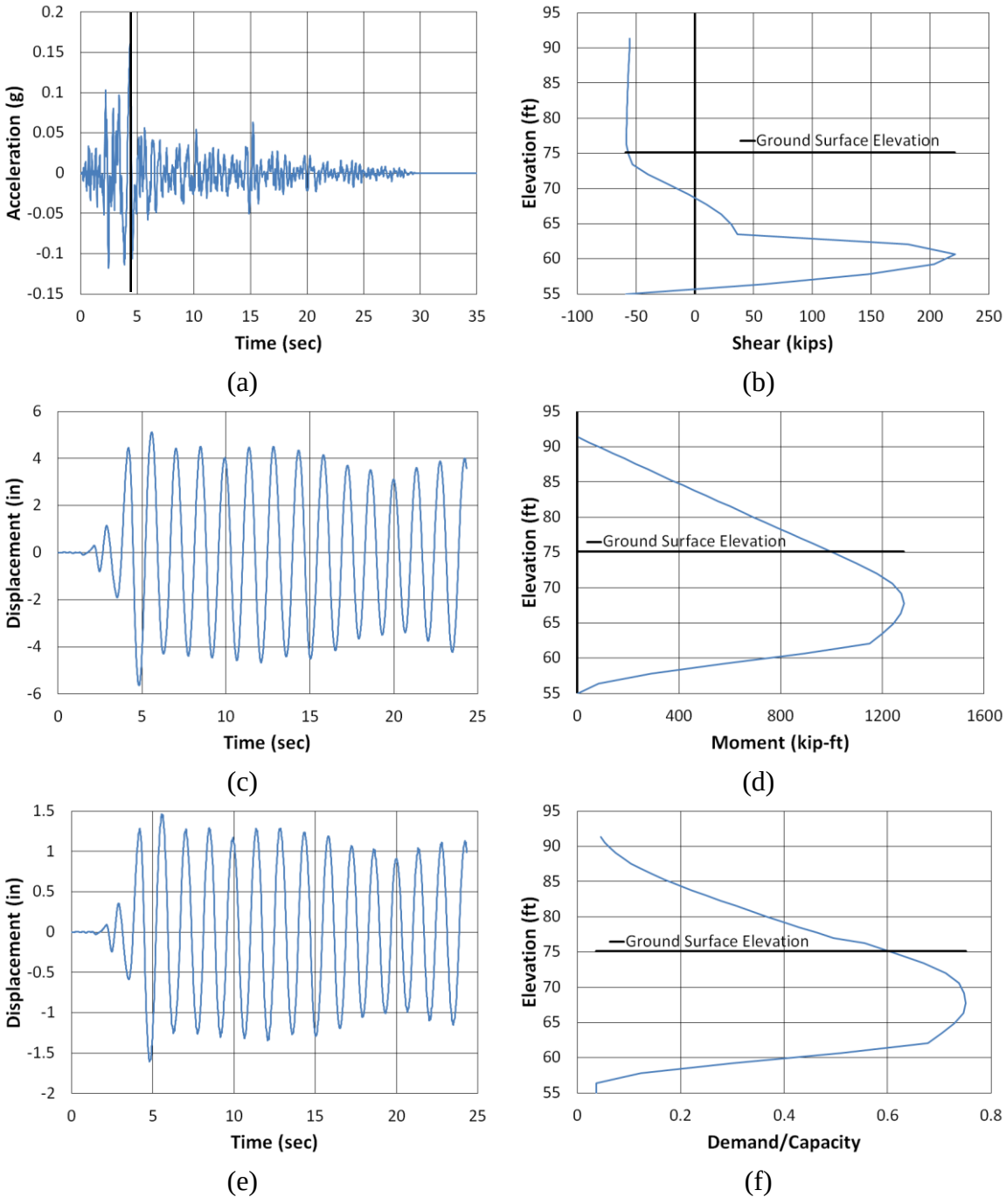

Figure B.17 Chambers County 25% Scour Longitudinal San Fernando2 North (a) time-history event, (b) shear distribution, (c) top of pier displacement, (d) moment distribution, (e) ground surface displacement, and (f) demand capacity ratio

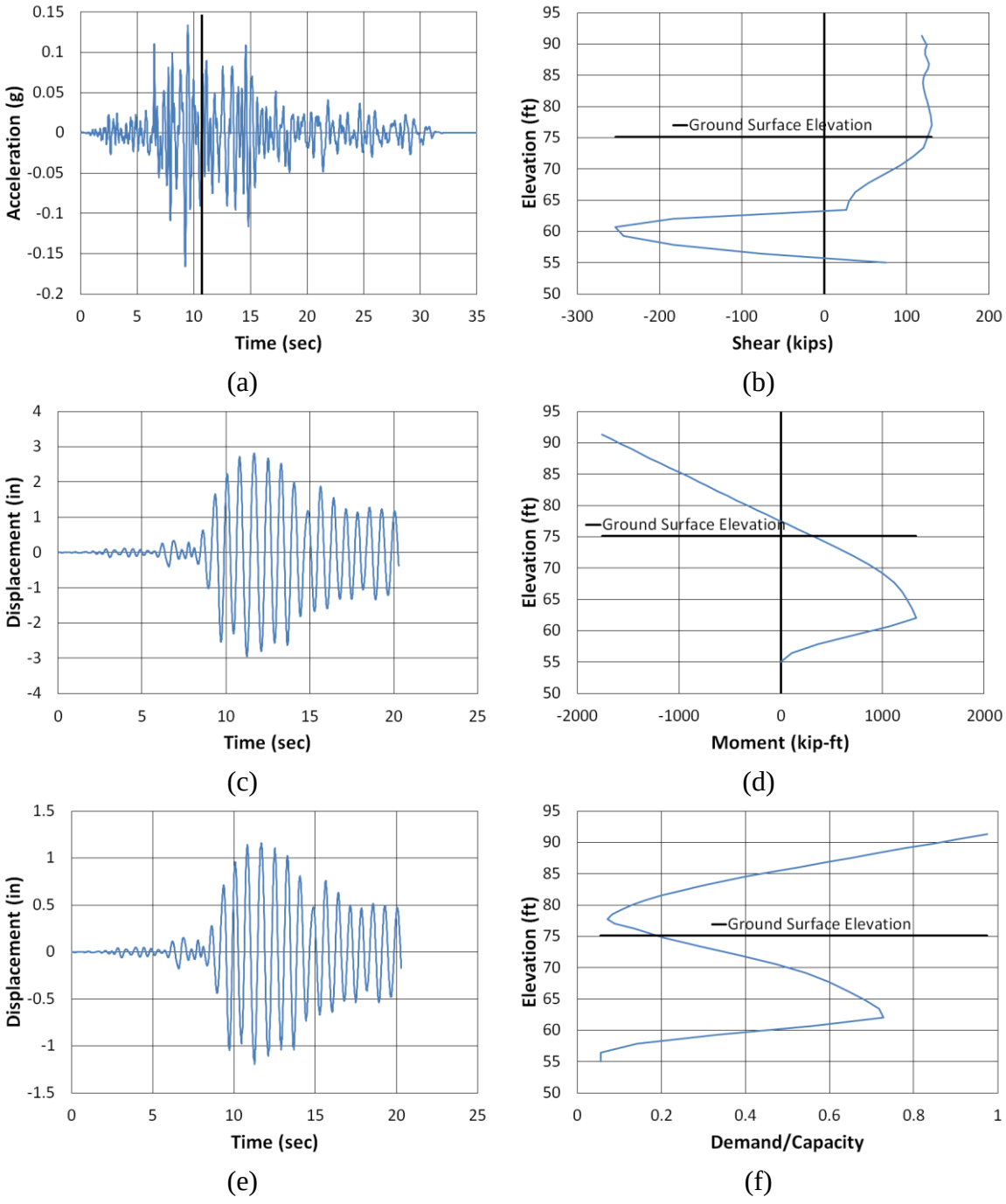

Figure B.18. Chambers County 25% Scour Transverse Coalinga North (a) time-history event, (b) shear distribution, (c) top of pier displacement, (d) moment distribution, (e) ground surface displacement, and (f) demand capacity ratio

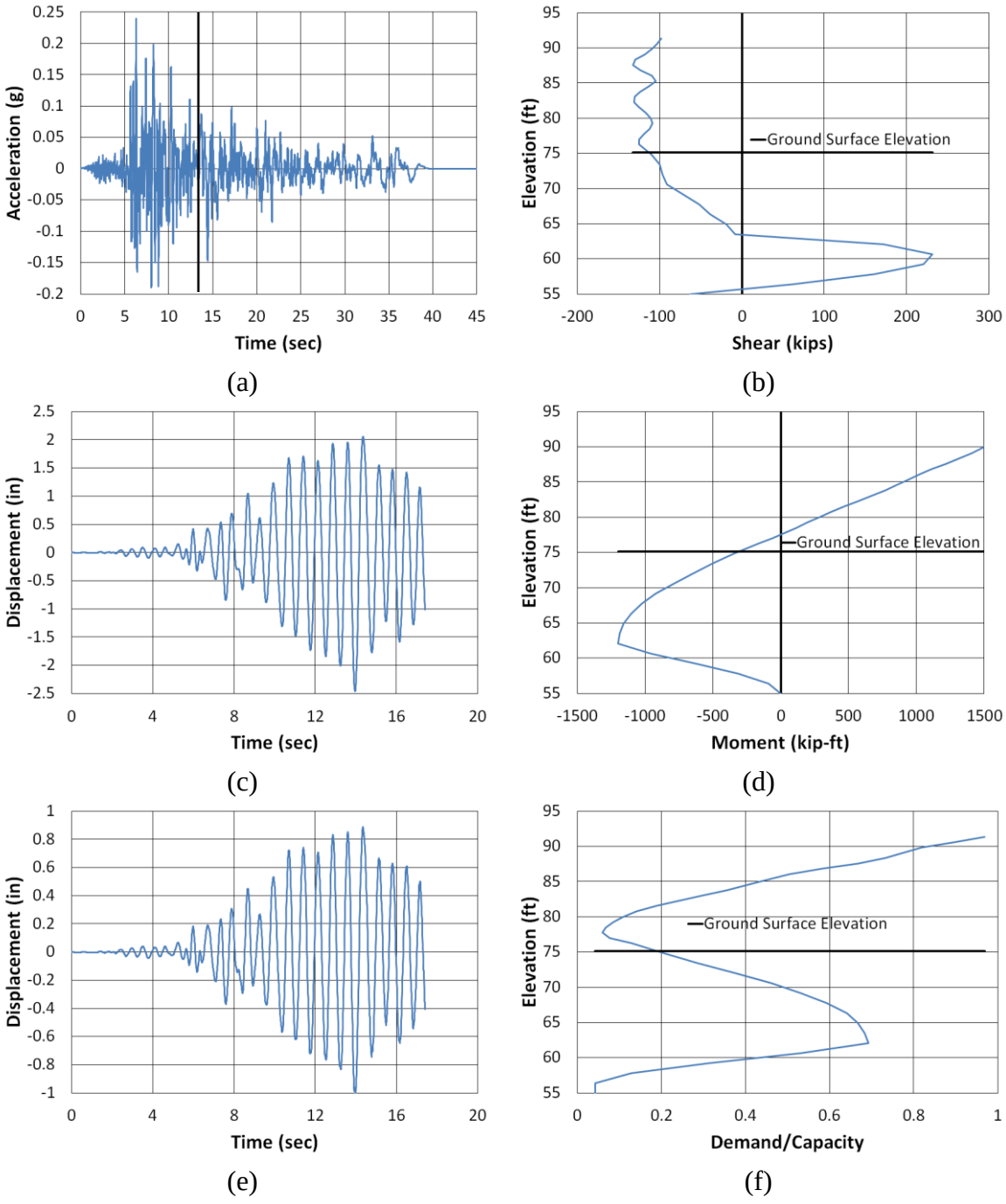

Figure B.19. Chambers County 25% Scour Transverse Imperial Valley NMCE (a) time-history event, (b) shear distribution, (c) top of pier displacement, (d) moment distribution, (e) ground surface displacement, and (f) demand capacity ratio

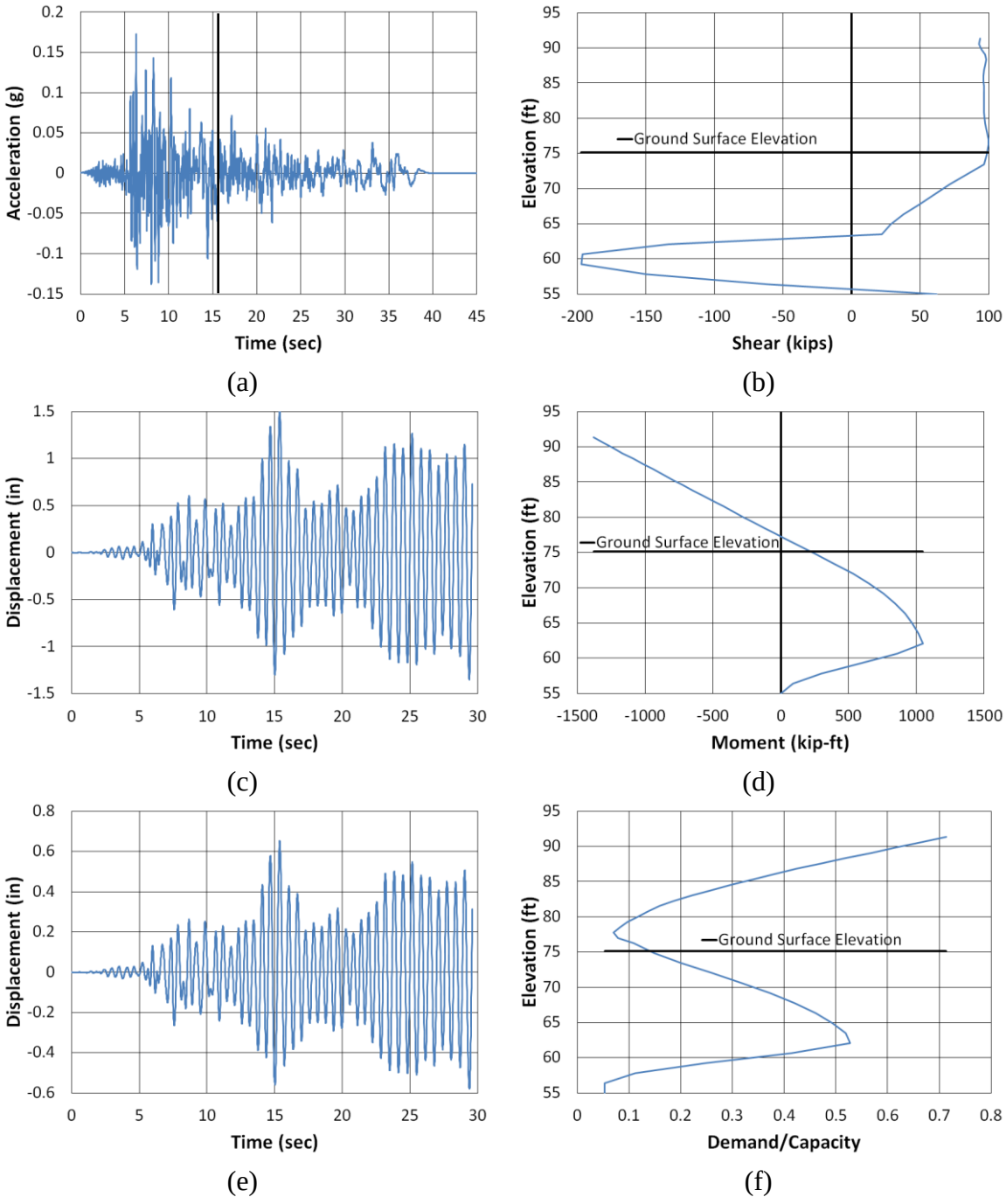

Figure B.20. Chambers County 25% Scour Transverse Imperial Valley North (a) time-history event, (b) shear distribution, (c) top of pier displacement, (d) moment distribution, (e) ground surface displacement, and (f) demand capacity ratio

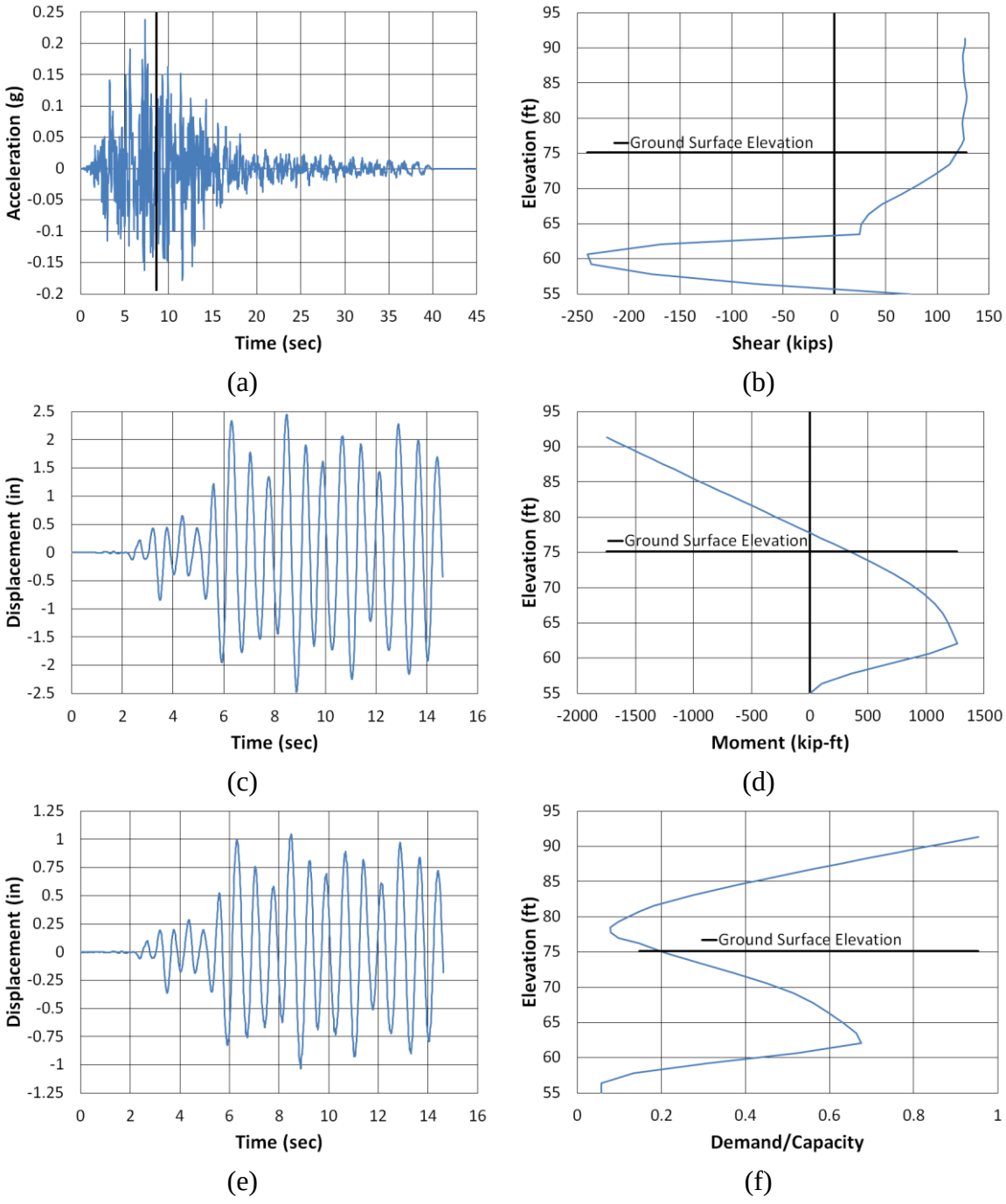

Figure B.21. Chambers County 25% Scour Transverse Kobe NMCE (a) time-history event, (b) shear distribution, (c) top of pier displacement, (d) moment distribution, (e) ground surface displacement, and (f) demand capacity ratio

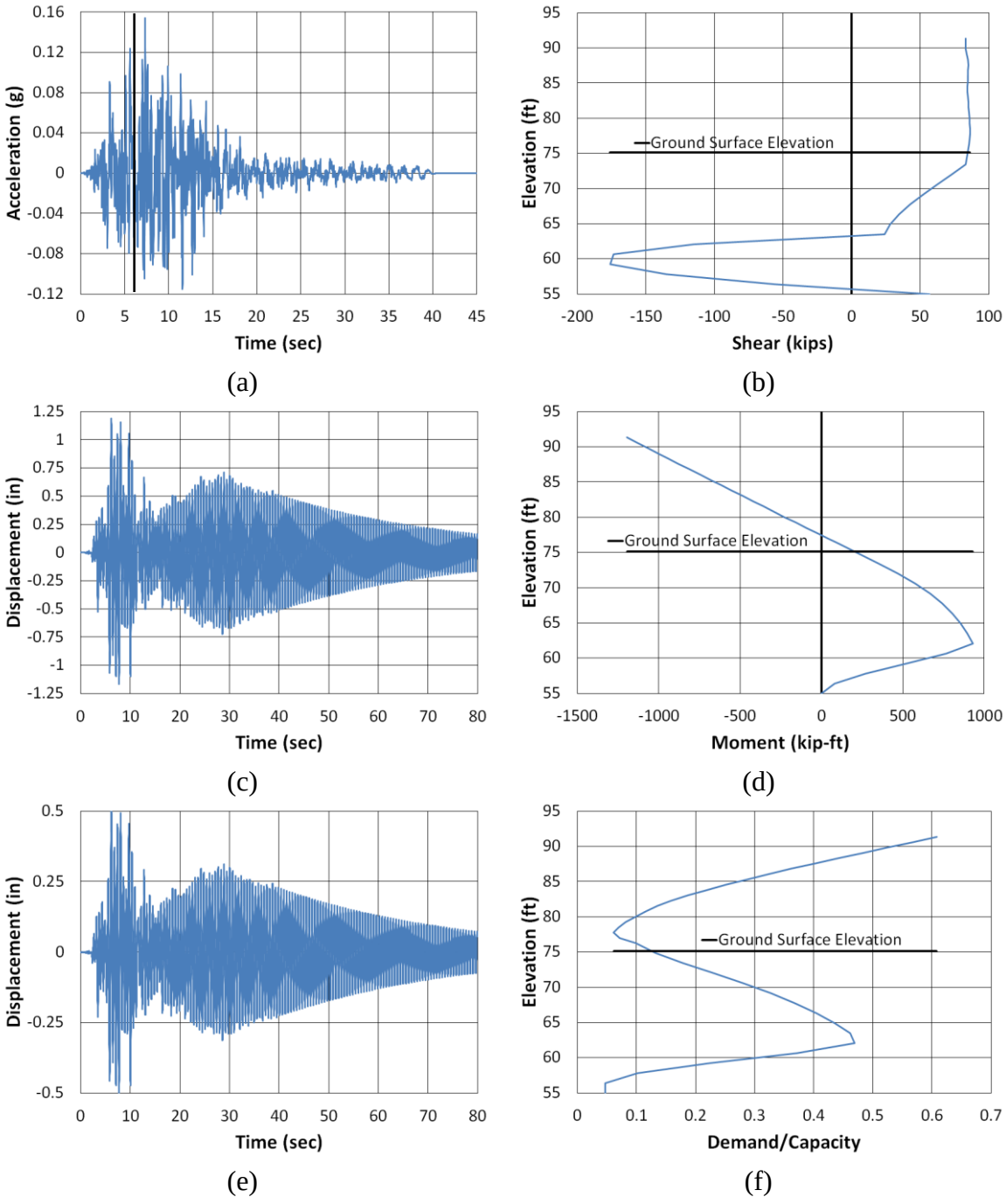

Figure B.22. Chambers County 25% Scour Transverse Kobe North (a) time-history event, (b) shear distribution, (c) top of pier displacement, (d) moment distribution, (e) ground surface displacement, and (f) demand capacity ratio

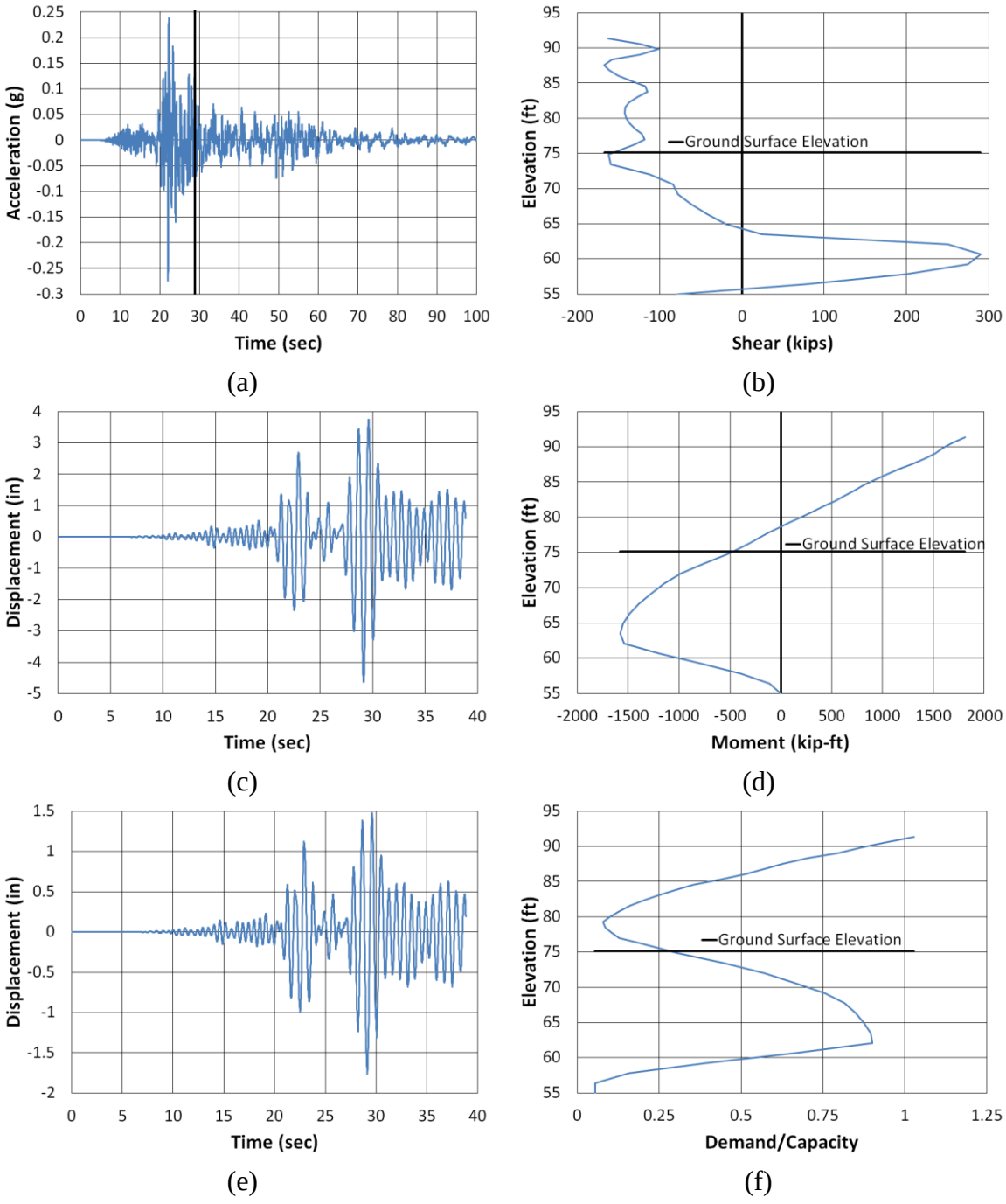

Figure B.23. Chambers County 25% Scour Transverse Kocaeli NMCE (a) time-history event, (b) shear distribution, (c) top of pier displacement, (d) moment distribution, (e) ground surface displacement, and (f) demand capacity ratio

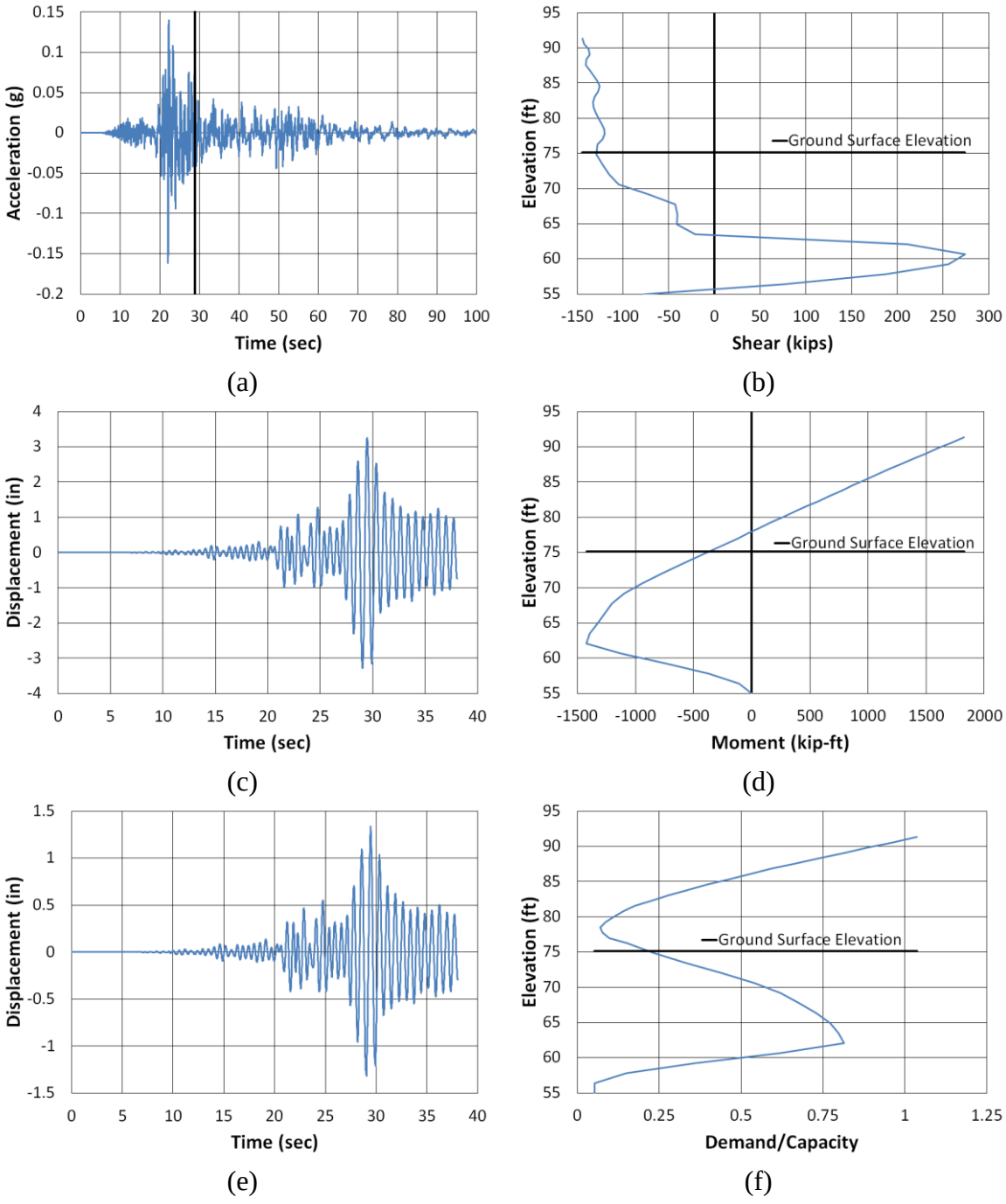

Figure B.24. Chambers County 25% Scour Transverse Kocaeli North (a) time-history event, (b) shear distribution, (c) top of pier displacement, (d) moment distribution, (e) ground surface displacement, and (f) demand capacity ratio

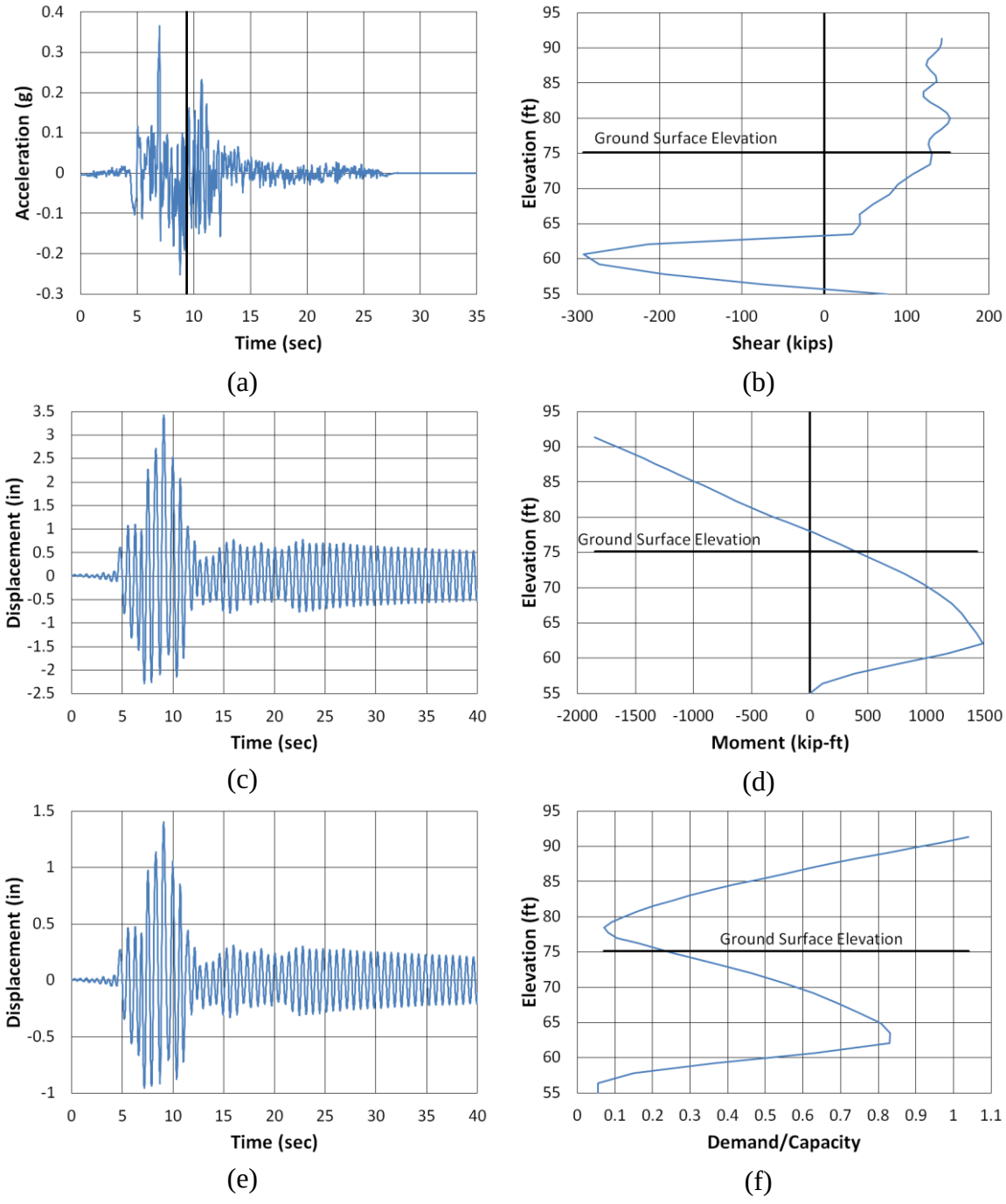

Figure B.25. Chambers County 25% Scour Transverse Kocaeli2 NMCE (a) time-history event, (b) shear distribution, (c) top of pier displacement, (d) moment distribution, (e) ground surface displacement, and (f) demand capacity ratio

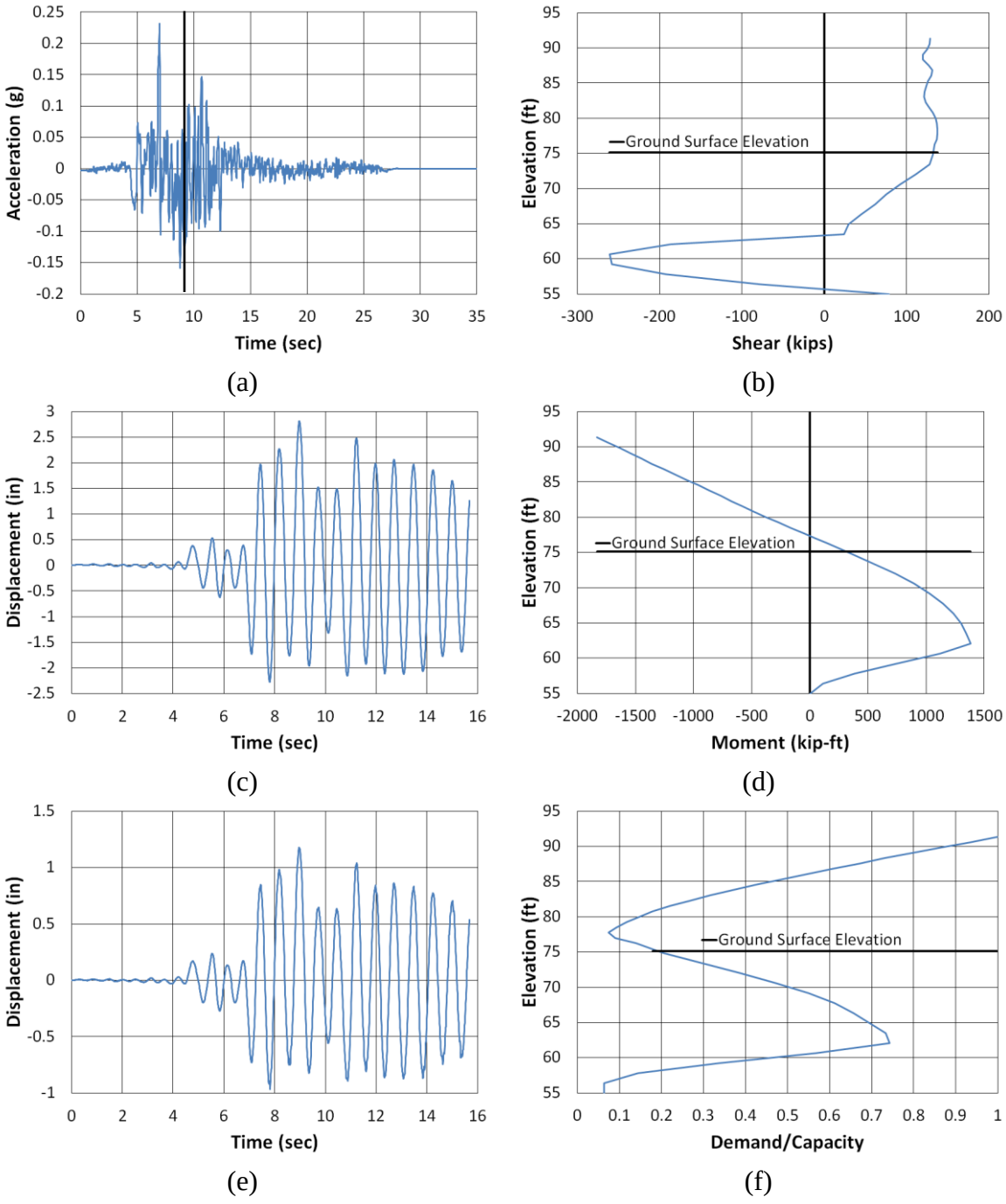

Figure B.26. Chambers County 25% Scour Transverse Kocaeli2 North (a) time-history event, (b) shear distribution, (c) top of pier displacement, (d) moment distribution, (e) ground surface displacement, and (f) demand capacity ratio

.

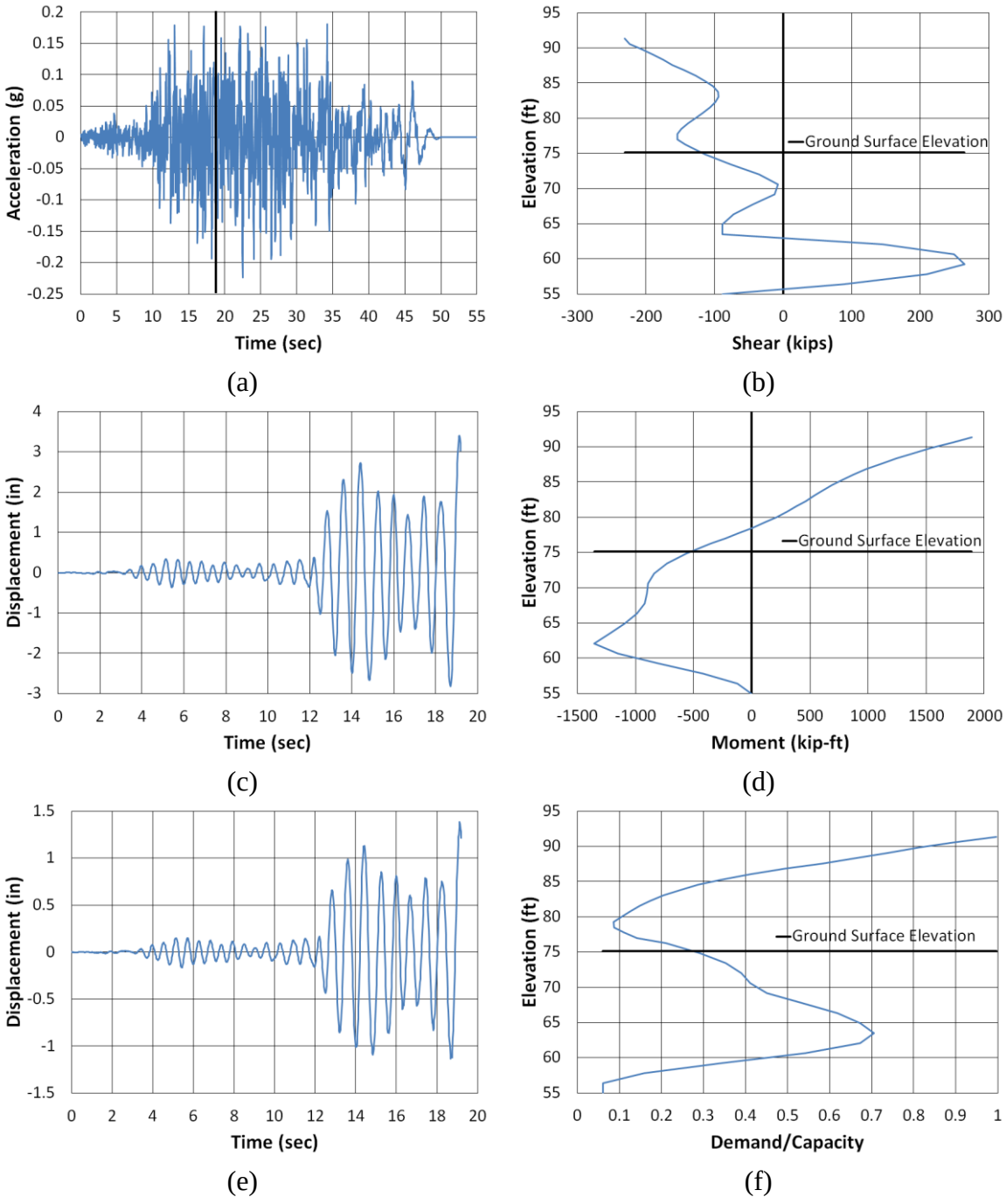

Figure B.27. Chambers County 25% Scour Transverse Landers NMCE (a) time-history event, (b) shear distribution, (c) top of pier displacement, (d) moment distribution, (e) ground surface displacement, and (f) demand capacity ratio

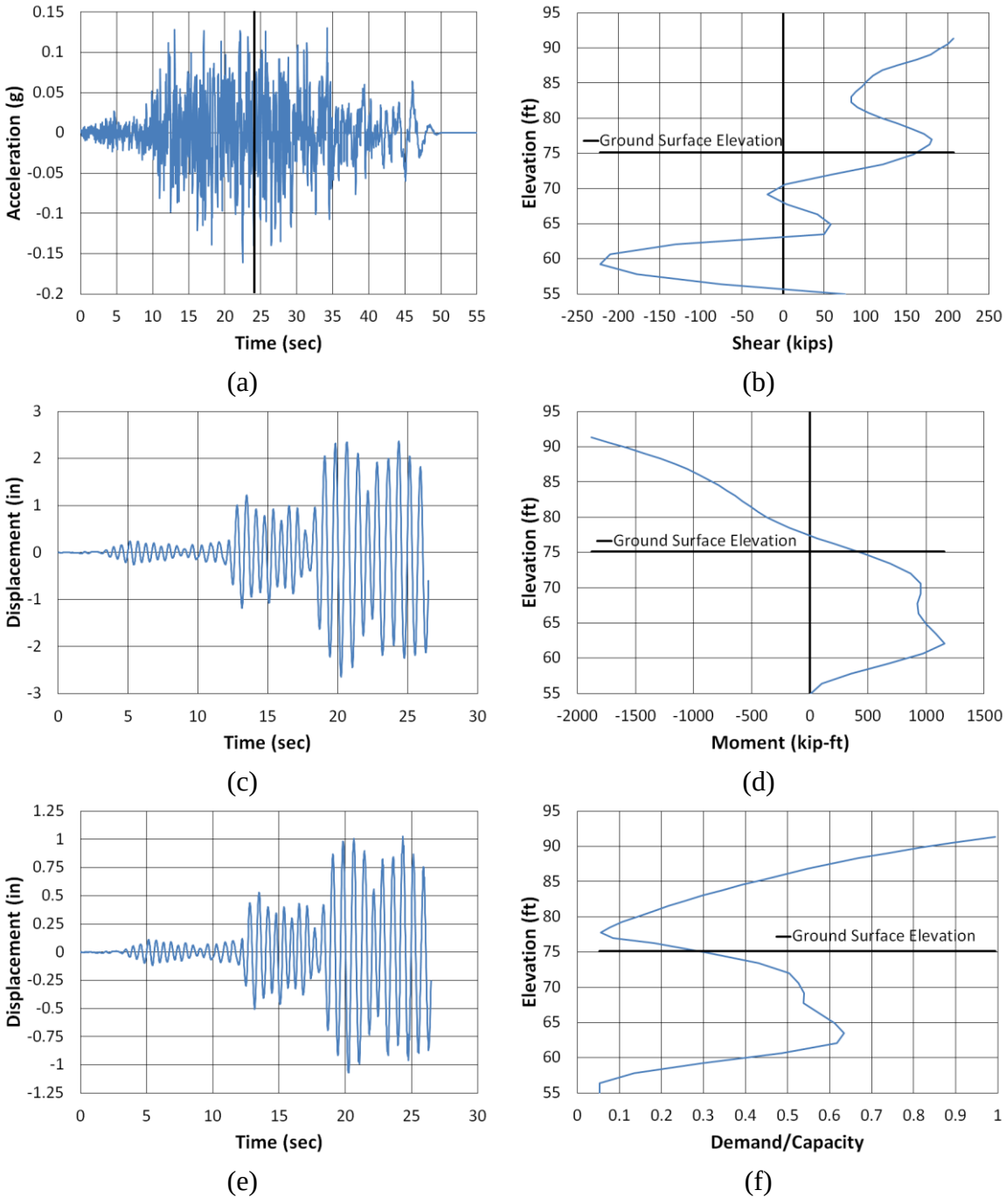

Figure B.28. Chambers County 25% Scour Transverse Landers North (a) time-history event, (b) shear distribution, (c) top of pier displacement, (d) moment distribution, (e) ground surface displacement, and (f) demand capacity ratio

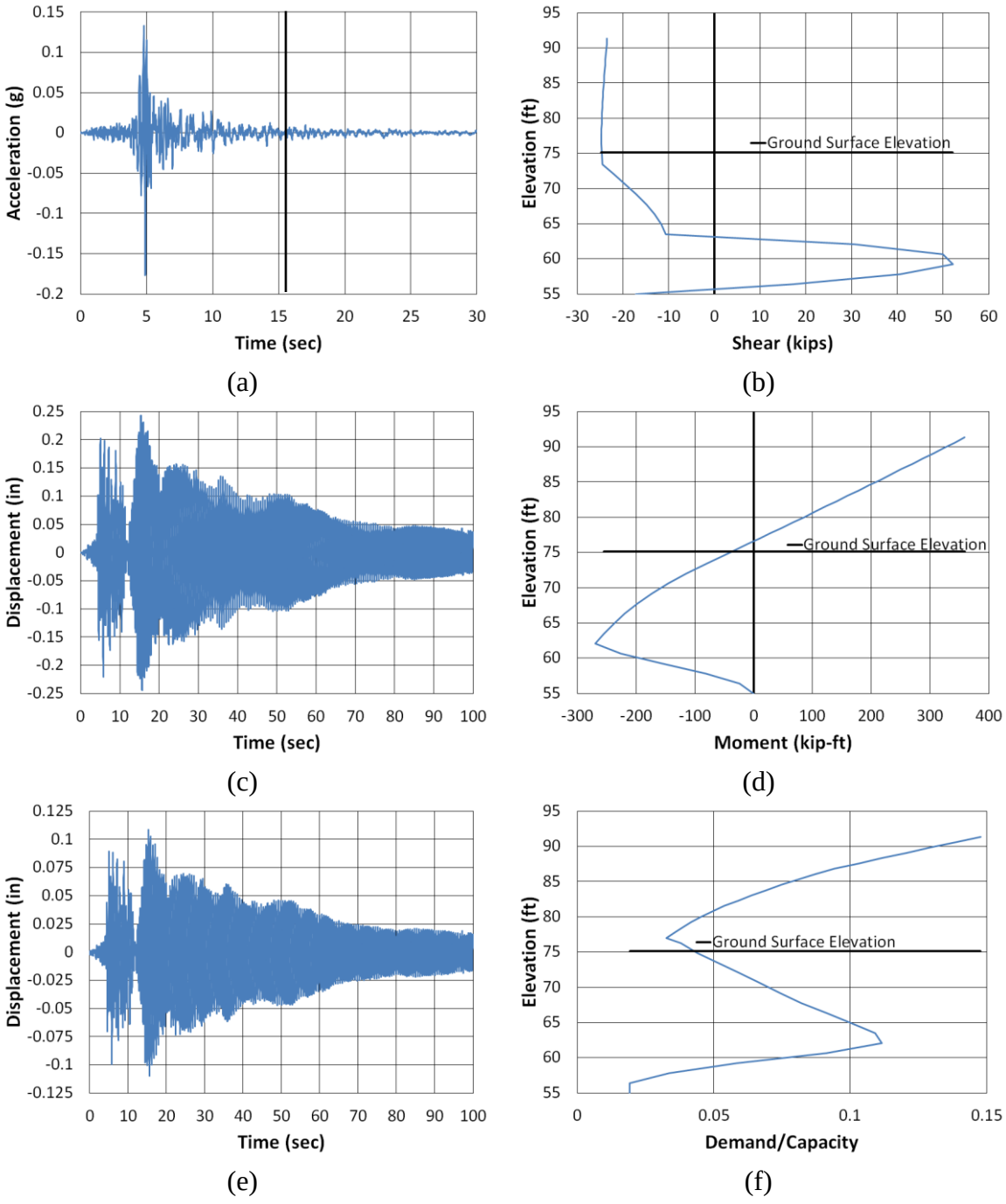

Figure B.29. Chambers County 25% Scour Transverse LSM North (a) time-history event, (b) shear distribution, (c) top of pier displacement, (d) moment distribution, (e) ground surface displacement, and (f) demand capacity ratio

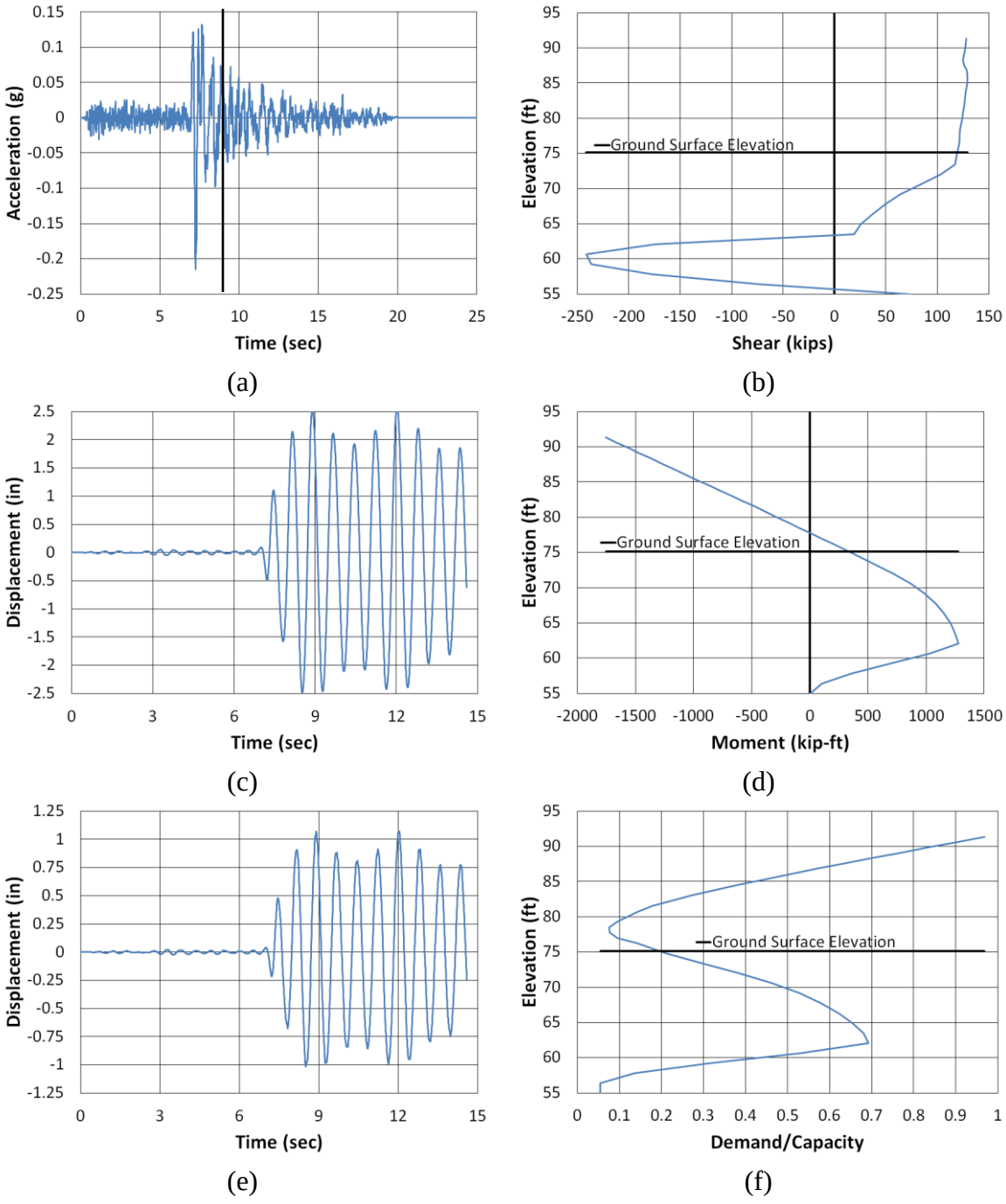

Figure B.30. Chambers County 25% Scour Transverse NPS North (a) time-history event, (b) shear distribution, (c) top of pier displacement, (d) moment distribution, (e) ground surface displacement, and (f) demand capacity ratio

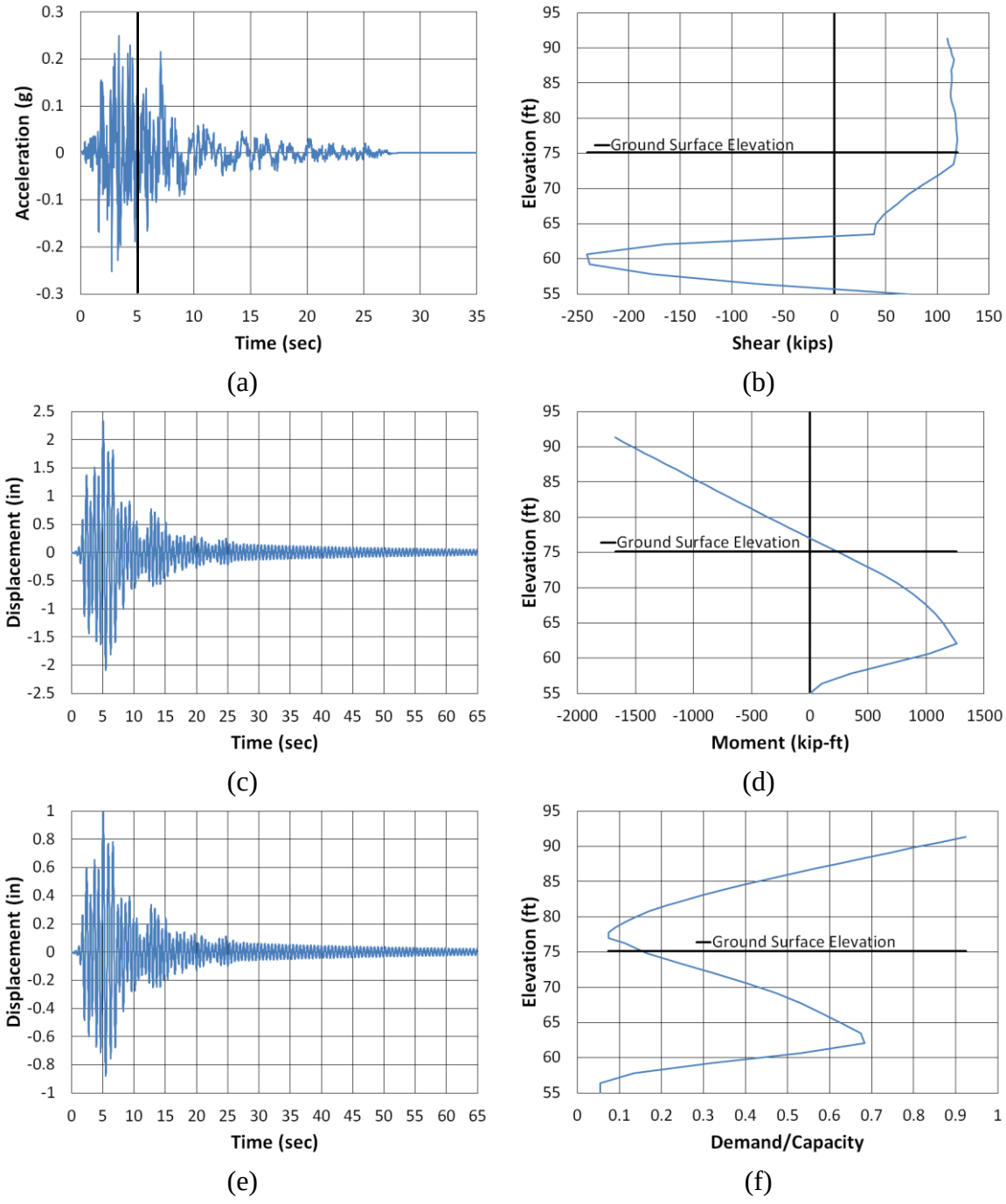

Figure B.31. Chambers County 25% Scour Transverse San Fernando NMCE (a) time-history event, (b) shear distribution, (c) top of pier displacement, (d) moment distribution, (e) ground surface displacement, and (f) demand capacity ratio

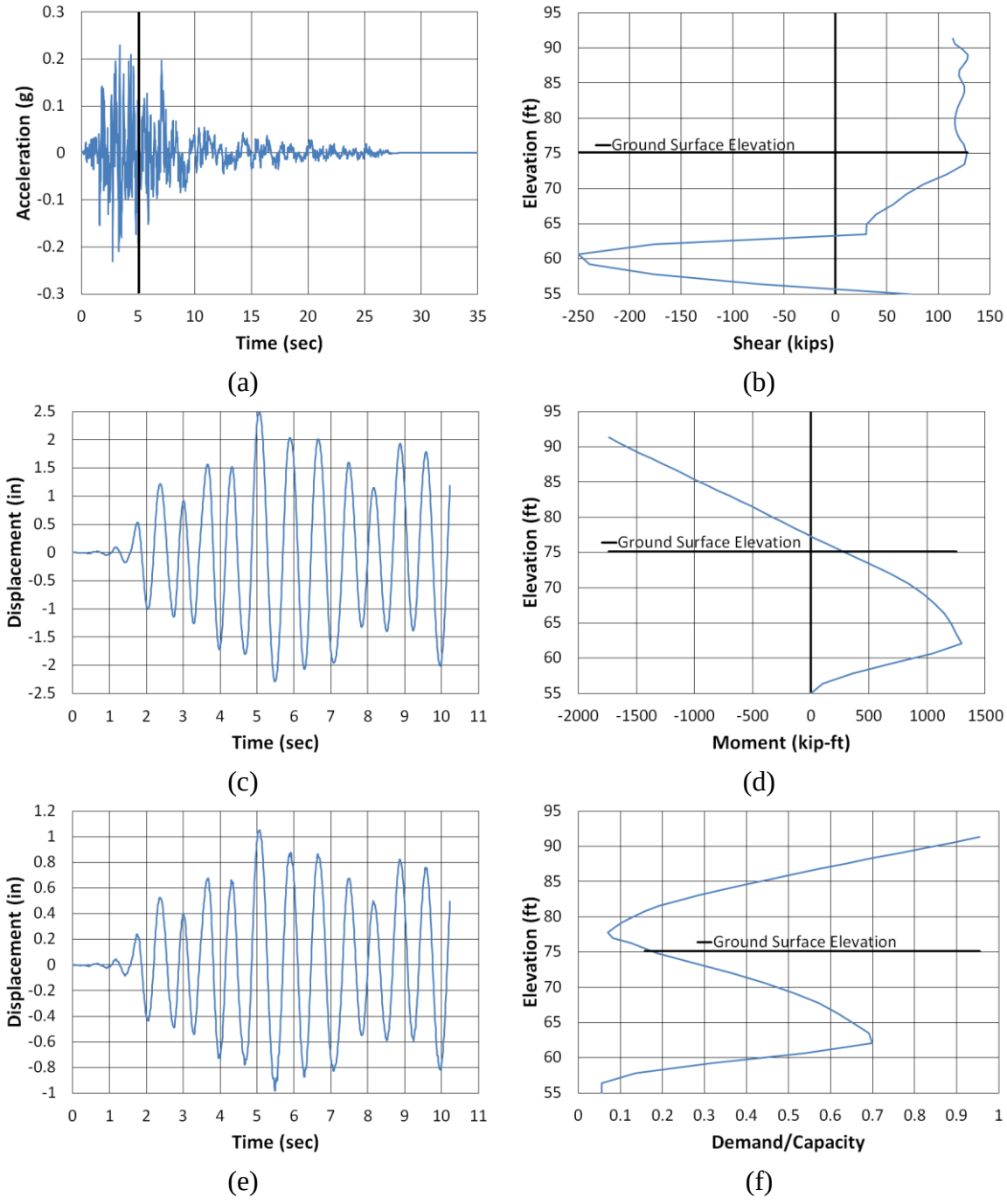

Figure B.32. Chambers County 25% Scour Transverse San Fernando North (a) time-history event, (b) shear distribution, (c) top of pier displacement, (d) moment distribution, (e) ground surface displacement, and (f) demand capacity ratio

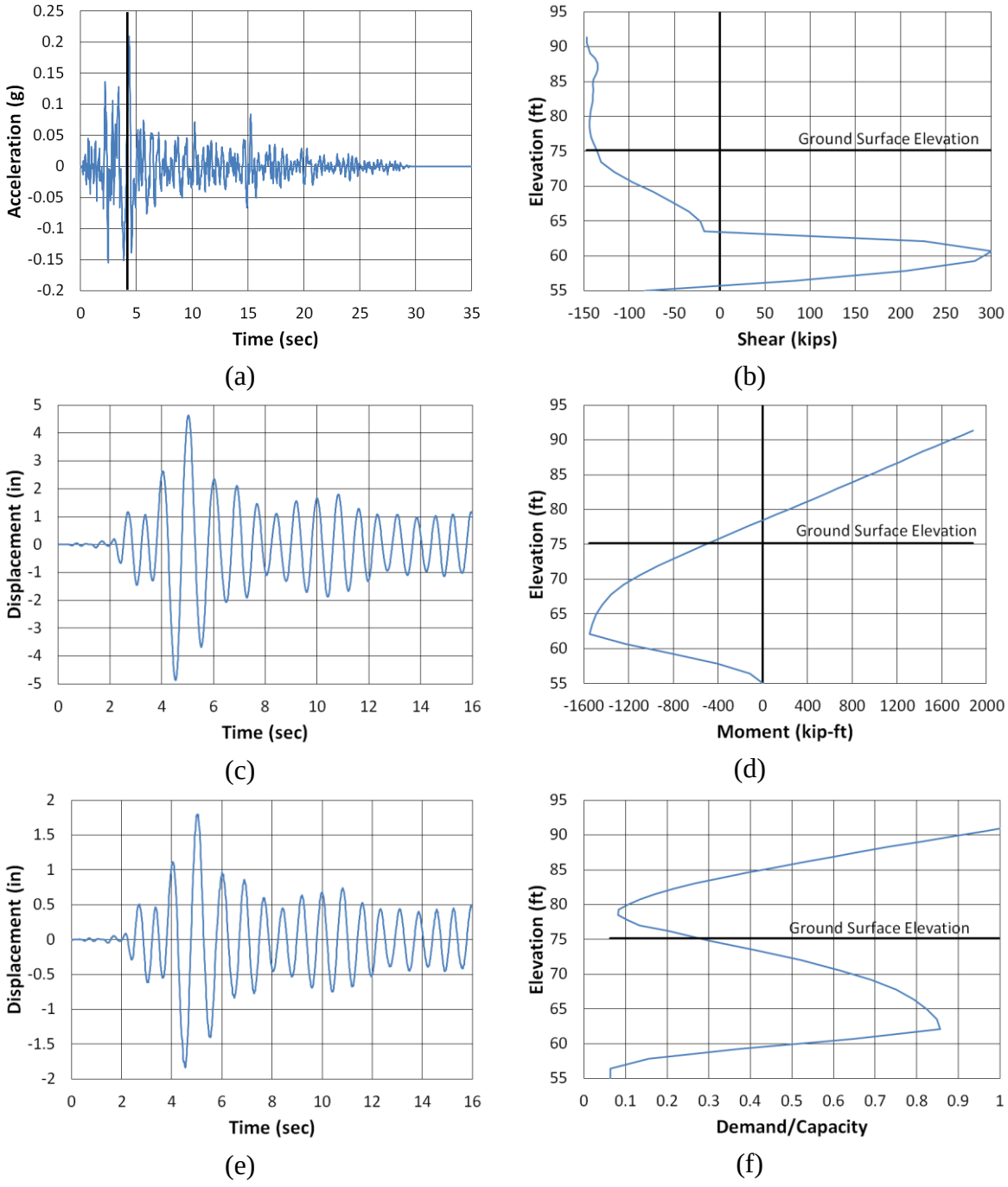

Figure B.33. Chambers County 25% Scour Transverse San Fernando2 NMCE (a) time-history event, (b) shear distribution, (c) top of pier displacement, (d) moment distribution, (e) ground surface displacement, and (f) demand capacity ratio

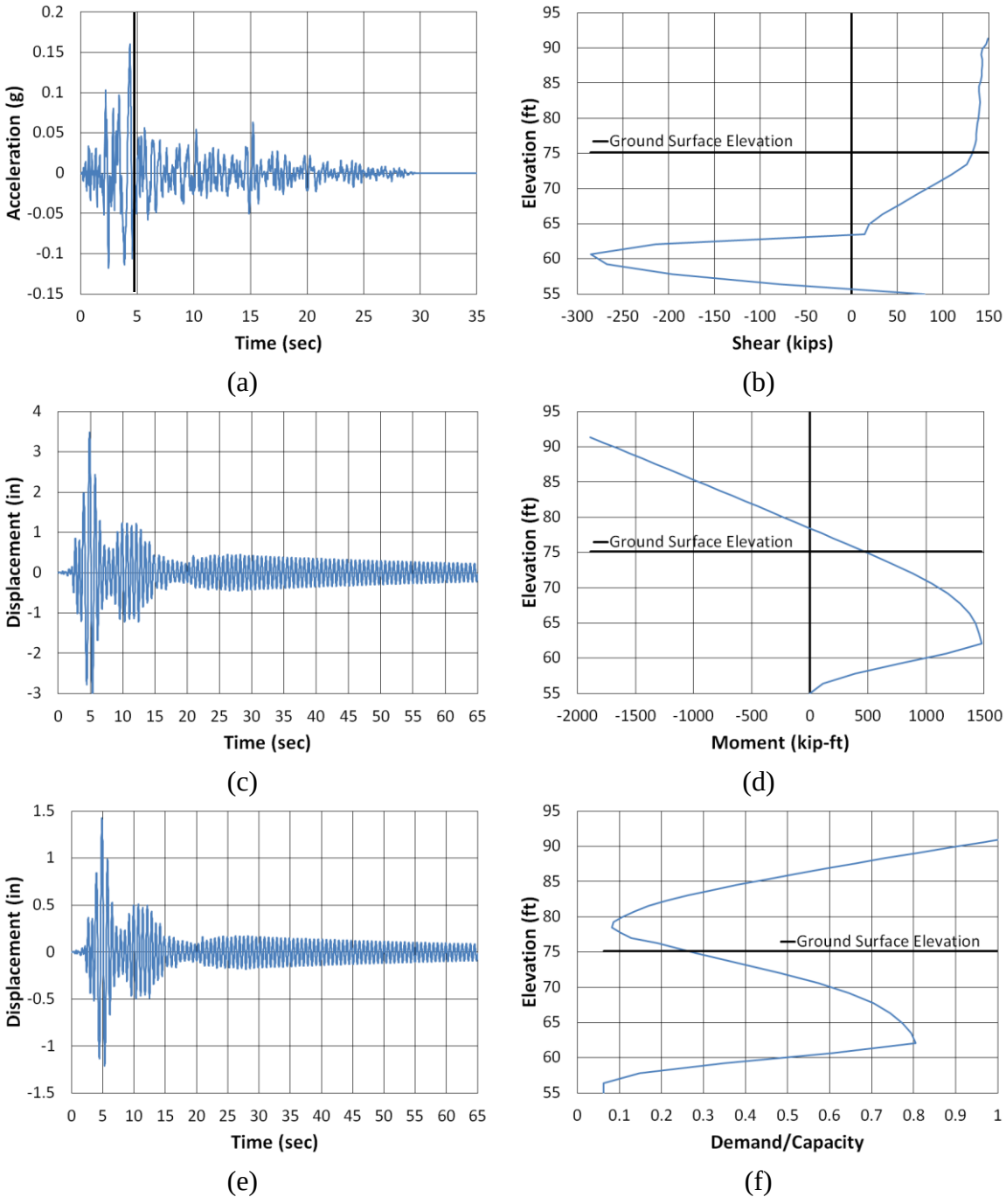

Figure B.34. Chambers County 25% Scour Transverse San Fernando2 North (a) time-history event, (b) shear distribution, (c) top of pier displacement, (d) moment distribution, (e) ground surface displacement, and (f) demand capacity ratio

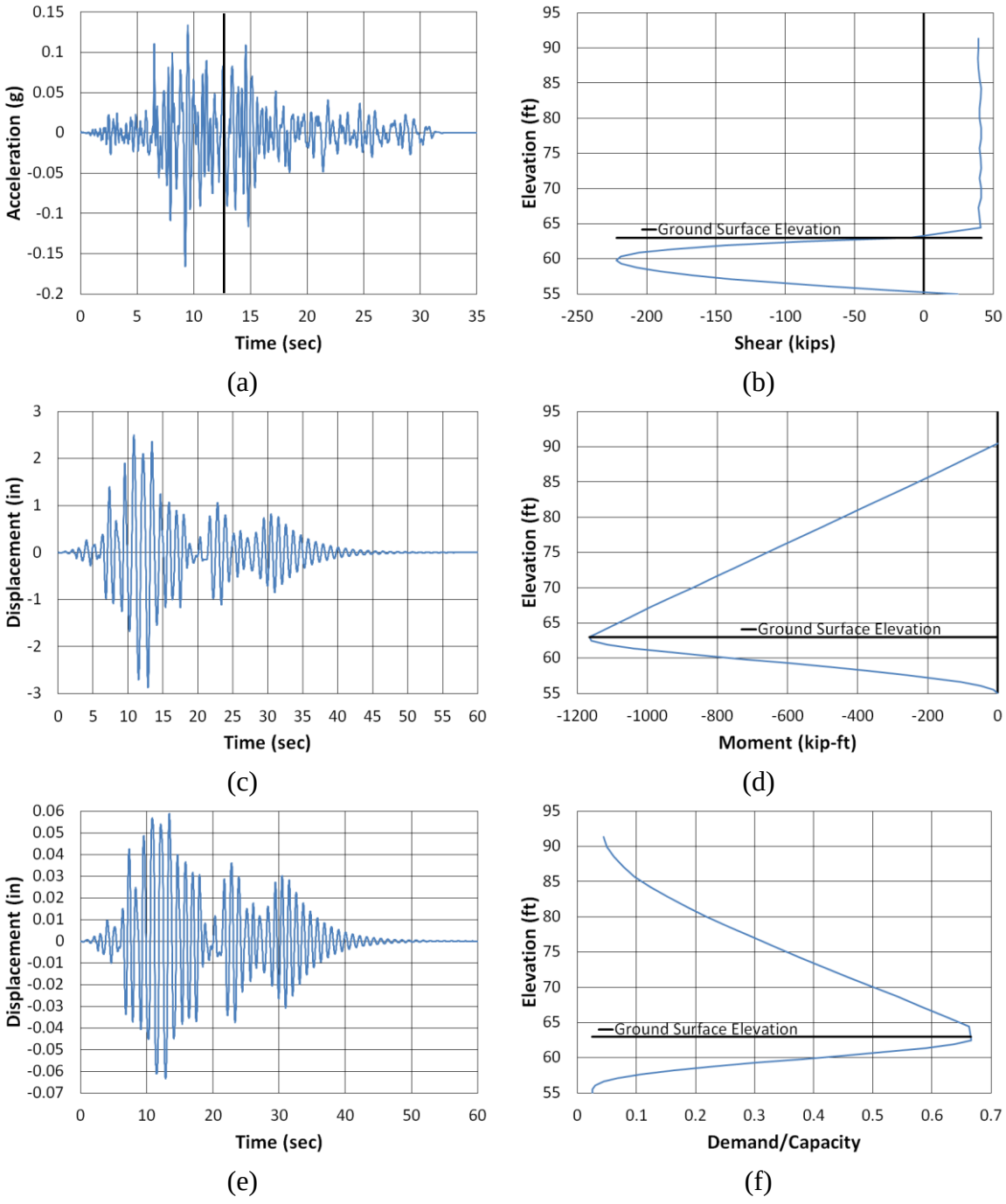

Figure B.35. Chambers County 100% Scour Longitudinal Coalinga North (a) time-history event, (b) shear distribution, (c) top of pier displacement, (d) moment distribution, (e) ground surface displacement, and (f) demand capacity ratio

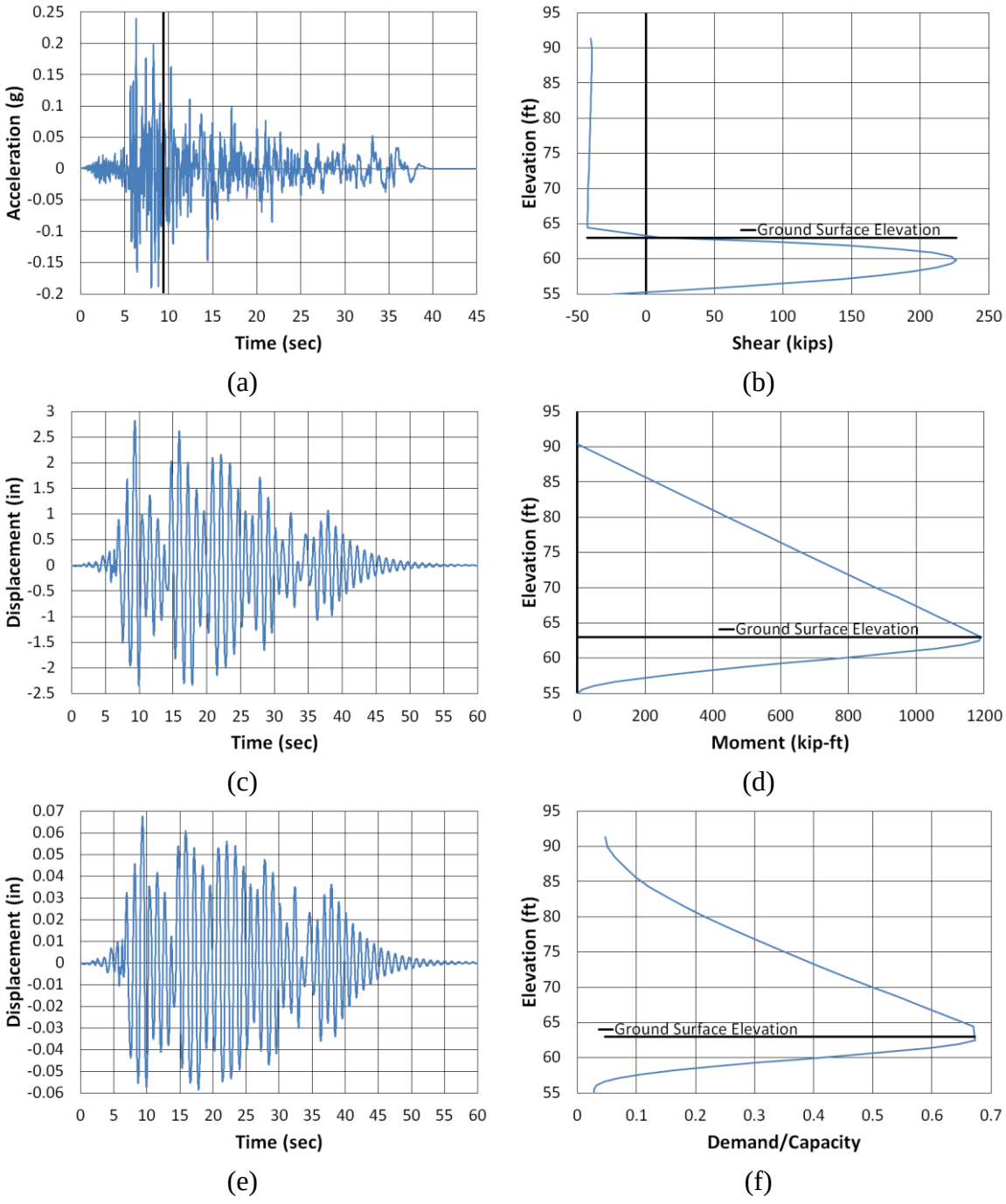

Figure B.36. Chambers County 100% Scour Longitudinal Imperial Valley NMCE (a) time-history event, (b) shear distribution, (c) top of pier displacement, (d) moment distribution, (e) ground surface displacement, and (f) demand capacity ratio

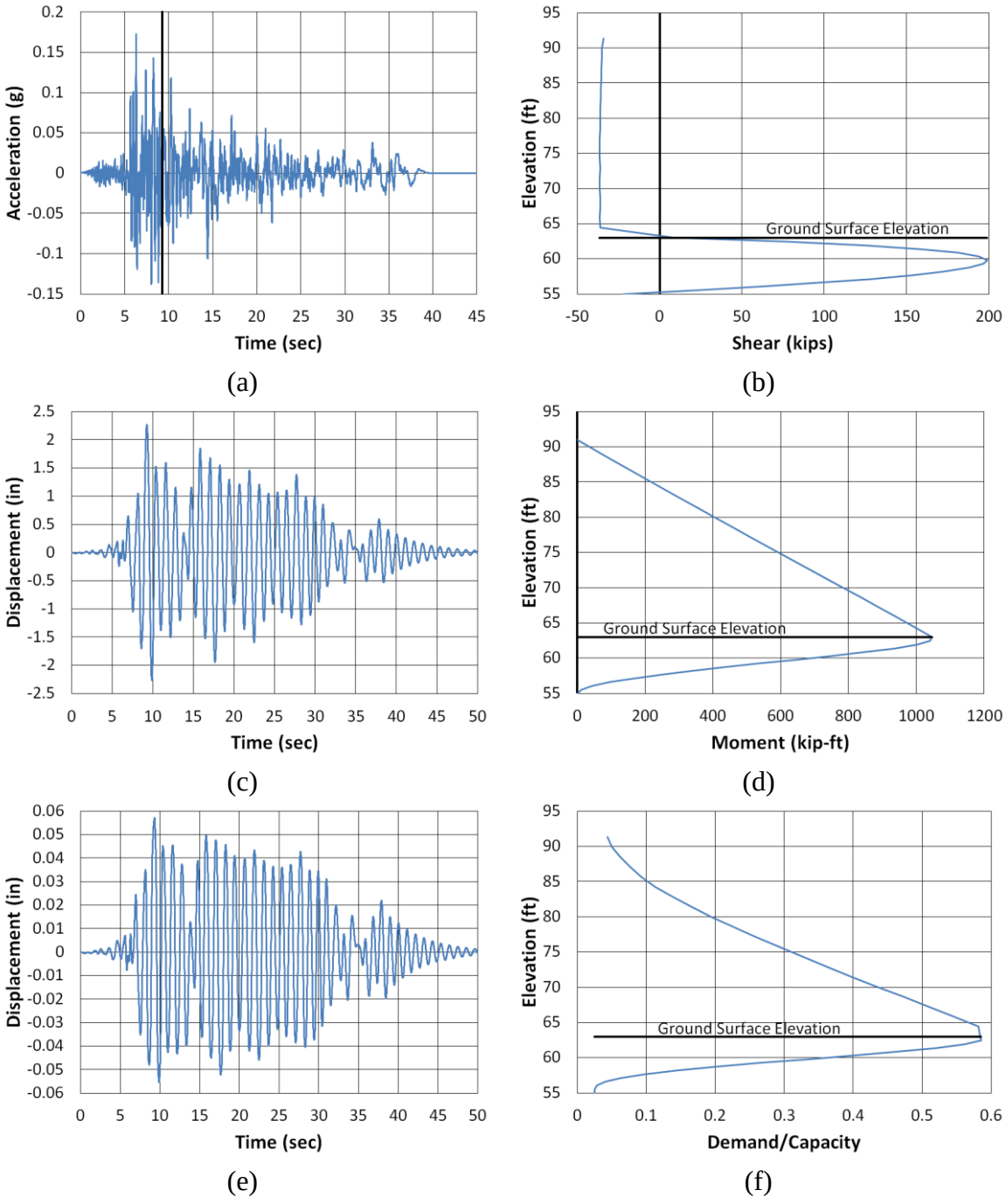

Figure B.37. Chambers County 100% Scour Longitudinal Imperial Valley North (a) time-history event, (b) shear distribution, (c) top of pier displacement, (d) moment distribution, (e) ground surface displacement, and (f) demand capacity ratio

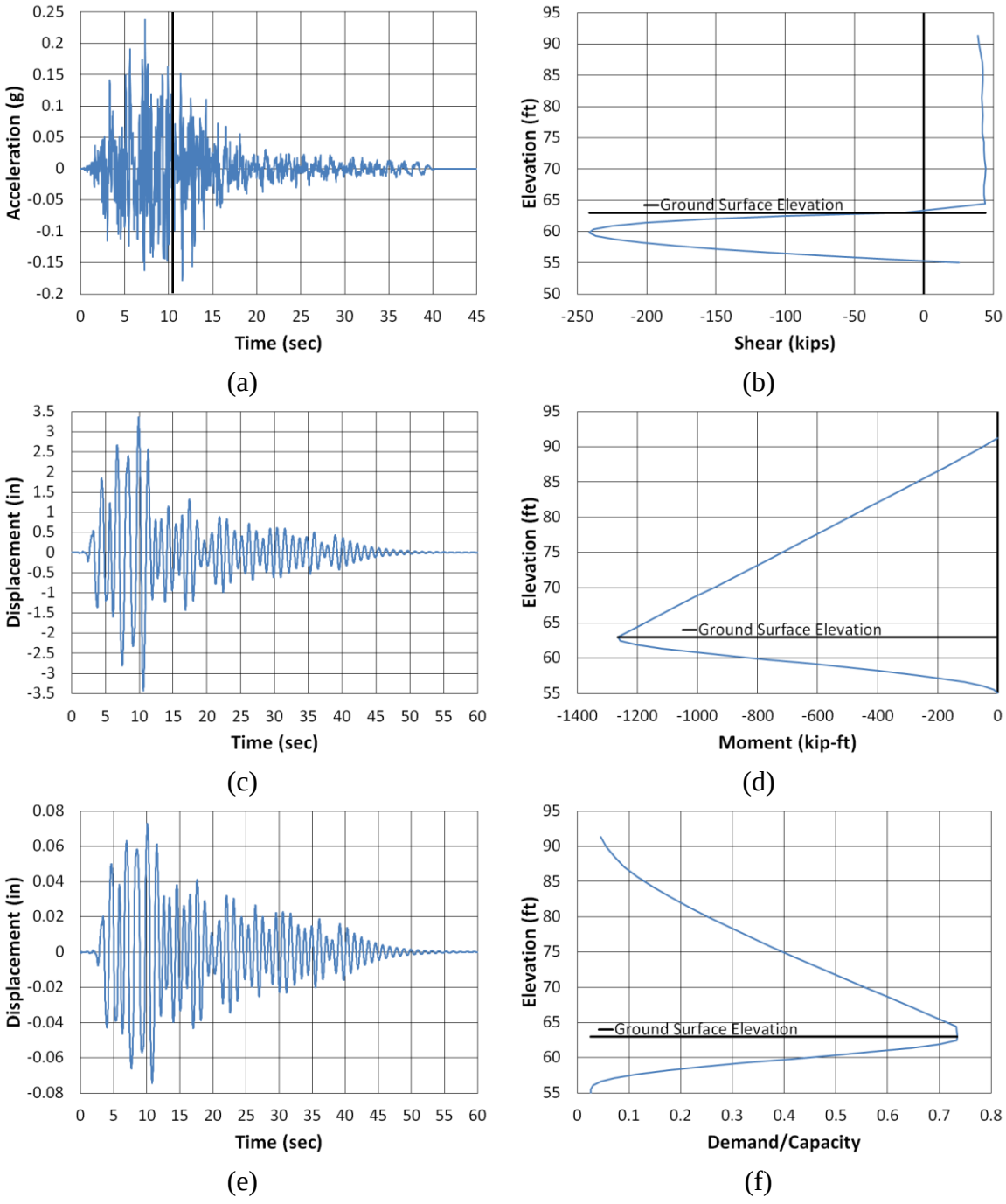

Figure B.38. Chambers County 100% Scour Longitudinal Kobe NMCE (a) time-history event, (b) shear distribution, (c) top of pier displacement, (d) moment distribution, (e) ground surface displacement, and (f) demand capacity ratio

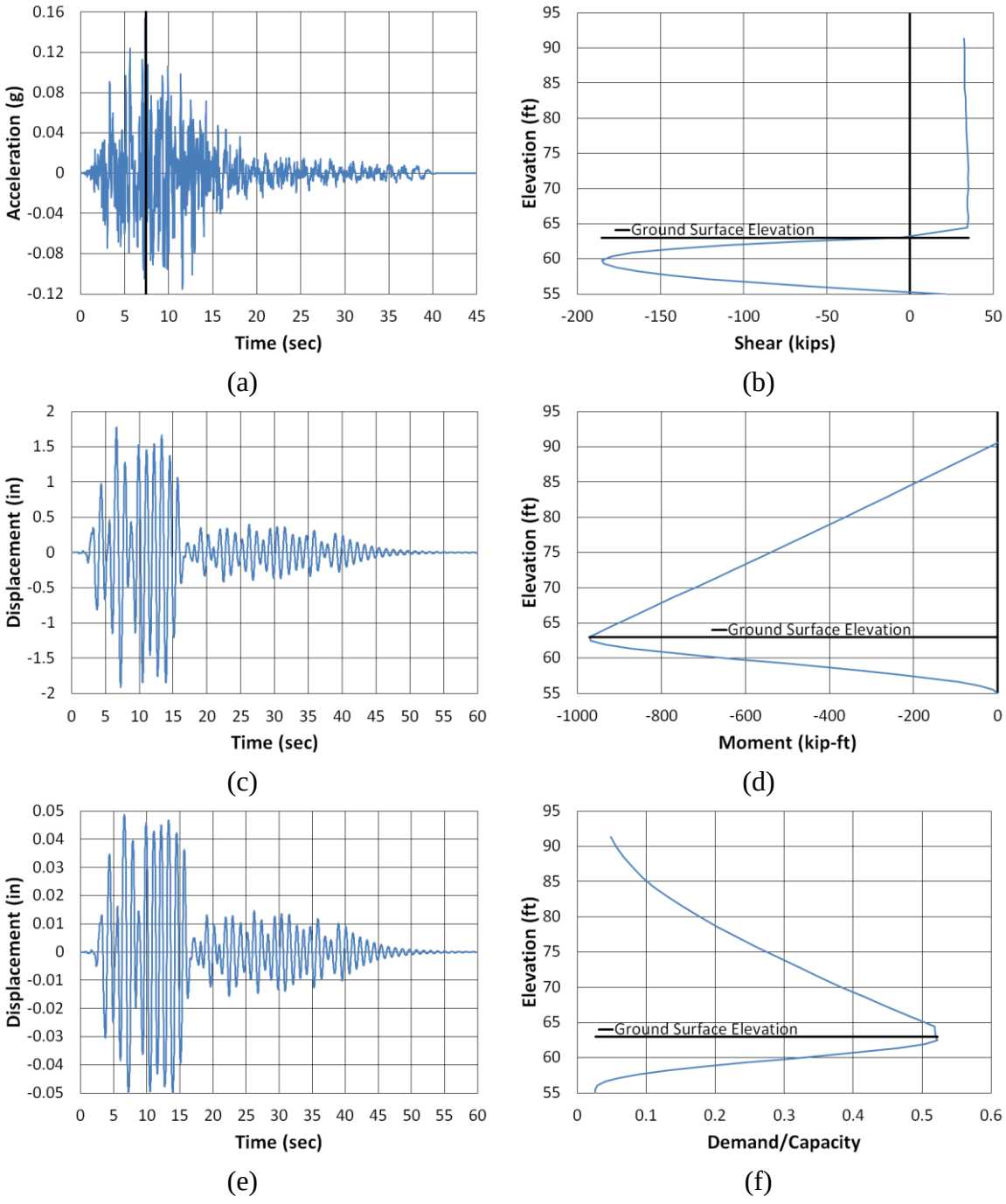

Figure B.39. Chambers County 100% Scour Longitudinal Kobe North (a) time-history event, (b) shear distribution, (c) top of pier displacement, (d) moment distribution, (e) ground surface displacement, and (f) demand capacity ratio

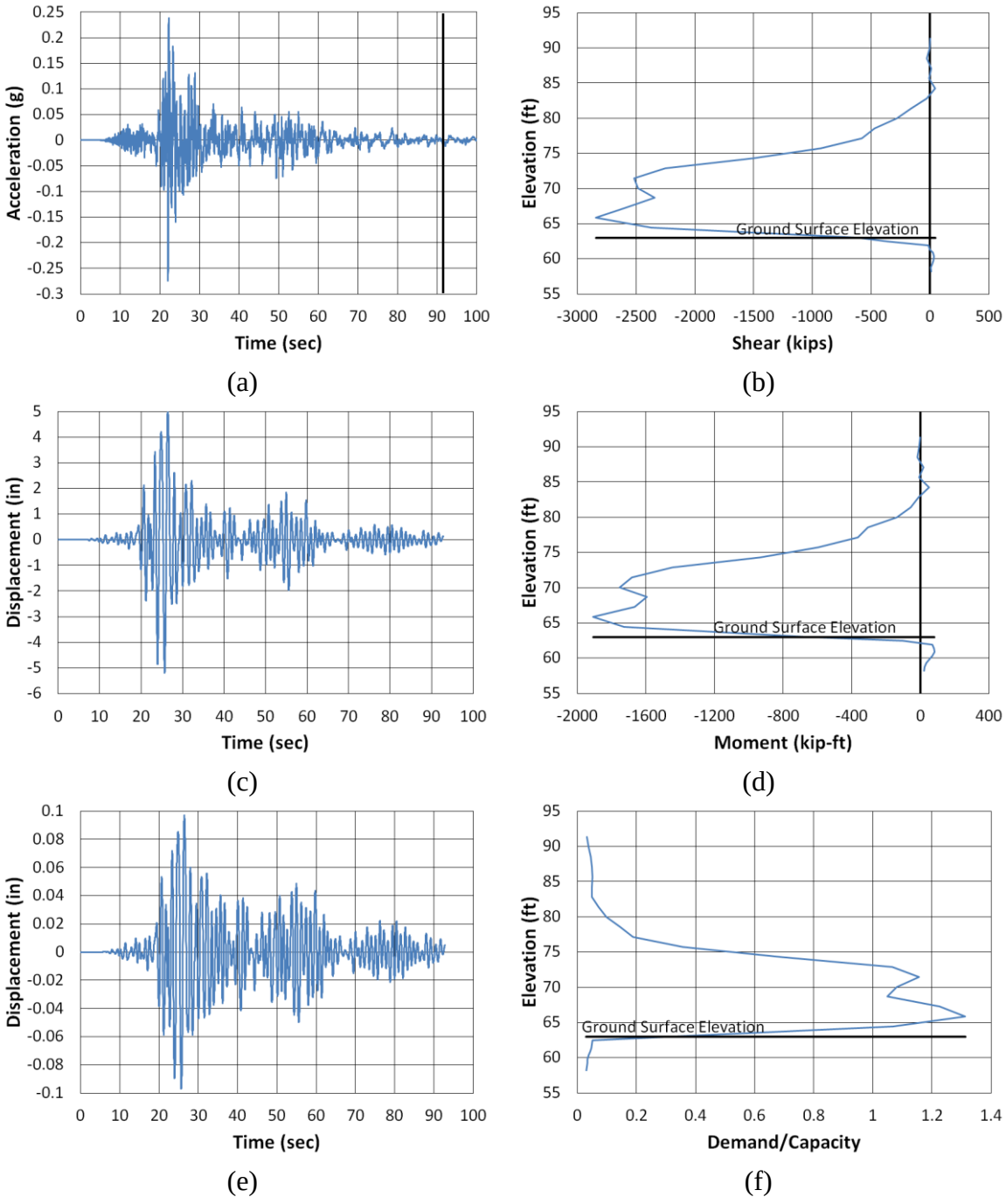

Figure B.40. Chambers County 100% Scour Longitudinal Kocaeli NMCE (a) time-history event, (b) shear distribution, (c) top of pier displacement, (d) moment distribution, (e) ground surface displacement, and (f) demand capacity ratio

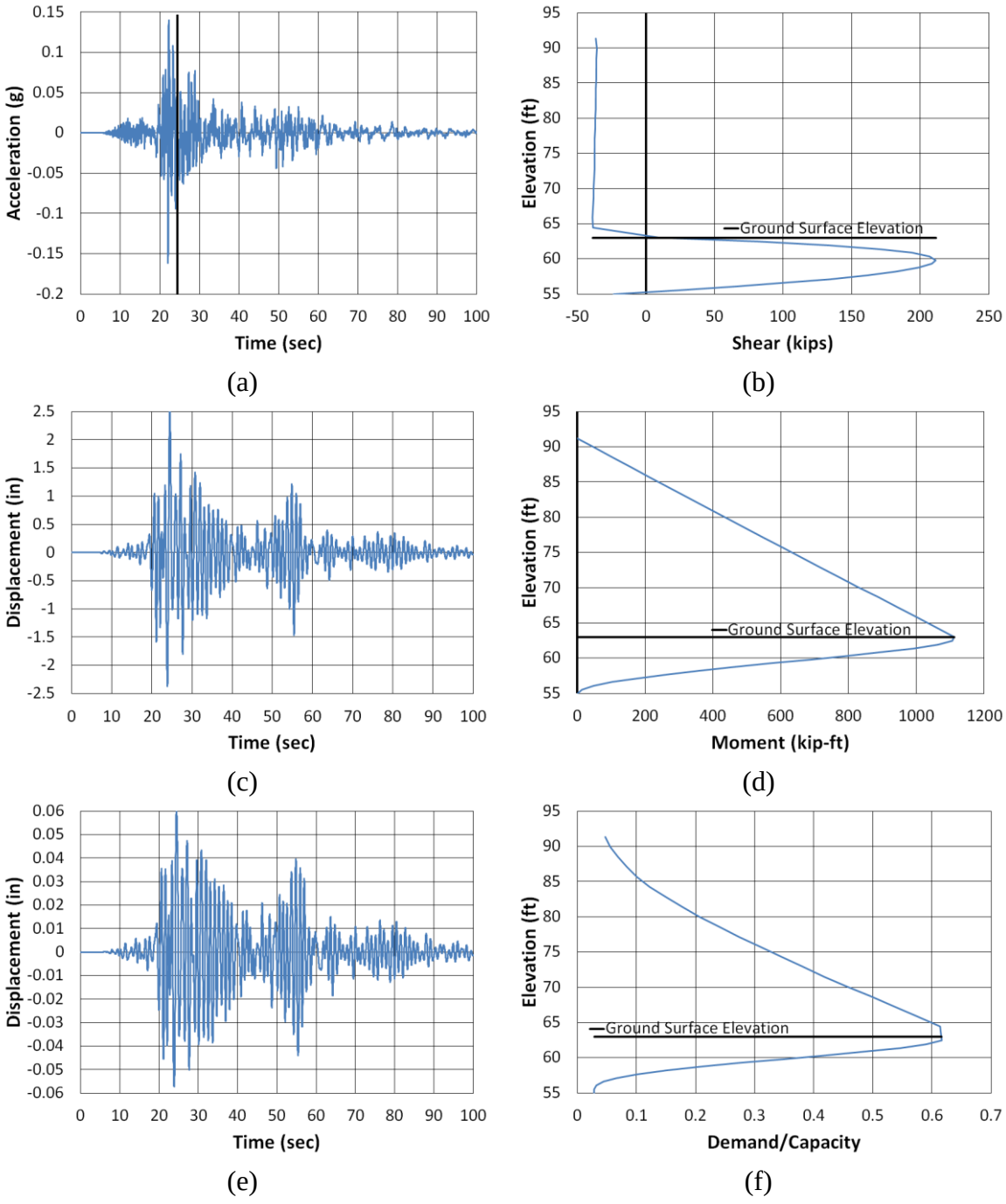

Figure B.41. Chambers County 100% Scour Longitudinal Kocaeli North (a) time-history event, (b) shear distribution, (c) top of pier displacement, (d) moment distribution, (e) ground surface displacement, and (f) demand capacity ratio

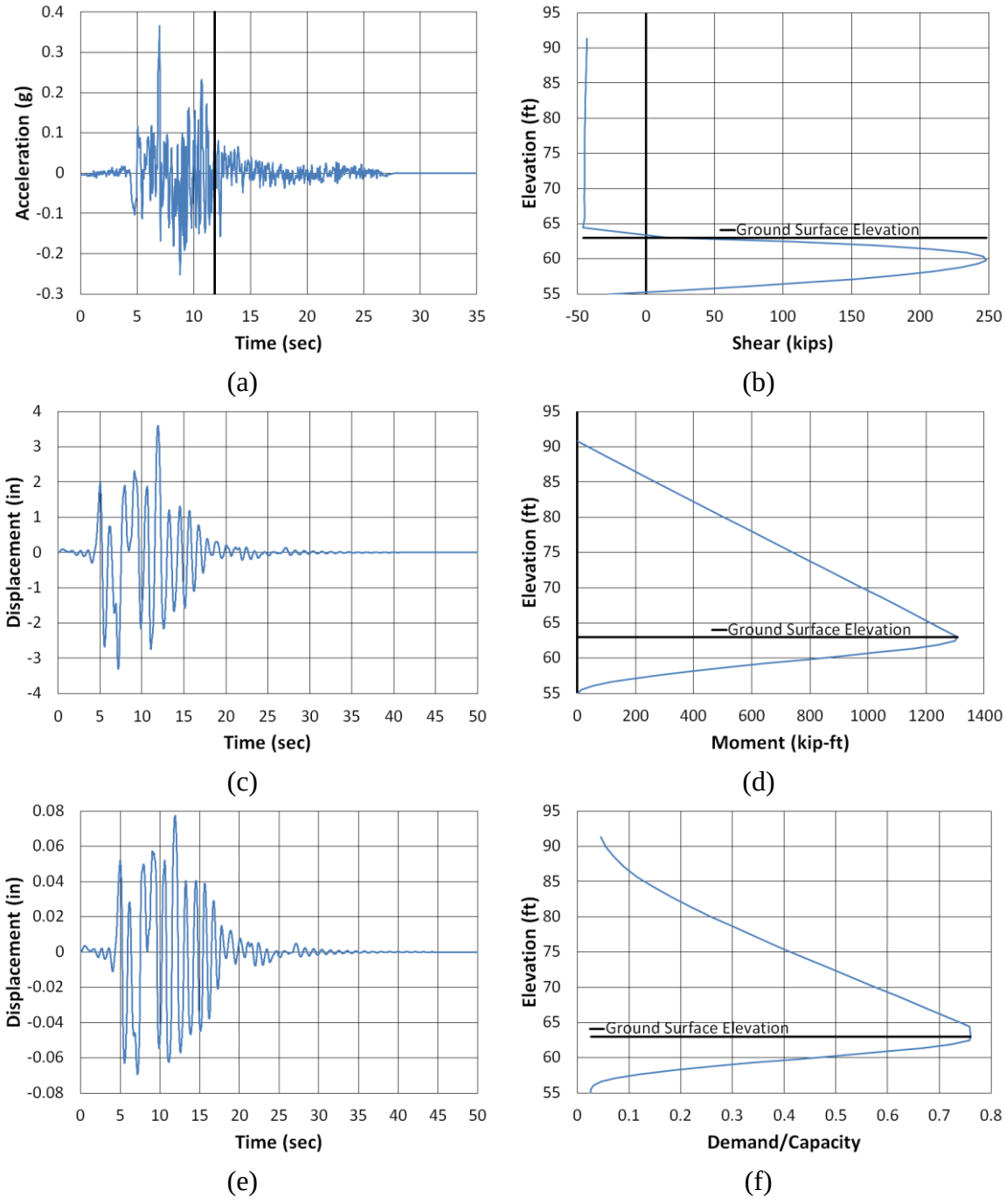

Figure B.42. Chambers County 100% Scour Longitudinal Kocaeli2 NMCE (a) time-history event, (b) shear distribution, (c) top of pier displacement, (d) moment distribution, (e) ground surface displacement, and (f) demand capacity ratio

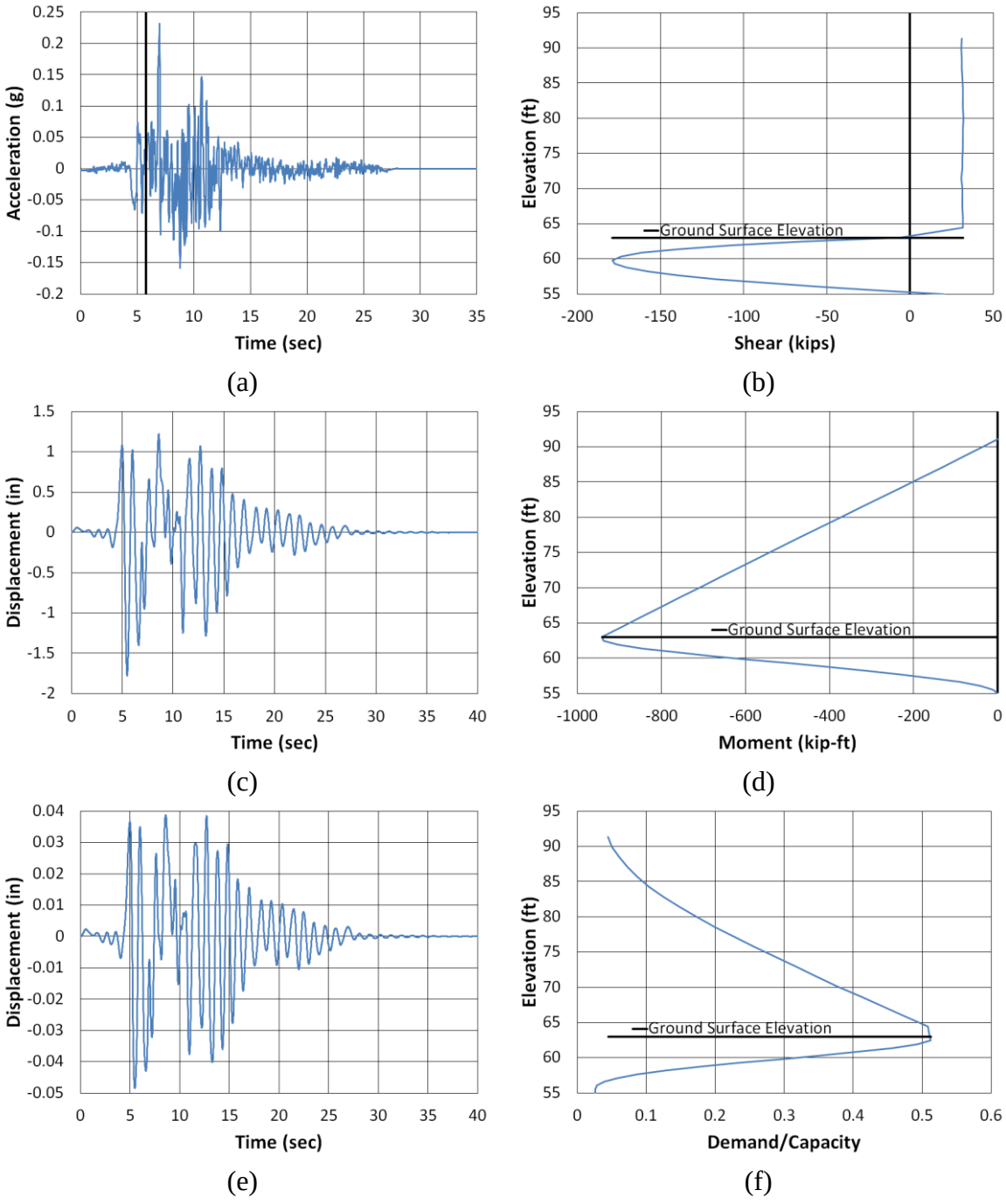

Figure B.43. Chambers County 100% Scour Longitudinal Kocaeli2 North (a) time-history event, (b) shear distribution, (c) top of pier displacement, (d) moment distribution, (e) ground surface displacement, and (f) demand capacity ratio

.

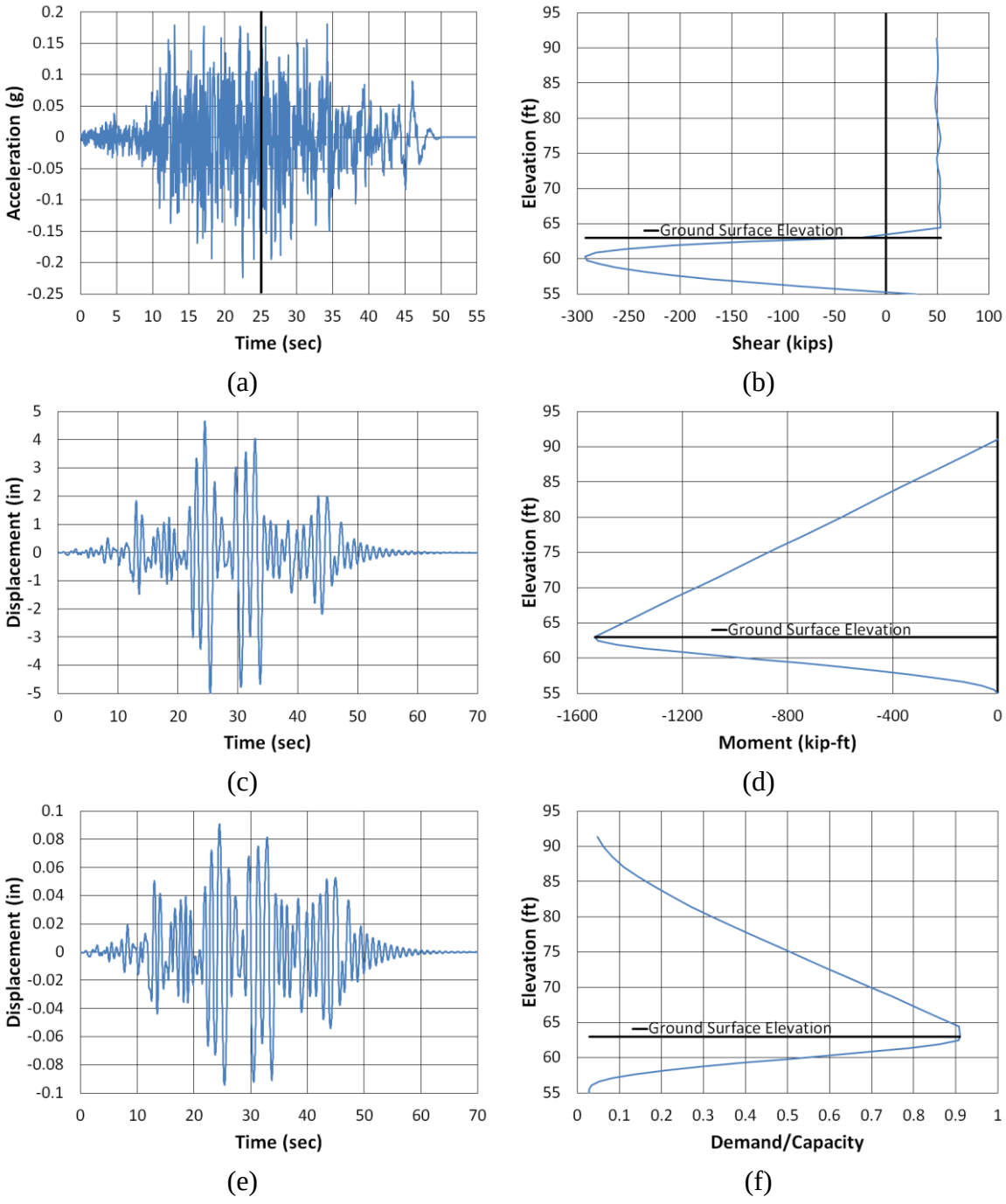

Figure B.44. Chambers County 100% Scour Longitudinal Landers NMCE (a) time-history event, (b) shear distribution, (c) top of pier displacement, (d) moment distribution, (e) ground surface displacement, and (f) demand capacity ratio

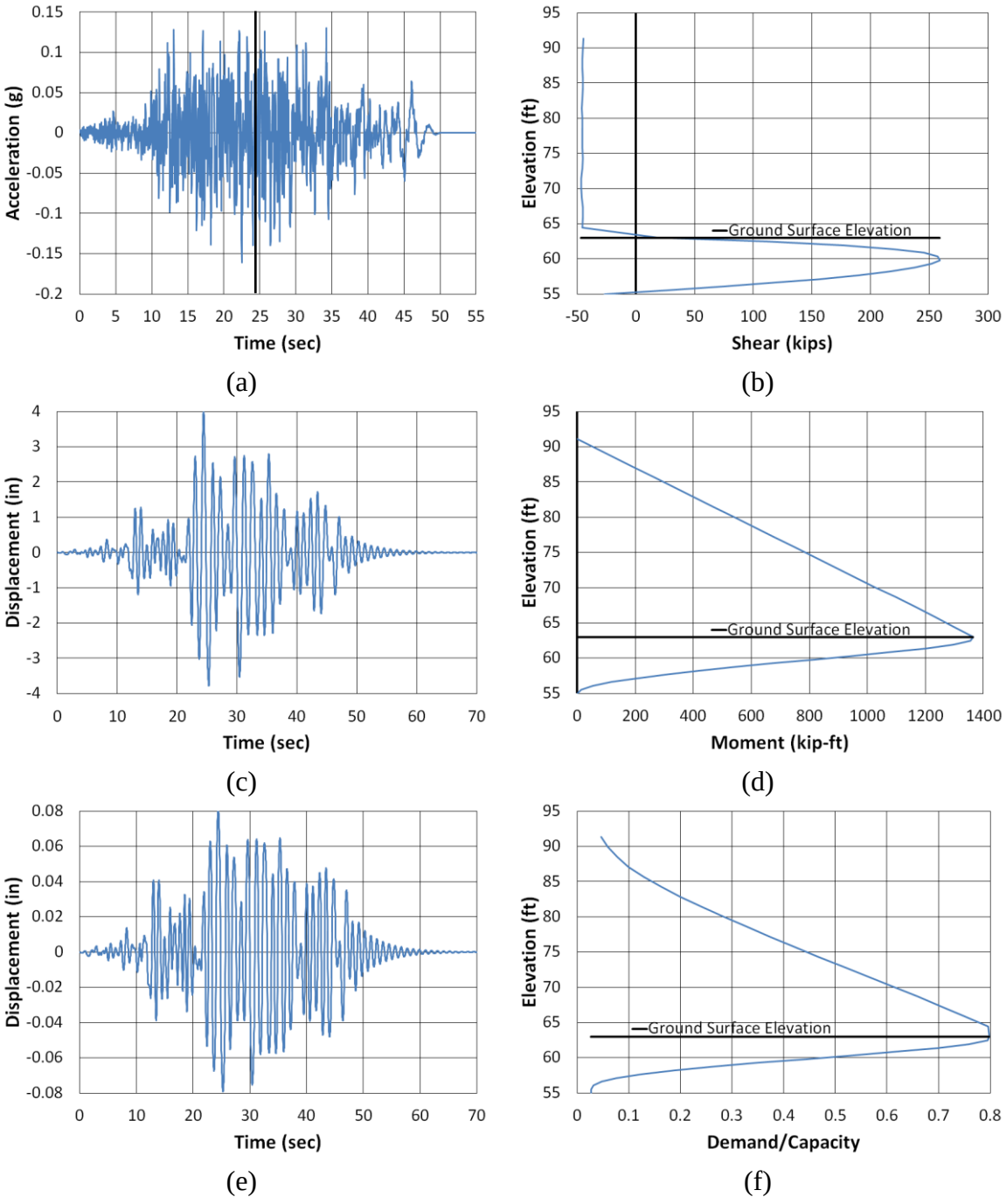

Figure B.45. Chambers County 100% Scour Longitudinal Landers North (a) time-history event, (b) shear distribution, (c) top of pier displacement, (d) moment distribution, (e) ground surface displacement, and (f) demand capacity ratio

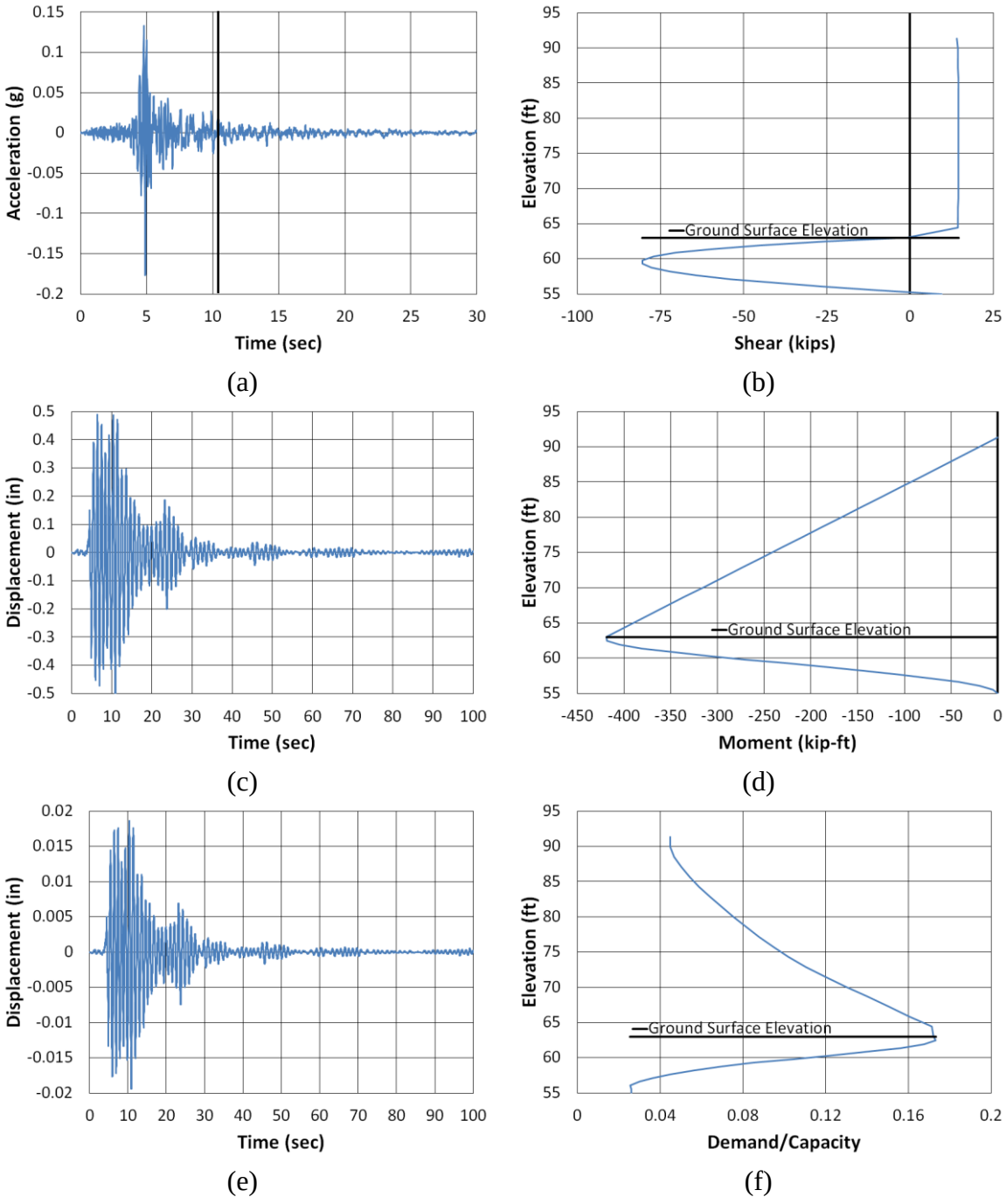

Figure B.46. Chambers County 100% Scour Longitudinal LSM North (a) time-history event, (b) shear distribution, (c) top of pier displacement, (d) moment distribution, (e) ground surface displacement, and (f) demand capacity ratio

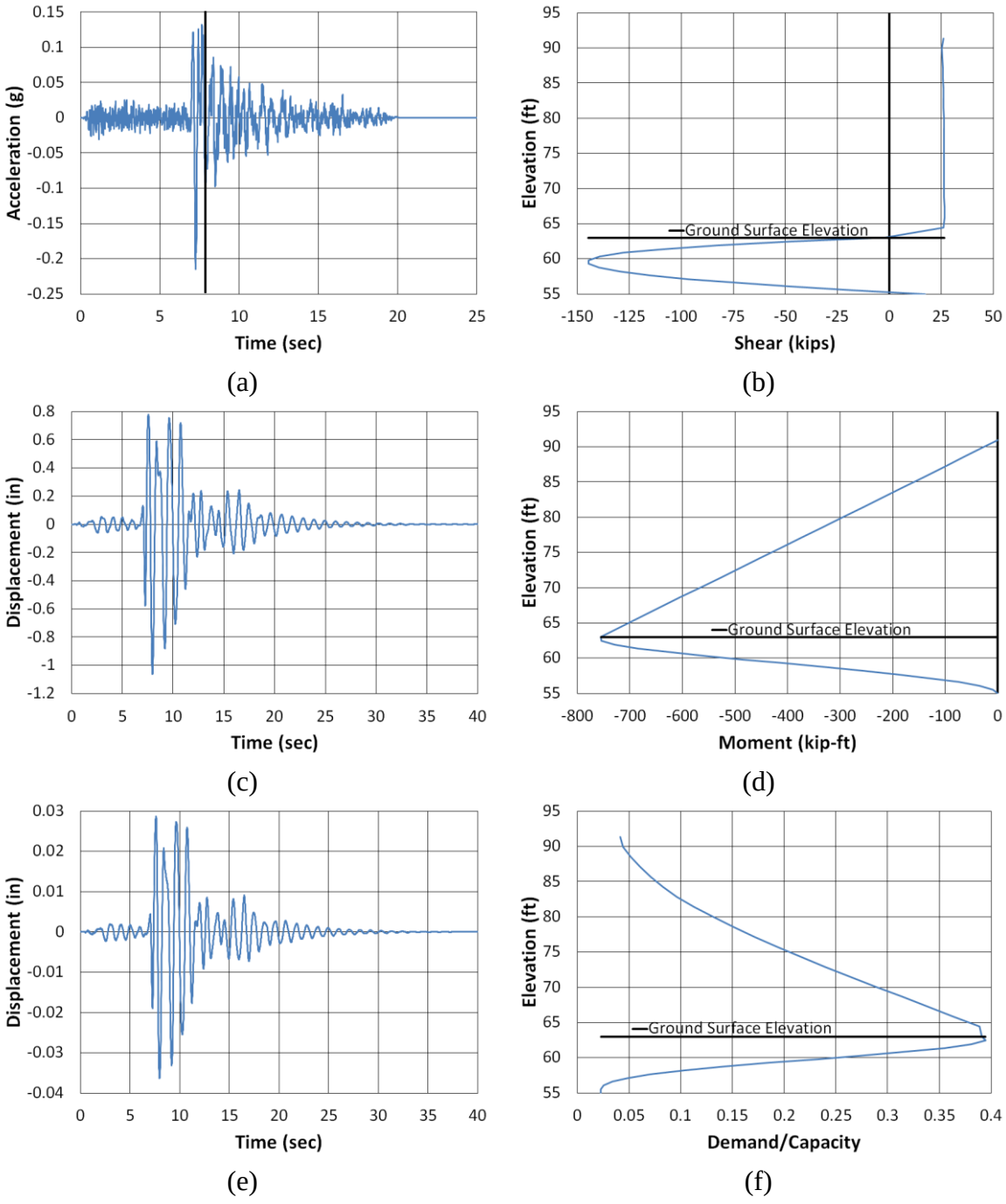

Figure B.47. Chambers County 100% Scour Longitudinal NPS North (a) time-history event, (b) shear distribution, (c) top of pier displacement, (d) moment distribution, (e) ground surface displacement, and (f) demand capacity ratio

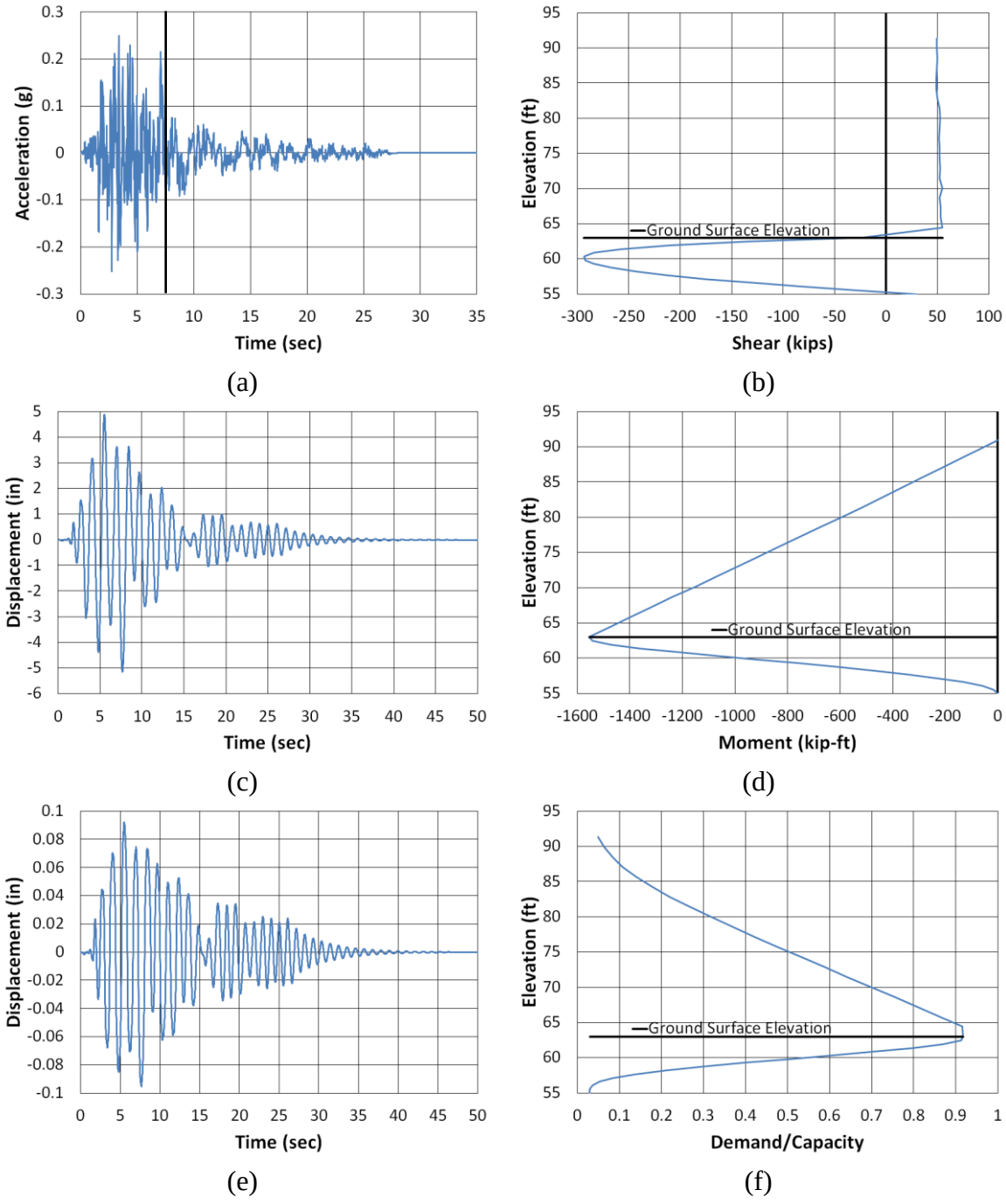

Figure B.48. Chambers County 100% Scour Longitudinal San Fernando NMCE (a) time-history event, (b) shear distribution, (c) top of pier displacement, (d) moment distribution, (e) ground surface displacement, and (f) demand capacity ratio

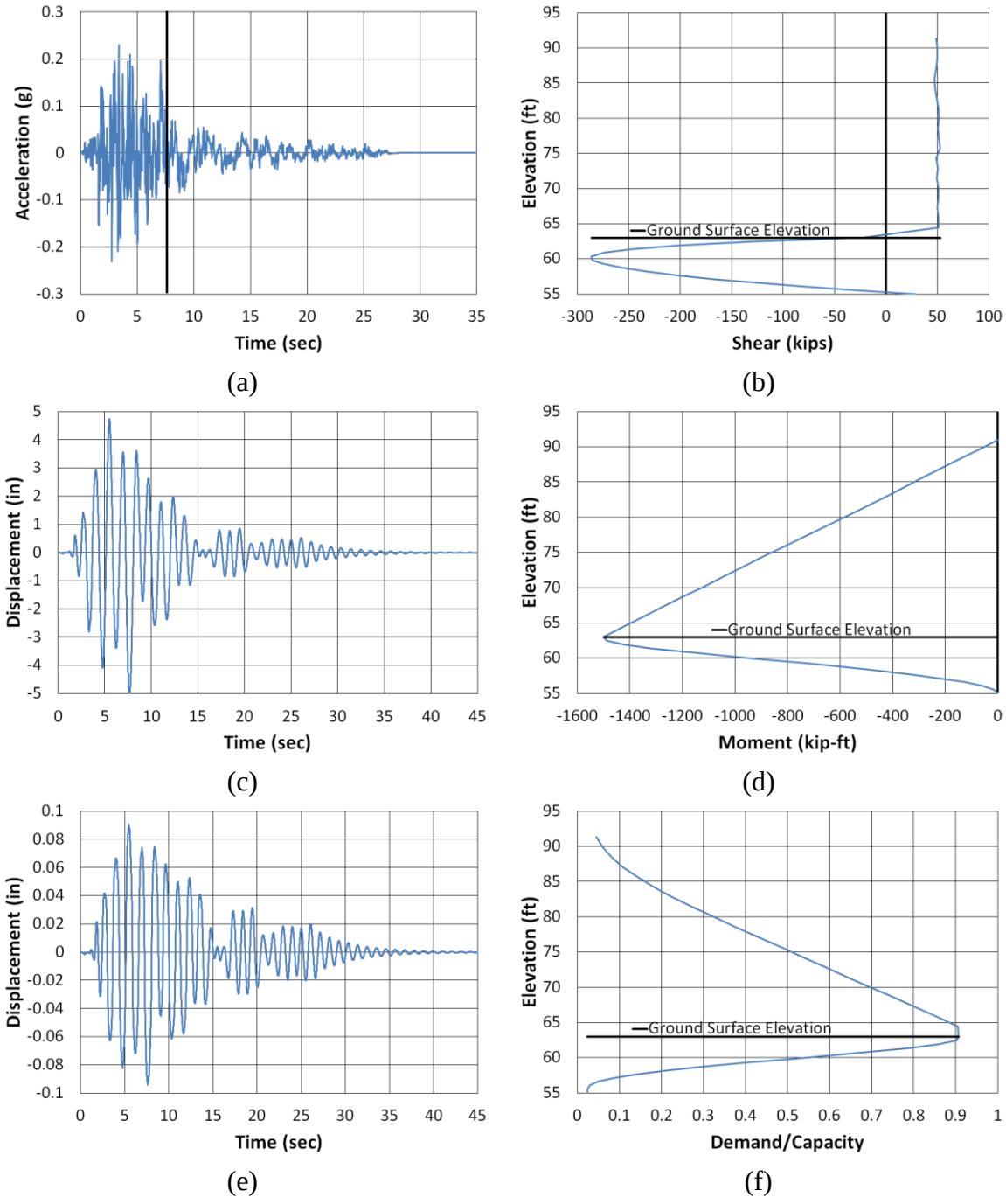

Figure B.49. Chambers County 100% Scour Longitudinal San Fernando North (a) time-history event, (b) shear distribution, (c) top of pier displacement, (d) moment distribution, (e) ground surface displacement, and (f) demand capacity ratio

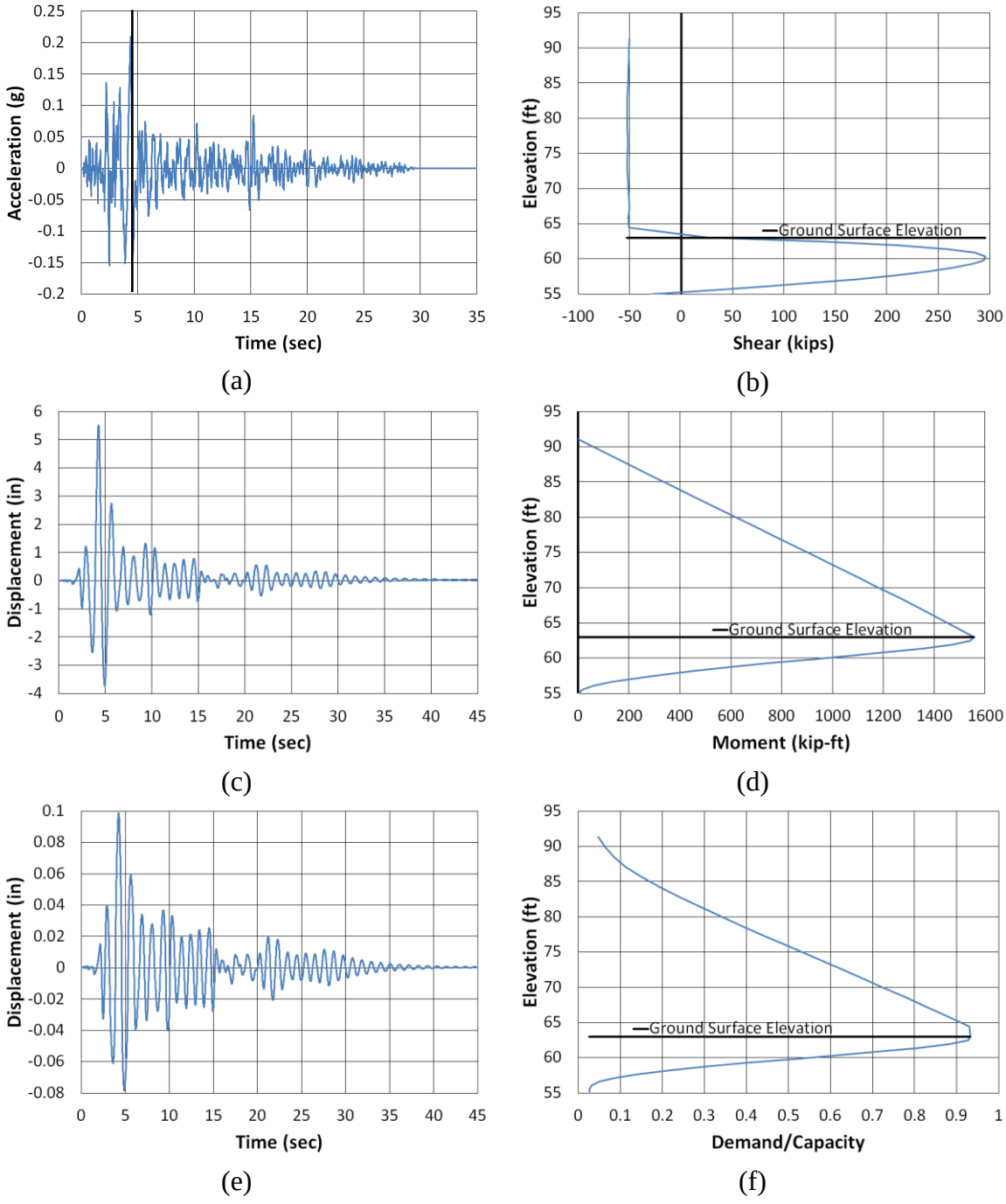

Figure B.50. Chambers County 100% Scour Longitudinal San Fernando2 NMCE (a) time-history event, (b) shear distribution, (c) top of pier displacement, (d) moment distribution, (e) ground surface displacement, and (f) demand capacity ratio

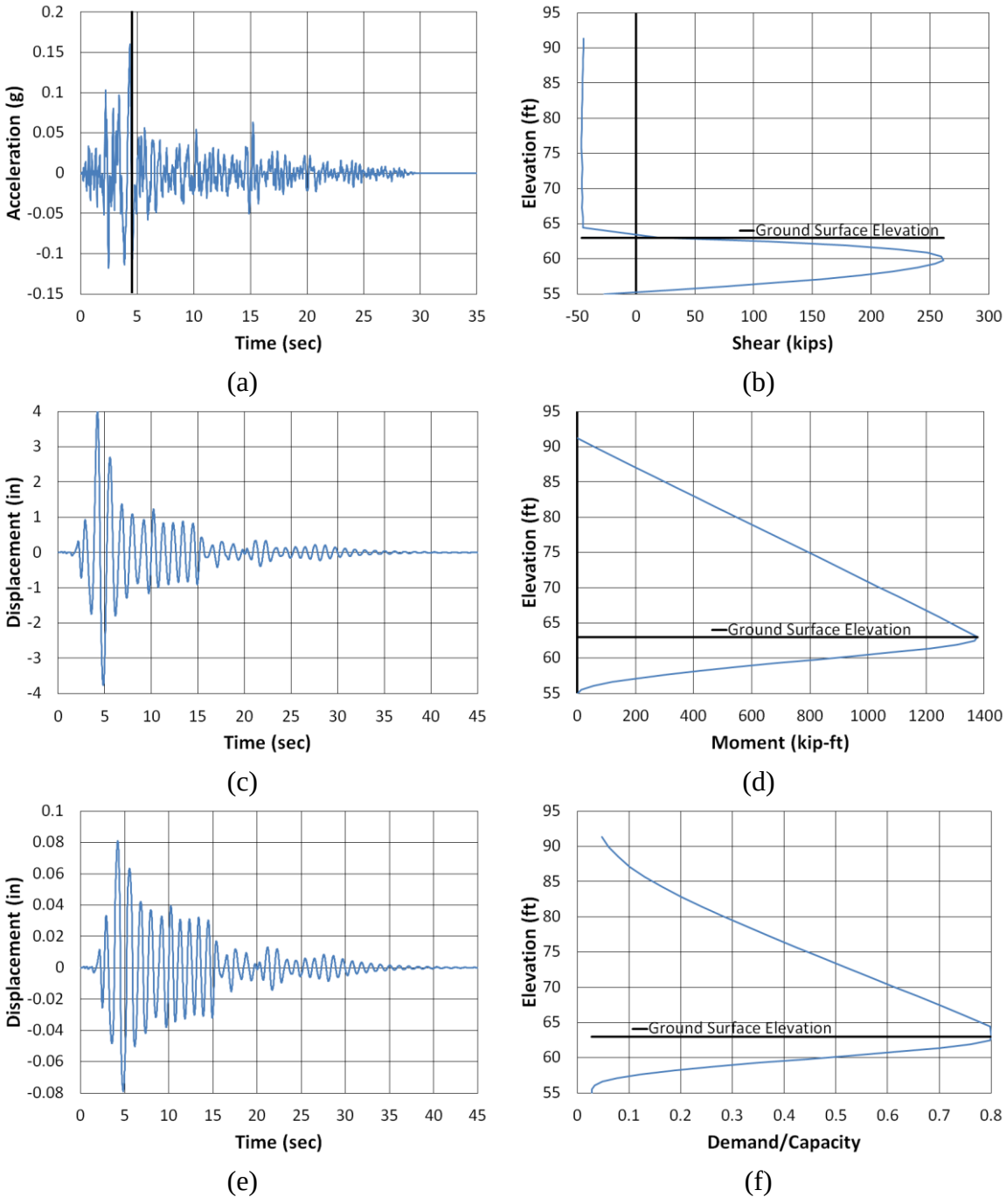

Figure B.51 Chambers County 100% Scour Longitudinal San Fernando2 North (a) time-history event, (b) shear distribution, (c) top of pier displacement, (d) moment distribution, (e) ground surface displacement, and (f) demand capacity ratio

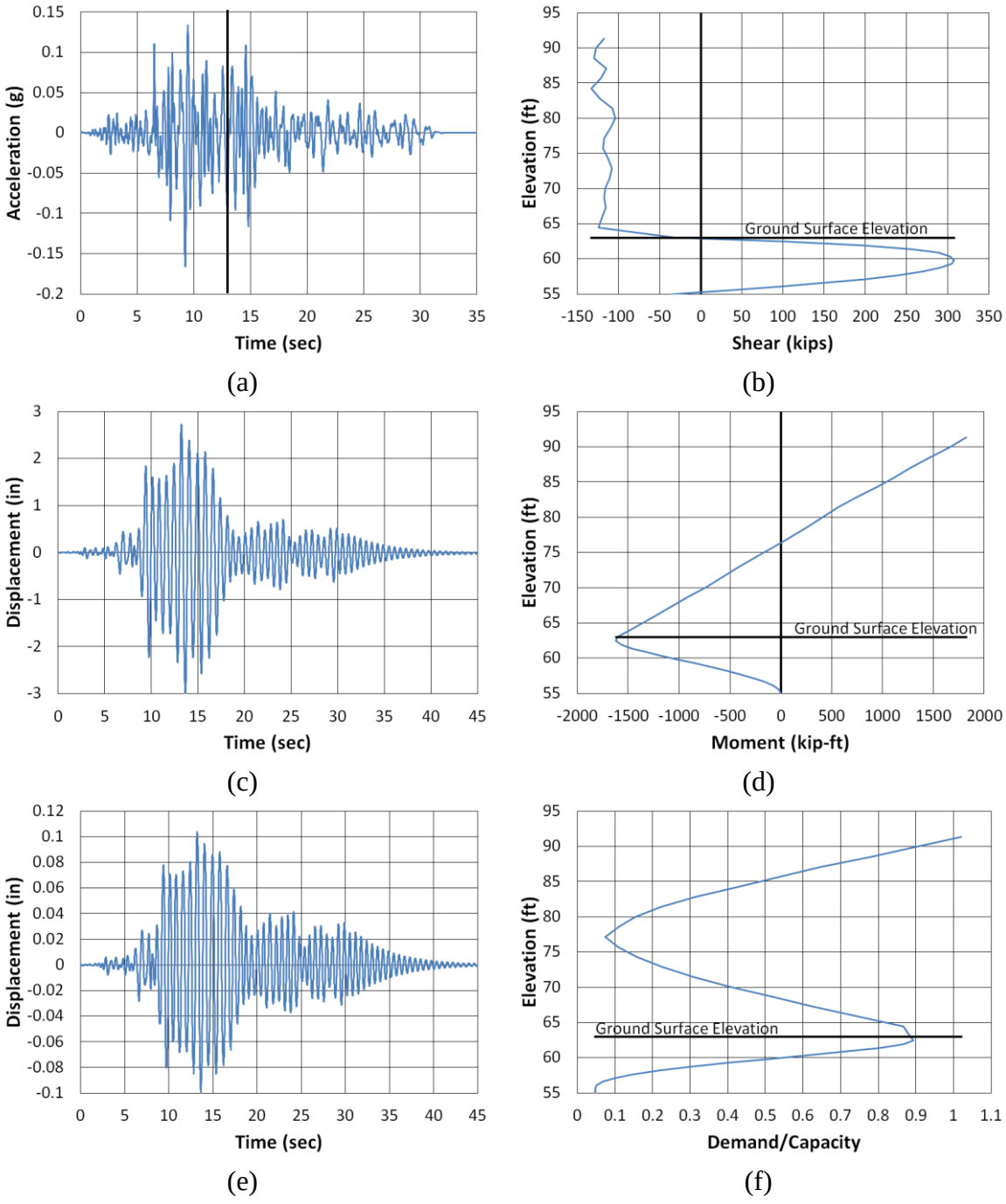

Figure B.52. Chambers County 100% Scour Transverse Coalinga North (a) time-history event, (b) shear distribution, (c) top of pier displacement, (d) moment distribution, (e) ground surface displacement, and (f) demand capacity ratio

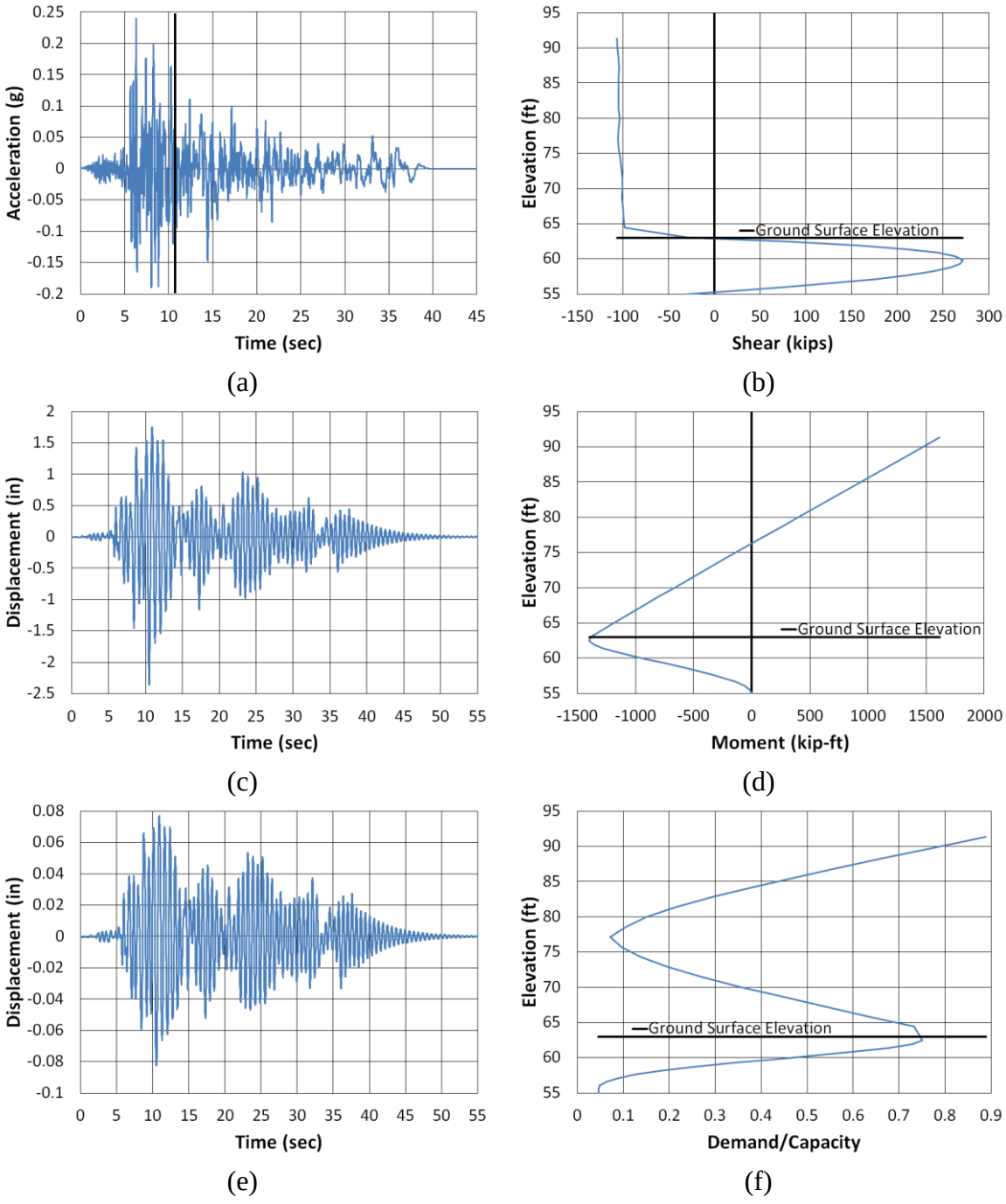

Figure B.53. Chambers County 100% Scour Transverse Imperial Valley NMCE (a) time-history event, (b) shear distribution, (c) top of pier displacement, (d) moment distribution, (e) ground surface displacement, and (f) demand capacity ratio

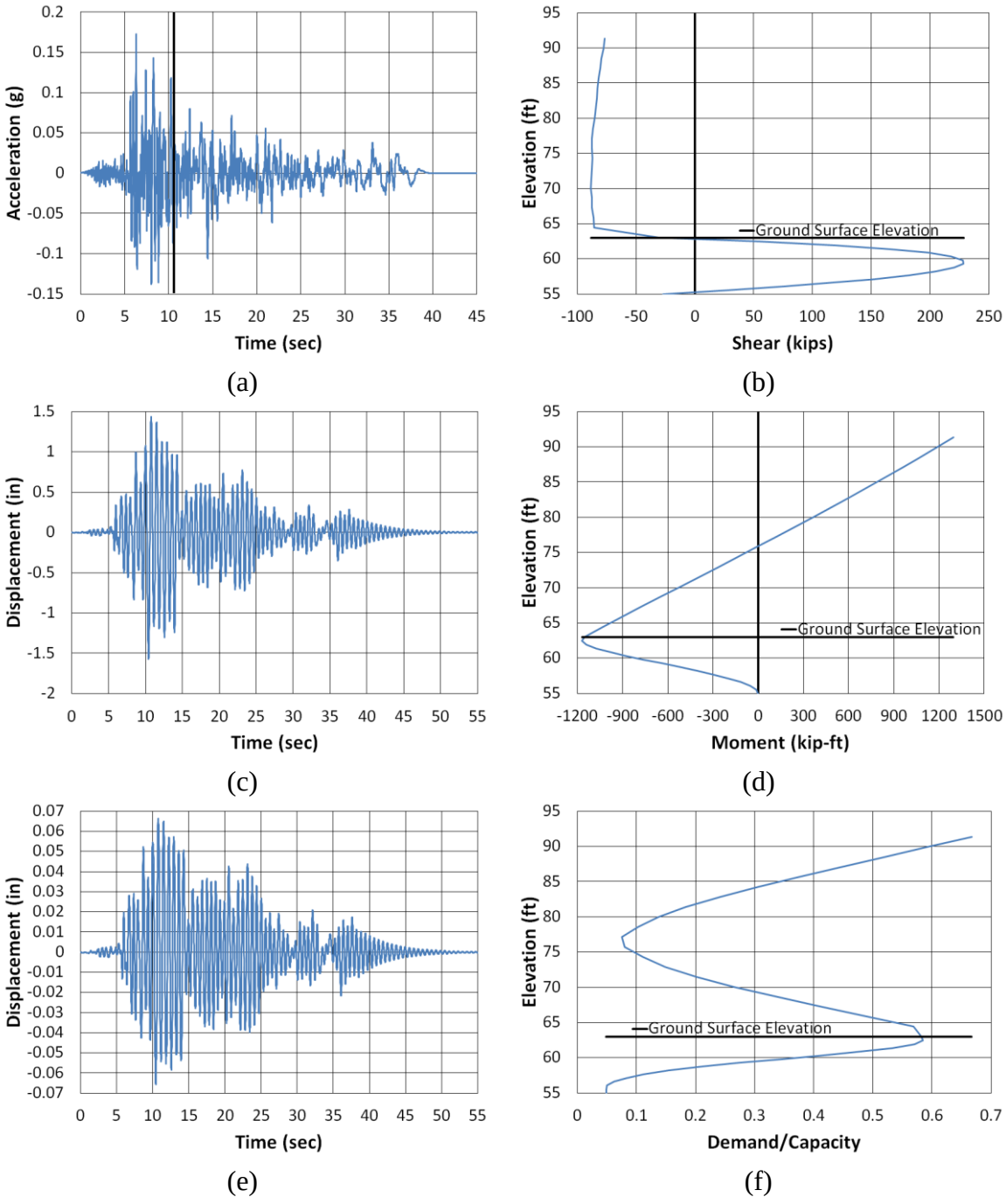

Figure B.54. Chambers County 100% Scour Transverse Imperial Valley North (a) time-history event, (b) shear distribution, (c) top of pier displacement, (d) moment distribution, (e) ground surface displacement, and (f) demand capacity ratio

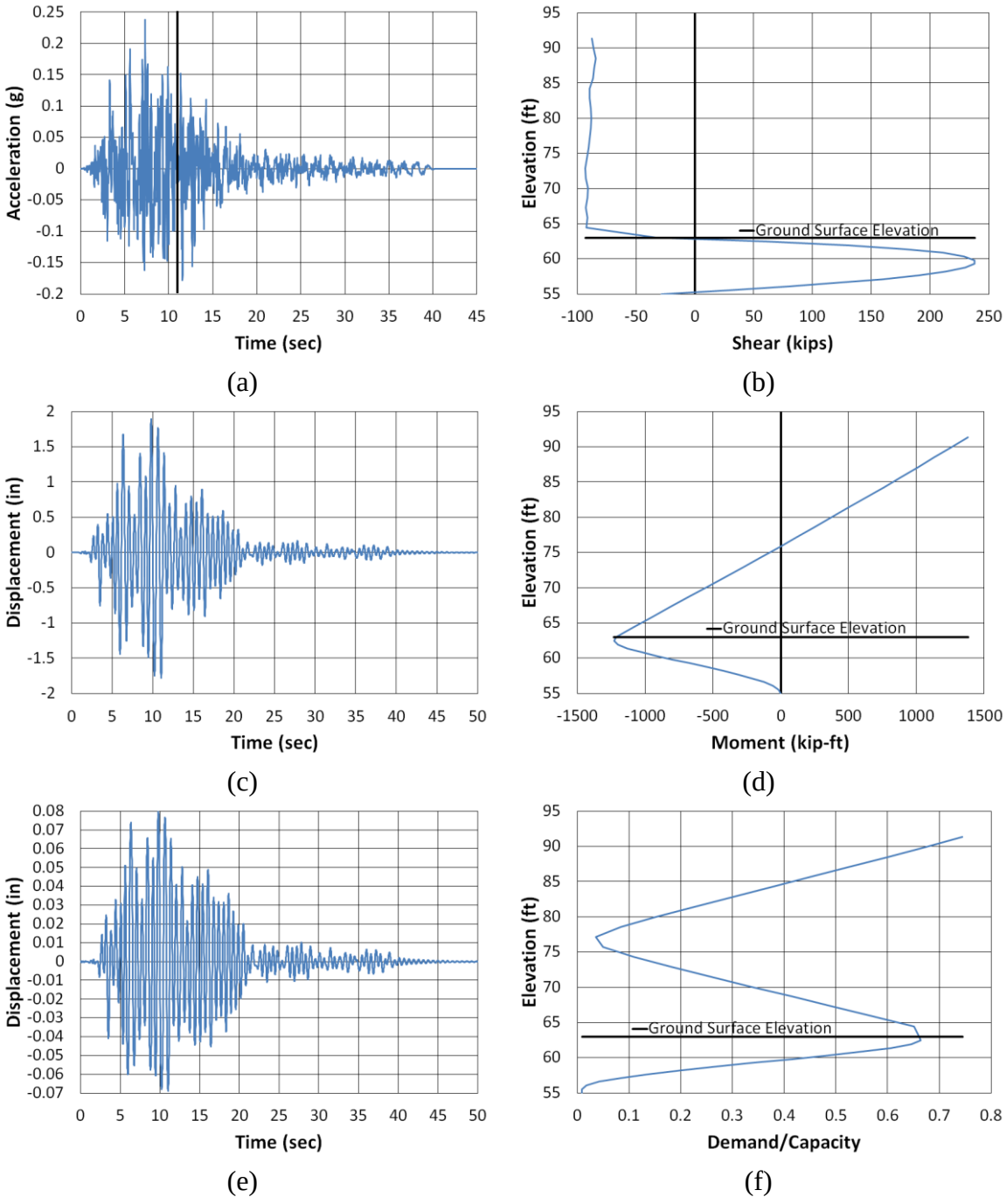

Figure B.55. Chambers County 100% Scour Transverse Kobe NMCE (a) time-history event, (b) shear distribution, (c) top of pier displacement, (d) moment distribution, (e) ground surface displacement, and (f) demand capacity ratio

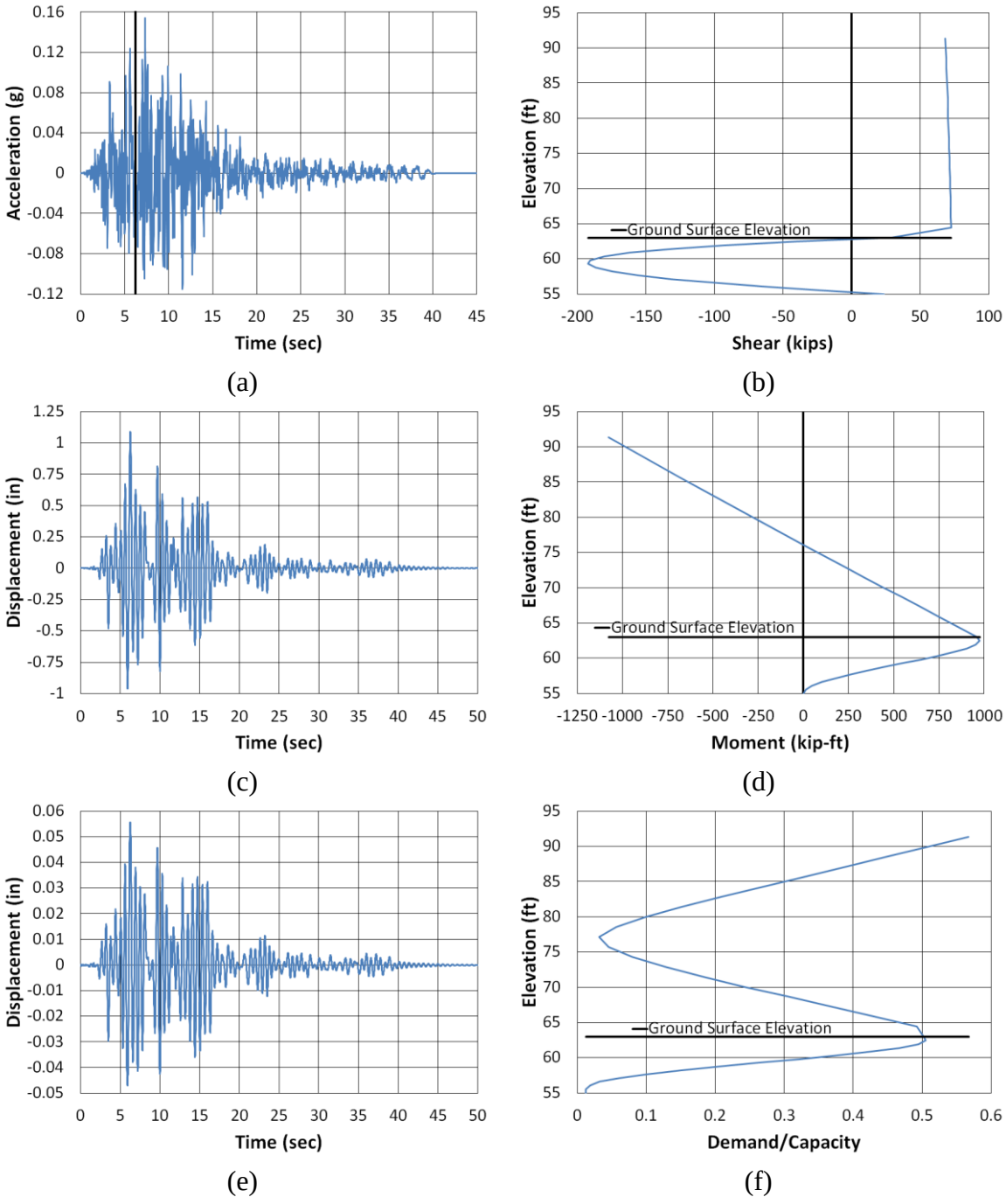

Figure B.56. Chambers County 100% Scour Transverse Kobe North (a) time-history event, (b) shear distribution, (c) top of pier displacement, (d) moment distribution, (e) ground surface displacement, and (f) demand capacity ratio

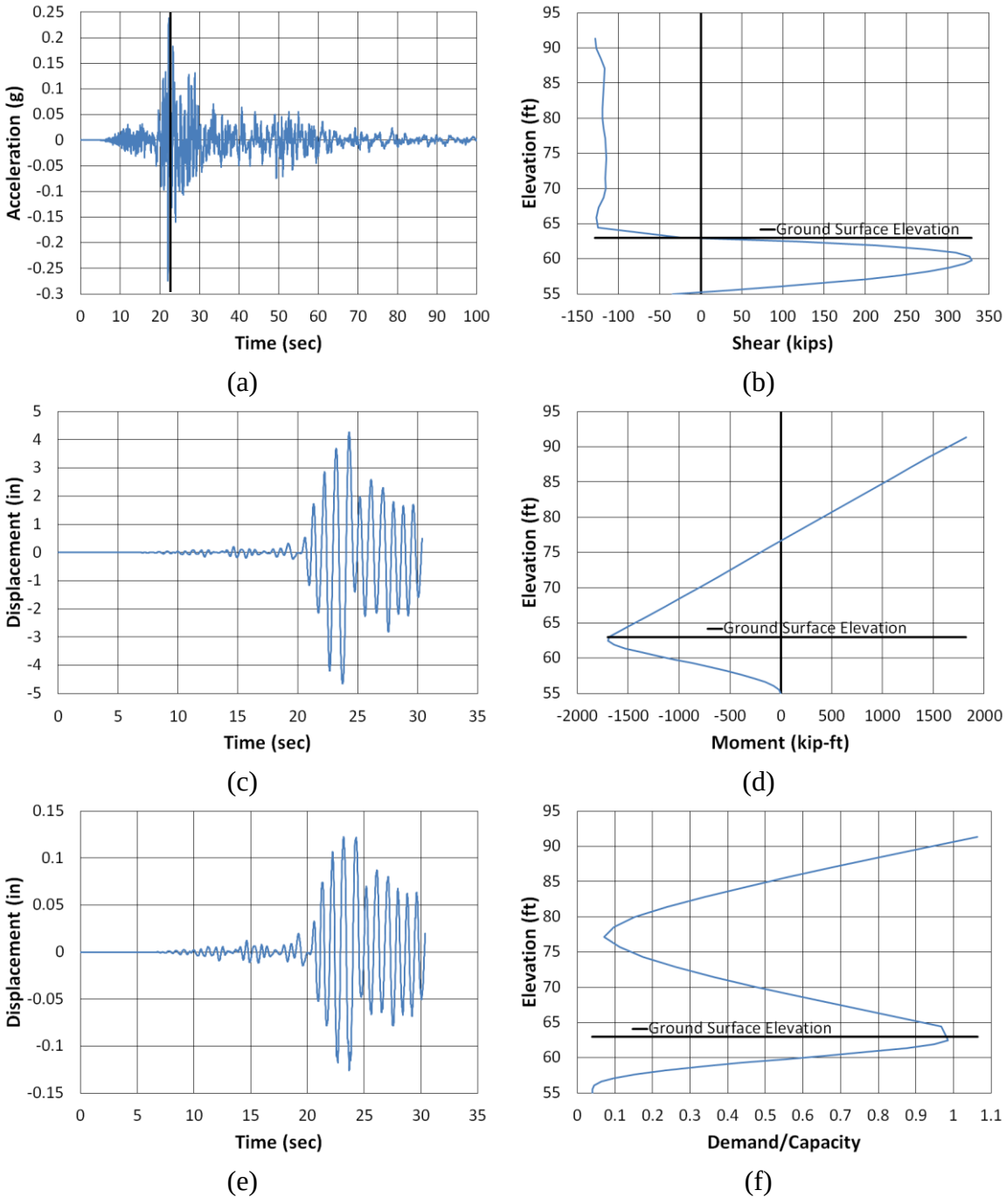

Figure B.57. Chambers County 100% Scour Transverse Kocaeli NMCE (a) time-history event, (b) shear distribution, (c) top of pier displacement, (d) moment distribution, (e) ground surface displacement, and (f) demand capacity ratio

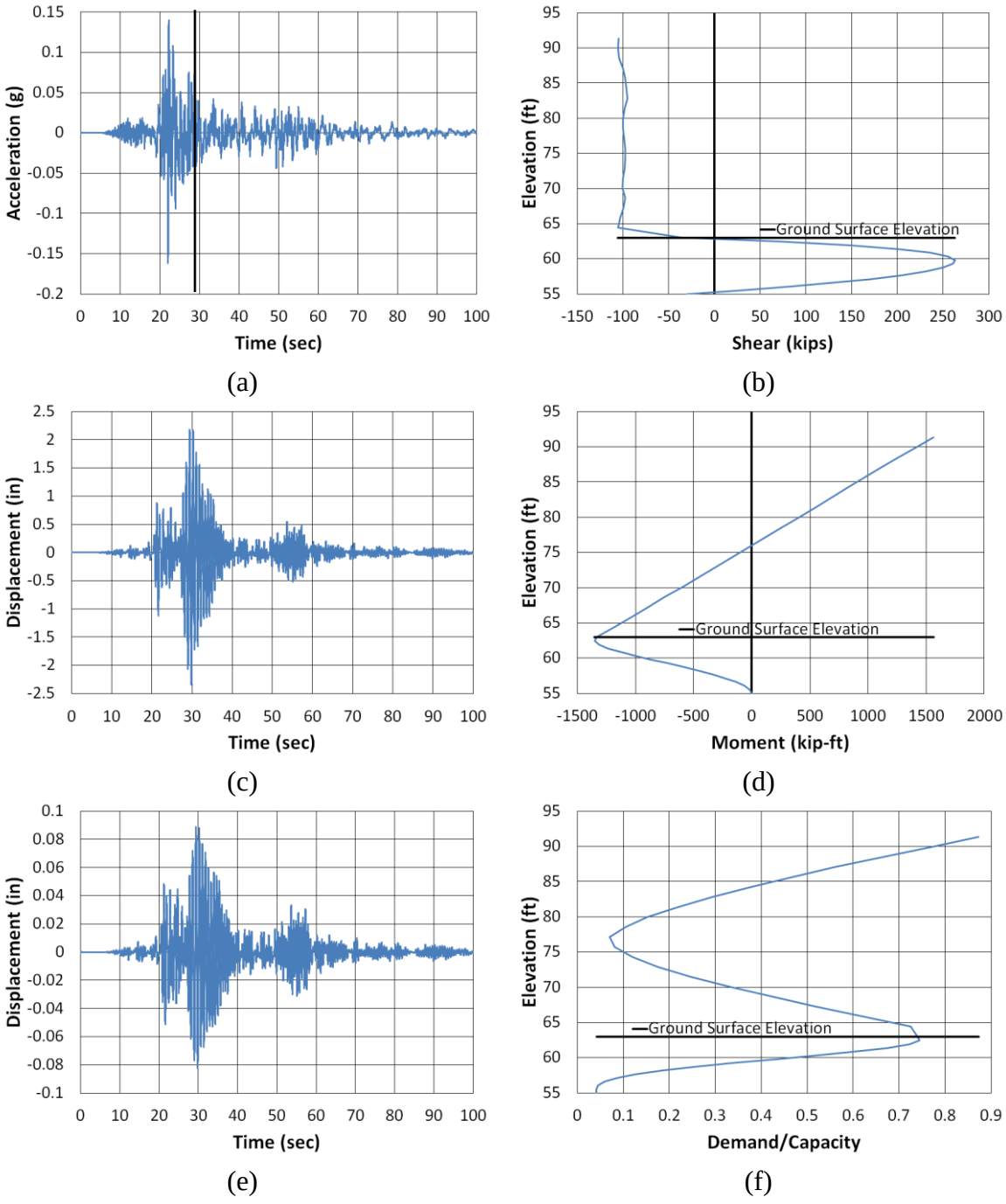

Figure B.58. Chambers County 100% Scour Transverse Kocaeli North (a) time-history event, (b) shear distribution, (c) top of pier displacement, (d) moment distribution, (e) ground surface displacement, and (f) demand capacity ratio

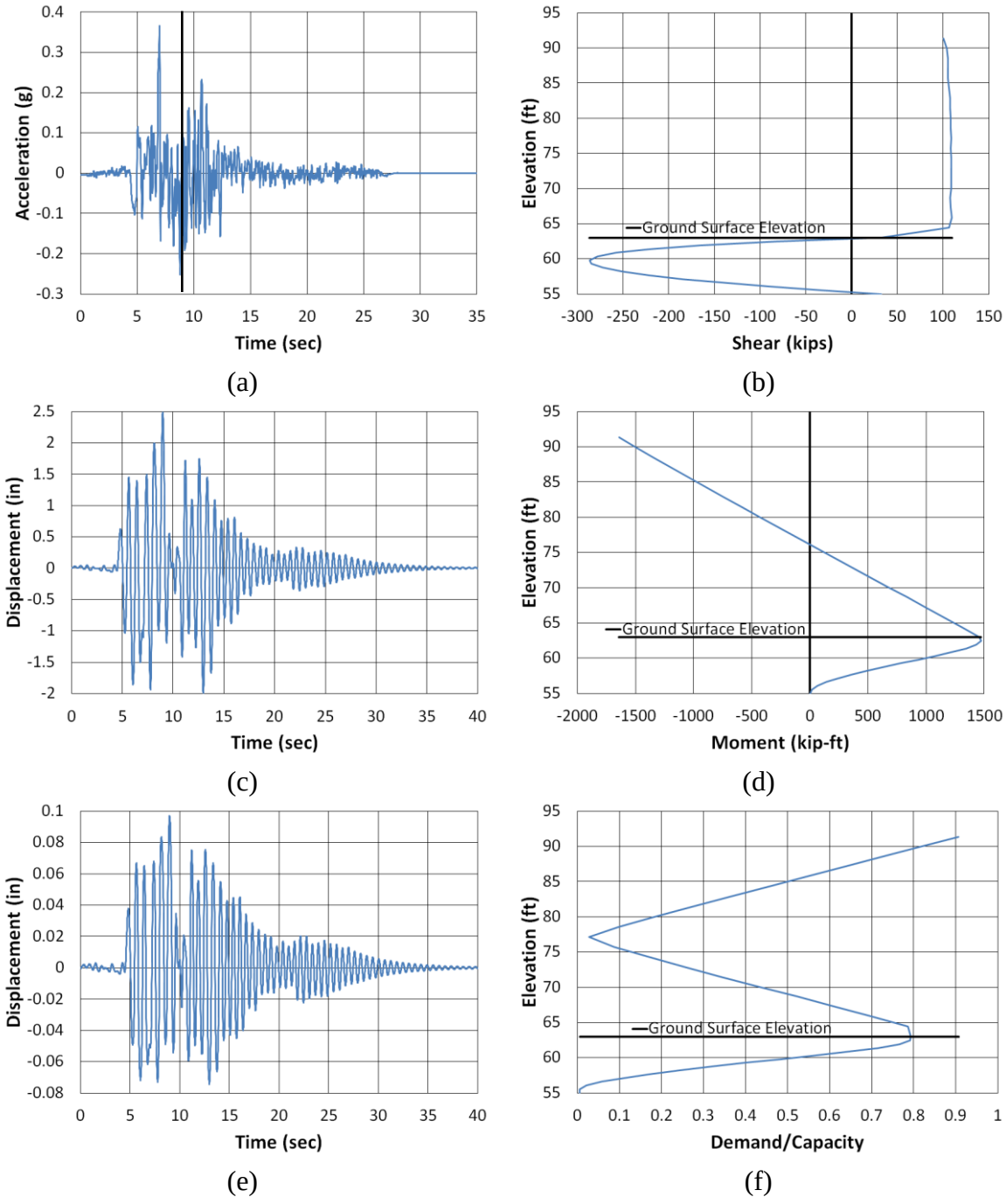

Figure B.59. Chambers County 100% Scour Transverse Kocaeli2 NMCE (a) time-history event, (b) shear distribution, (c) top of pier displacement, (d) moment distribution, (e) ground surface displacement, and (f) demand capacity ratio

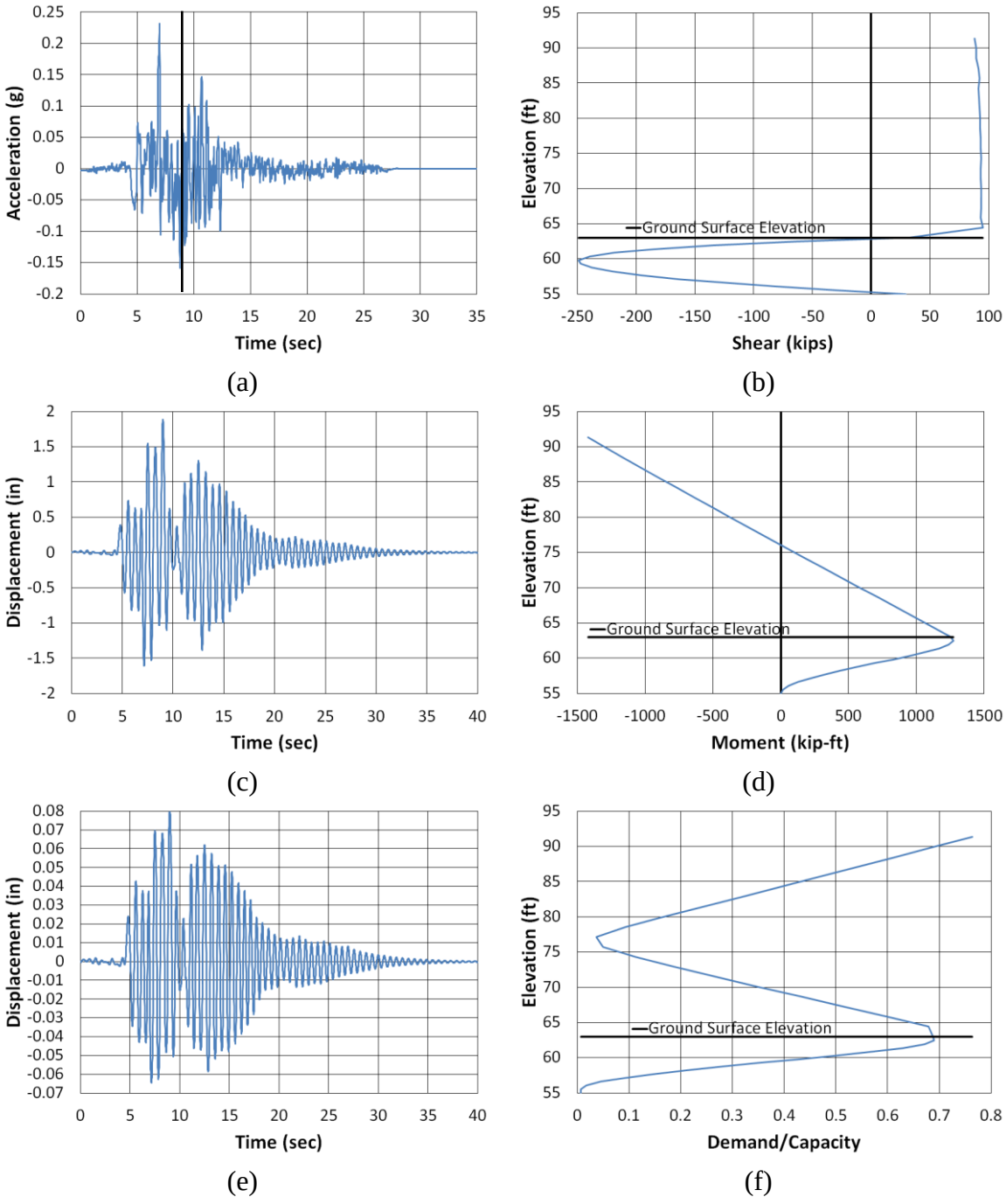

Figure B.60. Chambers County 100% Scour Transverse Kocaeli2 North (a) time-history event, (b) shear distribution, (c) top of pier displacement, (d) moment distribution, (e) ground surface displacement, and (f) demand capacity ratio

.

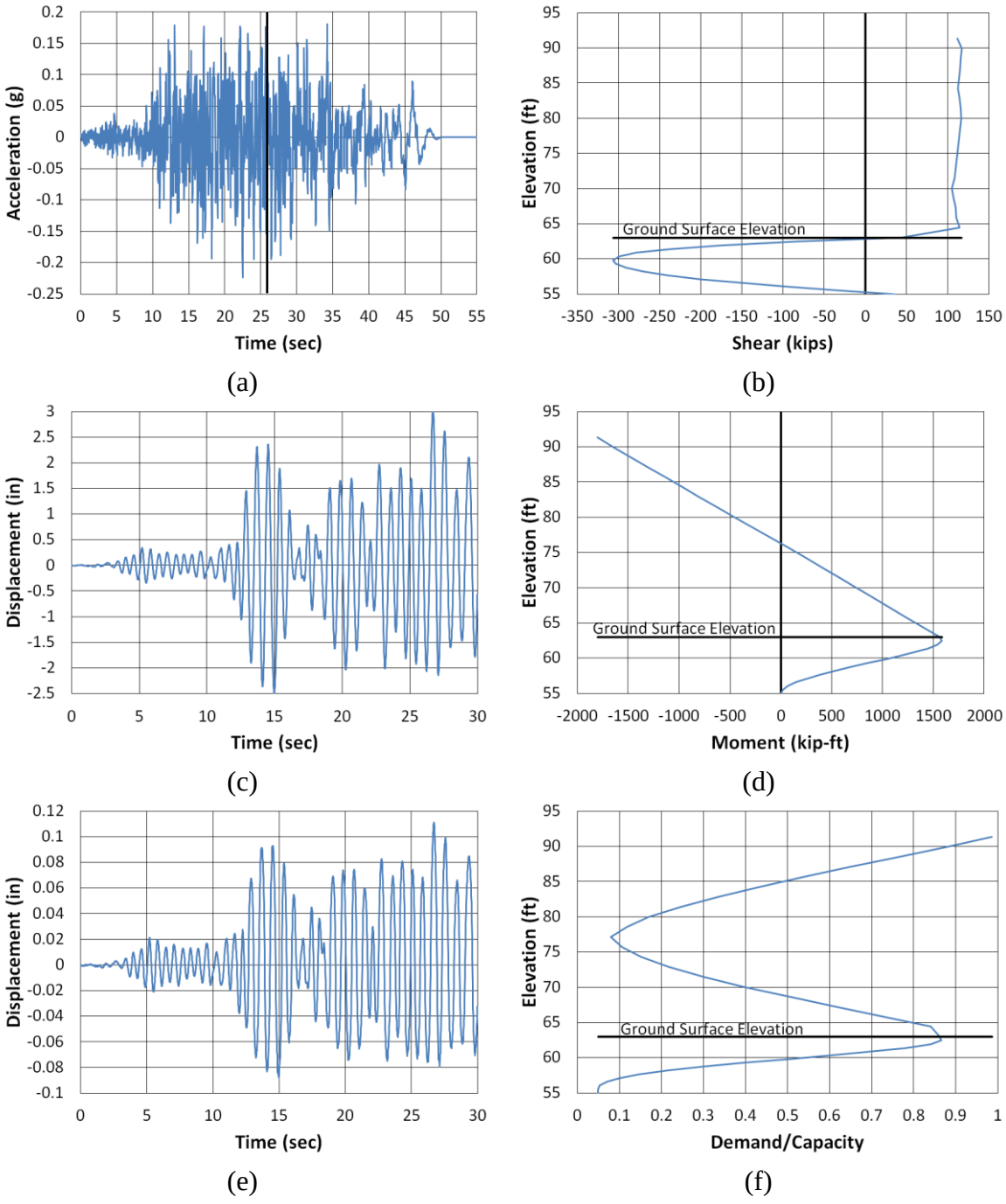

Figure B.61. Chambers County 100% Scour Transverse Landers NMCE (a) time-history event, (b) shear distribution, (c) top of pier displacement, (d) moment distribution, (e) ground surface displacement, and (f) demand capacity ratio

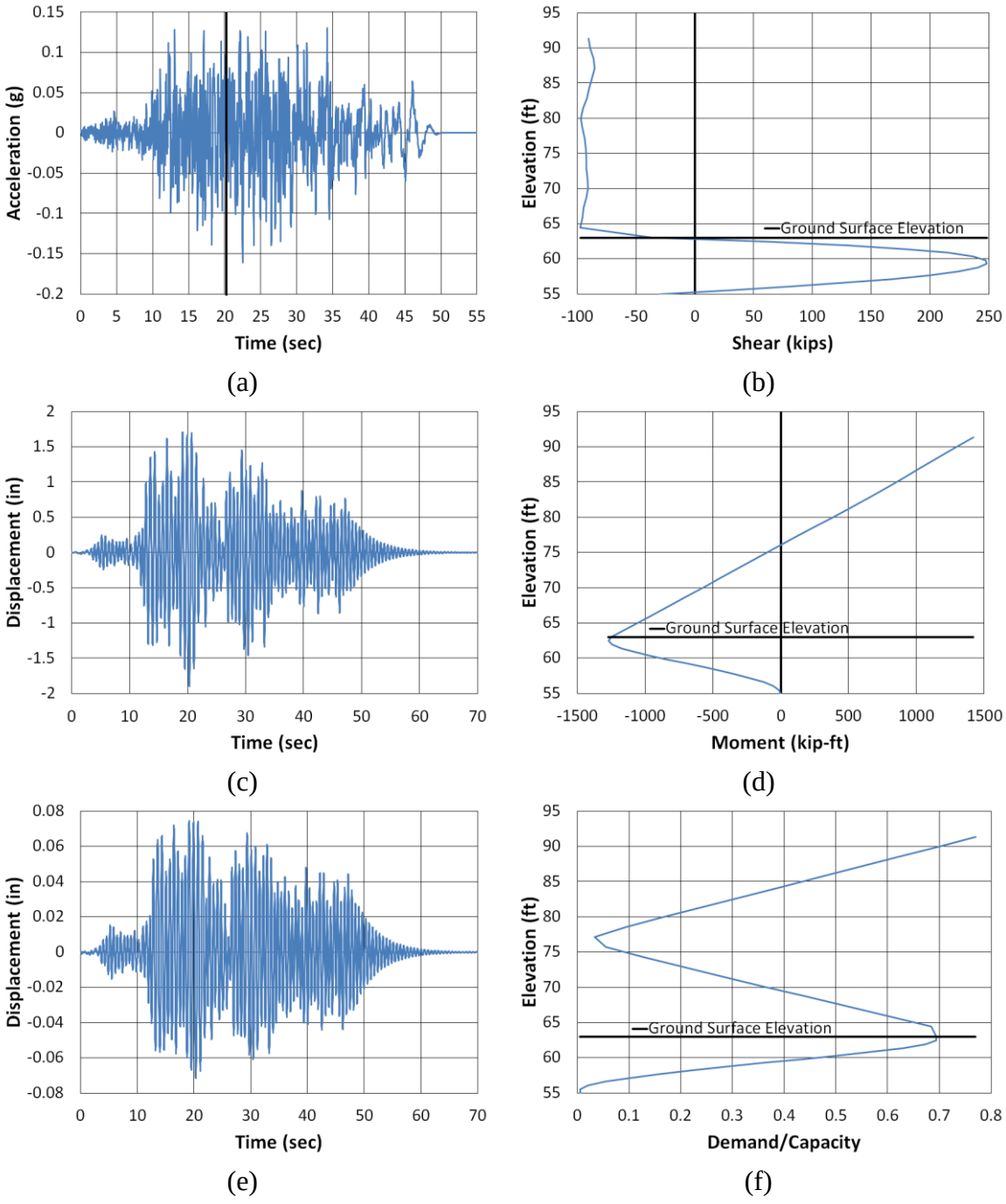

Figure B.62. Chambers County 100% Scour Transverse Landers North (a) time-history event, (b) shear distribution, (c) top of pier displacement, (d) moment distribution, (e) ground surface displacement, and (f) demand capacity ratio

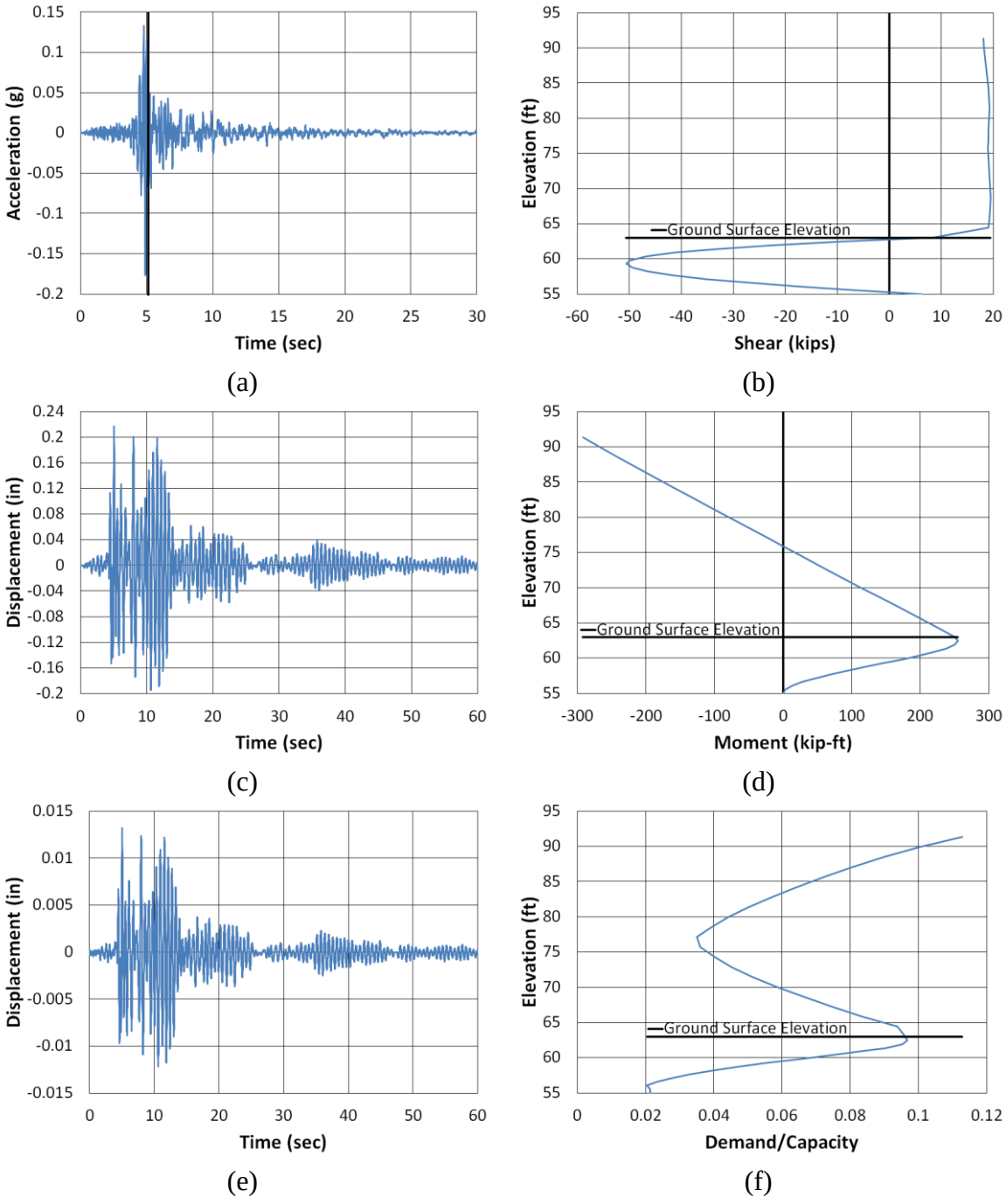

Figure B.63. Chambers County 100% Scour Transverse LSM North (a) time-history event, (b) shear distribution, (c) top of pier displacement, (d) moment distribution, (e) ground surface displacement, and (f) demand capacity ratio

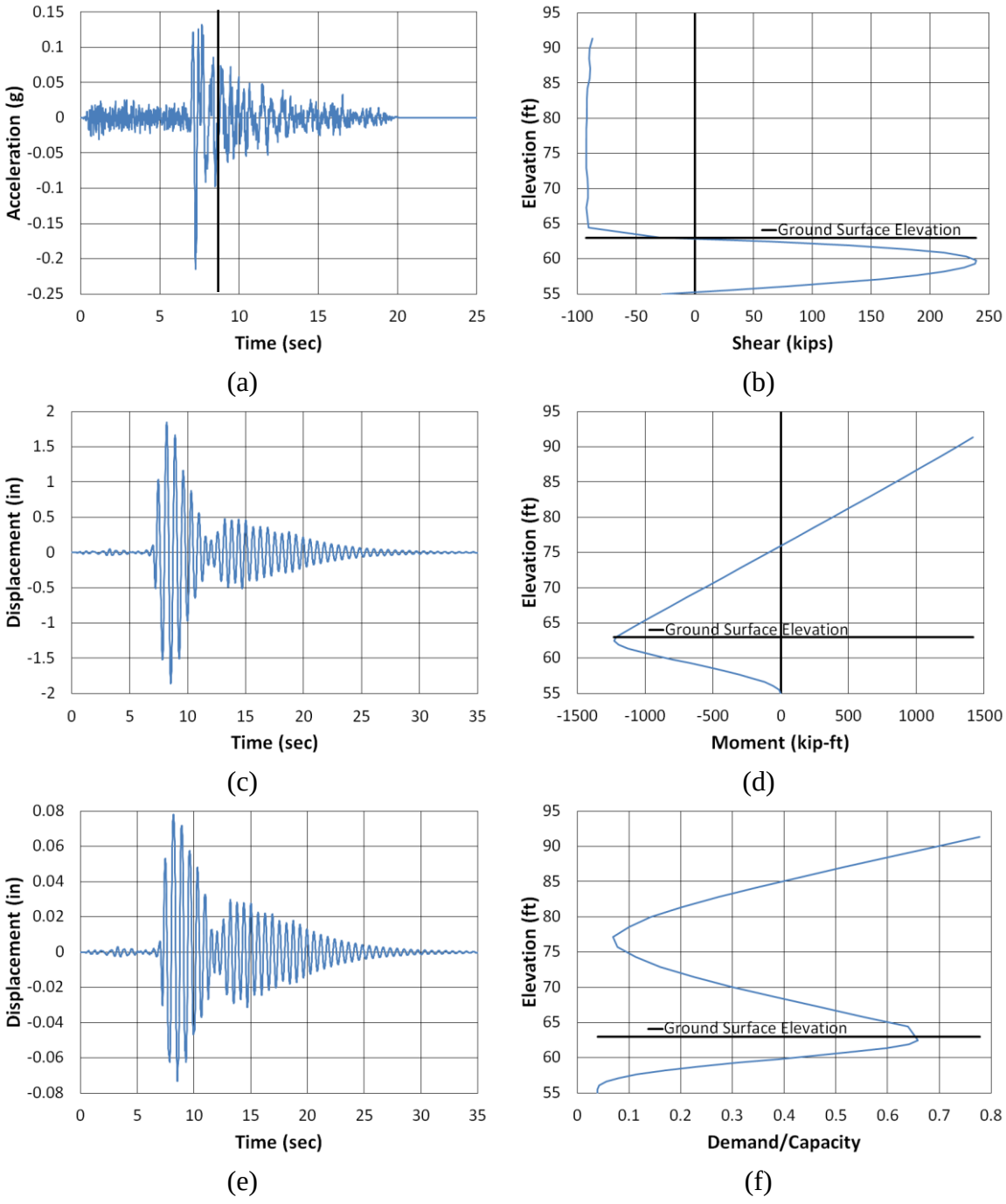

Figure B.64. Chambers County 100% Scour Transverse NPS North (a) time-history event, (b) shear distribution, (c) top of pier displacement, (d) moment distribution, (e) ground surface displacement, and (f) demand capacity ratio

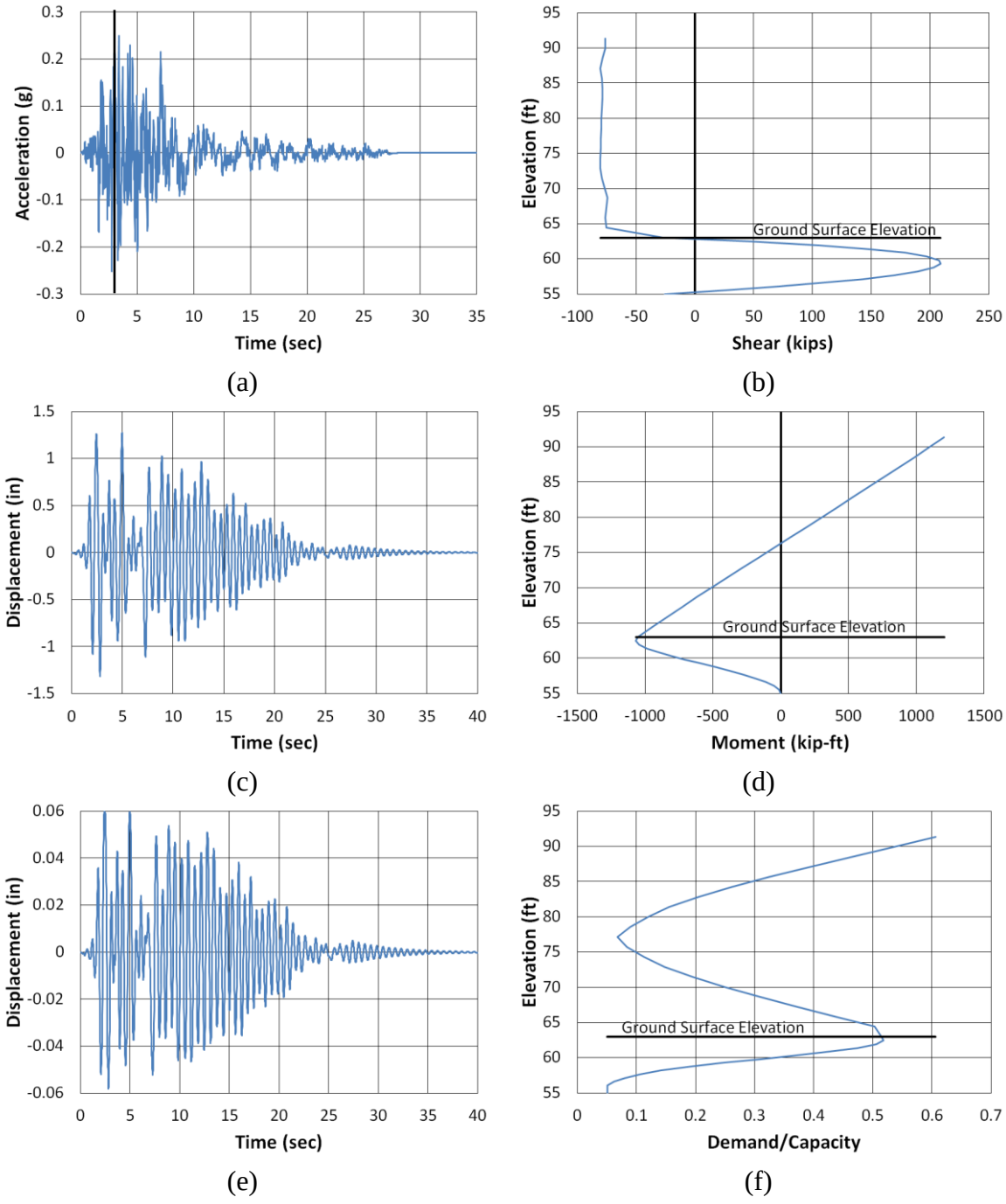

Figure B.65. Chambers County 100% Scour Transverse San Fernando NMCE (a) time-history event, (b) shear distribution, (c) top of pier displacement, (d) moment distribution, (e) ground surface displacement, and (f) demand capacity ratio

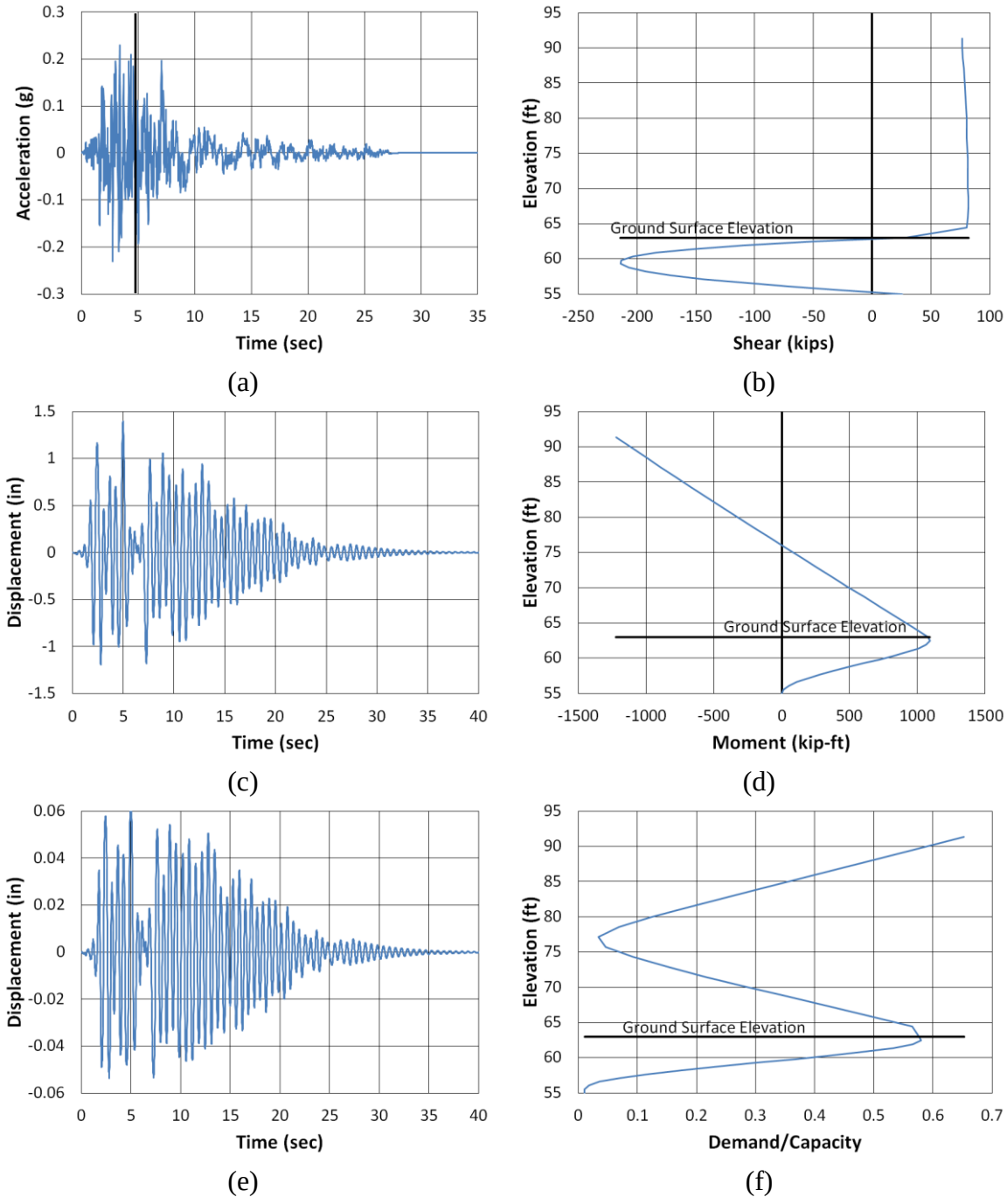

Figure B.66. Chambers County 100% Scour Transverse San Fernando North (a) time-history event, (b) shear distribution, (c) top of pier displacement, (d) moment distribution, (e) ground surface displacement, and (f) demand capacity ratio

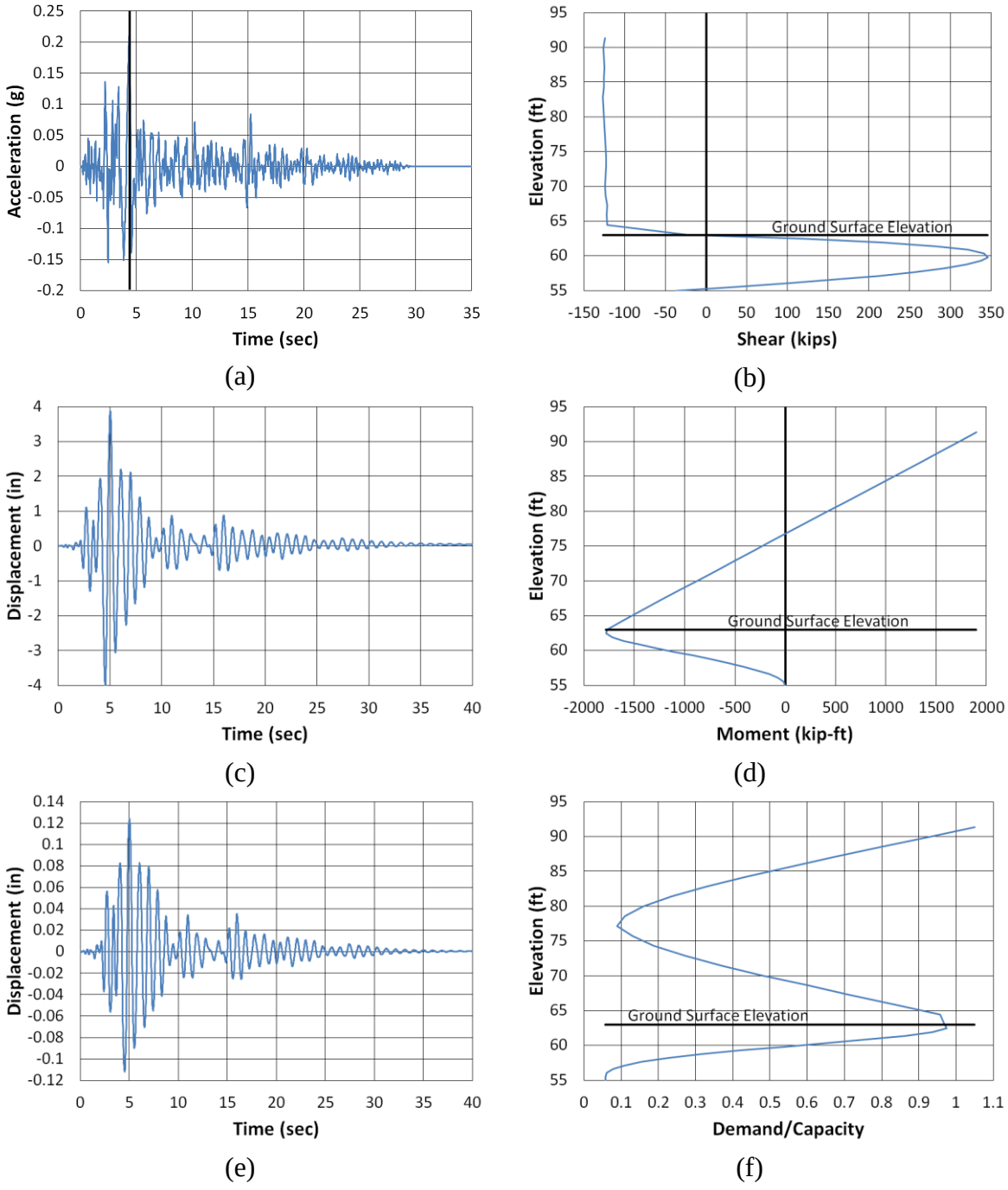

Figure B.67. Chambers County 100% Scour Transverse San Fernando2 NMCE (a) time-history event, (b) shear distribution, (c) top of pier displacement, (d) moment distribution, (e) ground surface displacement, and (f) demand capacity ratio

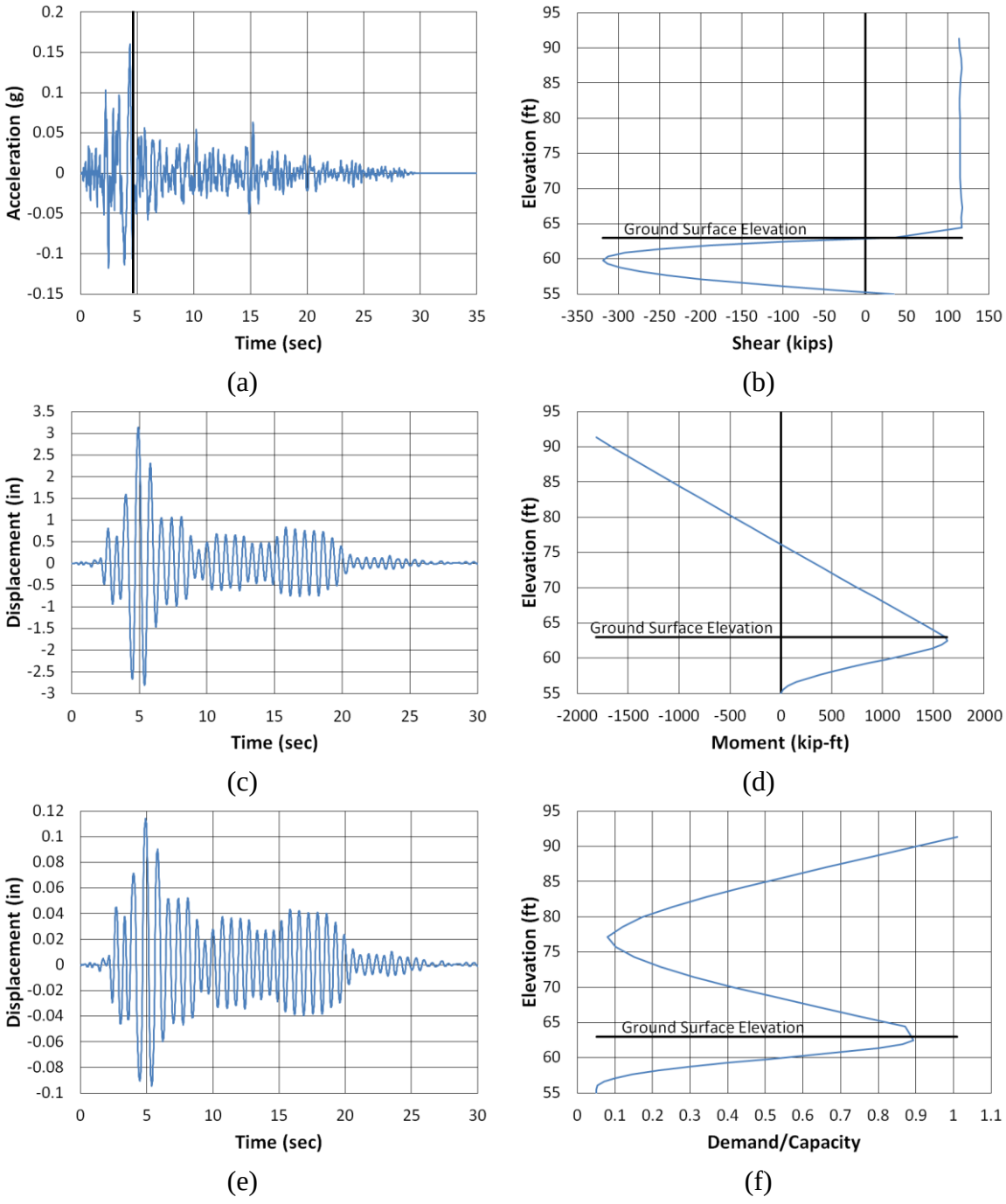

Figure B.68. Chambers County 100% Scour Transverse San Fernando2 North (a) time-history event, (b) shear distribution, (c) top of pier displacement, (d) moment distribution, (e) ground surface displacement, and (f) demand capacity ratio

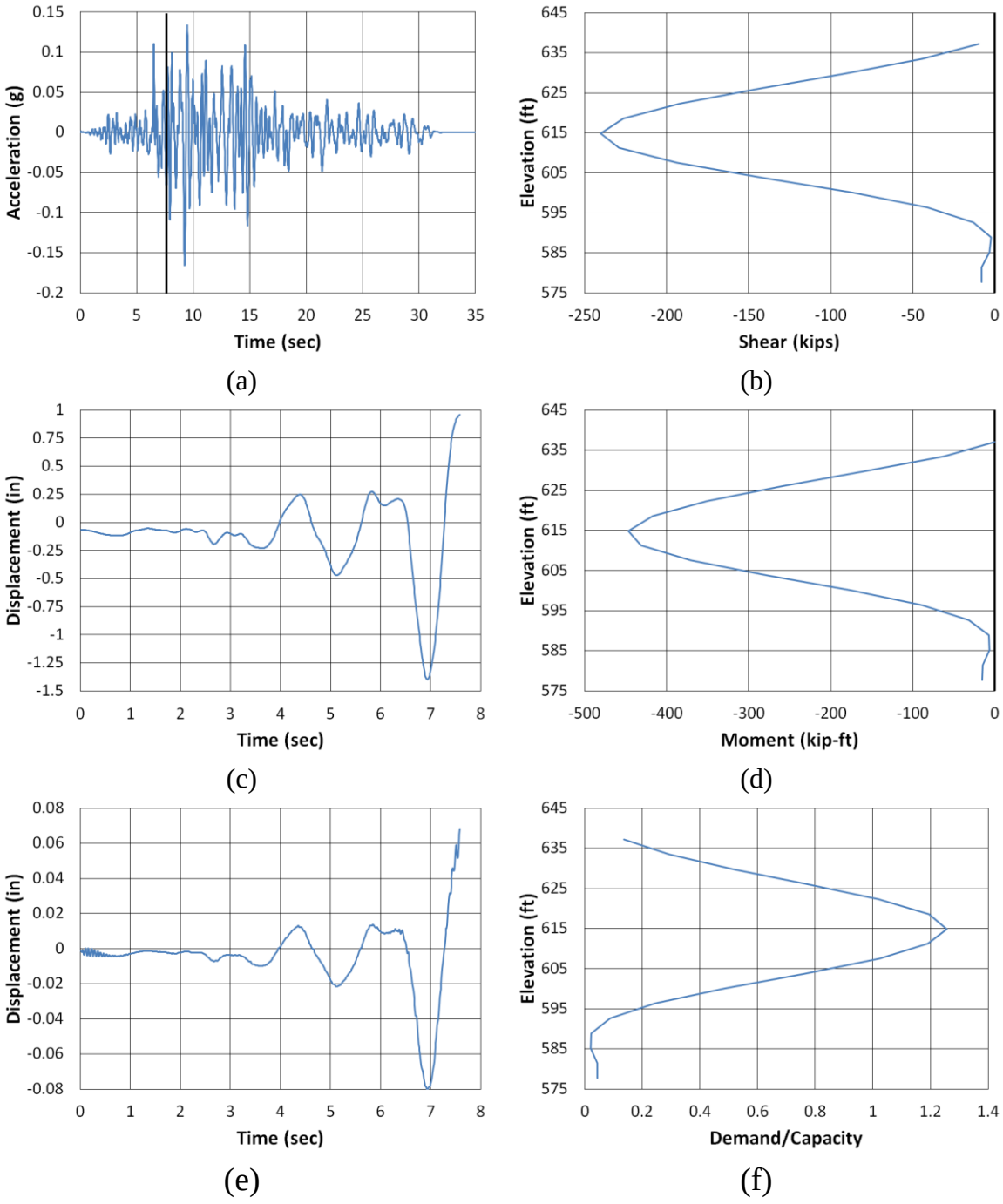

Figure B.69. Etowah County Longitudinal Coalinga North (a) time-history event, (b) shear distribution, (c) top of pier displacement, (d) moment distribution, (e) ground surface displacement, and (f) demand capacity ratio

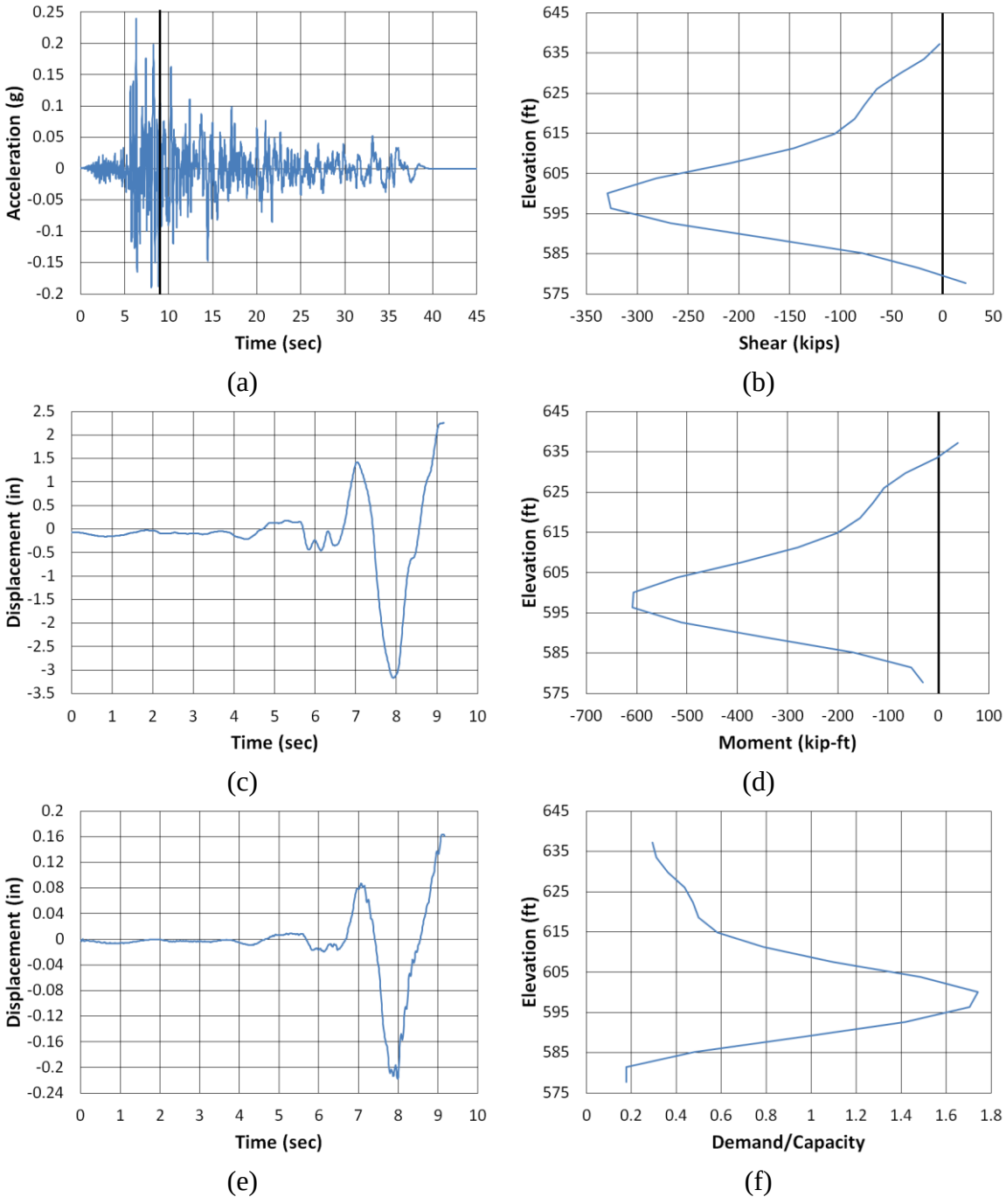

Figure B.70. Etowah County Longitudinal Imperial Valley NMCE (a) time-history event, (b) shear distribution, (c) top of pier displacement, (d) moment distribution, (e) ground surface displacement, and (f) demand capacity ratio

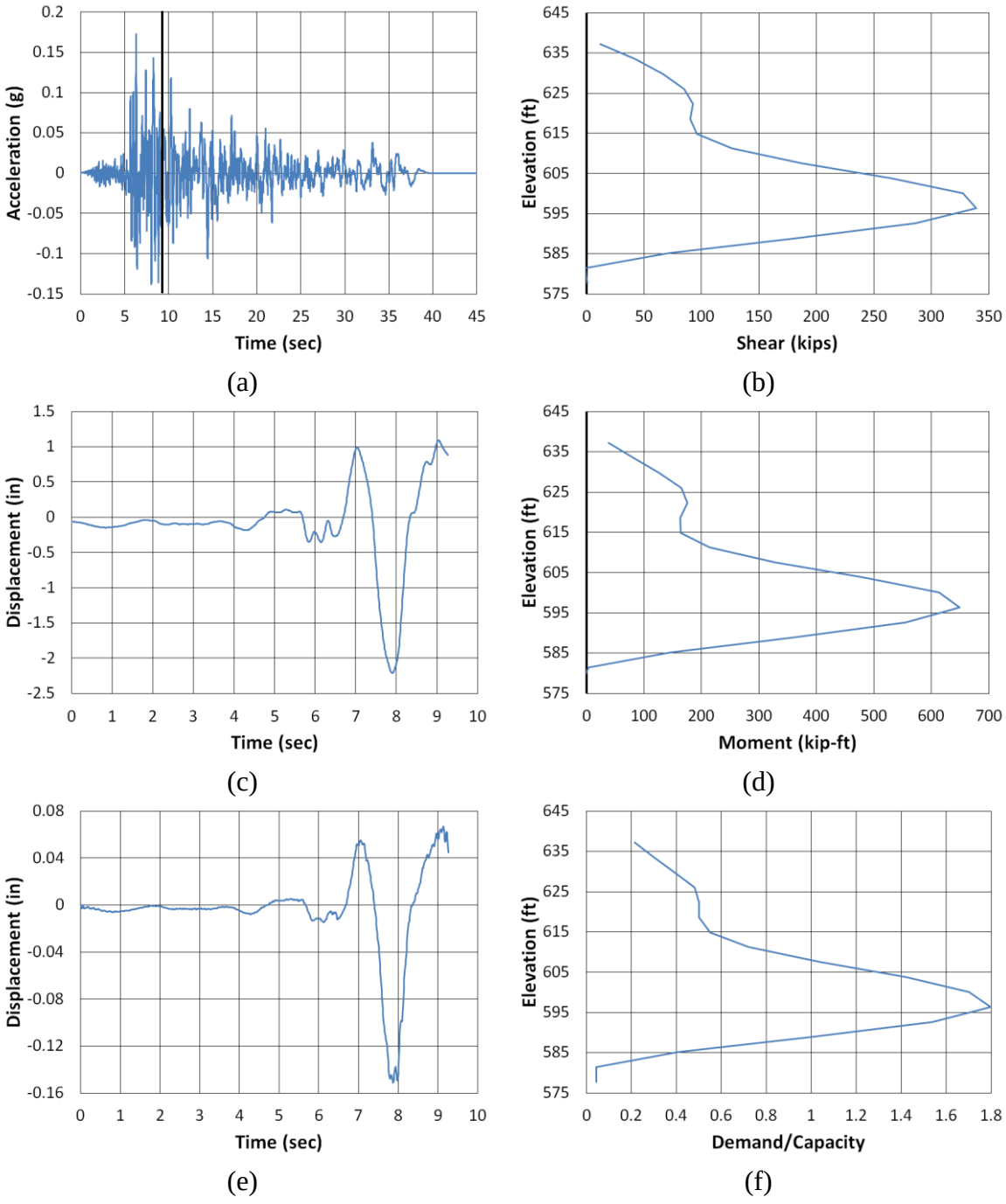

Figure B.71. Etowah County Longitudinal Imperial Valley North (a) time-history event, (b) shear distribution, (c) top of pier displacement, (d) moment distribution, (e) ground surface displacement, and (f) demand capacity ratio

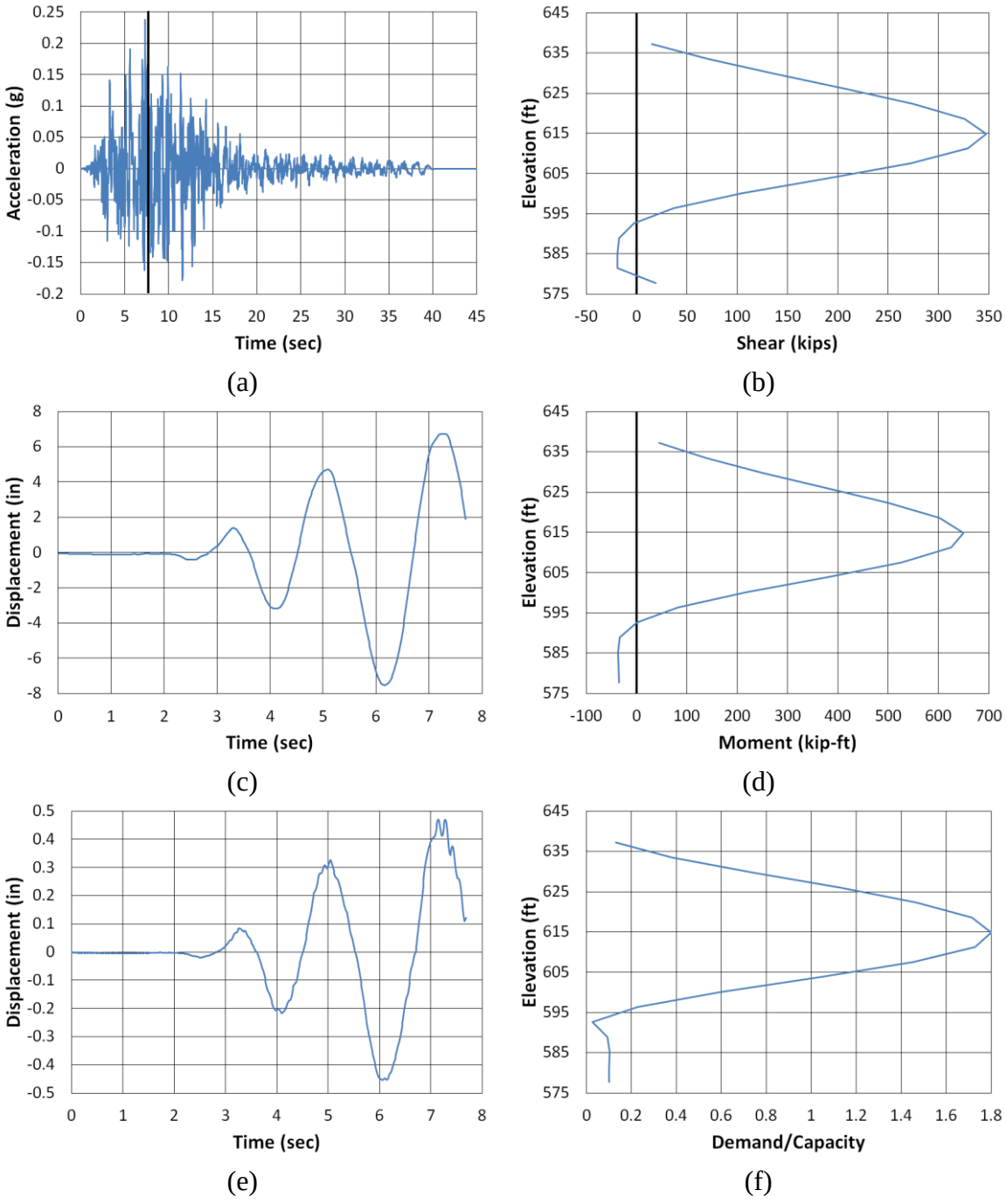

Figure B.72. Etowah County Longitudinal Kobe NMCE (a) time-history event, (b) shear distribution, (c) top of pier displacement, (d) moment distribution, (e) ground surface displacement, and (f) demand capacity ratio

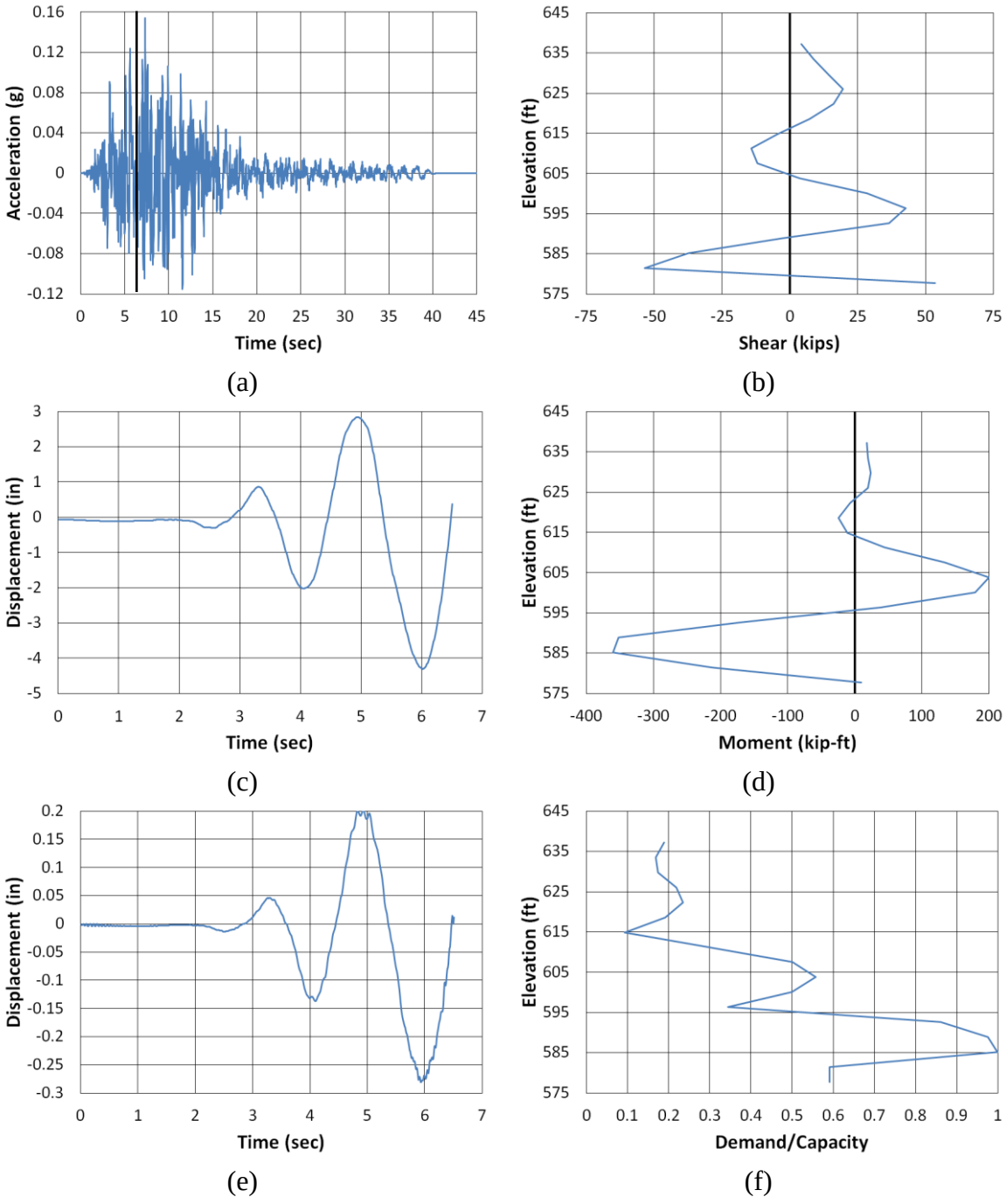

Figure B.73. Etowah County Longitudinal Kobe North (a) time-history event, (b) shear distribution, (c) top of pier displacement, (d) moment distribution, (e) ground surface displacement, and (f) demand capacity ratio

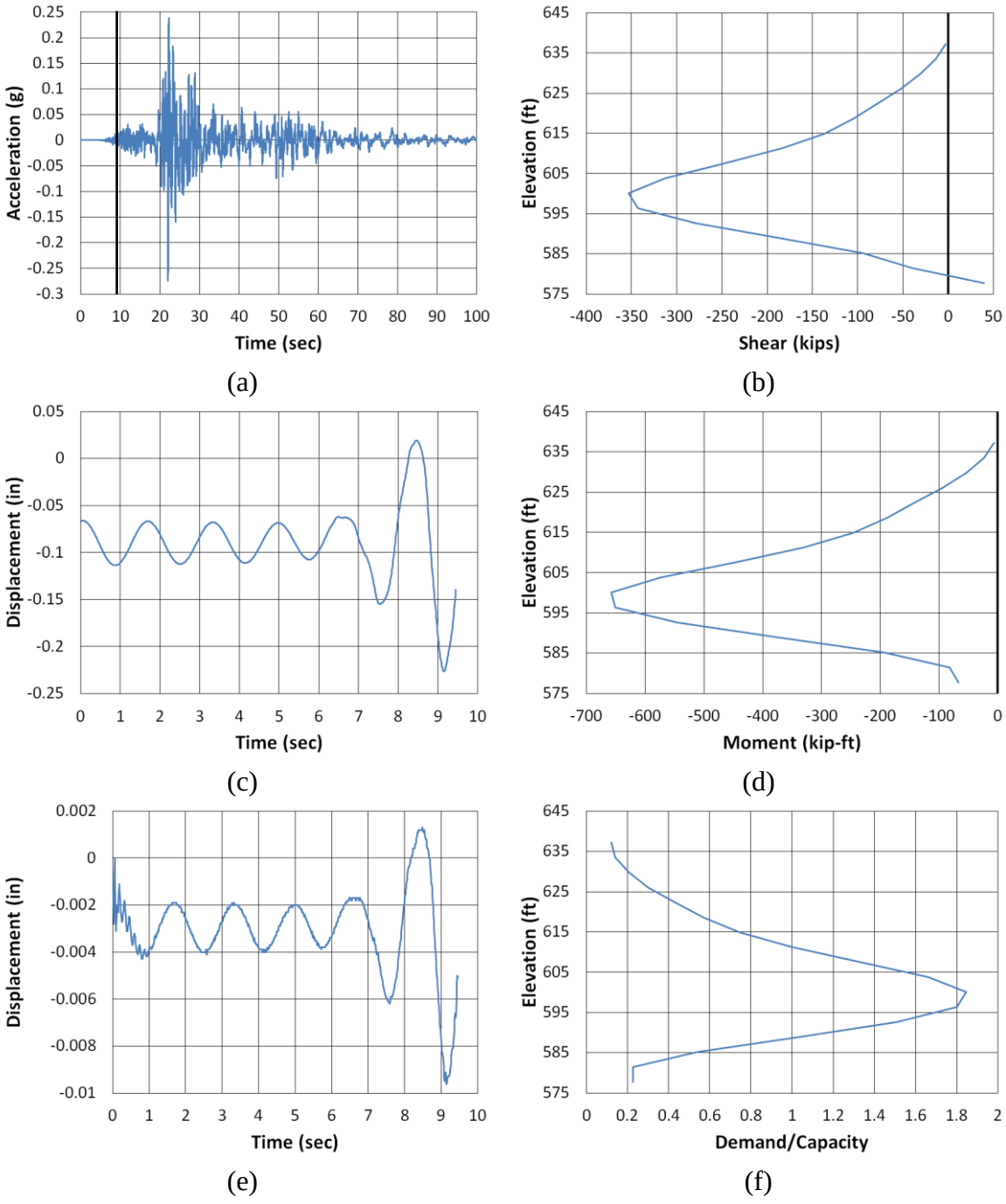

Figure B.74. Etowah County Longitudinal Kocaeli NMCE (a) time-history event, (b) shear distribution, (c) top of pier displacement, (d) moment distribution, (e) ground surface displacement, and (f) demand capacity ratio

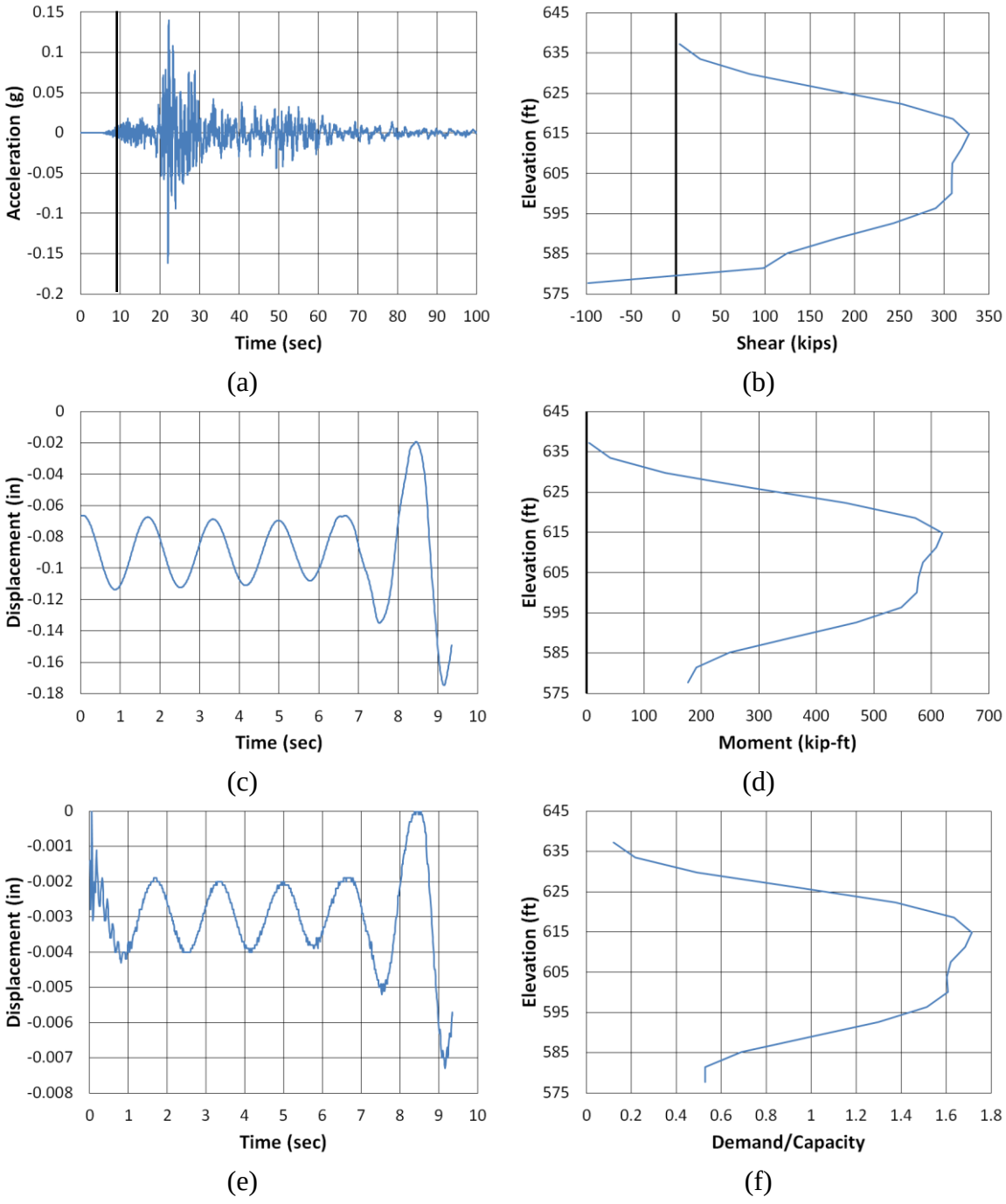

Figure B.75. Etowah County Longitudinal Kocaeli North (a) time-history event, (b) shear distribution, (c) top of pier displacement, (d) moment distribution, (e) ground surface displacement, and (f) demand capacity ratio

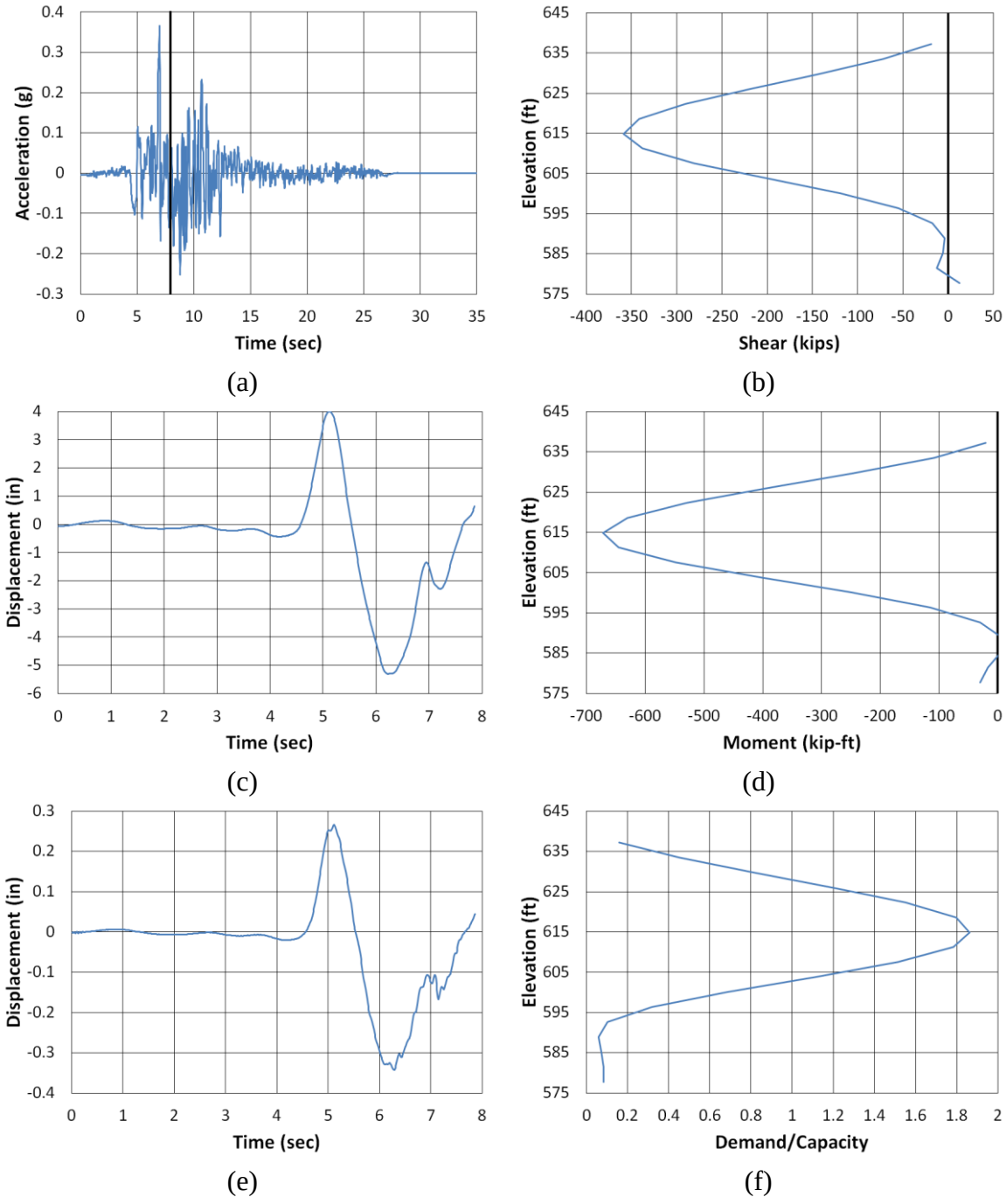

Figure B.76. Etowah County Longitudinal Kocaeli2 NMCE (a) time-history event, (b) shear distribution, (c) top of pier displacement, (d) moment distribution, (e) ground surface displacement, and (f) demand capacity ratio

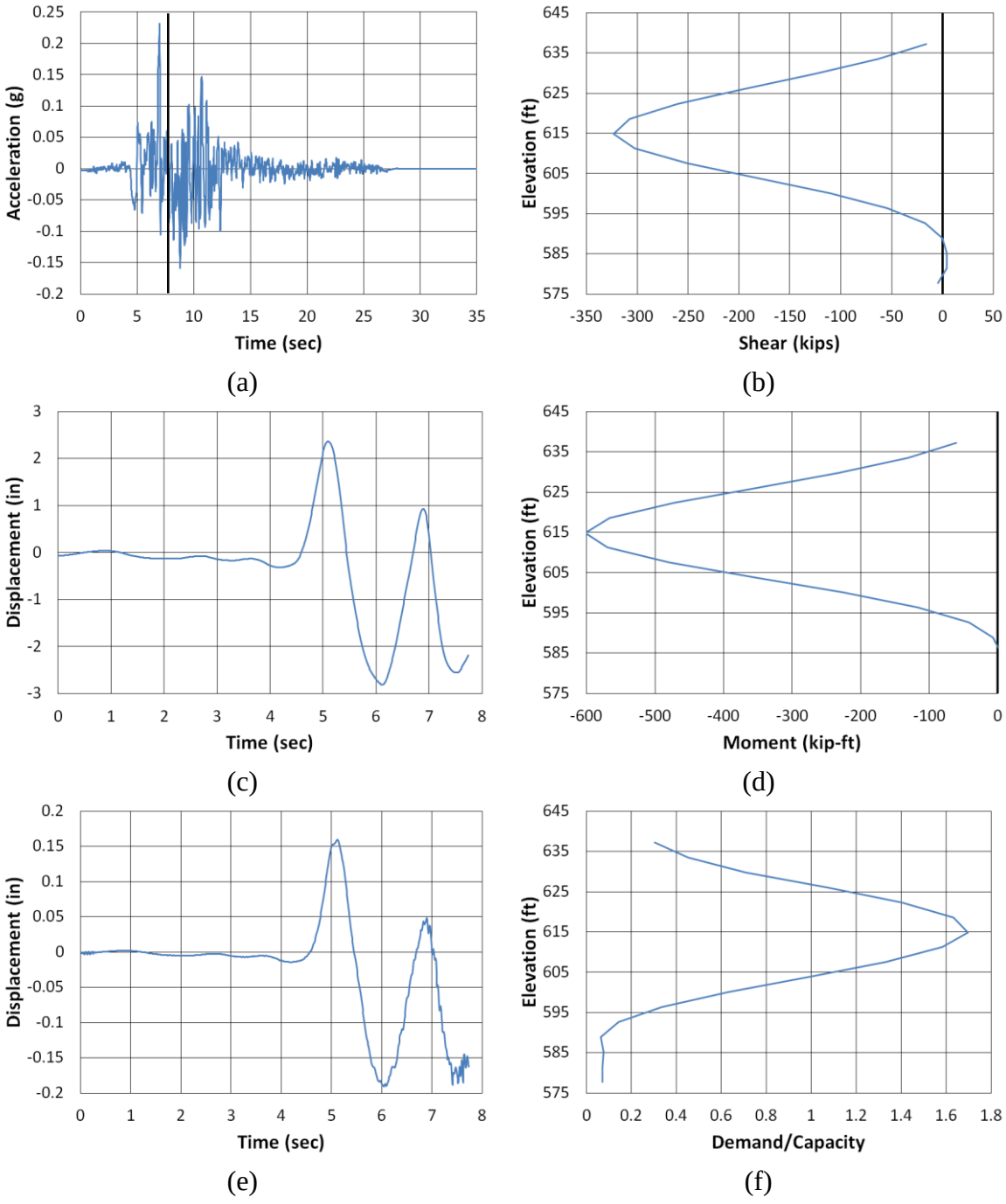

Figure B.77. Etowah County Longitudinal Kocaeli2 North (a) time-history event, (b) shear distribution, (c) top of pier displacement, (d) moment distribution, (e) ground surface displacement, and (f) demand capacity ratio

.

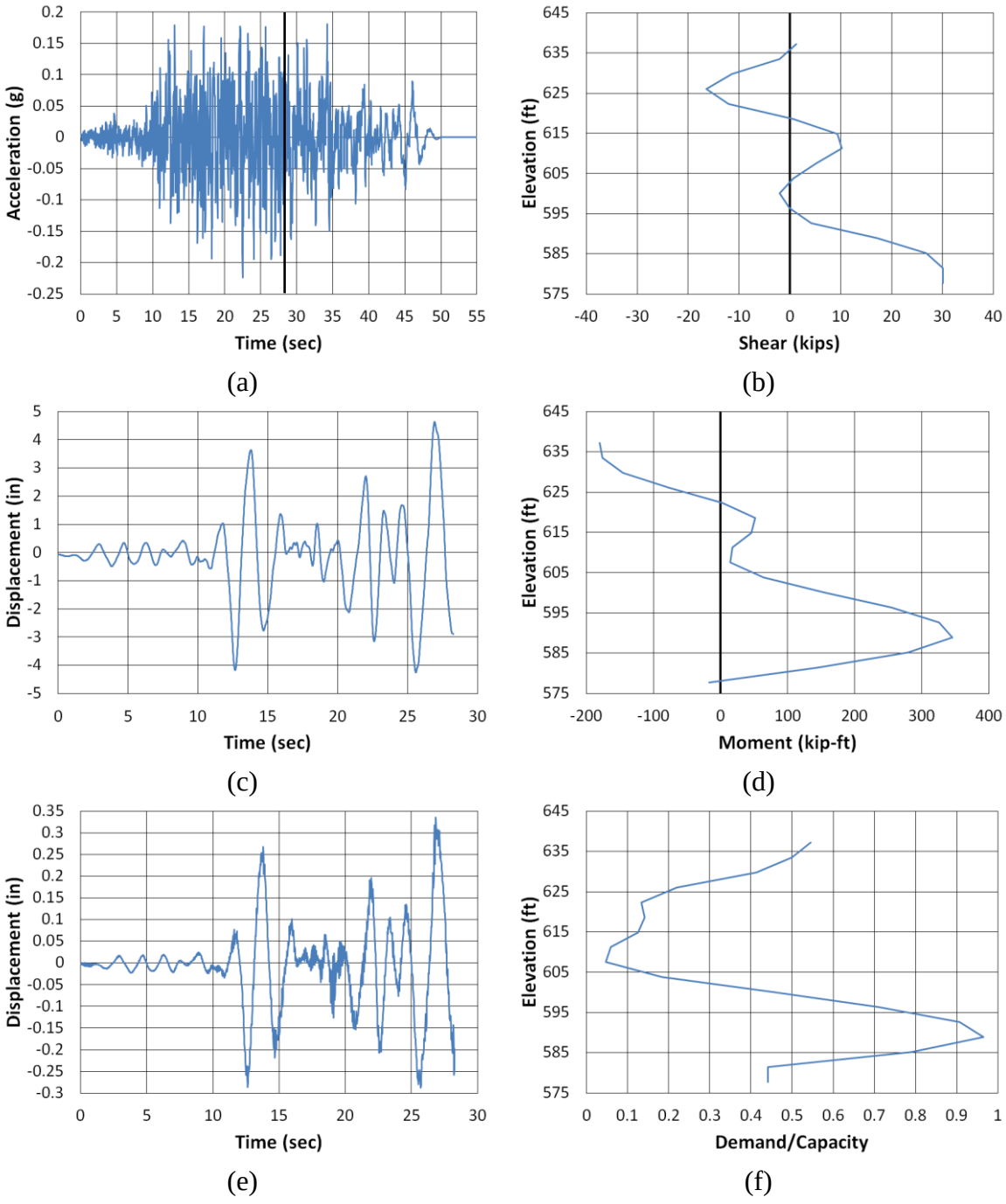

Figure B.78. Etowah County Longitudinal Landers NMCE (a) time-history event, (b) shear distribution, (c) top of pier displacement, (d) moment distribution, (e) ground surface displacement, and (f) demand capacity ratio

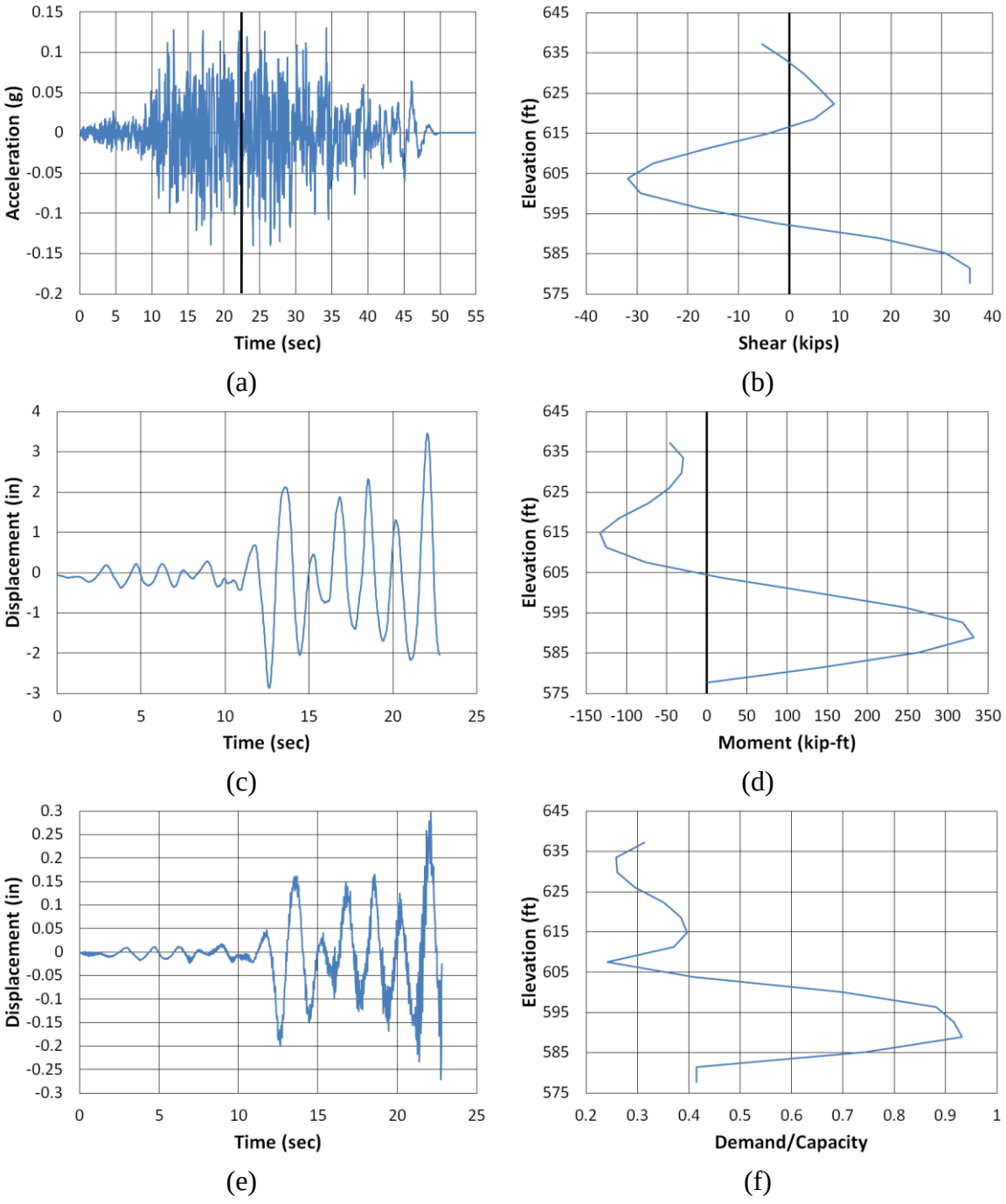

Figure B.79. Etowah County Longitudinal Landers North (a) time-history event, (b) shear distribution, (c) top of pier displacement, (d) moment distribution, (e) ground surface displacement, and (f) demand capacity ratio

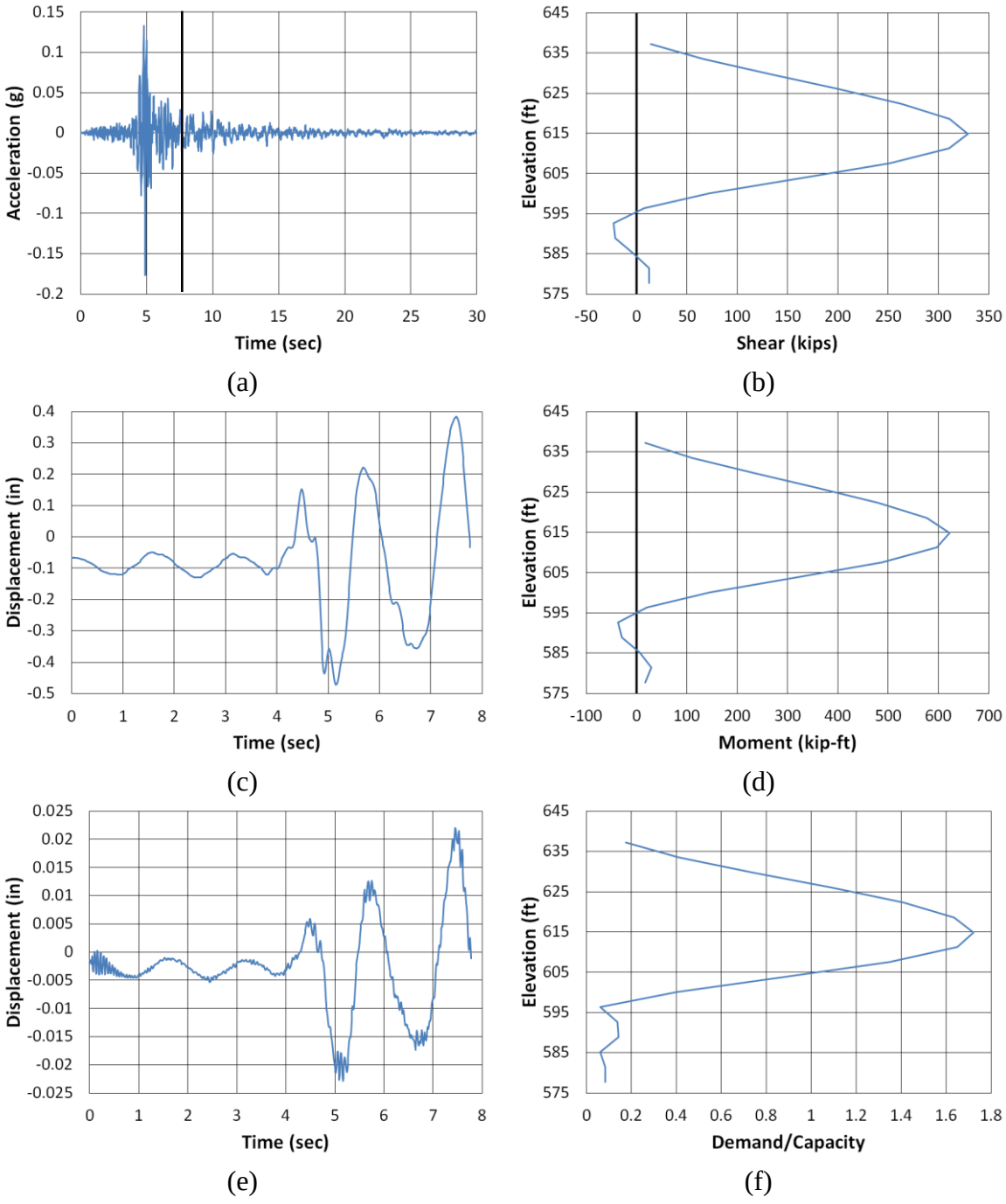

Figure B.80. Etowah County Longitudinal LSM North (a) time-history event, (b) shear distribution, (c) top of pier displacement, (d) moment distribution, (e) ground surface displacement, and (f) demand capacity ratio

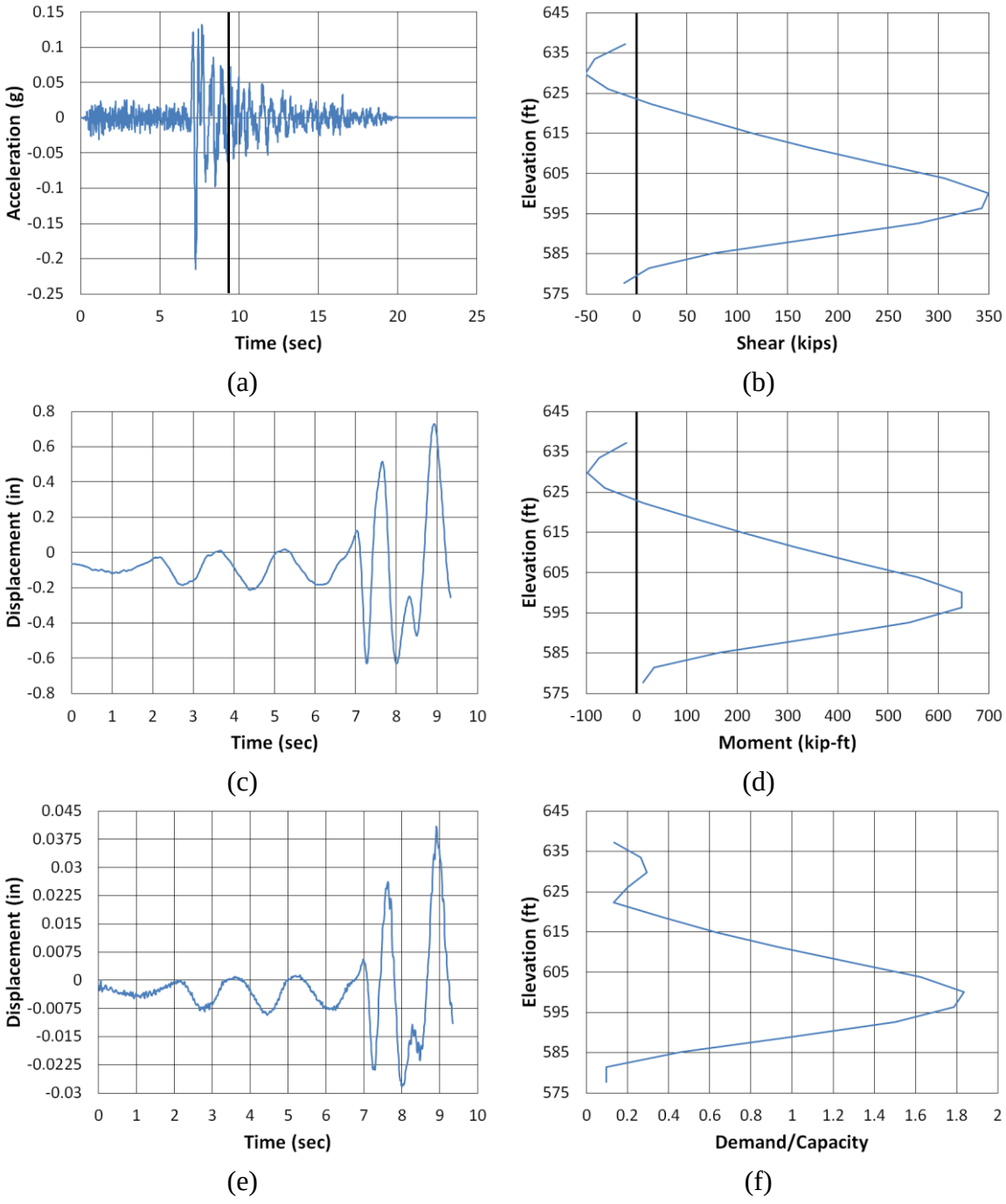

Figure B.81. Etowah County Longitudinal NPS North (a) time-history event, (b) shear distribution, (c) top of pier displacement, (d) moment distribution, (e) ground surface displacement, and (f) demand capacity ratio

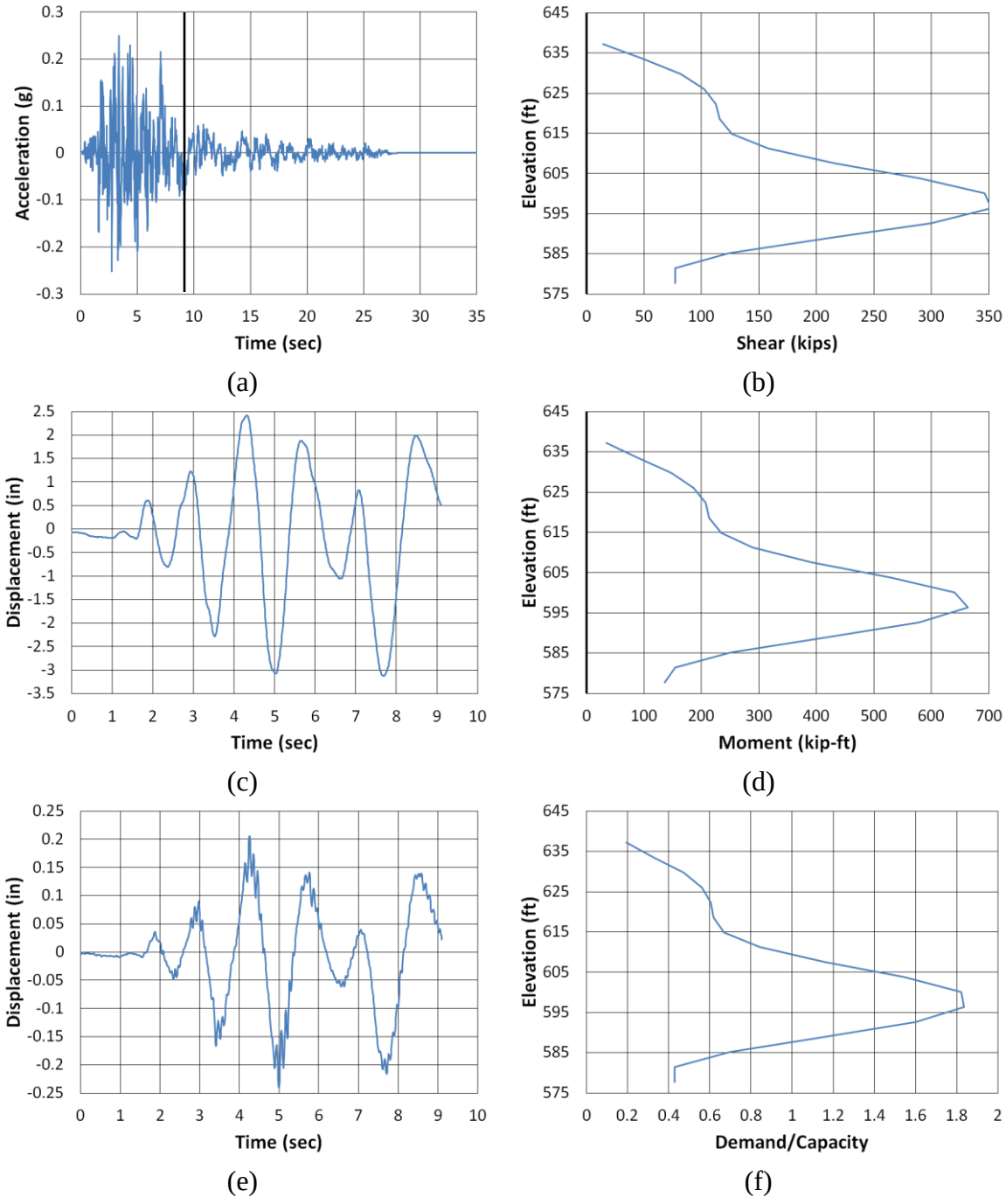

Figure B.82. Etowah County Longitudinal San Fernando NMCE (a) time-history event, (b) shear distribution, (c) top of pier displacement, (d) moment distribution, (e) ground surface displacement, and (f) demand capacity ratio

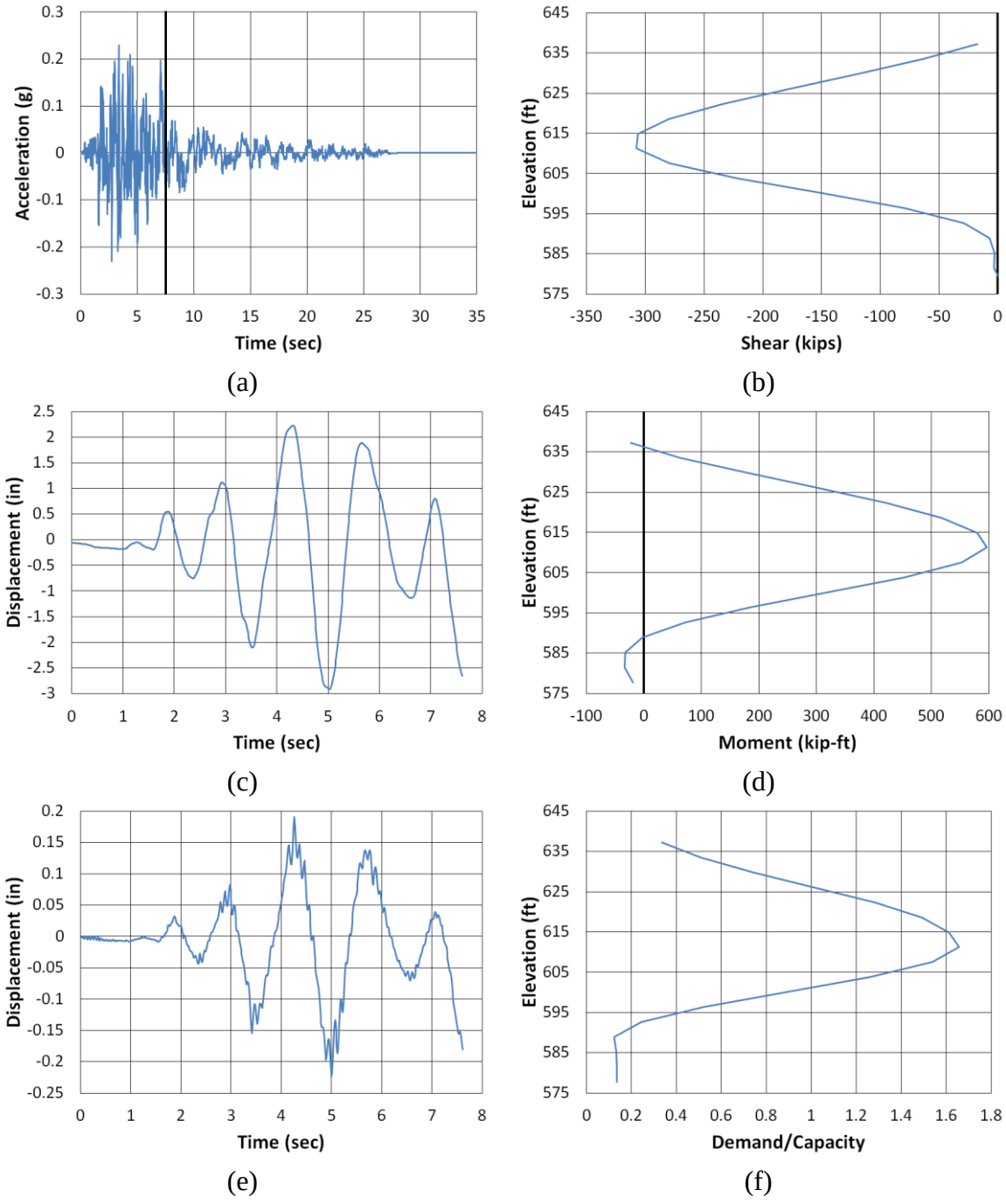

Figure B.83. Etowah County Longitudinal San Fernando North (a) time-history event, (b) shear distribution, (c) top of pier displacement, (d) moment distribution, (e) ground surface displacement, and (f) demand capacity ratio

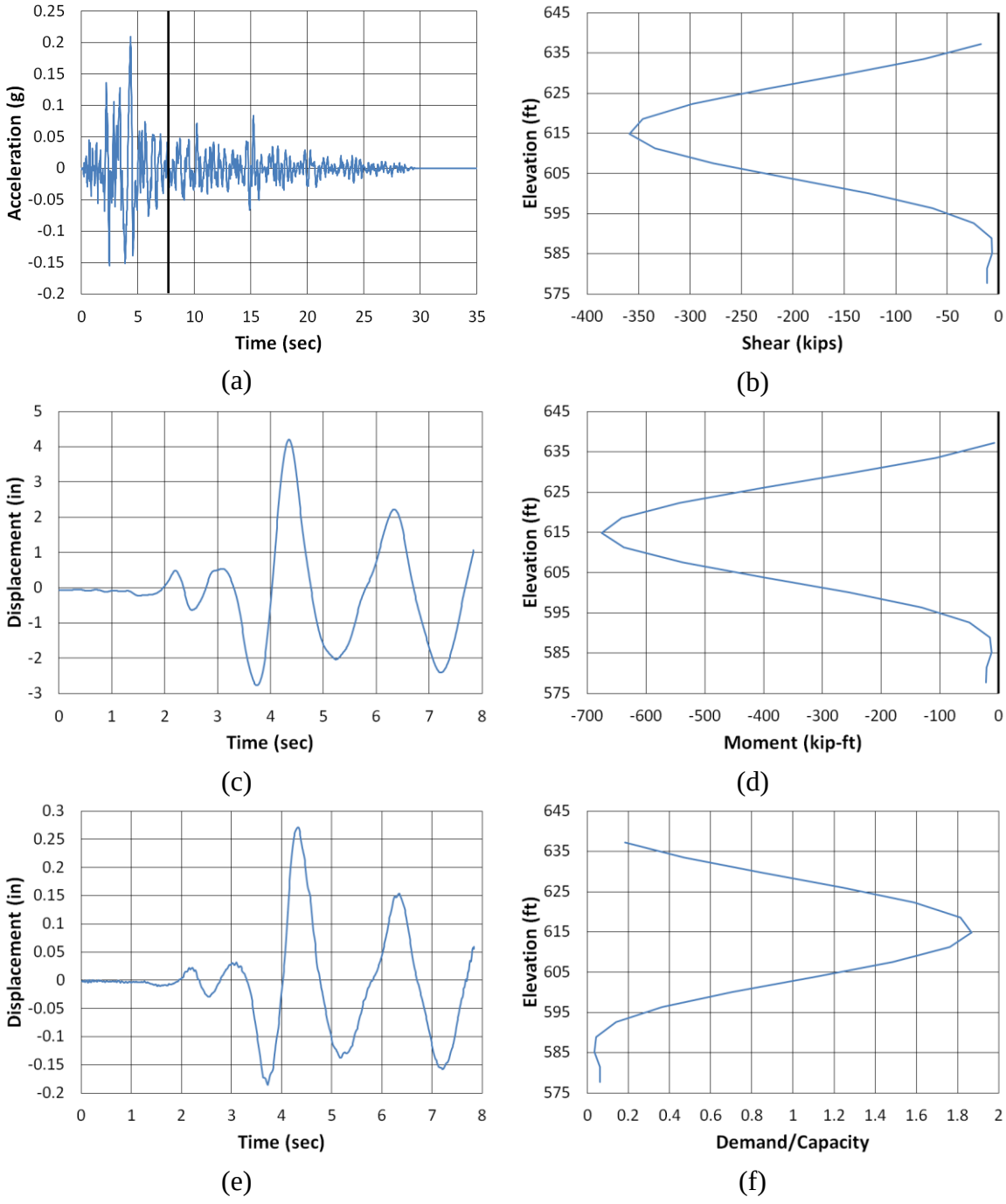

Figure B.84. Etowah County Longitudinal San Fernando2 NMCE (a) time-history event, (b) shear distribution, (c) top of pier displacement, (d) moment distribution, (e) ground surface displacement, and (f) demand capacity ratio

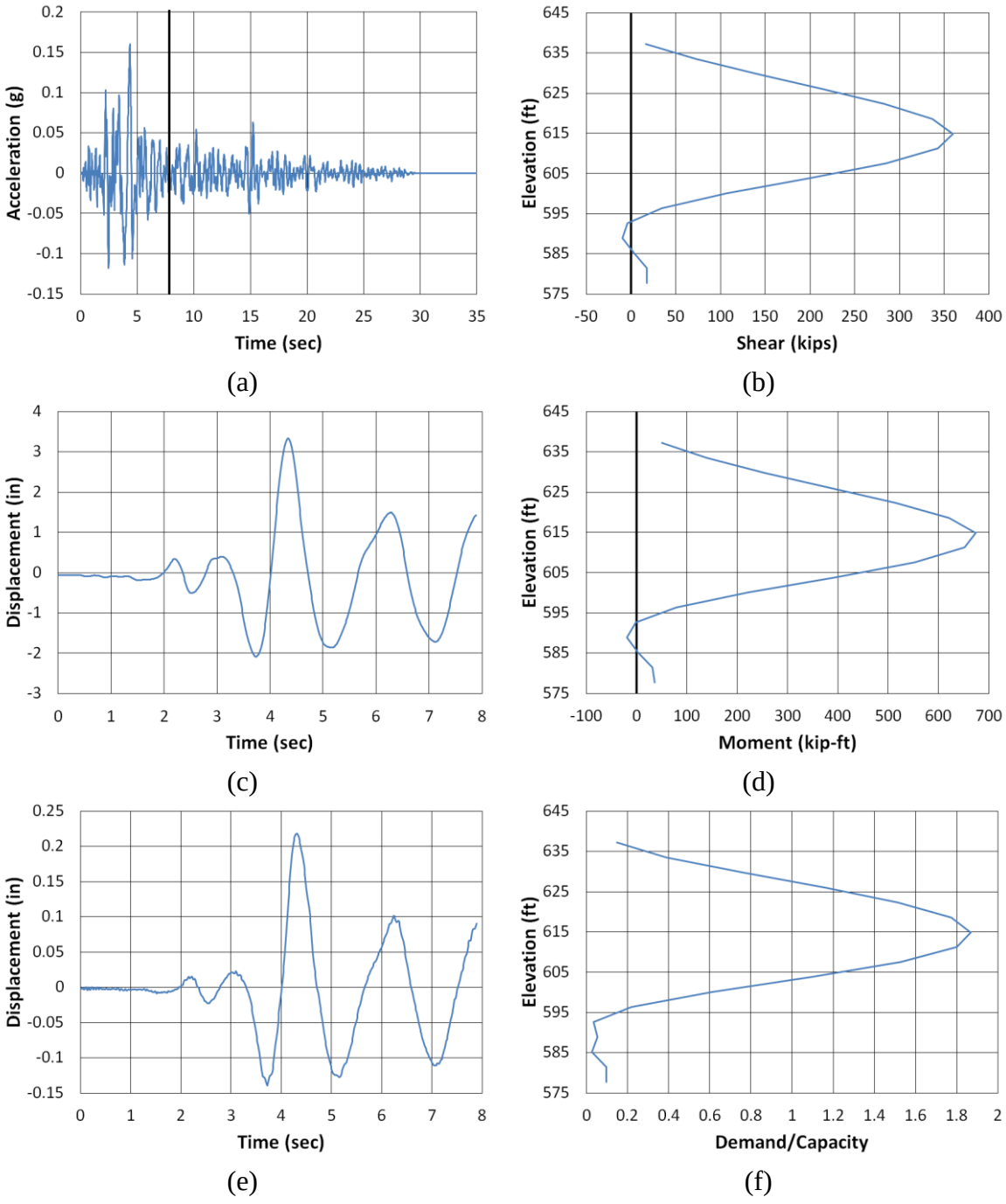

Figure B.85. Etowah County Longitudinal San Fernando2 North (a) time-history event, (b) shear distribution, (c) top of pier displacement, (d) moment distribution, (e) ground surface displacement, and (f) demand capacity ratio

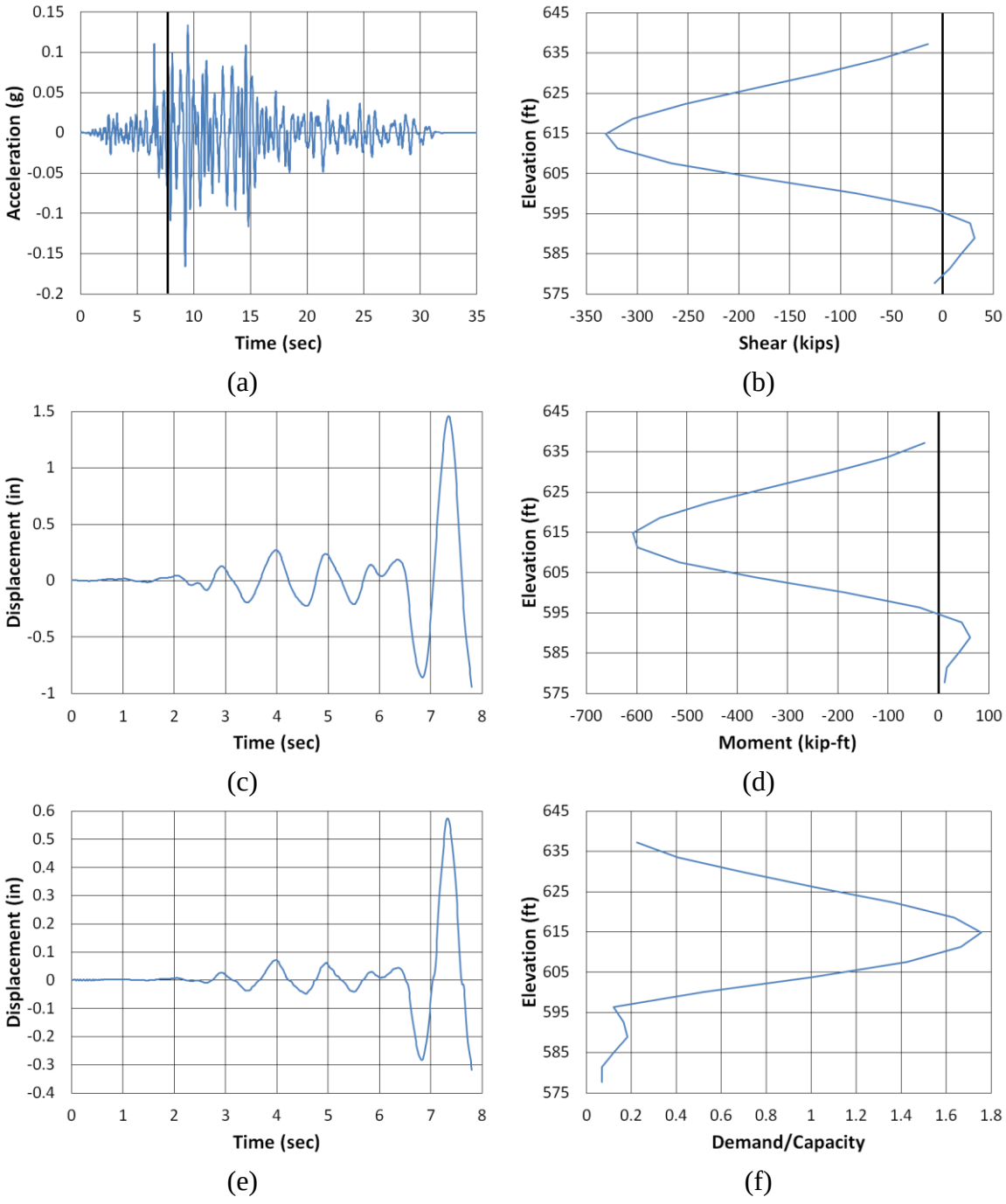

Figure B.86. Etowah County Transverse Coalinga North (a) time-history event, (b) shear distribution, (c) top of pier displacement, (d) moment distribution, (e) ground surface displacement, and (f) demand capacity ratio

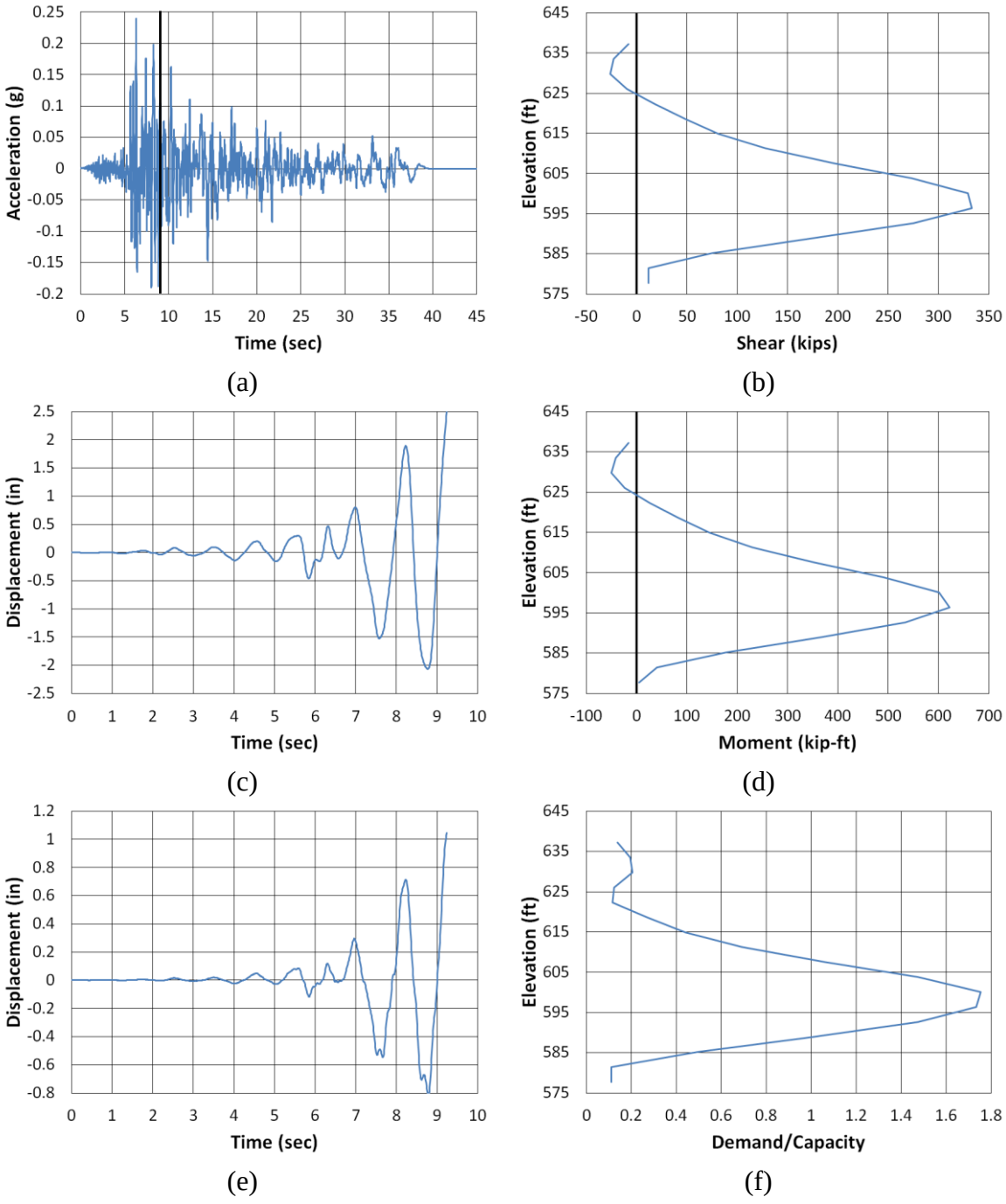

Figure B.87. Etowah County Transverse Imperial Valley NMCE (a) time-history event, (b) shear distribution, (c) top of pier displacement, (d) moment distribution, (e) ground surface displacement, and (f) demand capacity ratio

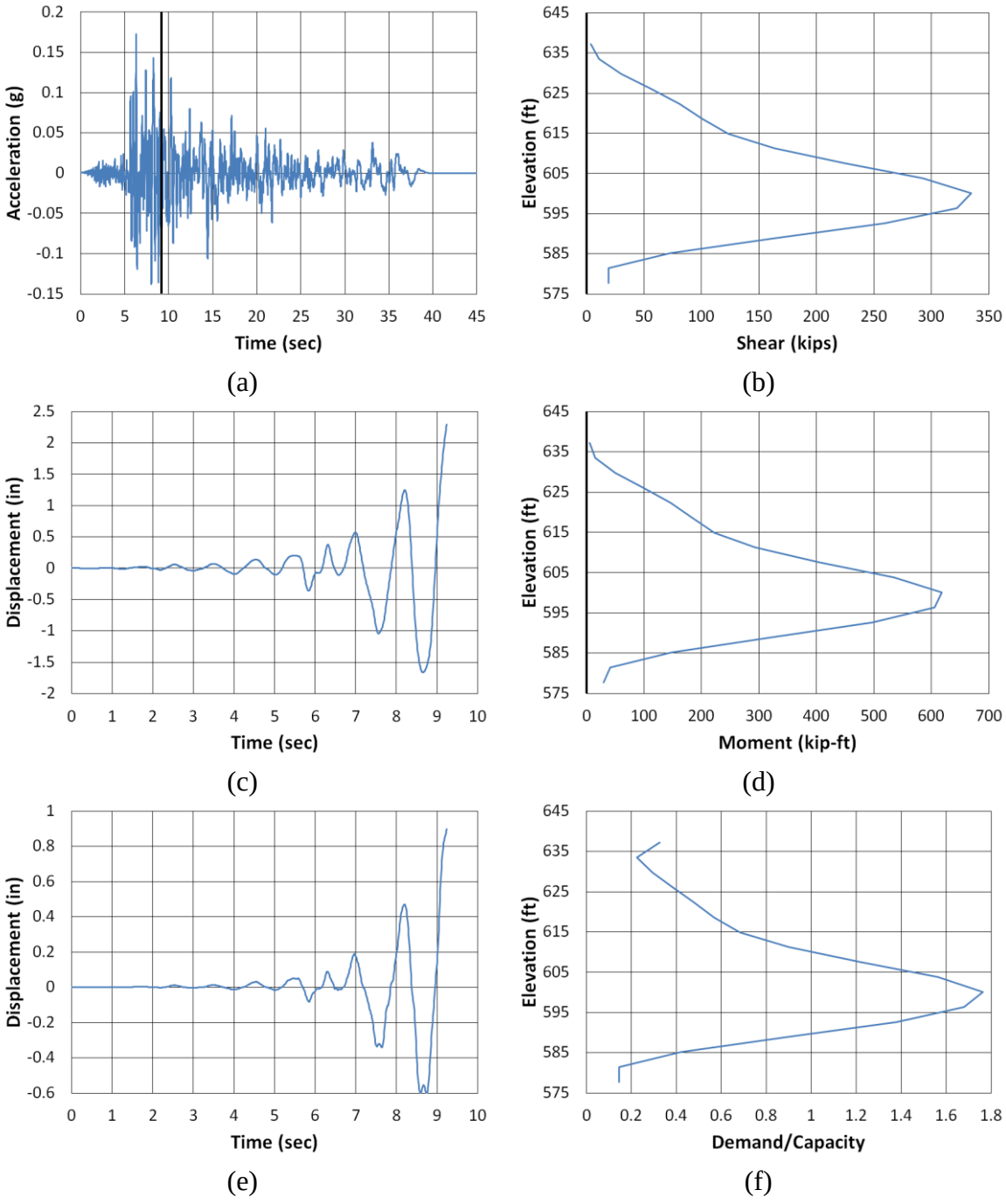

Figure B.88. Etowah County Transverse Imperial Valley North (a) time-history event, (b) shear distribution, (c) top of pier displacement, (d) moment distribution, (e) ground surface displacement, and (f) demand capacity ratio

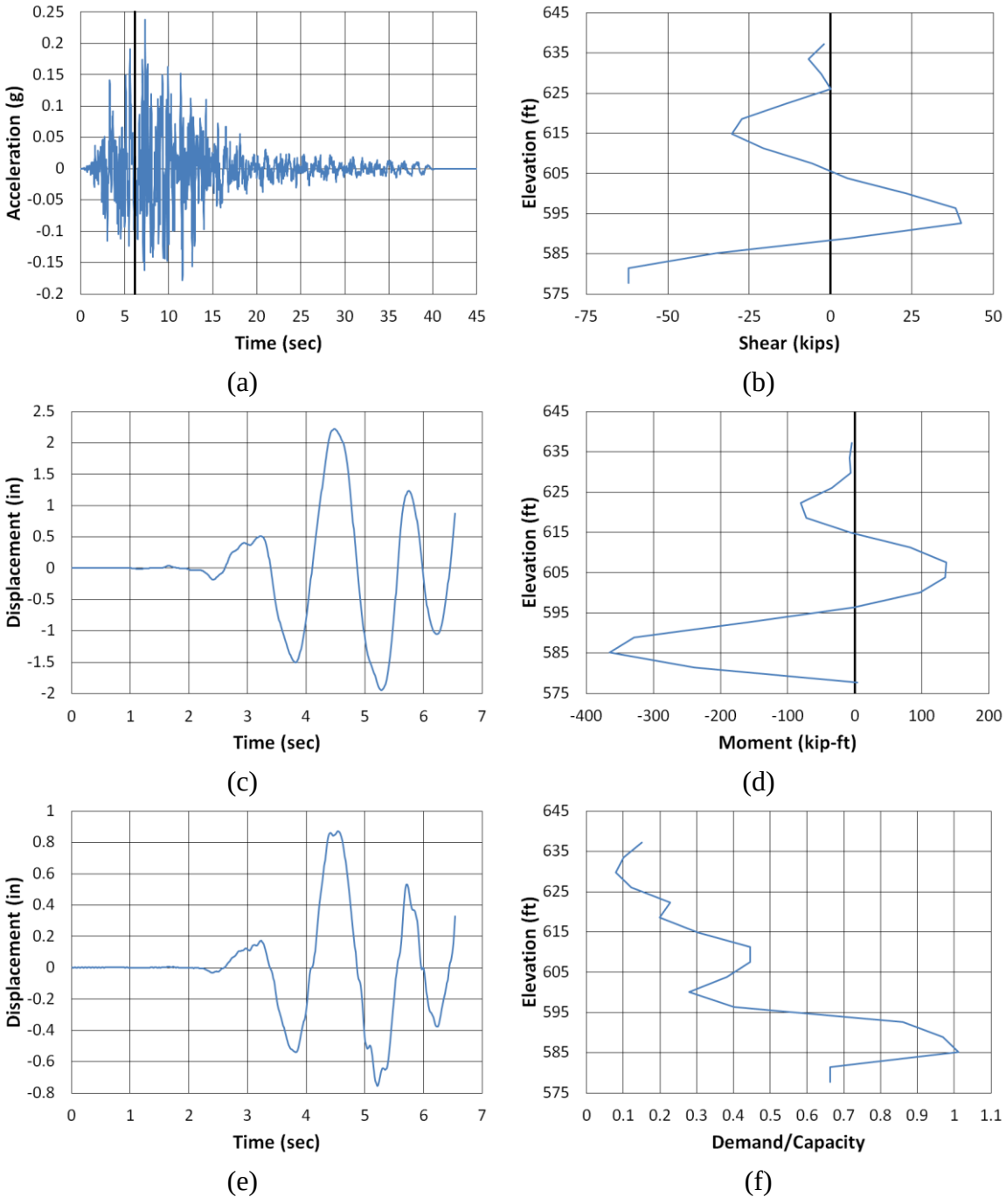

Figure B.89. Etowah County Transverse Kobe NMCE (a) time-history event, (b) shear distribution, (c) top of pier displacement, (d) moment distribution, (e) ground surface displacement, and (f) demand capacity ratio

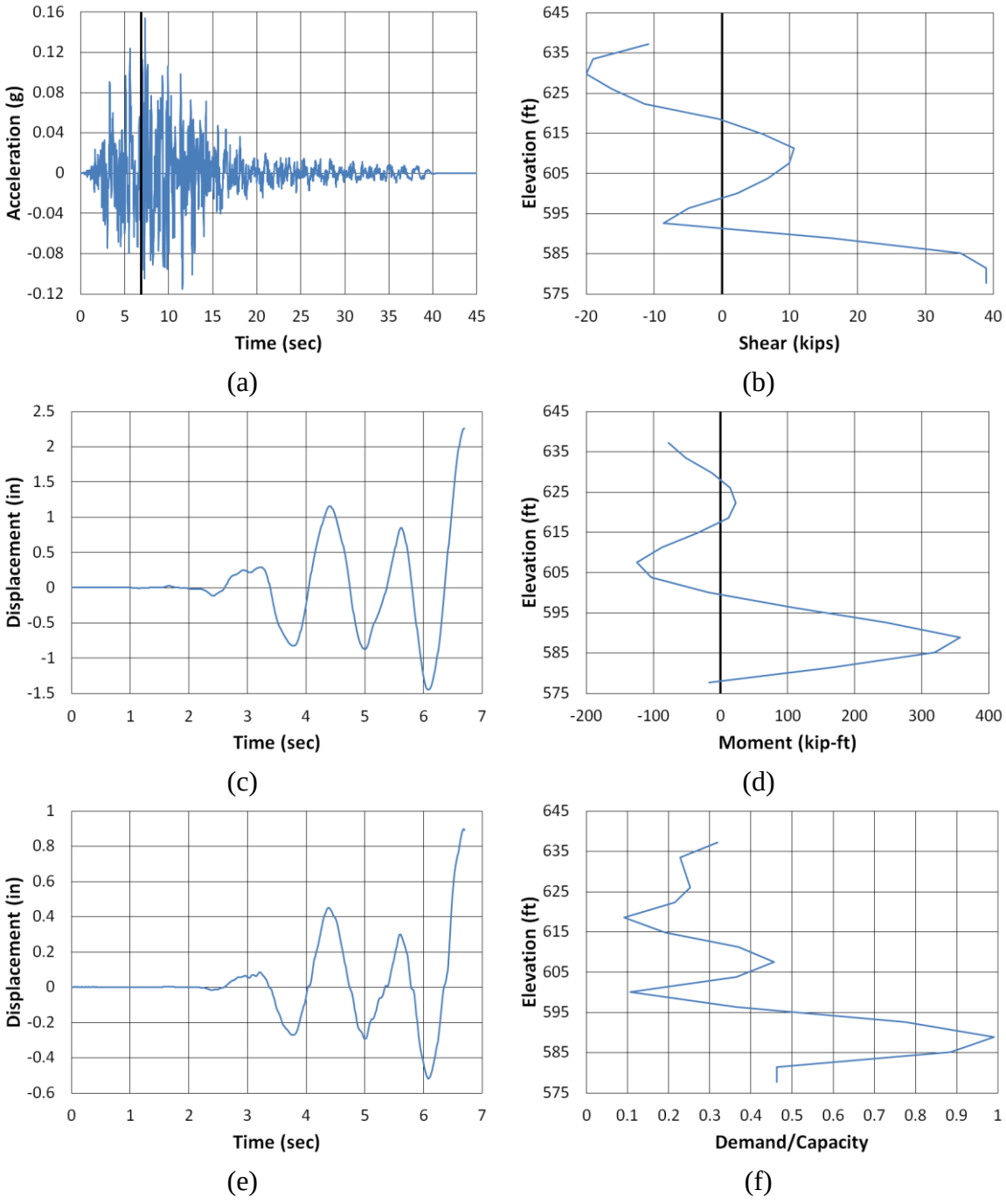

Figure B.90. Etowah County Transverse Kobe North (a) time-history event, (b) shear distribution, (c) top of pier displacement, (d) moment distribution, (e) ground surface displacement, and (f) demand capacity ratio

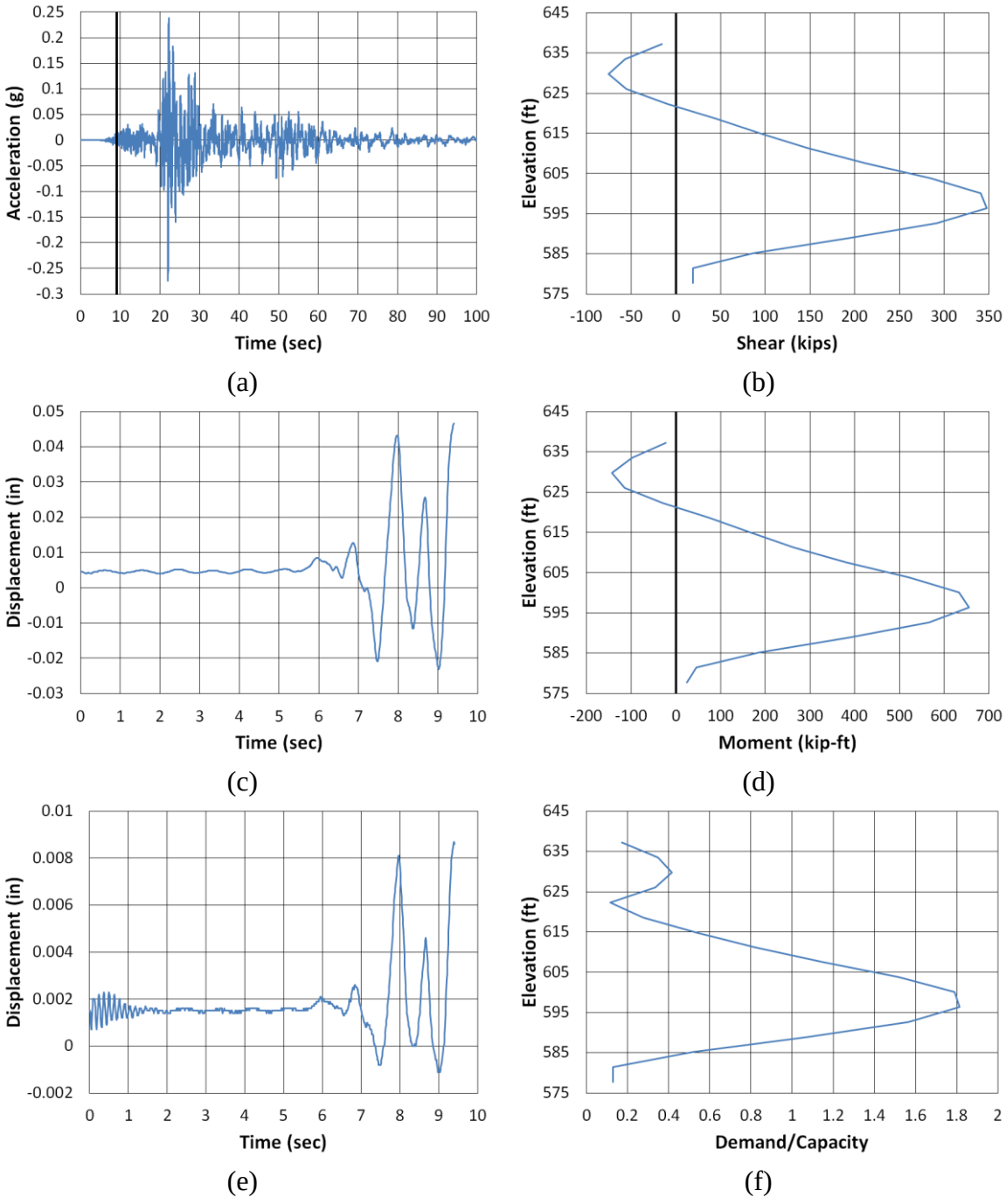

Figure B.91. Etowah County Transverse Kocaeli NMCE (a) time-history event, (b) shear distribution, (c) top of pier displacement, (d) moment distribution, (e) ground surface displacement, and (f) demand capacity ratio

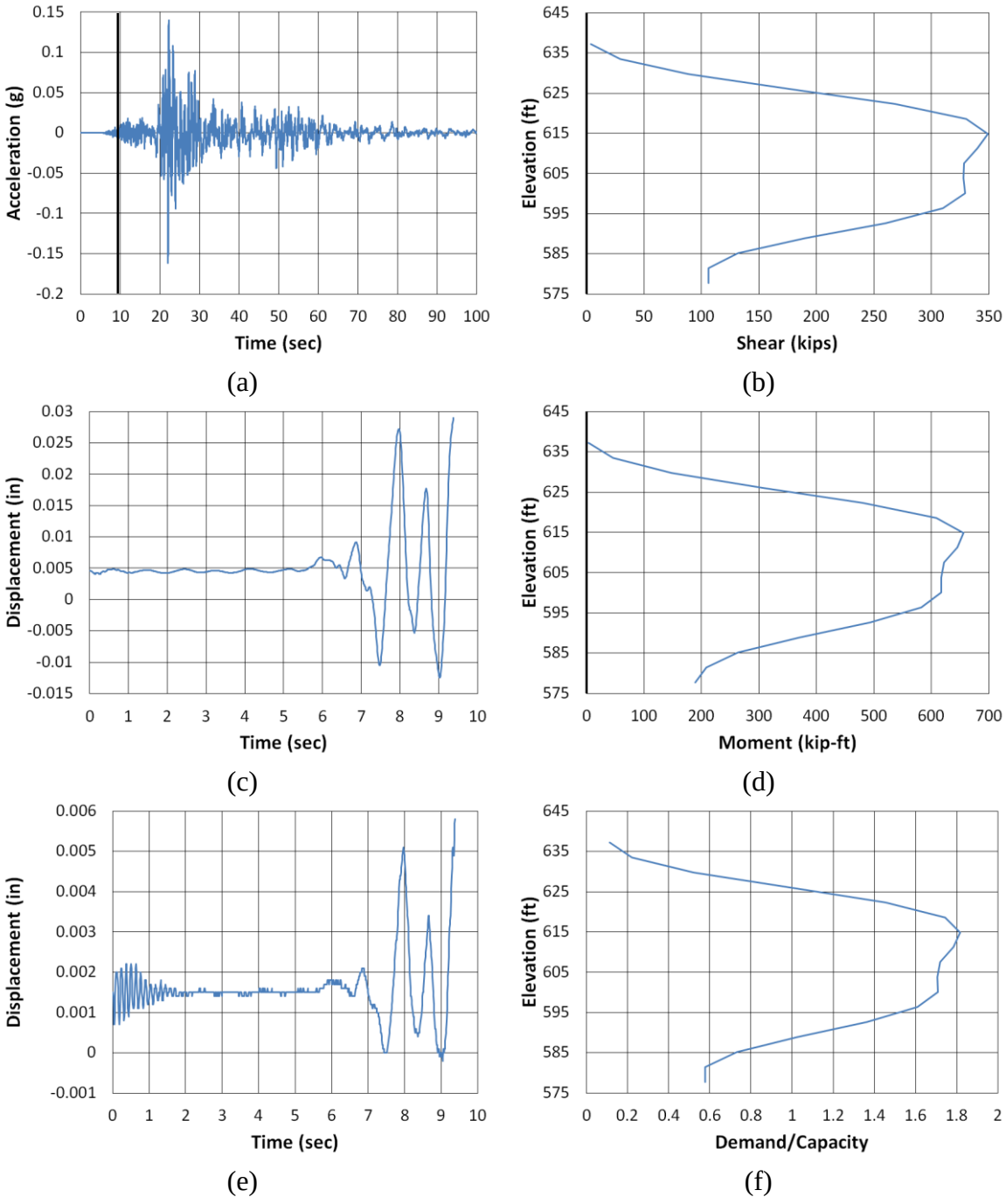

Figure B.92. Etowah County Transverse Kocaeli North (a) time-history event, (b) shear distribution, (c) top of pier displacement, (d) moment distribution, (e) ground surface displacement, and (f) demand capacity ratio

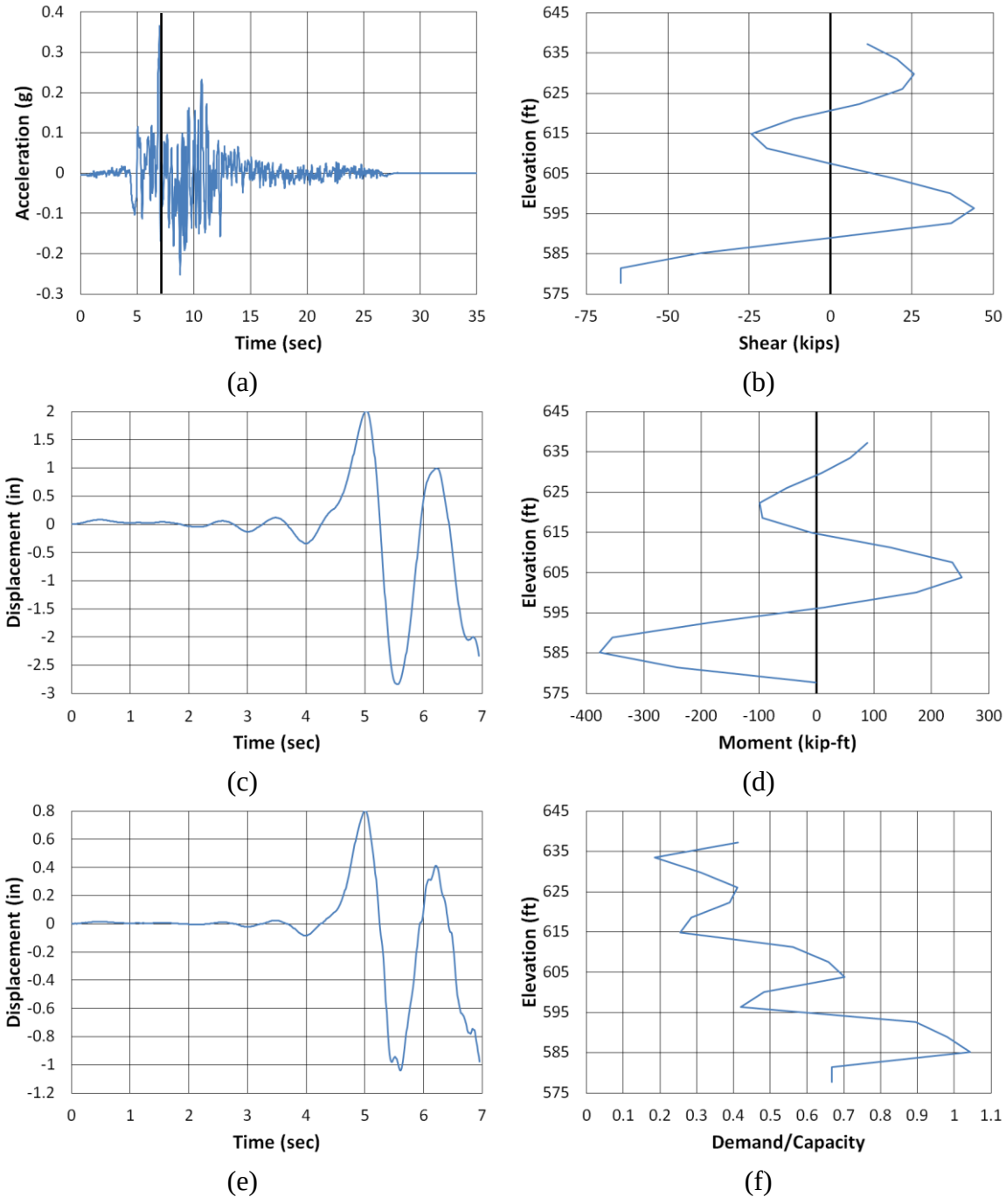

Figure B.93. Etowah County Transverse Kocaeli2 NMCE (a) time-history event, (b) shear distribution, (c) top of pier displacement, (d) moment distribution, (e) ground surface displacement, and (f) demand capacity ratio

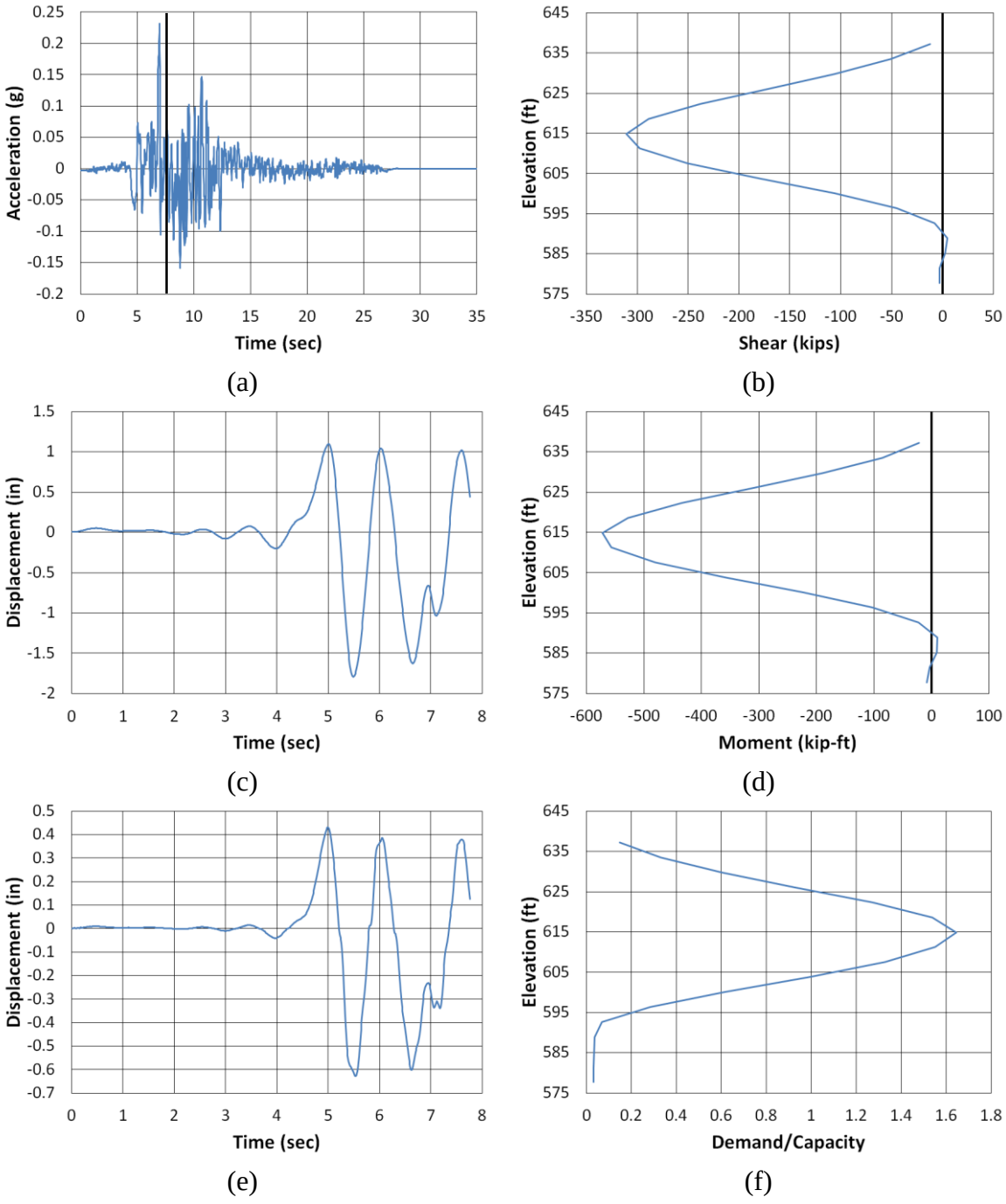

Figure B.94. Etowah County Transverse Kocaeli2 North (a) time-history event, (b) shear distribution, (c) top of pier displacement, (d) moment distribution, (e) ground surface displacement, and (f) demand capacity ratio

.

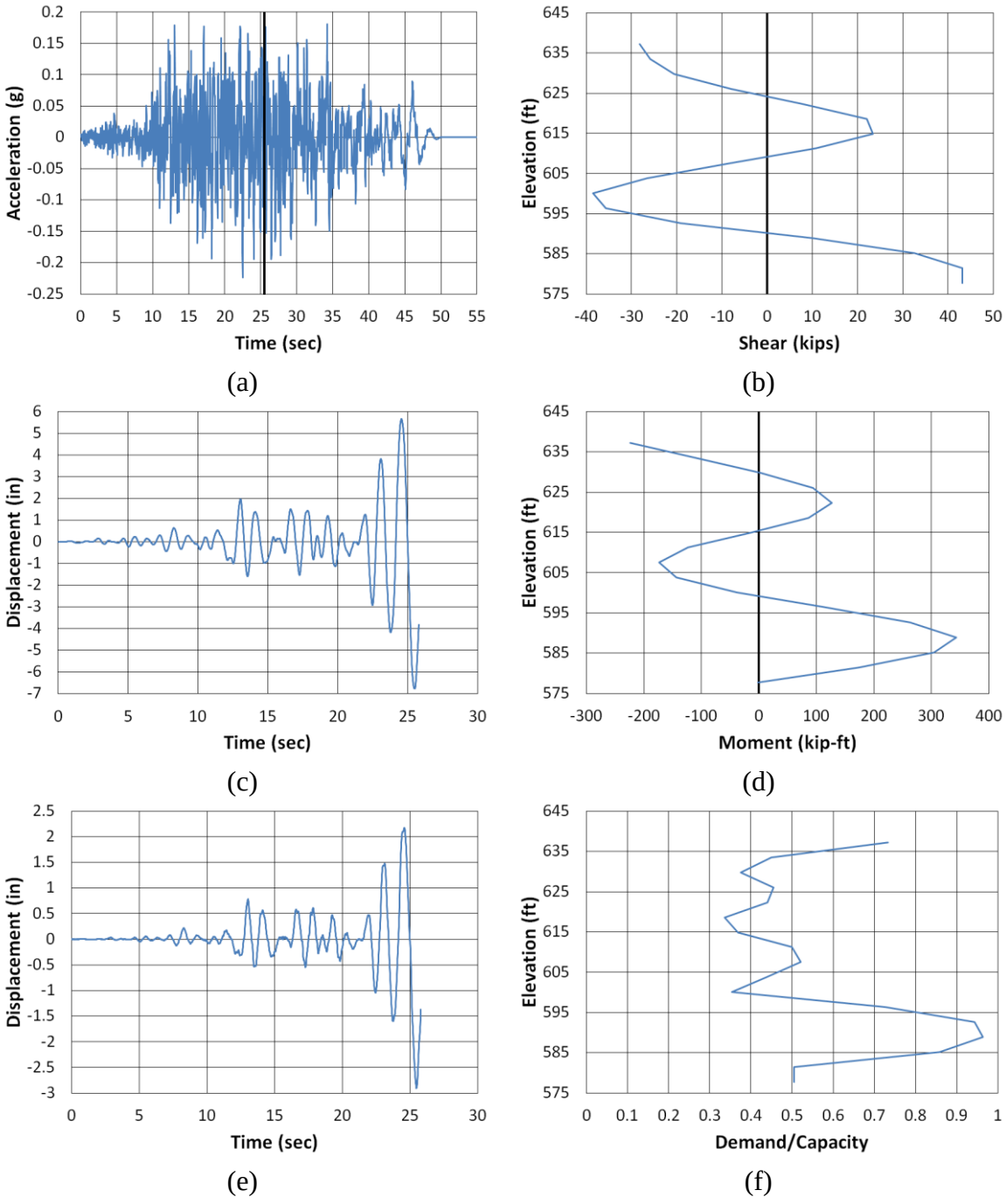

Figure B.95. Etowah County Transverse Landers NMCE (a) time-history event, (b) shear distribution, (c) top of pier displacement, (d) moment distribution, (e) ground surface displacement, and (f) demand capacity ratio

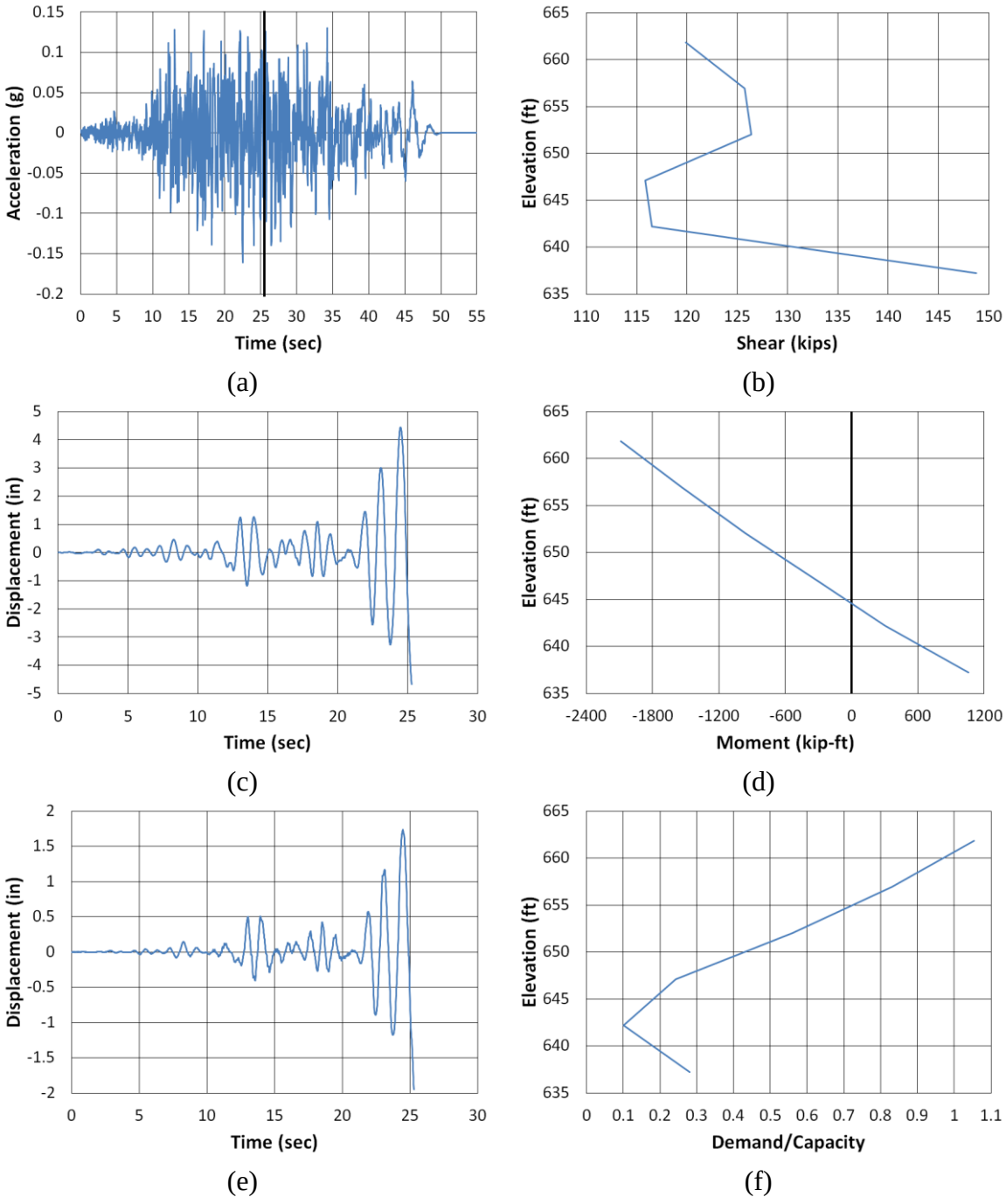

Figure B.96. Etowah County Transverse Landers North (column) (a) time-history event, (b) shear distribution, (c) top of pier displacement, (d) moment distribution, (e) ground surface displacement, and (f) demand capacity ratio

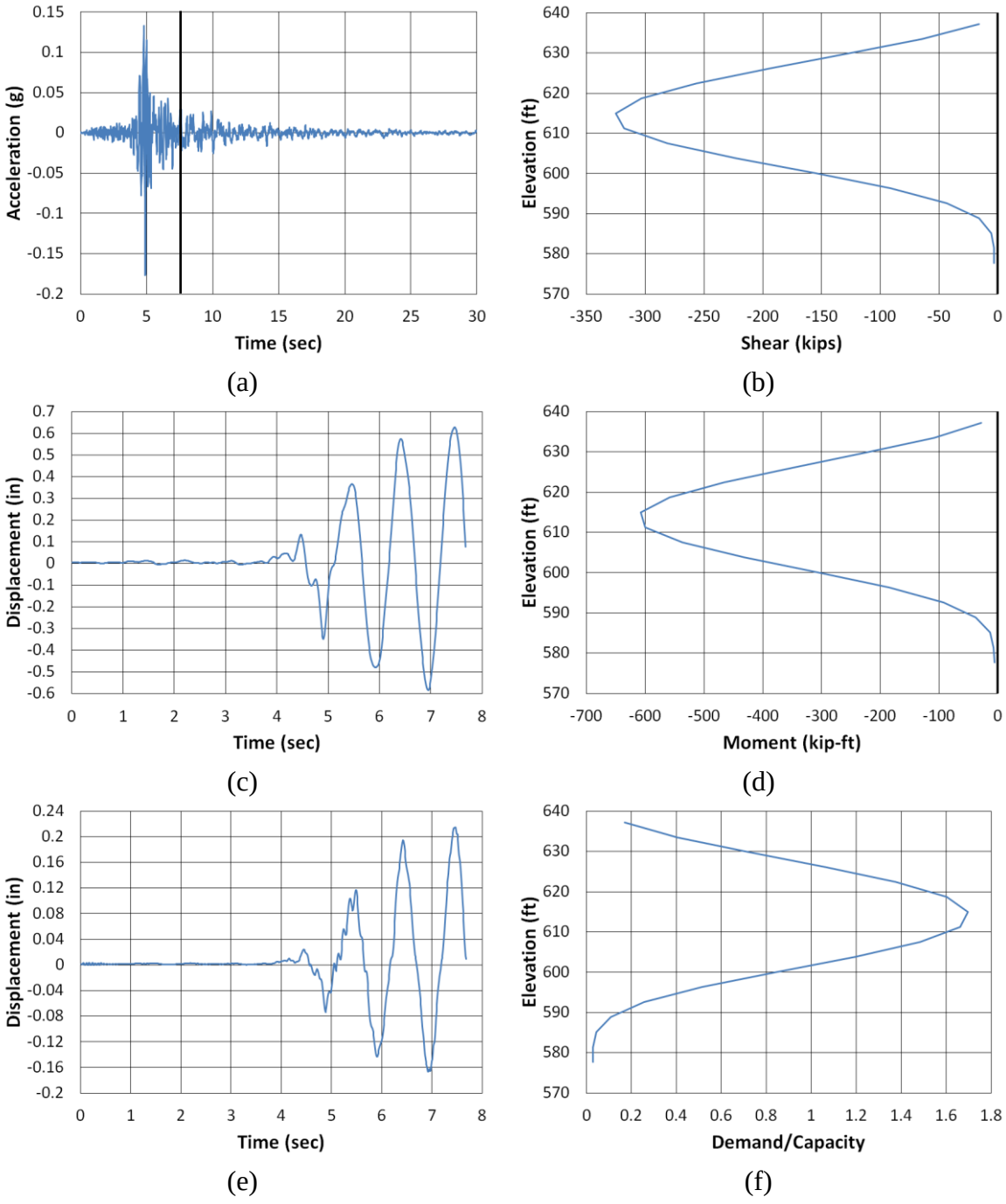

Figure B.97. Etowah County Transverse LSM North (a) time-history event, (b) shear distribution, (c) top of pier displacement, (d) moment distribution, (e) ground surface displacement, and (f) demand capacity ratio

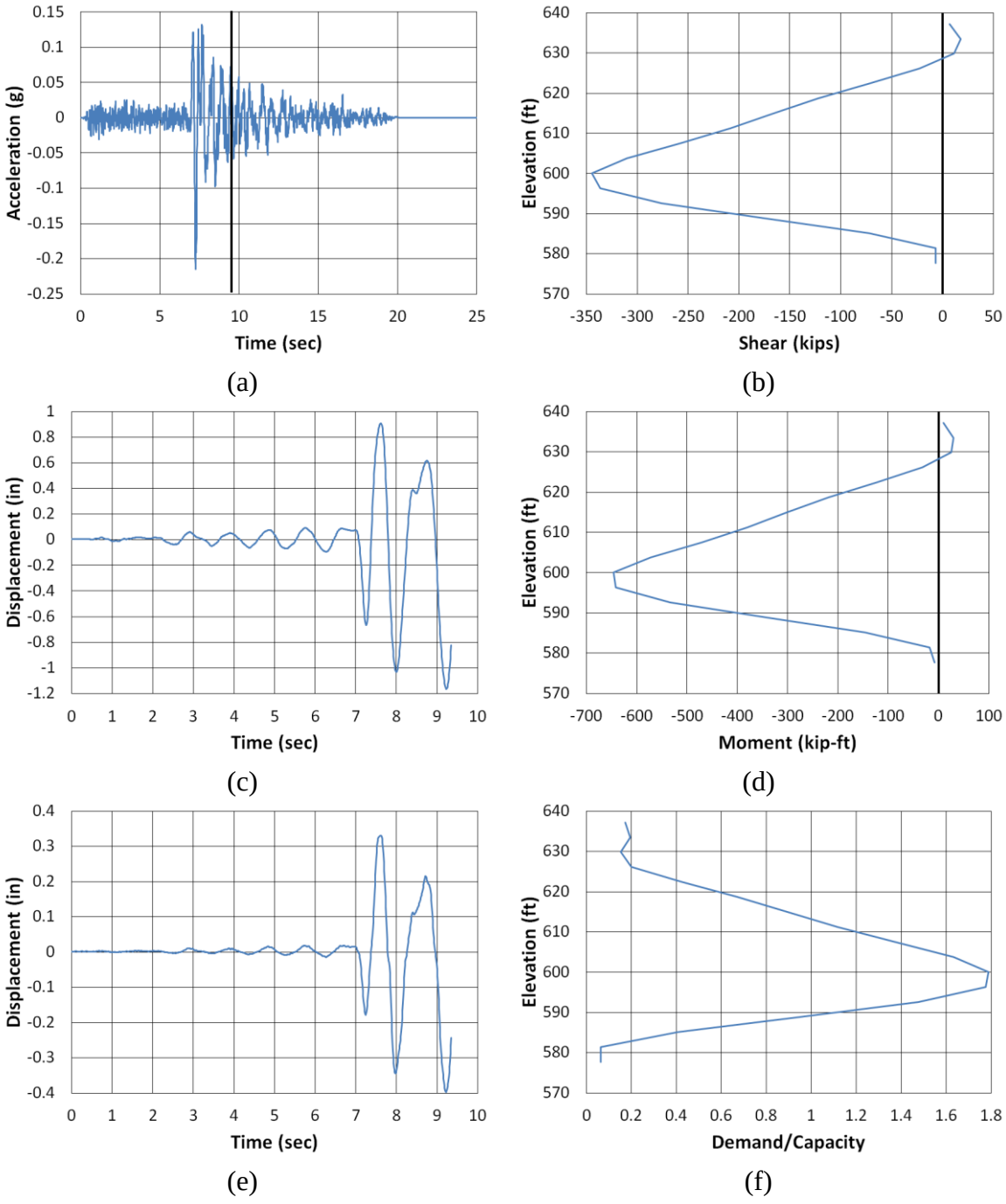

Figure B.98. Etowah County Transverse NPS North (a) time-history event, (b) shear distribution, (c) top of pier displacement, (d) moment distribution, (e) ground surface displacement, and (f) demand capacity ratio

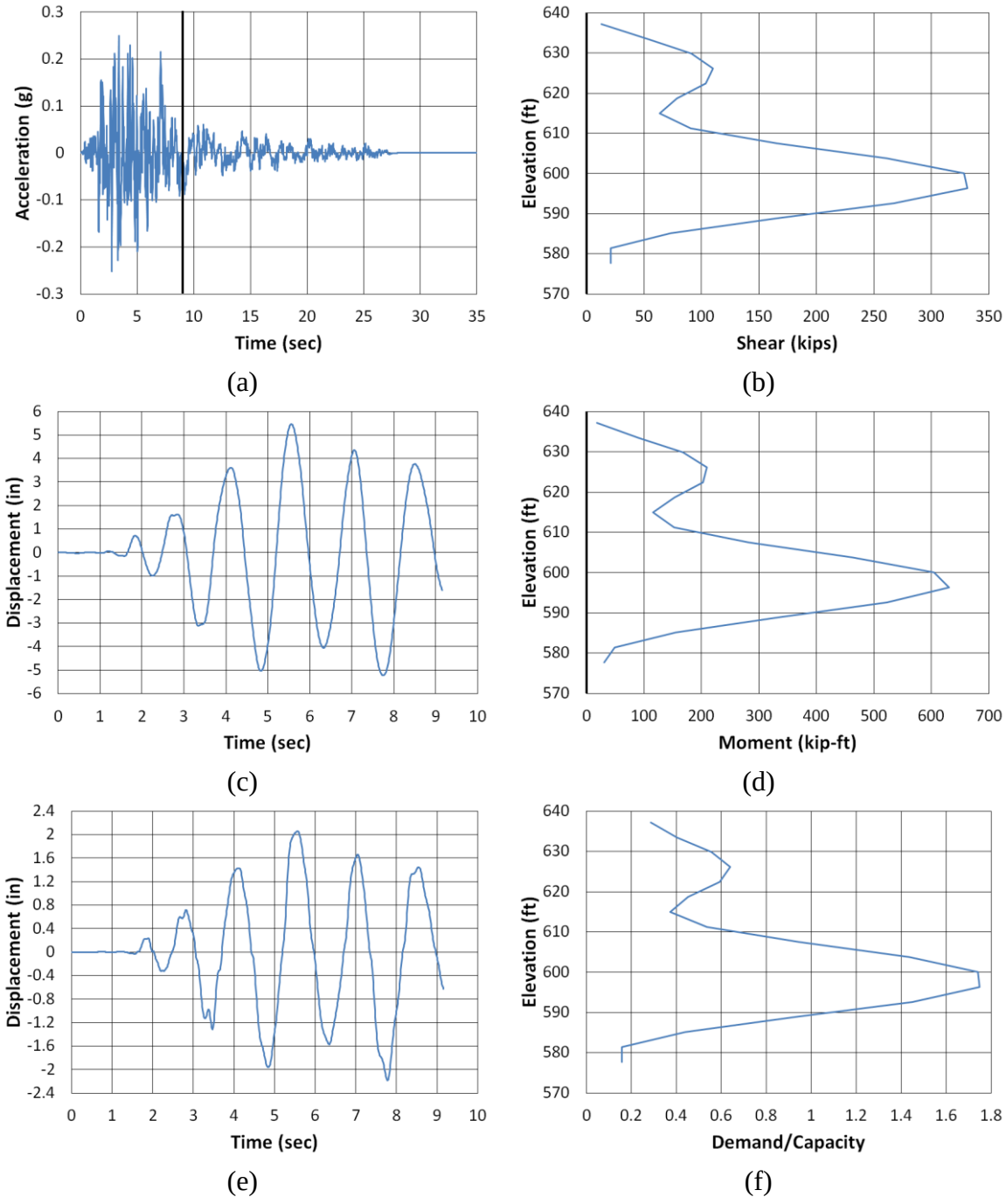

Figure B.99. Etowah County Transverse San Fernando NMCE (a) time-history event, (b) shear distribution, (c) top of pier displacement, (d) moment distribution, (e) ground surface displacement, and (f) demand capacity ratio

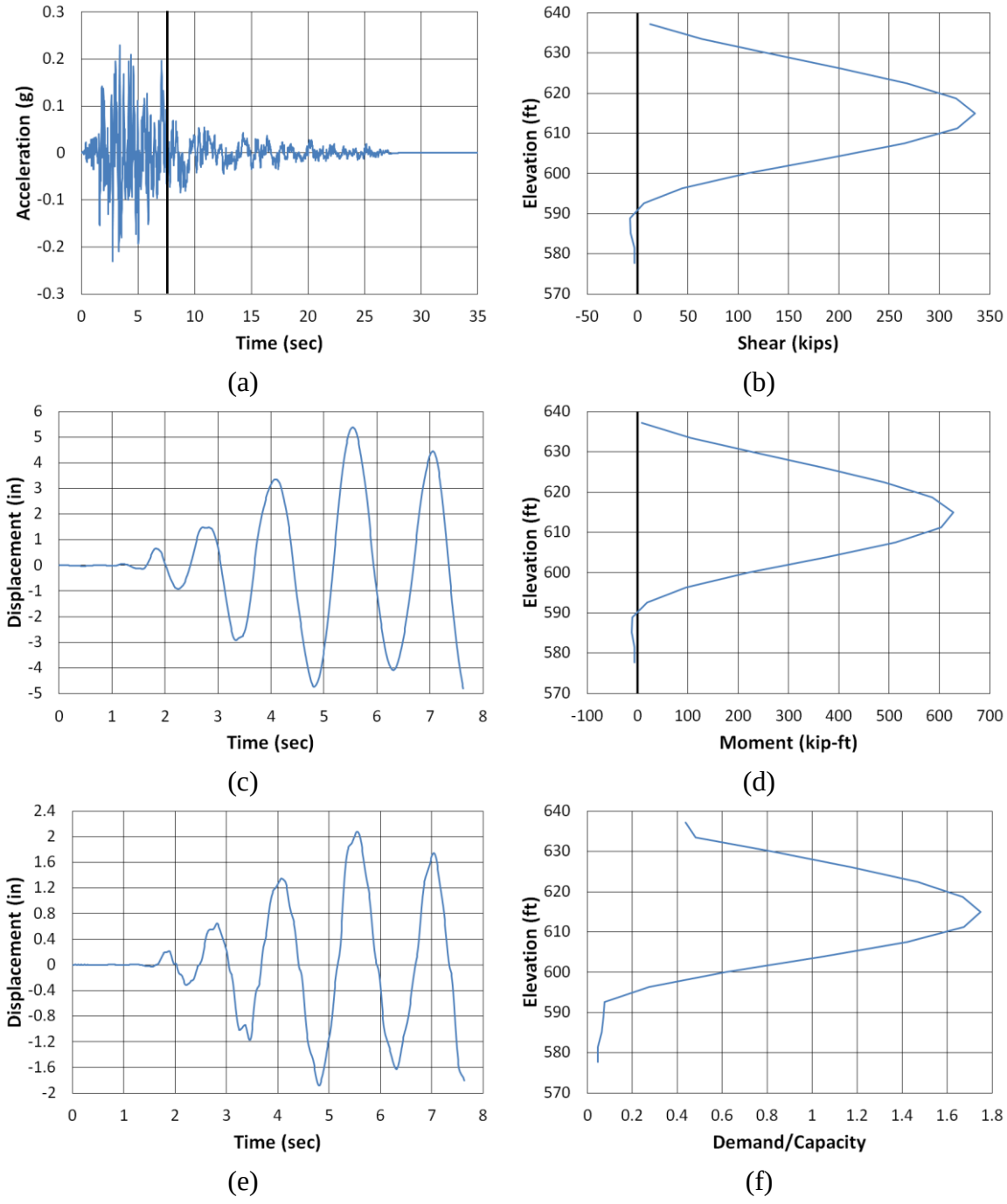

Figure B.100. Etowah County Transverse San Fernando North (a) time-history event, (b) shear distribution, (c) top of pier displacement, (d) moment distribution, (e) ground surface displacement, and (f) demand capacity ratio

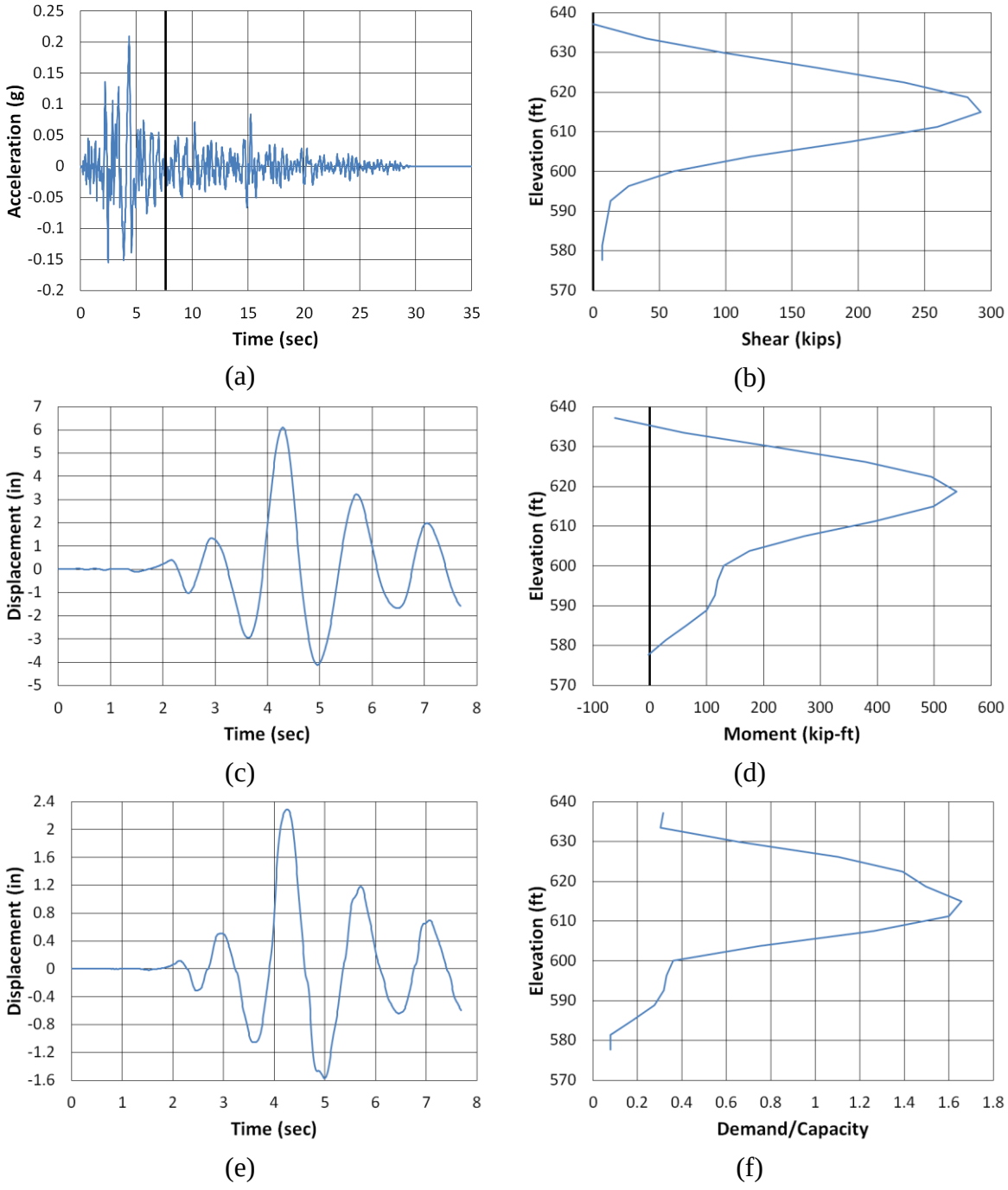

Figure B.101. Etowah County Transverse San Fernando2 NMCE (a) time-history event, (b) shear distribution, (c) top of pier displacement, (d) moment distribution, (e) ground surface displacement, and (f) demand capacity ratio

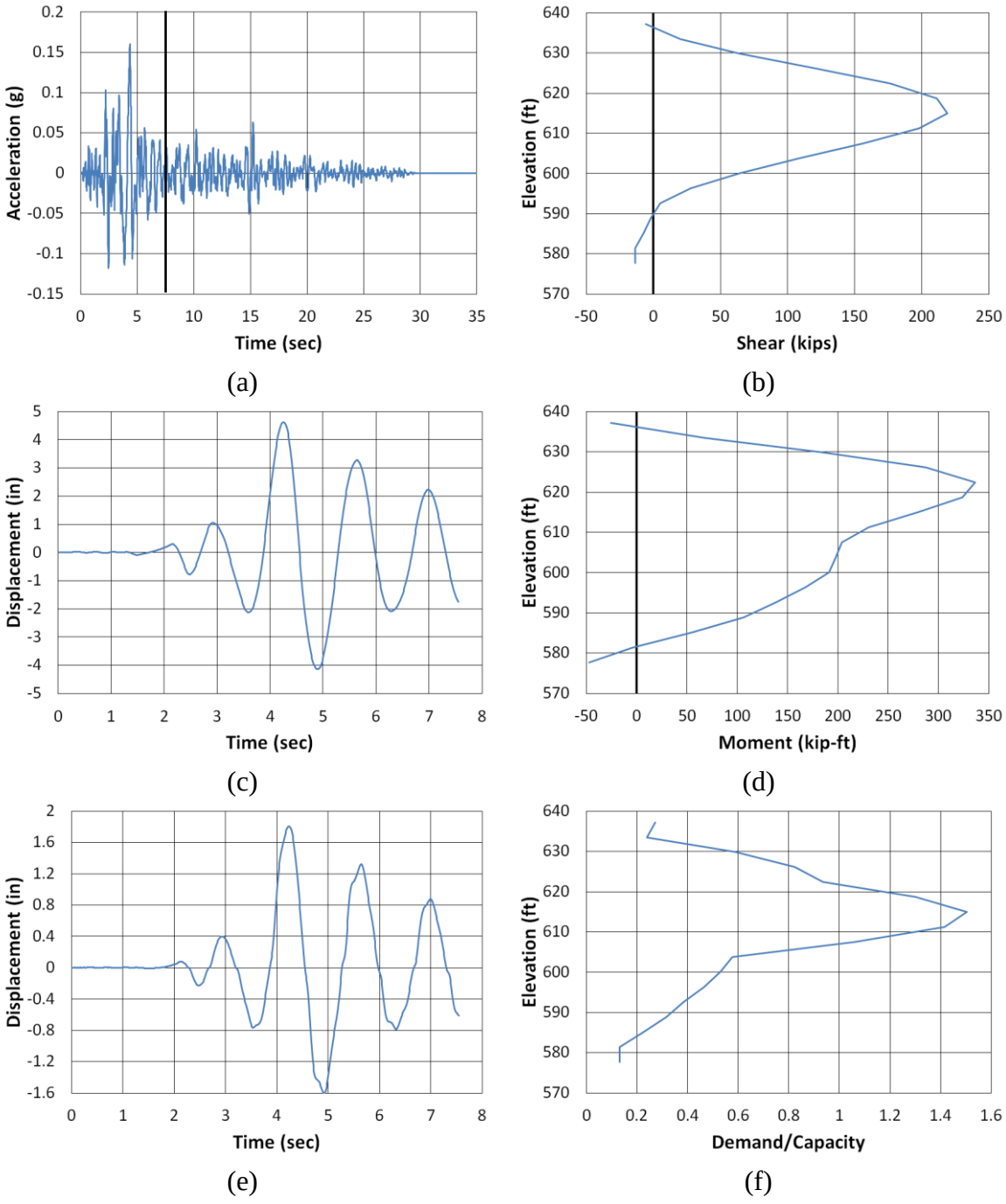

Figure B.102. Etowah County Transverse San Fernando2 North (a) time-history event, (b) shear distribution, (c) top of pier displacement, (d) moment distribution, (e) ground surface displacement, and (f) demand capacity ratio

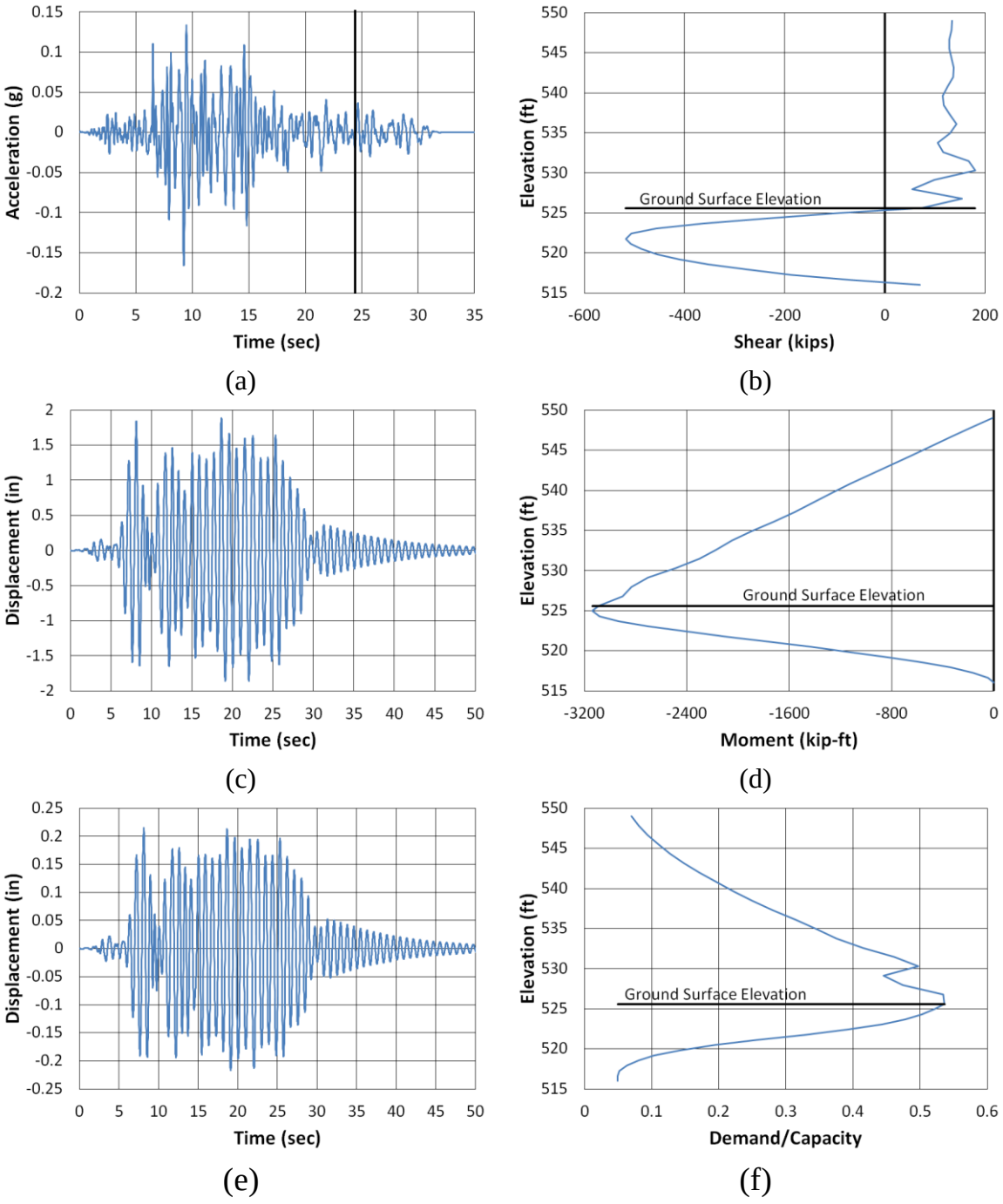

Figure B.103. Franklin County Longitudinal Coalinga North (a) time-history event, (b) shear distribution, (c) top of pier displacement, (d) moment distribution, (e) ground surface displacement, and (f) demand capacity ratio

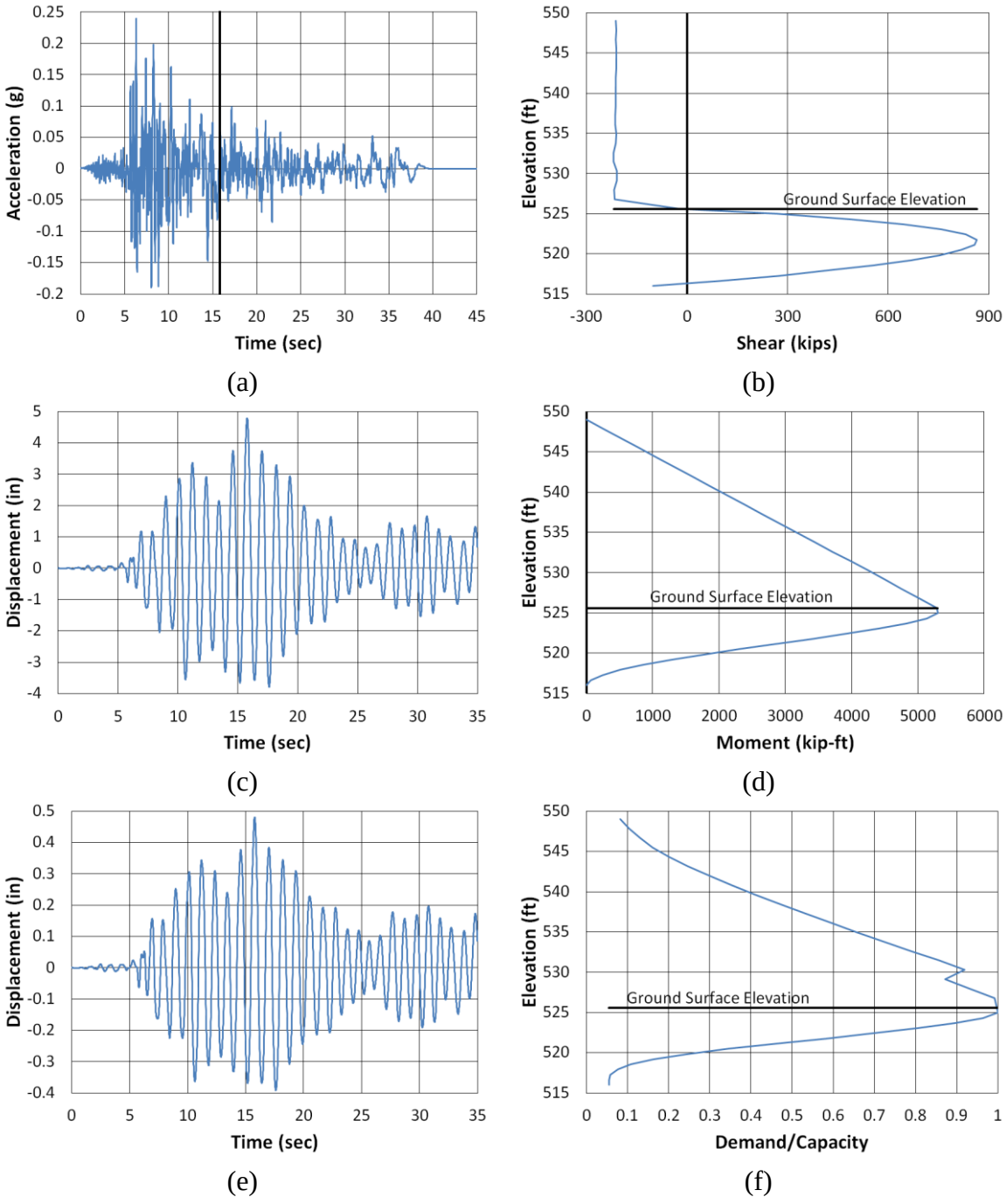

Figure B.104. Franklin County Longitudinal Imperial Valley NMCE (a) time-history event, (b) shear distribution, (c) top of pier displacement, (d) moment distribution, (e) ground surface displacement, and (f) demand capacity ratio

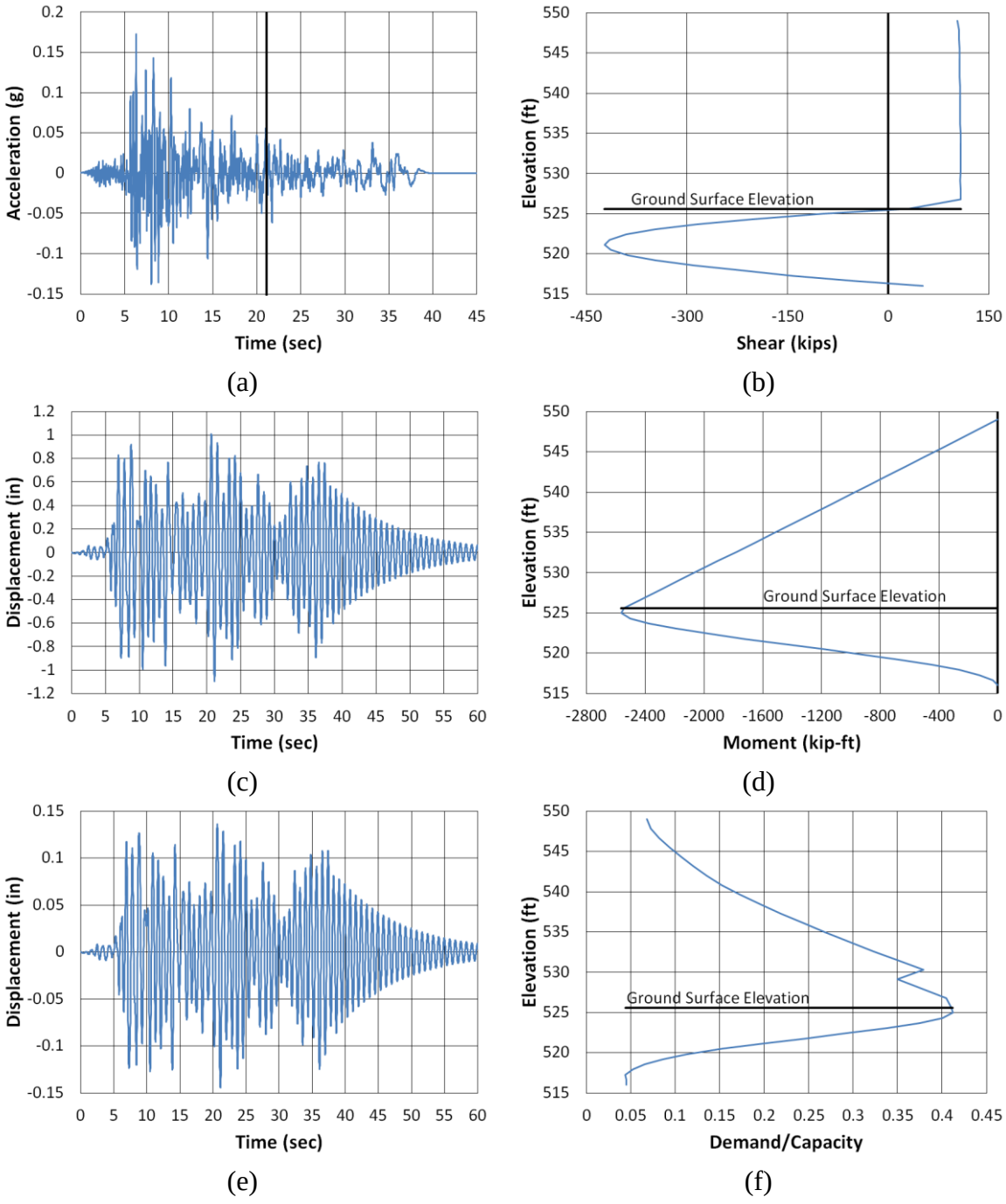

Figure B.105. Franklin County Longitudinal Imperial Valley North (a) time-history event, (b) shear distribution, (c) top of pier displacement, (d) moment distribution, (e) ground surface displacement, and (f) demand capacity ratio

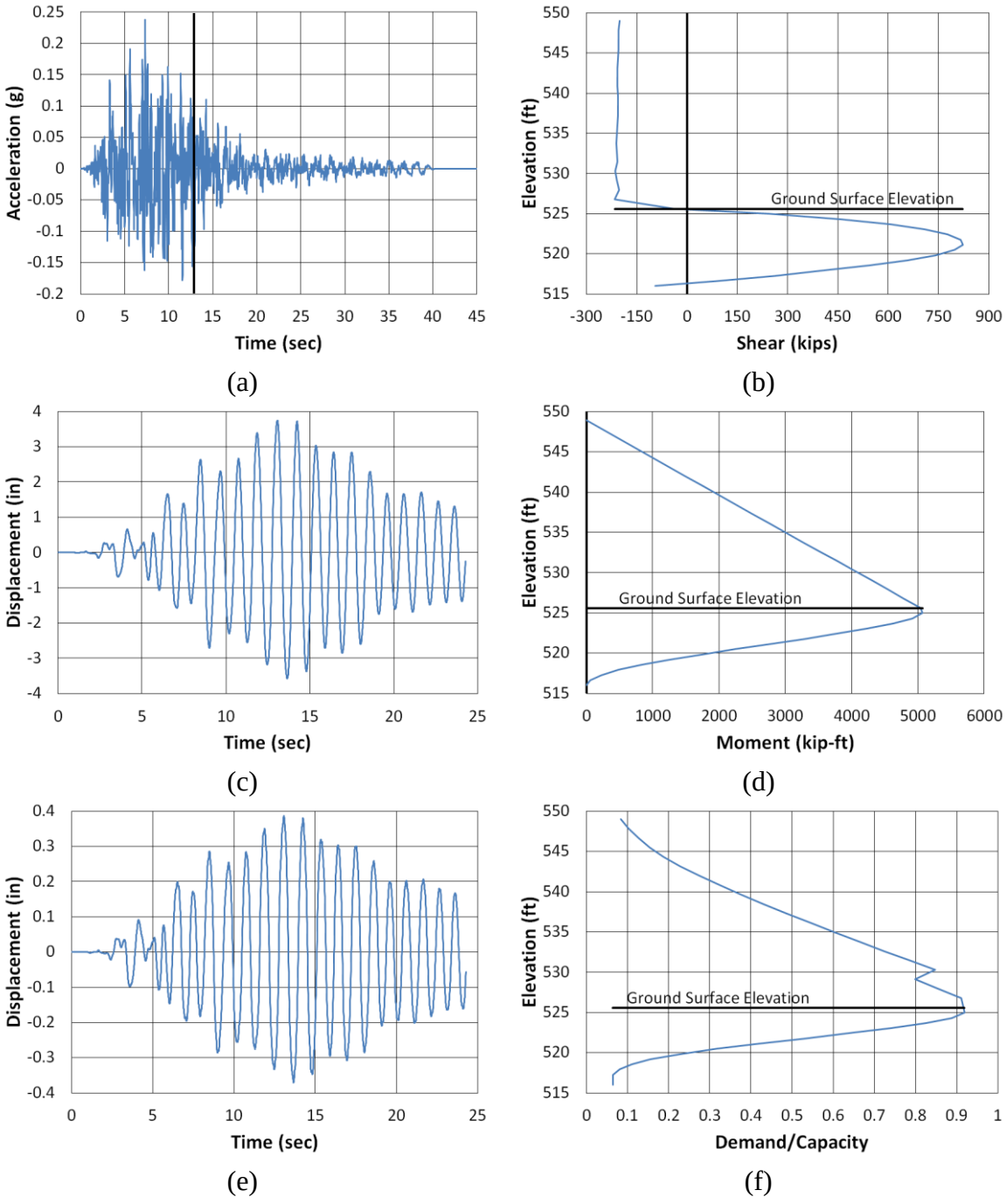

Figure B.106. Franklin County Longitudinal Kobe NMCE (a) time-history event, (b) shear distribution, (c) top of pier displacement, (d) moment distribution, (e) ground surface displacement, and (f) demand capacity ratio

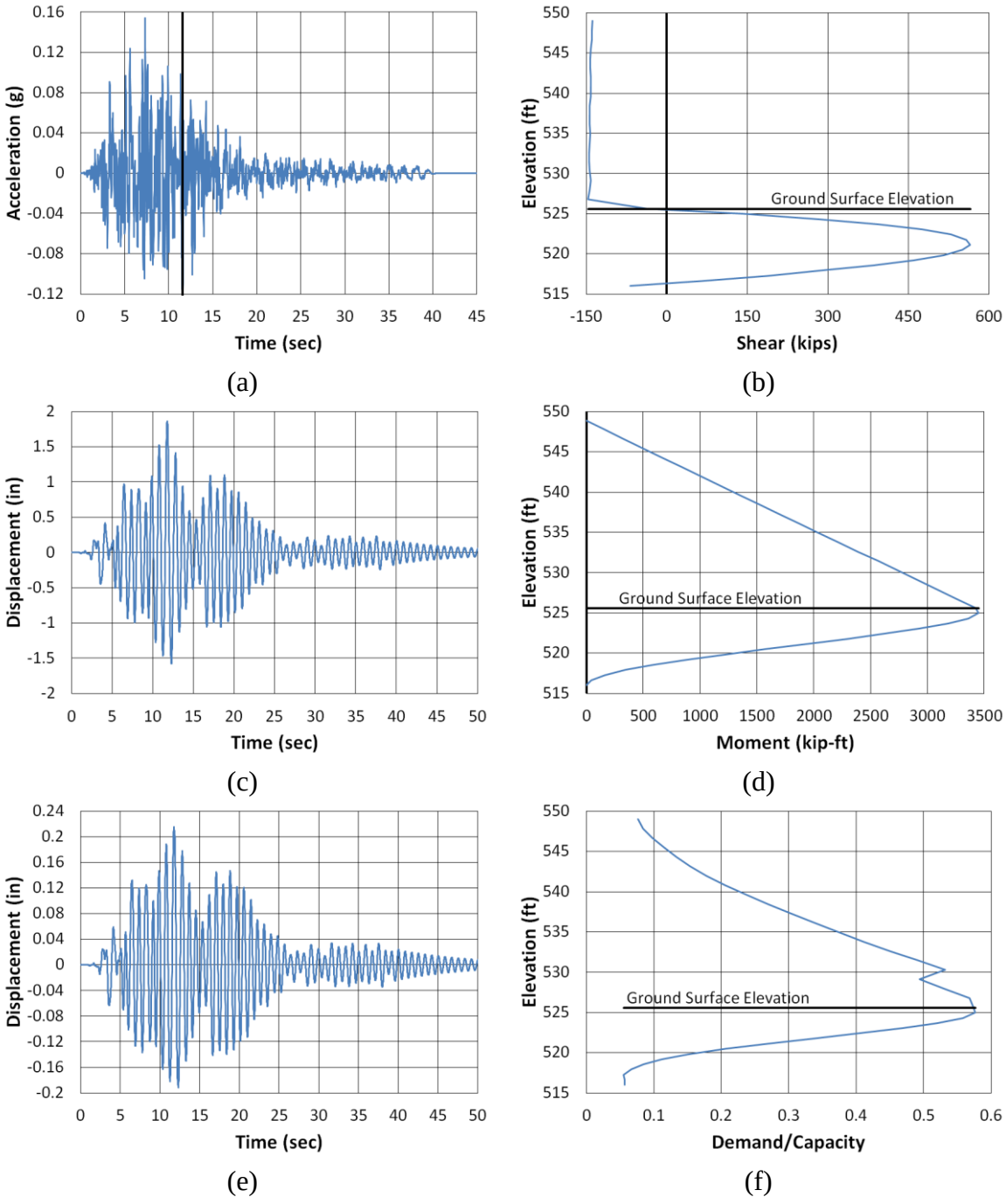

Figure B.107. Franklin County Longitudinal Kobe North (a) time-history event, (b) shear distribution, (c) top of pier displacement, (d) moment distribution, (e) ground surface displacement, and (f) demand capacity ratio

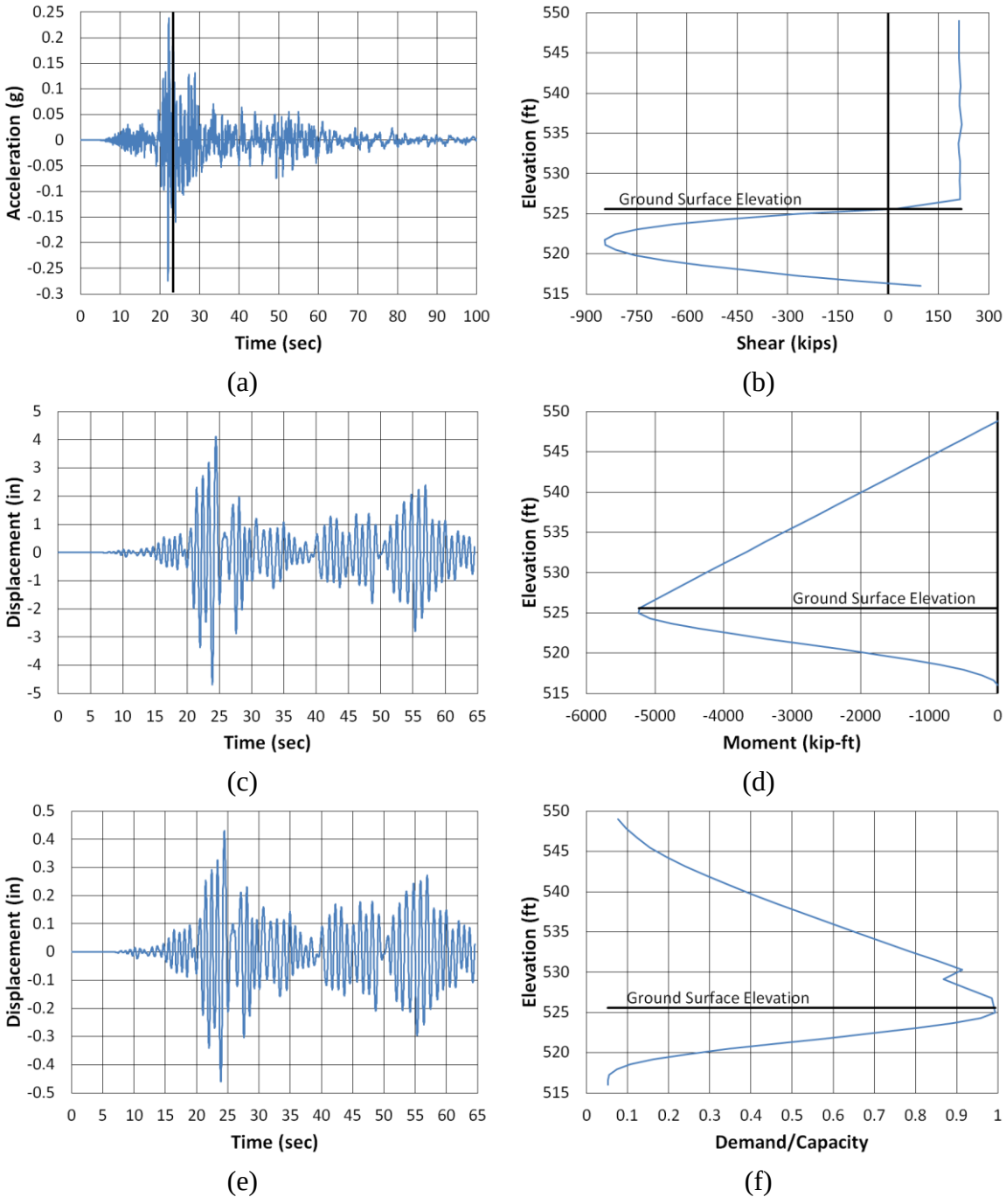

Figure B.108. Franklin County Longitudinal Kocaeli NMCE (a) time-history event, (b) shear distribution, (c) top of pier displacement, (d) moment distribution, (e) ground surface displacement, and (f) demand capacity ratio

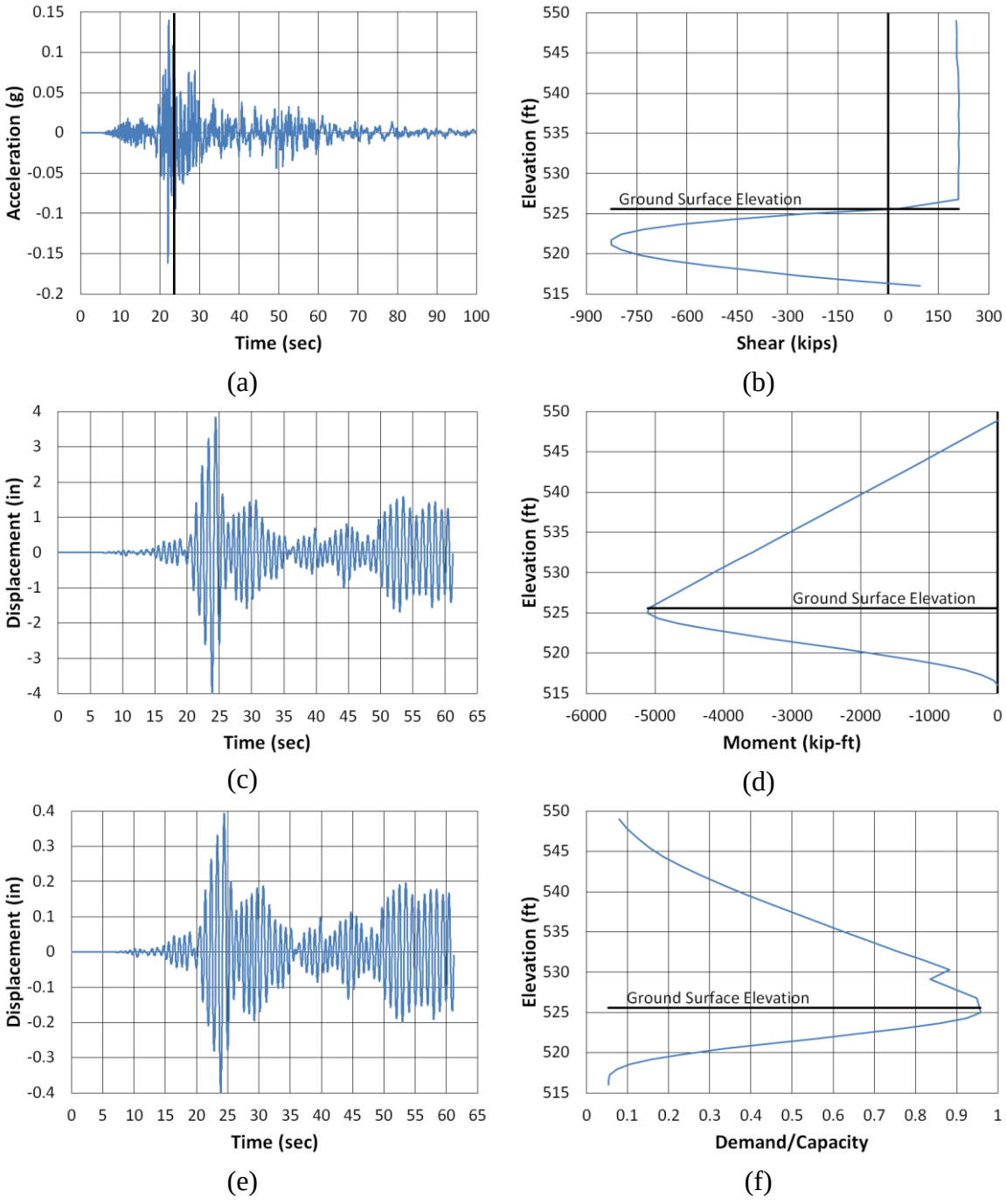

Figure B.109. Franklin County Longitudinal Kocaeli North (a) time-history event, (b) shear distribution, (c) top of pier displacement, (d) moment distribution, (e) ground surface displacement, and (f) demand capacity ratio

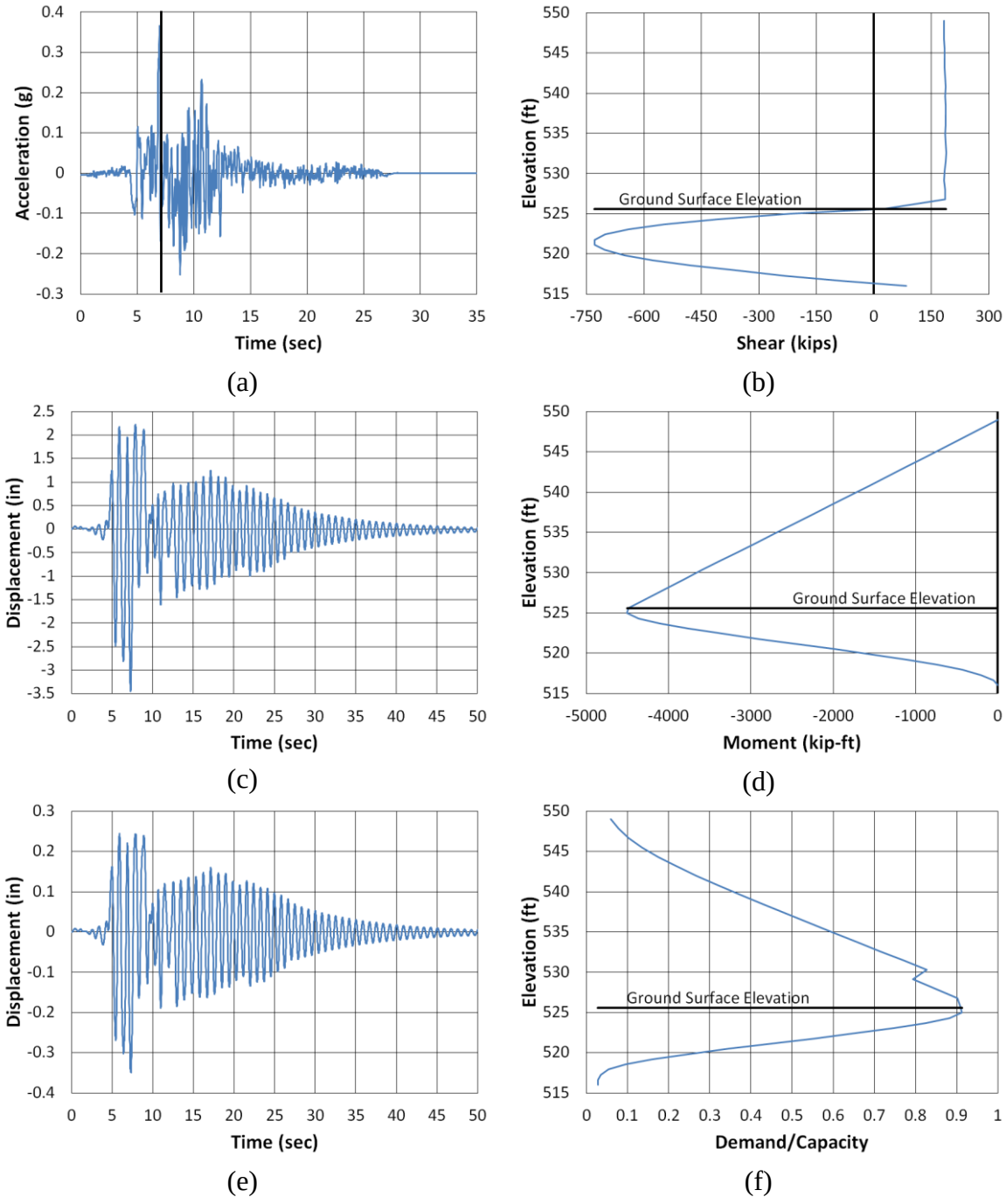

Figure B.110. Franklin County Longitudinal Kocaeli2 NMCE (a) time-history event, (b) shear distribution, (c) top of pier displacement, (d) moment distribution, (e) ground surface displacement, and (f) demand capacity ratio

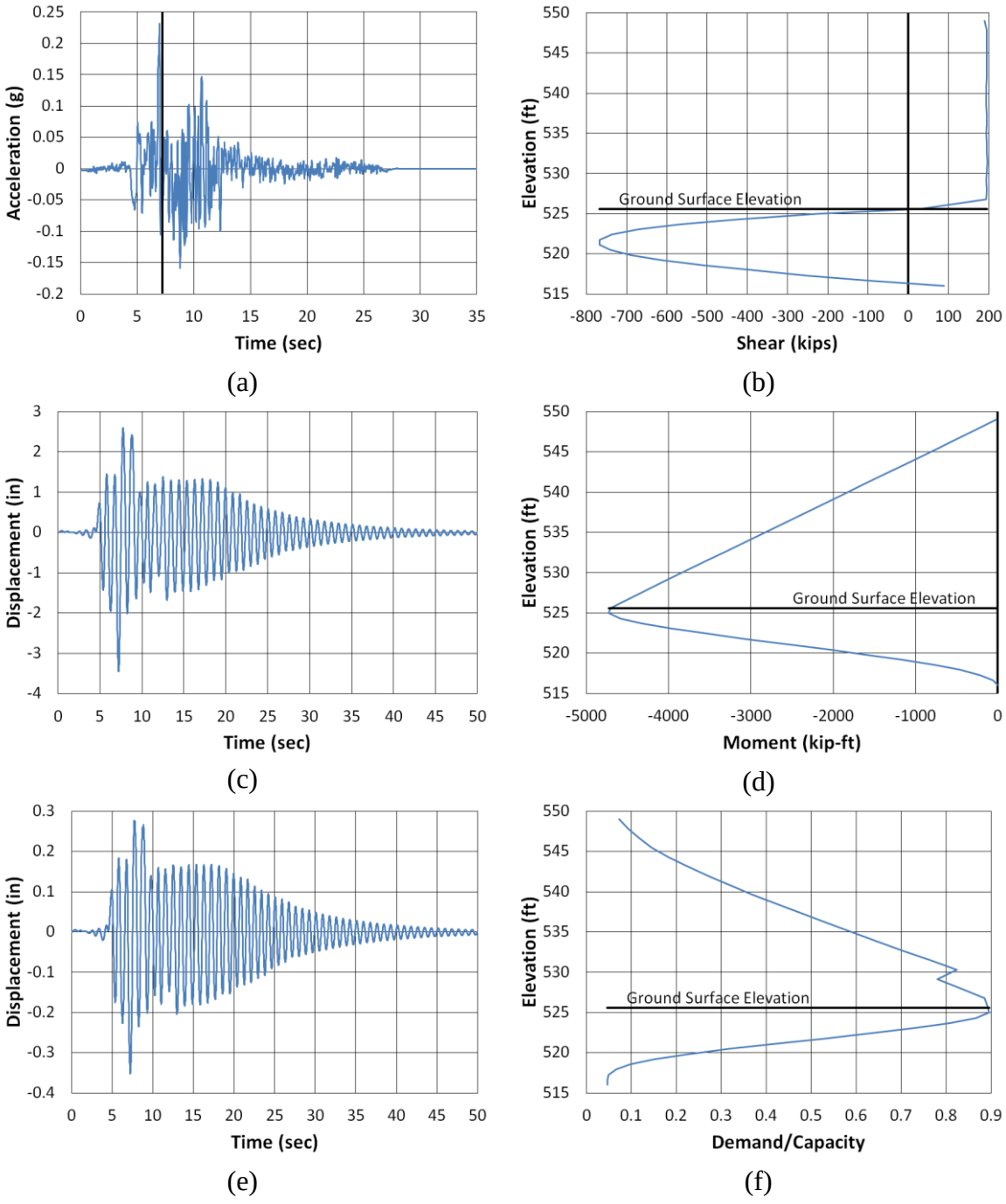

Figure B.111. Franklin County Longitudinal Kocaeli2 North (a) time-history event, (b) shear distribution, (c) top of pier displacement, (d) moment distribution, (e) ground surface displacement, and (f) demand capacity ratio

.

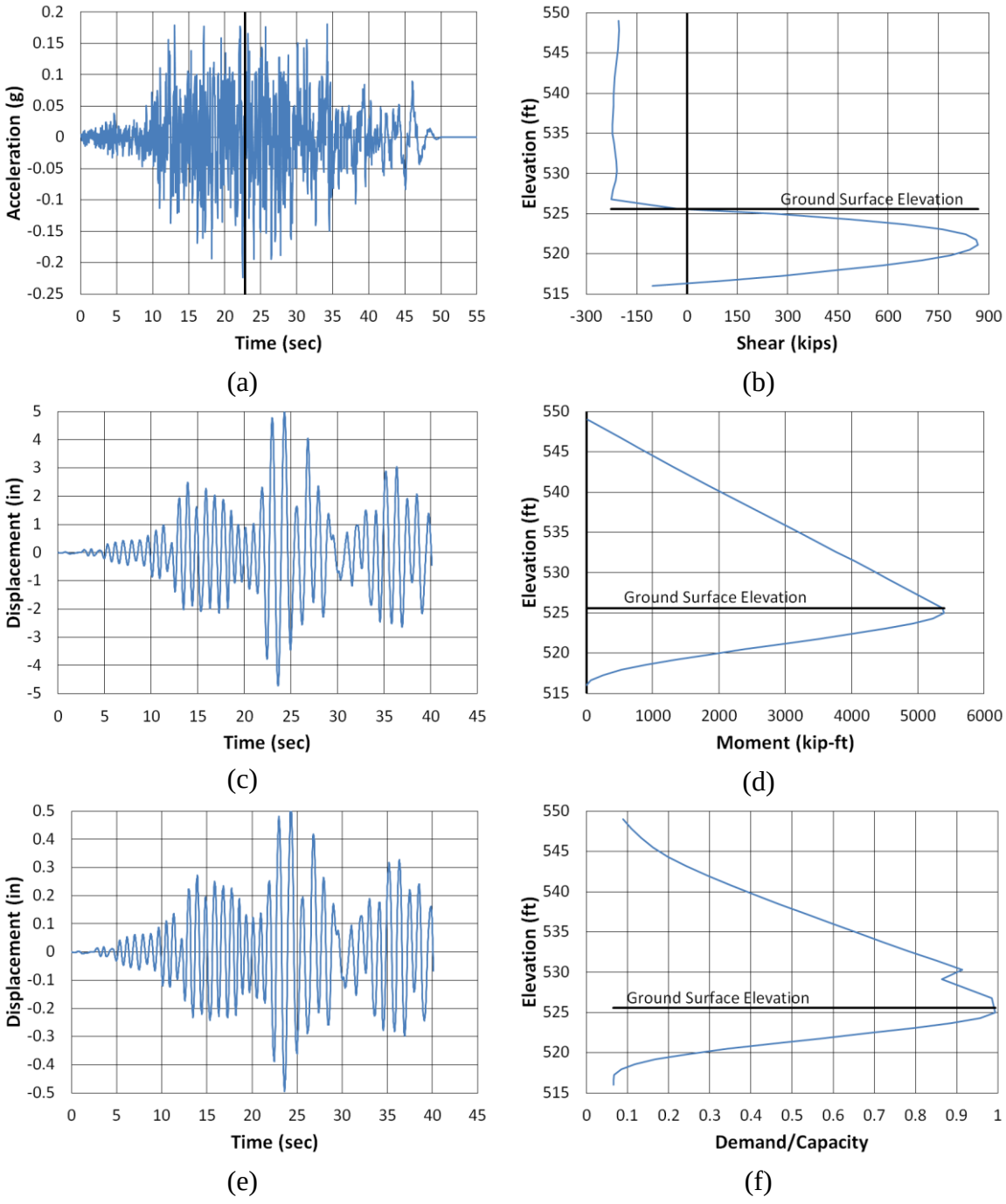

Figure B.112. Franklin County Longitudinal Landers NMCE (a) time-history event, (b) shear distribution, (c) top of pier displacement, (d) moment distribution, (e) ground surface displacement, and (f) demand capacity ratio

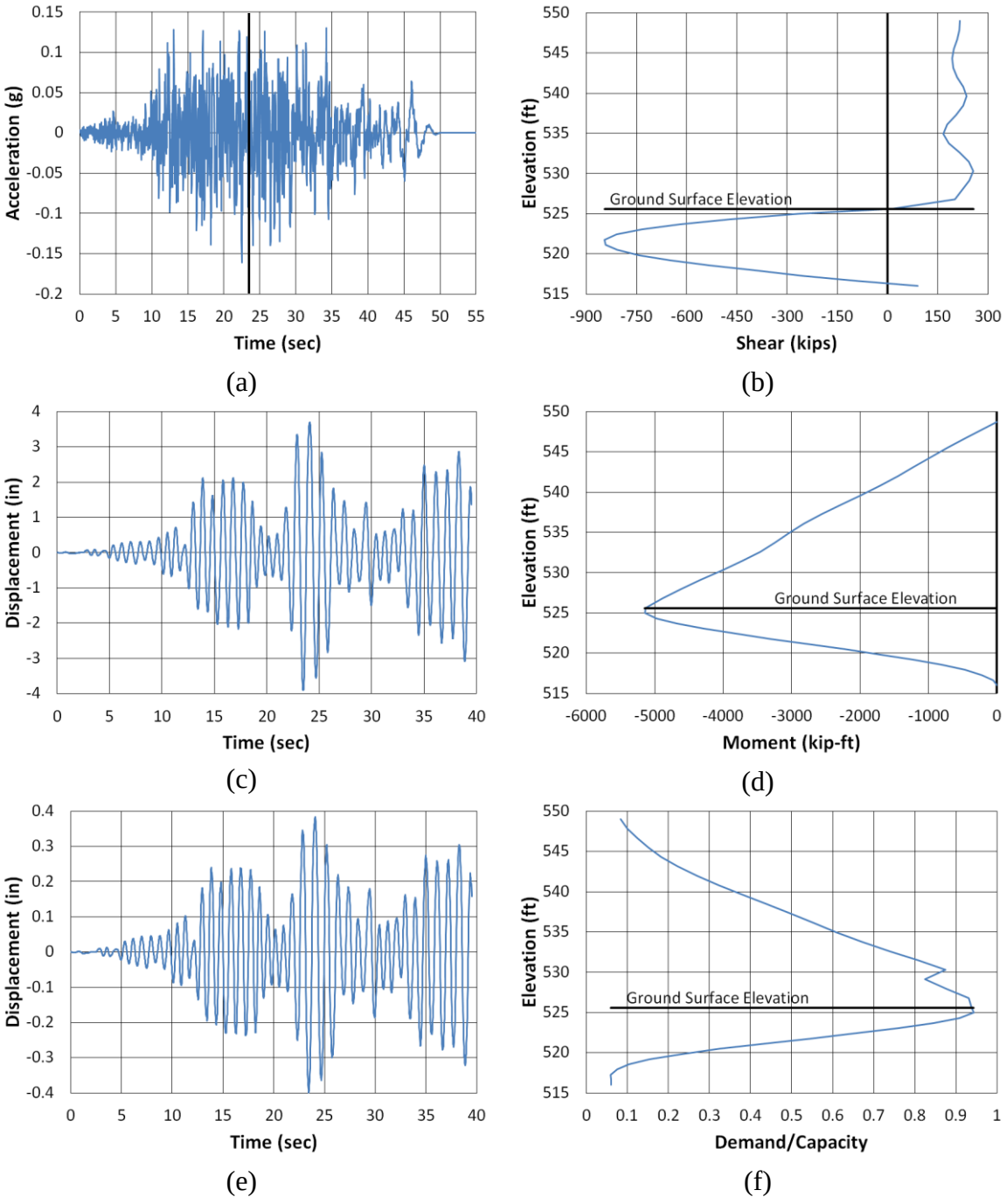

Figure B.113. Franklin County Longitudinal Landers North (a) time-history event, (b) shear distribution, (c) top of pier displacement, (d) moment distribution, (e) ground surface displacement, and (f) demand capacity ratio

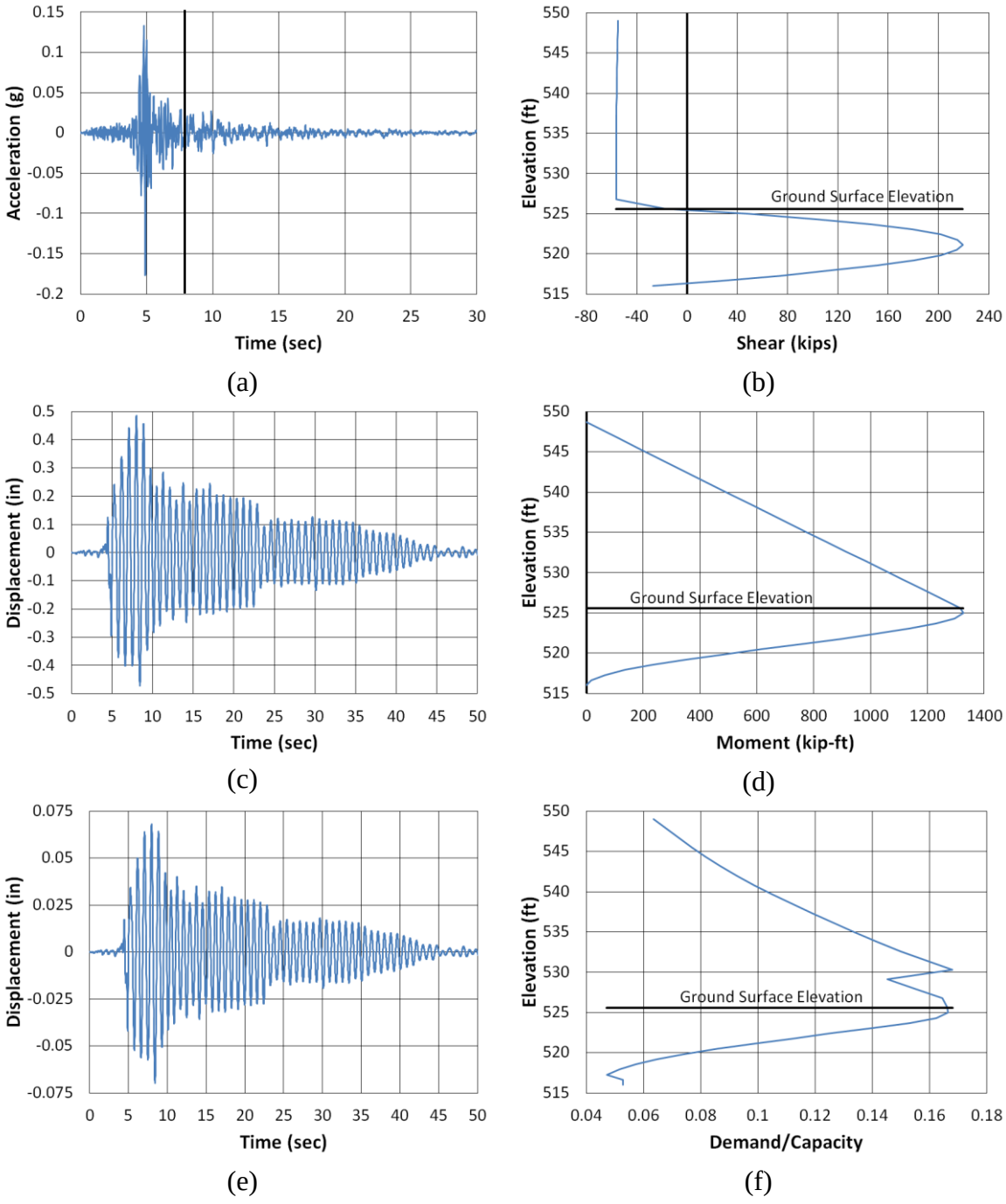

Figure B.114. Franklin County Longitudinal LSM North (a) time-history event, (b) shear distribution, (c) top of pier displacement, (d) moment distribution, (e) ground surface displacement, and (f) demand capacity ratio

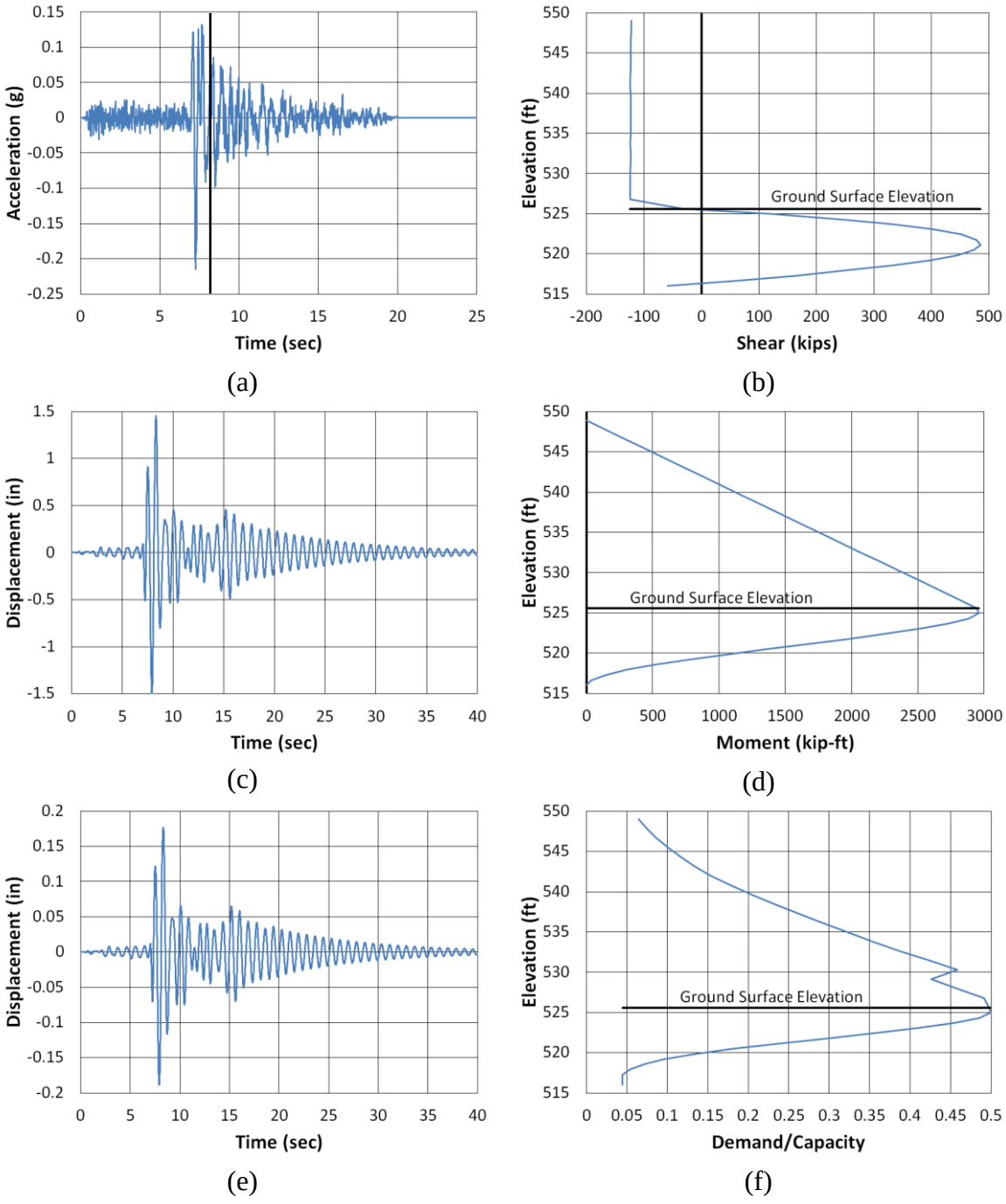

Figure B.115. Franklin County Longitudinal NPS North (a) time-history event, (b) shear distribution, (c) top of pier displacement, (d) moment distribution, (e) ground surface displacement, and (f) demand capacity ratio

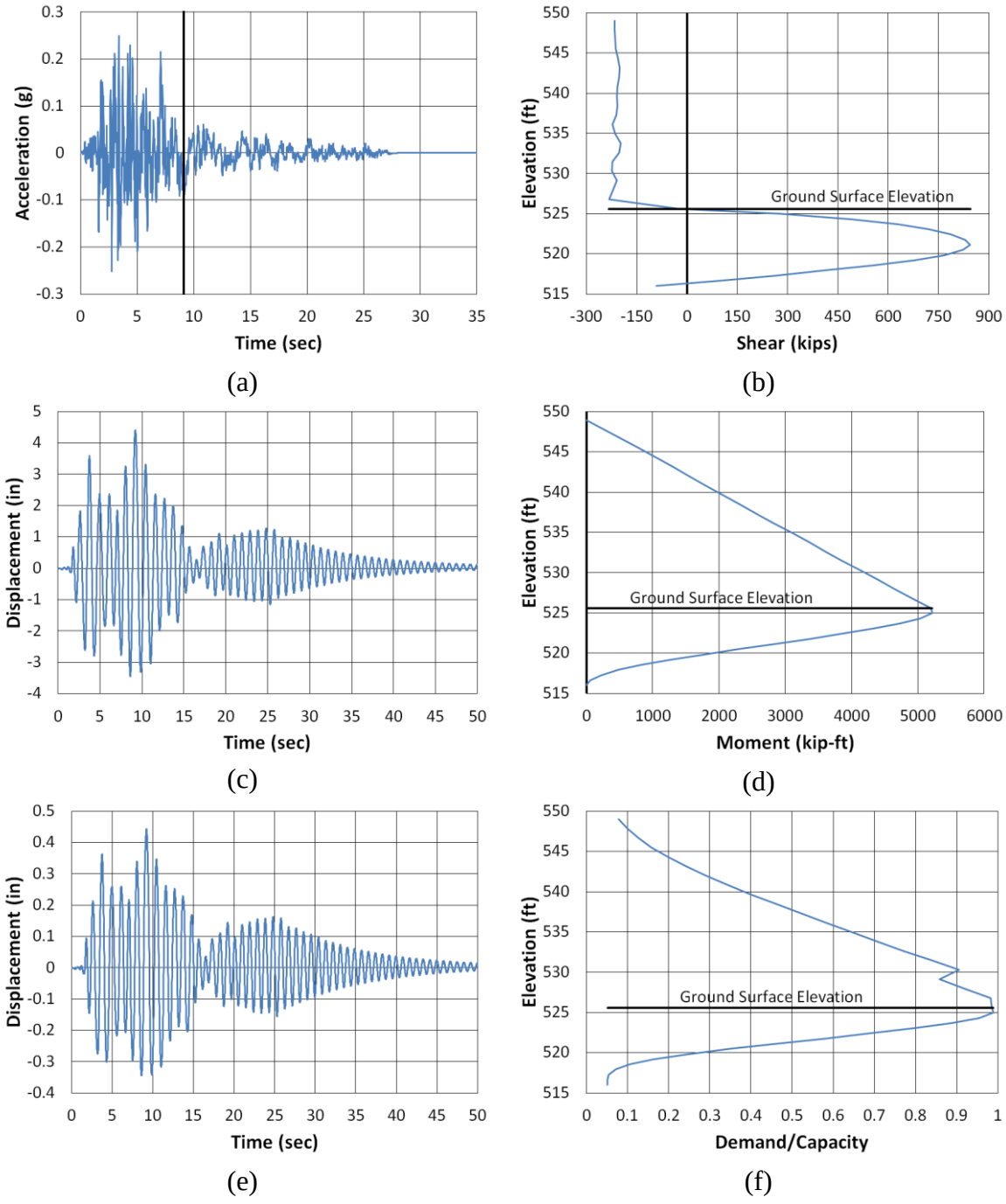

Figure B.116. Franklin County Longitudinal San Fernando NMCE (a) time-history event, (b) shear distribution, (c) top of pier displacement, (d) moment distribution, (e) ground surface displacement, and (f) demand capacity ratio

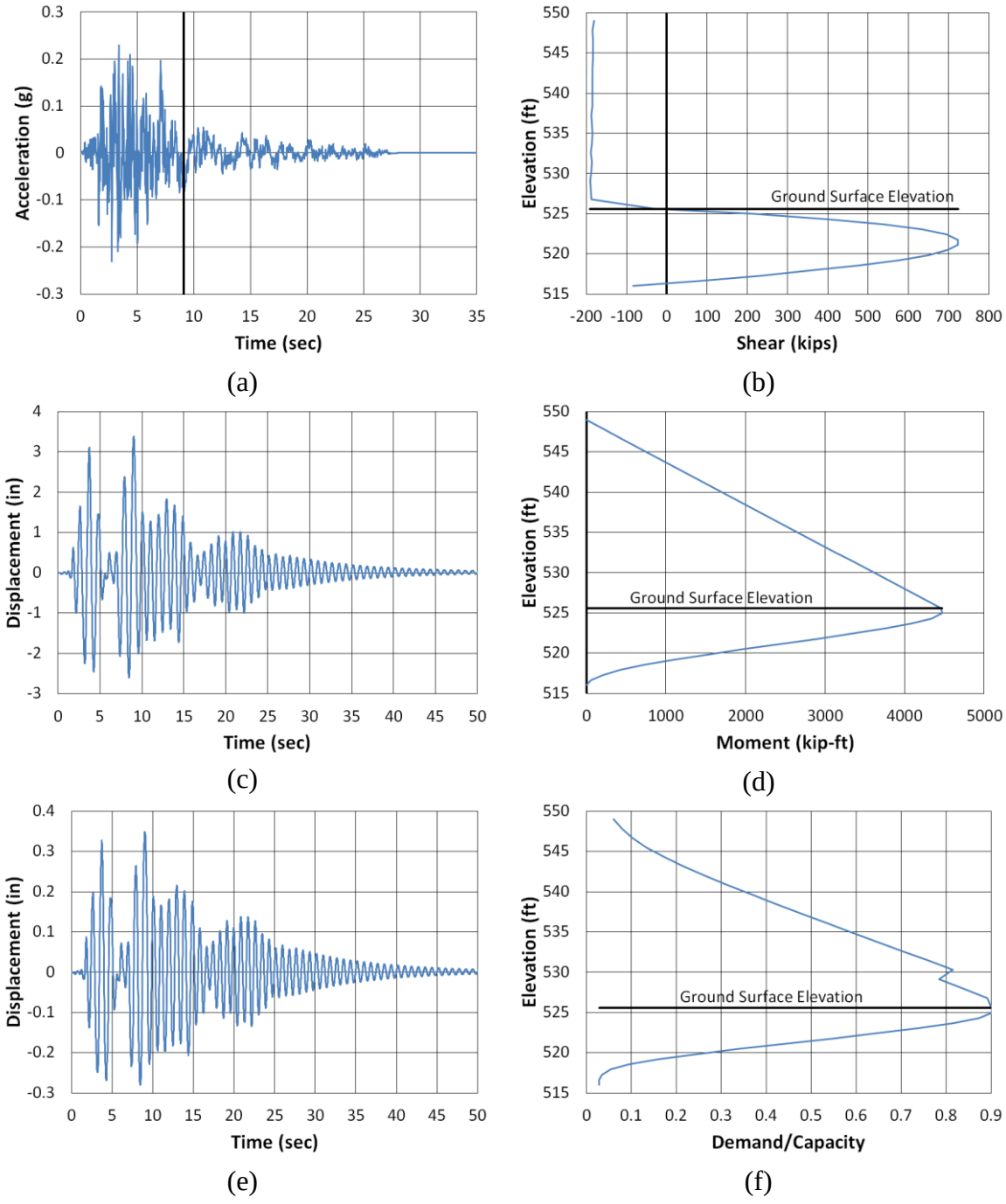

Figure B.117 Franklin County Longitudinal San Fernando North (a) time-history event, (b) shear distribution, (c) top of pier displacement, (d) moment distribution, (e) ground surface displacement, and (f) demand capacity ratio

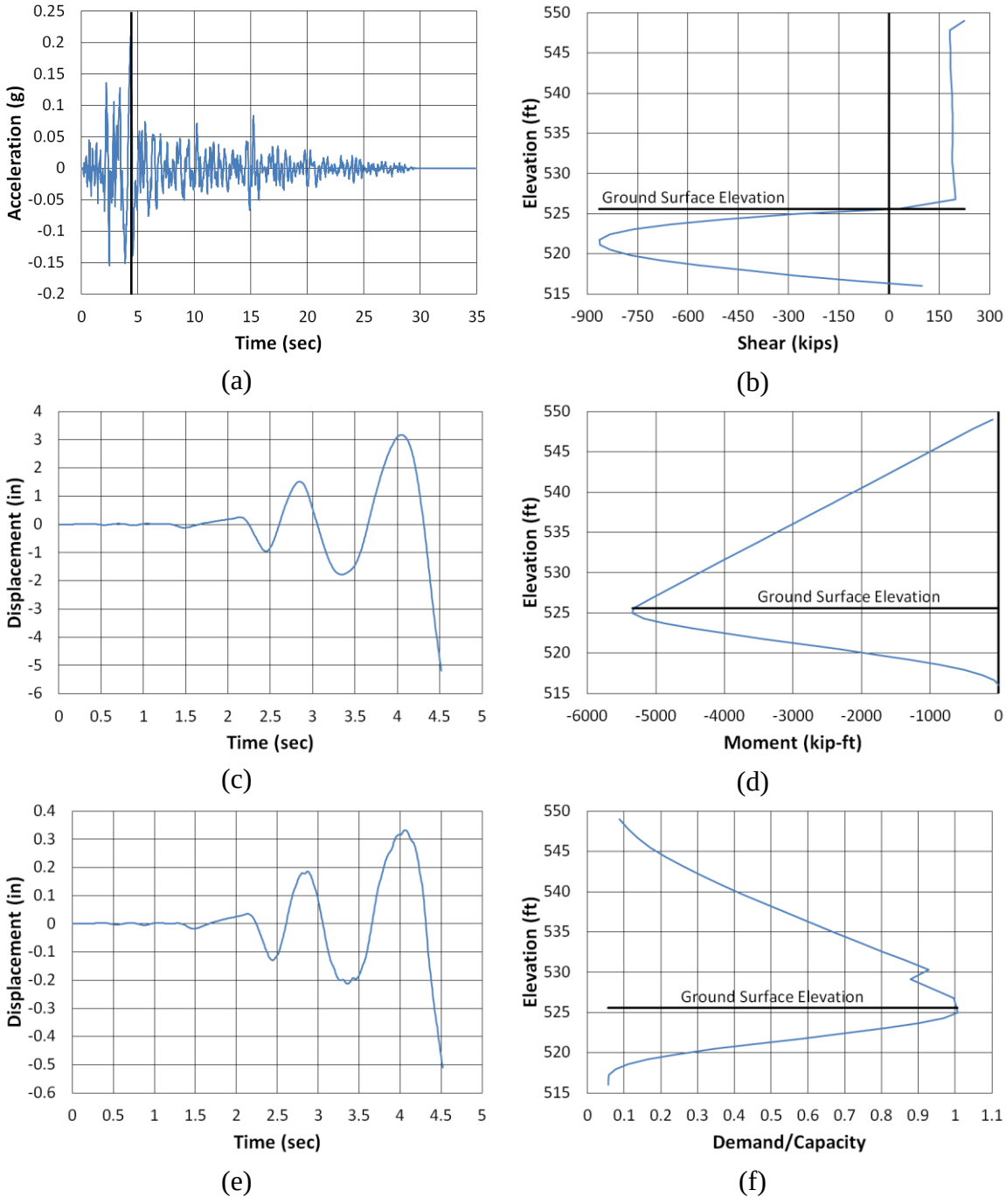

Figure B.118. Franklin County Longitudinal San Fernando2 NMCE (a) time-history event, (b) shear distribution, (c) top of pier displacement, (d) moment distribution, (e) ground surface displacement, and (f) demand capacity ratio

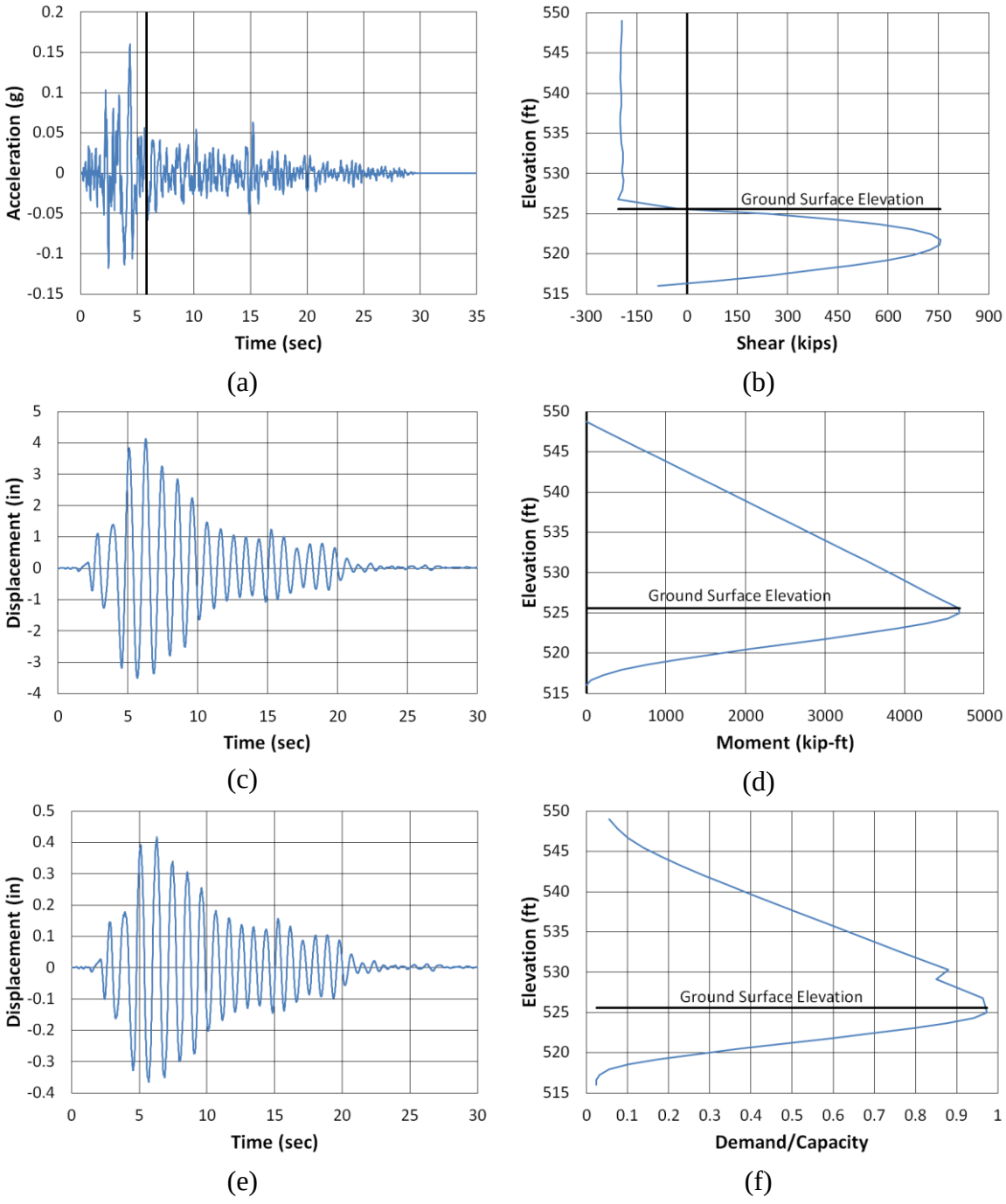

Figure B.119. Franklin County Longitudinal San Fernando2 North (a) time-history event, (b) shear distribution, (c) top of pier displacement, (d) moment distribution, (e) ground surface displacement, and (f) demand capacity ratio

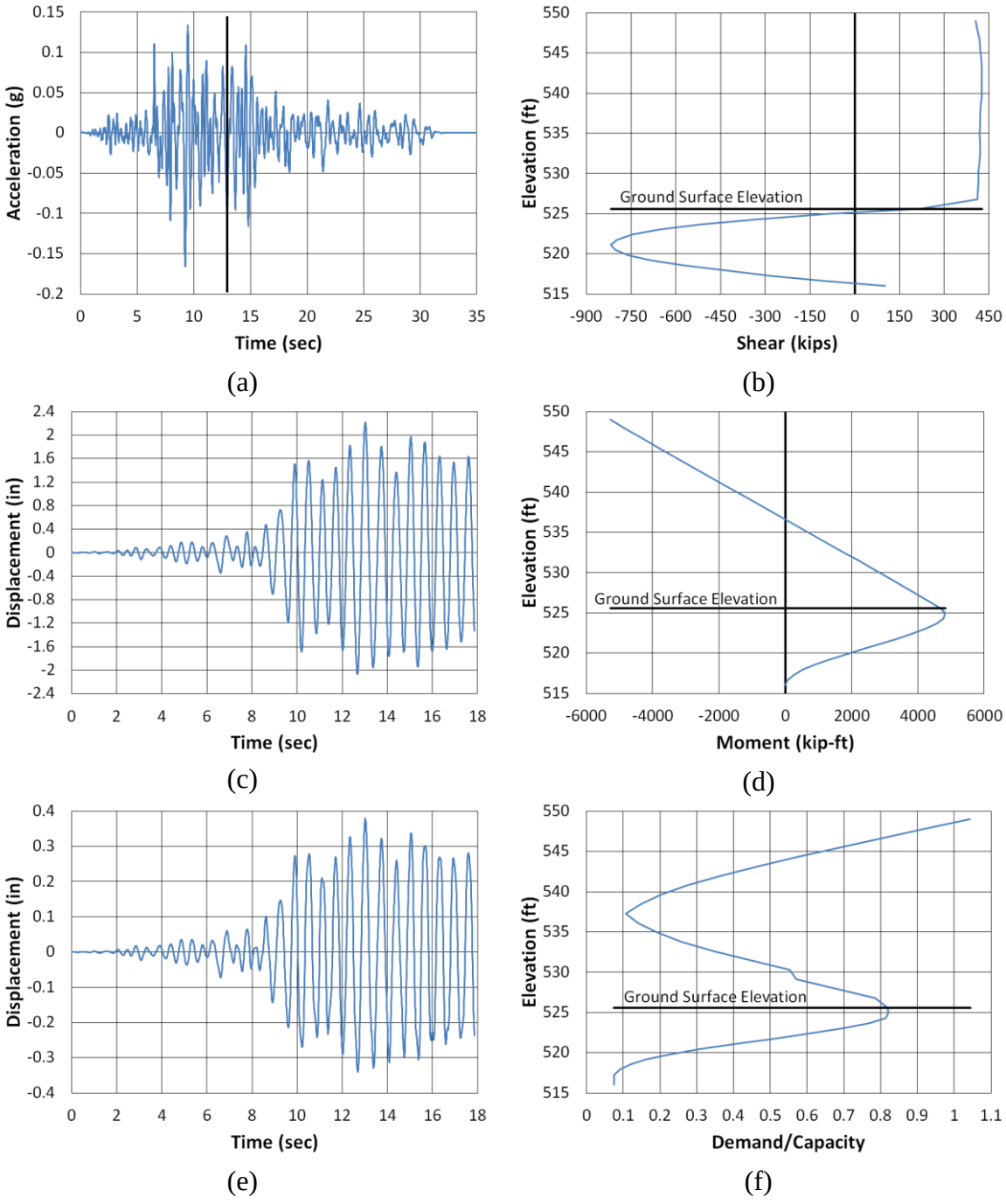

Figure B.120. Franklin County Transverse Coalinga North (a) time-history event, (b) shear distribution, (c) top of pier displacement, (d) moment distribution, (e) ground surface displacement, and (f) demand capacity ratio

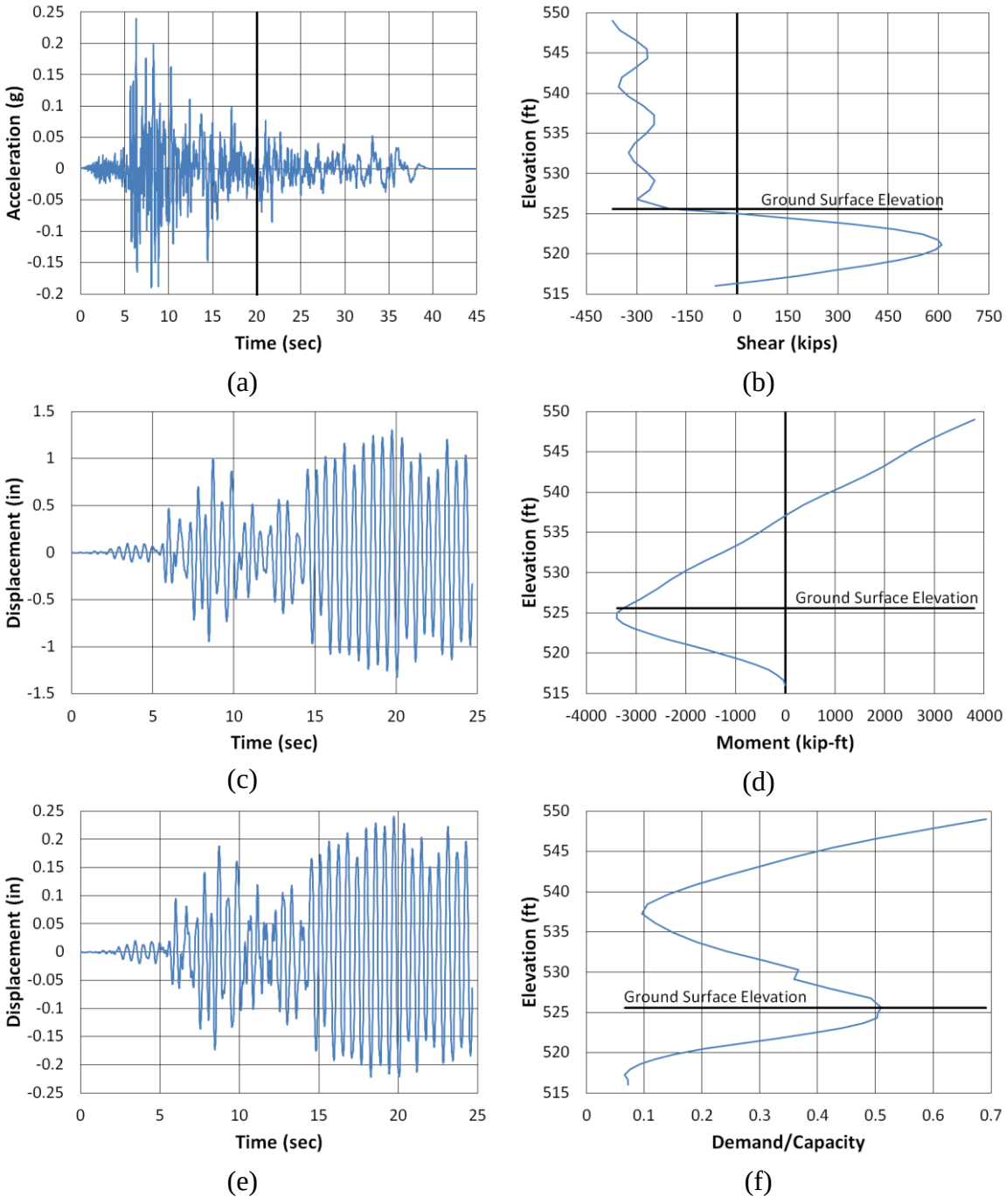

Figure B.121. Franklin County Transverse Imperial Valley NMCE (a) time-history event, (b) shear distribution, (c) top of pier displacement, (d) moment distribution, (e) ground surface displacement, and (f) demand capacity ratio

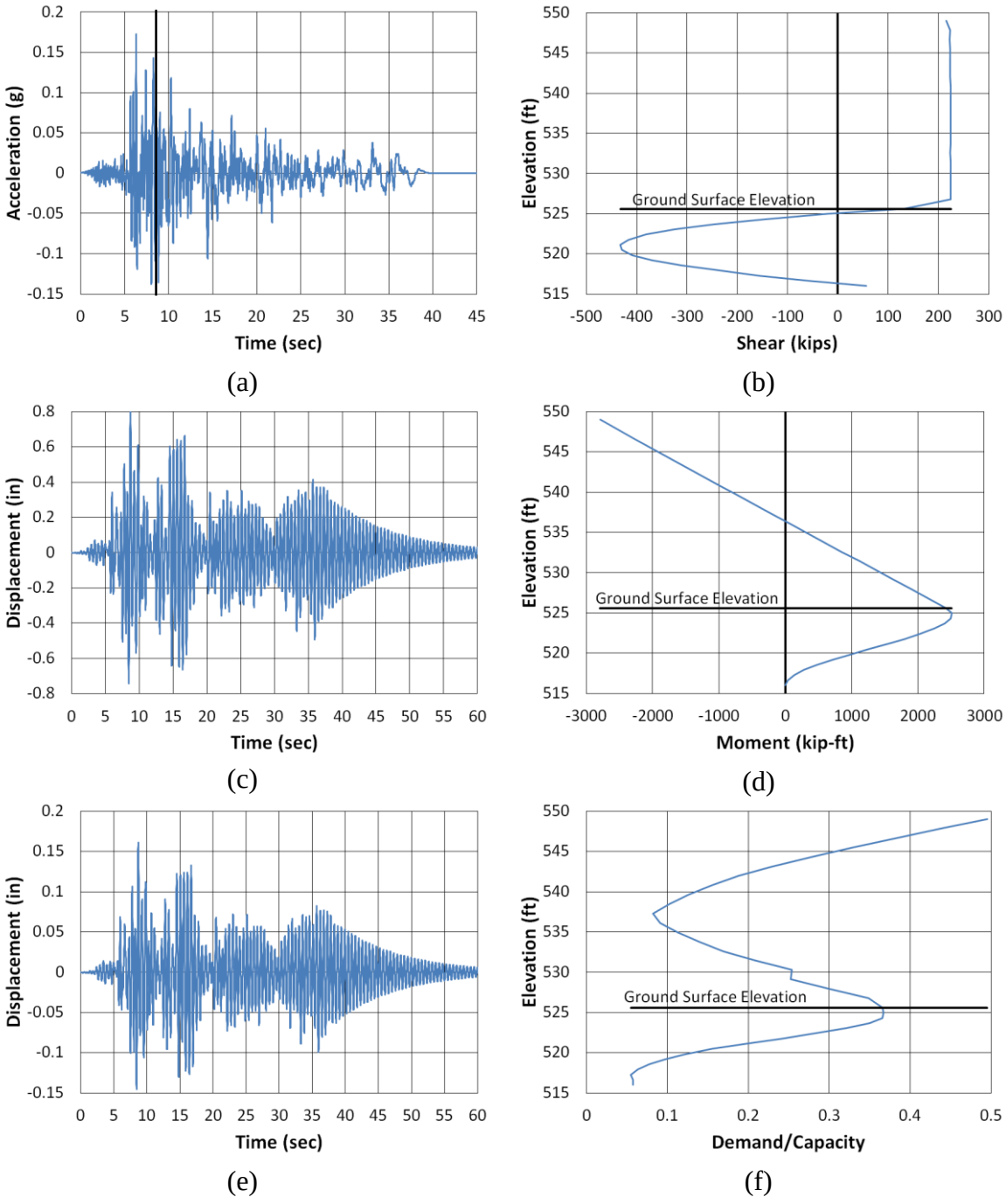

Figure B.122. Franklin County Transverse Imperial Valley North (a) time-history event, (b) shear distribution, (c) top of pier displacement, (d) moment distribution, (e) ground surface displacement, and (f) demand capacity ratio

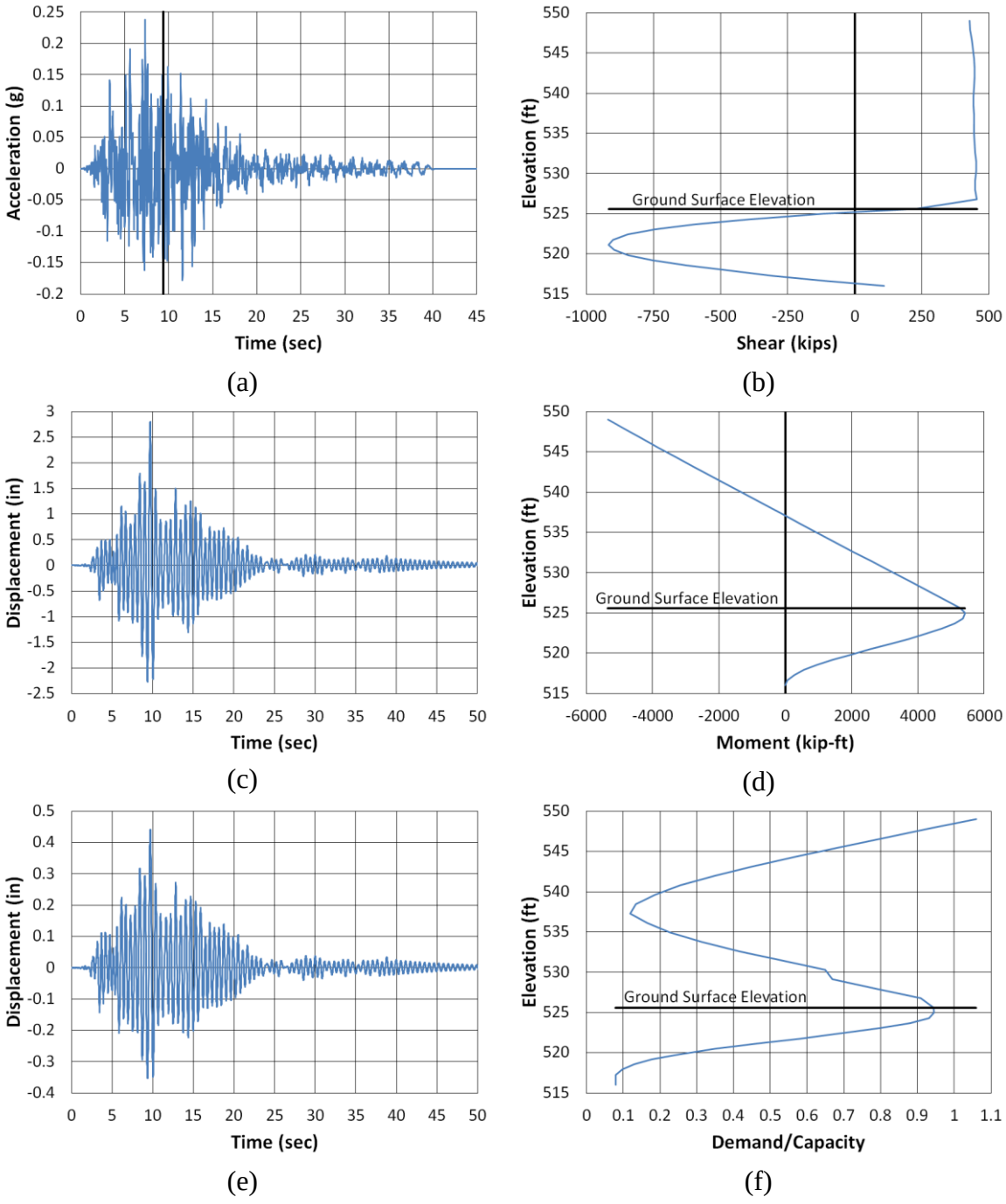

Figure B.123. Franklin County Transverse Kobe NMCE (a) time-history event, (b) shear distribution, (c) top of pier displacement, (d) moment distribution, (e) ground surface displacement, and (f) demand capacity ratio

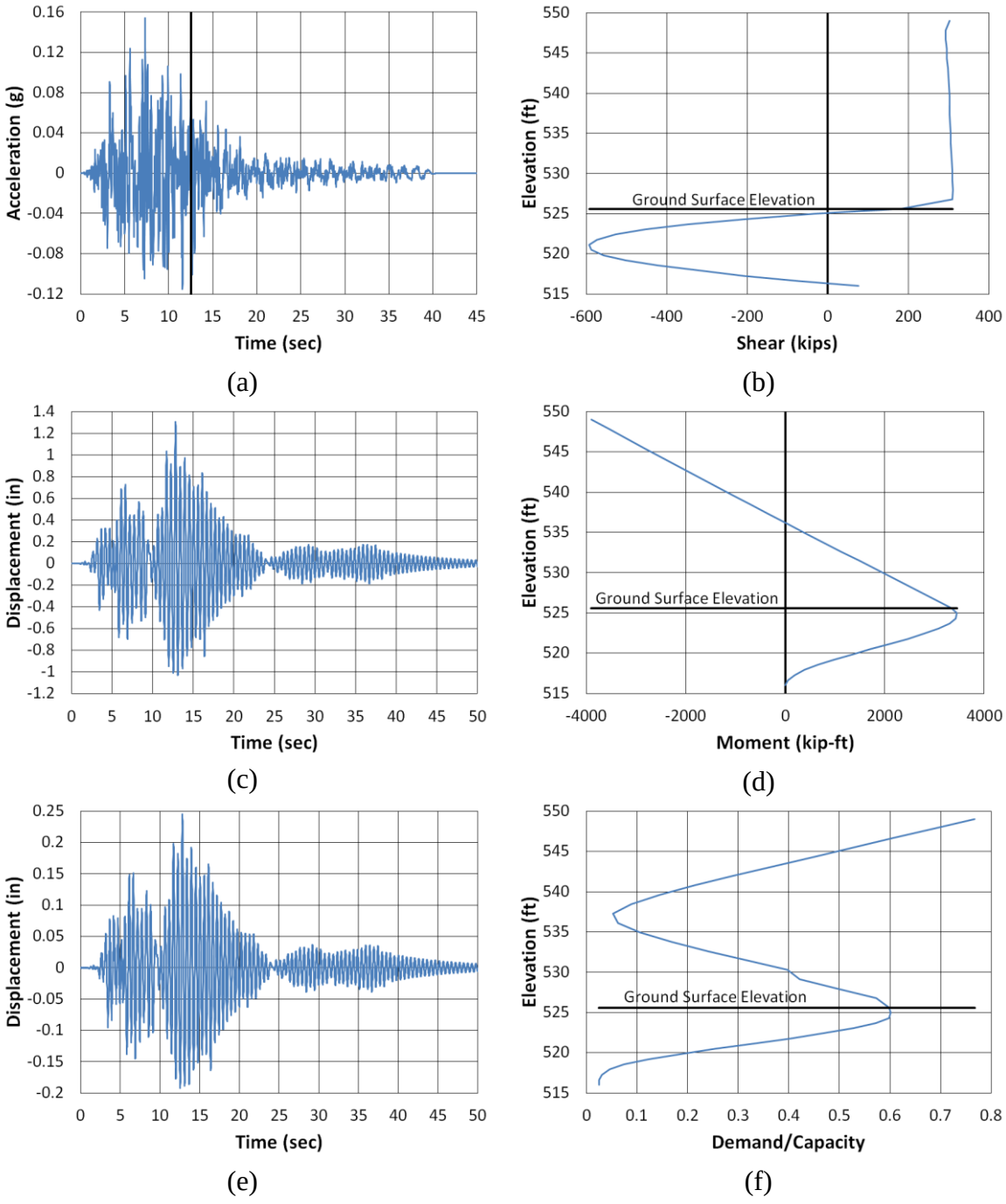

Figure B.124. Franklin County Transverse Kobe North (a) time-history event, (b) shear distribution, (c) top of pier displacement, (d) moment distribution, (e) ground surface displacement, and (f) demand capacity ratio

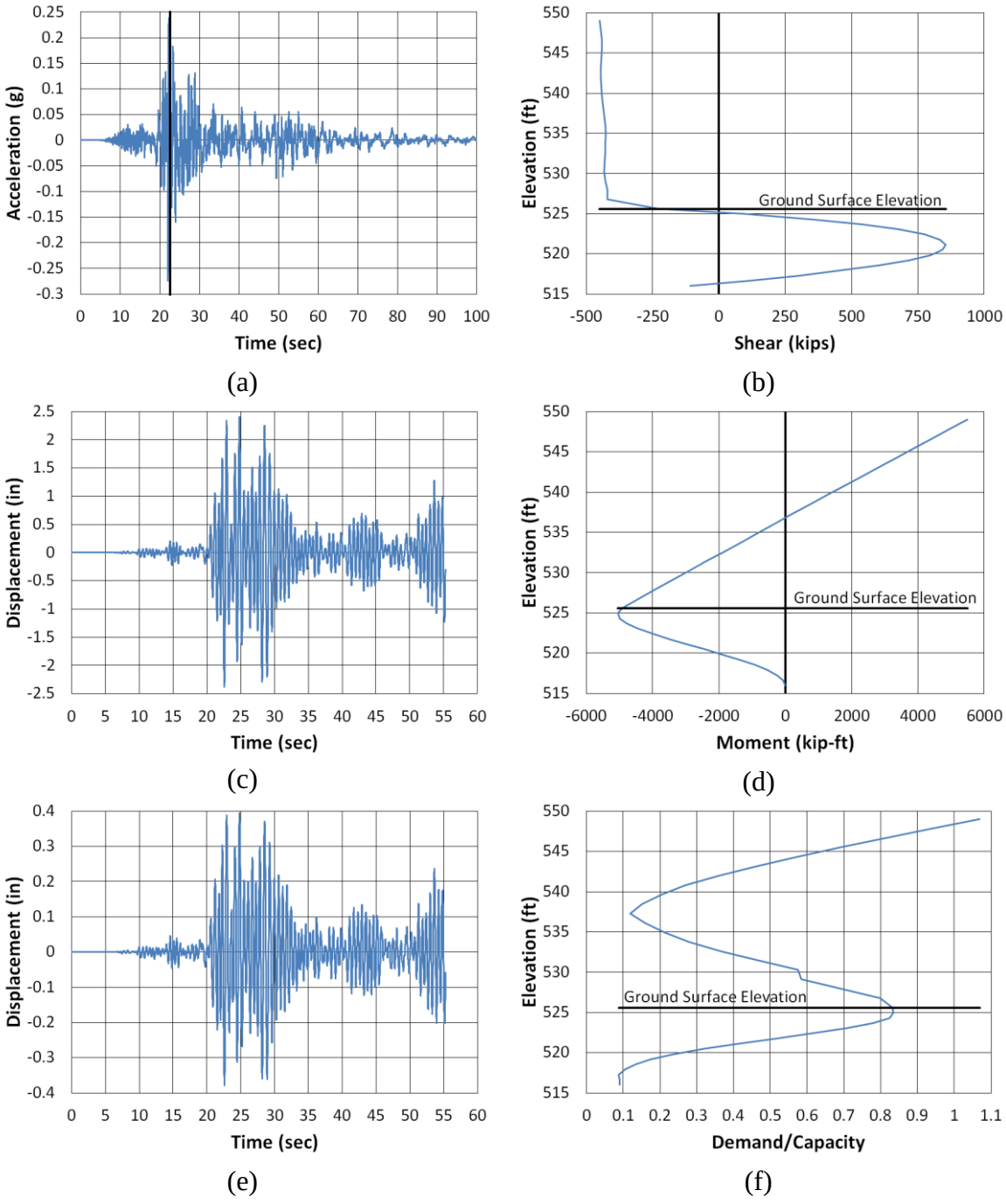

Figure B.125. Franklin County Transverse Kocaeli NMCE (a) time-history event, (b) shear distribution, (c) top of pier displacement, (d) moment distribution, (e) ground surface displacement, and (f) demand capacity ratio

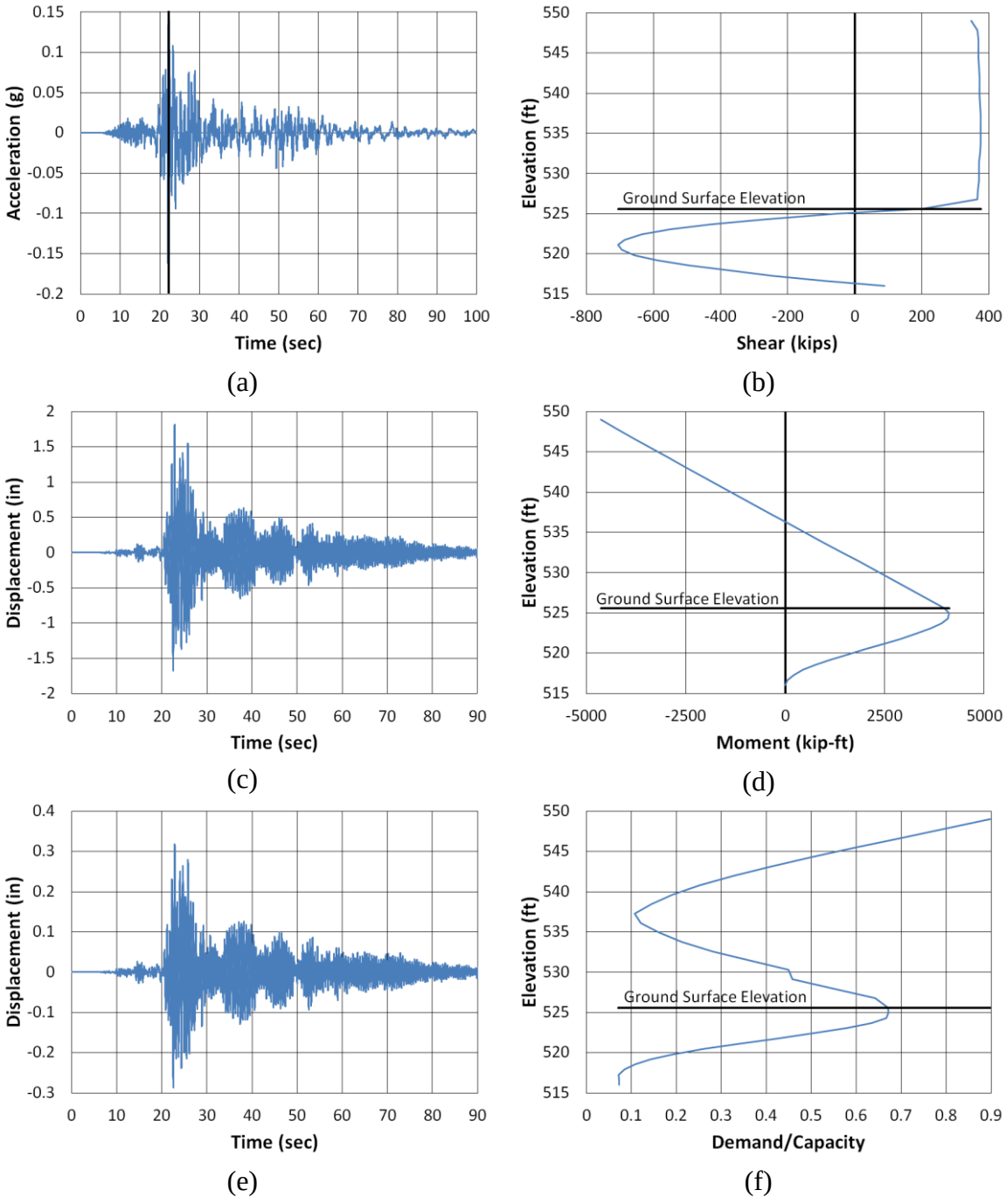

Figure B.126. Franklin County Transverse Kocaeli North (a) time-history event, (b) shear distribution, (c) top of pier displacement, (d) moment distribution, (e) ground surface displacement, and (f) demand capacity ratio

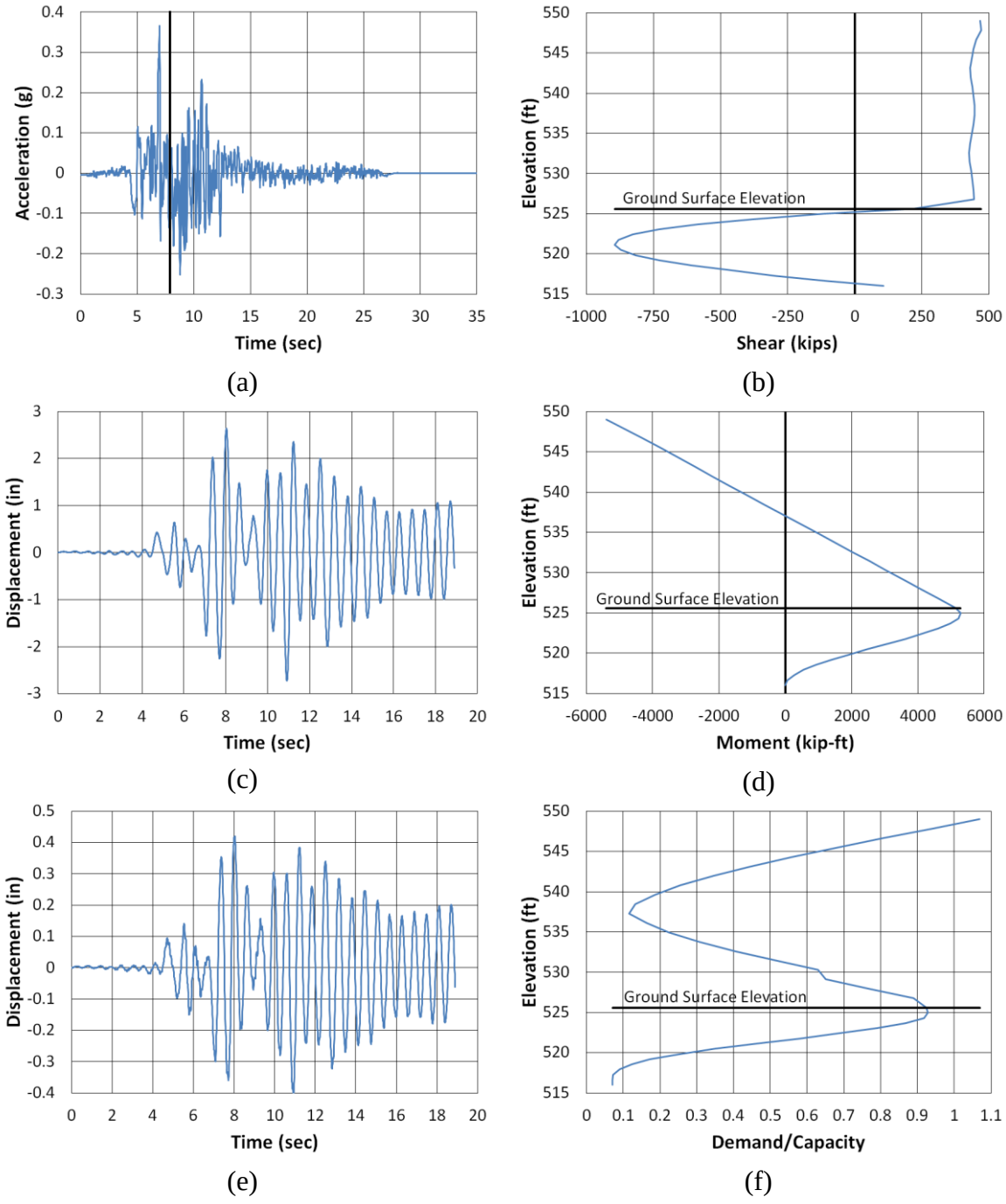

Figure B.127. Franklin County Transverse Kocaeli2 NMCE (a) time-history event, (b) shear distribution, (c) top of pier displacement, (d) moment distribution, (e) ground surface displacement, and (f) demand capacity ratio

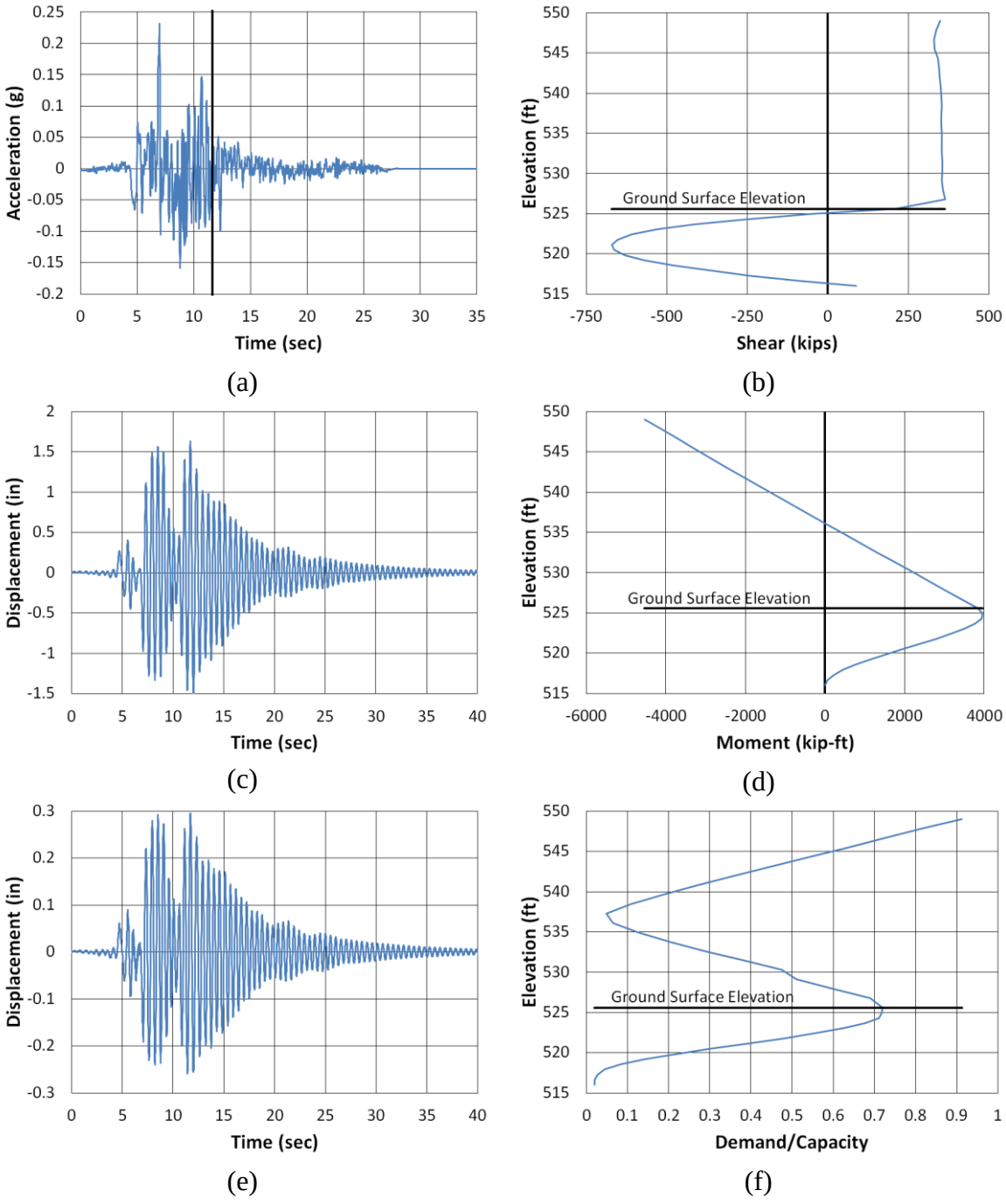

Figure B.128. Franklin County Transverse Kocaeli2 North (a) time-history event, (b) shear distribution, (c) top of pier displacement, (d) moment distribution, (e) ground surface displacement, and (f) demand capacity ratio

.

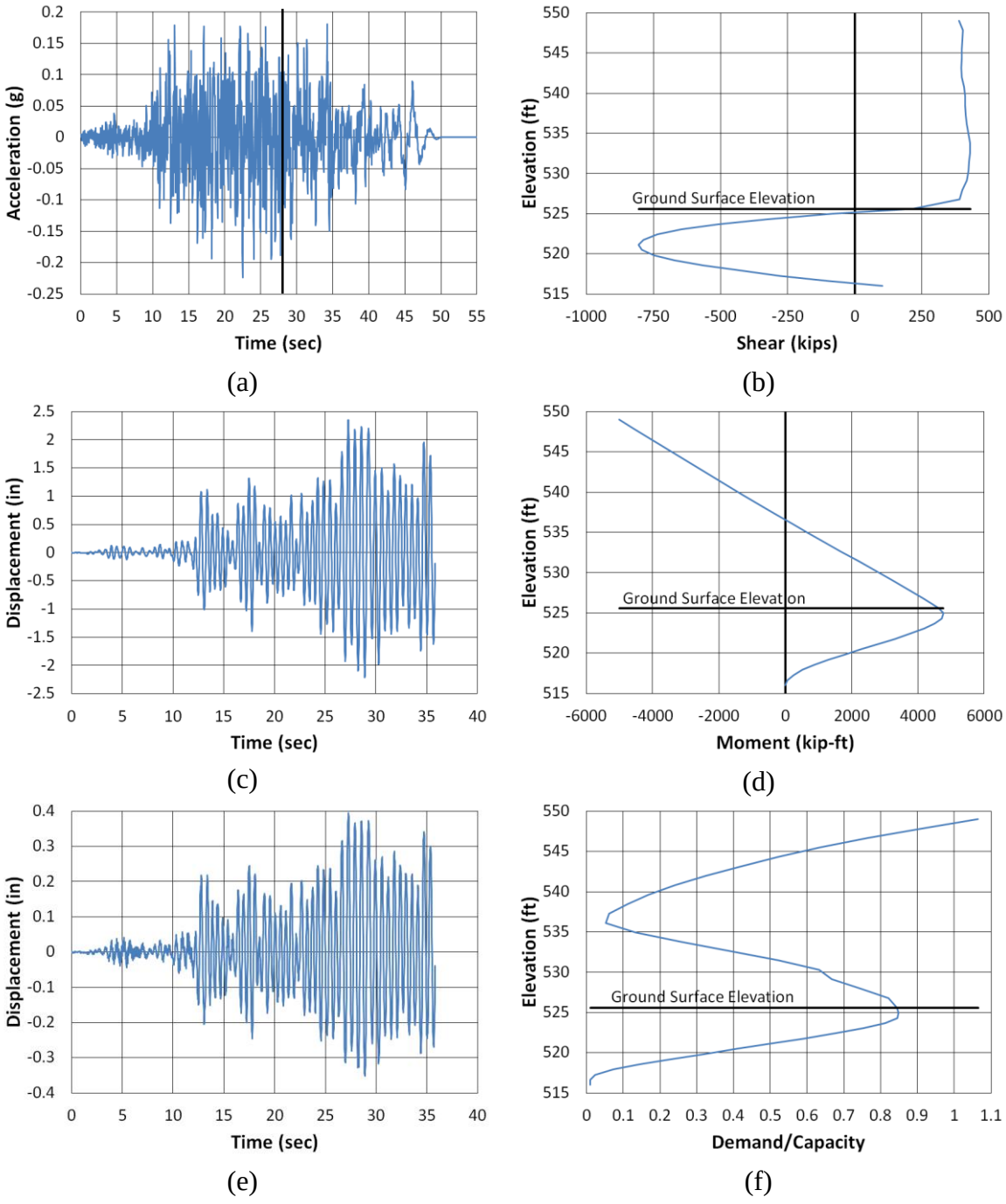

Figure B.129. Franklin County Transverse Landers NMCE (a) time-history event, (b) shear distribution, (c) top of pier displacement, (d) moment distribution, (e) ground surface displacement, and (f) demand capacity ratio

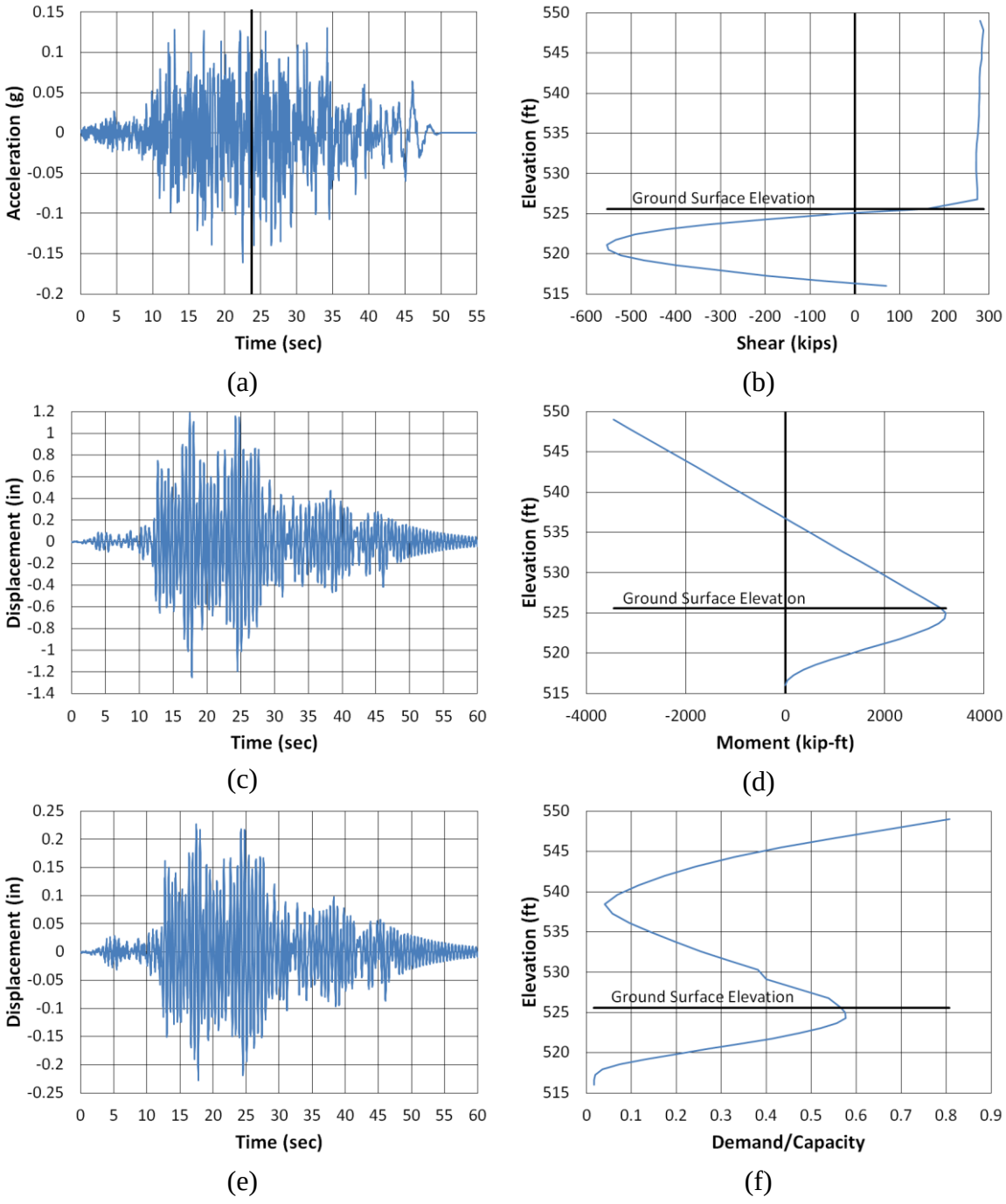

Figure B.130. Franklin County Transverse Landers North (column) (a) time-history event, (b) shear distribution, (c) top of pier displacement, (d) moment distribution, (e) ground surface displacement, and (f) demand capacity ratio

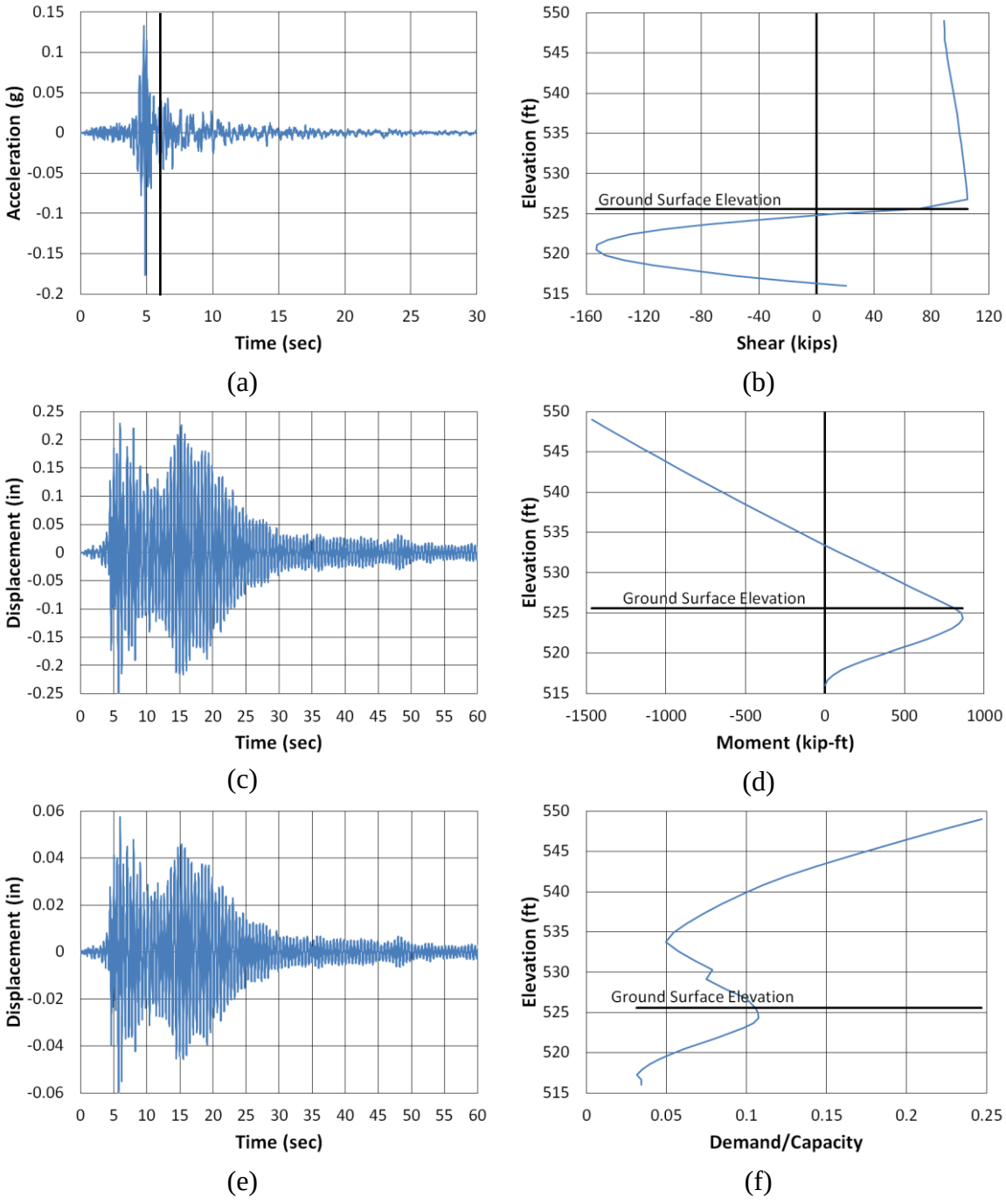

Figure B.131. Franklin County Transverse LSM North (a) time-history event, (b) shear distribution, (c) top of pier displacement, (d) moment distribution, (e) ground surface displacement, and (f) demand capacity ratio

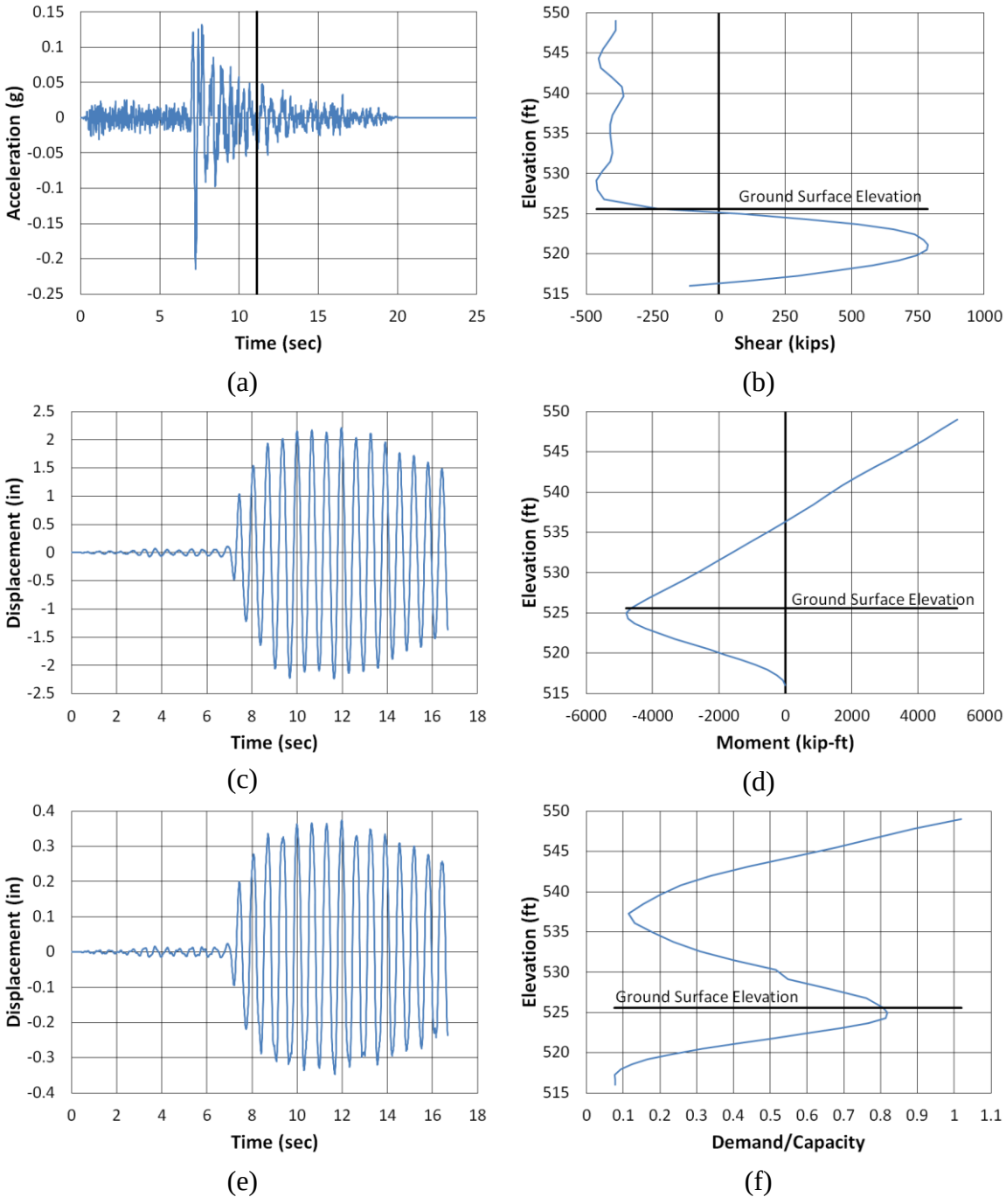

Figure B.132. Franklin County Transverse NPS North (a) time-history event, (b) shear distribution, (c) top of pier displacement, (d) moment distribution, (e) ground surface displacement, and (f) demand capacity ratio

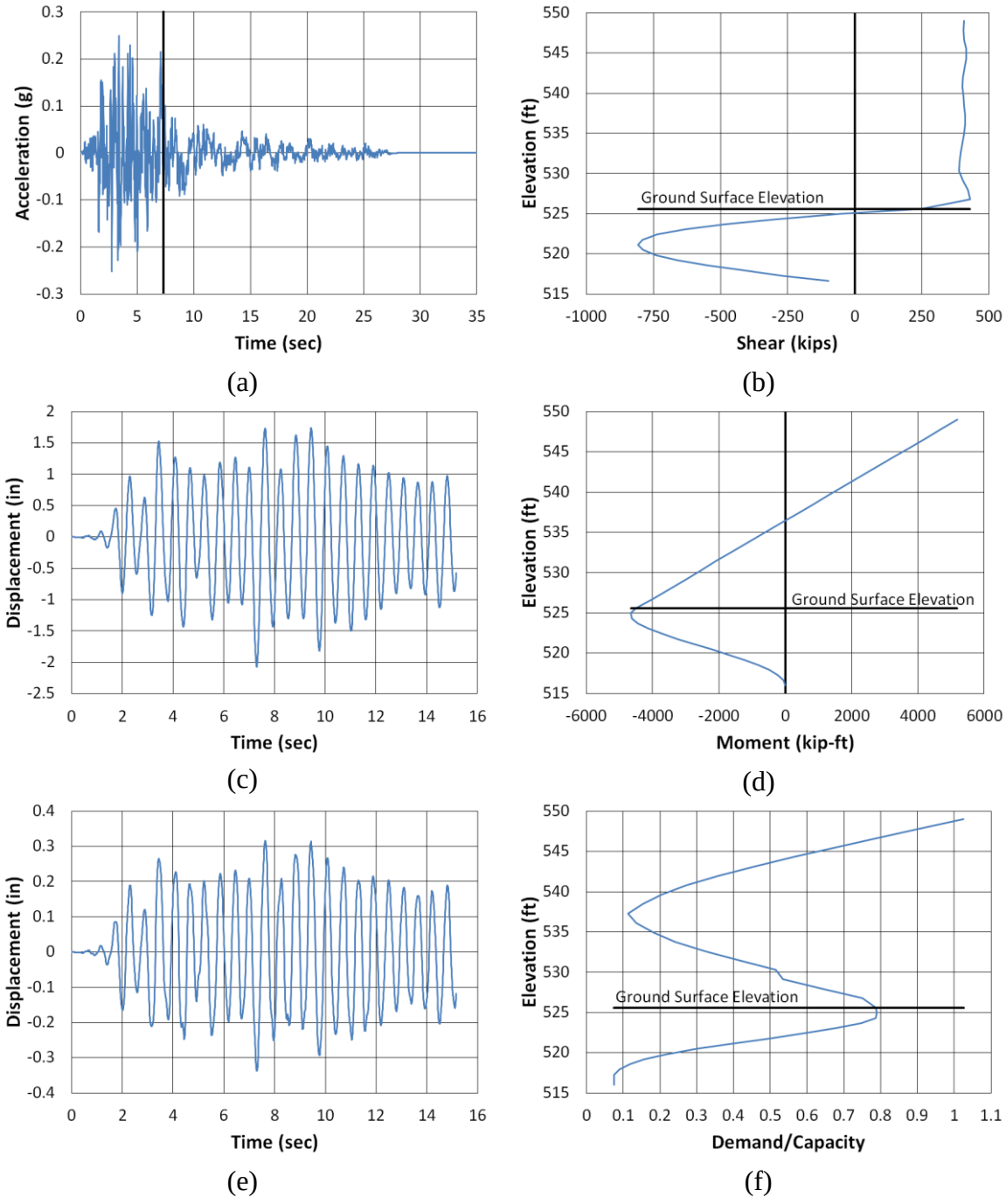

Figure B.133. Franklin County Transverse San Fernando NMCE (a) time-history event, (b) shear distribution, (c) top of pier displacement, (d) moment distribution, (e) ground surface displacement, and (f) demand capacity ratio

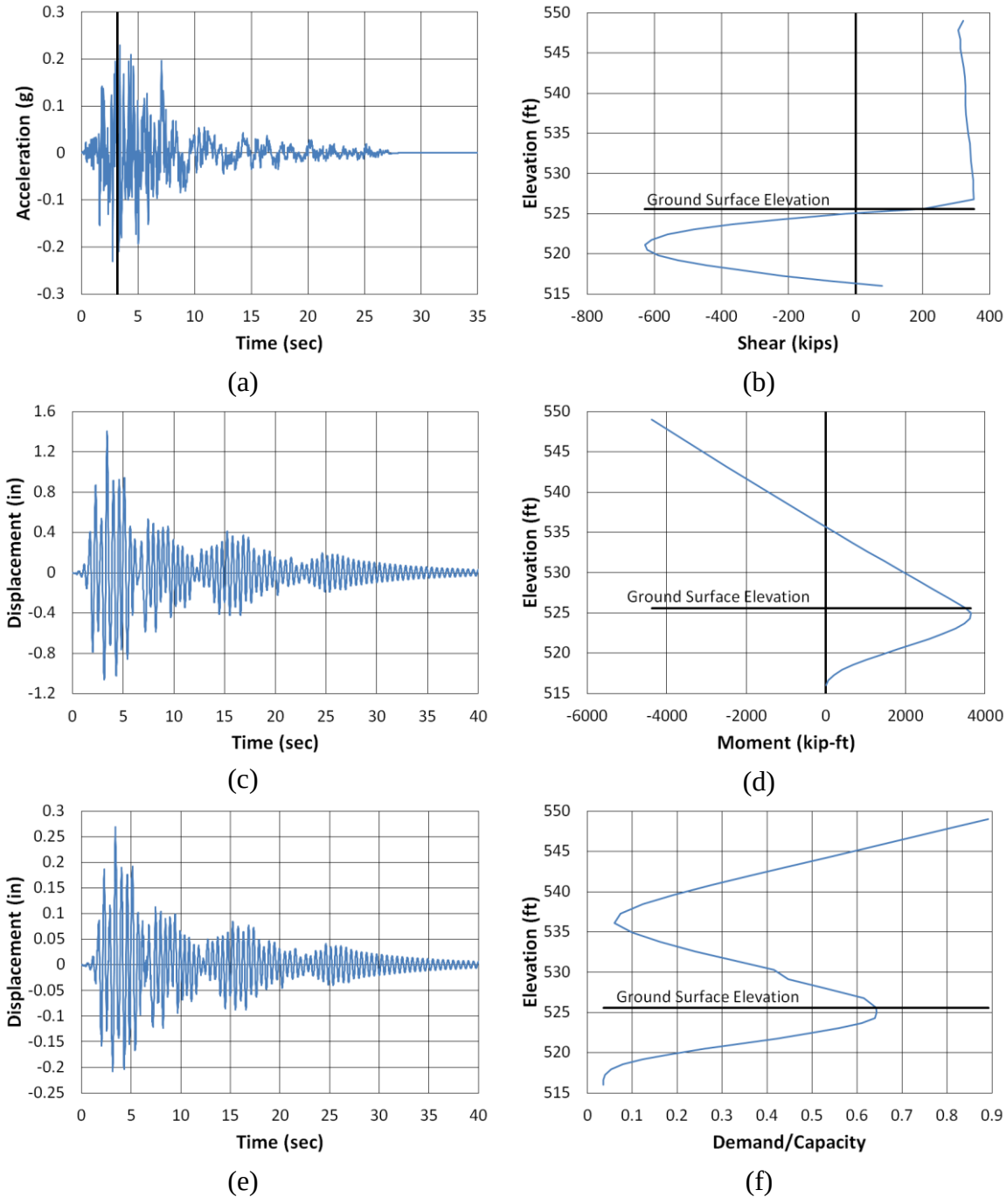

Figure B.134. Franklin County Transverse San Fernando North (a) time-history event, (b) shear distribution, (c) top of pier displacement, (d) moment distribution, (e) ground surface displacement, and (f) demand capacity ratio

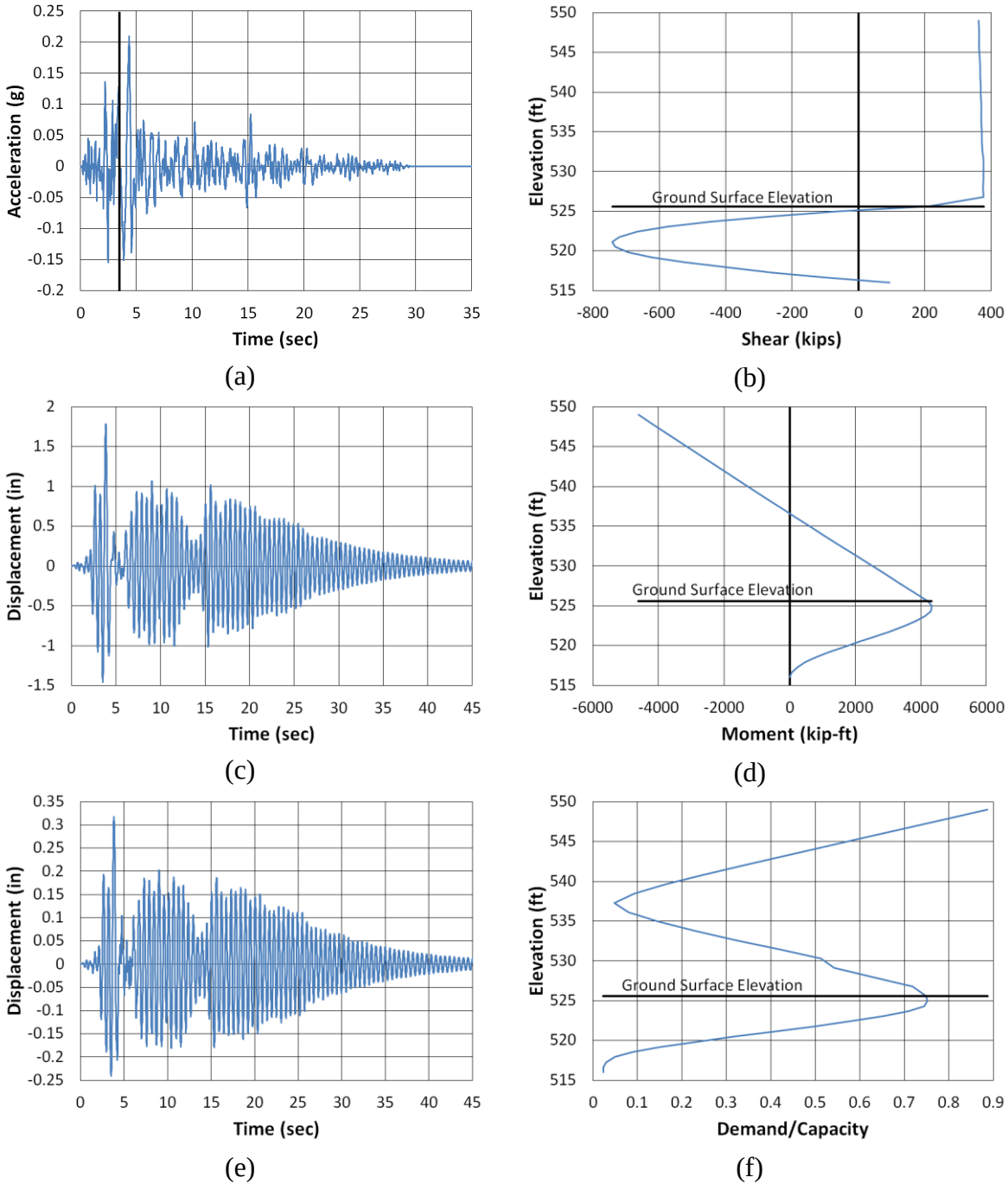

Figure B.135. Franklin County Transverse San Fernando2 NMCE (a) time-history event, (b) shear distribution, (c) top of pier displacement, (d) moment distribution, (e) ground surface displacement, and (f) demand capacity ratio

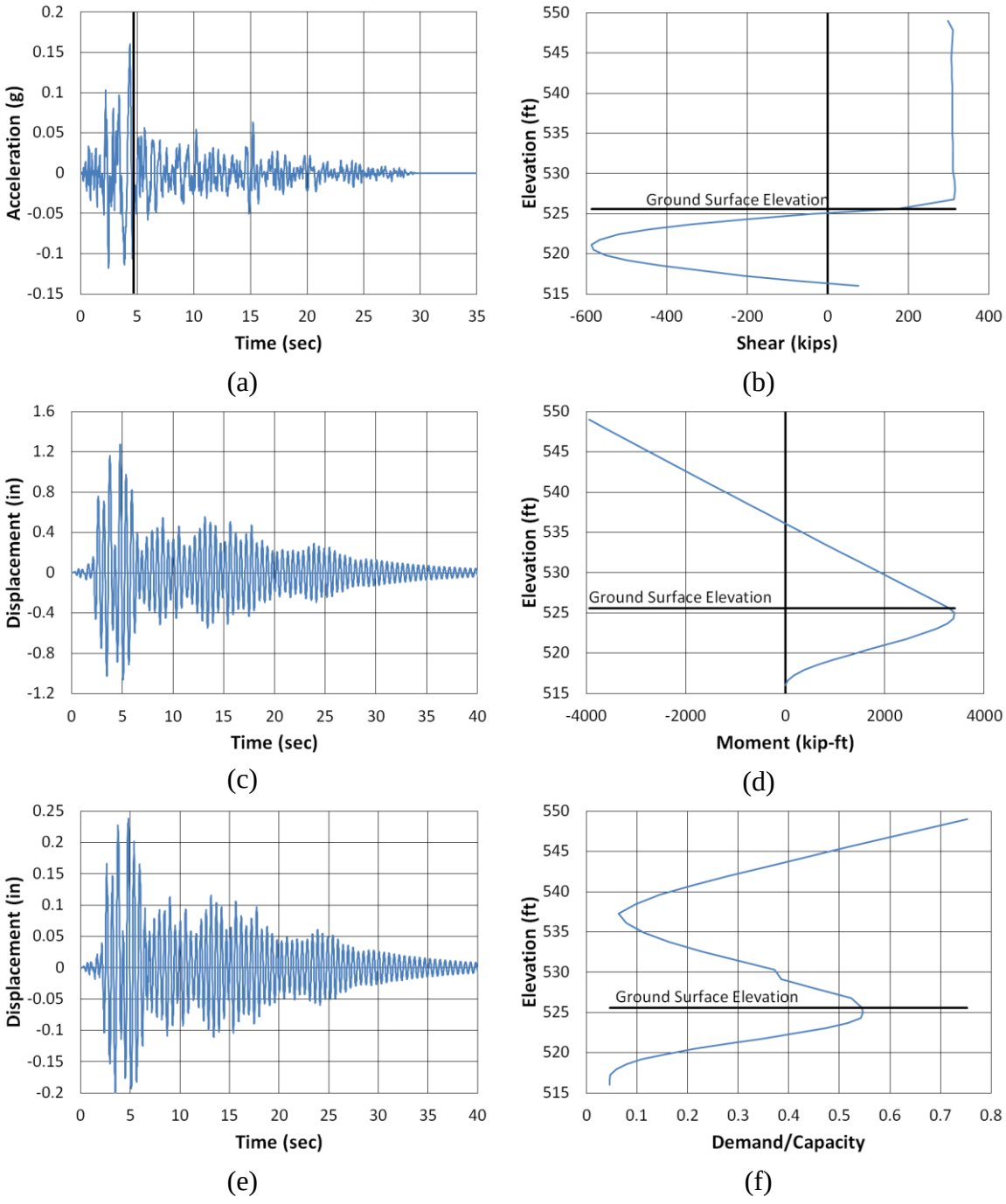

Figure B.136. Franklin County Transverse San Fernando2 North (a) time-history event, (b) shear distribution, (c) top of pier displacement, (d) moment distribution, (e) ground surface displacement, and (f) demand capacity ratio

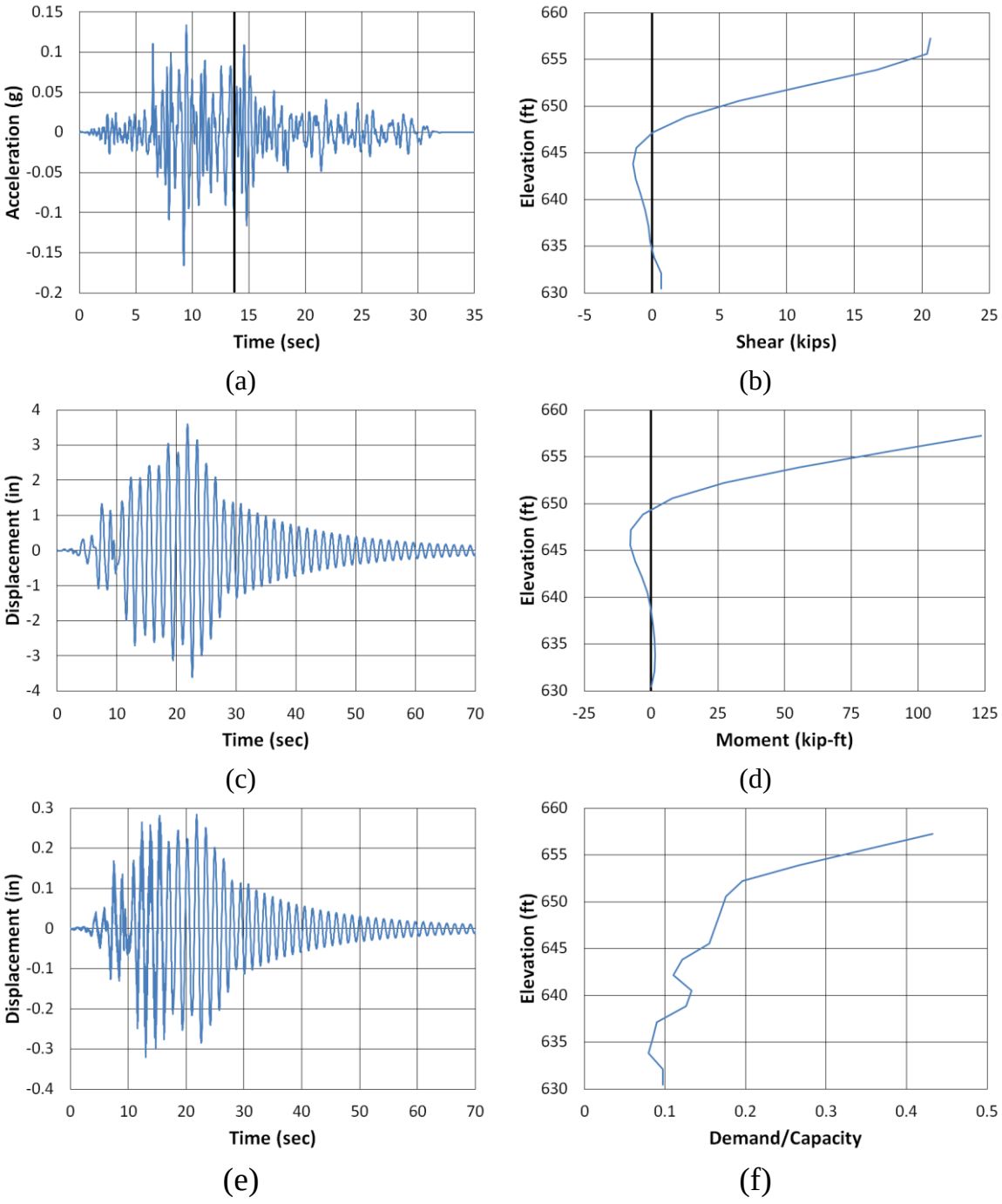

Figure B.137. Lee County Longitudinal Coalinga North (a) time-history event, (b) shear distribution, (c) top of pier displacement, (d) moment distribution, (e) ground surface displacement, and (f) demand capacity ratio

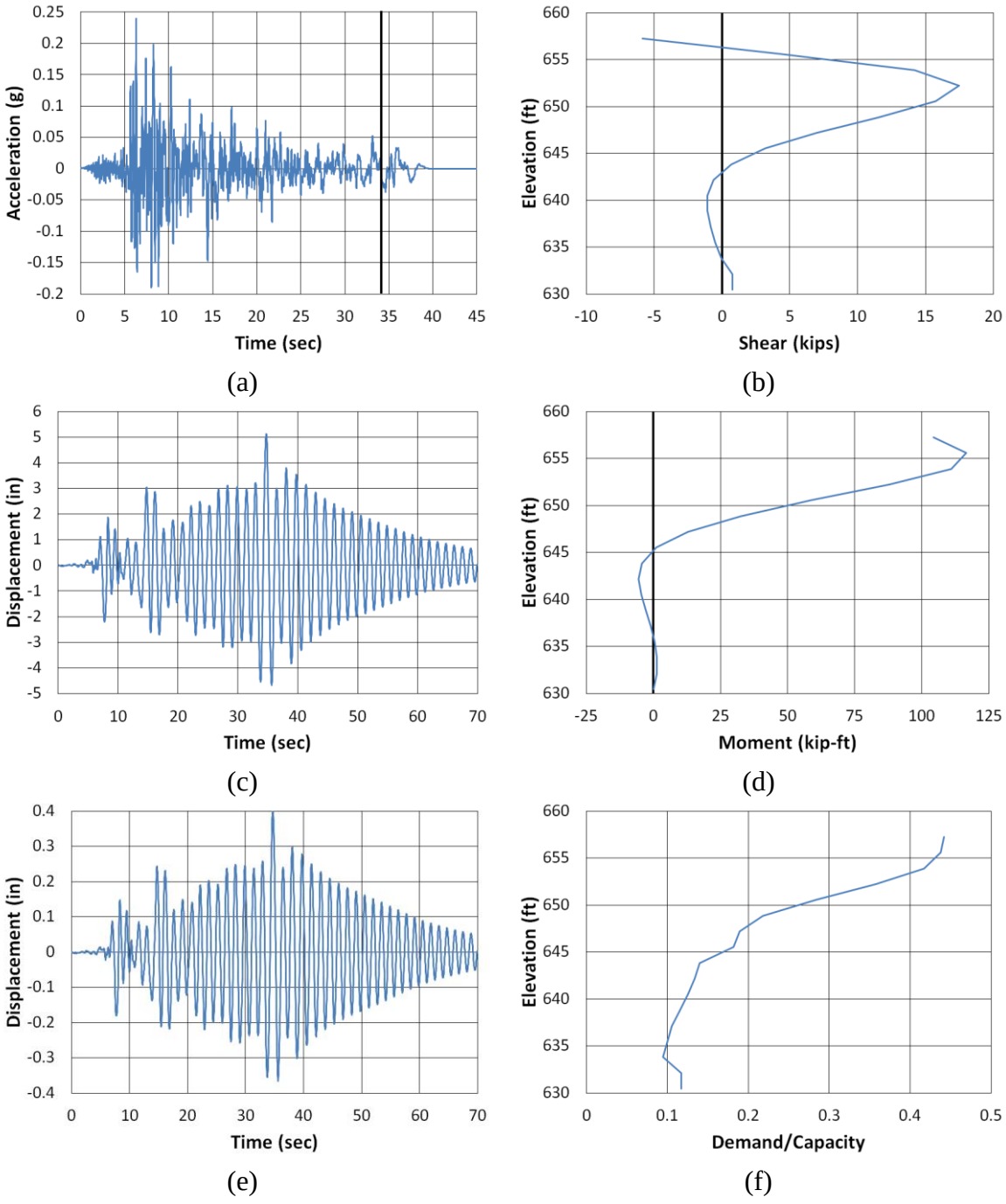

Figure B.138. Lee County Longitudinal Imperial Valley NMCE (a) time-history event, (b) shear distribution, (c) top of pier displacement, (d) moment distribution, (e) ground surface displacement, and (f) demand capacity ratio

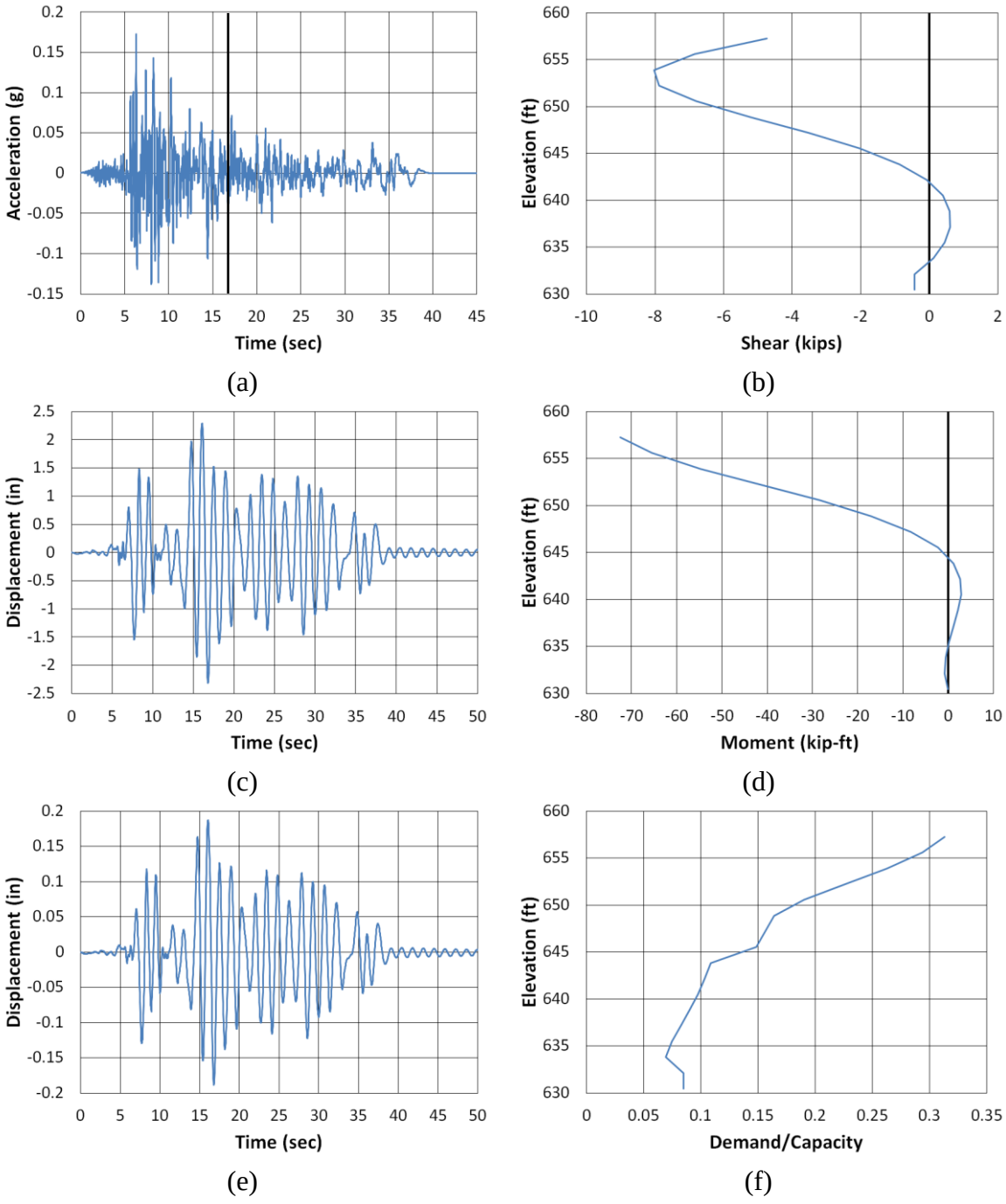

Figure B.139. Lee County Longitudinal Imperial Valley North (a) time-history event, (b) shear distribution, (c) top of pier displacement, (d) moment distribution, (e) ground surface displacement, and (f) demand capacity ratio

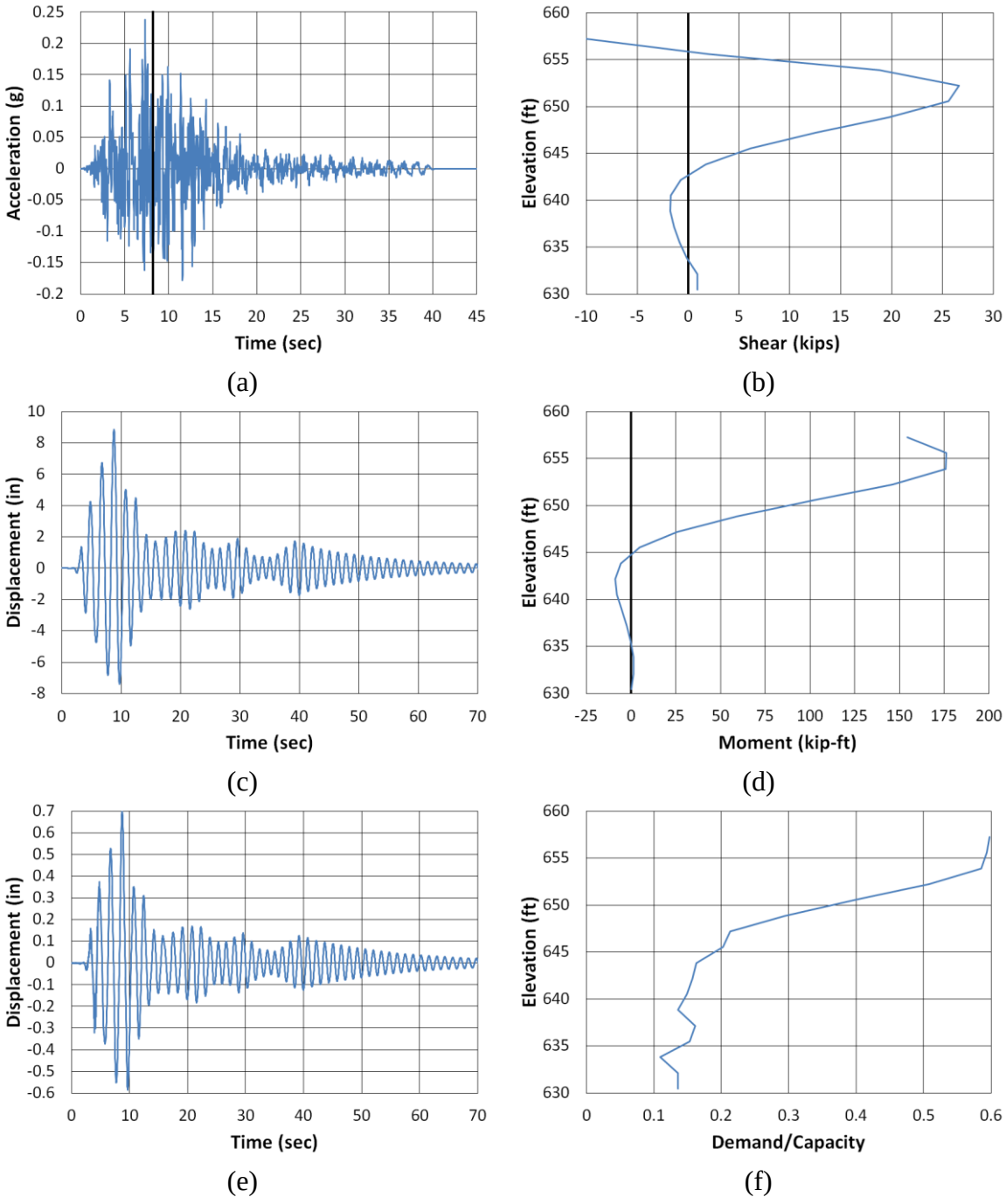

Figure B.140. Lee County Longitudinal Kobe NMCE (a) time-history event, (b) shear distribution, (c) top of pier displacement, (d) moment distribution, (e) ground surface displacement, and (f) demand capacity ratio

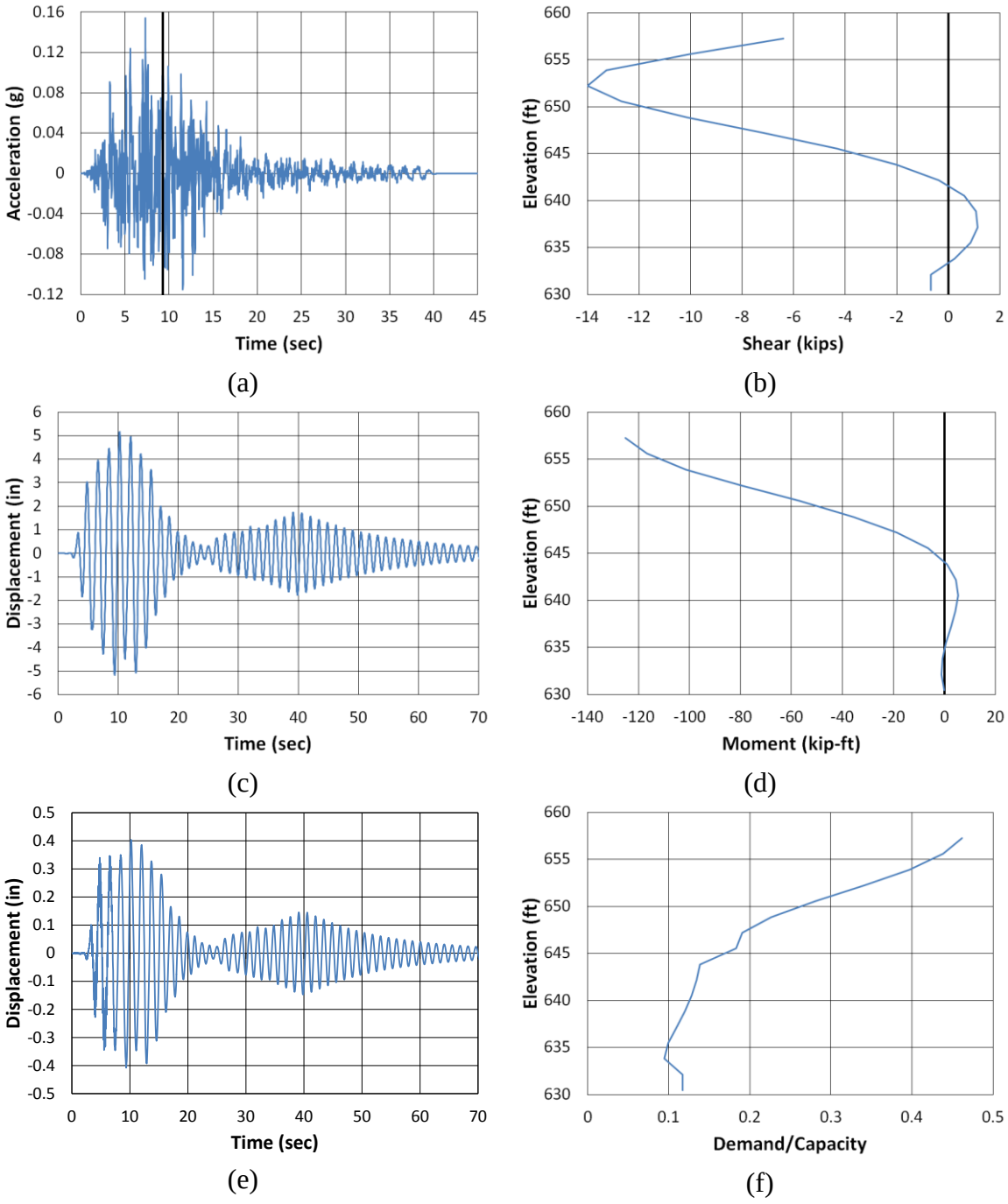

Figure B.141. Lee County Longitudinal Kobe North (a) time-history event, (b) shear distribution, (c) top of pier displacement, (d) moment distribution, (e) ground surface displacement, and (f) demand capacity ratio

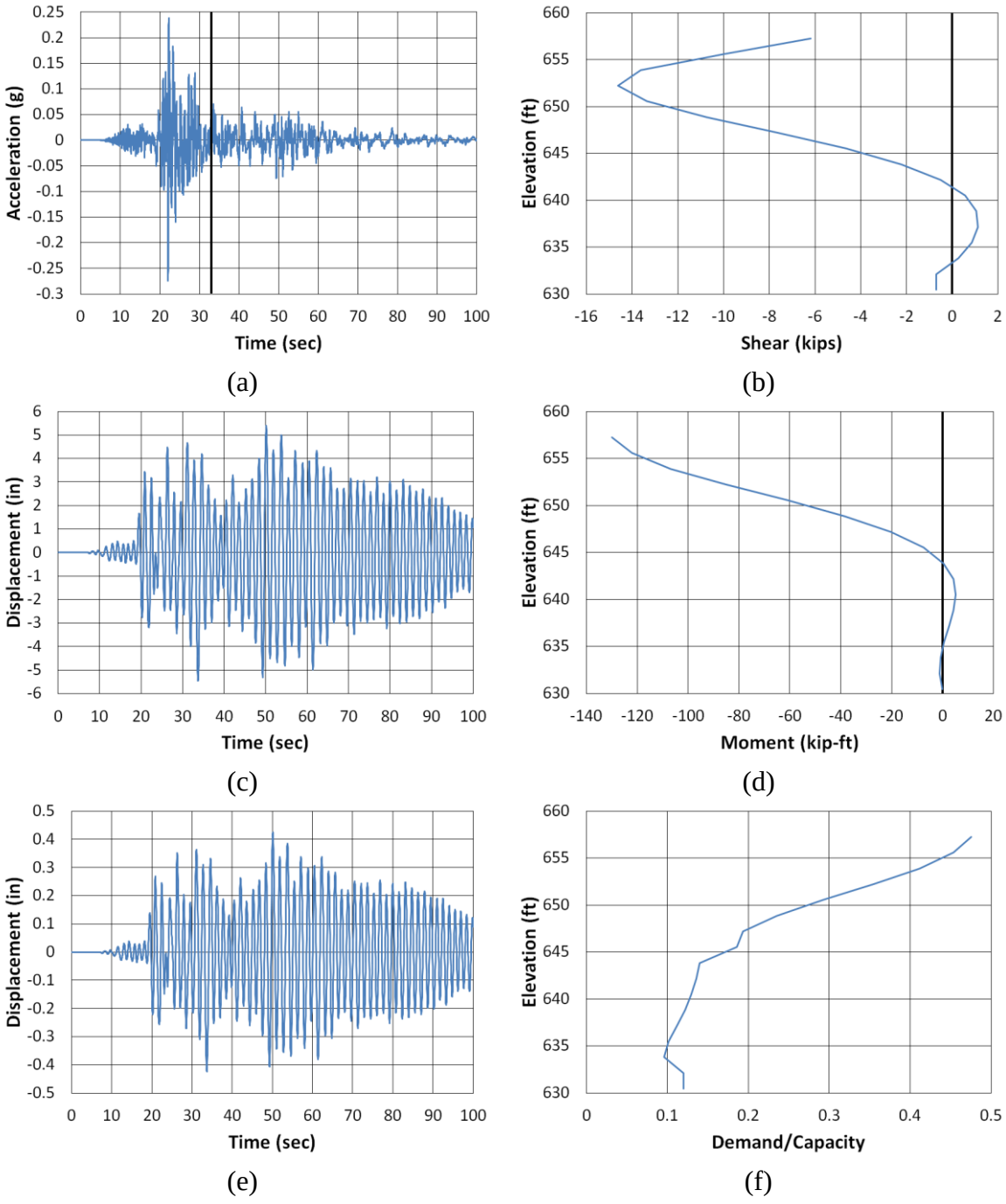

Figure B.142. Lee County Longitudinal Kocaeli NMCE (a) time-history event, (b) shear distribution, (c) top of pier displacement, (d) moment distribution, (e) ground surface displacement, and (f) demand capacity ratio

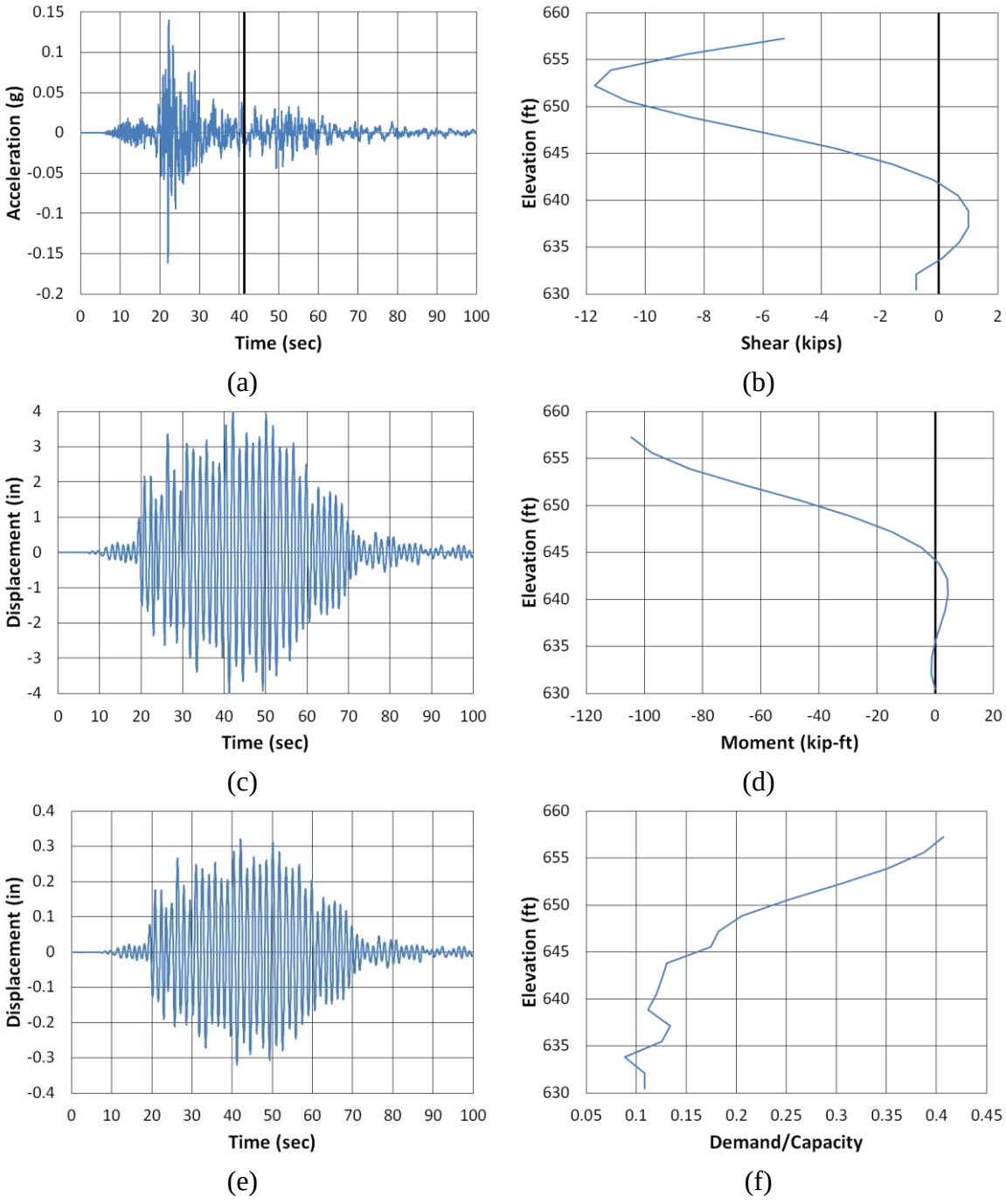

Figure B.143. Lee County Longitudinal Kocaeli North (a) time-history event, (b) shear distribution, (c) top of pier displacement, (d) moment distribution, (e) ground surface displacement, and (f) demand capacity ratio

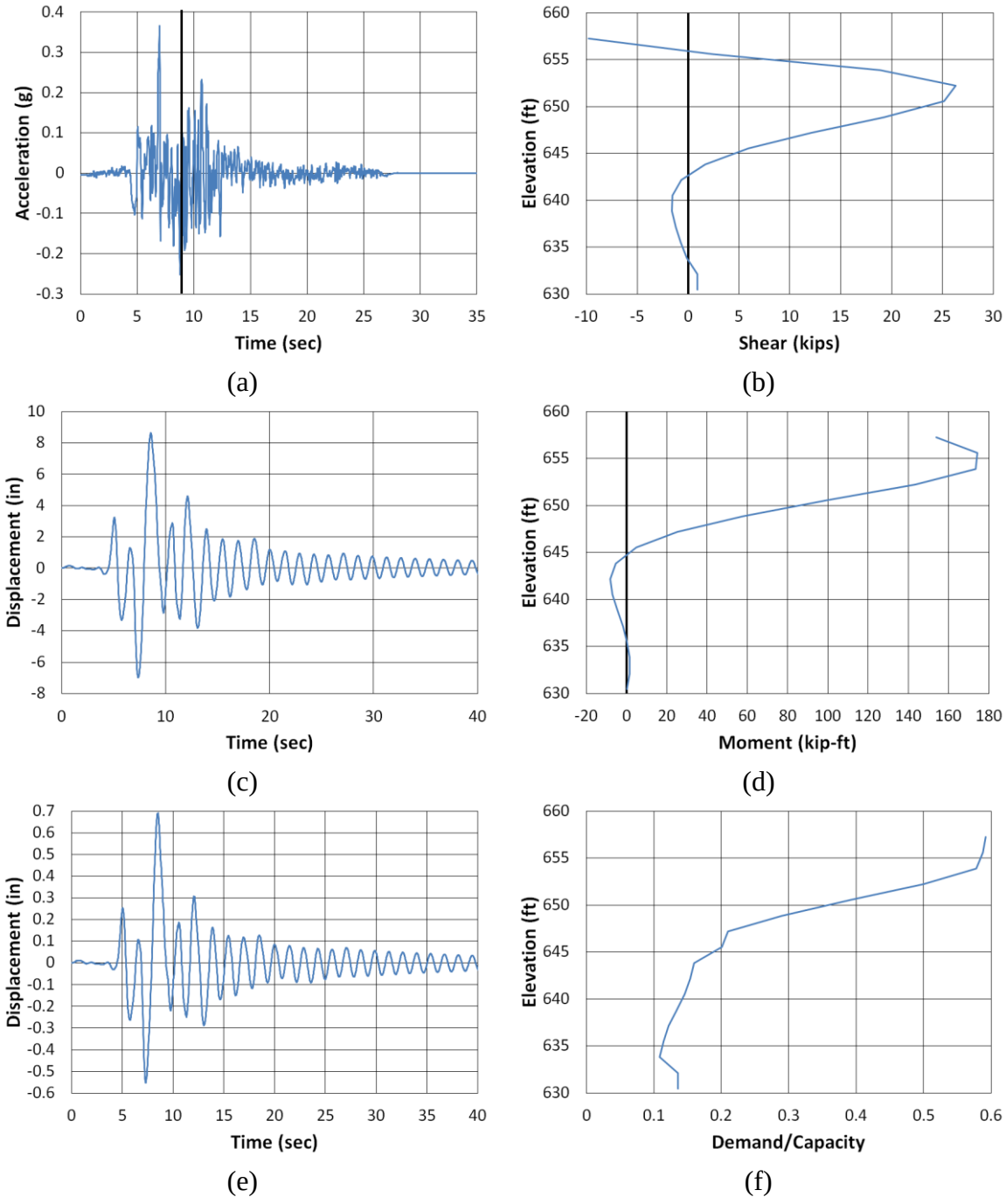

Figure B.144. Lee County Longitudinal Kocaeli2 NMCE (a) time-history event, (b) shear distribution, (c) top of pier displacement, (d) moment distribution, (e) ground surface displacement, and (f) demand capacity ratio

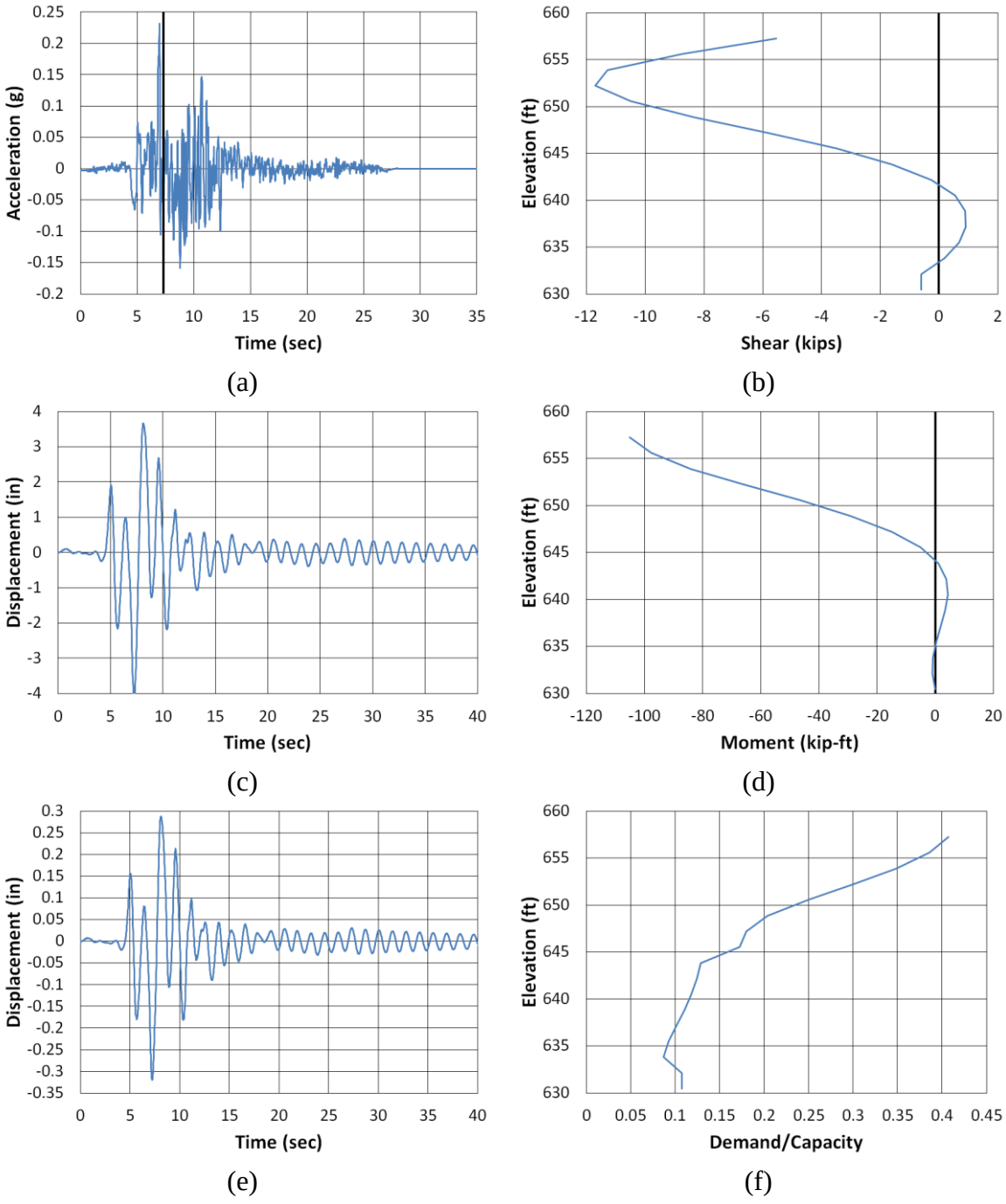

Figure B.145. Lee County Longitudinal Kocaeli2 North (a) time-history event, (b) shear distribution, (c) top of pier displacement, (d) moment distribution, (e) ground surface displacement, and (f) demand capacity ratio

.

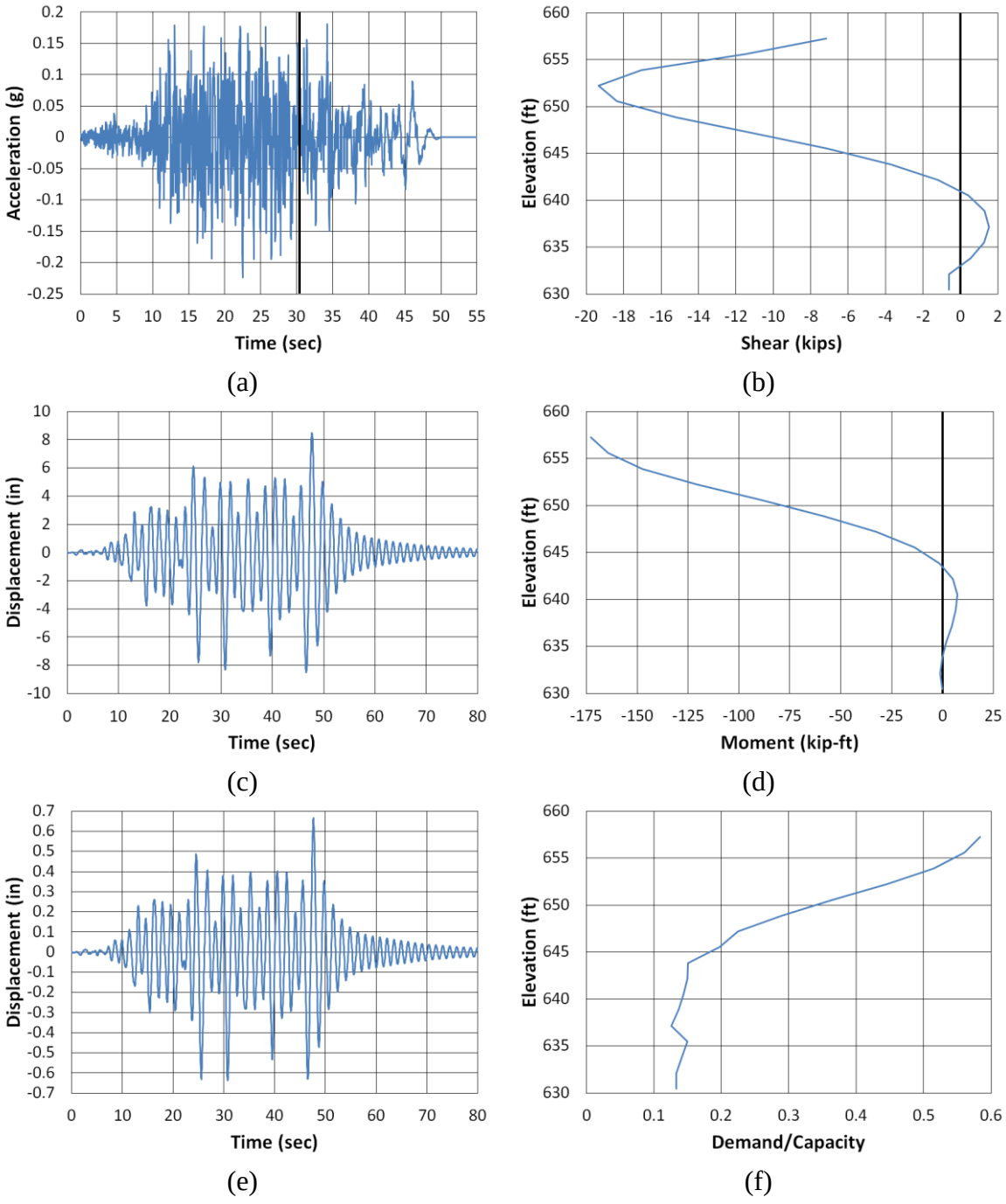

Figure B.146. Lee County Longitudinal Landers NMCE (a) time-history event, (b) shear distribution, (c) top of pier displacement, (d) moment distribution, (e) ground surface displacement, and (f) demand capacity ratio

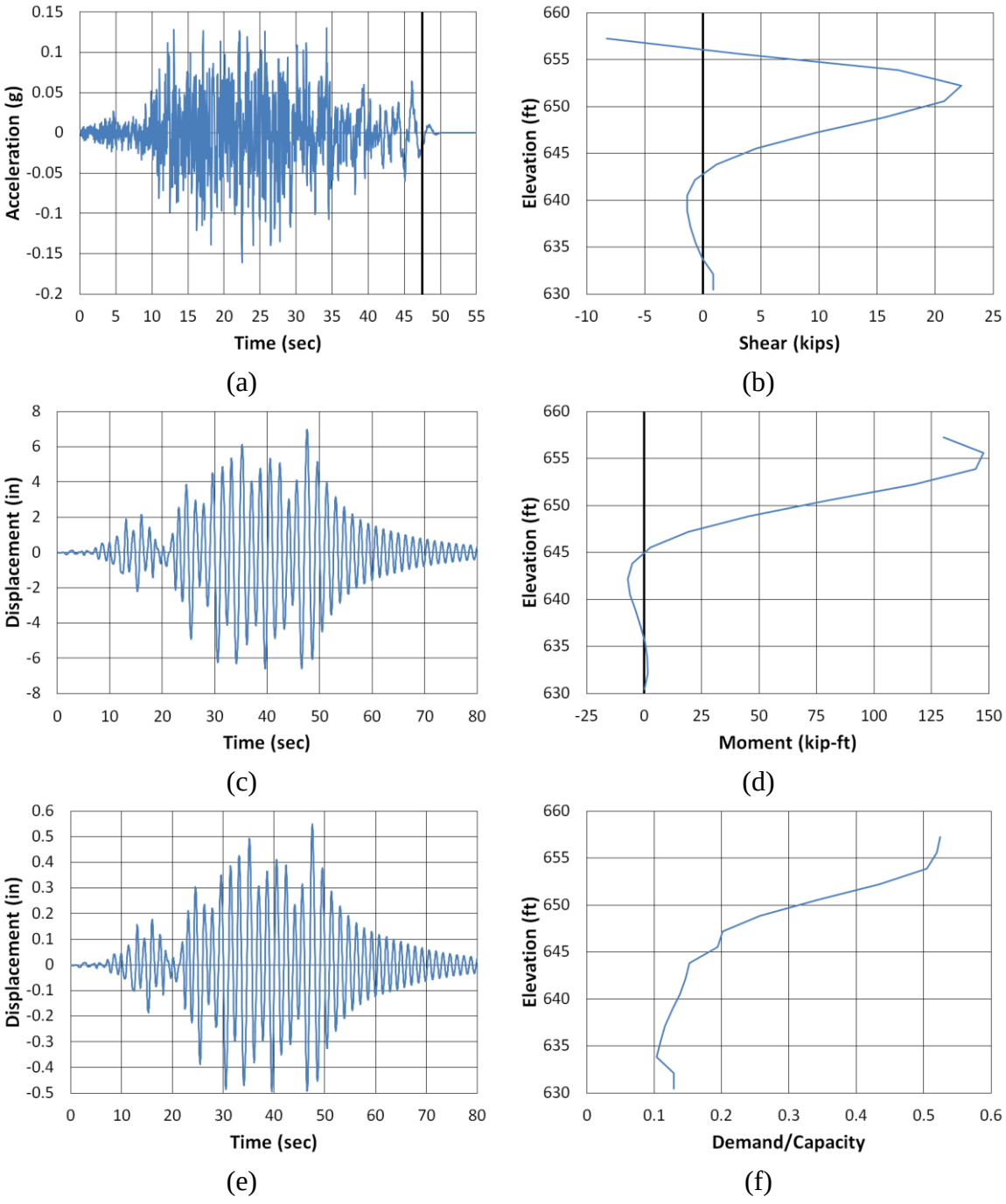

Figure B.147. Lee County Longitudinal Landers North (a) time-history event, (b) shear distribution, (c) top of pier displacement, (d) moment distribution, (e) ground surface displacement, and (f) demand capacity ratio

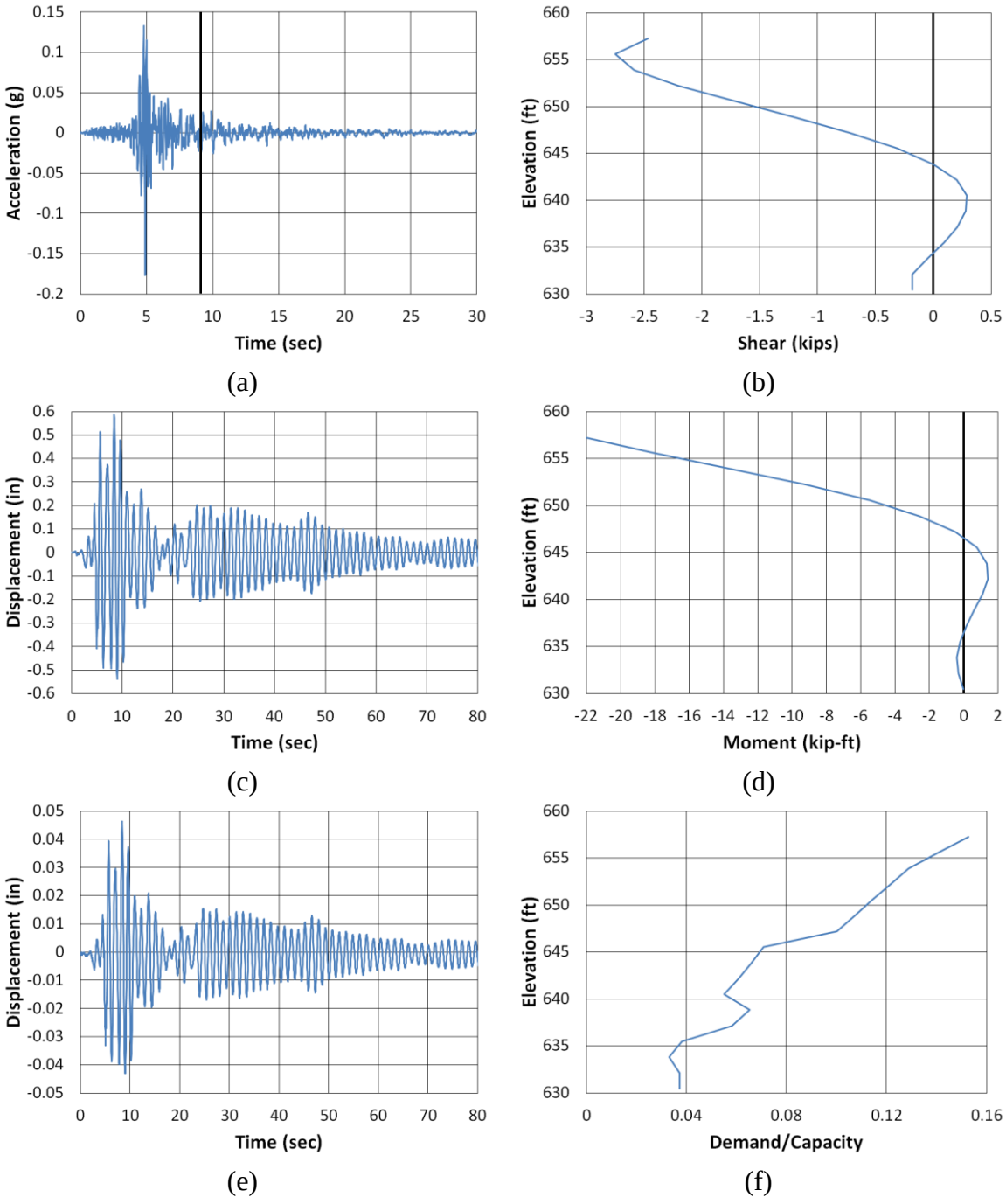

Figure B.148. Lee County Longitudinal LSM North (a) time-history event, (b) shear distribution, (c) top of pier displacement, (d) moment distribution, (e) ground surface displacement, and (f) demand capacity ratio

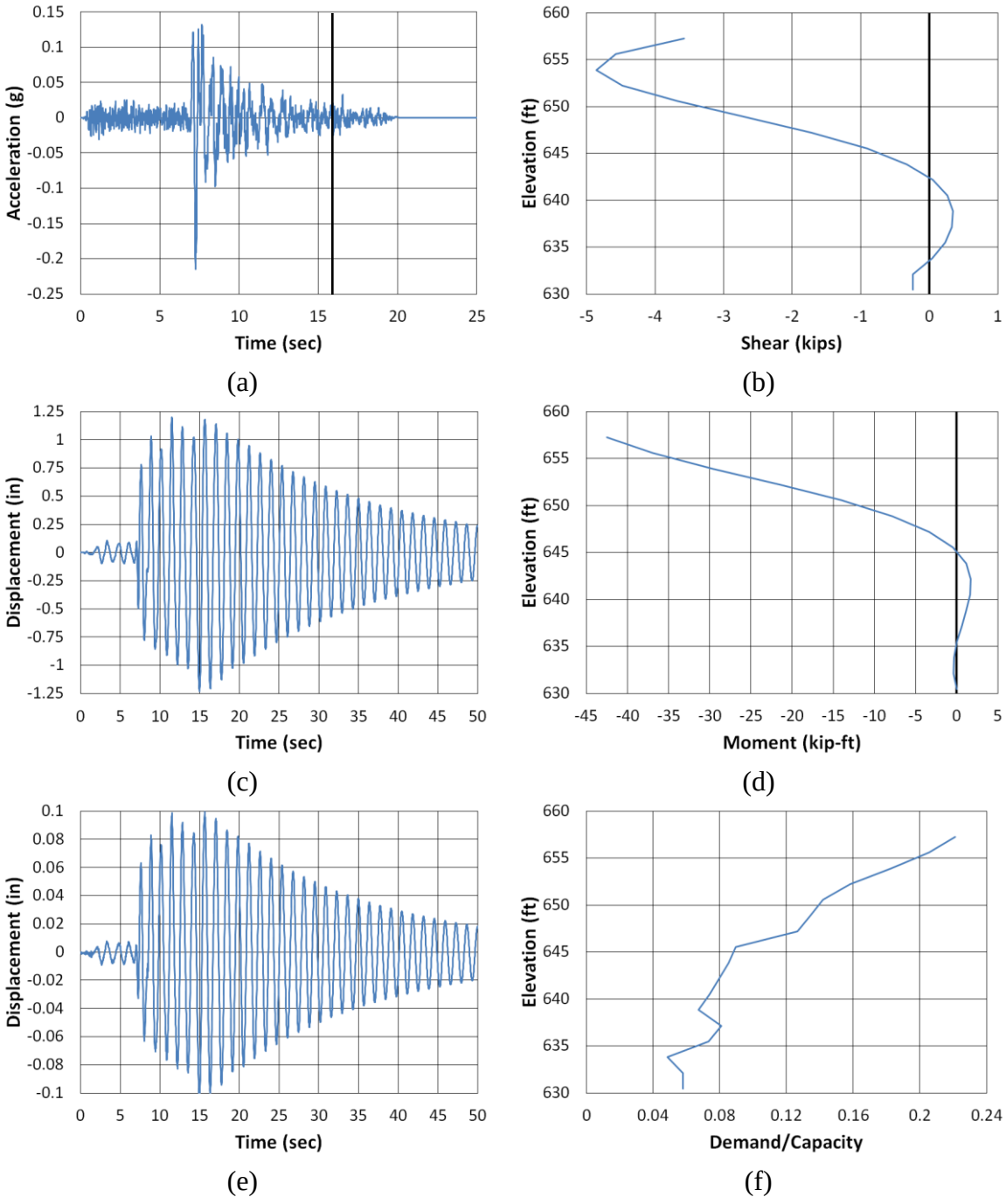

Figure B.149. Lee County Longitudinal NPS North (a) time-history event, (b) shear distribution, (c) top of pier displacement, (d) moment distribution, (e) ground surface displacement, and (f) demand capacity ratio

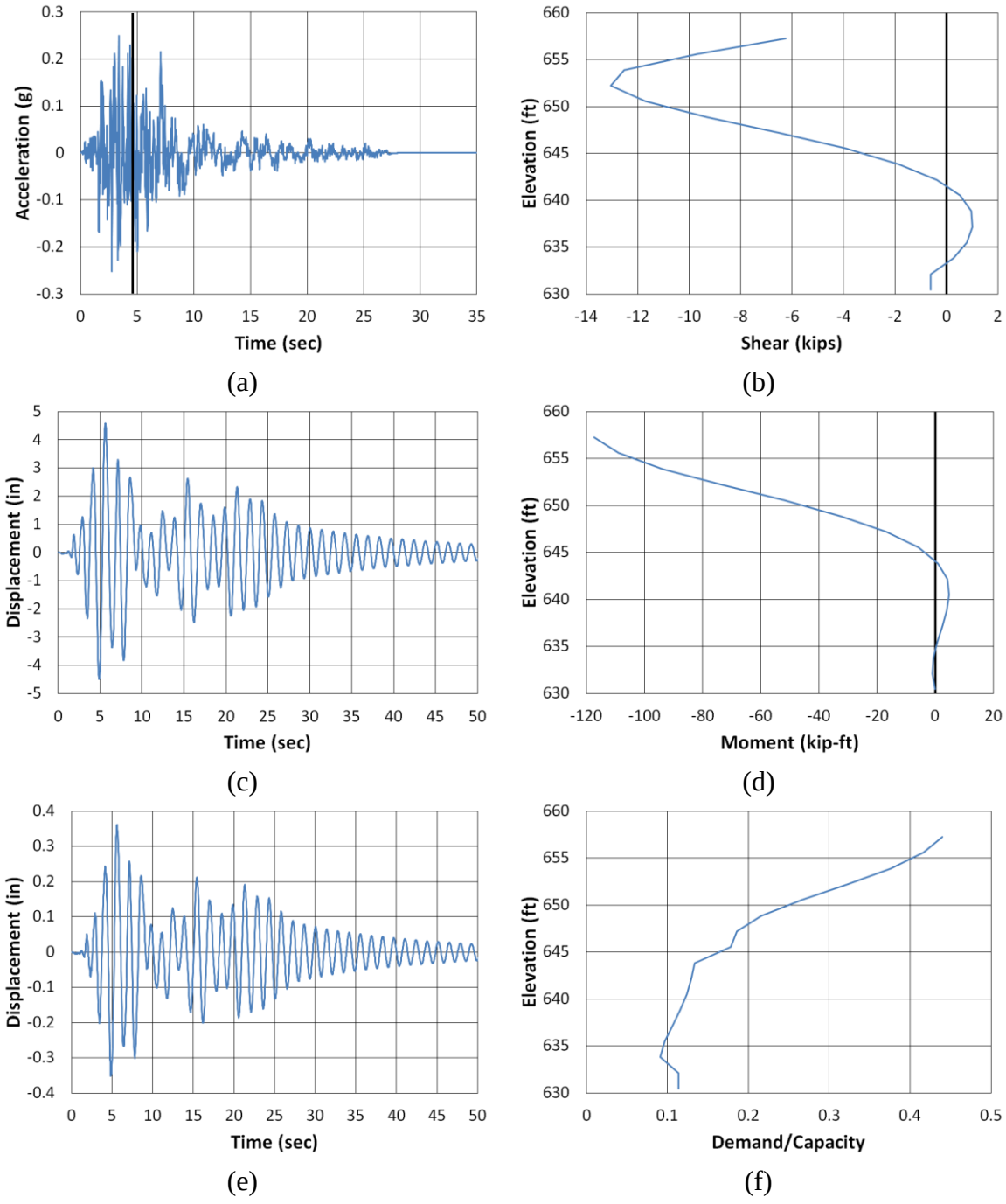

Figure B.150. Lee County Longitudinal San Fernando NMCE (a) time-history event, (b) shear distribution, (c) top of pier displacement, (d) moment distribution, (e) ground surface displacement, and (f) demand capacity ratio

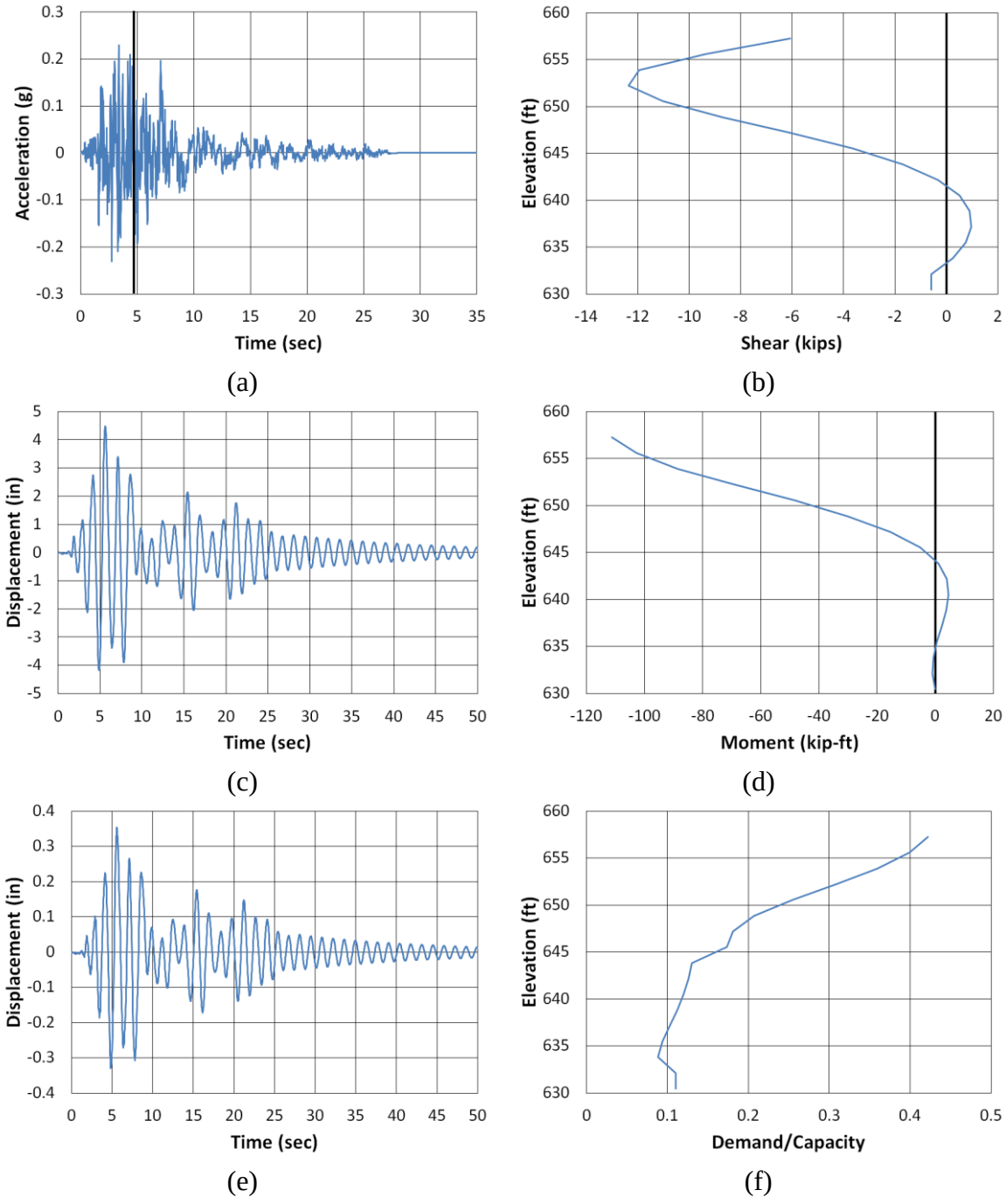

Figure B.151 Lee County Longitudinal San Fernando North (a) time-history event, (b) shear distribution, (c) top of pier displacement, (d) moment distribution, (e) ground surface displacement, and (f) demand capacity ratio

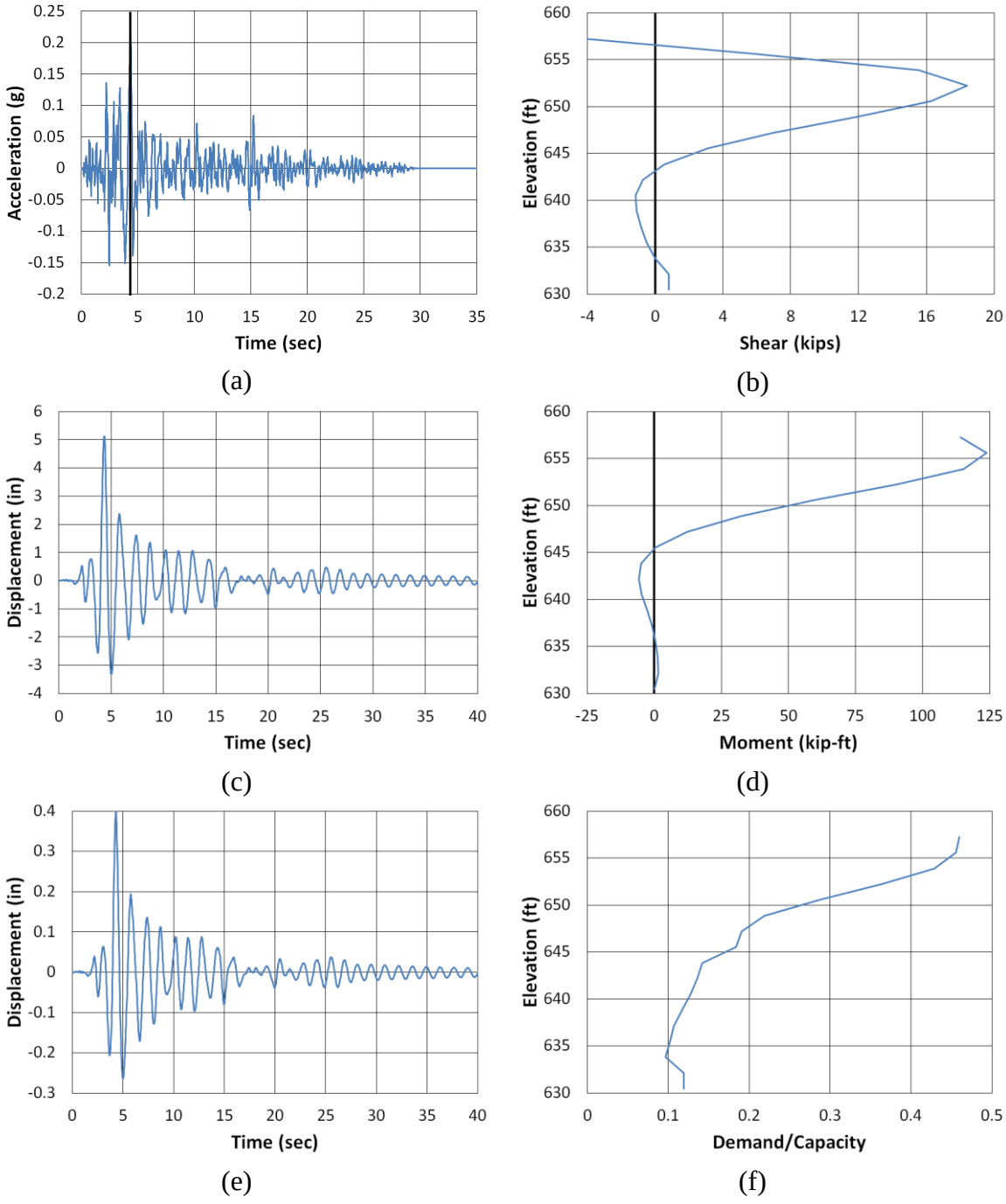

Figure B.152. Lee County Longitudinal San Fernando2 NMCE (a) time-history event, (b) shear distribution, (c) top of pier displacement, (d) moment distribution, (e) ground surface displacement, and (f) demand capacity ratio

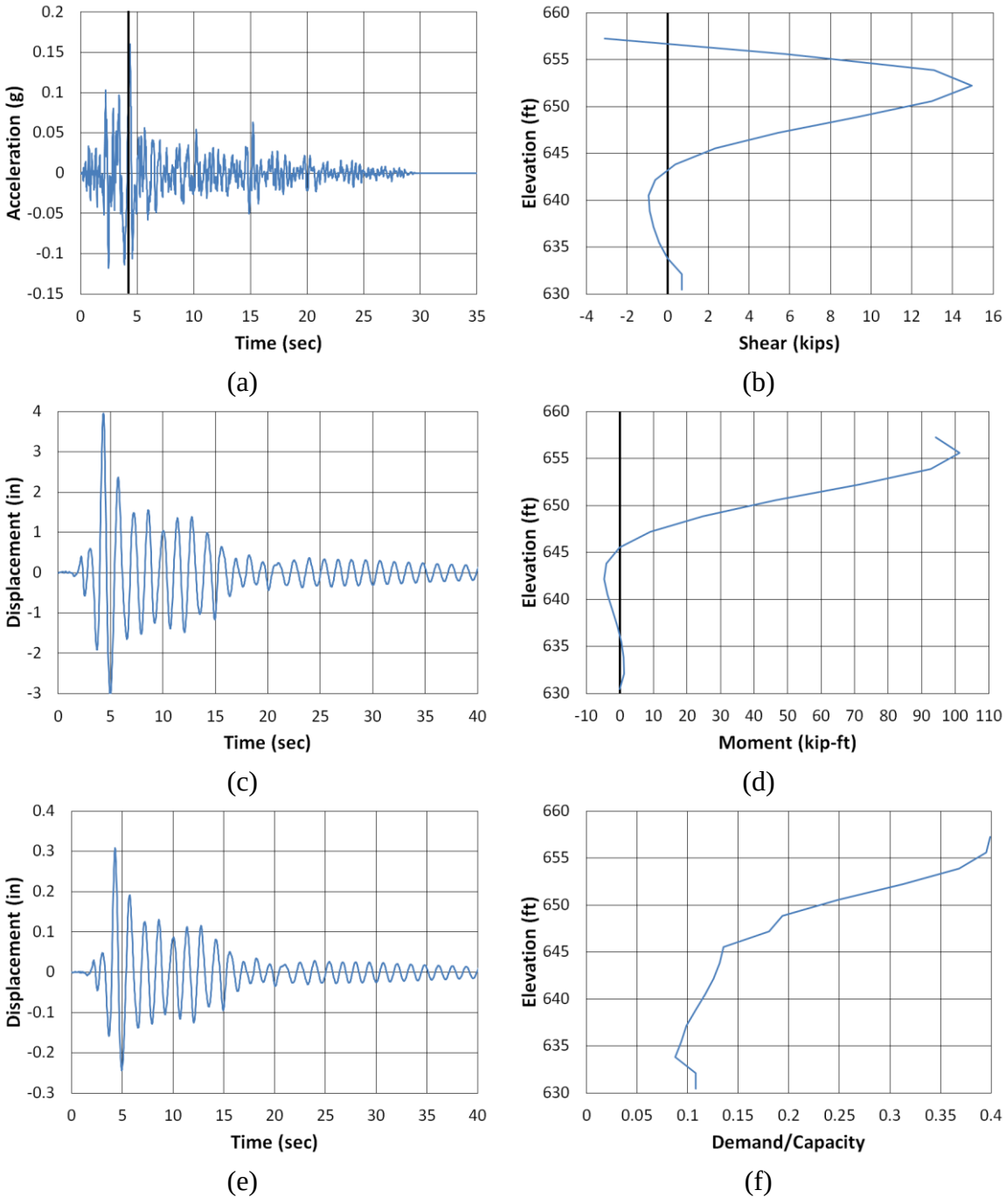

Figure B.153. Lee County Longitudinal San Fernando2 North (a) time-history event, (b) shear distribution, (c) top of pier displacement, (d) moment distribution, (e) ground surface displacement, and (f) demand capacity ratio

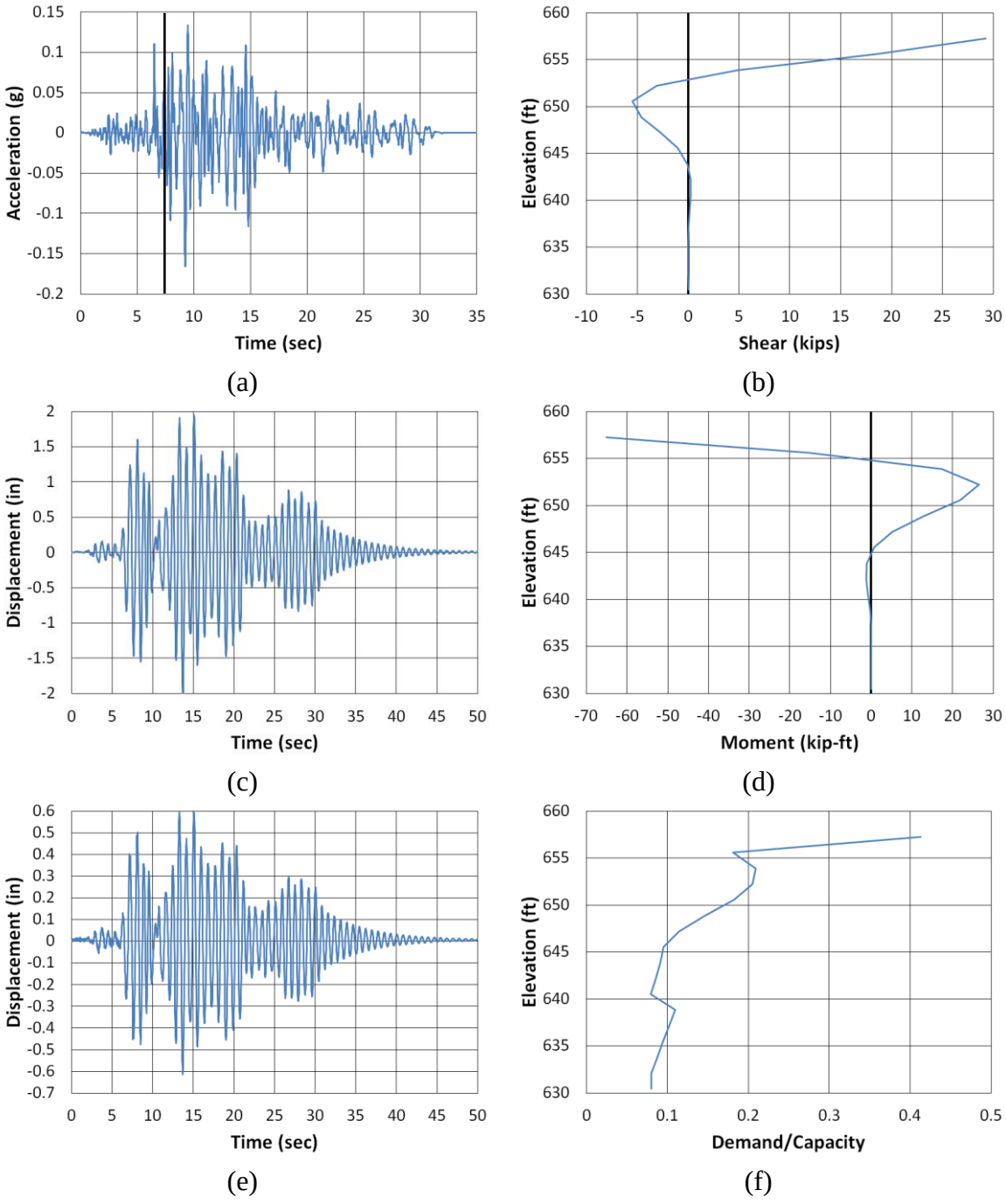

Figure B.154. Lee County Transverse Coalinga North (a) time-history event, (b) shear distribution, (c) top of pier displacement, (d) moment distribution, (e) ground surface displacement, and (f) demand capacity ratio

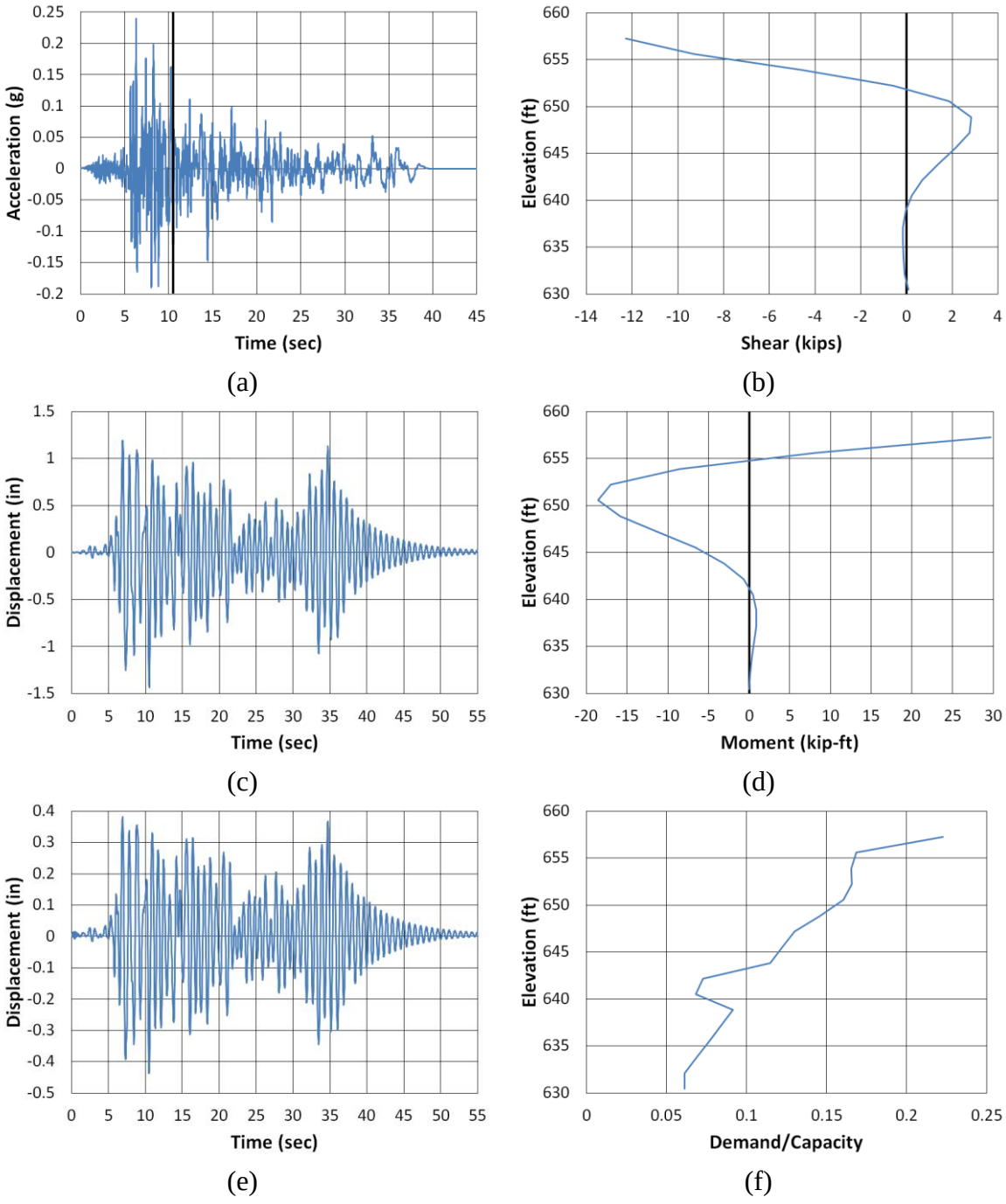

Figure B.155. Lee County Transverse Imperial Valley NMCE (a) time-history event, (b) shear distribution, (c) top of pier displacement, (d) moment distribution, (e) ground surface displacement, and (f) demand capacity ratio

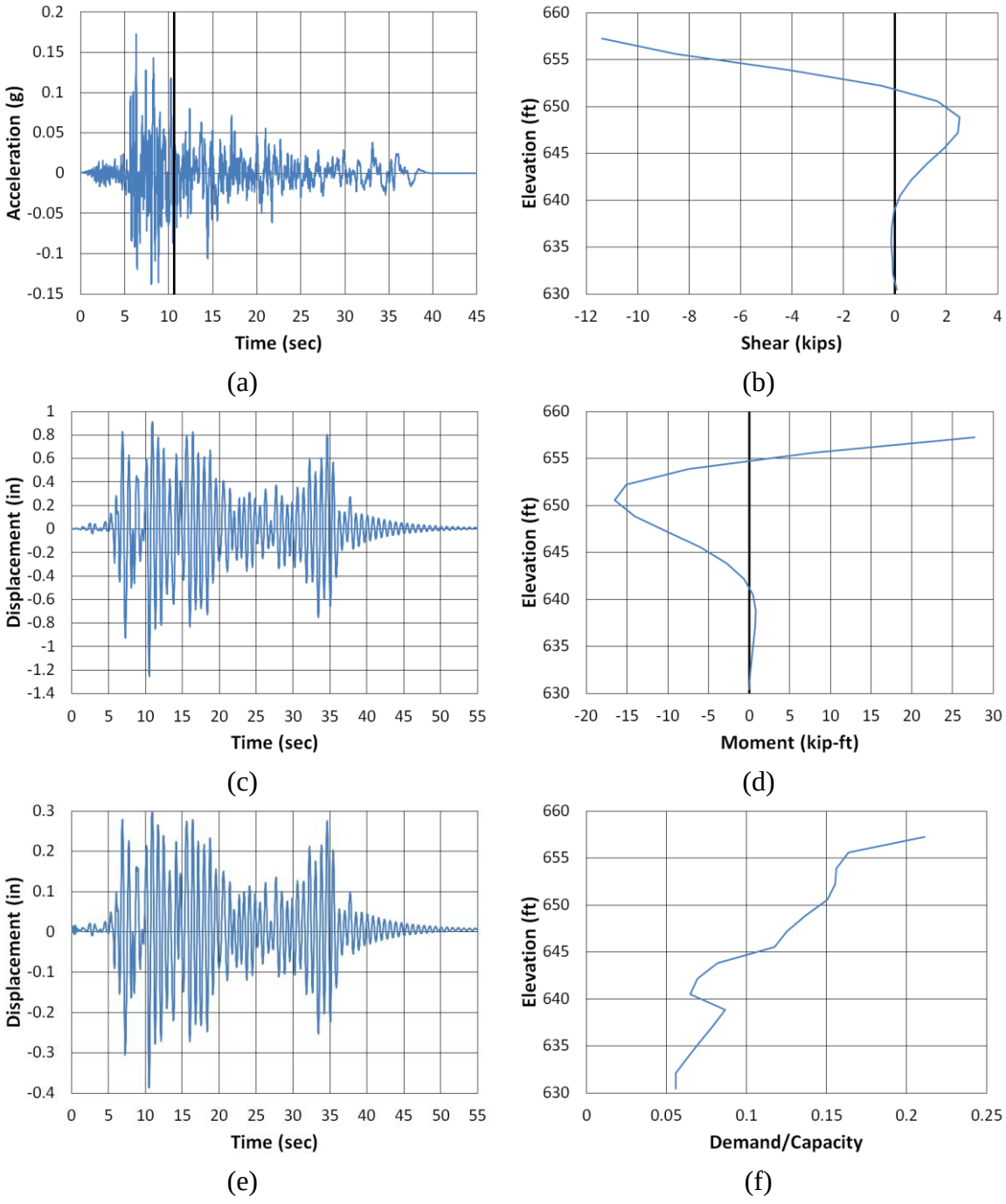

Figure B.156. Lee County Transverse Imperial Valley North (a) time-history event, (b) shear distribution, (c) top of pier displacement, (d) moment distribution, (e) ground surface displacement, and (f) demand capacity ratio

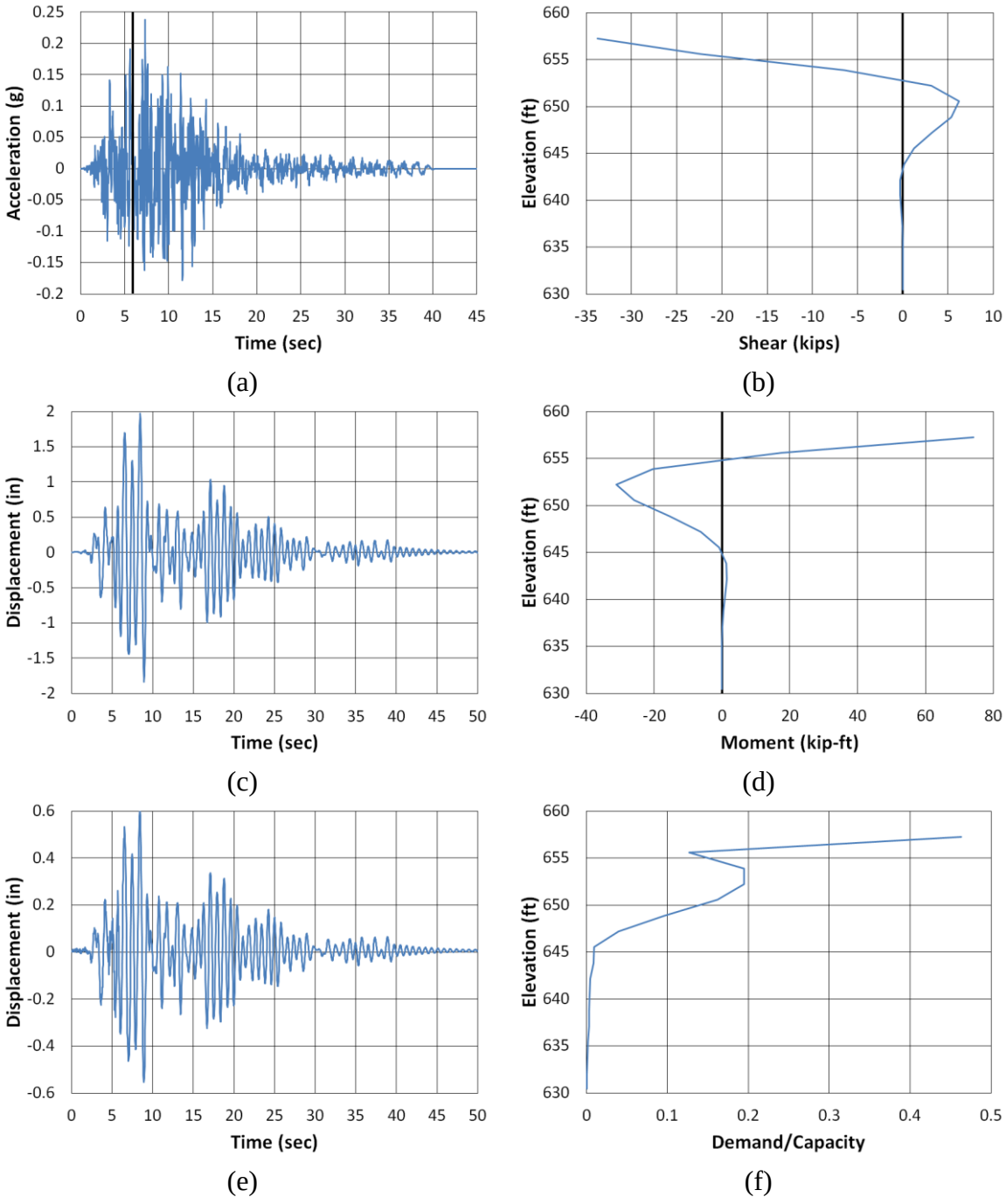

Figure B.157. Lee County Transverse Kobe NMCE (a) time-history event, (b) shear distribution, (c) top of pier displacement, (d) moment distribution, (e) ground surface displacement, and (f) demand capacity ratio

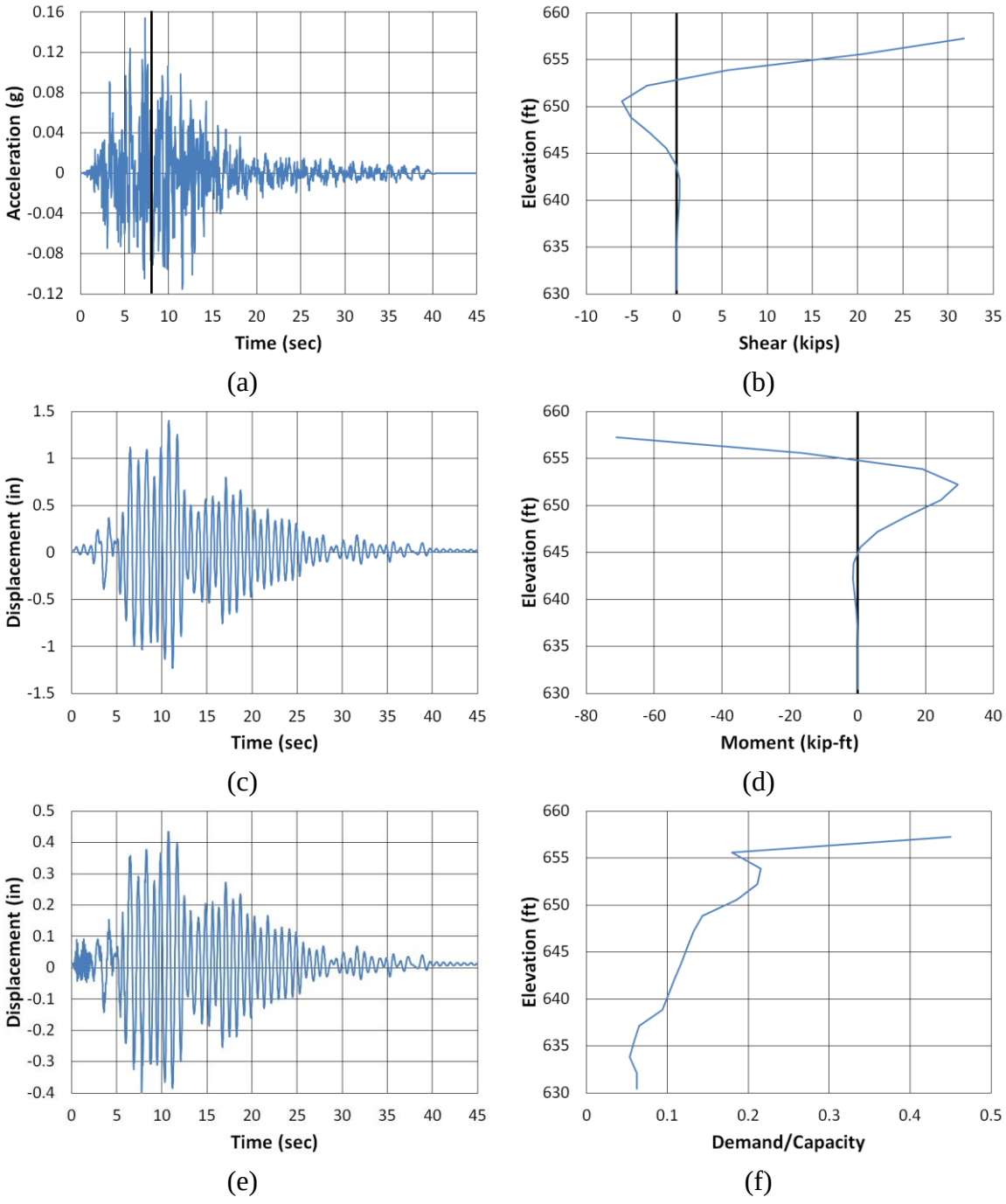

Figure B.158. Lee County Transverse Kobe North (a) time-history event, (b) shear distribution, (c) top of pier displacement, (d) moment distribution, (e) ground surface displacement, and (f) demand capacity ratio

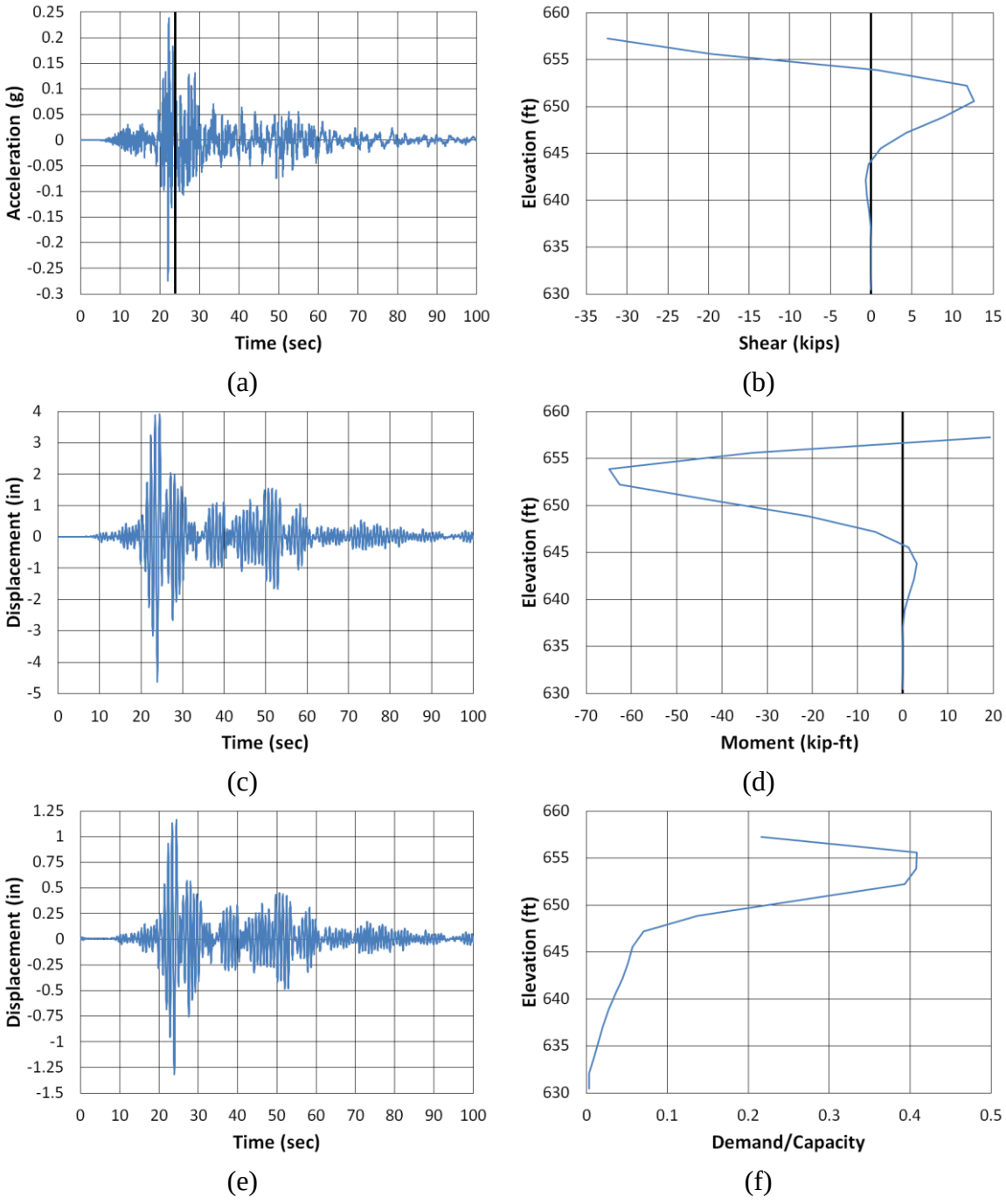

Figure B.159. Lee County Transverse Kocaeli NMCE (a) time-history event, (b) shear distribution, (c) top of pier displacement, (d) moment distribution, (e) ground surface displacement, and (f) demand capacity ratio

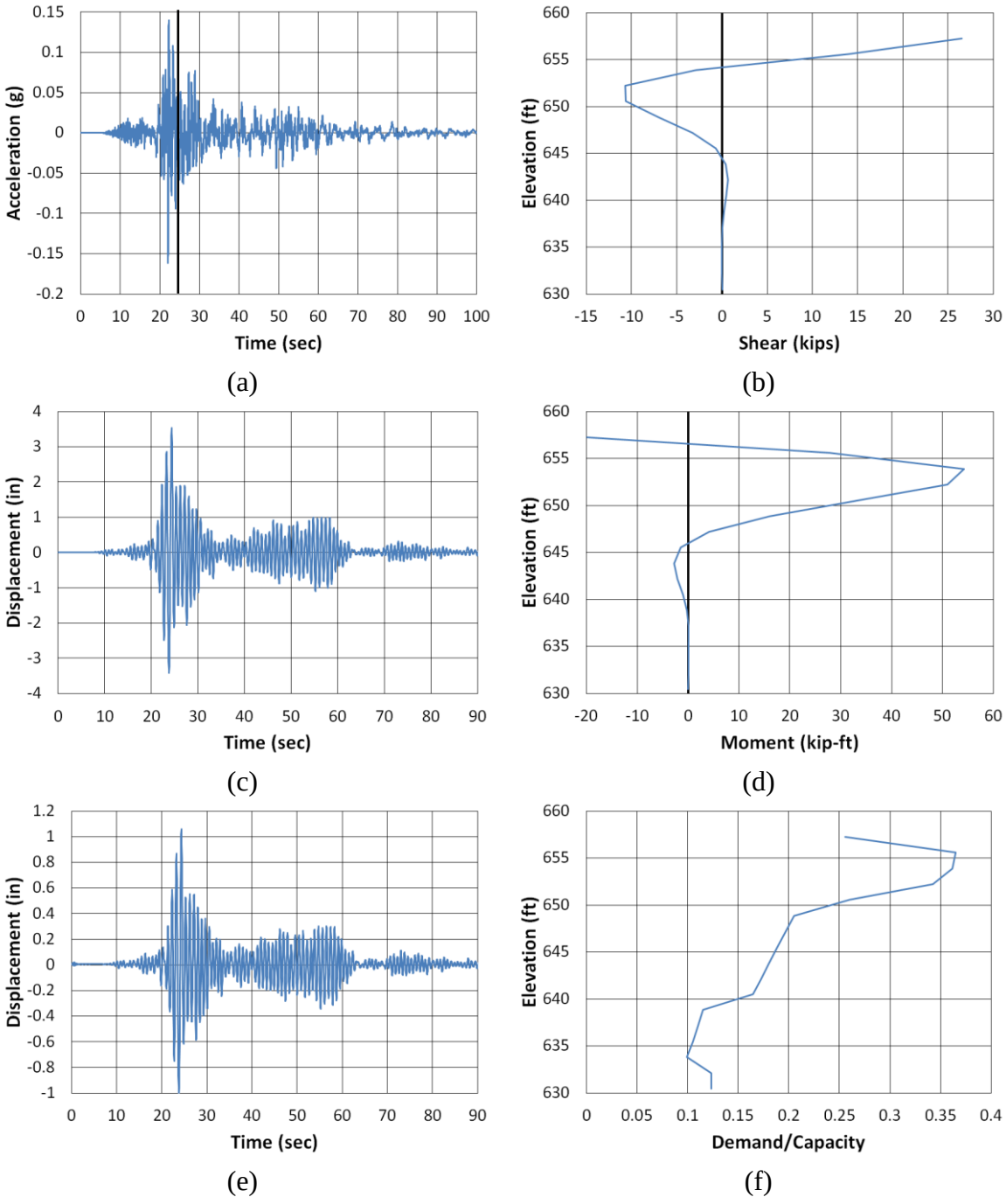

Figure B.160. Lee County Transverse Kocaeli North (a) time-history event, (b) shear distribution, (c) top of pier displacement, (d) moment distribution, (e) ground surface displacement, and (f) demand capacity ratio

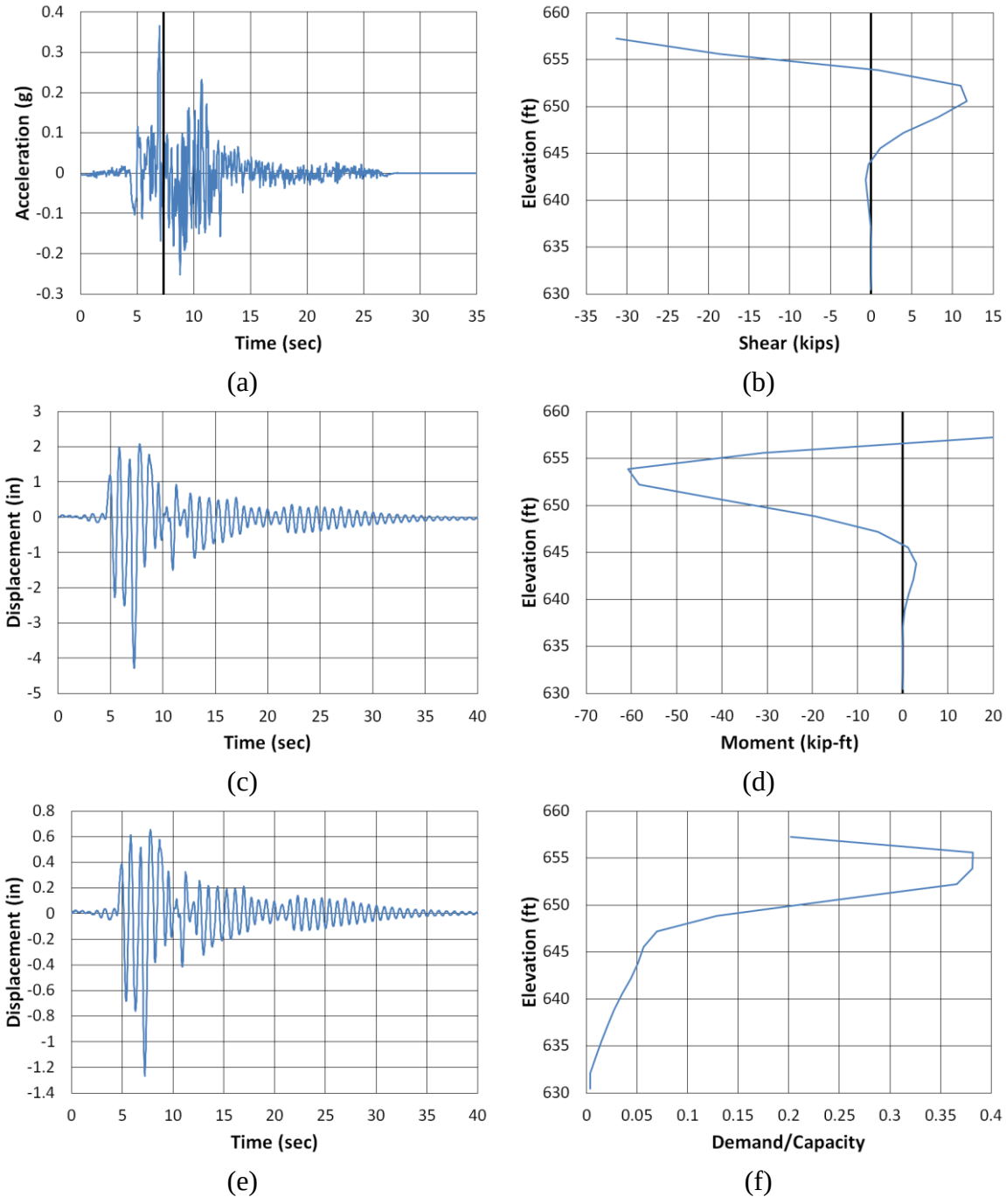

Figure B.161. Lee County Transverse Kocaeli2 NMCE (a) time-history event, (b) shear distribution, (c) top of pier displacement, (d) moment distribution, (e) ground surface displacement, and (f) demand capacity ratio

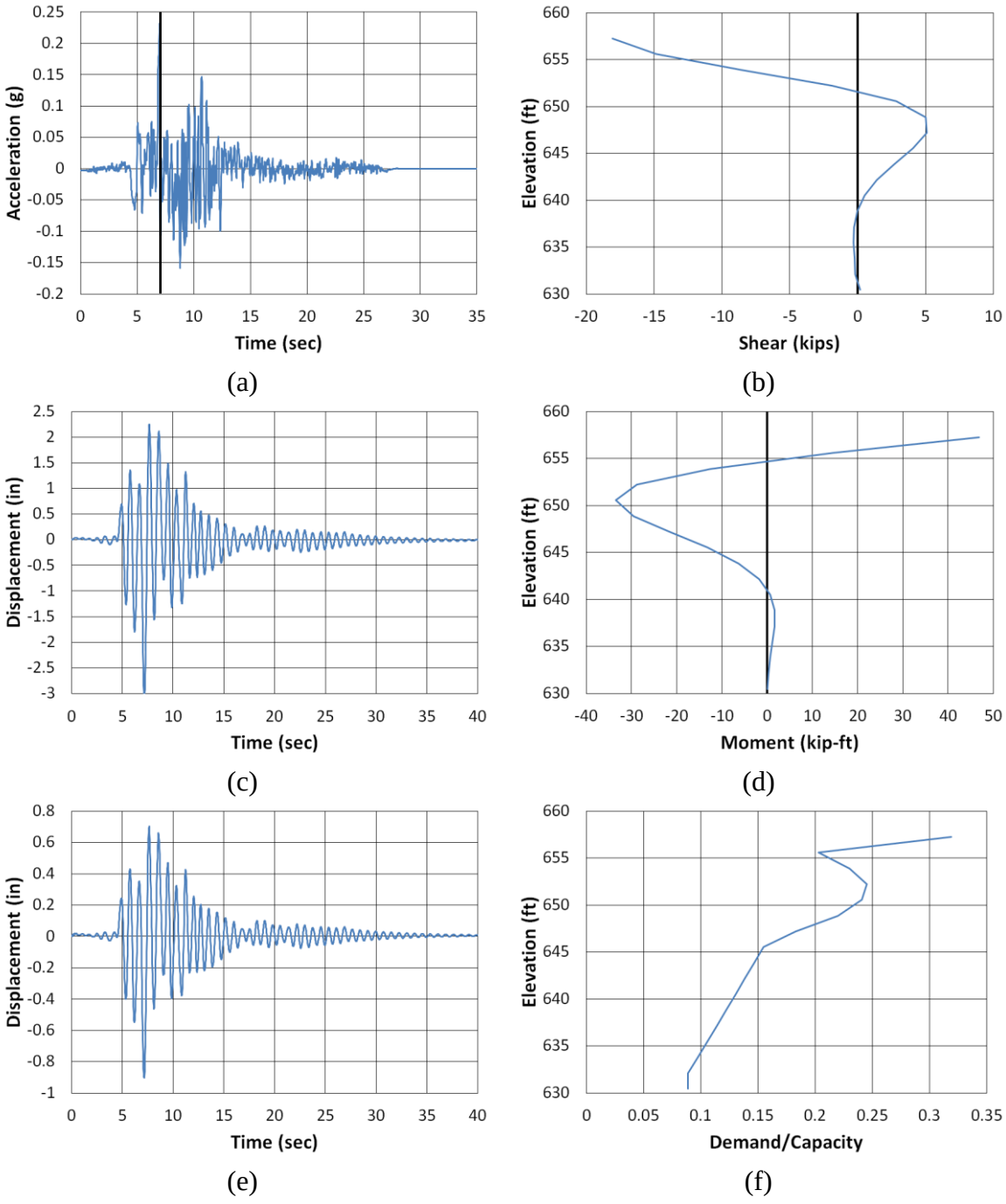

Figure B.162. Lee County Transverse Kocaeli2 North (a) time-history event, (b) shear distribution, (c) top of pier displacement, (d) moment distribution, (e) ground surface displacement, and (f) demand capacity ratio

.

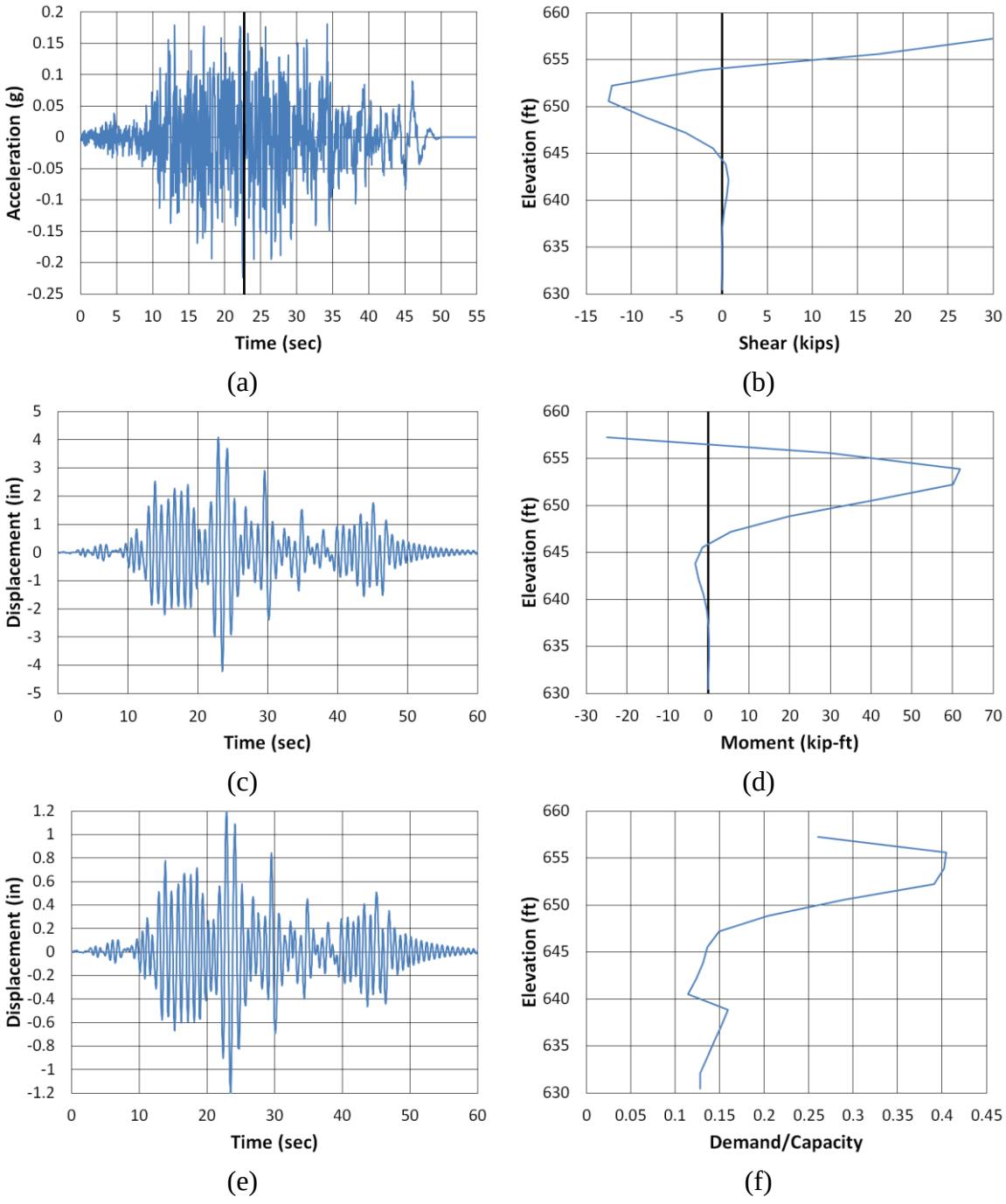

Figure B.163. Lee County Transverse Landers NMCE (a) time-history event, (b) shear distribution, (c) top of pier displacement, (d) moment distribution, (e) ground surface displacement, and (f) demand capacity ratio

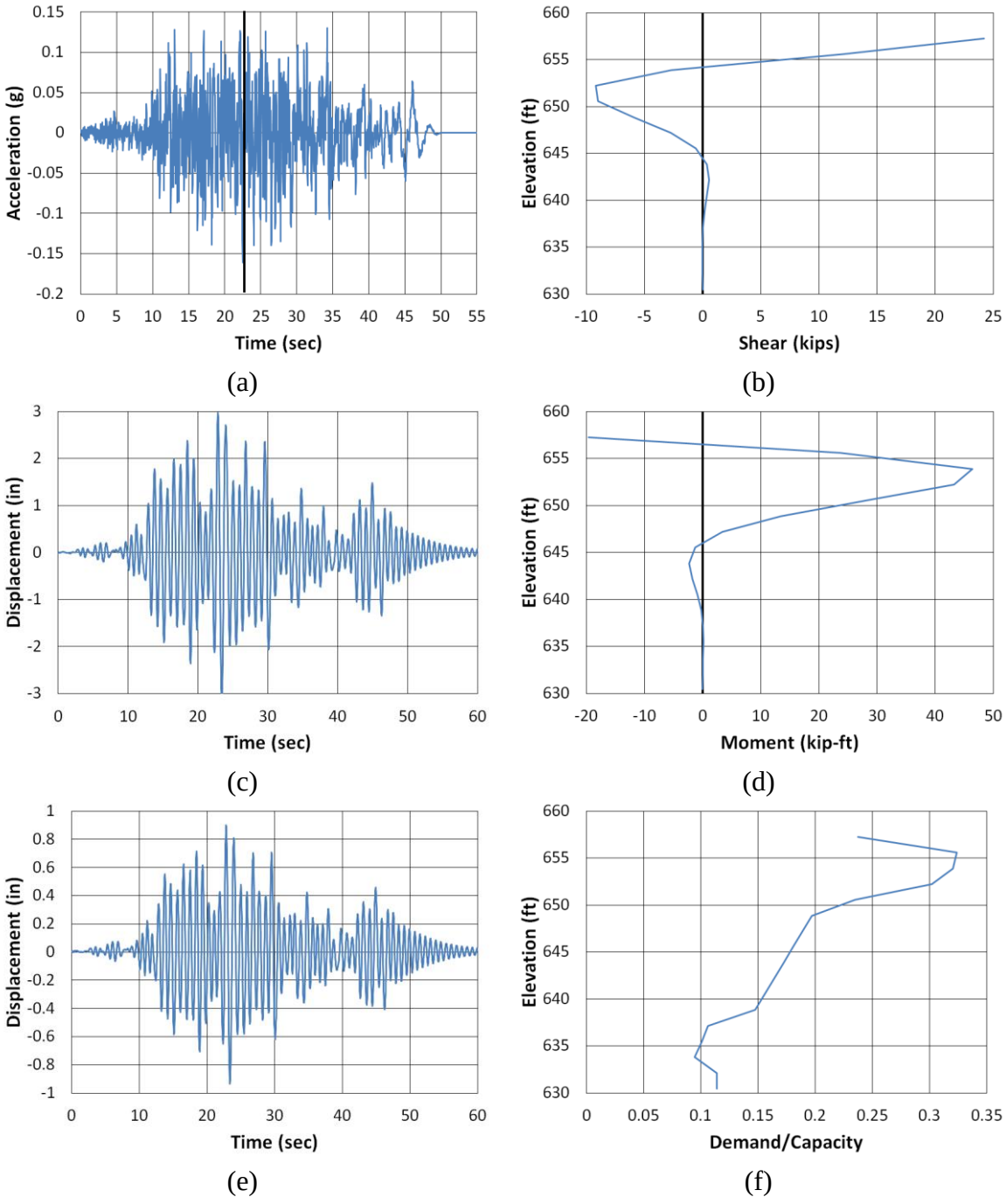

Figure B.164. Lee County Transverse Landers North (column) (a) time-history event, (b) shear distribution, (c) top of pier displacement, (d) moment distribution, (e) ground surface displacement, and (f) demand capacity ratio

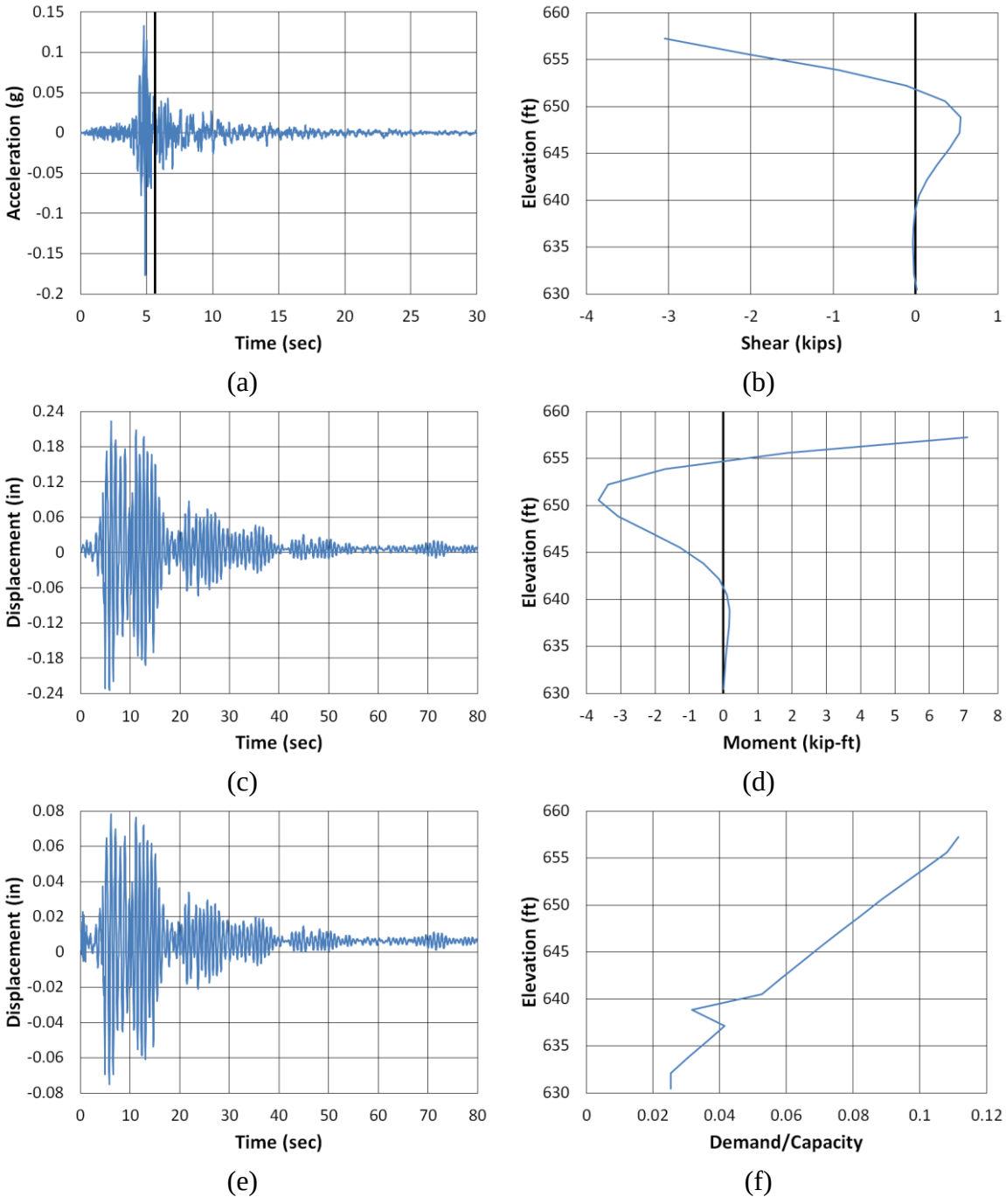

Figure B.165. Lee County Transverse LSM North (a) time-history event, (b) shear distribution, (c) top of pier displacement, (d) moment distribution, (e) ground surface displacement, and (f) demand capacity ratio

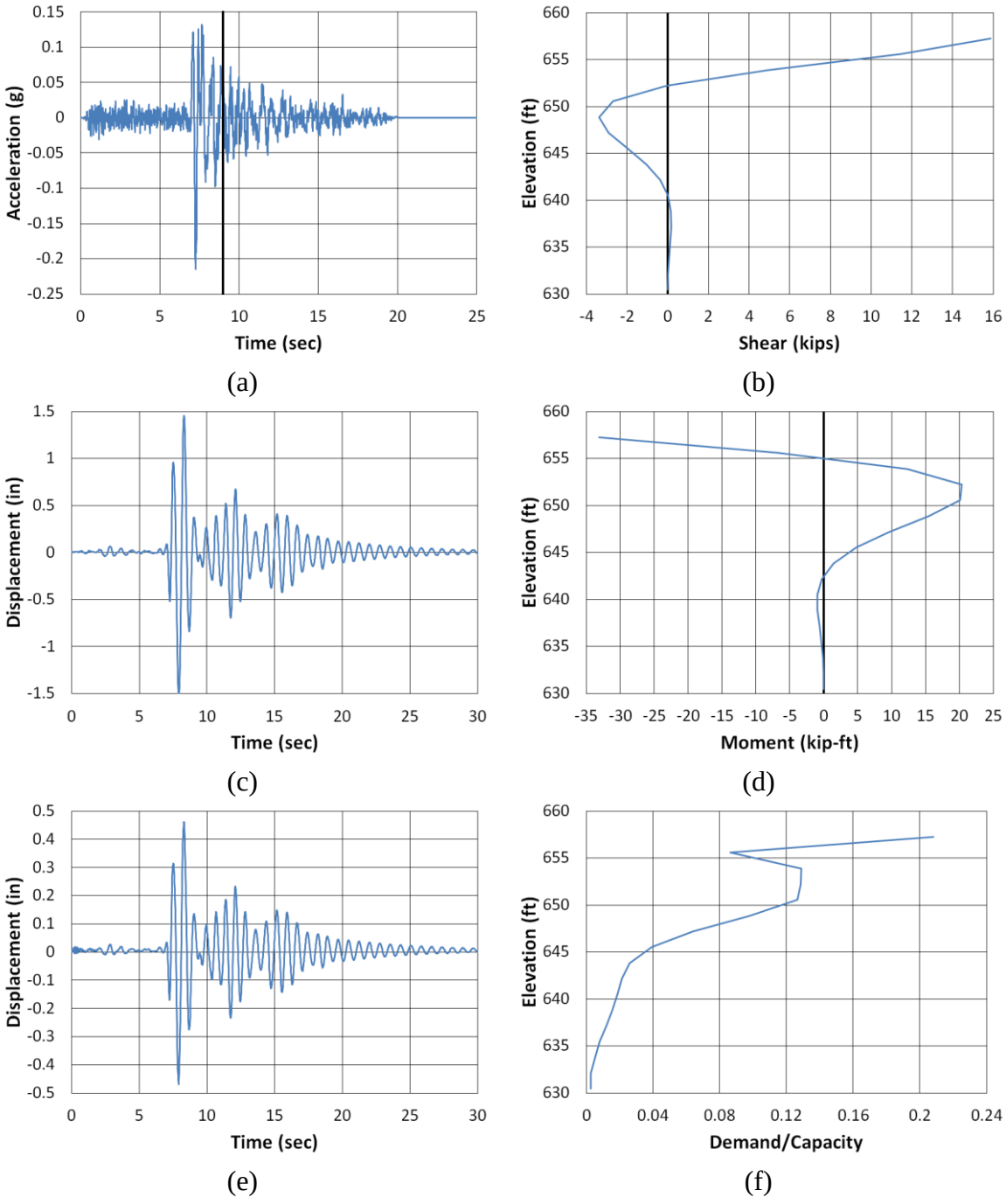

Figure B.166. Lee County Transverse NPS North (a) time-history event, (b) shear distribution, (c) top of pier displacement, (d) moment distribution, (e) ground surface displacement, and (f) demand capacity ratio

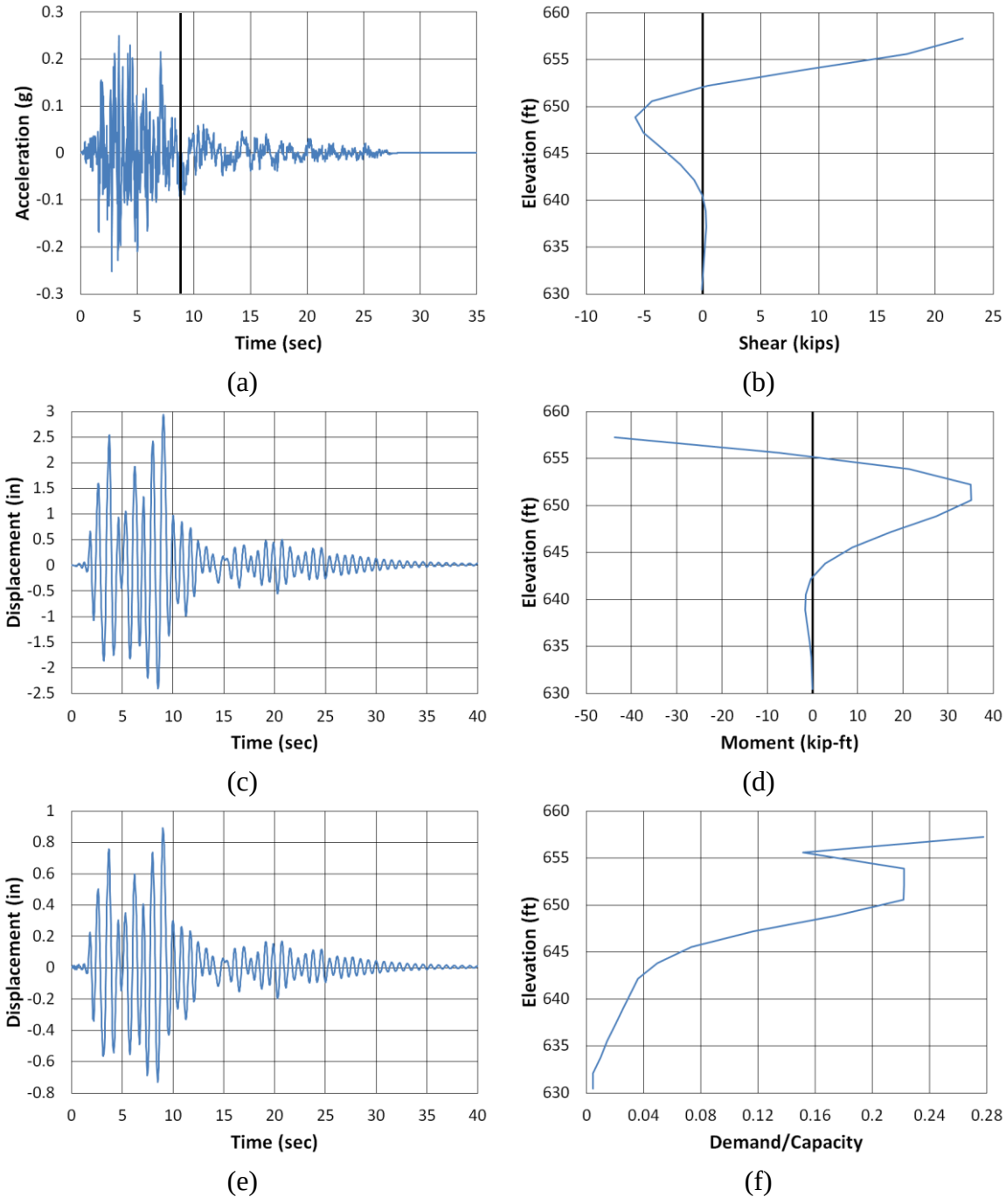

Figure B.167. Lee County Transverse San Fernando NMCE (a) time-history event, (b) shear distribution, (c) top of pier displacement, (d) moment distribution, (e) ground surface displacement, and (f) demand capacity ratio

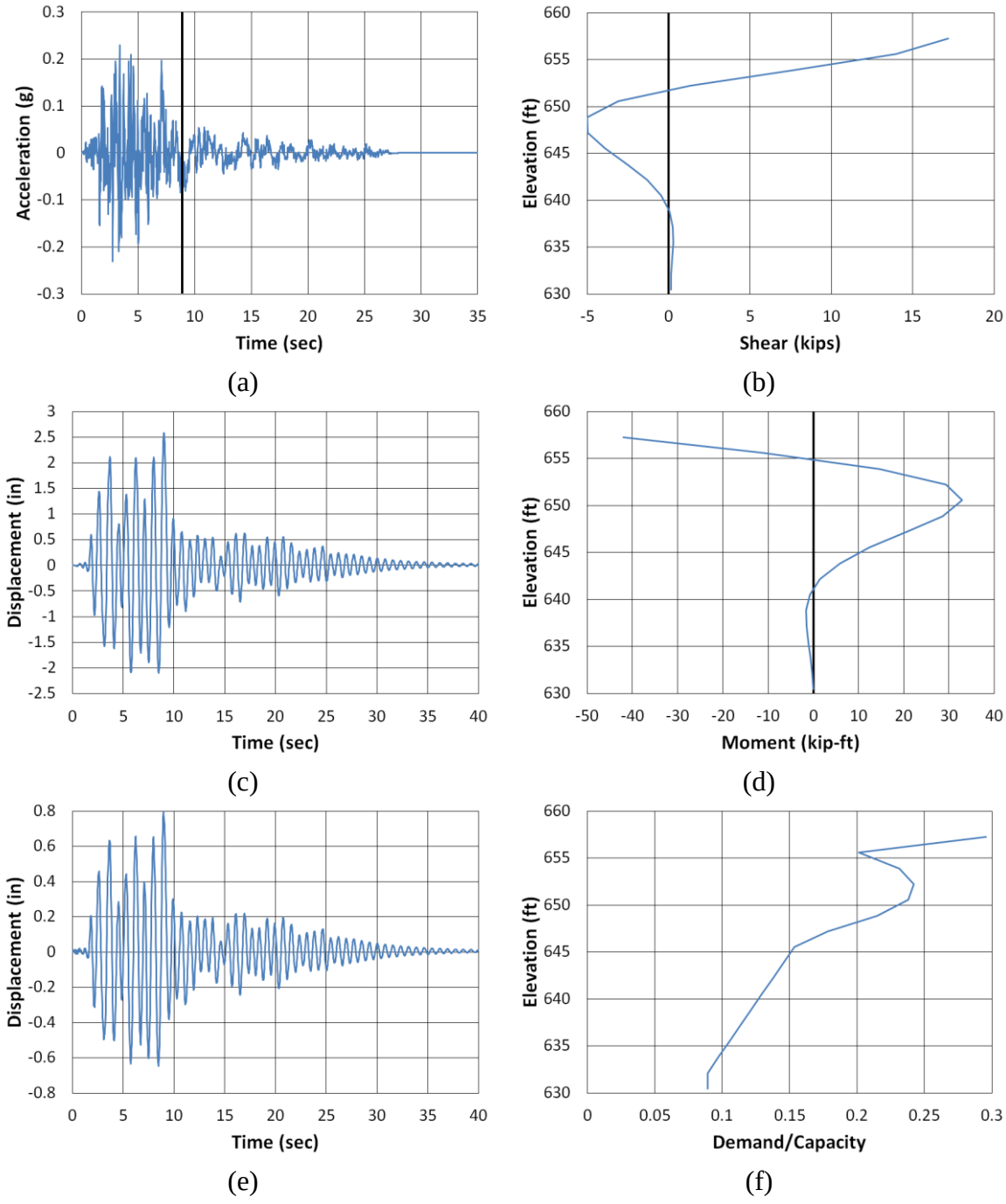

Figure B.168. Lee County Transverse San Fernando North (a) time-history event, (b) shear distribution, (c) top of pier displacement, (d) moment distribution, (e) ground surface displacement, and (f) demand capacity ratio

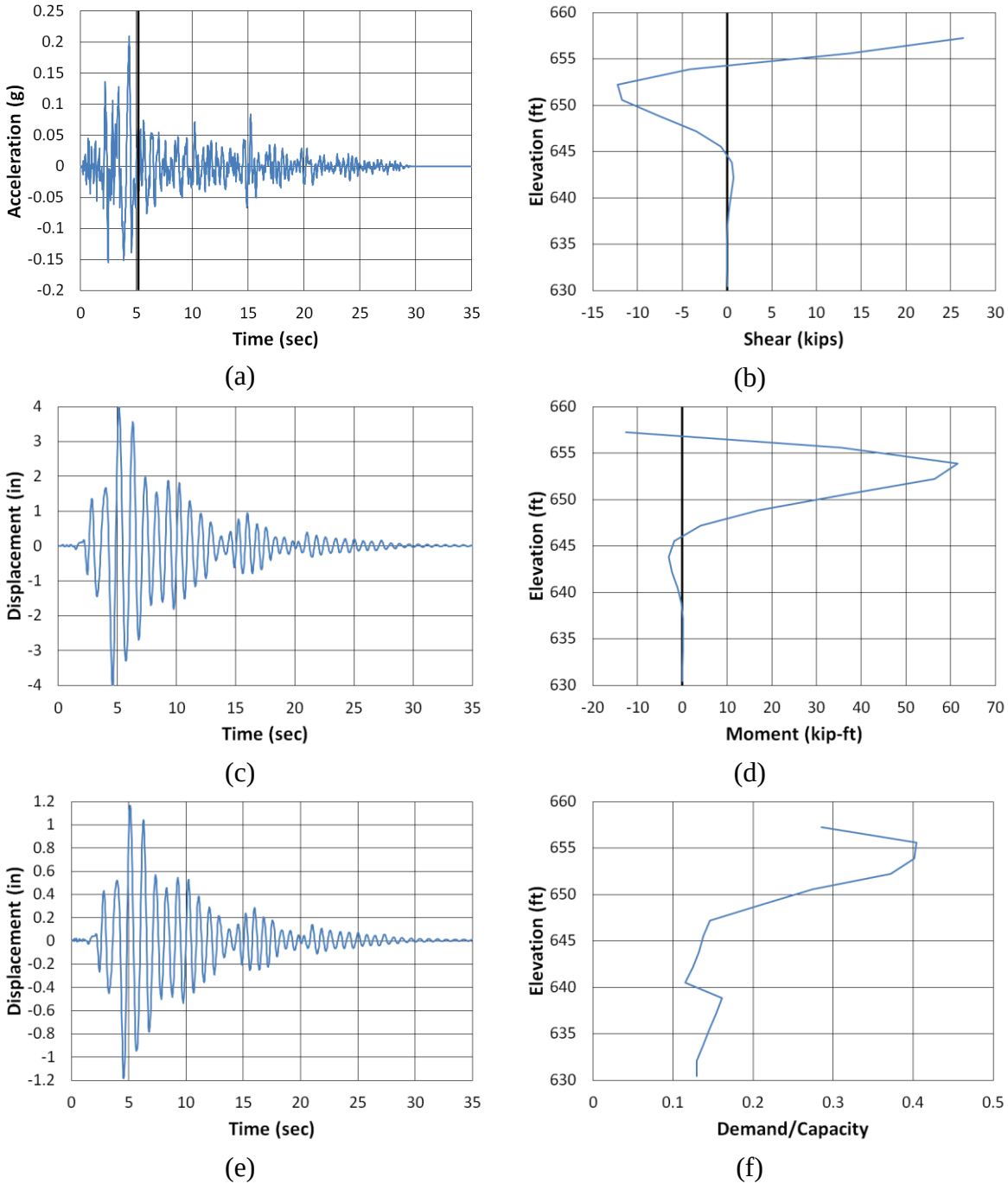

Figure B.169. Lee County Transverse San Fernando2 NMCE (a) time-history event, (b) shear distribution, (c) top of pier displacement, (d) moment distribution, (e) ground surface displacement, and (f) demand capacity ratio

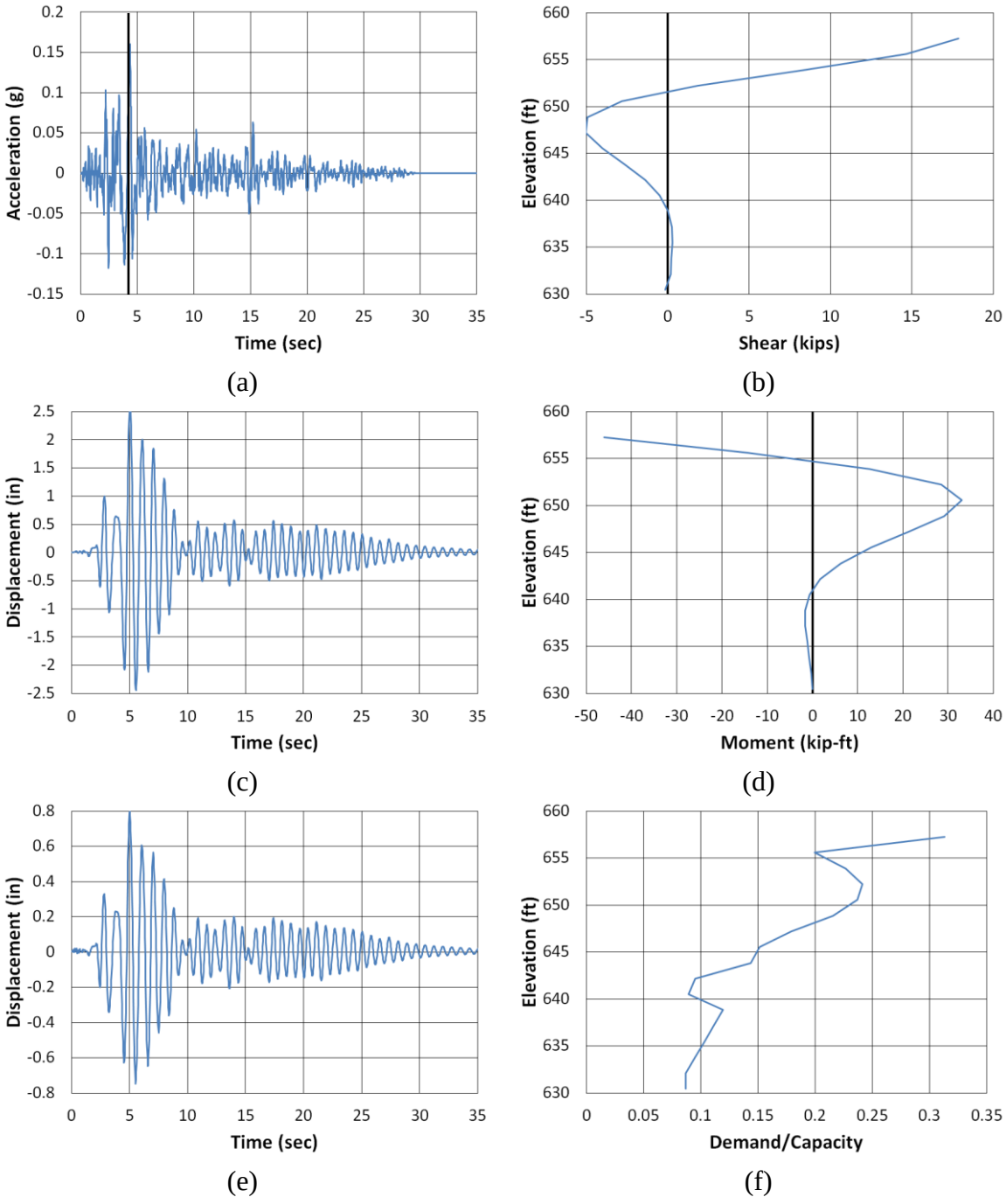

Figure B.170. Lee County Transverse San Fernando2 North (a) time-history event, (b) shear distribution, (c) top of pier displacement, (d) moment distribution, (e) ground surface displacement, and (f) demand capacity ratio

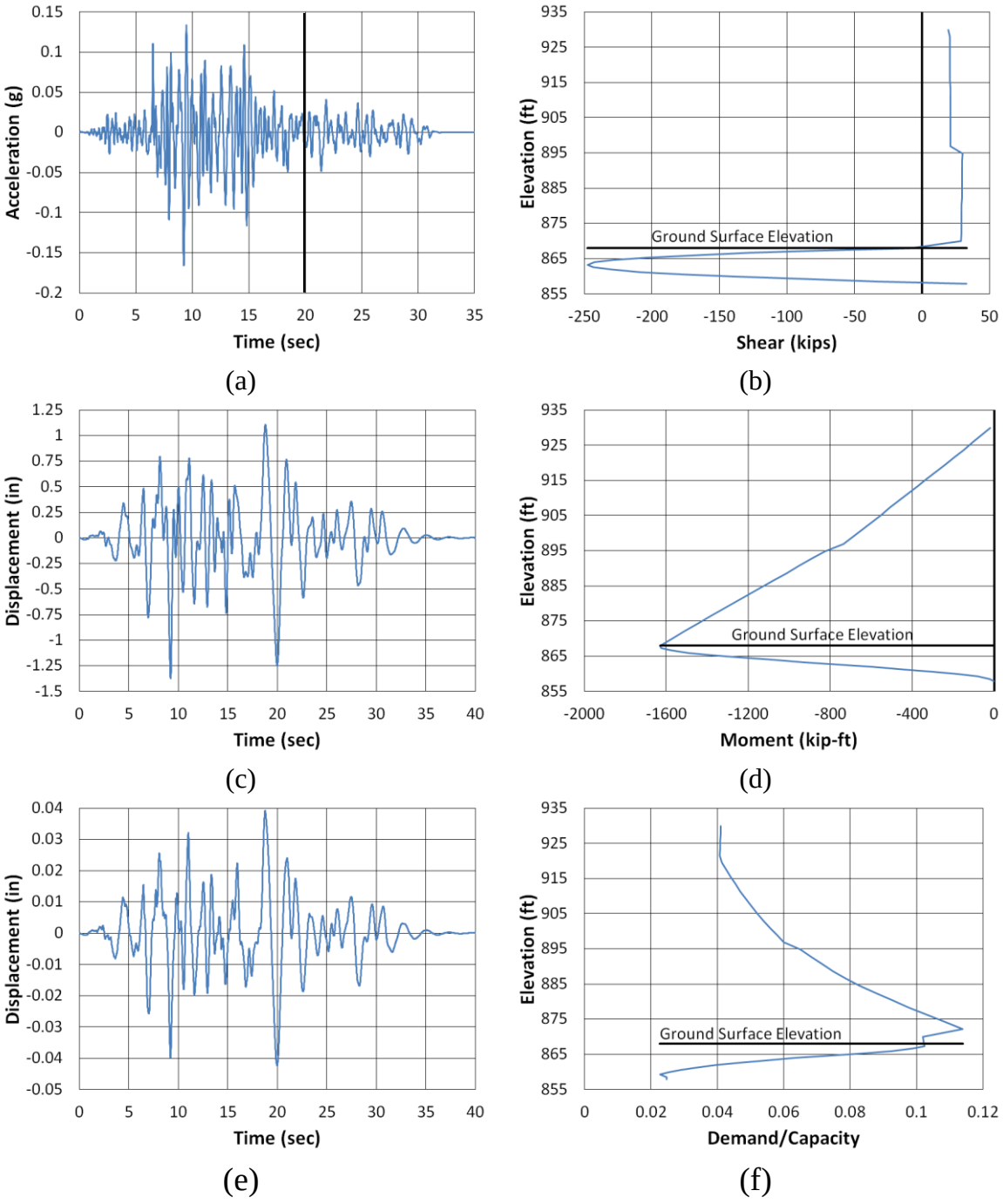

Figure B.171. Marshall County Longitudinal Coalinga North (a) time-history event, (b) shear distribution, (c) top of pier displacement, (d) moment distribution, (e) ground surface displacement, and (f) demand capacity ratio

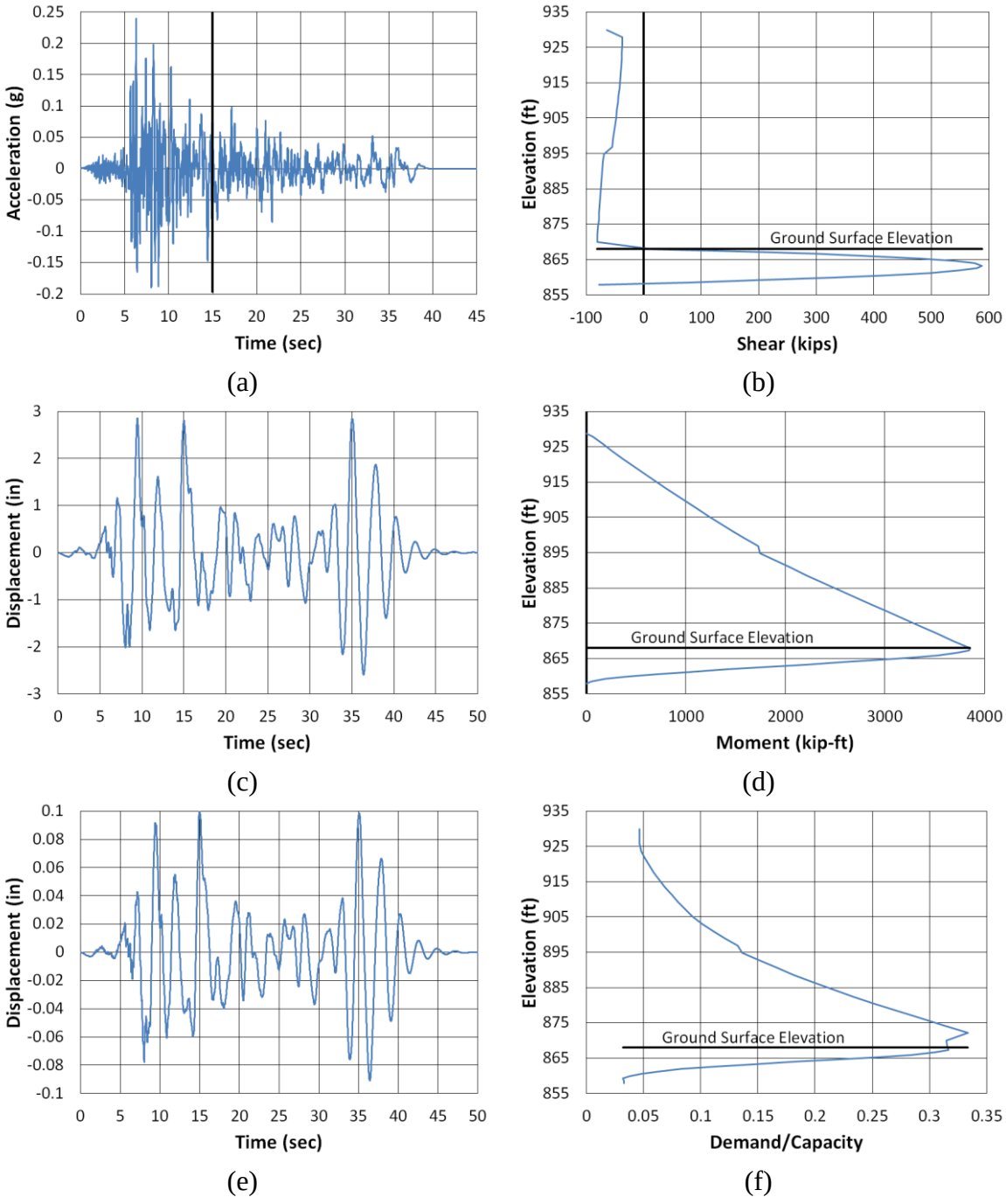

Figure B.172. Marshall County Longitudinal Imperial Valley NMCE (a) time-history event, (b) shear distribution, (c) top of pier displacement, (d) moment distribution, (e) ground surface displacement, and (f) demand capacity ratio

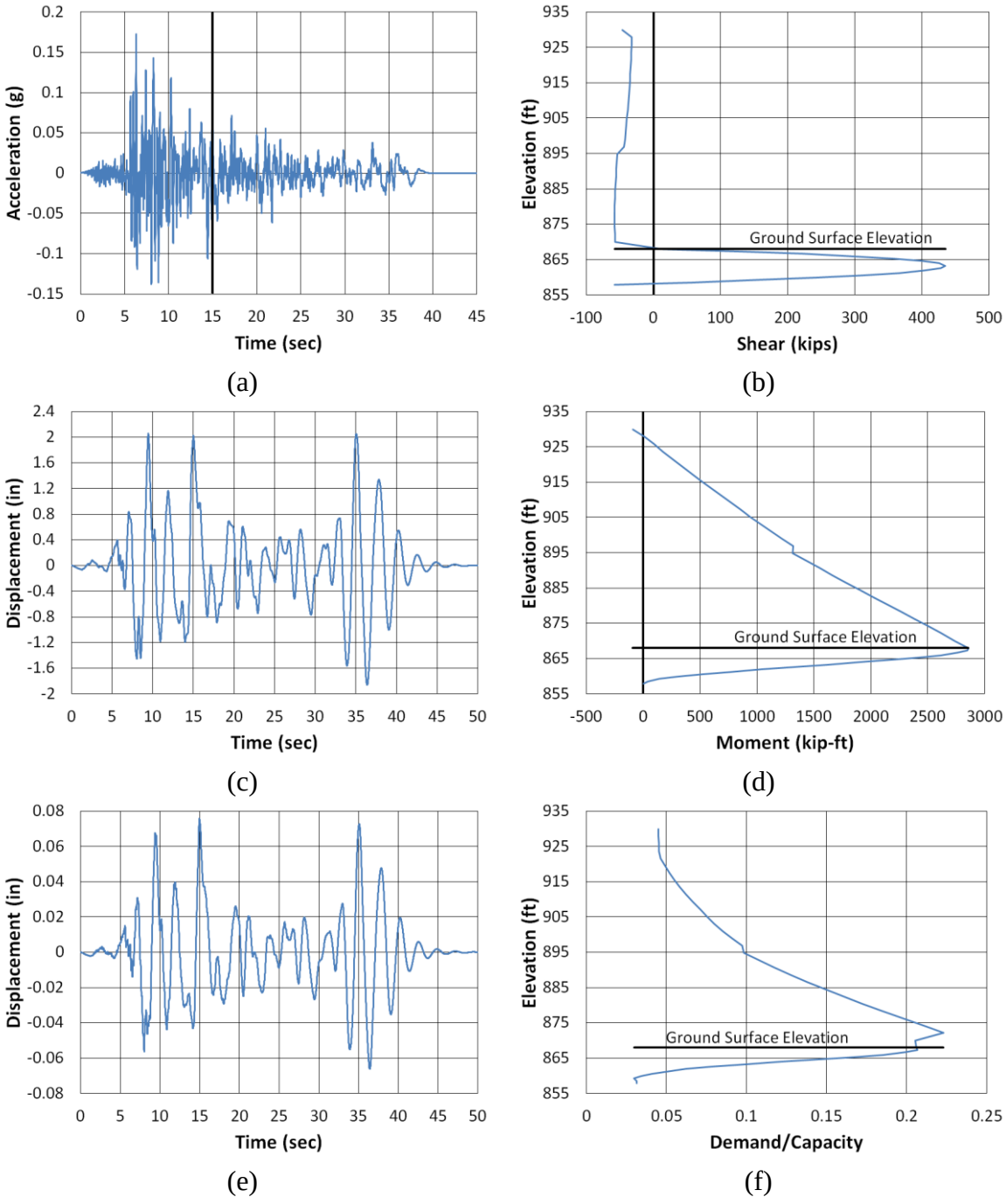

Figure B.173. Marshall County Longitudinal Imperial Valley North (a) time-history event, (b) shear distribution, (c) top of pier displacement, (d) moment distribution, (e) ground surface displacement, and (f) demand capacity ratio

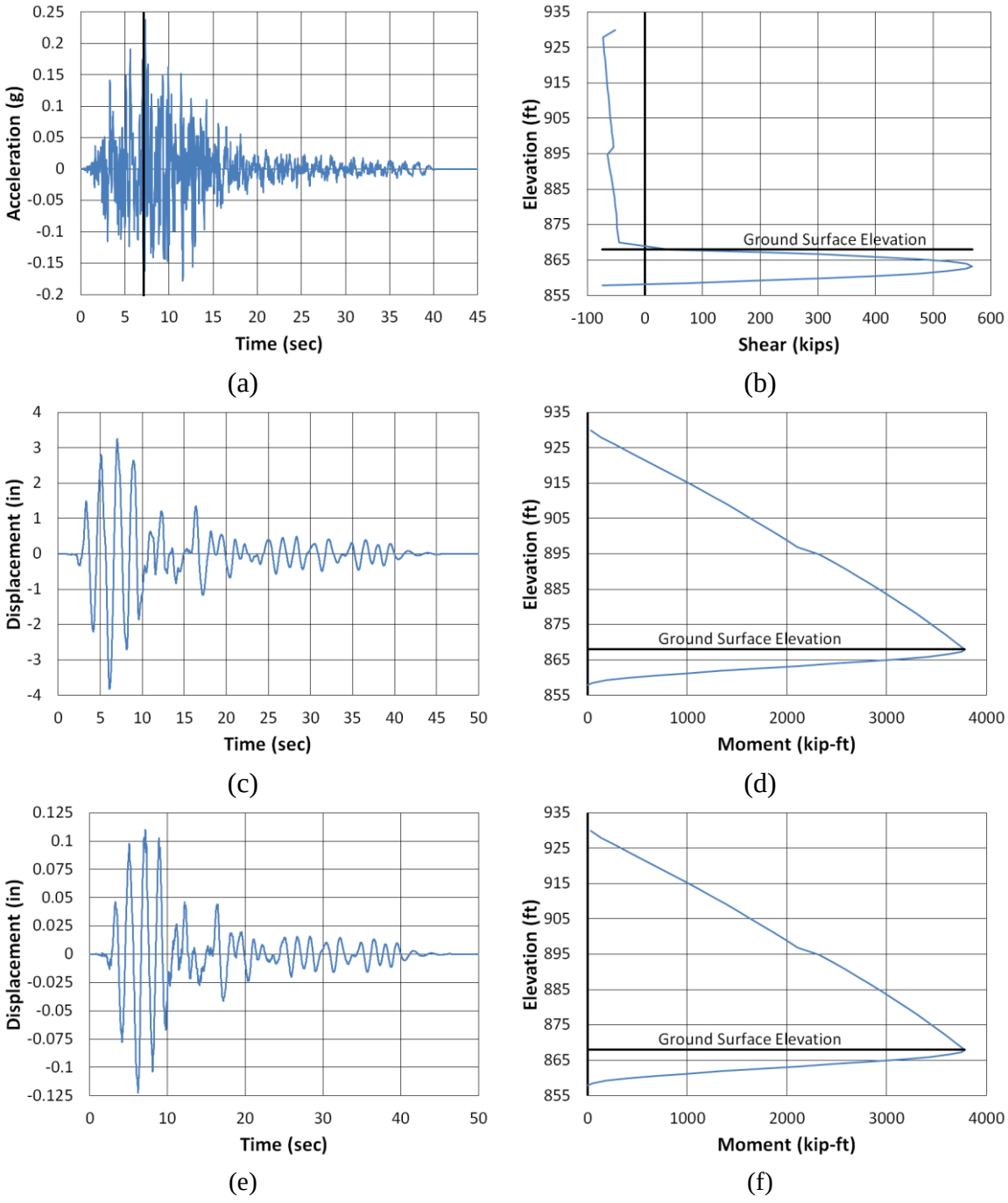

Figure B.174. Marshall County Longitudinal Kobe NMCE (a) time-history event, (b) shear distribution, (c) top of pier displacement, (d) moment distribution, (e) ground surface displacement, and (f) demand capacity ratio

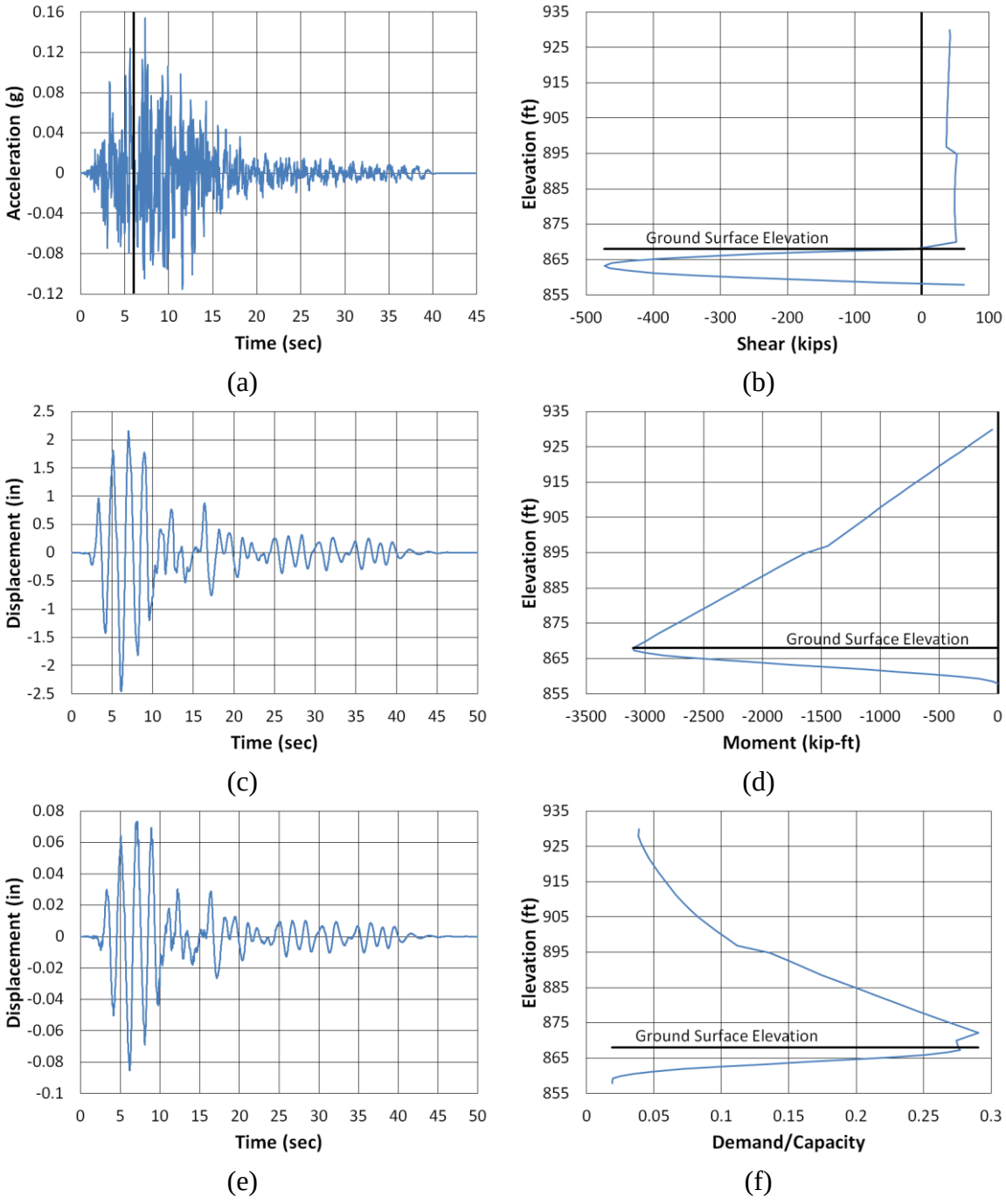

Figure B.175. Marshall County Longitudinal Kobe North (a) time-history event, (b) shear distribution, (c) top of pier displacement, (d) moment distribution, (e) ground surface displacement, and (f) demand capacity ratio

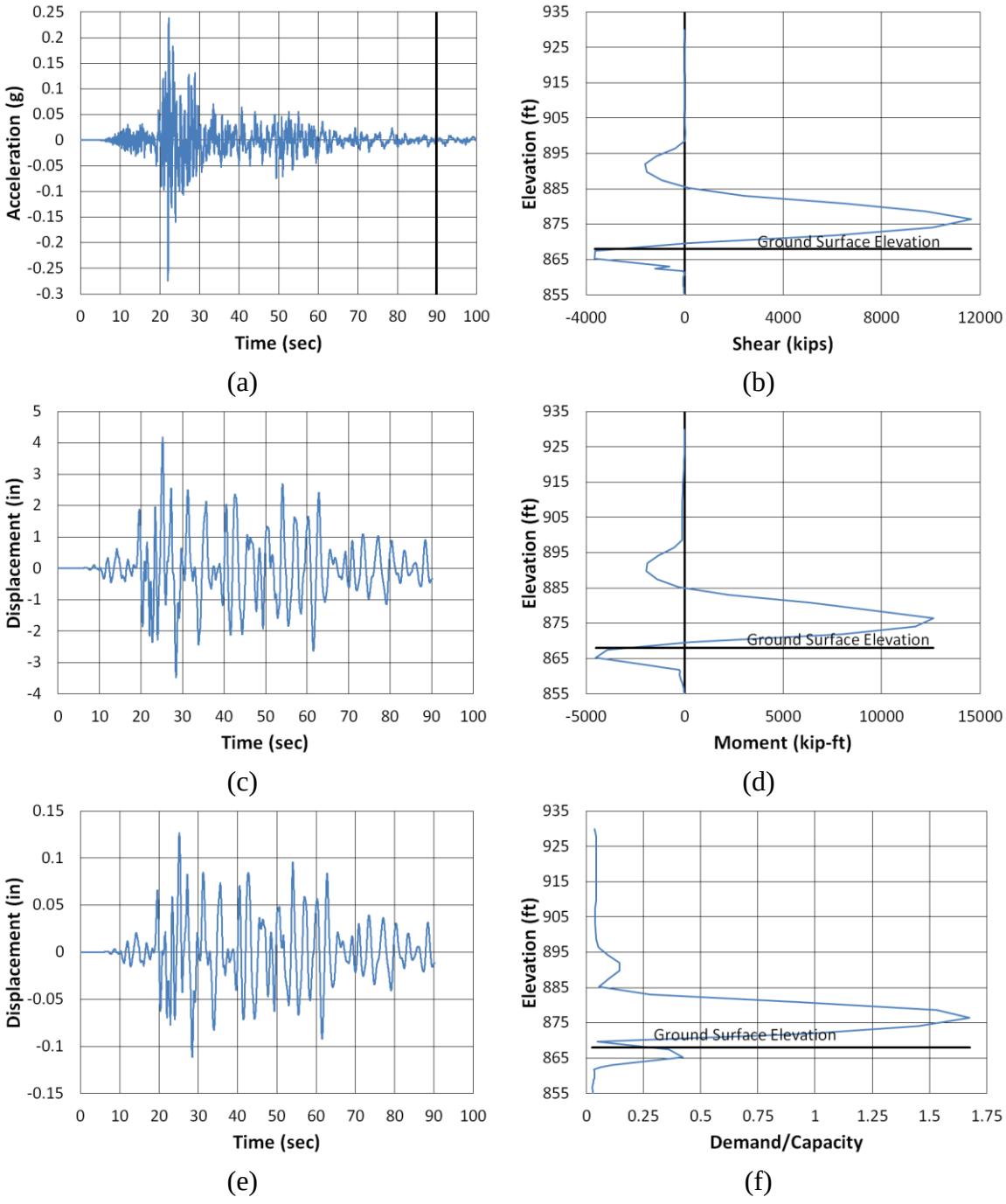

Figure B.176. Marshall County Longitudinal Kocaeli NMCE (a) time-history event, (b) shear distribution, (c) top of pier displacement, (d) moment distribution, (e) ground surface displacement, and (f) demand capacity ratio

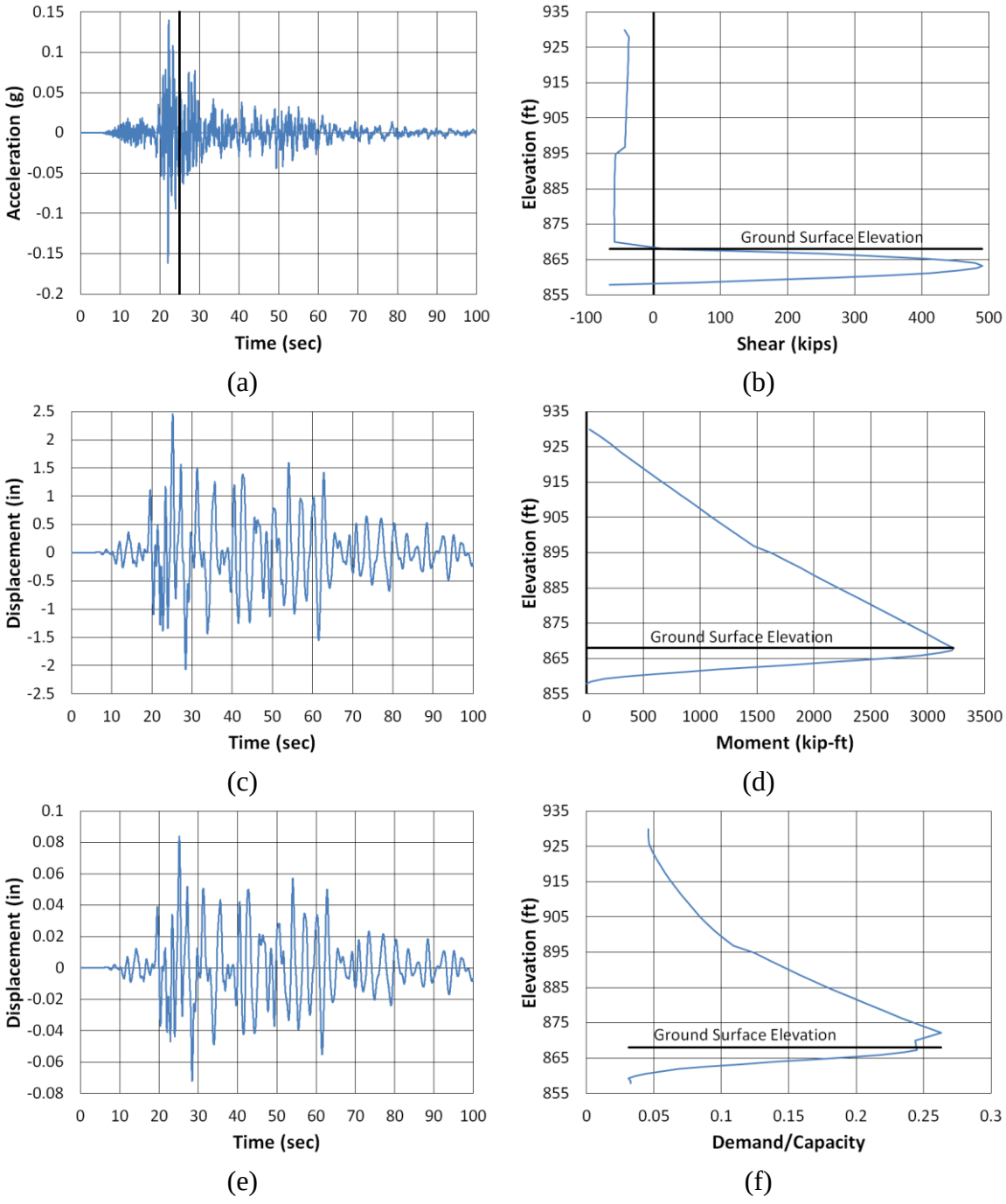

Figure B.177. Marshall County Longitudinal Kocaeli North (a) time-history event, (b) shear distribution, (c) top of pier displacement, (d) moment distribution, (e) ground surface displacement, and (f) demand capacity ratio

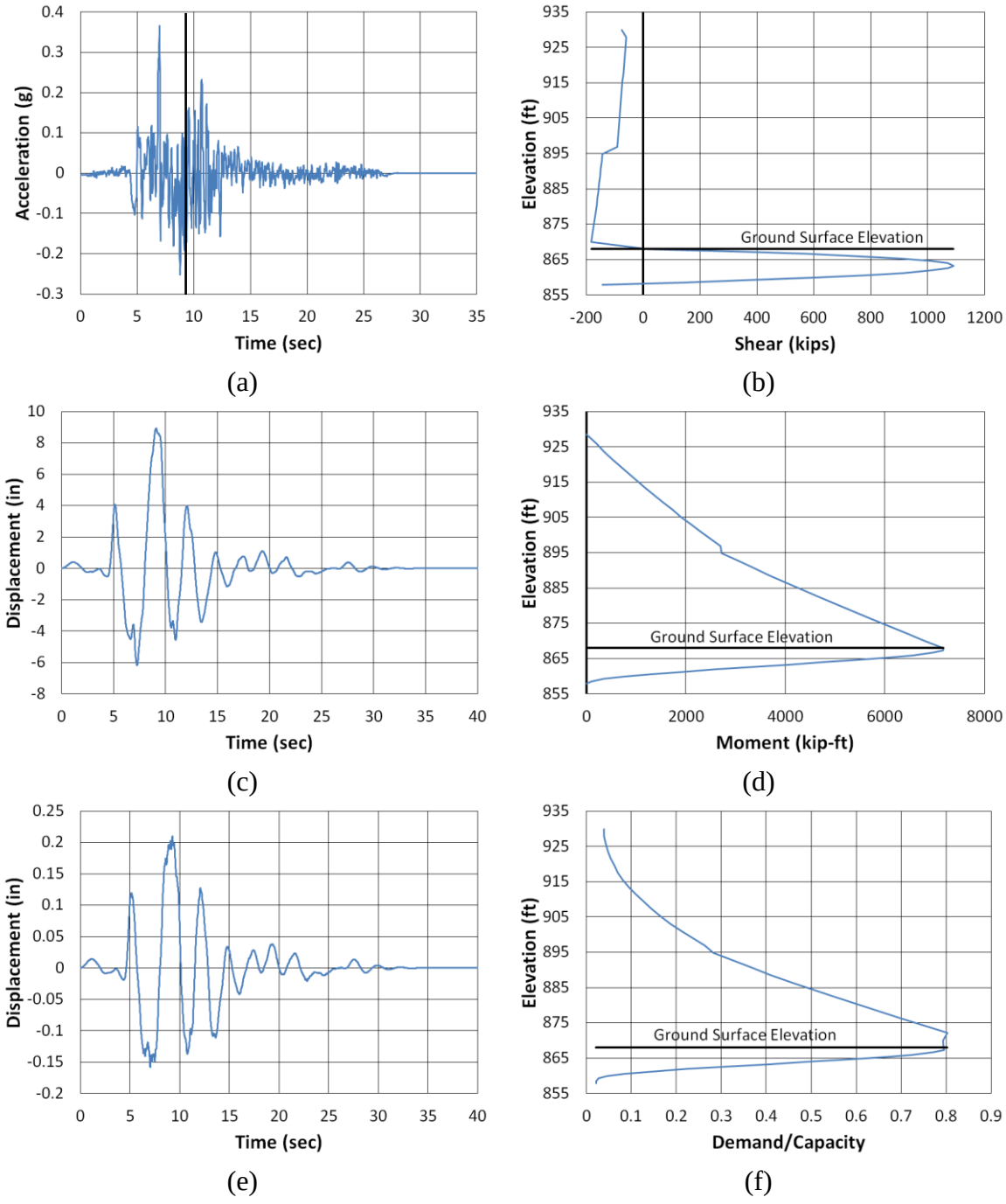

Figure B.178. Marshall County Longitudinal Kocaeli2 NMCE (a) time-history event, (b) shear distribution, (c) top of pier displacement, (d) moment distribution, (e) ground surface displacement, and (f) demand capacity ratio

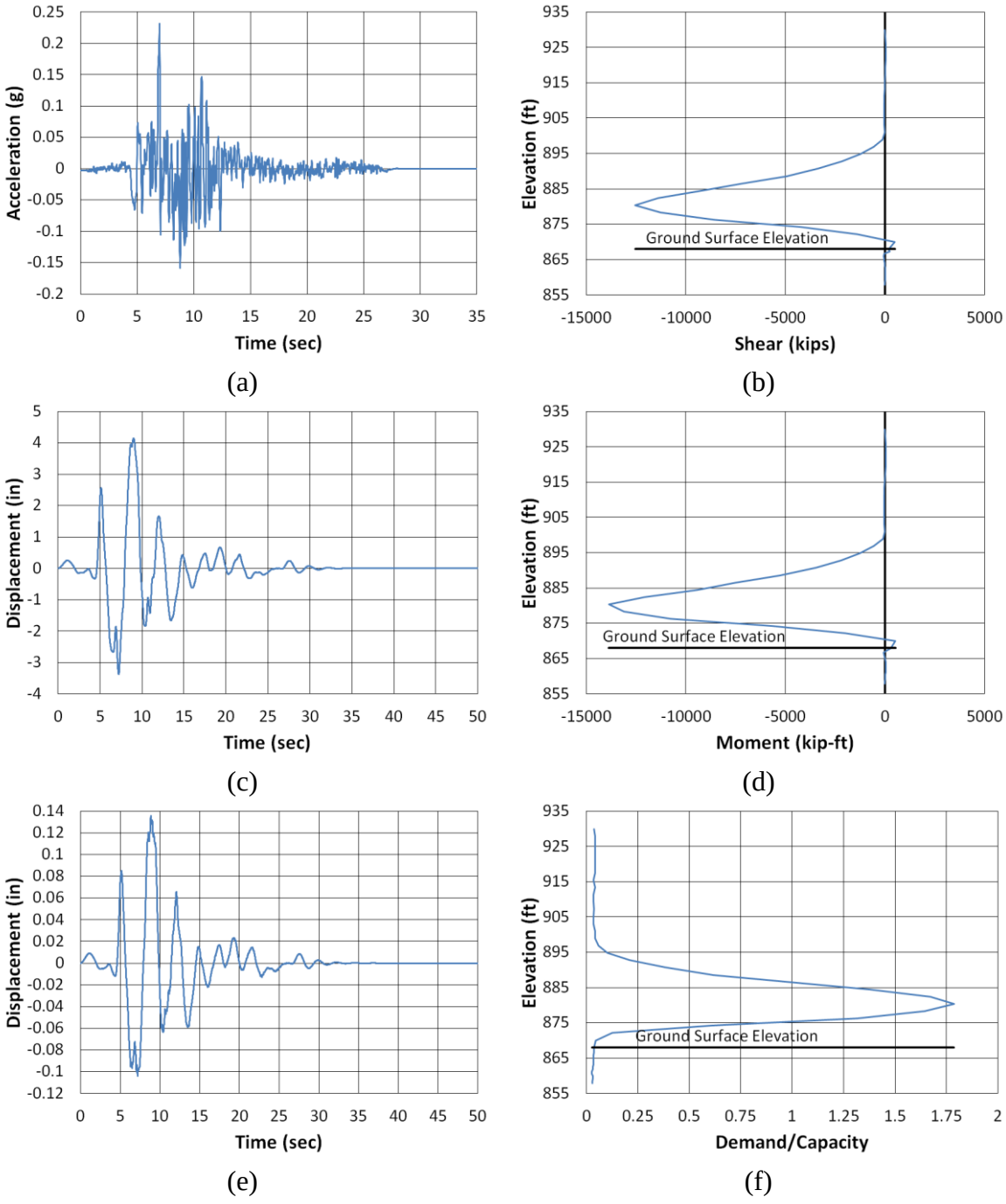

Figure B.179. Marshall County Longitudinal Kocaeli2 North (a) time-history event, (b) shear distribution, (c) top of pier displacement, (d) moment distribution, (e) ground surface displacement, and (f) demand capacity ratio

.

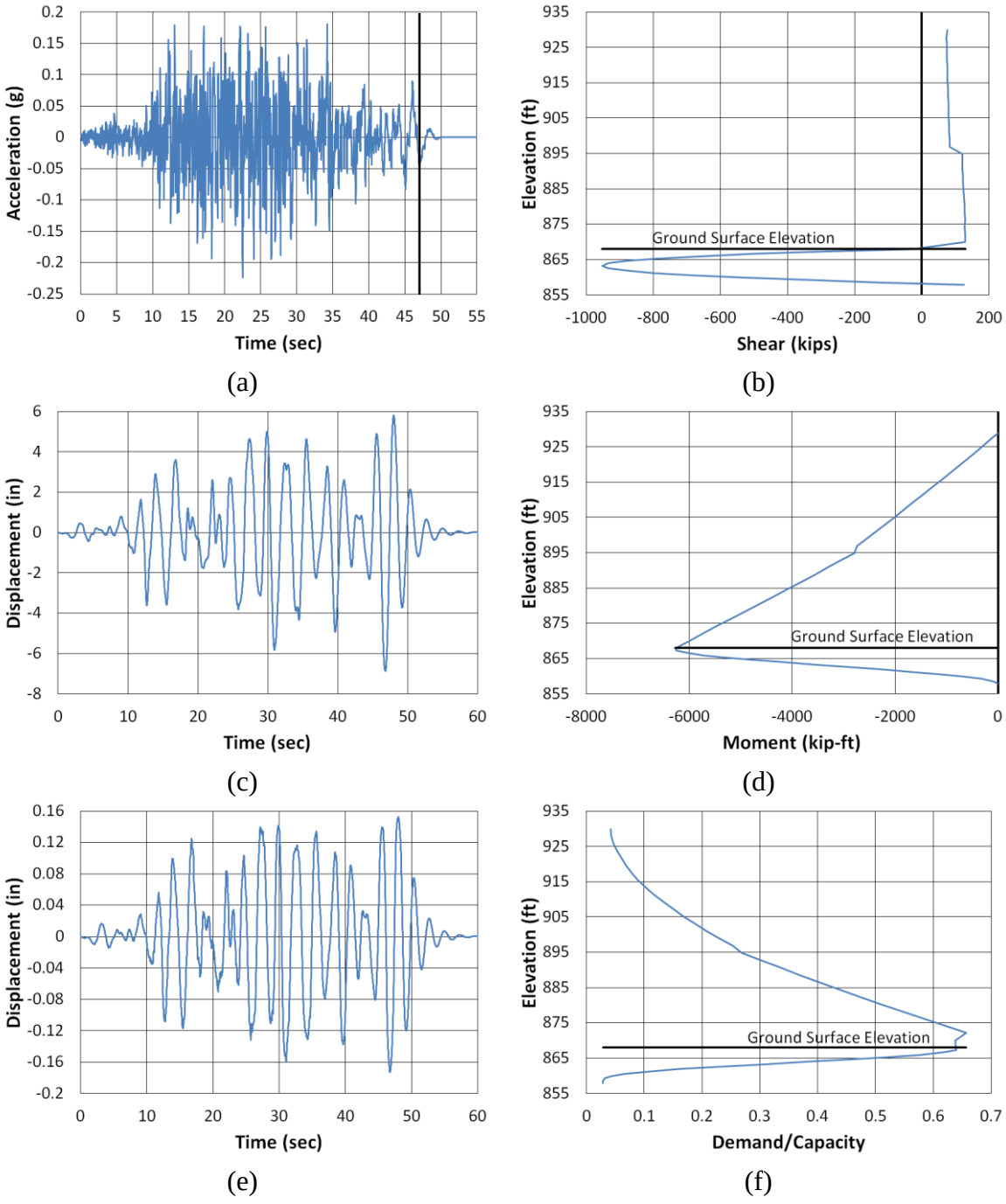

Figure B.180. Marshall County Longitudinal Landers NMCE (a) time-history event, (b) shear distribution, (c) top of pier displacement, (d) moment distribution, (e) ground surface displacement, and (f) demand capacity ratio

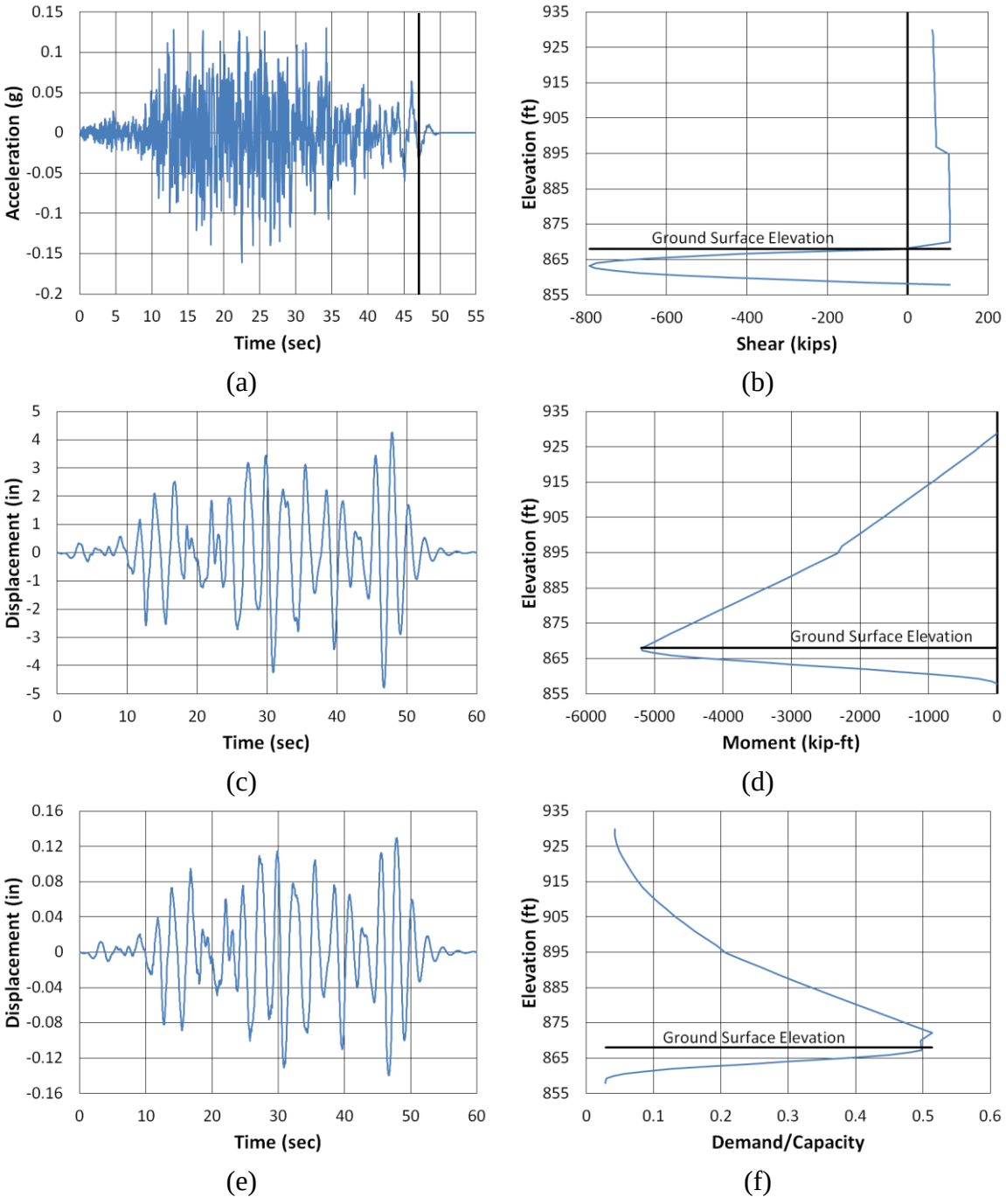

Figure B.181. Marshall County Longitudinal Landers North (a) time-history event, (b) shear distribution, (c) top of pier displacement, (d) moment distribution, (e) ground surface displacement, and (f) demand capacity ratio

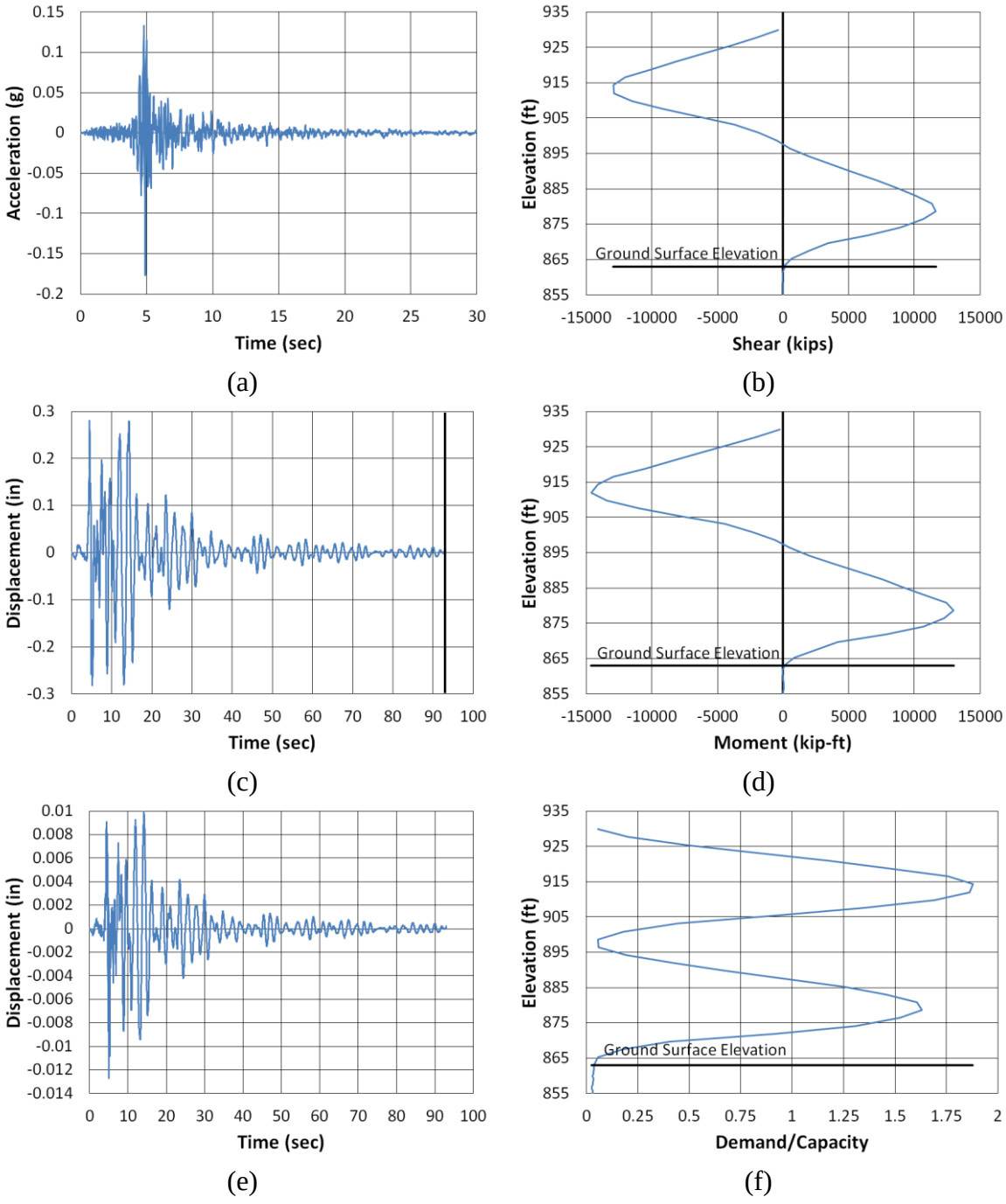

Figure B.182. Marshall County Longitudinal LSM North (a) time-history event, (b) shear distribution, (c) top of pier displacement, (d) moment distribution, (e) ground surface displacement, and (f) demand capacity ratio

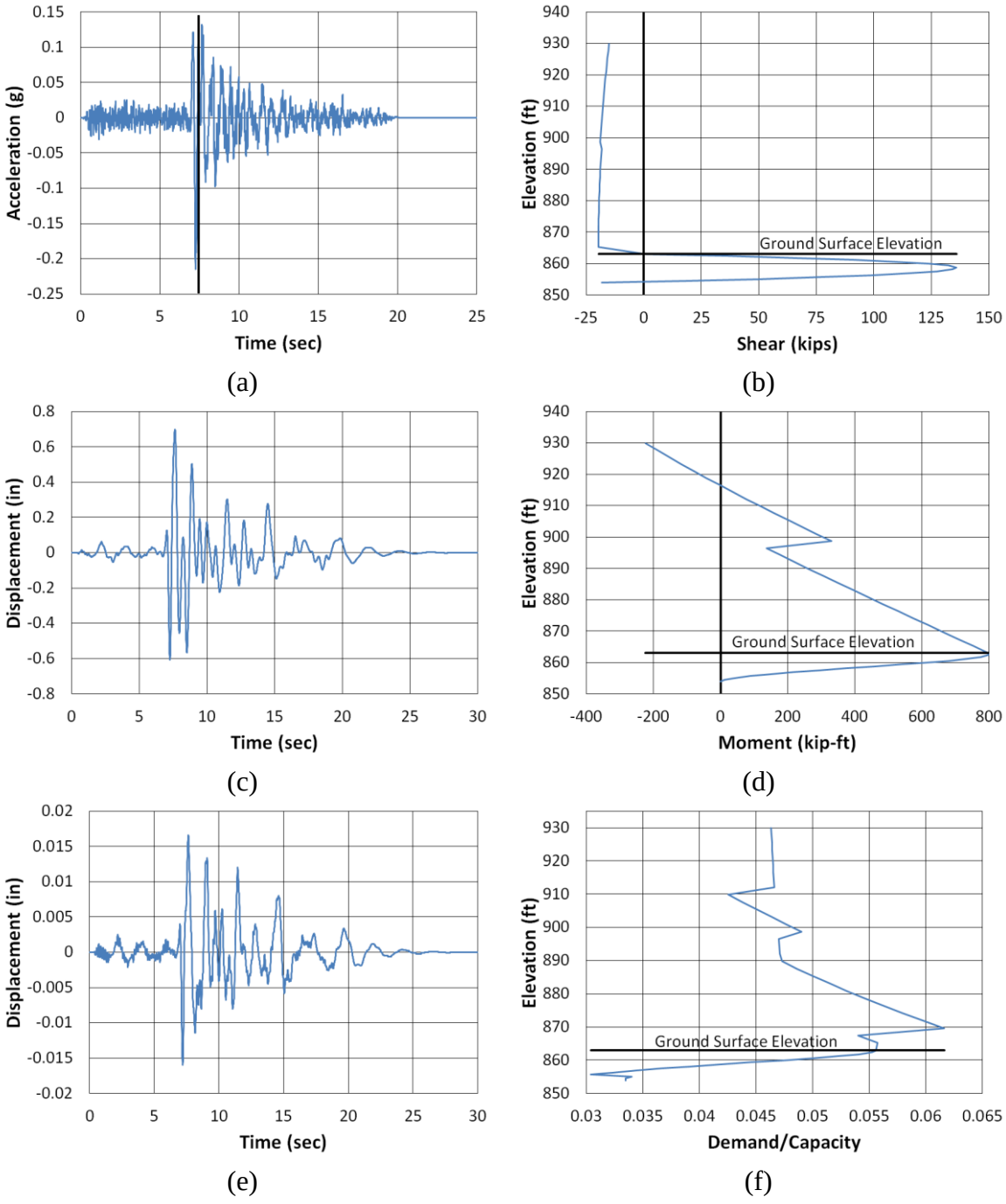

Figure B.183. Marshall County Longitudinal NPS North (a) time-history event, (b) shear distribution, (c) top of pier displacement, (d) moment distribution, (e) ground surface displacement, and (f) demand capacity ratio

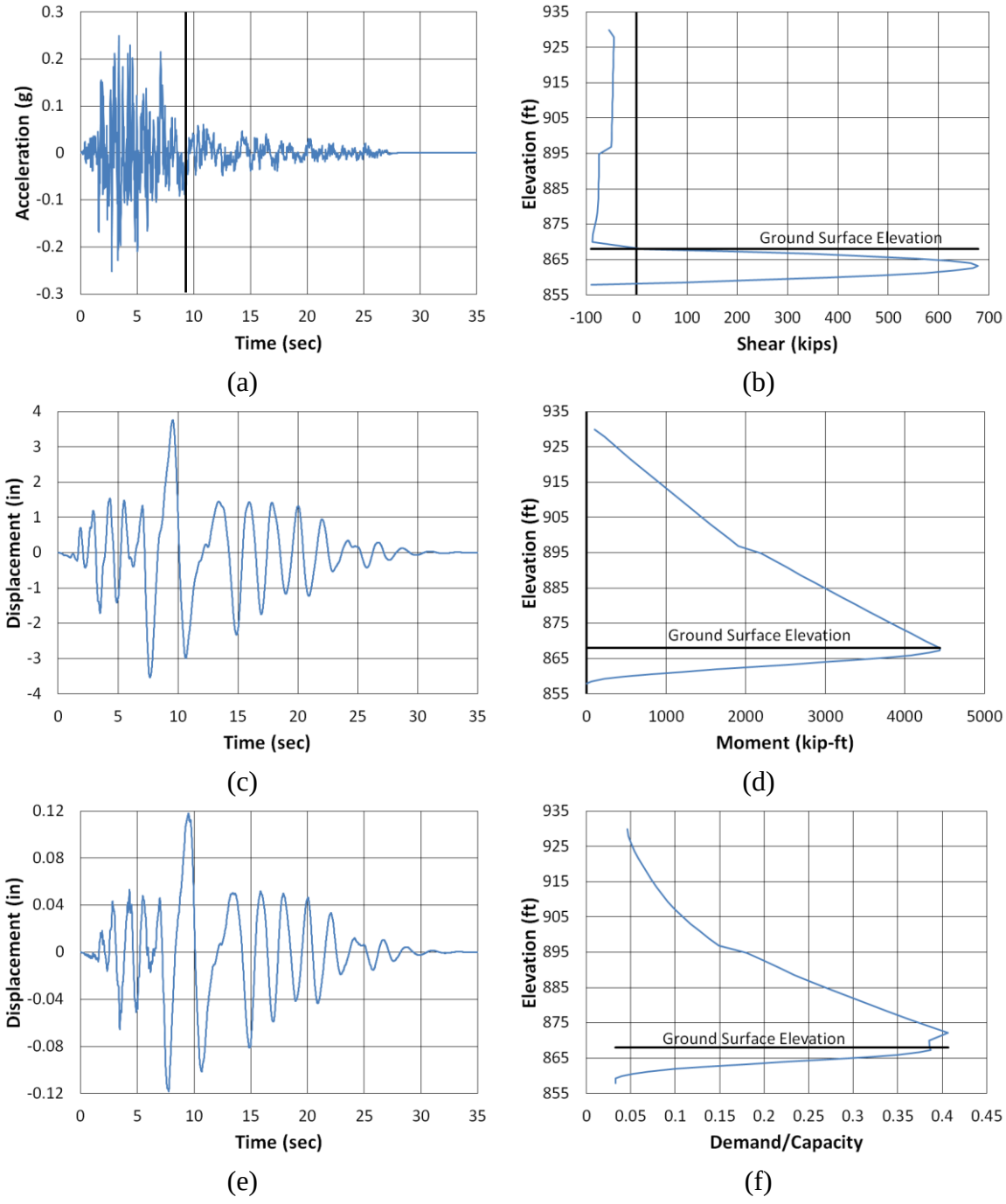

Figure B.184. Marshall County Longitudinal San Fernando NMCE (a) time-history event, (b) shear distribution, (c) top of pier displacement, (d) moment distribution, (e) ground surface displacement, and (f) demand capacity ratio

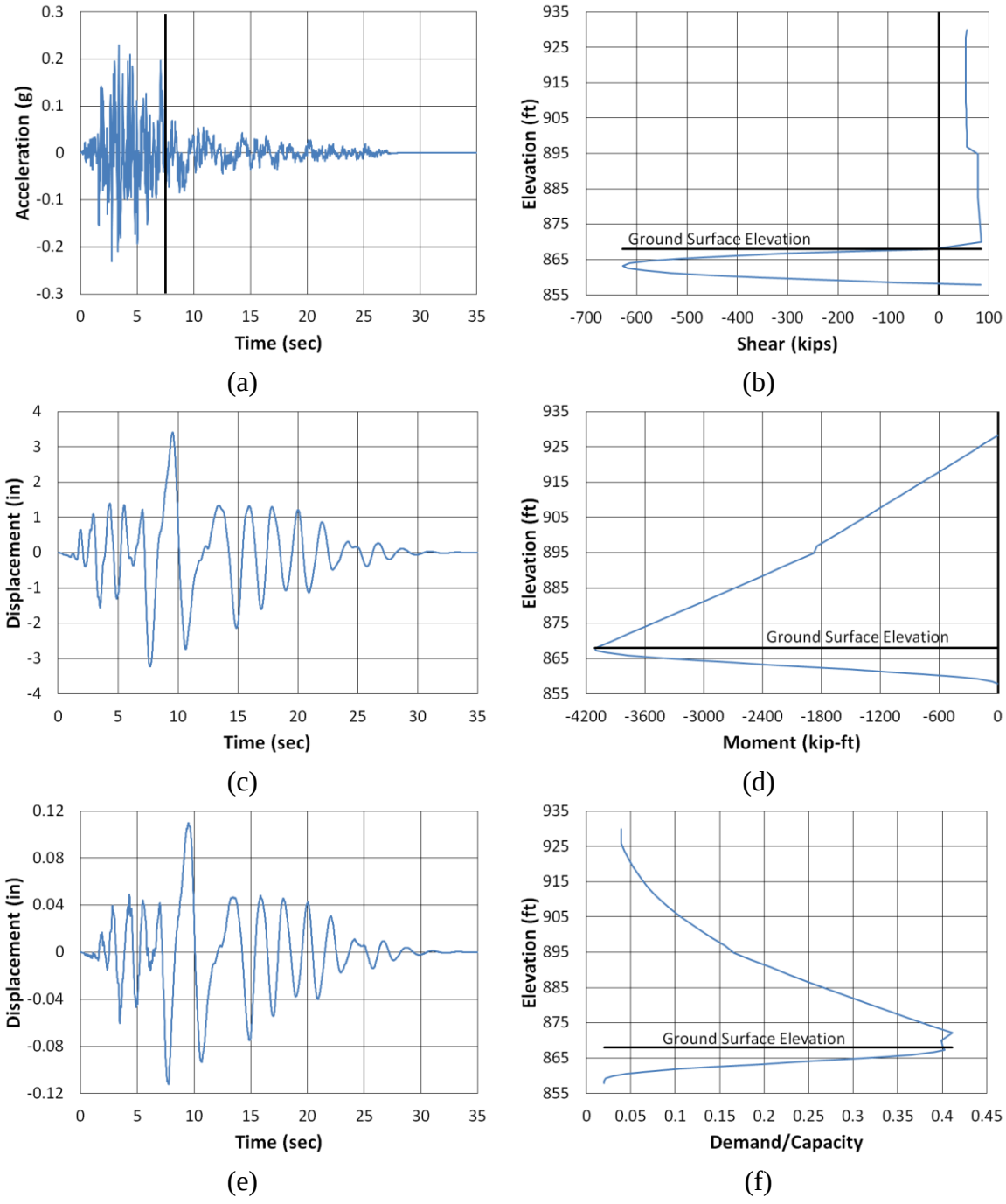

Figure B.185. Marshall County Longitudinal San Fernando North (a) time-history event, (b) shear distribution, (c) top of pier displacement, (d) moment distribution, (e) ground surface displacement, and (f) demand capacity ratio

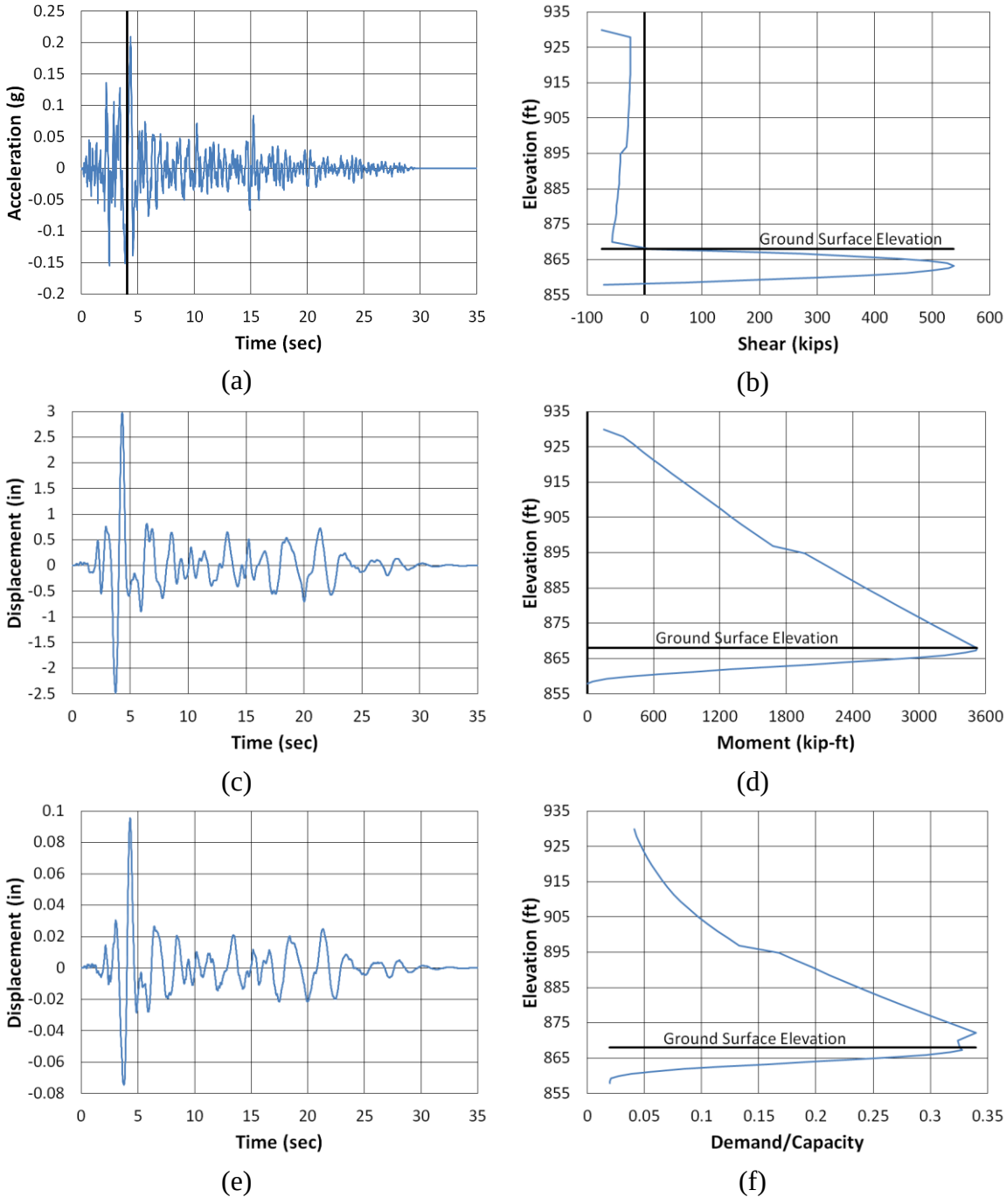

Figure B.186. Marshall County Longitudinal San Fernando2 NMCE (a) time-history event, (b) shear distribution, (c) top of pier displacement, (d) moment distribution, (e) ground surface displacement, and (f) demand capacity ratio

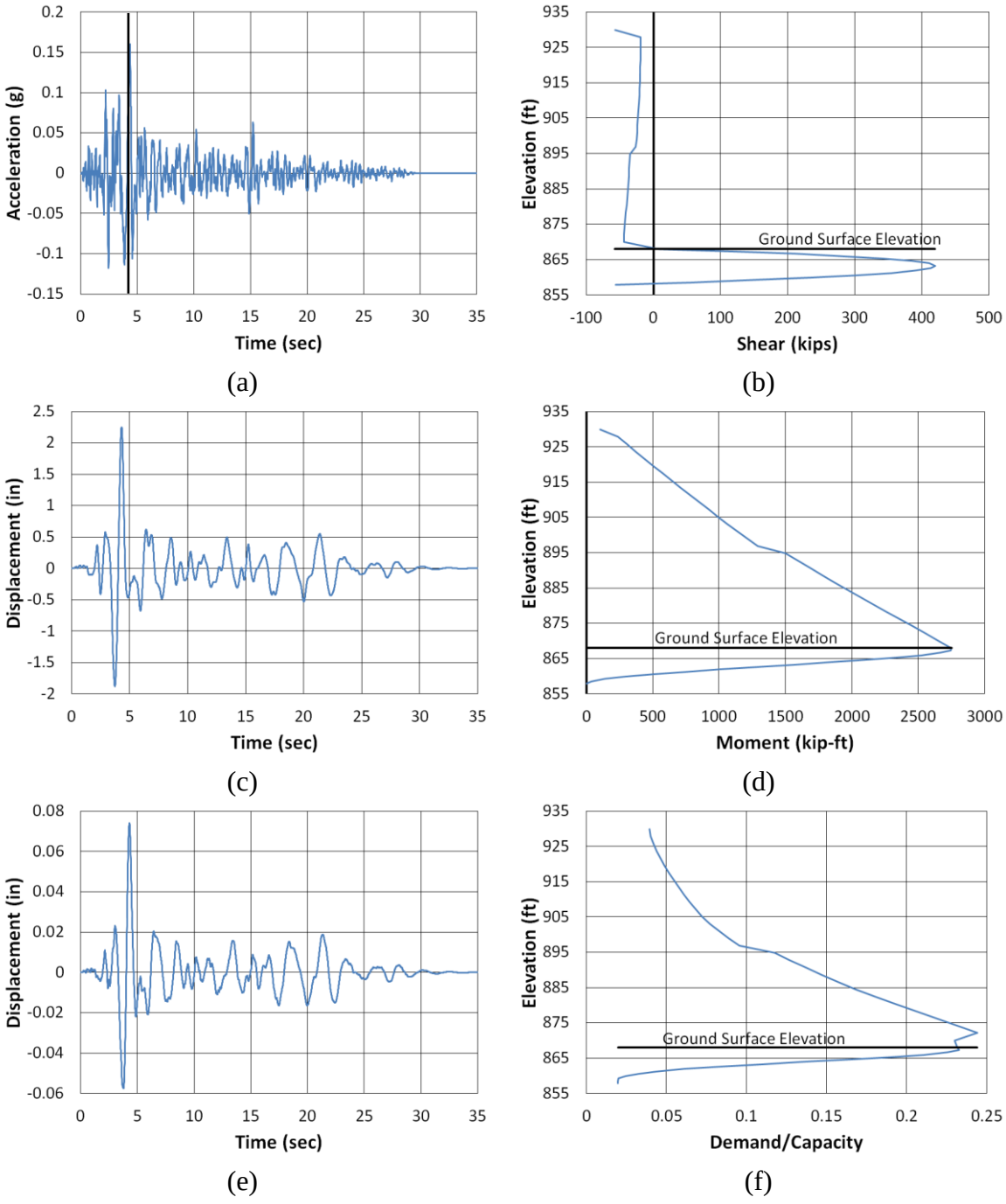

Figure B.187 Marshall County Longitudinal San Fernando2 North (a) time-history event, (b) shear distribution, (c) top of pier displacement, (d) moment distribution, (e) ground surface displacement, and (f) demand capacity ratio

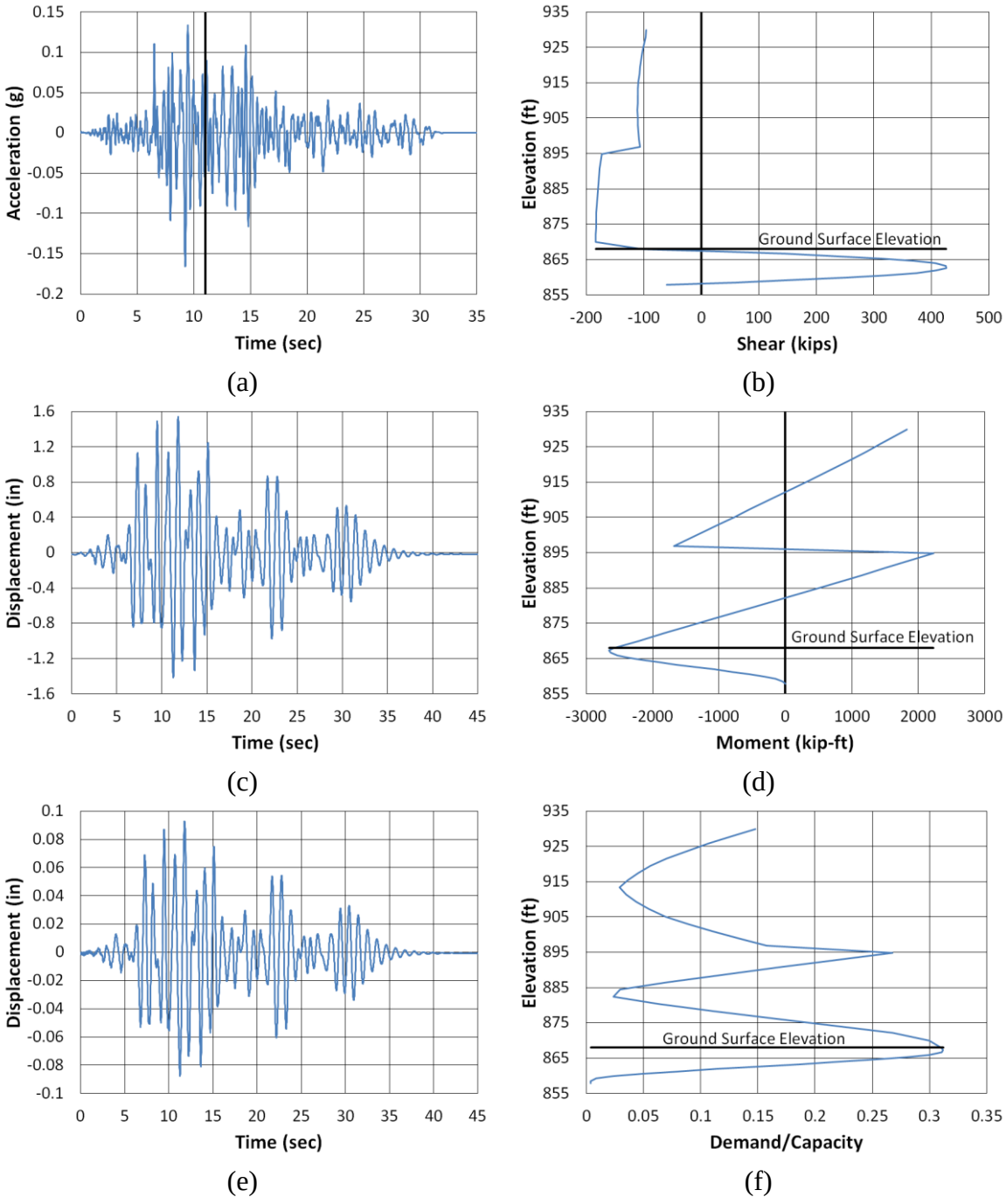

Figure B.188. Marshall County Transverse Coalinga North (a) time-history event, (b) shear distribution, (c) top of pier displacement, (d) moment distribution, (e) ground surface displacement, and (f) demand capacity ratio

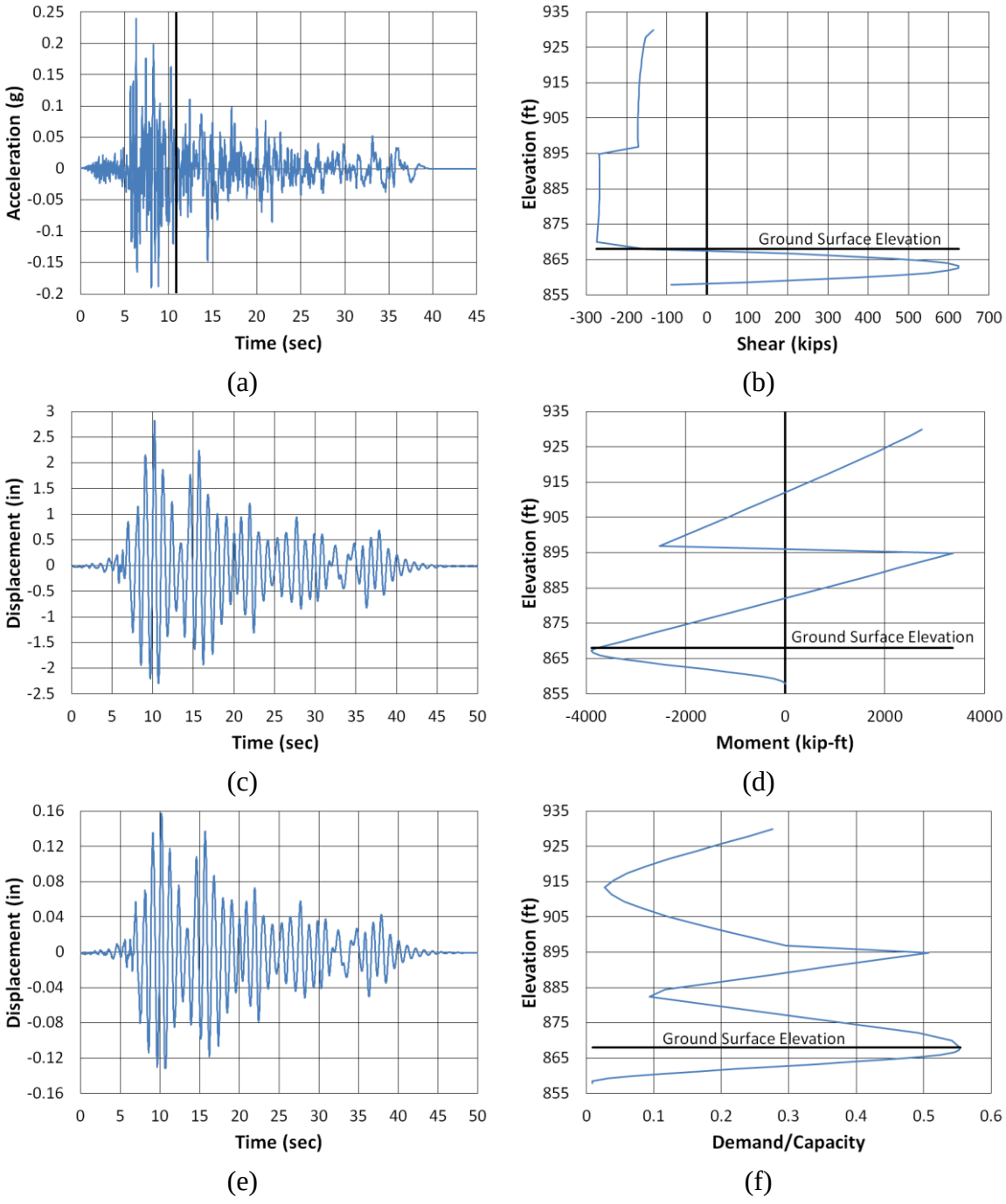

Figure B.189. Marshall County Transverse Imperial Valley NMCE (a) time-history event, (b) shear distribution, (c) top of pier displacement, (d) moment distribution, (e) ground surface displacement, and (f) demand capacity ratio

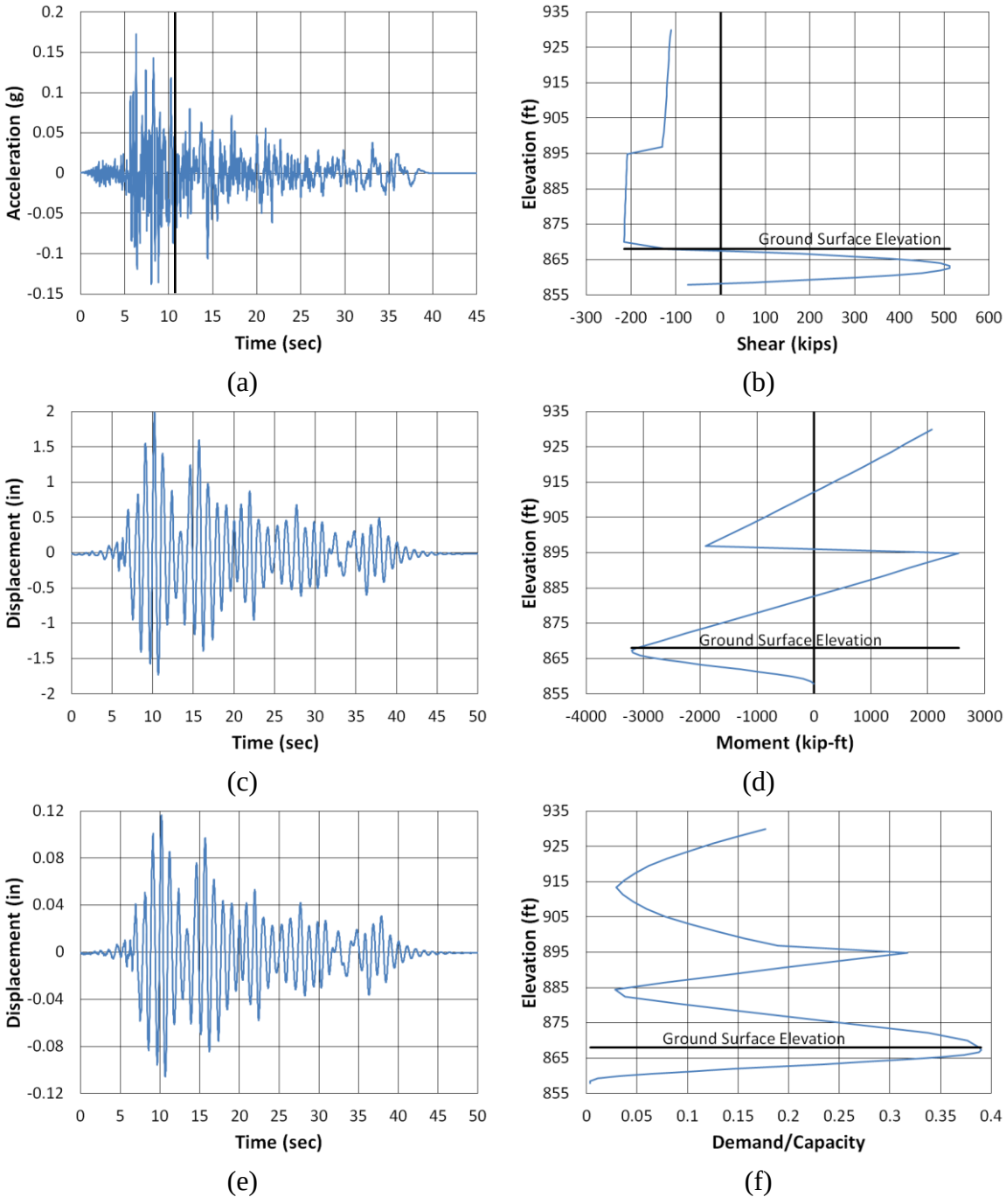

Figure B.190. Marshall County Transverse Imperial Valley North (a) time-history event, (b) shear distribution, (c) top of pier displacement, (d) moment distribution, (e) ground surface displacement, and (f) demand capacity ratio

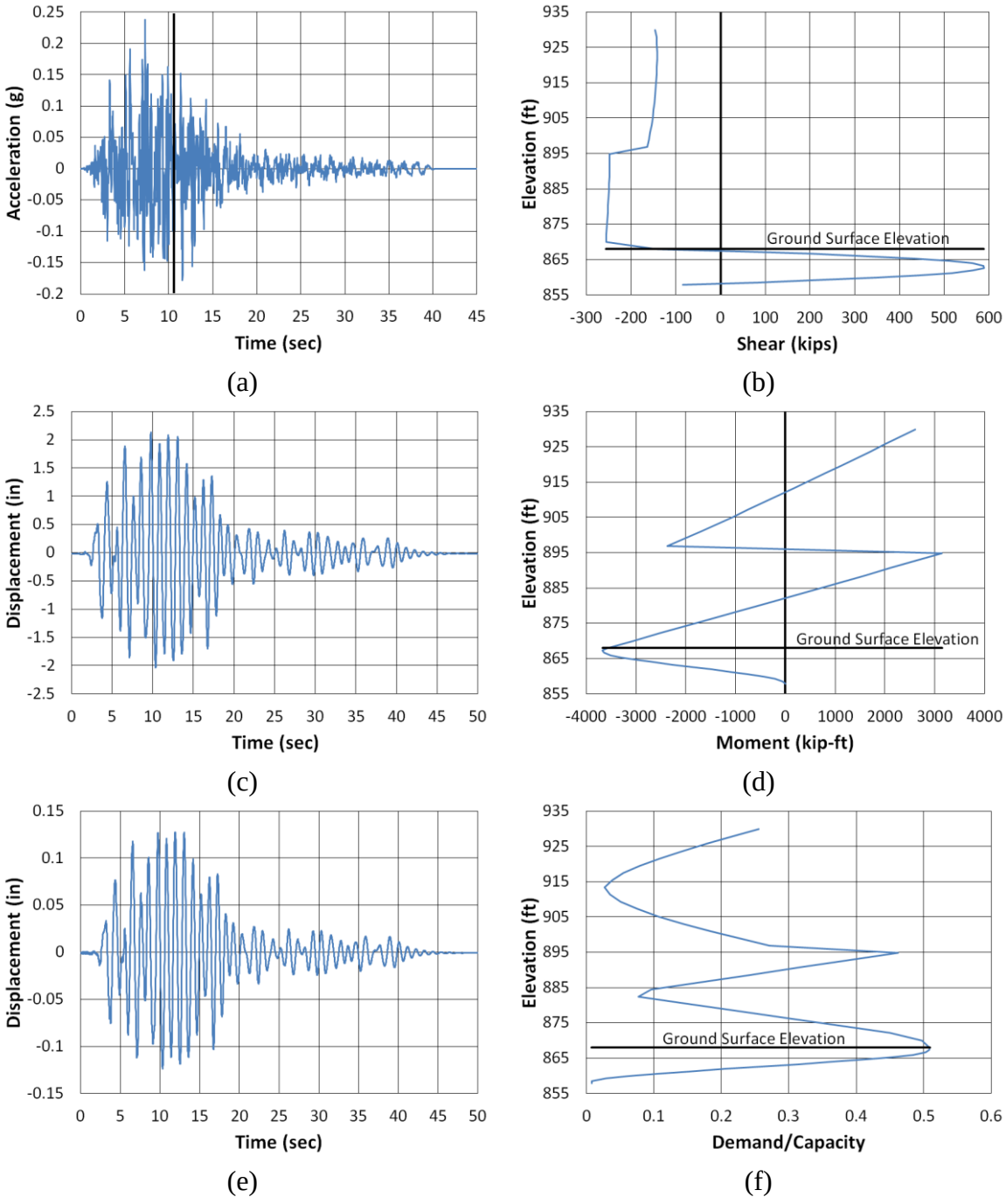

Figure B.191. Marshall County Transverse Kobe NMCE (a) time-history event, (b) shear distribution, (c) top of pier displacement, (d) moment distribution, (e) ground surface displacement, and (f) demand capacity ratio

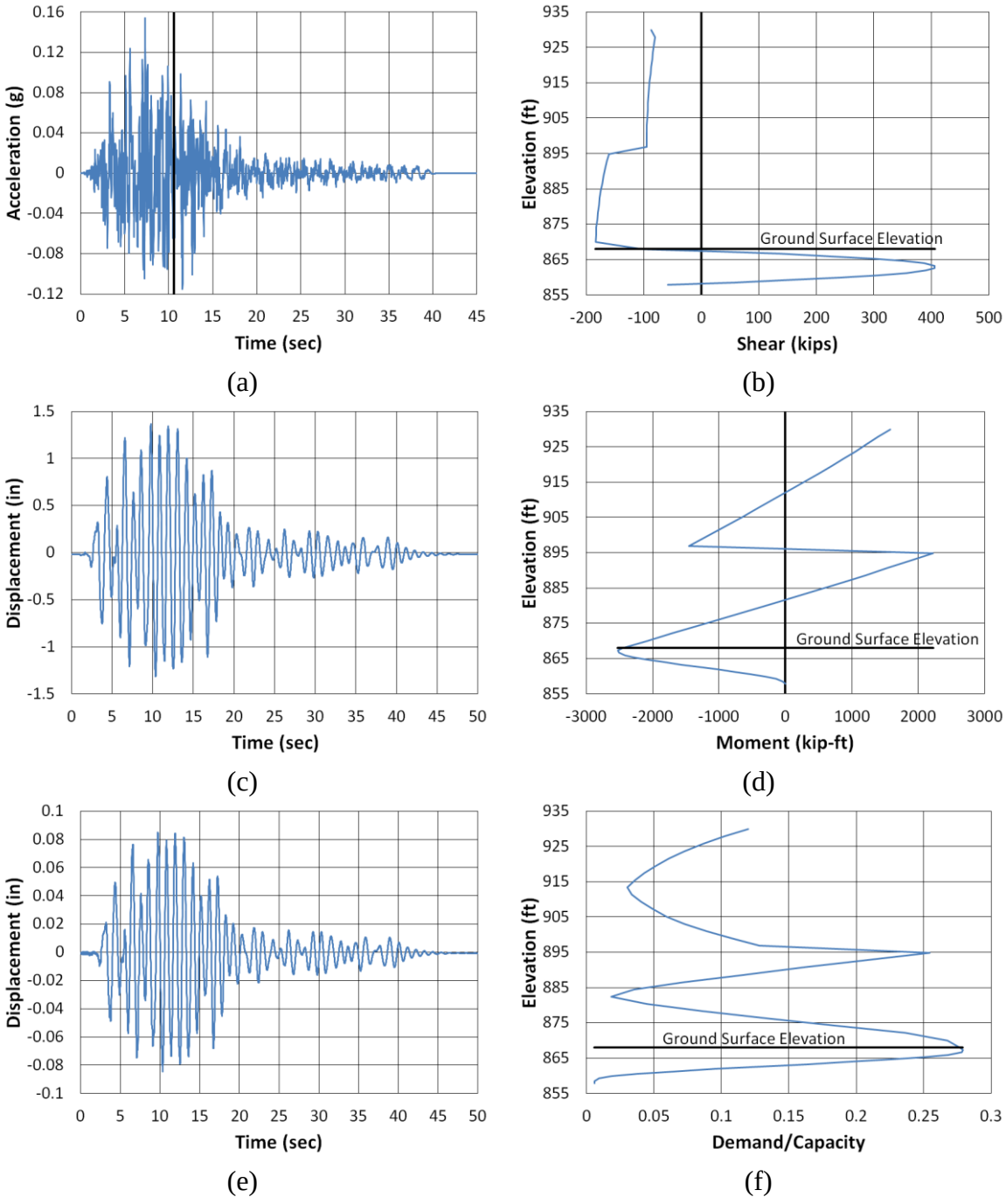

Figure B.192. Marshall County Transverse Kobe North (a) time-history event, (b) shear distribution, (c) top of pier displacement, (d) moment distribution, (e) ground surface displacement, and (f) demand capacity ratio

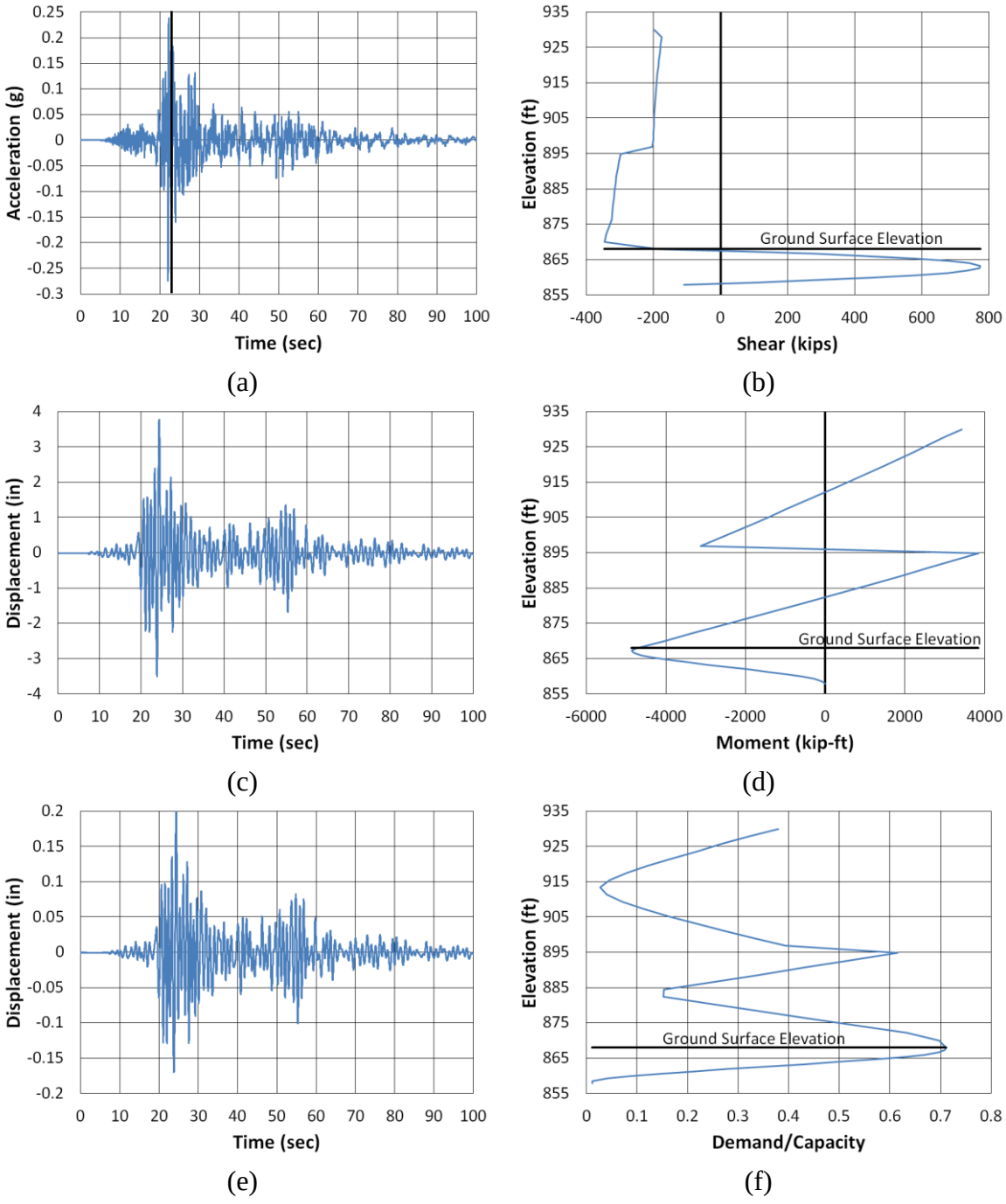

Figure B.193. Marshall County Transverse Kocaeli NMCE (a) time-history event, (b) shear distribution, (c) top of pier displacement, (d) moment distribution, (e) ground surface displacement, and (f) demand capacity ratio

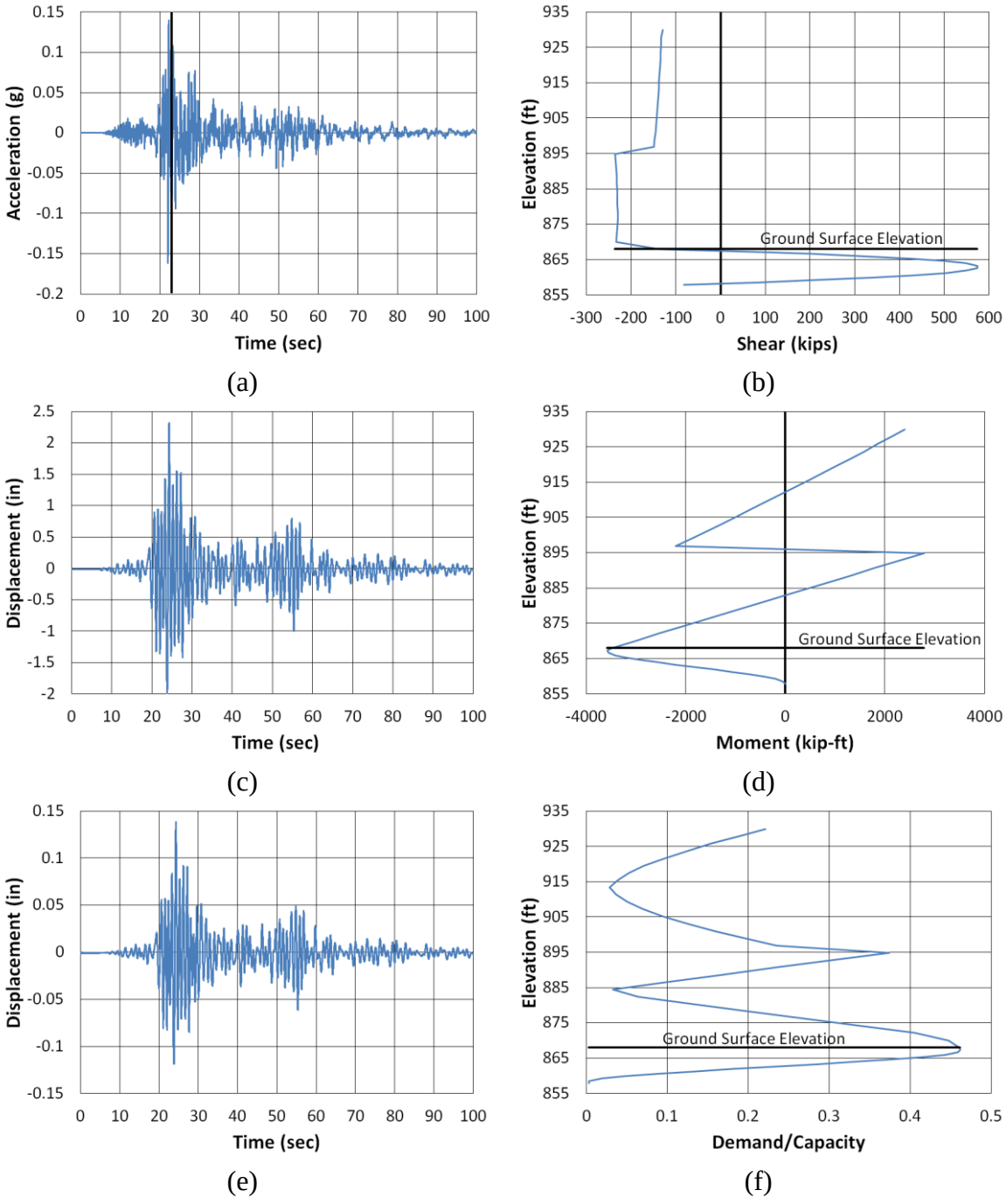

Figure B.194. Marshall County Transverse Kocaeli North (a) time-history event, (b) shear distribution, (c) top of pier displacement, (d) moment distribution, (e) ground surface displacement, and (f) demand capacity ratio

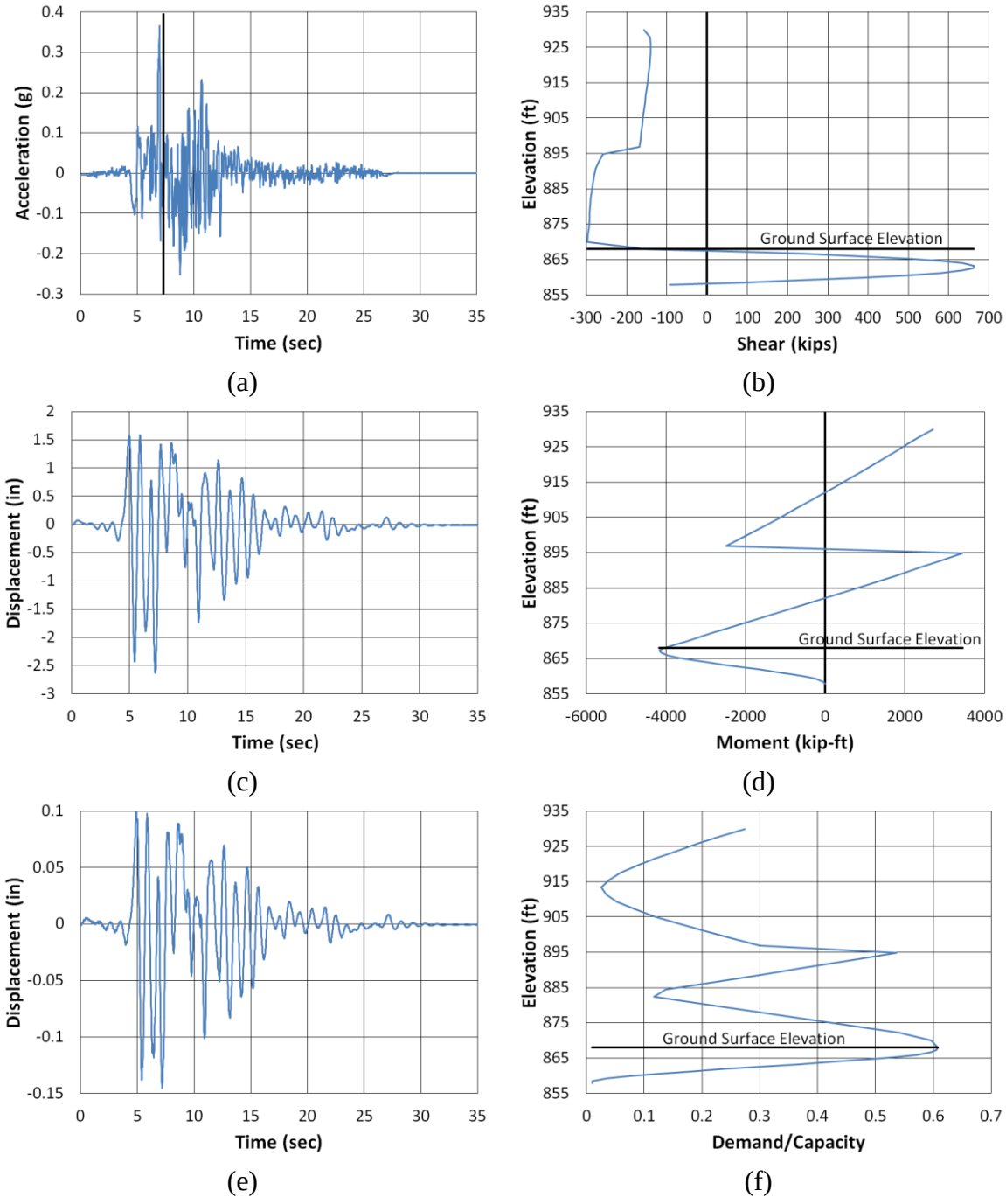

Figure B.195. Marshall County Transverse Kocaeli2 NMCE (a) time-history event, (b) shear distribution, (c) top of pier displacement, (d) moment distribution, (e) ground surface displacement, and (f) demand capacity ratio

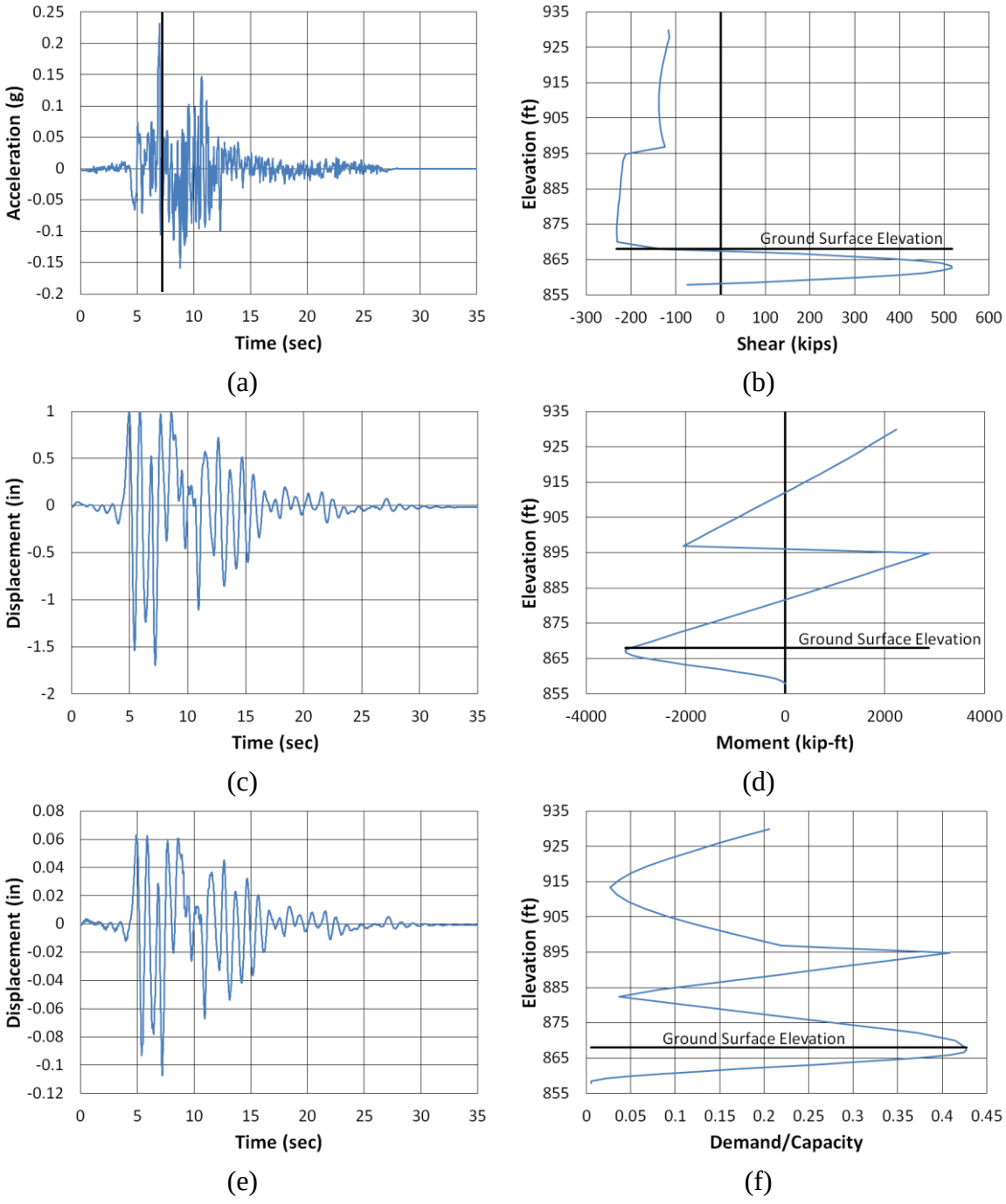

Figure B.196. Marshall County Transverse Kocaeli2 North (a) time-history event, (b) shear distribution, (c) top of pier displacement, (d) moment distribution, (e) ground surface displacement, and (f) demand capacity ratio

.

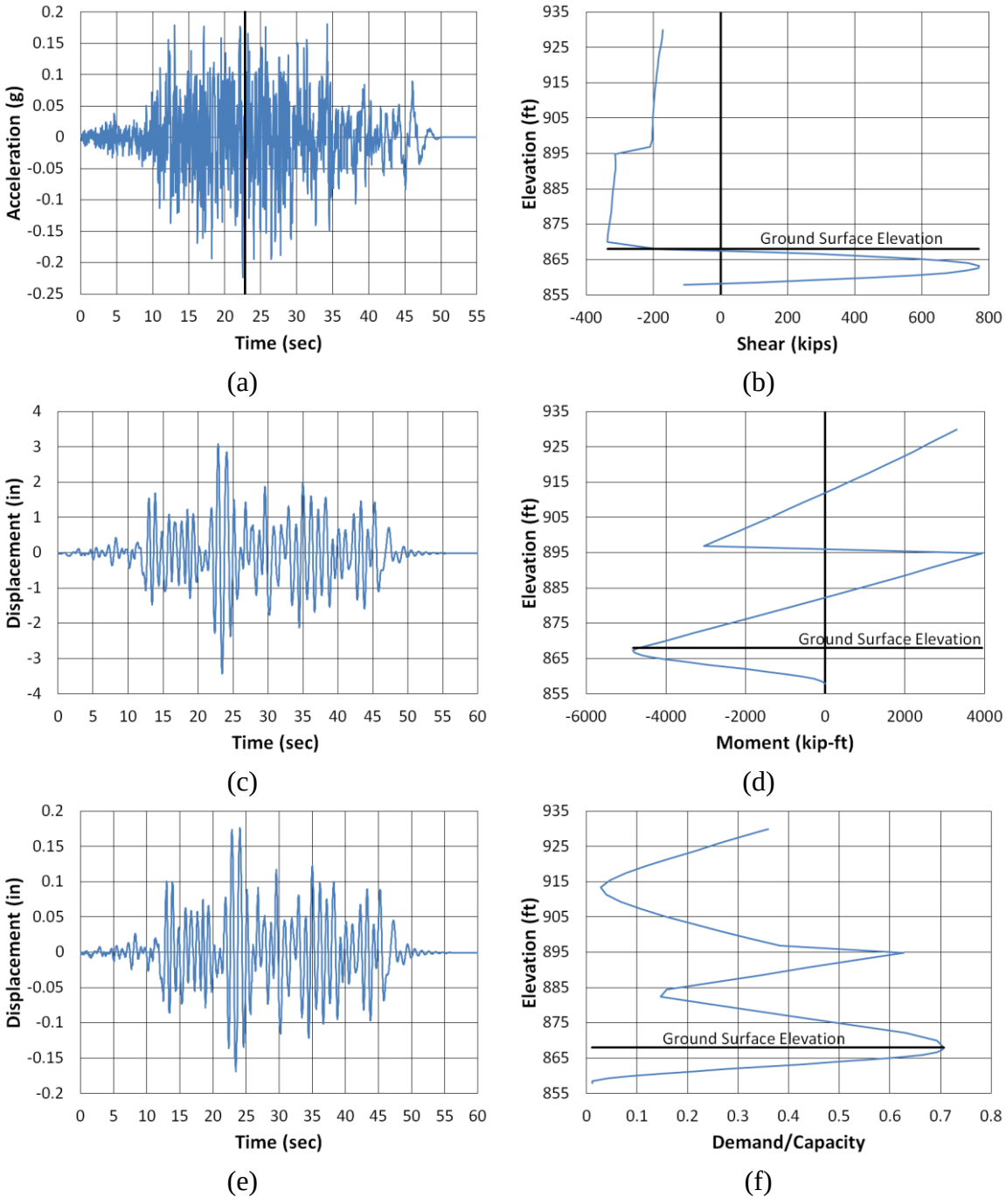

Figure B.197. Marshall County Transverse Landers NMCE (a) time-history event, (b) shear distribution, (c) top of pier displacement, (d) moment distribution, (e) ground surface displacement, and (f) demand capacity ratio

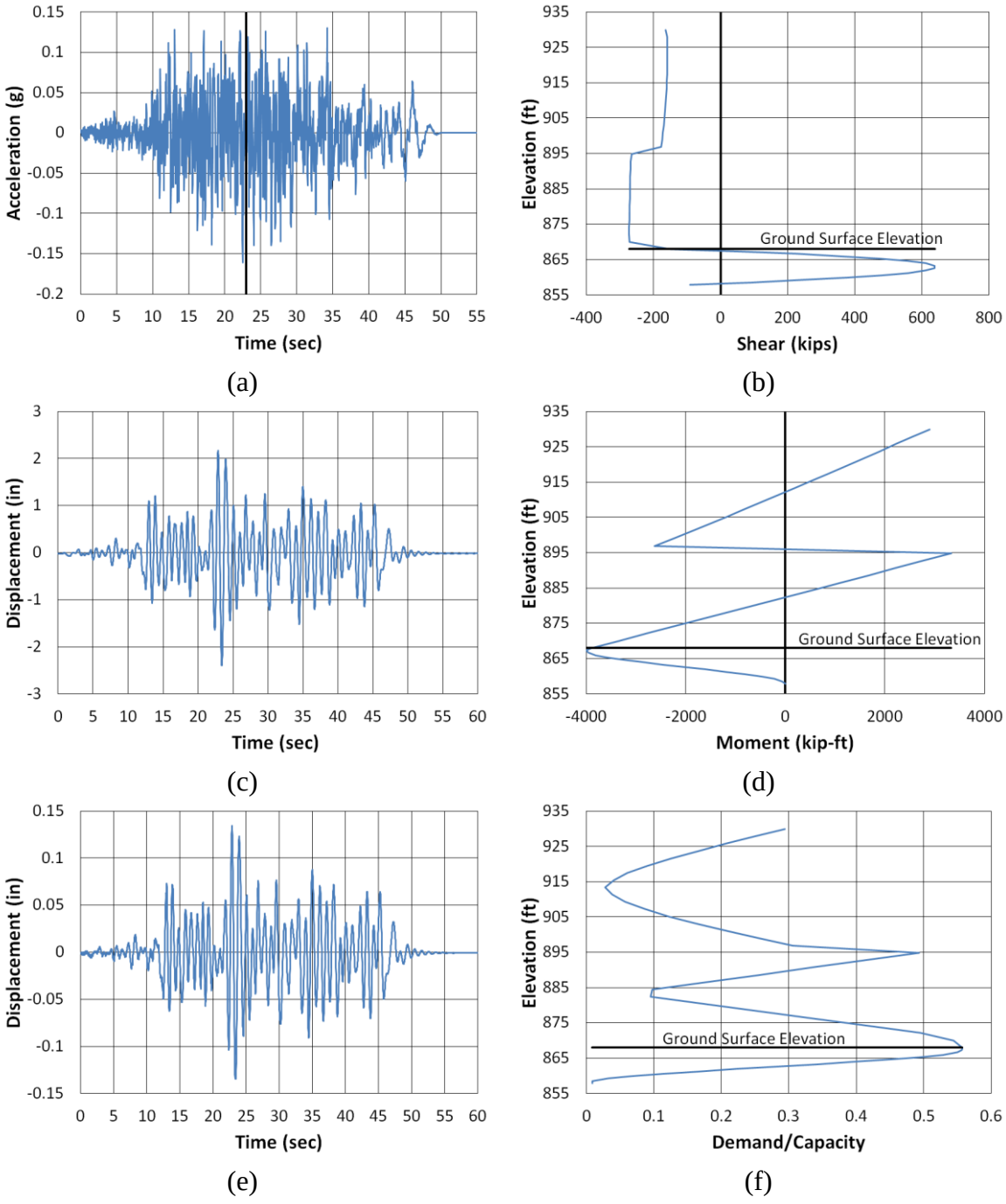

Figure B.198. Marshall County Transverse Landers North (column) (a) time-history event, (b) shear distribution, (c) top of pier displacement, (d) moment distribution, (e) ground surface displacement, and (f) demand capacity ratio

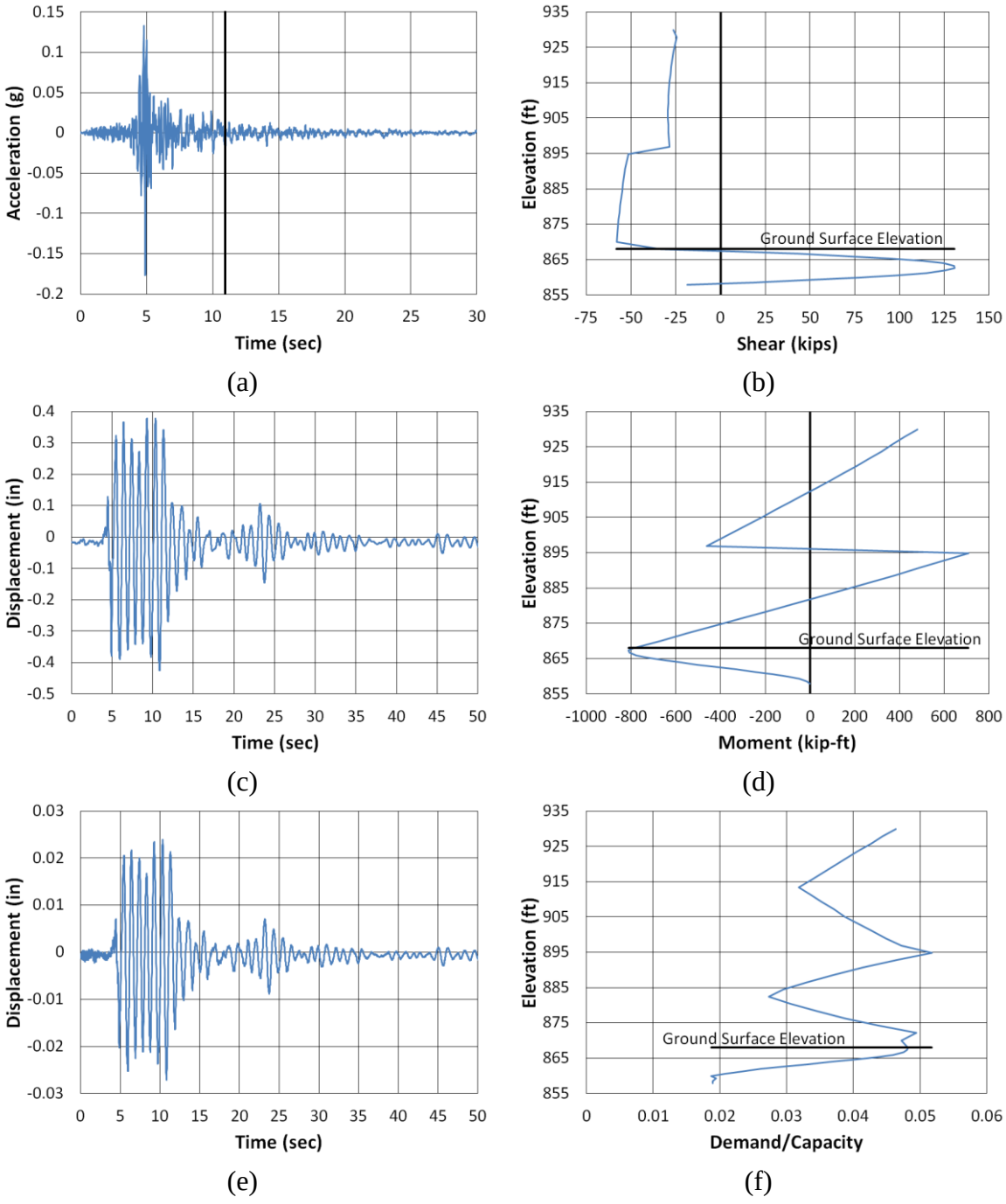

Figure B.199. Marshall County Transverse LSM North (a) time-history event, (b) shear distribution, (c) top of pier displacement, (d) moment distribution, (e) ground surface displacement, and (f) demand capacity ratio

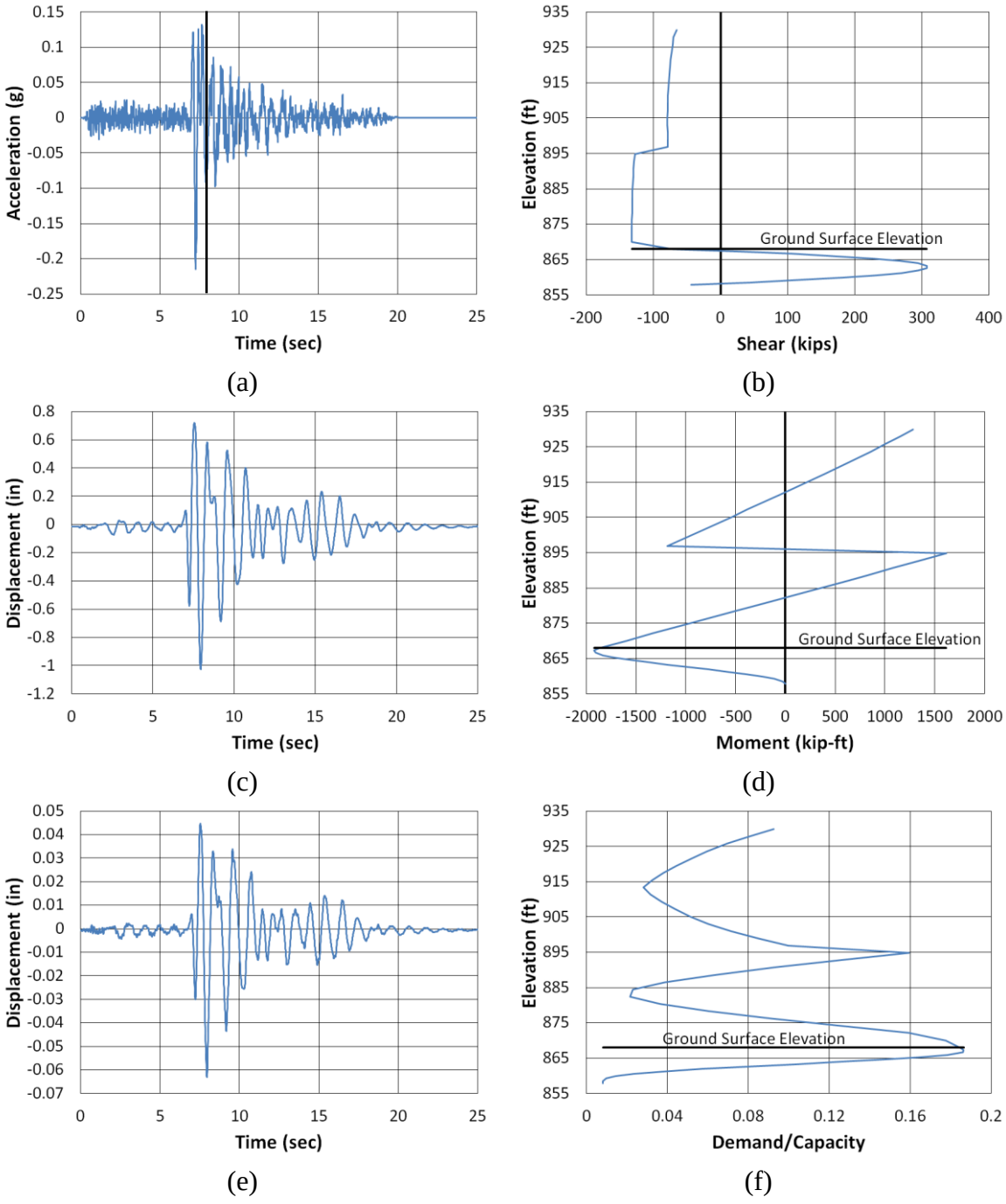

Figure B.200. Marshall County Transverse NPS North (a) time-history event, (b) shear distribution, (c) top of pier displacement, (d) moment distribution, (e) ground surface displacement, and (f) demand capacity ratio

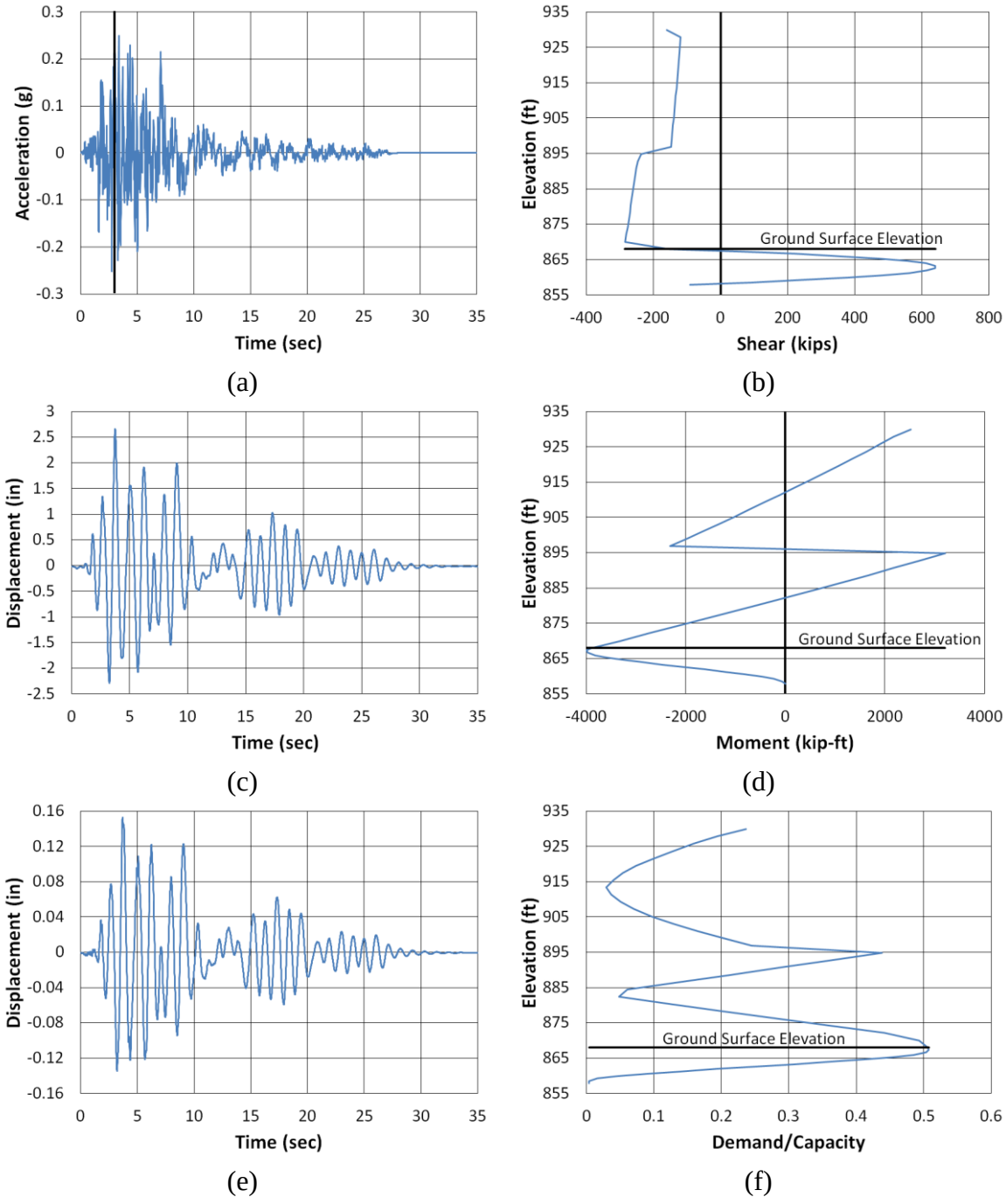

Figure B.201. Marshall County Transverse San Fernando NMCE (a) time-history event, (b) shear distribution, (c) top of pier displacement, (d) moment distribution, (e) ground surface displacement, and (f) demand capacity ratio

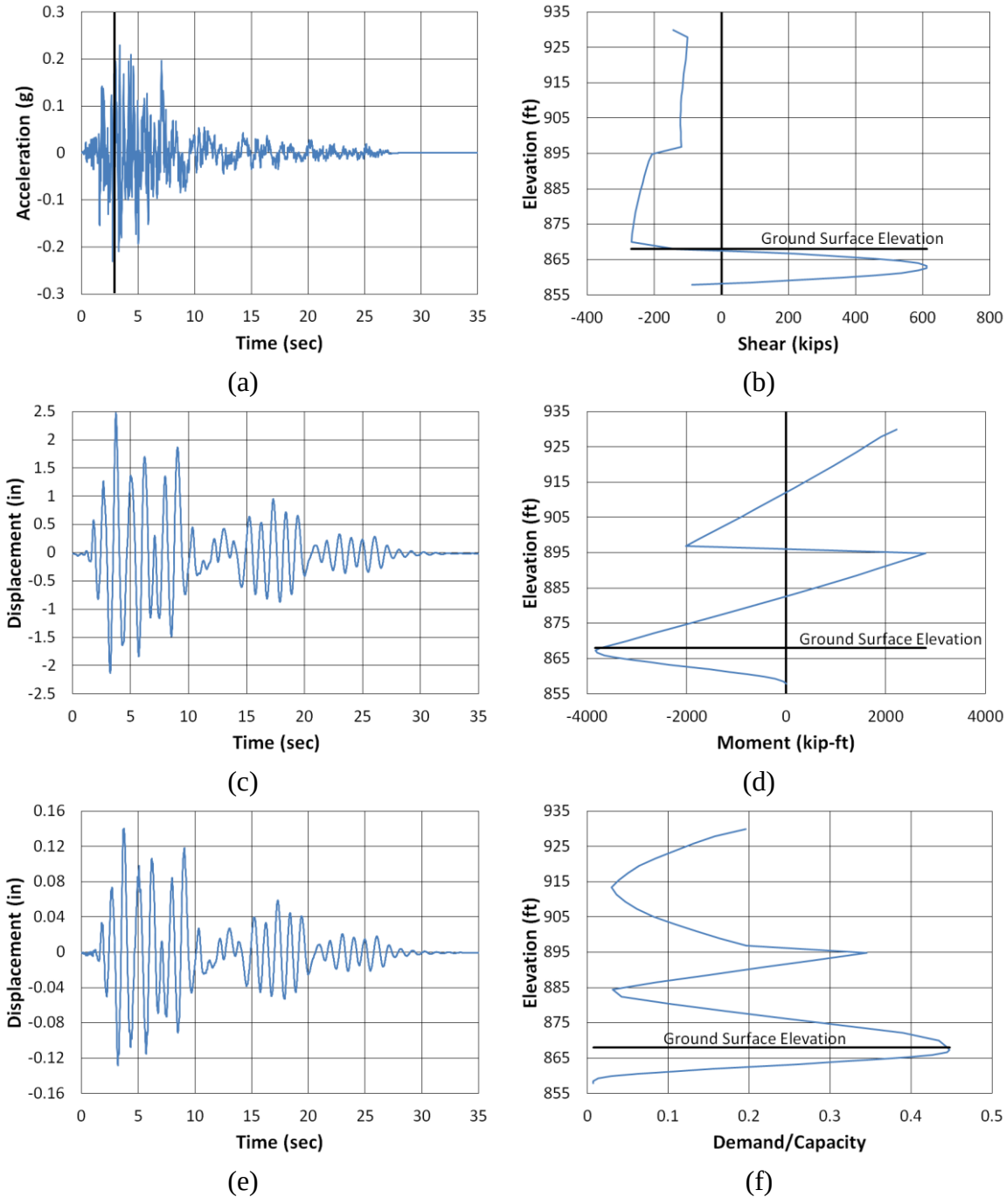

Figure B.202. Marshall County Transverse San Fernando North (a) time-history event, (b) shear distribution, (c) top of pier displacement, (d) moment distribution, (e) ground surface displacement, and (f) demand capacity ratio

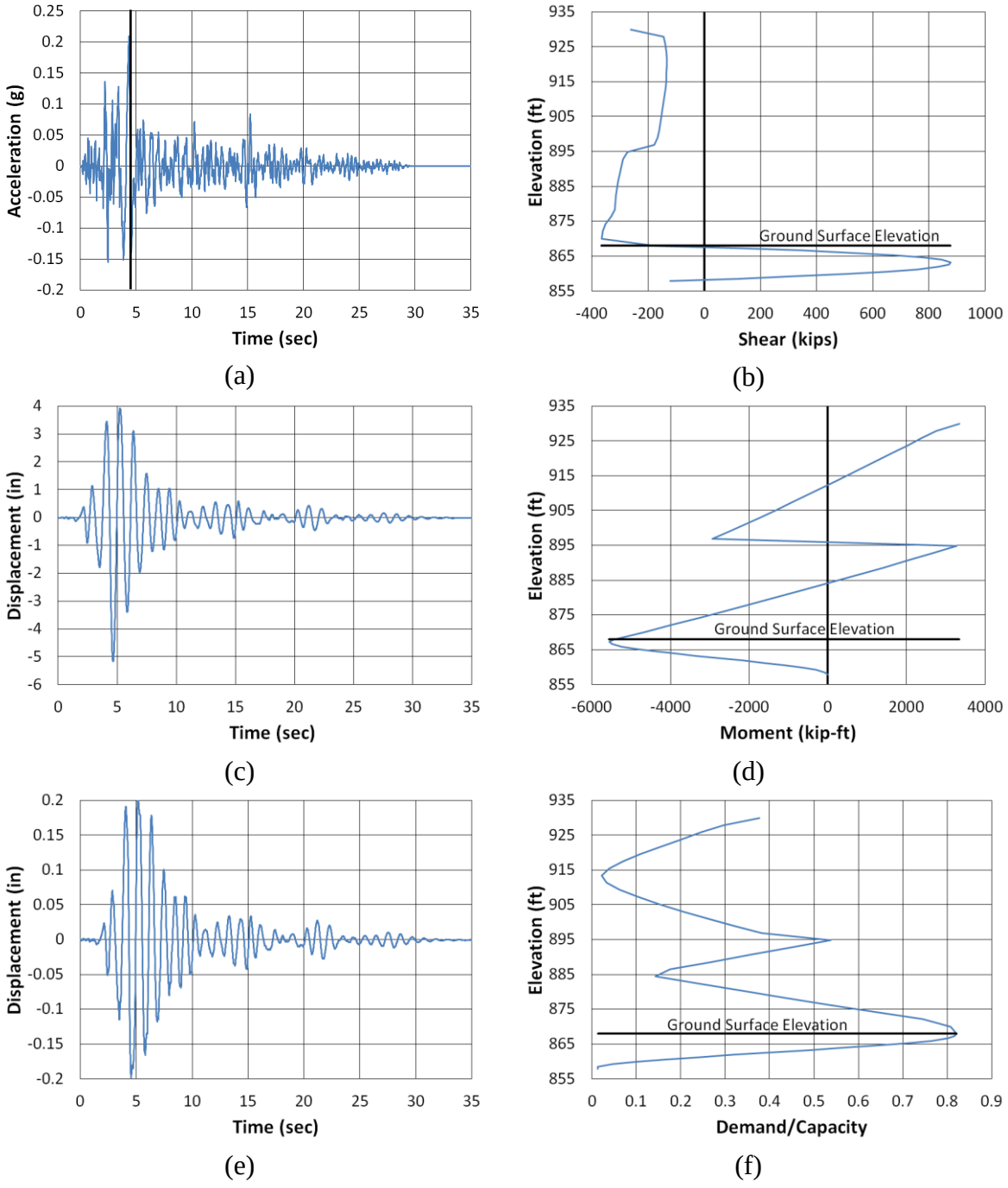

Figure B.203. Marshall County Transverse San Fernando2 NMCE (a) time-history event, (b) shear distribution, (c) top of pier displacement, (d) moment distribution, (e) ground surface displacement, and (f) demand capacity ratio

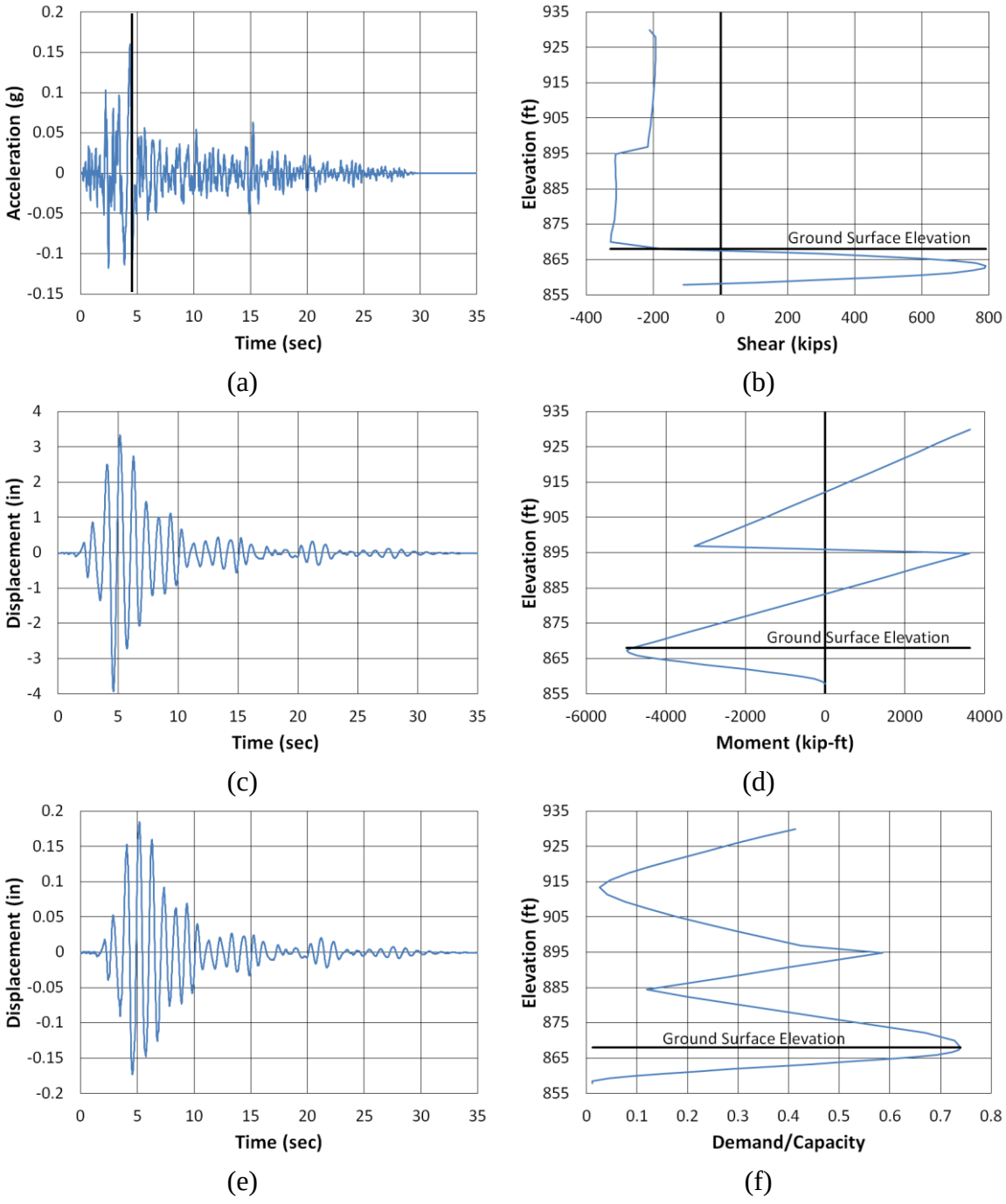

Figure B.204. Marshall County Transverse San Fernando2 North (a) time-history event, (b) shear distribution, (c) top of pier displacement, (d) moment distribution, (e) ground surface displacement, and (f) demand capacity ratio